Escola Tècnica Superior d'Enginyers
de Camins, Canals i Ports de Barcelona

UNIVERSITAT POLITÈCNICA DE CATALUNYA

Experimental and theoretical analysis of cracking in drying soils

PhD Thesis

by

Lakshmikantha, M. R.

Supervised by

Pere Prat Catalán

Alberto Ledesma Villalba

Enginyeria del Terreny, Cartogràfica i Geofísica
Universitat Politècnica de Catalunya

Barcelona, February - 2009

to my mother

Nagalakshmi

Abstract

The thesis focuses on the experimental and theoretical aspects of the process of cracking in drying soils. The results and conclusions were drawn from an exhaustive experimental campaign characterised by innovative multidisciplinary aspects incorporating Fracture Mechanics and classical Soil mechanics, aided with image analysis techniques. A detailed study of the previous works on the topic showed the absence of large scale fully monitored laboratory tests, while the existing studies were performed on already cracked soil, rather than focusing on the process of cracking. Also, the absence of a multidisciplinary approach was strongly felt.

The soil used in the present work is a Barcelona silty clay, extensively studied previously for its Thermo-Hydro-Mechanical (THM) behaviour. Tensile strength and fracture toughness are two important fracture parameters that were not characterized previously and which were determined for the soil used in the investigation. The effect of moisture content on tensile strength and fracture toughness was established. The variation of tensile strength with the degree of saturation was theoretically explored considering the concept of unsaturated cohesion, while the concepts of activation energy and rate process theory were used to explain the relation between the fracture toughness and moisture content.

Preliminary desiccation tests were conducted to gain basic knowledge of the cracking behaviour of Barcelona soil. Further experiments were conducted in a controlled laboratory environment with rectangular holding trays of similar geometry with five different surface areas. Crack initiation, temporal evolution of cracks resulting in the final crack pattern, meeting and bifurcation of cracks resulting in intersections, etc. were studied in detail. One of the objectives of the desiccation tests with similar geometry was to check the applicability of fracture mechanics. The results of the experiments showed existence of size-effect in soil cracking, thus justifying the use of fracture mechanics as a framework to model crack propagation.

A novel equipment capable of simulating the different combinations of climatic conditions with monitoring by sensors and a digital camera was designed and constructed. This en-

vironmental chamber can hold large specimens up to 80 cm in diameter and 20 cm thick. The results from experiments carried out with the environmental chamber have provided new knowledge about the process and mechanisms of desiccation cracking. Some observations made during the experiments prompted more detailed experiments on some aspects of crack formation. The morphology of cracks, fissures, and the presence of spiral and ripple-like cracks on the bottom surface demanded to explore a different theoretical point of view into the mechanism of cracking in soils. The possibility of using a theory based on either classical or unsaturated soil mechanics is critically examined, with emphasis on the importance of surrounding ambient conditions and seasonal variations.

Finally, detailed macro-morphology analysis of the crack patterns was performed. A theory was developed based on the morphology of crack patterns to explain the crack formation as a result of successive domain divisions or hierarchical nature of crack formation. To test the proposed theory, temporal evolution of cracks and crack pattern were studied in detail, showing the existence of hierarchy very clearly. An attempt has been made to explore a new way of analysing the cracking in soils as a process in transition from a disordered (at crack initiation) to a deterministic behaviour (at the end of drying resulting in a complex pattern). Finally, the possible mechanisms for the formation of cracks at the bottom of the specimens were examined, with emphasis on curling and synaeresis processes.

Resumen

La tesis se centra en los aspectos teóricos y experimentales del proceso de agrietamiento de suelos por desecación. Los resultados y las conclusiones fueron extraídos de una exhaustiva campaña de experimentación caracterizada por su aspecto multidisciplinario, incorporando las bases de la mecánica de fractura y la mecánica del suelo con la ayuda de técnicas de análisis de imagen.

Un estudio detallado de los trabajos anteriores sobre el tema puso de manifiesto la ausencia de experimentos a gran escala monitorizados en el laboratorio. Los estudios existentes se han realizado sobre suelos agrietados en lugar de centrarse en suelos en proceso de agrietamiento. Es remarcable, además, la ausencia de un enfoque multidisciplinario. El suelo utilizado en el presente trabajo es una arcilla limosa de Barcelona, ampliamente estudiada por su comportamiento Termo-Hidro-Mecánico (THM). Se recopilaron las características geológicas y geotécnicas reportadas en anteriores tesis doctorales y se determinaron dos nuevos importantes parámetros de fractura tales como la resistencia a tracción y la tenacidad de fractura del suelo estudiado. Fueron utilizados equipos específicos para cada parámetro. Se estableció el efecto del contenido de humedad en el suelo sobre la resistencia a tracción y tenacidad de fractura. Se estudió de forma teórica la variación de la resistencia a tracción con el grado de saturación, teniendo en cuenta el concepto de cohesión no saturada. Los conceptos de energía de activación y teoría de tasa de proceso se utilizaron para explicar la relación entre la tenacidad de fractura y el contenido de humedad.

Para conocer el comportamiento del suelo estudiado en cuanto a desecación y agrietamiento se realizaron unos ensayos preliminares. Adicionalmente, se realizó otra serie de experimentos con bandejas de geometría similar pero con diferente superficie, estudiando con precisión detalles como la iniciación y la evolución temporal de las grietas, sus intersecciones y el patrón final de agrietamiento. En general los resultados de los ensayos de desecación confirmaron los datos conocidos, excepto algunas observaciones que no correspondían a ningún resultado de estudios previos publicados. Uno de los objetivos de los ensayos de desecación con geometrías similares fue el de estudiar la aplicabilidad de

la teoría de Mecánica de Fractura. Los experimentos demostraron la existencia del efecto del tamaño en el agrietamiento del suelo, justificando el uso de la mecánica de fractura como marco teórico de referencia para modelar el proceso de propagación de las fisuras en suelos.

Se diseñó y construyó un nuevo equipo especial para el estudio del fenómeno del agrietamiento por desecación, la cámara ambiental, capaz de simular las diferentes combinaciones de condiciones climáticas con control por sensores y una cámara fotográfica digital integrada. En ella se pudieron estudiar muestras de gran tamaño, hasta 80 cm de diámetro y 20 cm de espesor. Algunas observaciones llevadas a cabo durante los experimentos mostraron la necesidad de realizar estudios ms detallados y de cambiar el punto de vista teórico del mecanismo de agrietamiento de suelos. Especialmente, teniendo en cuenta la presencia de grietas en forma de espiral en la superficie inferior de la muestra. La posibilidad de utilizar teorías basadas tanto en la mecánica de suelos clásica como en la no saturada fue examinada desde un punto de vista crítico, con énfasis en la importancia de las condiciones ambientales y las variaciones estaciónales.

Por último, se llevó a cabo un estudio sobre la macro-morfología detallada del patrón de agrietamiento. Una teoría basada en la morfología de las grietas fue desarrollada para explicar la formación de las grietas como resultado de las sucesivas divisiones de áreas integrales o de la naturaleza jerárquica de la formación de grietas. Para probar la nueva teoría, se estudió la evolución temporal de las grietas y el patrón de fisuras en detalle y los resultados mostraron la existencia de una jerarquía clara. Se realizó un intento de explorar una nueva forma de enfocar el agrietamiento de suelos como una conducta desordenada o determinista. Finalmente, los posibles mecanismos para la formación de grietas en la parte inferior de la muestra fueron examinados, dando importancia a los fenómenos de deformación por flexión y sinéresis.

Resum

La tesis es centra en els aspectes teòrics i experimentals del procés d'esquerdament en sòls per dessecació. Els resultats i les conclusions varen ser extretes d'una exhaustiva campanya d'experimentació caracteritzada pel seu aspecte multidisciplinari, incorporant les bases de la mecànica de fractura i la mecànica del sòl amb l'ajuda de tècniques d'anàlisis d'imatge.

Un estudi detallat dels treballs anteriors sobre el tema va posar de manifest l'absncia d'experiments a gran escala monitoritzats al laboratori. Els estudis existents s'han realitzat sobre sòls esquerdats en comptes de centrarse en sòls en procés d'esquerdament. s remarcable, a més, l'absència d'un enfocament multidisciplinar. El sòl utilitzat en el present treball és una argila llimosa de Barcelona, àmpliament estudiada pel seu comportament Termo-Hidro-Mecànic (THM). Es varen recopilar les característiques geològiques i geotècniques descrites en anteriors treballs i es varen determinar dos nous importants paràmetres de fractura tals com la resistència a tracció i la tenacitat de fractura del sòl estudiat. Van ser necessaris equips específics per a cada un dels paràmetres. Es va establir l'efecte del contingut d'humitat del sòl sobre la resistncia a tracció i la tenacitat de fractura. Es va explorar de forma teòrica la variació de la resistència a tracció amb el grau de saturació, tenint en compte el concepte de cohesió no saturada. Els conceptes d'energia d'activació i la teoria de velocitat del processos es varen utilitzar per a explicar la relació entre la tenacitat de fractura i el contingut d'humitat.

Per a conèixer el comportament del sòl estudiat en quan a dessecació i esquerdament es varen realitzar uns assaigs preliminars. Addicionalment, es varen realitzar una altra sèrie d'experiments amb safates de geometria similar però amb diferents superfícies, estudiant amb precisió detalls com l'inici i l'evolució temporal de les esquerdes, llurs interseccions i el patró final d'esquerdament. En general els resultats dels assaigs de dessecació varen confirmar les dades conegudes, exceptuant algunes observacions que no corresponien a cap resultat d'estudis previs publicats. Un dels objectius dels assaigs de dessecació amb geometries similars va ser el d'estudiar l'aplicabilitat de la teoria de mecànica de fractura. Els experiments varen demostrar l'existència del efecte del tamany en l'esquerdament de

sòls, justificant l'ús de la teoria de la mecànica de fractura com a marc de referència per a un model teòric de propagació d'esquerdes en sòls.

Es va dissenyar i construir un nou equip especial per a l'estudi del fenomen d'esquerdament per dessecació, la cambra ambiental, capaç de simular diferents combinacions de condicions climàtiques amb control per sensors i una càmera digital integrada. Amb ella es varen poder estudiar mostres de gran tamany, fins a 80 cm de diàmetre i 20 cm d'espessor. Algunes observacions dutes a terme durant els experiments varen mostrar la necessitat de realitzar estudis més detallats i de canviar el punt de vista teòric del mecanisme de d'esquerdament en sòls. Especialment, tenint en compte la presència d'esquerdes en forma d'espiral a la superfície inferior de la mostra. La possibilitat d'utilitzar teories basades tant en la mecànica de sòls clàssica com en la no saturada va ser examinada des d'un punt de vista crític, emfatitzant la importància de les condicions ambientals i les variacions estacionals.

Per últim, es va estudiar la macro-morfologia detallada del patró d'esquerdament. Una teoria basada en la morfologia de les esquerdes va ser desenvolupada per explicar la formació de les esquerdes com a resultat de les successives divisions d'àrees integrals o de la naturalesa jeràrquica de la formació d'esquerdes. Per a provar la nova teoria, es va estudiar l'evolució temporal de les esquerdes i el patró d'esquerdament en detall i les resultats varen mostrar l'existència d'una jerarquia clara. Es va realitzar un intent d'explorar una nova manera d'observar l'esquerdament de sòls com una conducta desordenada o determinista. Finalment, els possibles mecanismes per a la formació d'esquerdes a la part inferior de la mostra varen ser examinats, donant importància als fenòmens de deformació per flexió i la sinèresi.

Acknowledgements

I would like to convey my profound gratitude to my tutors, Pere Prat and Alberto Ledesma for their guidance and cooperation during this thesis. I like to express my gratitude to Pere Prat for the initiative and eagerness showed when I was still in India and looking for an opportunity to do further studies and to Ravindra Gettu who introduced me to Pere Prat.

Special thanks to Toni Lloret for all those suggestions and the discussions I had with him during the course of this thesis. I wish to thank Eduardo Alonso and Antonio Gens. Thanks to Enrique Romero for his cooperation and suggestions during the experimental work.

I would like to thank Marcelo Sanchez for all the encouragement and words of experience.

Thanks to Pierre Delage, Emanuel de Laure and the people from CERMES, ENPC, Paris. My gratitude to Vincenzo and Jean-Michel for the cooperation and the friendship they extended.

I would like to thank administrative team of the department: Eva, Mari Carmen, Oscar, and Victor. Thanks to Albert and Joan for keeping me virus free and always connected. Thanks to Fernando, Jose and Manel for their support in the laboratory work. Very big thanks to Tomas for his invaluable collaboration in the design of experimental equipment. Thanks to Maria Jose from the administrative section of the school.

I thank all those persons I met during my stay in Barcelona, especially Daniel, Juan, Beti and Olga.

Thanks to Imma Llort and the group of Escola de Bambu from Casa Asia, Barcelona.

Finally, I would like to thank my parents in Bangalore, Ranga & Ramya, and Olga.

Table of Contents

List of Figures

List of Tables

Chapter 1

Introduction

1.1 Background

Seasonal variations in climatic conditions affect water retention in soils and as a result they swell and shrink. During droughts shrinkage of soils is commonly associated with the formation of cracks. Physical properties and behaviour of cracked soils are quite different from those of the intact soil. Cracking is a complex phenomenon in general and especially for materials such as soils, which are inherently heterogeneous and multi-phase materials with history, time, temperature and water content dependent behaviours. The presence of desiccation cracks in the soil mass changes soil behaviour in many ways. Hydraulic conductivity increases due to crack formation which has several adverse effects in different situations such as rapid and direct movement of water and solutes from the soil surface to the permeable sub-strata [Rounsevell et al., 1999];[Armstrong et al., 1994];[Flury et al., 1994]: in mine waste deposits contributing to the contamination of surface and subsurface water resources [Rodríguez, 2002]; in the case of landfill liners and covers cracking may affect its stability and integrity apart from the leachate infiltration [Yesiller et al., 2000]; in earth embankments cracking reduces strength and may lead to seepage and percolation problems. Complex networks of cracks give way to the formation of preferential paths for transport of pollutants to the subsoil [Drumm et al., 1997]. Deep vertical cracks during prolonged and intense drought increase the infiltration capacity of the soil, mobilising the shrinkage or swelling potential of deeper soils, and thus increasing the risk to construction. Cracks induced by environmental agents also reduce the bearing capacity of the soil and increase its propensity to erosion. Soils that shrink and swell cause damage to building foundations through subsidence, creating a problem for householders and the housing insurance industry (Building Research Establishment;[BRE, 1990]). In

addition, drier climatic conditions will increase the frequency and size of crack formation in soils, especially those in temperate regions of Europe, which currently do not reach their full shrinkage potential (Climate Change Impacts Review Group;[CCIRG, 1991];[CCIRG, 1996]).

Considerable work has been done in the last two decades to study experimentally the physical phenomenon of cracking in soils. Researchers have worked to give an acceptable reasoning to the process of cracking; nevertheless, the process is highly complicated. The majority of the studies are spread across several disciplines and they have been performed mostly on already cracked soils, instead of focusing on the cracking process (crack formation and propagation). Since the work of Corte and Higashi [Corte and Higashi, 1960] there have been no significant large scale laboratory experiments. Even in their work, relevant parameters such as temperature and relative humidity were not controlled. However these in turn affect suction and the soil's tensile strength.

In a drying soil, a crack initiates when the tensile stresses exceed the soil strength. The tensile strength is dependent on the moisture content of the soil and on the suction. This interrelationship between the main factors makes the process very complicated. Crack propagation may be considered to be governed by the stress state in the crack front and subsequent dissipation of energy, for which the fracture mechanics theory can be used. Some research has been reported with application of linear elastic fracture mechanics (LEFM) concepts to explain the propagation, depth, and spacing of the cracks. The theories explaining the cracking phenomena using LEFM have many shortcomings and are far from being general application. Very few published work can be found on the experimental determination of fracture parameters (tensile strength, fracture toughness) which are essential in determining the cracking behaviour. It is known that the tensile strength of soils varies with the degree of saturation (moisture content) as well as with density. Though the tensile strength determines crack initiation, crack propagation seems to be a fracture driven process wherein concepts of fracture mechanics can be of extreme importance in defining a numerical and theoretical framework.

Studies on desiccation and cracking from the point of view of soil mechanics are few, while application of unsaturated soil mechanics is minimal. But cracking in drying soils is an unsaturated soil mechanics problem, where suction plays a key role. Earlier studies have not focused on this area and new concepts and advanced knowledge of experimentation with unsaturated soils could be used to explain the cracking mechanism.

Characterization of crack patterns is useful in different fields of science and engineering. In Soil Mechanics, structural cracks are of much interest: their shape, size, and ruggedness carry with them clues to past stresses and strains imposed to the soil, with implications

into their future stability and functionality [Preston et al., 1997]. In Agriculture, study of crack patterns can help determine whether different soil management treatments are having an effect on soil structure. Crack patterns act as an indicator of the state of soil structure. If the crack patterns are different between soil treatments, other structural properties of the soil are also likely to be different, but not vice-versa. Crack pattern measurements, together with bulk density, can be used to calculate the volume changes during drying and this can increase the accuracy of water balance calculations for soils which shrink as they dry.

1.2 Objectives and research methodology

The main objective of the present investigation was to advance the understanding on the physical processes and phenomena involved in the desiccation and cracking of soils. More specific objectives are:

- To identify the mechanisms and main causes of cracking.
- To determine the effect of drying on tensile strength and fracture toughness.
- To check the applicability of linear elastic fracture mechanics (LEFM)
- To identify the state of soil at crack initiation and during propagation.
- Effect of extrinsic variables such as temperature and relative humidity.
- Contribute to explain the observed processes from a theoretical point of view.

The research methodology adopted to achieve these objectives is explained as follows:

1. To summarise the published data on desiccation and cracking of soils from all available sources and fields of research.
2. To find the basic cracking behaviour of the Barcelona soil using some simple desiccation tests (preliminary tests).
3. To characterise the Barcelona soil for its fracture parameters (tensile strength and fracture toughness), considering the effect of moisture content and density. The specimens were prepared at different moistures within a defined range taking into account the variation of moisture in a desiccation test.

4. Because qualitative analysis of cracks was not sufficient, a quantitative analysis of the cracks and crack patterns was undertaken using image analysis techniques.

5. Developing a low-cost image acquisition system capable of obtaining good undistorted images prior to image analysis.

6. The applicability of fracture mechanics could be checked by looking for energy-related size-effect in cracking of soils. Therefore experiments with specimens of similar geometry and changing size (in case of cracking the surface area) were carried.

7. Design and construction of a special equipment capable of imposing desired temperature and relative humidity on the desiccating soil. The equipment should monitor all aspects of desiccation and cracking in real-time. For this purpose the environmental chamber was designed and constructed.

8. It has been noticed that there exists a similarity in crack patterns from millimetre to kilometre scale; hence macro-morphology analysis of cracks and crack patterns was also undertaken.

9. An attempt has been made to give a reasonable theoretical explanation in each of the behaviour observed during the experiments.

1.3 Organisation of the Thesis

The Thesis has been divided into nine chapters and two appendices. The chapters contain the different aspects contributing to the totality of the present research work. The chapters are organised in such a manner that individually they fulfil an objective of the investigation and at the same time are independent and self-contained. At the beginning of each chapter a brief introduction explaining the background of the issues addressed in the chapter is given. The following section (in all chapters) gives details of either the experimental equipment or basics of theoretical methods used in the investigation. The experimental procedure adopted is explained. The results and analysis upon comparisons with published data is followed by the theoretical formulation to explain the observed experimental details.

Chapter 1 is this Introduction that shows the background to the present research work, justifying the necessity and impact of the findings to the advancing of the knowledge on the desiccation and cracking in drying soils. The scope and objectives of the present work is explained. The organisation of the thesis is briefly explained.

Chapter 2 gives an account of the published data covering a broad spectrum of research on soil desiccation, cracking and drying soils, etc. Different points of view of diverse research backgrounds emphasising the use of theories based on soil mechanics and fracture mechanics have been compiled. The implication of presence and formation of cracks to different natural and man-made structures, environment, agriculture, etc. is explained along with the important factors responsible for the processes.

In Chapter 3 the geological and geotechnical properties of the Barcelona soil are given. The information is a summary of various research works carried out at the Department of Geotechnical Engineering and Geosciences of UPC.

In Chapter 4, the Barcelona soil is characterised for its fracture behaviour by both experimental and theoretical approaches. Tensile strength and fracture toughness were determined using two different equipments at varying moisture contents and densities. The concept of unsaturated cohesion was used to explain the tensile behaviour of drying soils, while concepts of activation energy and rate process theory were used to explain the variation of fracture toughness with moisture content.

Chapter 5 explores the effect of specimen size, shape and geometry on the initiation, propagation of cracks and the final crack pattern for a desiccating soil starting from same initial state of moisture under the same drying conditions (temperature and relative humidity). The main results were obtained from image analysis techniques of the photos taken during the experiments.

Chapter 6 focuses on the size-effect in soil cracking. Specially designed experiments were performed to observe size-effect during the cracking process in soils. The results and observations from the experiments showed the evidence of existing energy-related size-effect in soil cracking.

Chapter 7 deals with the development of an environmental chamber especially designed and constructed to study the desiccation and cracking behaviour of soils under controlled or imposed climatic conditions. The tests have provided some new insights into the mechanics of the process of formation of cracks in a drying soil. Some observations made during the experiments prompted more detailed (on some aspects of crack formation) experiments. The morphology of cracks, fissures, and the presence of spiral and ripple-like cracks on the bottom surface demanded to explore a different theoretical point of view into the mechanism of cracking in soils.

Chapter 8 analyses the macro-morphology of cracks and crack networks from a new approach based on the theory of successive domain divisions or hierarchical nature of crack

pattern formation. Experimental observations were analysed for temporal changes during the crack pattern formation due to desiccation. Some new ideas were developed: crack formation seen as a system changing from a disorder to deterministic, curling and synaeresis as possible mechanisms of crack formation at the bottom surface of the specimens.

Chapter 9 contains a summary of the conclusions drawn from the investigation. The present research is a clear example of how the combination of different disciplines and experimental techniques help to a better understanding of a complex problem. The chapter also contains the suggestions for future lines of investigation. Also, some suggestions for mathematical modelling and numerical implementation are given.

Appendix A gives details of the image analysis techniques used in the present investigation. Image analysis techniques can be applied to study the crack patterns that appear in cohesive soils under drying conditions due to changes in the environmental conditions. The appendix describes a simple technique to process sequences of images obtained during the laboratory tests, and how information can be gathered by means of image analysis, providing values for such parameters as average crack width, total crack length, total area of cracks, number, area and aspect ratio of un-cracked cells, or evolution of surface shrinkage with time.

Details of publications directly related to the present investigation are presented in Appendix B.

Chapter 2

From physical phenomenon to practical implications

2.1 Introduction

Cracks in soils are naturally occurring phenomena resulting from the seasonal variations in the environment. The cracks in soils are as old as the soil itself. Since ages it has been an object of study for many, to start, the cracks in the irrigated lands and dried water-courses. With the advancement in use of soil for an earthen bund to the clay barriers, liners for repositories, waste containment facilities, the cracks have travelled along, as well. There are two main objectives of the study of cracks in soils, the causes and the implications; quite obviously in the early studies the later was the main objective, in the recent past the former became another main objective along with the later. With the changing time the objectives are becoming more refined, resulting in deeper research to solve the puzzle.

To break or snap apart is the first general meaning of crack in most of the dictionaries.

In technical terms cracking in soils are:

The cracks are result of an internal energy imbalance in the soil mass caused by non-uniform moisture distribution, temperature distribution, or distribution of compaction energy during construction [Fang, 1997].

Shrinking soil often cracks when they dry. Cracking occurs under different conditions and it cannot be explained in the same way [Towner, 1987b].

Crack initiation and propagation in soils is a complex problem involving the mechanics of strain localization and the hydraulics of water flow in saturated and un-saturated media, as well as their interaction [Prat et al., 2002].

Cracking in soils that are undergoing drying is controlled by soil suctions and by soil properties such as compression modulus, Poisson's ratio, shear strength, tensile strength, and specific surface energy [Morris et al., 1994].

Soil mechanical strength is an important indicator of soil physical properties that reflects the soil-cracking characteristics [Nichols and Grismer, 1997].

Cracking is a fracture problem, which is not adequately treated by a strength-of-material approach in which failure is defined in terms of tensile strength [Harison and Hardin, 1994].

The interchange of moisture required for the soil water balance to adjust itself both seasonally and in the long term takes place mainly by the transfer of energy and water through the soil surface. As this transfer takes place, the soil is alternatively wetted & dried, and swells & shrinks in sympathy. The shrinkage results in surface cracking, and the subsequent wetting and swelling causes the cracks to close again [Blight, 1997].

The mechanical response of clays is dictated by their fabric as well as by flaws or discontinuities that may exist in the material. These flaws, often in the form of cracks(or notches) and inclusions, result in shear bands that spread from the crack and form a zone in which most of the deformation is localized [Saada et al., 1994a].

Where and how does the crack initiates?

Cracking was found to begin from the center of the soil layer and to propagate to the surface or bottom with non-uniform speed [Corte and Higashi, 1960].

The crack is generally initiated at a surface of great stress (often at or near the ground surface) and is propagated toward the interior of the medium where the tension diminishes and ultimately passes in to compression [Lachenbruch, 1961].

Cracks are developed as soil is restrained against the volume change resulting from the soil suction generated with in a desiccating soil mass [Nahlawi and Kodikara, 2002].

The development of significant tensile strain causes tension cracks in well-developed tension zones in brittle soils [Lee et al., 1988].

Soils generally dry downwards from the surface, where matrix suctions are generally largest and self-weight stresses are zero. The micro-cracking that is present throughout bodies of soil in the form of inter-particle voids is of course also present at the soil surface. Thus, conditions for crack growth are most favourable at the surface of the soil [Morris et al., 1992].

Cracking occurs at the surface when the relationship between effective overburden stress and the horizontal shear stress is such that the soil fails or fractures [Blight, 1997].

During desiccation, cracks initiated at the bottom and propagated vertically upward toward the free surface and laterally outward toward adjacent cracks [Weinberger, 1999].

Why the study of cracks in soils is so difficult?

Previous studies on desiccation cracking are spread across several disciplines and they date back to the early twentieth century. These studies have been predominantly qualitative and behavioral in nature. The field evidence reported covers a wide range of research areas. The reported data are generally incomplete in details and in some cases they are conflicting with one another. Crack spacing varying from about 75 mm to 76 m have been reported. Similarly, the depth of desiccation cracks ranging from several centimeters to over 10 m have been reported in literature. The relationship between the crack depth and spacing was also not clearly defined, although a general trend of larger spacing with deeper cracks seems to exist [Kodikara et al., 1999].

After an extensive literature review Vallejo [Vallejo, 1994] found that, two basic approaches have been taken to examine fissures in clays. The *first approach* is from geological point of view and is concerned with the genesis and classification of fissures. While, the *second approach* concentrate on the effects of fissures on the in-situ strength or strength measured in the laboratory and using these value the relative performance of the fissured clays in slopes and earth dams were determined.

Many researchers have given different definitions for the process of desiccation and cracking, which confuses the reader at first. The probable reason for this may be because of the different objectives behind each work.

2.2 Definition and soil cracking types

Cracking in soils is a complex phenomenon involving physical, chemical, mechanical, hydraulic parameters of soil with respect to its climatic situations and surrounding geo-environment. Considering this coupling of different phenomenon, it would be ideal to explore some of the basics of desiccation and cracking staring from: definitions, types and classification of the cracks.

2.2.1 Definition of the characteristics of cracking soil

Definitions and explanations of some basic terminologies generally used while referring to: desiccation, cracks and crack pattern are given below.

Cracking moisture content, is the moisture content of the soil at the moment when cracking starts. This is obtained by sampling the soil when the cracking is first noted or interpolated on a desiccation curve. For a thicker layer of soil, this moisture content is taken as the one at surface.

Thickness of the soil, is defined as the thickness of the soil when it is completely dry. It is observed that the thickness changed very little after the cracking started.

Cells, are the fragments of soil separated by crack which intersect each other.

Size of cell, is the area of each cell. Generally it is the area after the cracked soil is completely dry, unless it is mentioned that the change of size during desiccation is considered.

Area of cracks, is equal to the area of containers (in which the tests are carried out) minus total area of cells.

Length of cracks, is the total linear dimension which is measured along the cracks.

Specific length of cracks, is defined as the length of cracks per unit area or the length of cracks divided by the total area of the container.

Dry density of the soil, is defined as the weight of solids per unit volume of the soil.

The above definitions were given by Corte and Highashi [Corte and Higashi, 1960].

2.2.2 Classification after [Frookes and Denness, 1969]

The discontinuities in clays were classified based up on their: size, surface geometry, surface roughness, and the intensity and spacing of the fissures. Tables 2.1 to 2.5 show in detail the classifications explained earlier. In tables 2.1 and 2.2, the surface geometry of cracks is measured in terms of area of fissures, the radius of curvature and curved length of the fissure. In table 2.2 L is the curved length of the fissure, R is the radius of curvature of fissure of length L. Table 2.3 show the classification based on the surface roughness of the fissures. The surface roughness is determined in comparison with the roughness grade of standard sand papers. Tables 2.4 and 2.5 show the classification based on the crack intensity and their spacing respectively, the intensity is measured in terms of area of fissures to the total volume of soil.

Table 2.1: Size classification of fissures [Frookes and Denness, 1969]

Type	Size (area)
Very large fissure	$\geq 100m^2$
Large fissure	1 - 100 m^2
Normal fissure	0.01 - 1 m^2
Small fissure	1 - 100 cm^2
Very small fissure	$\leq$ 1 cm^2

Table 2.2: Surface geometry classification of fissures [Frookes and Denness, 1969]

Type	Description*
Planar	L/R $\leq \pi/8$
Semi-curved	$\pi/8$ < L/R < $\pi/4$
Curved	L/R $\geq \pi/4$
Hinged	Combination of planar and semi-curved
Semi-undulose	Combination of two or more alternatively convex and concave semicurved
Undulose	Combination of two or more alternatively convex and concave curved
Conchoidal	As a conchoid

Table 2.3: Fissure surface roughness classification [Frookes and Denness, 1969]

Type	Sand Paper Grade	Height of Asperity, H, above main plane of fissure (mm)
Slickensided	00	0
Very smooth	00	$0 < H \leq 2$
Smooth	00 - 01	$2 < H \leq 4$
slightly rough	01 - 02	$2 < H \leq 4$
Rough	02 - 03	$4 < H \leq 6$
Very rough	03 - 04	$4 < H \leq 6$
Pock marked	04	$6 < H \leq 8$
Pitted	-	$H > 8$

Table 2.4: Intensity classification of fissures [Frookes and Denness, 1969]

Intensity type	Area of fissure per unit volume (m^2/m^3)
Very low	≤ 3
Low	3 - 10
Moderate	10 - 30
High	30 - 100
Very high	100 - 300
Excessive	≥ 300

Table 2.5: Spacing classification of fissures [Frookes and Denness, 1969]

Description	Spacing of fissures
Very thickly	> 2 m
Thickly bedded	0.6 m - 2 m
Medium bedded	0.2 m - 0.6 m
Thinly bedded	60 mm - 0.2 m
Very thinly bedded	20 mm - 60 mm
Laminated	6 mm - 20 mm
Thinly laminated	< 6 mm

2.2.3 Classification after [Fang, 1997]

The types of soil cracking have been classified in to four types: shrinkage, thermal, tensile, and fracture cracks. Explanation to the four types of cracks is presented in the following paragraphs, note that the explanation given is referring to Fang [Fang, 1997].

2.2.3.1 Shrinkage cracking

It is the most common cracking found in earth structures and the phenomena can be observed on drying mud flats as shown in figure 2.1. As water is lost from the surface of a soil mass, tensile forces are established in the drying surface layer. Because of the water loss soil also loses its ability to receive these tensile forces by plastic flow. These stresses are finally relieved by the formation of shrinkage cracks that break up the surface layer into pieces of more or less distinct geometric shapes. This geometric shape of the cracks depends on the clay mineral composition, the heating process, pore fluids, and other factors. As shown in figure 2.1, Illite shows finer cracks than Muscovite, and oven dried samples give more irregular cracking patterns than air-dried samples. If the soil material is homogeneous, the cracking pattern is hexagonal in accordance with the law of the triple angle, which is a special form of the law of least energy. This phenomenon can also be explained by linear elastic fracture mechanics (LEFM) concepts. If the soil system is non homogeneous, as in the case of the presence of organic matter or different water affinity and greater mobility than the mineral soil components, then the hexagons will tend to become rounded and the organic matter will become concentrated at the surface fissures.

2.2.3.2 Thermal cracking

Thermal cracks are caused by the change of the thermal stresses of material. The stresses are developed when material is heated and then suddenly cooled, a significant change in temperature such as freezing-thawing or wet-dry process in soil. The thermal cracks for soil are somewhat different than other construction material because the temperature and moisture in the soil are so closely related and the state of stress of soil is so sensitive to the influence by both temperature and moisture behavior simultaneously.

The plastic deformation occurs in different zones of the soil mass as a result of differential temperature with accompanying volume changes arising during the cooling cycle. If the deformations arising are within the elastic strength range of the soil mass, then no stress

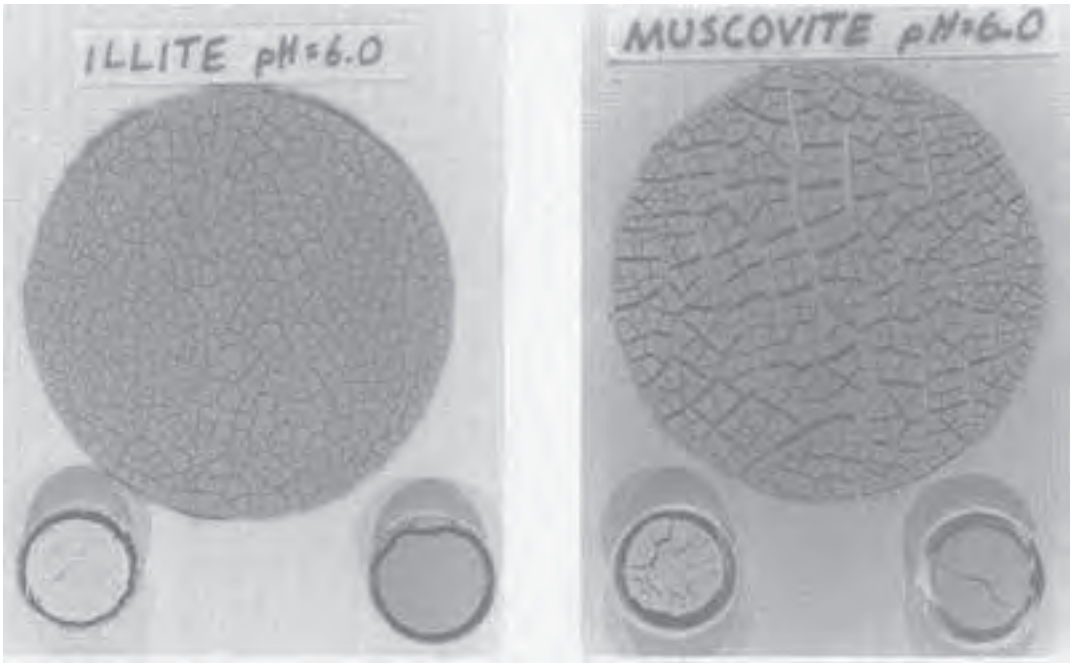

Figure 2.1: Comparison of cracking patterns between Illite and Muscovite clays [Fang, 1997]

remains after temperature equilibrium is reached. As indicated in figure 2.1, the cracking patterns between oven and air dried soil sample of Illite and Muscovite are different because the rate of heating process in the oven is more intense and less uniform than the air-dried process. Other factors that contribute to the thermal cracks are soil types, unit weight, grain size distribution, void ratio, and geometry of the primary and secondary drying surfaces.

2.2.3.3 Tensile cracking

Tensile cracks are caused mainly by overburden pressures including structural loading, rainfall, and ice & snow loads, vegetation, and seasonal creep loads. Sometimes, they are also associated with changes in moisture or thermal stresses, as discussed earlier, and related with fracture loads.

2.2.3.4 Fracture cracking

In a soil mass either man made or in the natural state, there always exist some cracks due to daily moisture or temperature changes or caused by seasonal ground-water table fluctuation, rainfall or melting snow which will fill into the cracks or voids, and consequently,

produce the pore-water pressures. These pore-water pressures vary with changes of these environmental conditions as does the capillarity tension produced from pore-water between the soil particles. When a saturated soil dries, a meniscus develops in each void of the soil structure which produces the tension in the soil water system and a corresponding compression force in the soil skeleton. This compression stress is just as effective as stress commonly used in soil mechanics in producing soil compression as an external load. Pressure of 200 to 300 kPa can be produced in fine-grained soils. This internal cyclic-type load caused by the combination of shrinkage and thermal stresses and the fluctuation of the pore water pressure between soil particles is called fracture load in soil. The cracks produced from the fracture load are referred to as fracture cracks in soil.

2.3 Causes

Williams and Jennings,1977 (as cited by [Vallejo, 1994]) found that fissures develop in clays under, among others, the following circumstances:

(a) fissures develop during the consolidation process,

(b) as a result of a decrease in overburden pressure during swelling of the clay,

(c) as a result of synaeresis, a colloidal phenomena,

(d) chemical reactions in the clay can induce volume distortions with fissures thus being the end result,

(e) as a result of tectonic stresses,

(f) fissures develop as the clay dries,

(g) fissures can be inherited from the bedrock, and

(h) large lateral stresses can induce fissuring of the clay.

There are several causes for desiccation and cracking, researchers have tried to focus on each one of them. Starting from, the composition of the soils to the weather conditions and as well the placement i.e. may be a part of a land fill liner, a clay cover, an earthen bund of a reservoir or simply a mine tailing. Also, different pore fluids causes different patterns of crack, but at this stage it is not relevant to consider the effect of different pore fluids. Although the location and weather conditions are variable factors, the inherited

properties of soils (mineralogy, grain size, etc) are of significant importance. The following subsection explain the effect of soil composition on desiccation.

2.3.1 Soil composition

Soil is a product of weathering, in the process it inherits the original and as well modified properties of the parent rock or mineral. Soil composition has a direct bearing on the shrinkage and swelling properties, which in turn influences the cracking behaviour.

2.3.1.1 Clay content

Volumetric shrinkage strain increases with increasing clay content and plasticity index. The volumetric shrinkage strain increases because soils with higher clay content or plasticity index have a greater affinity for water. The greater affinity for water is reflected in the increase in optimum water content and decrease in maximum dry unit weight (see table 2.6) as the plasticity index increases. which is evident in figure 2.2 a and b, [Albrecht and Benson, 2001].

2.3.1.2 Clay mineralogy

The soils containing larger percentages of Smectite or mixed layer of Illite/Smectite (see table 2.6) showed highest volumetric shrinkage strains. Smectite typically adsorb more water and undergo greater shrinkage before the clay particles come in to contact. The smallest shrinkage strains were observed for soils which contained less Smectite, and more Illite, Kaolinite, and Quartz [Albrecht and Benson, 2001]. Similar observations were made by Omidi et al [Omidi et al., 1996] for a soil with highest clay content and Smectite mineralogy, volumetric shrinkage of 16.4% was observed. But, for Illite soil a volumetric shrinkage of 11.7% was observed. For both the soils an addition of 30% sand resulted in a volumetric shrinkage of 10.3 and 6.2% for Smectite and Illite soils respectively.

2.3.1.3 Soil structure

Corte and Highashi [Corte and Higashi, 1960] conducted laboratory drying tests for soils with loose packing and close packing structure. From the experimental data (see figure 2.3) the time required for crack initiation showed a linear relation with thickness of drying

Table 2.6: Properties of soils used in the study [Albrecht and Benson, 2001]

Depositional environment	Soil							
	Houston Red	Sauk County	Denver	Green Lakes	Wilson Ville	Detroit	Lodgement	New Orleans
	Marine Sediment	Residual Soil	Marine Sediment	Glacial Till	Alluvial	Glacial lacustrine	Glacial	Beach deposit
(a) Classification								
USCS Classification	CH	CH	CL	CL	CL	CL	CL	CL
Liquid limit	67	67	49	35	24	27	18	29
Plasticity index	46	32	26	19	11	15	11	16
% Sand and Gravel	6	47	6	11	38	24	57	48
% fines (0.075mm)	94	53	94	89	62	76	43	52
% Clay (2 μm)	53	40	40	41	20	28	12	16
(b) Mineralogy (%)								
Quartz	24	24	32	33	33	24	46	73
P feldspar	2	0	4	3	3	2	4	1
K feldspar	1	Trace	2	2	6	1	3	Trace
Calcite	12	0	2	8	10	17	12	0
Kaolinite	Trace	0	4	3	7	10	13	Trace
Chlorite	3	4	4	5	2	8	3	2
Illite	8	3	4	22	14	27	4	Trace
Smectite	0	0	43	0	0	0	0	0
Mixed layer Smectite/Illite (% Illite)	44(10-20)	43(20-30)	0	18(70-80)	23(50-60)	9(70-90)	13(60-70)	22(10-40)
(c) Compaction								
$\gamma_{dmax}(kN/m^3)$								
Reduced Proctor	15.5	14.8	NA	NA	NA	NA	NA	NA
Standard Proctor	16.2	15.5	17.6	17.4	20.4	19.1	20.6	19.0
Modified Proctor	17.5	17.7	NA	NA	NA	NA	21.8	NA
$W_{opt}(\%)$								
Reduced Proctor	21	24	NA	NA	NA	NA	NA	NA
Standard Proctor	19	21	18	17	10	13.5	9	12
Modified Proctor	16	16	NA	NA	NA	NA	7.3	NA

NOTE: NA=not applicable

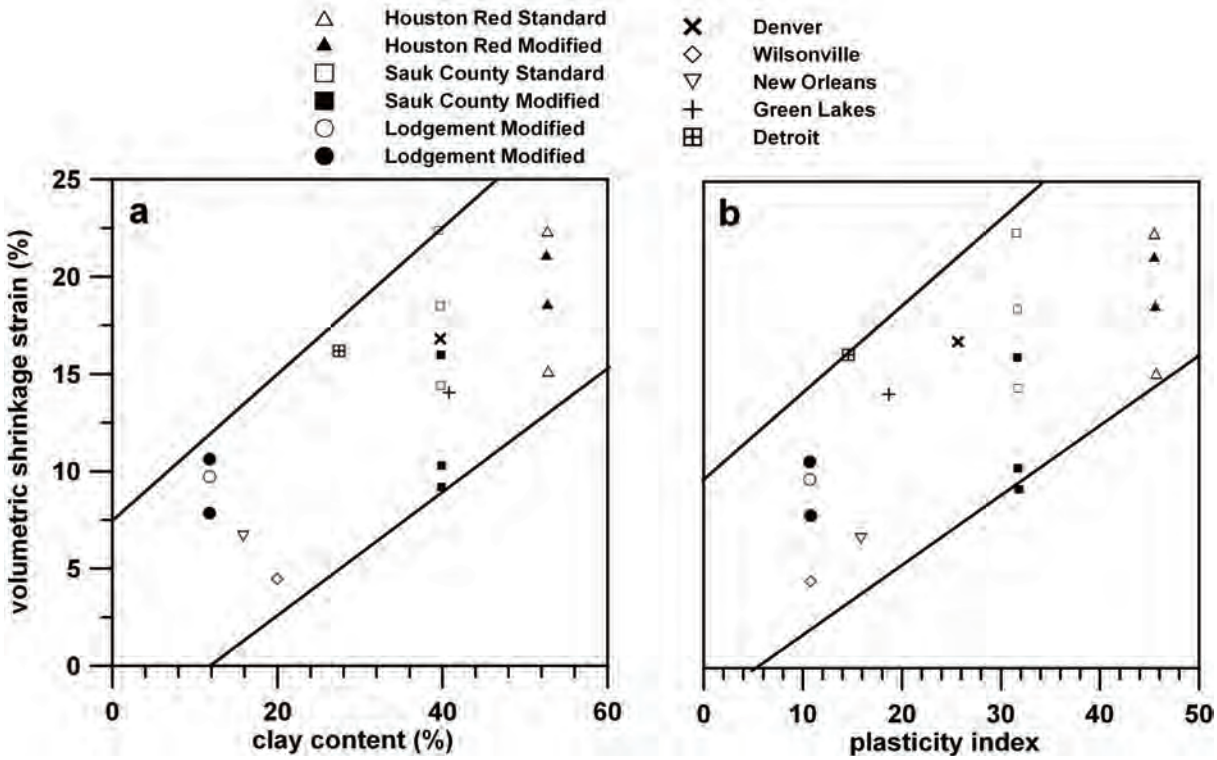

Figure 2.2: Volumetric shrinkage strain versus soil properties: (a) clay content;(b) Plasticity index [Albrecht and Benson, 2001]

layer for close packing soils (denser soils). For loose packing soils, the relation was a saturation curve type, i.e. after some threshold value (of drying layer thickness) the relation is no more linear. The different behaviour for loose and close packing may be due to the difference of speed of evaporation from the surface and the speed of vapour diffusion in the soil. Another observation made was, the cracking (first crack) in the loose packing soil started at a higher moisture content than the close packing soil.

Fang [Fang, 1997] in their study on desiccation and cracking, referring to other researchers points out that the different soil structures like flocculating or dispersive structures when filled with different pore fluids if subjected to desiccation create different types of cracking patterns. The illustration in figure 2.4 shows a soil structure where flocculating structure hypothetically produces larger areas of cracking than dispersive structures.

2.3.1.4 Density

The density of the soil seems to have an effect on the cracking behaviour of soils. The effect of density on the cracking behaviour is reported in the work of Albrecht and Benson [Albrecht and Benson, 2001]. For details of the properties of the different soils used in

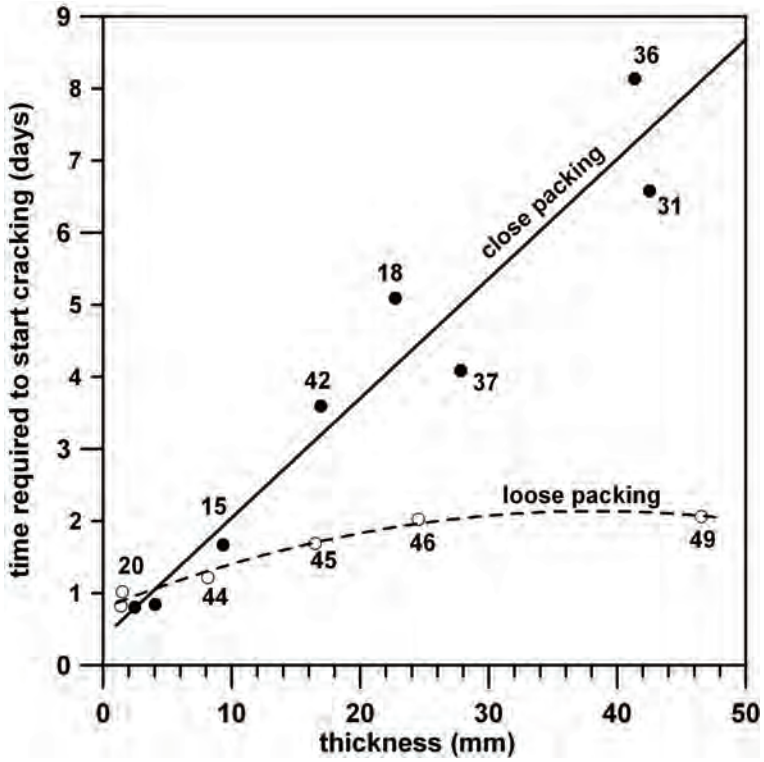

Figure 2.3: Thickness of soil vs time required to start cracking [Corte and Higashi, 1960]

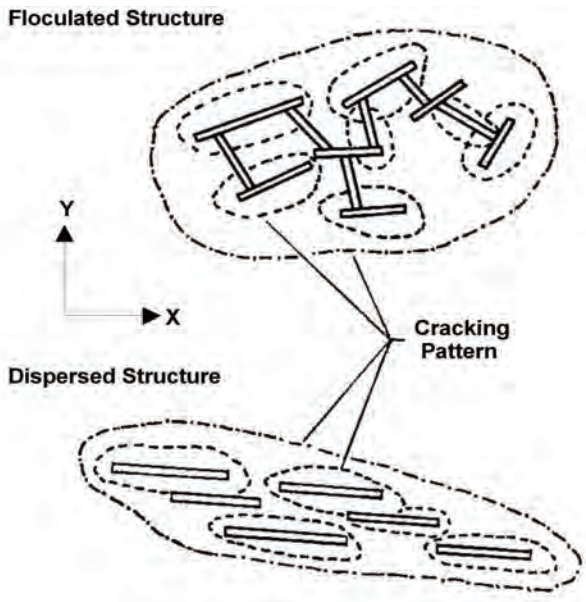

Figure 2.4: Schematic diagram illustrates the effect of soil structure on cracking behaviour [Fang, 1994]

their study is given in table 2.6. The variation of volumetric shrinkage strain for different dry densities is shown in figure 2.5 and the volumetric shrinkage was observed to be higher for lower dry density and vice versa. A different approach to show the effect of density is from the work of Corte and Highashi [Corte and Higashi, 1960]. A plot relating thickness with cracking moisture content is shown in figure 2.6, where for same thickness of drying layer the cracking moisture content is lower for higher density and visa versa.

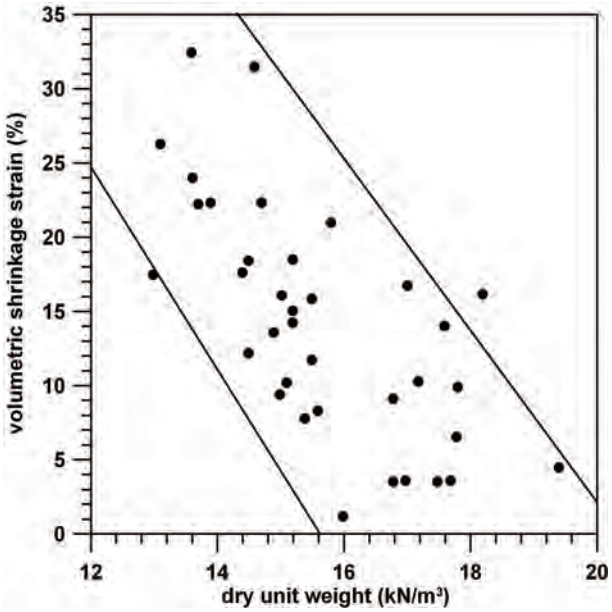

Figure 2.5: Volumetric shrinkage strain and dry unit weight [Albrecht and Benson, 2001]

2.3.2 Compaction

Barriers and liners are engineered components of a system with a purpose to serve, their integrity and durability is a matter of concern. Albrecht and Benson [Albrecht and Benson, 2001]) showed that clay barriers in earthen covers typically became very moist or field saturated each year by late winter, even in seasonal semi arid climates. The barriers then dry as water is extracted during spring, summer, and early fall. Though, the process of compaction and the compaction water content does not matter in desiccation of soils occurring naturally or a tailing, but is significant in the case of clay barriers and liners. Albrecht and Benson [Albrecht and Benson, 2001] conducted studies to determine how factors such as number of drying cycles, compaction conditions, and soil composition and mineralogy affect shrinkage and cracking of compacted clays subjected to desiccation. Omidi et al [Omidi et al., 1996] and Sivakumar and Gartung [Babu and Gartung, 2001] conducted experiments to study the effects of desiccation cracking on the hydraulic

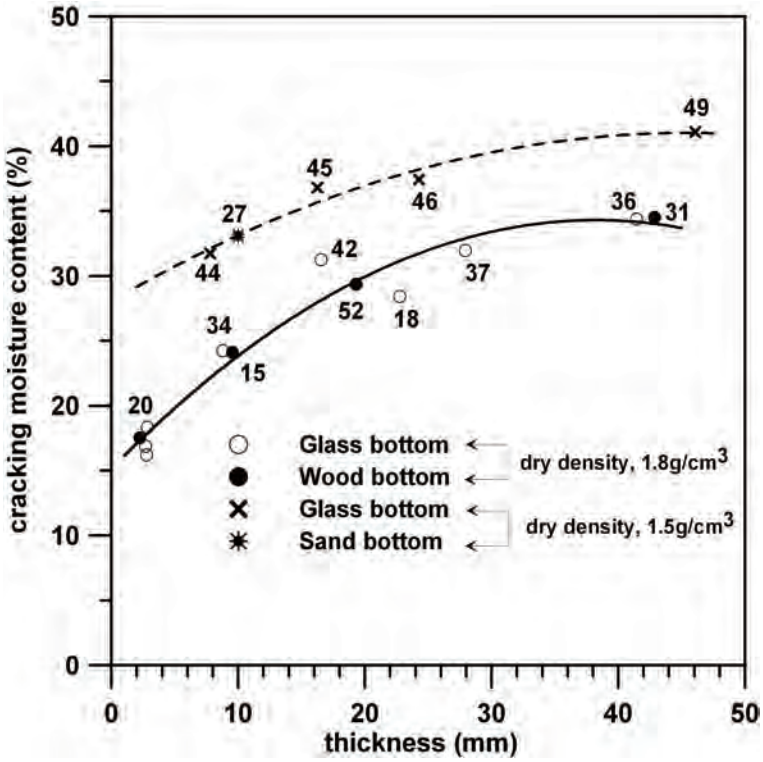

Figure 2.6: Cracking moisture content and thickness of drying layer [Corte and Higashi, 1960]

conductivity of the compacted clay liner. The summary of the above mentioned works is presented in the following paragraphs.

2.3.2.1 Compaction effort and water content

From the work of Albrecht and Benson [Albrecht and Benson, 2001] the specimens compacted with the lowest compaction effort shrank the most and specimens with the lowest volumetric shrinkage strain typically were compacted near optimum water content irrespective of the compaction effort (see figure 2.7). Volumetric shrinkage strain increased with an increase in compaction water content relative to optimum. Volumetric shrinkage strains as large as 30% were observed at water contents 5% wet of optimum. Like wise, the volumetric shrinkage strain increases as the compaction water content becomes dry of optimum, with a volumetric shrinkage strains above 15%. The lowest volumetric shrinkage strains generally occurred for specimens compacted near optimum content. Sivakumar and Gartung [Babu and Gartung, 2001] from their work referring to the suction observed that standard proctor effort resulted in lesser suction pressures compared to modified proctor effort, indicating the effect of compaction effort on the macro structure.

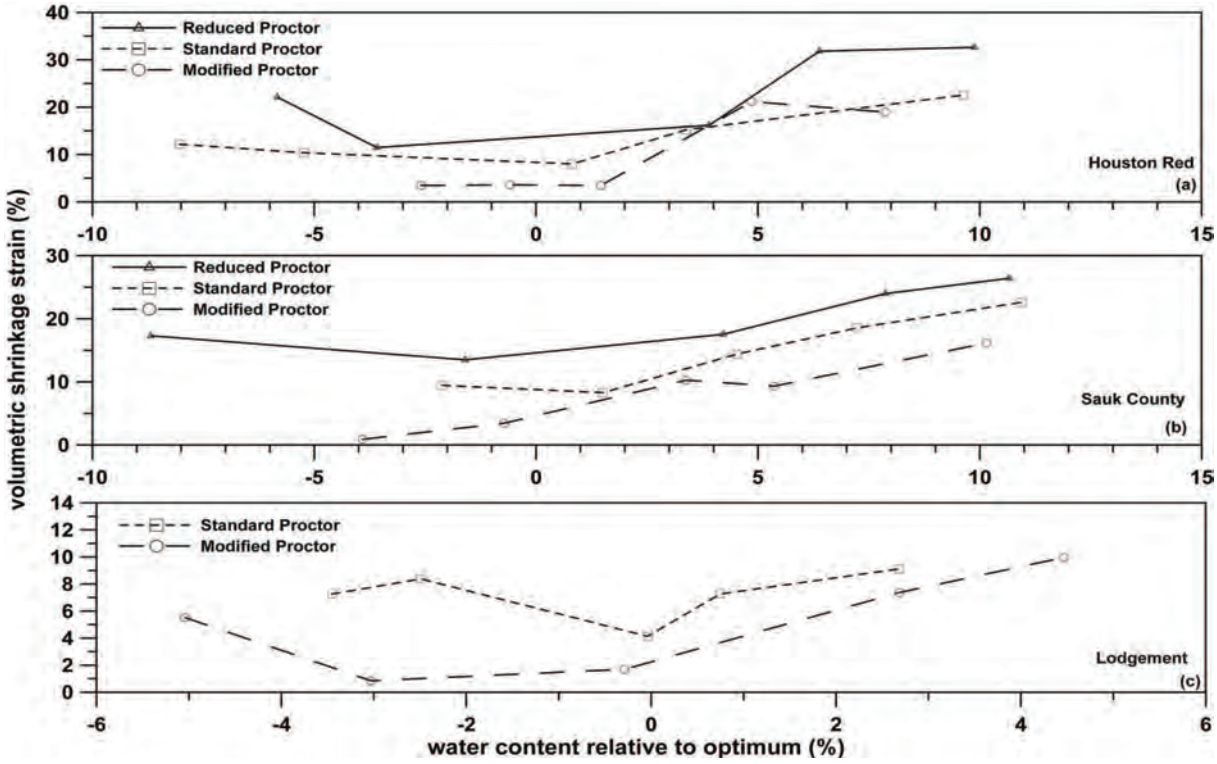

Figure 2.7: Volumetric shrinkage strain versus compactive effort for (a) Houston Red, (b) Sauk County, and (c) Lodgment soils [Albrecht and Benson, 2001]

2.3.3 Water content and thermal energy

This section explores the effect of initial moisture content and the evolution of the moisture content during desiccation. The rate of desiccation and the factors affecting the speed of desiccation are also examined. Also, some important soil moisture terms are explained.

2.3.3.1 Soil moisture terminology

The soil moisture terminology gives a clear picture of soil moisture existence under different states. Figure 2.8 show the approximate relationship of commonly used soil moisture terms. This scale is proposed by Olmstead and referred and explained by Fang [Fang, 1997]).

Suspensions: Above point **A** are the soil suspensions. The settling volume is marked by point **A** which is space-occupied by a unit weight of soil after settling from a suspension.

Gravitational water: From point **A** to **B** is the region of gravitational water. The

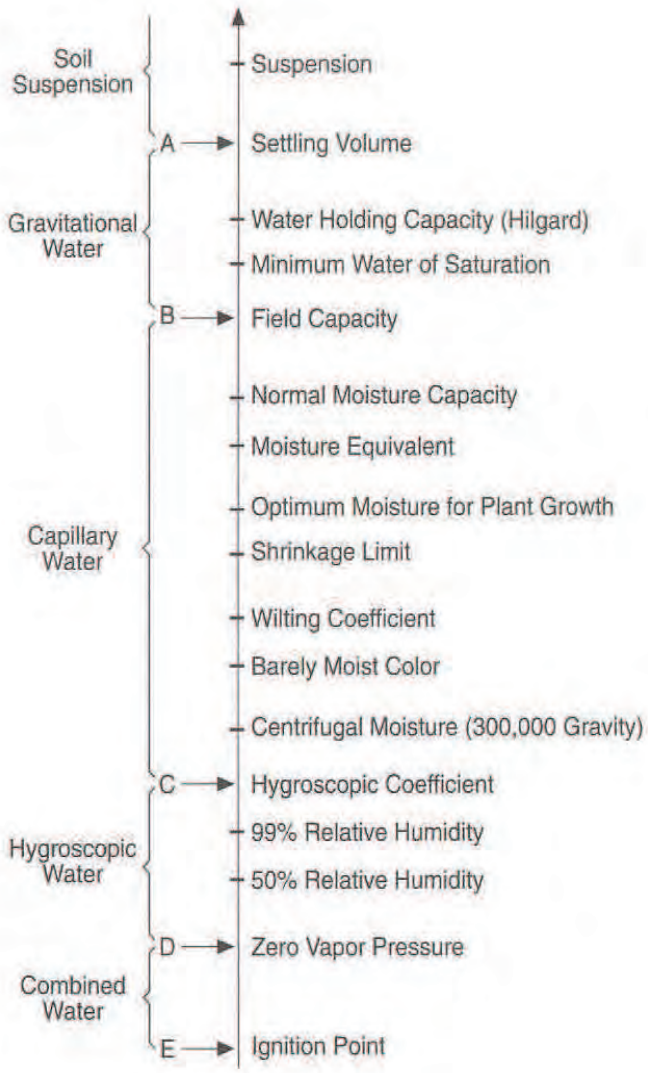

Figure 2.8: Soil moisture scale showing the approximate relationship of commonly used soil moisture terms (After Olmstead,L.B and Smith,W.O.[1938], Soils and Men, Yearbook of Agriculture, U.S. Agriculture,pp.897-910) As referred by [Fang, 1997]

maximum water-holding capacity is the moisture content of a 1 inch layer of loose soil after gravitational water has drained from the largest pores. The minimum water of saturation is the lowest moisture content at which a soil may be saturated with water when the soil grains are worked into the position of closet packing.

Capillary range: From **B** to **C** is the capillary range. Capillary tensions vary from zero at point **B** to several mega Pascal at point **C**. In this region, several important terms must be pointed out as:

Field capacity, representing maximum amount of water that can be held against the force

of gravity.

Moisture equivalent representing the adsorption water.

Optimum moisture content.

Shrinkage limit.

Wilting coefficient, is the moisture content just low enough to cause plants to wilt. The points at which soils show a barely perceptible difference in colour from the air-dry condition is indicated for reference.

Hygroscopic range and Ignition point: From points **C** to **D** is the hygroscopic range. The hygroscopic range marks the upper limit of this range. The water remaining after all hygroscopic water has been removed is called combined water. It is held by chemical rather than physical forces and can be driven off only by heating. At Ignition point, a bright red heat, all soil water is finally lost.

2.3.3.2 Initial and evolution of moisture content

Soils in nature can have a varying range of moisture content, starting from a dry soil which has no moisture to a fully saturated state depending on the surrounding environmental conditions and geology. In this section a review of studies on soils which are either saturated or unsaturated subjected to desiccation and the effect of initial moisture content and how the moisture evolves is presented.

Initial water content is a term which creates ambiguity as moisture content varies constantly in naturally occurring soils. It would be difficult to say at what initial water content the soil desiccation started. For the purpose of analysis in this work the moisture content at the start of the experiments are considered to be initial moisture content. Albrecht and Benson [Albrecht and Benson, 2001] conducted desiccation tests on compacted soils with an objective to study the hydraulic conductivity as affected by desiccation. In their experimental work the specimens were compacted at 3% wet of optimum, at optimum and at 3% dry of optimum. The specimens were subjected to four cycles of wetting and drying.

The hydraulic conductivity increased for all the specimens after desiccation, but largest increase in hydraulic conductivity and shrinkage strains occurred for specimens compacted wet of optimum water content (see figure 2.9). The experimental observation made by

Albrecht and Benson [Albrecht and Benson, 2001] on effect of desiccation on hydraulic conductivity is in agreement with the theory of Haines [Haines, 1923]. According to this theory the specimens compacted at optimum water content have the largest volume of soil particles and the least volume of water per unit volume of soil at any given compactive effort, and thus undergo the smallest volume change during drying. Whereas specimens compacted wet of optimum contain the most water and therefore will undergo larger volume changes during primary drying relative to specimens compacted dry of optimum that have much lesser water.

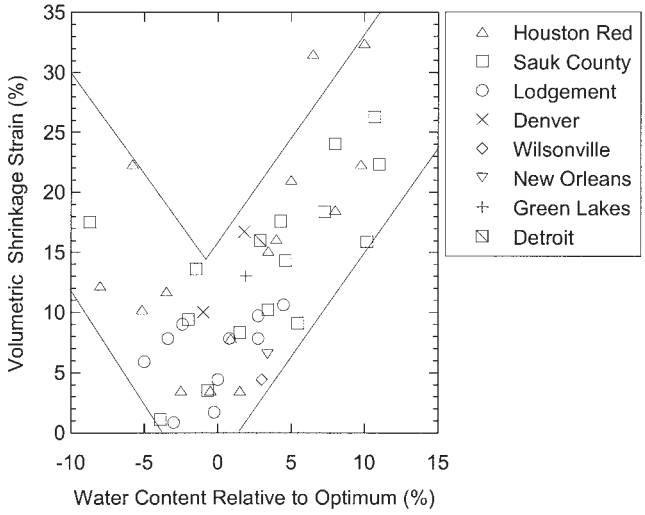

Figure 2.9: Volumetric shrinkage strain variation with compaction water content relative to optimum [Albrecht and Benson, 2001]

Once the process of drying starts the water content changes dynamically until the process of drying or the water content is stabilised. The evolution of water content is mainly affected by hydraulic conductivity of the soil, thickness of the drying soil layer and the surrounding environmental conditions. Cracking moisture content is the moisture content at the moment when the cracking starts, this plays an important role as this depends on many physical parameters like the thickness of the drying layer and the desiccation speed coefficient. The following definition was adopted (originally proposed by Corte and Highashi [Corte and Higashi, 1960] and modified by Nahlawi and Kodikara [Nahlawi and Kodikara, 2006]) to mathematically describe the desiccation rate:

$$(w - w_t) = (w_i - w_r)e^{-kt} \tag{2.1}$$

Hence,

$$\frac{dw}{dt} = -k(w_i - w_r) \tag{2.2}$$

where, w_i is the initial water content, w is the water content at desiccation time t, and w_r is the residual water content at the final stage. The desiccation rate is defined by (dw/dt) and k is a parameter signifying desiccation rate and is termed desiccation coefficient (1/t). It can be inferred that the desiccation rate is directly proportional to the desiccation coefficient.

The effect of thickness and desiccation speed or coefficient on cracking moisture content can be seen in the figures 2.6 and 2.10. From figure 2.6 it can be observed that the cracking moisture content increases with increasing depth of the drying layer. Corte and Highashi [Corte and Higashi, 1960] found that the tendency for the cracking moisture content to increase with the thickness of the soil layer may be due to desiccation speed from the surface of the soil, because the soil dries faster as the thickness decreases. Towner [Towner, 1987b] expressed the cracking water content as a function of initial water content (see table 2.7). From the table it can be observed that there is no significant difference between the sets of samples from different initial water contents. The effect of desiccation speed or coefficient on cracking moisture content is explained in next heading.

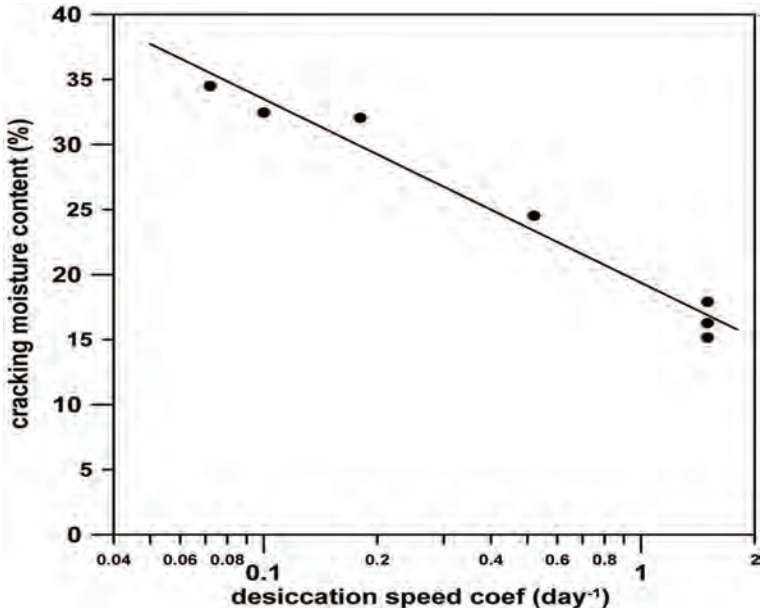

Figure 2.10: Cracking moisture content and desiccation speed coefficient [Corte and Higashi, 1960]

2.3.3.3 Rate of desiccation

The time required to desiccate a soil mass of same thickness in two different weather conditions is not the same, and even the same soil mass with different thickness in the same weather conditions is also not same. Thus rate of desiccation, depth of drying soil

Table 2.7: Water content at cracking [Towner, 1987b]

Initial water content (kg/kg)	Observed water content at cracking (kg/kg)	Mean water content at cracking (kg/kg)
0.62	0.328,0.313,0.312,0.314	0.317
0.64	0.322,0.325,0.318,0.316	0.320
0.71	0.336,0.317,0.321,0.304	0.319
0.83	0.333,0.311,0.317,0.310	0.318
0.91	0.322,0.309,0.318,0.288	0.309(0.316)

and the weather conditions have interdependence. Moreover rate of desiccation has a notable effect on the pattern of cracking.

Figure 2.11a show a reduction of moisture content for three samples of close packing soils and figure 2.11b shows for loose packing soils. The close packing soils show an exponential decrease in moisture content. Coefficient of desiccation (k) was calculated by fitting the curves (to equation 2.1).

The curves showing reduction in moisture for loose packed soils follow linear tendency in comparison with the curves for close packing. The reason may be due to the low temperature of the water in the first few days (as observed by Corte and Highashi [Corte and Higashi, 1960]). During the preparation of specimens with loose packing the method used was by keeping ice sheet over dry soil. From the results of the experiments, the desiccation rate also depends on the thickness of drying soil. Figure 2.10, shows a relation between desiccation speed coefficient and cracking moisture content, as the desiccation speed increases there is a decrease in cracking moisture content.

In a different work the phenomena of evaporation, potential evapotranspiration and actual evapotranspiration is illustrated by figure 2.12. The figure shows moisture losses with time from the surfaces of four identical plastic containers, three filled with soil and one with water [Blight, 1997]. From figure 2.12 it can be observed that there is a initial linear and later a curved behaviour for bare soil surface loosing moisture due to desiccation.

2.3.4 Tensile strength

Tensile strength of soils is an important indicator, as it depends on various other properties of soil. Determination of tensile strength has not received as much attention that it deserves, may be because of the difficulty in its experimental determination. Tensile

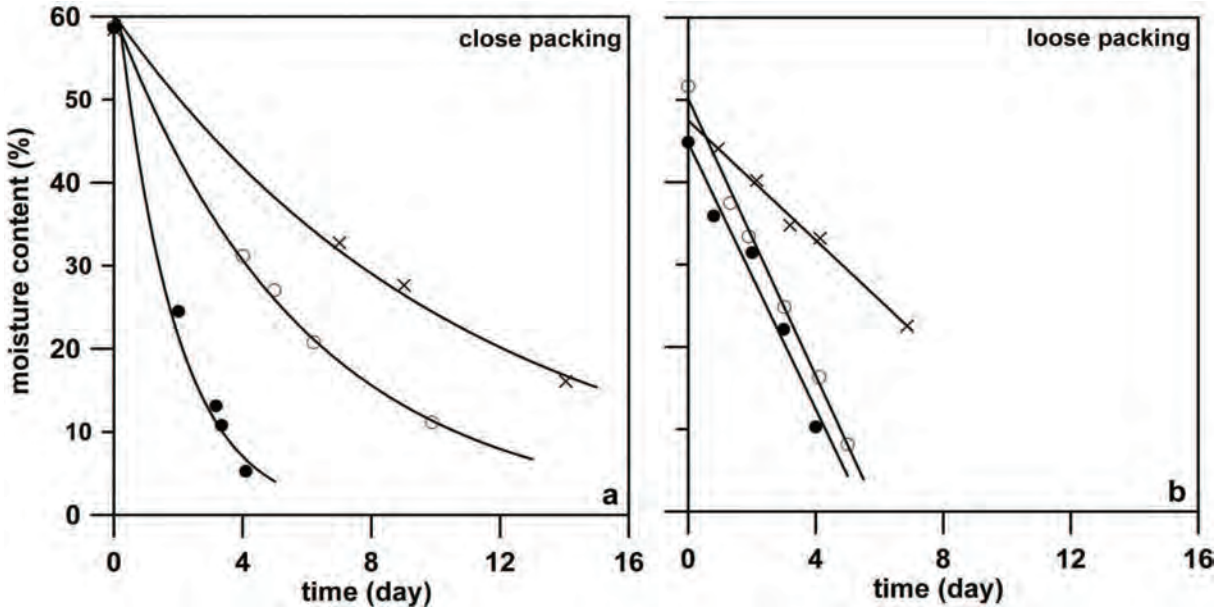

Figure 2.11: Process of desiccation at the surface of soil [Corte and Higashi, 1960]

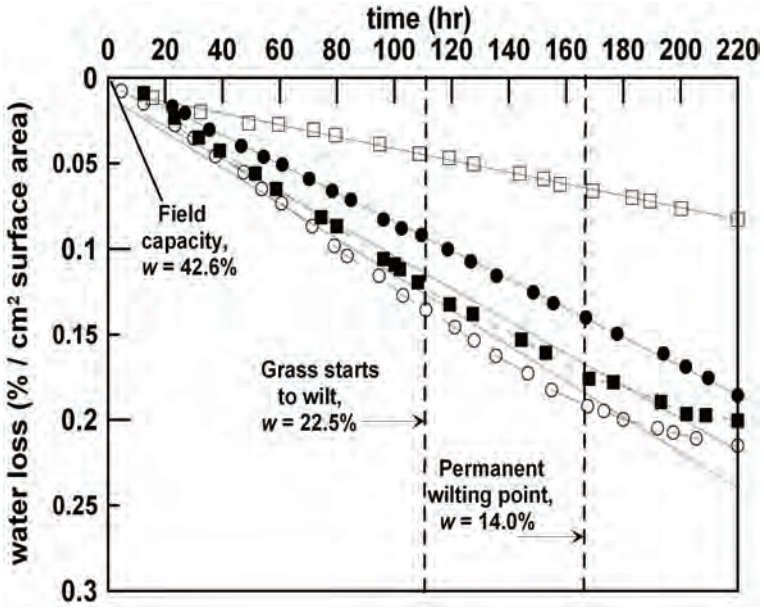

Figure 2.12: Moisture loss with time from soil in containers with various surface conditions [Blight, 1997]

strength determination for saturated and unsaturated soils is from different experimental methods. This is due to the problems in sample preparation and testing procedure / equipments for saturated and unsaturated soils [Nearing et al., 1991]. Also, tensile strength determination is different for unconsolidated and consolidated or over-consolidated soils. Table 4.1 summarises the observed variation in measured tensile strength for different test methods is presented [Harison et al., 1994].

For certain types of soils under particular climatic conditions crack initiation occurs under saturated or quasi saturated conditions, whereas for some soils under a different climatic conditions the crack initiation is under unsaturated conditions. Keeping this in view the tensile strength determination for application in the study of desiccation cracking should be in both saturated and unsaturated conditions.

Table 2.8: Variation of tensile strength with test method [Harison et al., 1994]

Test method	Specimen dimensions (mm)	$V_{95}(mm^3)$	Strength ratio
Ring test	$R_\circ/R_i = 8; R_\circ = 50, and\ t = 25$	8.29	1
Three-point bending	$200 \times 50 \times 25$; $100 \times 50 \times 25$	156; 78.1	1.78; 1.56
Four-point bending	$200 \times 50 \times 25$	2187	3.00
Brazilian test	$R_\circ = 50, and\ t = 25$	10596	4.10
Direct-pull dog bone	$d = 25$; $L = 35$	17181	4.50

Note : $R_\circ$ = Outside radius; R_i = Inside radius; t = Thickness; d = Diameter; and L = Length

V_{95} = Volume of that part of the specimen subjected to at least 95% of maximum tensile stress

Towner [Towner, 1987b] explains tensile strength as a material property which depends in general on both the soil-water suction and water content. Moreover the relationship also depends on the degree of anisotropy that may exist initially in the physical properties of the clay or be induced subsequently by, for example the application of anisotropic loading system. Figure 2.13 shows tensile load at failure against water content: there is a trend of increasing tensile load at failure with decreasing water content.

Figure 2.14, shows tensile strength variation with degree of saturation. Figure 2.13 show the variation of tensile strength for a small range of water content of 0.30 to 0.5 kg/kg, whereas the figure 2.14 (from the work of Rodríguez [Rodríguez, 2002]) gives the complete picture of tensile strength variation with degree of saturation.

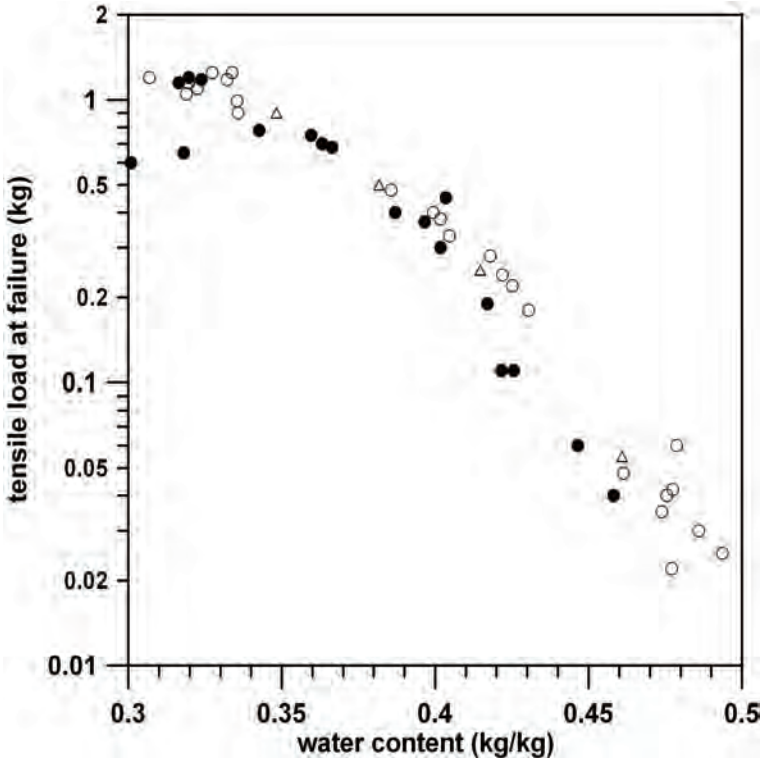

Figure 2.13: Plot of the measured tensile load at failure versus water content [Towner, 1987b]

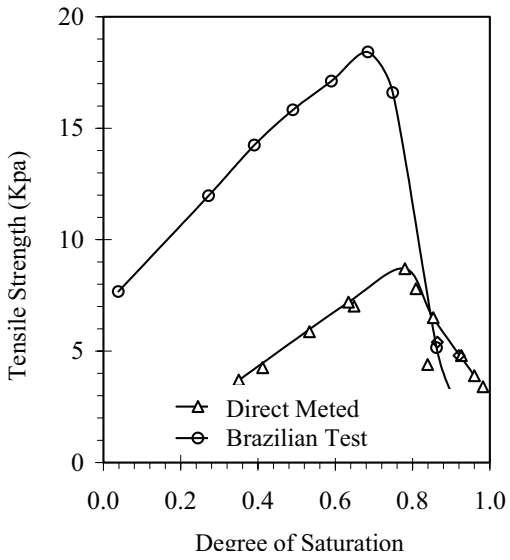

Figure 2.14: Variation of Tensile strength with Degree of saturation [Rodríguez, 2002]

2.3.5 Suction

Many geotechnical problems arise from volume and moisture changes due to capillarity: the shrinkage and swelling of expansive clays and collapse of some loams are the most conspicuous. One of the major parameters controlling these phenomena is the matric capillary pressure or suction [Fleureau et al., 1993]. From the work of Konrad and Ayad [Konrad and Ayad, 1997b] and Abu-Hejleh and Znidarcic [Abu-Hejleh and Znidarčić, 1995] the critical suction at crack initiation near the soil surface during the shrinkage-desiccation process depends on: the soil tensile strength, the initial stress state, the total and effective stress paths, and the stress history of the soil. Shear strength data from the research literature suggests that there is a nonlinear increase in strength as the soil desaturates as a result of an increase in matric suction [Vanapalli et al., 1996b].

The recent work by Rodríguez [Rodríguez, 2002] on the desiccation of a mining waste summarised in figure 2.15 gives a complete picture of the effect of suction on the process of cracking.

2.3.6 Vegetation

When the soil surface is covered with vegetation the transfer of soil water to the atmosphere occurs mainly from plant canopies by a process called transpiration. Transpiration is caused by a vapor pressure gradient between the normally water-saturated leaf cells and generally quite dry atmosphere. Soil water is extracted by the roots which permeate the soil and is transmitted through the stems to the continuously transpiring leaves. Thus, in the presence of vegetation the soil may dry more rapidly and to greater depths than a bare soil. Hence, vegetation can increase shrinkage and cracking [Ravina, 1983].

The effect of different species of trees on drying of clay has been studied by Biddle [Biddle, 1983]. 36 trees of 4 different types growing on 5 different types of soil isolated from trees of other species were studied. The conclusion was, the effect of different species on drying pattern is different depending on the water requirement of the trees. There was no significant effect by different soil type, apart from the usual effect of index properties on shrinkage behaviour.

The effect of vegetation on the swelling and shrinking; of soils in Australia has been studied by Richards et al [Richards et al., 1983], study on clays in Britain was done by Driscoll [Driscoll, 1983], and on clays in the USA has been studied by Holtz [Holtz, 1983]. Most of the studies agree that the presence of vegetation increases the rate of shrinkage

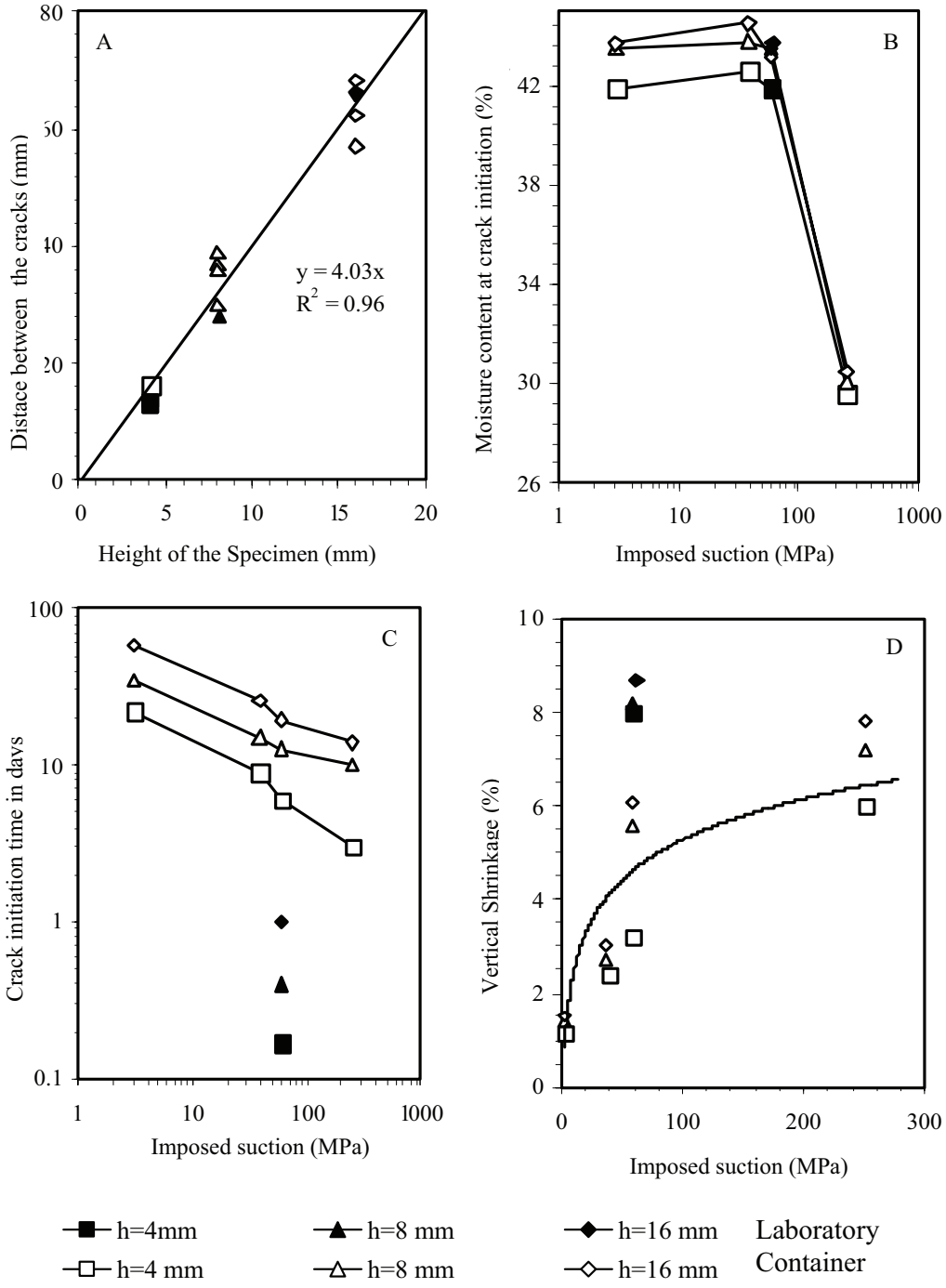

Figure 2.15: Relationship between: (A) Height of Specimen and Distance between the cracks (B) Moisture content at crack initiation and Suction imposed (C) Crack initiation time and Imposed suction (D) Vertical shrinkage and Imposed suction [Rodríguez, 2002]

by reducing the soil moisture.

Biddle [Biddle, 1983] from the extensive series of field measurements around individual trees conluded that the vertical and lateral extent of the moisture deficit depend on the soil permeability and the tree species/height. However, other studies suggests that a group of trees will cumulatively extract a larger volume of water from the ground than an individual tree and as a consequece greater moisture deficit may result.

Alonso and Lloret [Alonso and Lloret, 1995] are also of the same opinion that the presence of vegetation causes a faster loss of soil moisture.

2.4 Implications

The effect of presence and formation of cracks in soils is far reaching, altering the strength and characteristics of the intact soil. The effects can be broadly grouped as environmental, agricultural and effects on properties of soil.

2.4.1 Properties of soil

The propeties of cracked soil seems different when compared with the intact soil. In this section the changes to the geotechnical properties brought by the presence of cracks is explored.

2.4.1.1 Physical and Index properties

No published data was found (with experimental evidences) on the effect of cracking to the index properties of soil, but there can be an effect on some of the physical properties. It is well known that the soil can be a two phase or a three phase system depending on the degree of saturation. During the process of cracking (due to desiccation) there is a continuous change in the degree of saturation and volume of the desiccating soil mass, thus the cracking may affect all weight-volume relations.

2.4.1.2 Strength properties

Significant effect of cracking on the strength properties of soils was found from the available literature.

Desiccation may result in over consolidation with a over consolidation ratio (OCR) value up to three. Mesri and Ali [Mesri and Ali, 1999] studied the effect of desiccation on the consolidation properties of soil, they conducted experiments on Boston Blue clay which is a glacial silty clay. The Boston Blue clay was overconsolidated by desiccation with a OCR equal to 3. Some important interpretaion drawn form the tests are: opening of microfissures due to sampling disturbance probably reduced the value of undrained shear strength when subjected to insitu effective stress condition. Then, closing of the microfissures in the recompression range from effective overburden pressure to preconsolidation pressure resulted in an increase in undrained shear strength. Another observation was, undrained shear strength of the desiccated glacial stiff clay moved towards zero as the vertical consolidation pressure decreased starting from the in-situ condition.

Other studies with similar objectives like that of Mesri and Ali [Mesri and Ali, 1999] can be found, an example is the work of Thorne [Thorne, 1984]. Experiments were conducted to determine the strength and stability for fissured clays. The conclusions drawn are in agreement with other studies, indicating a decrease in strenth due to the presece of fissures and important alteration to the soil structure.

2.4.1.3 Hydraulic conductivity

Soil cracks can be considered as macropores and as a consequence the hydraulic conductivity may not be the same for the intact soil and a soil with fractures/cracks. Then it would be interesting to quantify the change in hydraulic conductivity.

The objective of the work from Omidi et al [Omidi et al., 1996] was experimental study on effects of desiccation cracks on the hydraulic conductivity of the compacted soil. Two soils of diverse mineralogy and some typical soils used in the clay liner construction were selected for testing. Each one was tested in its natural state and after adding 30% sand. Volumetric shrinkage of each soil was measured during the laboratory tests in addition to the hydraulic conductivity determined using 10 cm diameter fixed wall permeameters. In table 2.9 a summary of the experimental results showing the effect of desiccation on the hydraulic conductivity of the soil is given.

The summary of the other studies on the effect of cracking on the hydraulic conductivity

Table 2.9: The average measured hydraulic conductivity for unamended and sand-amended soils [Omidi et al., 1996]

Soil	Hydraulic conductivity, cm s^{-1}			
	Smectite Soil	Illite Soil	Smectite + 30% sand	Illite + 30% sand
Undesiccated: Laboratory (Small permeameters)	$7.8X10^{-10a}$ ($4.8X10^{-10}$)	$9.3X10^{-9}$ ($7.0X10^{-10}$)	$7.3X10^{-9}$ ($2.0X10^{-9}$)	$1.2X10^{-8}$ ($1.1X10^{-9}$)
Large permeameters	$3.1X10^{-8}$ ($1.6X10^{-8}$)	$7.7X10^{-8}$ ($1.3X10^{-8}$)	$7.5X10^{-8}$ ($2.9X10^{-8}$)	$8.0X10^{-8}$ ($4.1X10^{-8}$)
Desiccated: (Large permeameters) 1^{st}Cycle	$8.9X10^{-8}$ ($3.0X10^{-8}$)	$1.7X10^{-7}$ ($8.4X10^{-8}$)	$7.8X10^{-8}$ ($3.2X10^{-8}$)	$8.7X10^{-8}$ ($3.9X10^{-8}$)
2^{nd}Cycle	$3.5X10^{-7}$ ($2.7X10^{-7}$)	$2.0X10^{-7}$ ($1.7X10^{-7}$)	$9.7X10^{-8}$ ($3.5X10^{-8}$)	$1.0X10^{-7}$ ($4.5X10^{-8}$)

[a]Each value is the mean of three permeameters with standard deviation beneath in parenthesis.

of the soils are presented in the following paragraphs.

Mckay et al [McKay et al., 1993a] studied the hydraulic conductivity in fractured till. The field horizontal hydraulic conductivity values were up to 3 orders of magnitude greater than the mean value for the unfractured clay matrix (2×10^{-10} m/s) determined from laboratory tests.

Drumm et al [Drumm et al., 1997] carried out experiments with laboratory Lysimeters to study the effect of drying on the hydraulic conductivity. The conclusion form the study was, to properly assess the long-term integrity of compacted clay barriers and to develop appropriate maintenance measures, an understanding of the shrinkage induced volume changes and the development of preferential flow paths must be obtained. In order to accomplish this idea, the Lysimeter outflow collector was divided in to sectors, the detailed lay out is shown in figure 2.16. The results of the experiments (figure 2.17) clearly show that the desiccation cracks results in preferential flow paths.

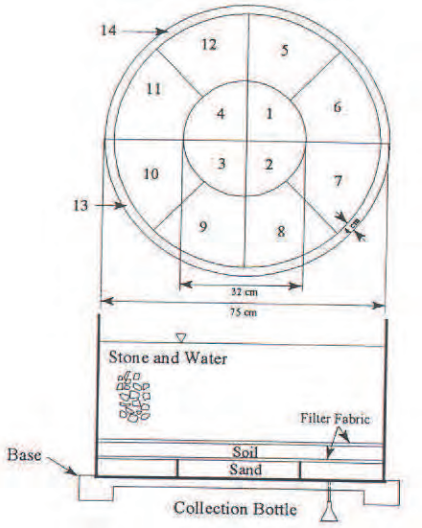

Figure 2.16: Plan view of individual chambers of Lysimeters (top), cross-section of Lysimeter (bottom) [Drumm et al., 1997]

2.4.2 Environmental

The fractured zone in soils has been observed to have a depth ranging from a few centimeters to tens of meters and this can increase both hydraulic conductivity of the deposit and the potential for rapid migration of contaminants. Flow in individual fractures may be very rapid, reaching up to an order of several meters per day and could significantly influence contaminant migration even in deposits where the bulk hydraulic conductivity is low [McKay et al., 1993b].

Cracks in the soil´s upper layer increase the permeability due to the formation of preferential flow paths. This is a severe problem in many engineering situations such as mine tailing dams or closure caps of waste disposal sites where transport of pollutants may be significantly increased [Drumm et al., 1997].

It is recognised since long that leaching of agrochemicals such as pesticides and ferilizers to groundwater and surface water sources is a serious threat to the environmental quality of water. Hendrik et al [Hendriks et al., 1999] did some simulations of Bromide tracer and Nitrogen transport in cracked clay. Apart from other reasons for contaminant transport, shrinkage cracks proved to be important for solute transport under relatively wet conditions.

Millions of tons of waste material is produced by the mining industry world wide, these wastes are deposited as tailing dams open to the atmosphere. During the depositon and subsequent years these tailings experience a dry-wet cycle due to seasonal variations.

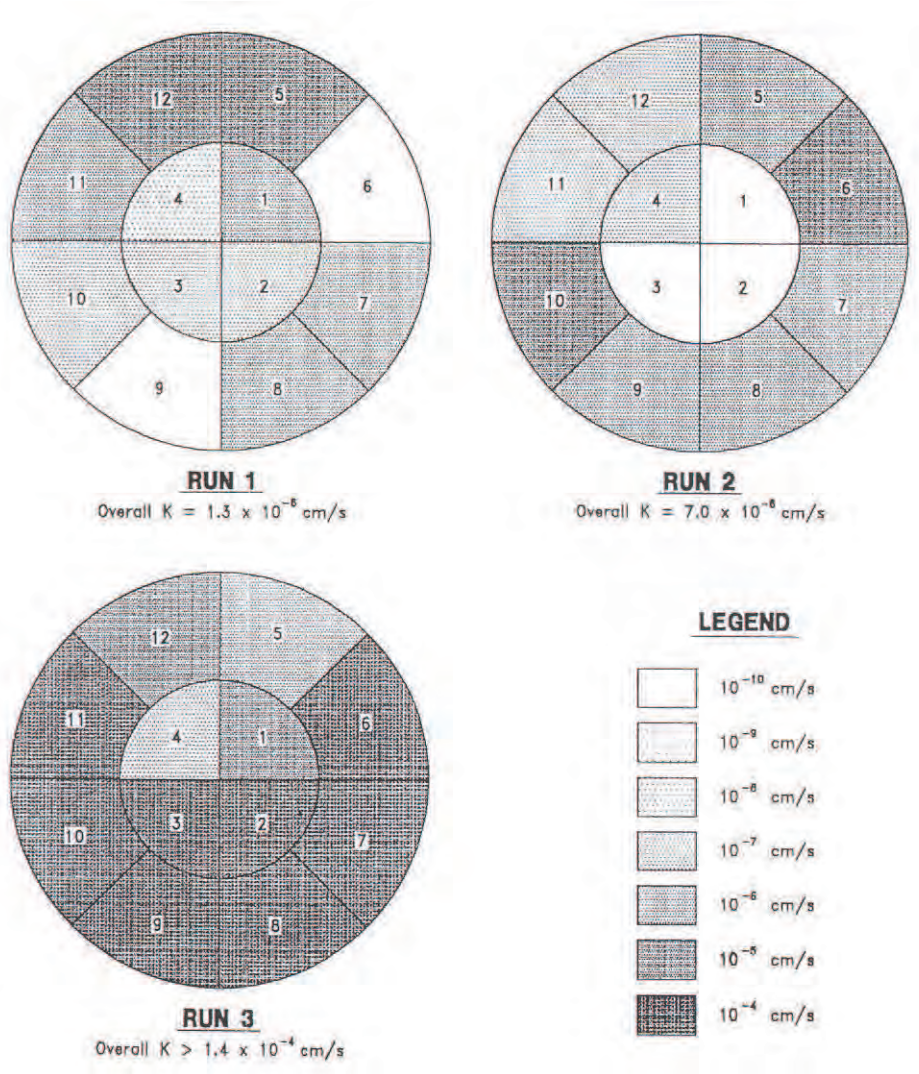

Figure 2.17: Measured hydraulic conductivity by Lysimeter sector [Drumm et al., 1997]

The deposits crack during the summer and when it rains the rain water infiltrates and contaminates the ground and surface water. The doctoral investigation of Rodríguez [Rodríguez, 2002] with laboratory experiments to characterize and study the behaviour of Metallurgical waste produced by the Cuban Nickel industry in the Moa district of Cuba showed some very interesting results on the effect of cracking. The conclusions from the work were: cracking of the metallurgical waste by desiccation can significantly increase the permeability, even if fissures are sealed by additional filling or by means of a mechanical confinement. The effect of layering and crack formation increases hydraulic conductivity more than one order of magnitude compared to the initial continuous sample of metallurgical waste. These factors should be taken into account when simulating flow and transport processes in the deposits. Also, hydraulic conductivity had an important dependence on sample thickness.

2.4.3 Agricultural

Drying of clay soils results in the formation of shrinkage cracks and subsidence of the soil surface. Water and solutes flow rapidly through the cracks into the subsoil, thus bypassing the relatively dry root zone. This process may lead to, water and nutrient shortage for crops, and pollution of subsoil and ground-water [Bronswijk, 1991b].

After brief compilation of differetn research works on the effect of desiccation on crop growth in agricultural fields Yoshida and Adachi [Yoshida and Adachi, 2001] suggested that the cracks in clayey agricultural fields play an important role in water balance affecting various factors. The factors affected were: efficiency of drainage, irrigation, or the rate of evapo-transpiration. Thus controlling the crack´s location, width, and depth is of practical concern in various situations related to agricultural activities.

Soil mechanical strength is an important indicator of soil physical properties that affect agricultural production and reflects the soil's cracking characteristics important to water management and salt leaching of clay soils [Nichols and Grismer, 1997]. Seedling emergence, root penetration and reaction to tillage implements, also may be useful indicator of quality of soil because it depends on adsorbed cations, water content, bulk density and aggregate size.

2.5 Experiments

It is not rare, but difficult to find experimental work only focusing on the process of desiccation and cracking especially at a larger scale (bigger size specimens comparable with cracks occuring in nature) in the laboratory. After an extensive compilation of available published work, the experimental work of Corte and Highashi [Corte and Higashi, 1960] found to be the most comprehensive series of laboratory tests undertaken on the desiccation of soil layers. In this section a compilation of the important works both at laboratory and in-situ conditions are presented.

2.5.1 Laboratory / Small scale

Laboratory tests on cracking soil are mostly qualitative in nature, the laboratory tests can be grouped into two based on the approach of analysis and on the application.

2.5.1.1 Based on approach

The laboratory work is again subdivided into two. One, the experiments concentrate determining the cracking characteristics of the soil with soil mechanics approach. Two, the experiments based on a different approach (other than soil mechanics) like fracture mechanics.

Soil mechanics:

The laboratory experiments conducted by Corte and Highashi [Corte and Higashi, 1960] are the most comprehensive series of laboratory tests. A brief description of the experiments: the experiments were carried out with fairly large containers to avoid the wall/boundary effect. The desiccation process was observed carefully throughout, before and after cracking has started, by measuring the water content of the soil and by taking pictures at various stages of crack growth. These observations were very useful for clarifying the dynamic mechanism of crack formation. The final stage of crack formation was examined on pictures taken after the soil became completely dry. Various parameters were defined based on the observation of final crack pattern. The features observed were: the number of cells surrounded by the cracks, the shape, number of sides, size distribution of the cells, total length of the cracks, and area of the cracks. These quantities are considered both as characteristics of the cracks themselves and also for the cracking phenomena.

Variables such as, temperature and humidity (of the air), thickness of the soil layer, and the material of the bottom of the containers were considered as extrinsic parameters. Intrinsic conditions studied were: initial moisture content and initial degree of packing. Experiments were carried out with free shrinkage (no adhesion at the bottom contact surfce) and with adhesion of the soil to the bottom material of the containers.

The total number of experiments conducted were around sixty. The objectives of the study include: the effect of thickness (of drying layer), bottom material (on the contact surface), desiccation speed, degree of packing, ground water, humidity, freezing, cycle of wetting-drying, etc. The soil used for the experiments was Bloomington till obtained from a till deposit near Lily Lake, Illinois. Most of the experiments were carried out with flat wooden containers of size $600mm$ X $840mm$ plan area and $70mm$ deep. The soil was prepared in two initial states: (1) as a slurry with initial water content of 60% and a dry density of $1800kg/m^3$, and (2) as a loosely compacted soil with initial water content of about 45% and a dry density of about $1500kg/m^3$. Different materials were used at the base of the containers in order to provide different base adhesion characteristics. The base material used included plain wood, greased wood, and sheet of glass. For majority

of the tests, the room temperature was kept around 22°C and the relative humidity was in the range of 30 to 40%.

The work of Lloret et al [Lloret et al., 1998]: Two preliminary desiccation tests (series A) were performed measuring continuously the weight and vertical strains during drying under laboratory conditions (temperature of 22°C, relative humidity of 60%). In the first case, a cylindrical specimen (diameter of 38 mm and thickness of 76 mm) compacted initially at saturation state with dry density of 1.53 g/cm^3. In the second case, the soil in slurry state (water content 50%) was poured into a cylindrical container (250 mm dia with 40 mm thick) with a smooth base and with the upper soil surface exposed to laboratory conditions.

In series B, tests were performed by preparing soil (initial water content of 50%) on circular holding tray of diameter 225 mm with different thickens of soil and circular groves (1.5 mm deep) at the bottom contact surface in order to assure adhesion with soil. The specimens were kept in different hermetic container where a predetermined relative humidity was imposed (by means of a salt or sulphuric acid solutions). Different suctions (corresponding to a value of relative humidity) were imposed to the each container. The material used in these tests is a mining waste.

Albrecht and Benson [Albrecht and Benson, 2001]: Eight types of soils were selected for the experimental study (details of properties given in table 2.6). The desiccation tests were carried out on compacted specimens. Specimens were prepared for each soil type. The compaction scheme adopted was either one or more of the three compactive efforts: standard, modified, and reduced proctor effort. After compaction the specimens were either immediately placed in permeameters for saturation or wrapped in plastic sheets to prevent drying until they could be saturated.

Specimens were prepared to include a wide range of compaction conditions and soil properties. Saturation was ensured by permeating the specimens in flexible-wall permeameter using a hydraulic gradient of 10 and an average effective stress of 10.5 kPa. Each specimen was dried after initially being saturated by permeation. When a specimen was removed from the permeameter, measurements were made for height, diameter, and weight. The specimens were then placed in a pan on a shelf in the laboratory at room temperature (approximately 20°C) and allowed to dry slowly.

Towner [Towner, 1987b] proposed a theory explaining the mechanism of cracking of a drying clay. The experiments performed to test the theory consisted of three parts:

(1) Measurement of the water content at cracking of clay bars of fixed length for a range

of initial water contents.

(2) Measurements of the tensile strength at different water contents.

(3) Measurement of the drying limb of the water characteristic curves.

Fracture mechanics:

Application of concepts of fracture mechanics to explain cracking in soils is not new, according to Vallejo [Vallejo, 1994] Bishop in 1967, and Skempton et al. in 1969 were the first to suggest that fracture mechanics concepts might shed light on the process of progressive failure of slopes made of stiff fissured clays.

Lee et al [Lee et al., 1988]: Proposed a finite element model for tension crack propagation in soils. In the model the criterion for crack propagation is based on fracture mechanics principle. So, in order to determine the fracture parameters of the soil experiments were conducted to evaluate the critical energy release rate G_C. The experimental setup was adopted for soils from established fracture mechanics test procedures [ASTM E399-78(1986) and BS 5447 (1977)]. Figure 2.18, shows the schematics of test specimen and loading.

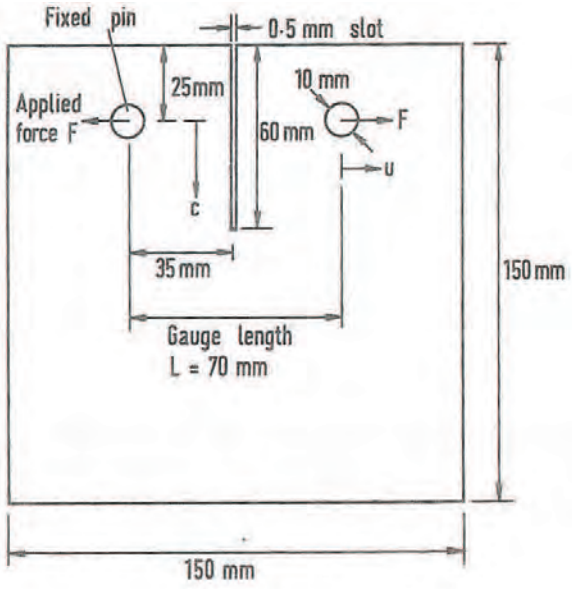

Figure 2.18: Schematic diagram of test specimen and loading [Lee et al., 1988]

Chudnovsky et al [Chudnovsky et al., 1988]: Formulated the concept of crack layer and its propagation for overconsolidated clays. To examine the applicability of the proposed theory they conducted experiments. Kaolinite clay slurries consolidated to approximately

280 kPa were first cut into the shape of a hollow cylinder. A special lathe (is a machine tool which spins a block of material to perform various operations such as cutting, sanding, knurling, drilling, or deformation with tools that are applied to the workpiece to create an object which has symmetry about an axis of rotation) was used to reduce them to the size and shape shown in figure 2.19. Next, a horizontal notch was cut into the specimen. The specimen was consolidated in a special cell to an overconsolidation ratio of 6.0 and 4.5. Then the specimen is tested undrained under cyclic torsional loads. During the test, torque with rotation and the crack sliding displacement at the center of the notch were recorded. From these data subsequent computation of the potential energy and the irreversible work were made at specified intervals using the torque against rotation plot and integration technique.

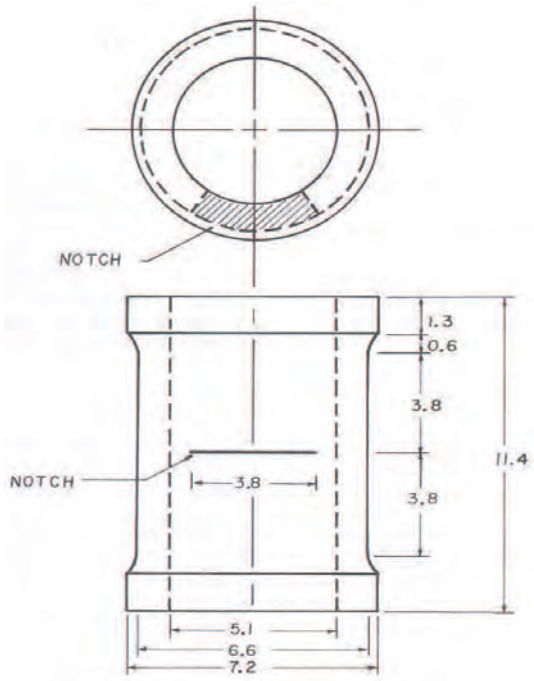

Figure 2.19: Hollow cylindrical specimen geometry (all dimensions in cm) [Chudnovsky et al., 1988]

Konrad and Ayad [Konrad and Ayad, 1997a]: Conducted experiments to determine soil properties for the model proposed by Konrad and Ayad [Konrad and Ayad, 1997b] using the priciples of fracture mechanics. The experimental set-up to determine the critical energy release rate was adopted from established fracture mechanics test procedures recommended in ASTM E399-78 (1983). The specimen, fitted with the two aluminum rods was mounted between two perspex plates and installed vertically on a conventional direct shear box apparatus. The procedure adopted by Konrad and Ayad [Konrad and Ayad, 1997b] is different from the tests performed by Lee et al [Lee et al., 1988] where the sample was sheared horizontally developing an additional frictional component.

Fang [Fang, 1994]: Conducted laboratory tests to calculate fracture mechanics parameters of soils. The tests were conducted following the established fracture mechanics test procedures (ASTM E399-83). The specimens used in the test were prepared with a mould developed at Lehigh University. The mould consists of a steel base with removable sides and interior walls. It can accommodate up to four specimens at a time. The experiments were conducted on three types of soils, Soft Marine clay, Compacted Fine-grained soil, and solidified sludge waste.

Work of Sadda and Bianhini [Saada et al., 1994a]; Sadda and Liang [Saada et al., 1994b]: A hollow cylindrical specimen was used in the experiments. The experiments are aimed at studying the effect of cracks or fissures or inclusions on the bifurcation and shear band propagation in saturated clays.

Harison et al [Harison et al., 1994]: Conducted experiments to study the fracture toughness of compacted cohesive soils using Ring test.

Li et al [Li et al., 2000]: Conducted experiments on frozen soil to determine the fracture toughness K_{IIC}. A four point bending device is used to test the rectangular specimens (thickness of 0.08m, width of 0.1m and span of 0.3m) with a notch at the center of span.

Avila et al [Ávila et al., 2002]: Carried out experiments to measure fracture mechanics parameters of a clay soil (from Bogotá, Colombia). The tests were performed using strain controlled and stress controlled techniques. The test specimen preparations and testing procedure is adopted from ASTM E399 (1983).

2.5.1.2 Based on application

This section gives an account of experiments performed with an objective to solve a particular engineering situation like: the desiccation and cracking of clay liners, tailing dams and processes like hydraulic fracture, etc.

Clay/soil liner/cover:

Wendling and Meibner [Wendling and Meibner, 2001]: Studied the sealing effect of compacted clay layers which are used as a cover or liner for landfills. The functionality of the liner is directly affected as soon as cracks appear. The focus of the study was on the relationship between the formation of cracks in clayey soils (due desiccation) and the soil-water suction in relation to the parameters such as temperature, water content and void ratio.

Yesiller et al [Yesiller et al., 2000]: Three compacted liner soils obtained from local landfills in southeast Michigan were investigated to know the desiccation behaviour. The soils had low plasticity with varying content of fines. The test samples were very large, which were subjected to wetting and drying cycles. All the samples were first subjected to a compaction-drying cycle and a subsequent wet-dry cycles. Surficial dimensions of cracks and suction in the soils were monitored. Dimensions of cracks at the surface were quantified using the crack intensity factor (CIF), which is the ratio of the surface area of cracks to the total surface area of the soil.

Tailing dam:

Swarbrick and Fell [Swarbrick and Fell, 1992] studied desiccation and cracking of mine tailings by using small scale laboratory experiments. Swarbrick [Swarbrick, 1994] studied using a Drying box and simulation by a numerical model. Fujiyasu et al [Fujiyasu et al., 2000] did field investigation of evaporation from freshwater tailing.

Hydraulic fracturing:

Murdoch [Murdoch, 1993] conducted laboratory experiments to study the hydraulic fracturing of soils, the findings were published in three parts as methods and observations, propagation, and theoretical analysis.

2.5.2 Field / Large scale

Published work on large scale desiccation experiments are scarce. Normally the publshed work is on the study of desiccation and cracking of naturally occuring processes.

Konrad and Ayad [Konrad and Ayad, 1997a] conducted the field experiment exclusively to study the formation of shrinkage cracks in an intact and weathered sensitive marine clay. An excavation with three different levels was exposed to continuous evaporation during 35 days. To study the formation of desiccation (shrinkage) cracks in soils with different properties, three test sections were excavated at three different depths. Figure 2.20, shows a plan view and longitudinal cross section of the excavations. As shown in the figure that the first level was located in top soil at a depth of 0.4 m, the second level of excavation is in weathered clay at a depth of 1.2 m, finally at 2.0 m depth the intact clay was found. The main objective of the experiment was to study the behaviour of intact clay which was not exposed to any desiccation-drying or freeze-thaw cycle and to do this the layer was instrumented. The other layers were not instrumented and were used to gather information on desiccation crack formation in soils which were already subjected

to thousands of cycles of drying and weeting.

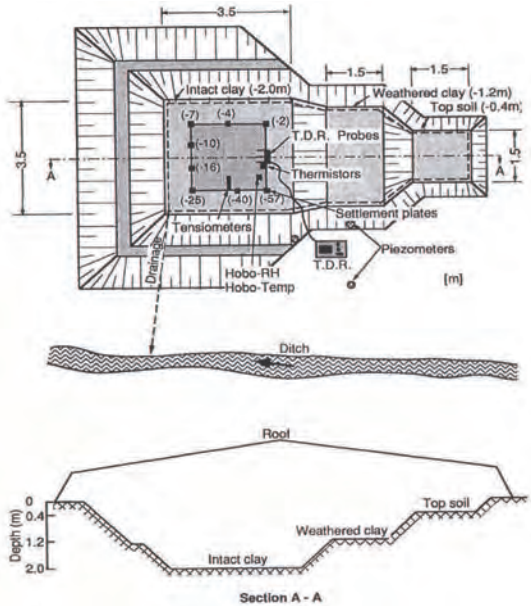

Figure 2.20: Characteristics of test sections [Konrad and Ayad, 1997a]

Weinberger [Weinberger, 1999]: Studied the fracture characteristics of mud cracks in dehydrating mud puddles in the Dead Sea region, Israel. The mud consists mainly of carbonate and clay particles typically displaying fining upward. The morphology showed a distinct surface discontinuity between the upper desiccated layers and the uncracked lower layers. The surface morphology of hundreds of cracks which were lifted from the field were examined under optimal oblique illumination, figures 2.21, 2.22 and 2.23 show some of the observed cracks. The initiation of the cracks were observed to be from the bottom of the desiccating layer and propagate vertically upward towards the free surface and laterally outward toward adjacent cracks. This is a striking contrast to the reported literature where in the initiation of the cracks are at or near the surface [Lachenbruch, 1961], [Morris et al., 1992], [Morris et al., 1994], [Prat et al., 2002], or from the middle of the drying layer [Corte and Higashi, 1960] and in most of the cases propagte downwards.

Wells et al [Wells et al., 2001] examined the modes of cracking in expansive soils of the Mississipi delta and their impact on infiltration. Soil for the experiments were obtained from a depth of 0 to 30 cm of Sharkey silty clay. The air dried and crushed soil passed through a 2 mm sieve were packed in a rectangular box of size 20cm $\times$ 94.3cm $\times$ 20cm, fitted with a sub-surface driange system. The soil was packed to a depth of 16cm over a 4cm layer of fine sand. The packing density varied from $1.4g/cm^3$ to $1.5g/cm^3$. The box was fitted with a centeral divider parallel to the sidewalls, providing two identical

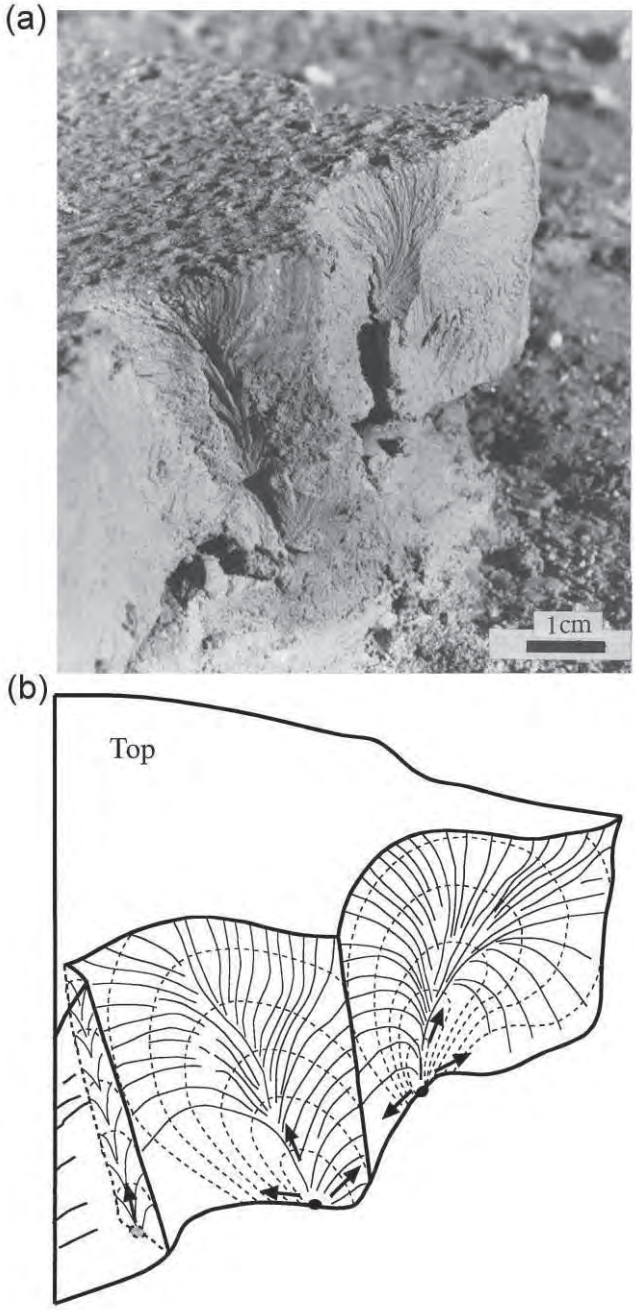

Figure 2.21: Oblique view of two adjacent mud cracks (a) and their surface morphology interpretation (b). Crack origins (solid dots) are located at the bottom [Weinberger, 1999]

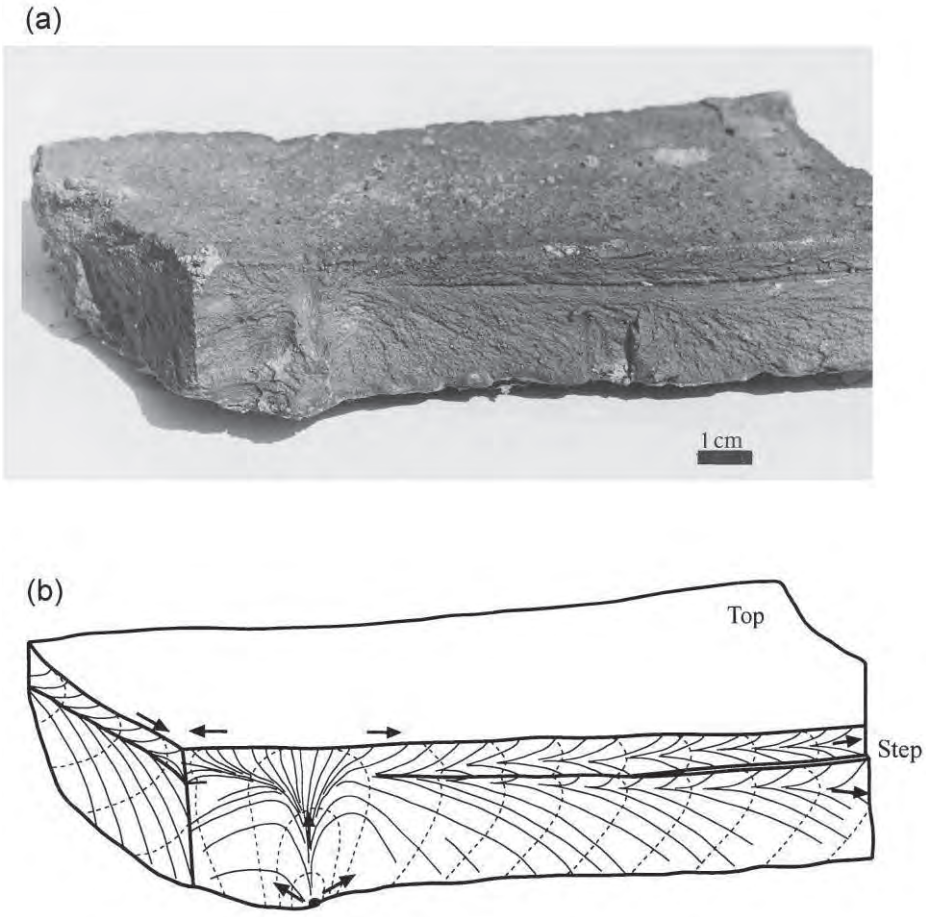

Figure 2.22: Oblique view of a recovered polygon (a) and surface morphology interpretation of an associated bounded crack (b). A single vertical plume axis branches in to separate sub-horizontal axes (along whcih cracks are propagated at opposite direction) that are obliquely oriented with respect to bedding [Weinberger, 1999]

test surfaces. To study the process of seal (due to process of healing) development during rewetting in dry-wet cycle and as an effect of rain storm. The simulation of rain storm over one of the test surfaces was done with out protection and on the other with protection.

It is evident from several researchers who have conducted numerous experiments, that though the main object of study is the same but the point of view and application is so diverse. This shows the wide range of implications cracks in soils has got.

2.5.3 Shrinkage, Subsidence, Water balance, and Cracking

Bronswijk [Bronswijk, 1991b] refering to (Haines,1923; Keen,1931; Stick,1954) distinguishes the phases during shrinkage as:

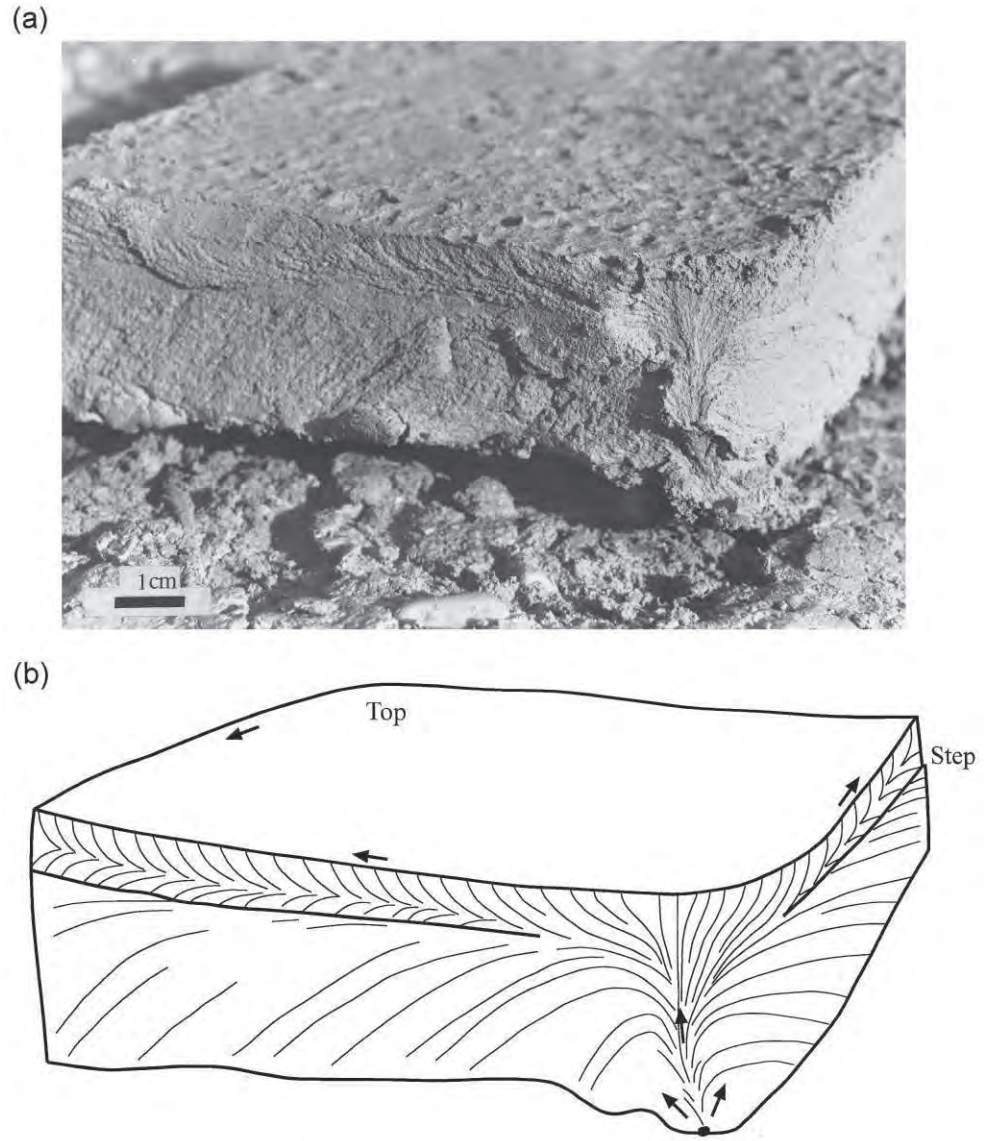

Figure 2.23: Oblique view of a polygon (a) and interpretation of surface morphology of an associated mud crack (b). The crack nucleates at depth, ruptures the desiccated layers, and subsequently propagate bi-laterally away from the origin along curved paths [Weinberger, 1999]

1.*Stuctural shrinkage*: when saturated soils dry, large water-filled pores may be emptied without accompanying volume changes.
2.*Normal shrinkage*: volume decrease of soil aggregates is equal to water loss. The soil aggregates remain fully saturated.
3.*Residual shrinkage*: In the process of drying, although the volume of the soil aggregates decreases, water loss exceeds volume decrease. Air enters the pores of the soil aggregates.
4.*Zero shrinkage*: the soil particles have reached their densest configuration. The water loss is equal to the increase of the air volume in the soil aggregates. Aggregate volume do not decrease any further.

Sridharan and Prakash [Sridharan and Prakash, 2000] explains the process of shrinkage as: volume reduction that takes place due to capillary pressures induced by the evaporation of water from the soil. As the evaporation continues, the radius of the meniscus developed in water in every pore where there is air-water interface continues to decrease, and the menisci will retreat into the soil mass until the shear stresses induced by the capillary pressures are equalized by the shear strength at the particle level.

Sridharan and Prakash [Sridharan and Prakash, 2000] are of the opinion that the shrinkage limit of a soil is not a plasticity characteristic of the soil. Instead it is the result of packing phenomenon and is primarily controlled by the relative grain size distribution of the soil. Further, for the systems having the same grain size distribution, the one which has higher shearing resistance at the particle level will shrink less.

A list of some of the important publication on the phenomenon of shrinkage is listed here, which are of interest. Mainly the work of Bronswijk and Evers [Bronswijk and Eversvermeer, 1990], and Bronswijk [Bronswijk, 1990], [Bronswijk, 1991a], [Bronswijk, 1991b].

2.6 Models

The very idea of modelling is to explain the naturally occurring phenomena with mathematical equations in a rational, logical and above all in a generalized way.

2.6.1 Conceptual models

The first step in modelling is the theoretical formulations based on the experimental observation and apllying basic concepts of fundamental theories. There are several conceptual models which explain the process of cracking in soils, some of them have formulated mathematical models and put in to test. Some of the important conceptural models are explained in the following paragraphs.

Lachenbruch [Lachenbruch, 1961]: Theoretical model presented was to study the tension cracks in a semi-infinite solid. The crack is generally initiated at a surface of great stress (often at or near the ground surface) and is propagated towards the interior of the medium where the tension diminishes and ultimately passes in to compression. The depth and spacing of such tension cracks are measurable quantities which contain information about the mechanical conditions under which the cracks formed, and hence about the history

of the medium in which they occur. The effect of the crack in relieving stress at the ground surface bears on the problem of crack spacing, and the rate of energy dissipation at the advancing crack tip bears on the problem of crack depth. For this a physical model provided by the modified Griffith´s theory (by Irvin,1948 and Orowan,1950) in which the surface energy considered by Griffith is replaced by the energy of plastic deformation near the advancing crack tip may be used. Before the theory can be applied to geologic problems, however, it is necessary to have a mathematical model of stress in the cracked ground. An elastic model of the stress perturbation caused by cracking should give a very good approximation to the stress conditions that exist immediately after the crack has formed.

Towner [Towner, 1987b]: Considering the changes that occur as the clay soil dries and assuming that the clay is initially saturated and remains saturated at least until it cracks, so that the changes in its bulk volume is equal to the volume of water evaporated. Considering these assumptions some simple experiments of drying with restriction to shrinkage in one direction were conducted. From these simple experiments an hypothesis was formulated. When clay dries, it will shrink anisotropically if the shrinkage is prevented or restricted in any direction; it will crack when the tensile stresses in some direction become greater than the tensile strength. Intuitively assuming that both the induced tensile stresses and the tensile strength increases with decreasing water content. Indeed, both depend on the soil-water suction.

Chudnovsky et al [Chudnovsky et al., 1988]: The approach adopted is called as Crack Layer Theory. The crack together with its surrounding damage are referred to as a crack layer [Chudnovsky et al.,1983]. As in all other approaches based on principles of thermodynamics, the crack layer theory requires experimental observation to describe the fracture as applied to overconsolidated clay. Once this is done, a criterion for local instability and ultimately constitutive equations for predicting failure can be obtained. To achieve this goal the following steps were formulated:

(1) Identification and characterization of the changes in the microstructure of overconsolidated clay in the vicinity of the propagating crack.

(2) Identification of the dominant thermodynamic driving forces within the context of the crack layer theory.

(3) Formulation of the kinetic equations describing the fracture process throughout stable crack propagation.

Tension effects at air-water-soil contacts inside the soil generate negative pressures (or

matrix suctions) below atmospheric pressure in the remaining pore water. These matrix suctions produce two counteracting effects. One, in a selected point, the soil tends to contract more or less isotropically, assuming at this stage that the pore water remains interconnected and the pore air is discontinuous. This shrinkage produces vertical cracks below horizontal drying surface. Two, the soil gains strength and provides increased resistance to crack formation.

Abu-Hejleh and Znidarcic [Abu-Hejleh and Znidarčić, 1995]: The theory is based on four assumptions. First, the soft fine-grained soils undergoing desiccation remain saturated until the void ratio reaches the shrinkage limit void ratio, that is the void ratio at which the shrinkage is terminated. There after, the desiccated soil becomes rigid and its response is not modelled in the present theory. Second, the theory considers a homogeneous soil that does not vary in properties from point to point horizontally. Third, the soil skeleton exhibits no intrinsic time effects with incompressible water and solid phases. Fourth, during the overall consolidation and desiccation process, the lateral and vertical planes through any point in the cracked and uncaracked soil columns are principal planes. A key element of this model is to consider the principle of effective stress in the slurry to relate total stress induced by a condition of zero lateral strain during shrinkage to the suction and the effective stress path followed by any soil element during consolidation.

The overall consolidation and desiccation process of soft soils is modelled in the theory with four consecutive segments, which correspond chronologically to the phases that a soft soil layer undergoes in the field after deposition. These phases are:

(1) Consolidation under one dimensional compression

(2) One dimensional shrinkage

(3) Propagation of desiccation vertical cracks with tensile stress release

(4) Three dimensional shrinkage

Konrad and Ayad [Konrad and Ayad, 1997b]: The general outline of the their model, illustrated as a flow chart in figure 2.24, revels that the approach uses interactively three distinct known models in close association with the principle of effective stress to describer stress partitioning in the soil. First, a one-dimensional mass transfer model enabling the determination of the suction profile with time for a given surface evaporation flux provides the input to determine the condition of crack initiation using total and effective stress paths during desiccation consolidation assuming restrained conditions. Second, the LEFM theory allows for the determination of the ultimate depth of crack under a given later stress

field. Third, the theory of linear elasticity is used to compute the stress redistribution around the crack in order to determine the extent of the stress relief zone which in turn relates directly to the spacing of these primary cracks.

It is emphasized that the model does not consider subsequent deepening of these primary cracks as further moisture extraction occurs with time.

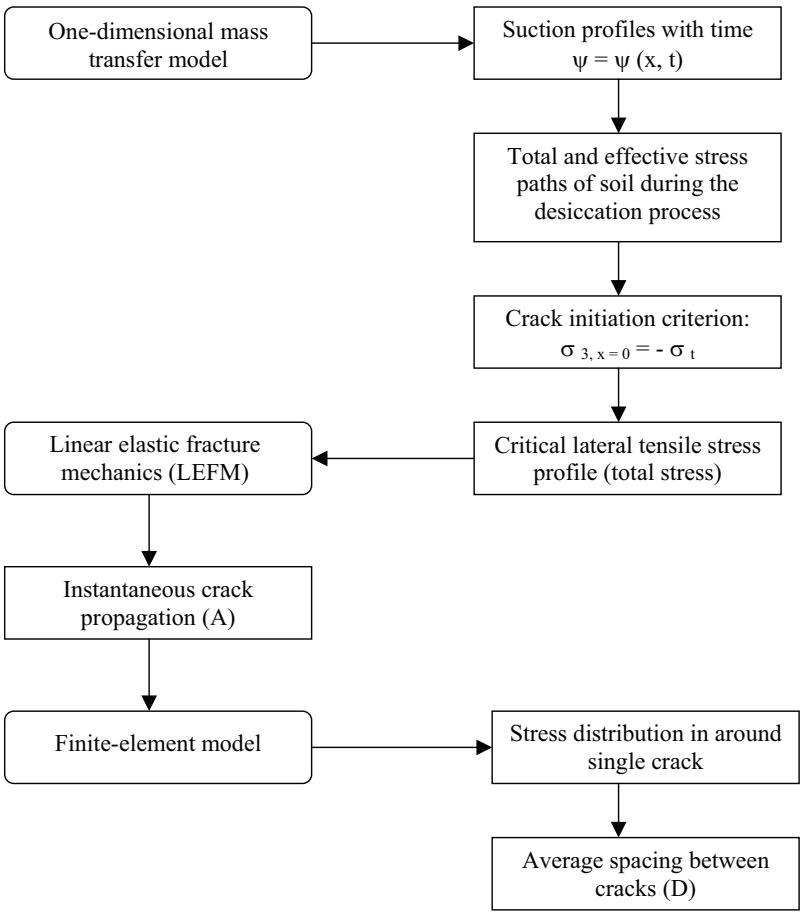

Figure 2.24: Flow chart of the model [Konrad and Ayad, 1997b]

Prat et al [Prat et al., 2002]: Crack initiation and propagation in soils, and particularly in compacted soils, and the influence of flow and pore water pressure is a complex problem involving the mechanics of strain localization and the hydraulics of water flow in saturated and unsaturated media, as well as their interaction.

Desiccation of the soil surface induces volume and tensional changes that favors crack formation in the soil mass that starts from the surface and penetrates into the soil up to a depth dependent on the particular boundary conditions. During drying, crack formation and propagation is mainly controlled by the horizontal tensile stresses that appear during

the process, and that are associated to the volumetric strains produced by water loss in the soil. These tensile stresses, as well as the soil stiffness, vary considerably with the degree of saturation of the soil.

2.6.2 Classical and unsaturated soil mechanics

After reviewing some of the very widely accepted research papers, disagreement was seen regarding the applicability of classical saturated or unsaturated soil mechanics for the desiccation cracking in soils. In fact, cracks can occur in nature in saturated or unsaturated states, but the disagreement for desiccation cracking is evident in the literature.

Clay soils tend to crack when they dry. In early stages of drying from horizontal surface from a soft, initially saturated soil, decreases in water content are largely accommodated by reorganization of the soil particles in to successively closer arrangements. Experiments have shown that the void spaces between the particles do not remain indefinitely filled with water, and successively larger proportions of air gradually enter the void spaces. Surface tension effects at air-water-soil contacts inside the soil generate negative pressures (or matrix suctions) below atmospheric pressure in the remaining pore water. These matrix suction produce two counter acting effect, one, in a selected point, the soil tends to contract more or less isotropically, this shrinkage produces vertical cracks below horizontal drying surfaces. Two, the soil gains strength and provides increased resistance to crack formation. This concept of mechanism of desiccation of soil by Morris et al [Morris et al., 1992] clearly shows that the soil is unsaturated when it cracks. Further, to express the shear strength of unsaturated soil they utilize the equations of Fredlund (1979) with some reservations on the validity of effective stress concept and Fredlund´s state variables to link the pore-air and pore-water pressures in the soil.

Saturated clay subjected to evaporation experiences a continuous decrease in water content, negative pressures or suctions are developed in the porous network of the soil. If the soil is unrestrained, the developed suctions impose an increase in effective stresses, which in turn, produces a decrease in the soil volume by consolidation. The relationship between moisture content and void ratio is often referred to as the shrinkage characteristics of a given soil. Figure 2.25, presents a typical shrinkage curve for a soil with a high clay content. During the drying process, several stages can be identified. In the first stage, the volume decrease of the soil is equal to the moisture loss and the soil remains saturated over a wide range of water contents. The second stage begins when the capillary tension reaches the bubbling pressure or the air entry pressure of the soil. As the air enters progressively in to the soil pore network, further moisture loss occurs, and the liquid phase

becomes more and more discontinuous. In this stage, the moisture loss is greater than the volume decrease, and the shrinkage curve becomes progressively horizontal. In the third stage called zero shrinkage stage, the soil does not show any further volumetric change. The moisture loss is then equal to the increase in the soil air volume. The above description of mechanism of shrinkage in clays was give by Konrad and Ayad [Konrad and Ayad, 1997b] clearly remarks the state of soil as stages with instantaneous moisture content and voids ratio of the shrinking soil. Konrad and Ayad clearly states that the cracking begins when the soil is in stage-I, i.e. soil is still saturated, further, quote that the equations developed for crack initiation and initial depth by Morris et al [Morris et al., 1992] can not be used as the approach followed is of unsaturated one.

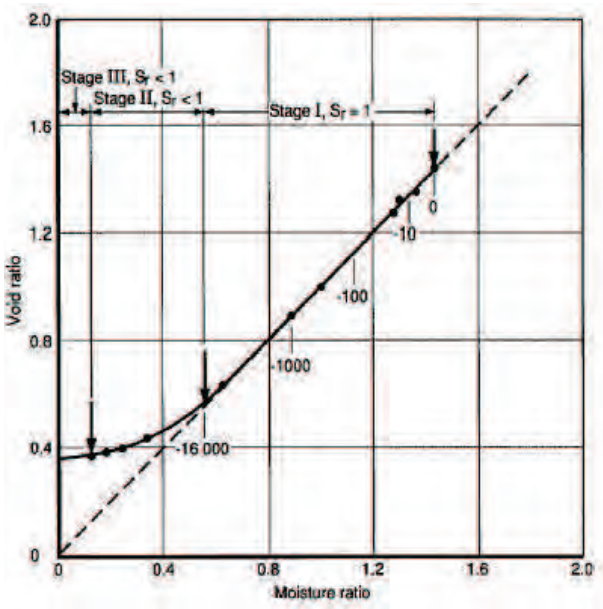

Figure 2.25: Typical shrinkage characteristics of clay soil (after Bronswijk-1988) as referred by [Konrad and Ayad, 1997b]

Kodikara et al [Kodikara et al., 1998] in their discussion on the framework by Konrad and Ayad [Konrad and Ayad, 1997b] agrees that some clays (for example slurried Regina clay) does not desaturate until the soil is subjected to more than 1 MPa, but referring to Bronswijk [Bronswijk, 1988] quotes that there is evidence that some light clays deviate from this behaviour and primarily show residual shrinkage as the soil desaturates. Further, heavily over consolidated clays as well as compacted clays predominantly behave in an unsaturated manner during the desiccation, to substantiate this claim they point to the work of Vanapalli et al [Vanapalli et al., 1996a]. In the work of Vanapalli et al, soil-water characteristics measured for compacted soil specimens of Indian Head till have shown that the air entry value is less than 100 kPa even for specimens compacted about 6% wet of optimum. Since the tensile strength of these clays is higher than that for unconsolidated

clays, suctions exceeding 100 kPa can develop at the point of initial cracking. Under these suctions, these soils are most likely to be unsaturated. Regarding the comment by Konrad and Ayad [Konrad and Ayad, 1997b] on the use of equations for crack initiation and initial depth of propagation given by Morris et al [Morris et al., 1992], Kodikara et al [Kodikara et al., 1998] points that the equation for net horizontal stress used by Morris et al [Morris et al., 1992] can be modified for K_0 loading and saturated conditions will be the same as the effective stress relation used by Konrad and Ayad [Konrad and Ayad, 1997b]. The only difference is that the vertical to horizontal stress ratio, K_0, will be given by $\nu/(1-\nu)$ instead of $(1-\sin\phi)$, as commonly used for normally consolidated soils. This arises from inherent disparity between continuum mechanics elasticity and particulate soil mechanics. On the discussion of Kodikara et al[Kodikara et al., 1998], Konrad and Ayad [Konrad and Ayad, 1998] in their reply totally agree that the model should also consider the unsaturated soil mechanics, but they mentions that the model presented holds for soils with a high clay content in which the desiccation cracks from while the soil is still saturated.

The comments from Kodikara et al[Kodikara et al., 1998] can be substantiated by the experimental work on the crack initiation in drying soils by Lloret et al[Lloret et al., 1998]. According to Lloret et al cracking occurs in quasi-saturated conditions. They did experiments with different initial water content and different imposed suction, they conclude that the soils with high initial water content, the initiation of cracks is observed when the saturation is near to 1, and 0.8 for soils with lower initial water content. Which ever the case the initiation of crack is under quasi-saturated or unsaturated conditions.

Bronswijk and Evers [Bronswijk and Eversvermeer, 1990] conducted shrinkage experiments on Dutch clay soil aggregates, they noted that some clay soils show normal shrinkage from saturation till a pressure head much lower than $-16,000cm$ (a suction of $1.57Mpa$). An extreme example of this is the Bruchem C11g horizon (one of the clay soil they tested). They say that under Dutch climatic circumstances, the aggregates in this soil horizon always remain fully saturated. Air is only present in inter-aggregate pores like shrinkage cracks.

Another example of saturated soils with suction is from the work of Fleureau et al [Fleureau et al., 1993]. They have conducted experiments on 11 different types of soils, from natural loams' to pure kaolinites and montmorillonites. In their experiments they observed that, when the water content is reduced below the air entry point, the degree of saturation decreases very sharply, almost linearly with water content as long as the void ratio remains approximately constant. The point of saturation at which the curve begins to deviate from the straight line corresponds to the shrinkage negative pressure as in figure 2.26B. Figure 2.26D shows the variation of the degree of saturation with pF (The

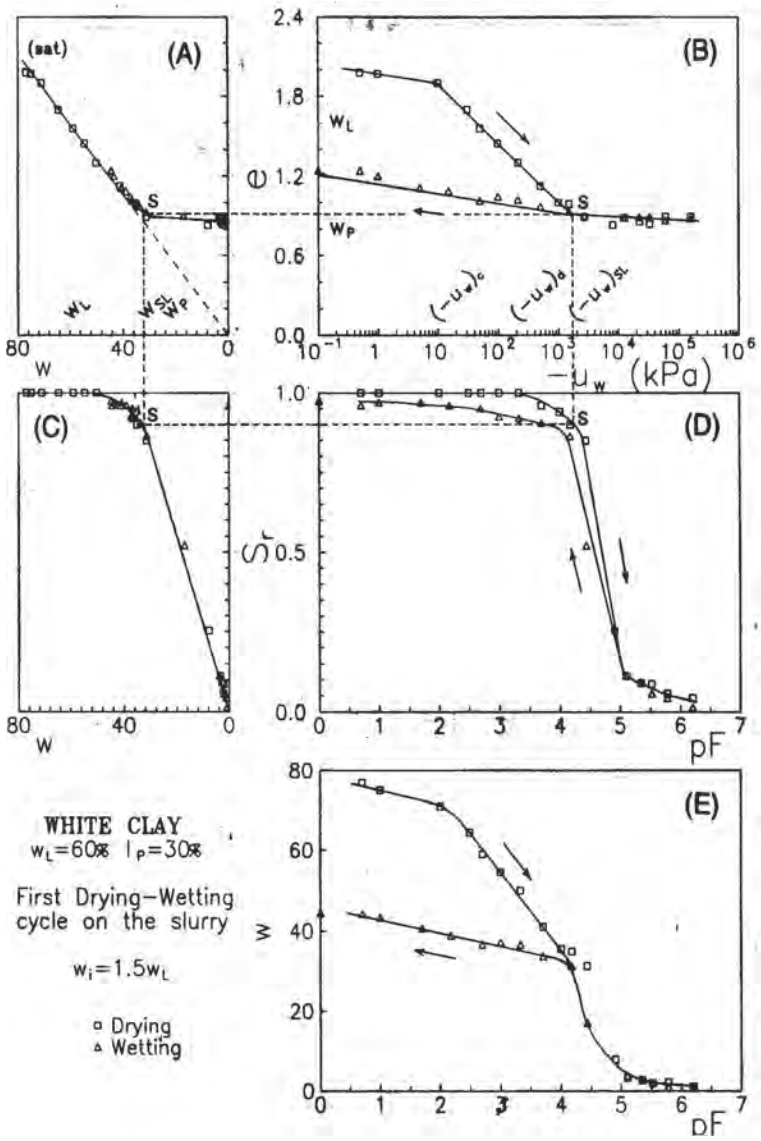

Figure 2.26: Synthesis of drying-wetting paths on the white clay [Fleureau et al., 1993]

logarithm of negative pressure expressed in cm of water): the soil remains quasi-saturated up to the desaturation negative pressure of 1MPa, then the degree of saturation decreases rapidly to reach approximately 0.1 for negative pore pressure of 10MPa.

2.6.3 Stochastic

Hoegan and Young [Horgan and Young, 2000] have presented an empherical model for the fragmentation of drying soil, based on the geometry of two-dimensional crack growth. The model is restricted to only two dimensional cracks. The parameters used to generate cracking patterns include those used to characterize crack growth development as a

random walk, fragmentation of peds above certain size threshold and attraction of cracks within defined distances. Figure 2.27 shows the three stages of crack growth as explained in the model. The model has many parameters, the final geometry of the cracking pattern is defined by defining these simple parameters.

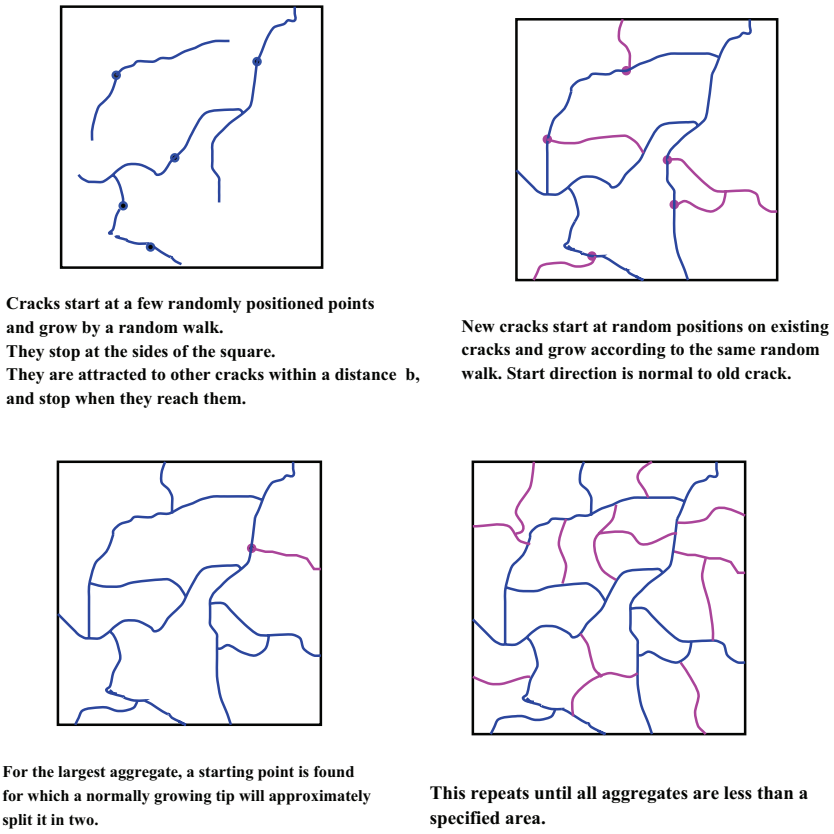

Figure 2.27: Stages of crack formation [Horgan and Young, 2000]

Lecocq and Vandewalle [Lecocq and Vandewalle, 2002], designed a simple experiment to study both the dynamical and statistical properties of cracking that occurs in a one-dimensional system composed of wet clay exposed to shrinkage induced by desiccation.

2.7 Conclusions

The following are the conclusions after the extensive literature survey.

Definition and mechanism:

(1) The definition on how the mechanism of cracking occurs, each researcher has his own definition of mechanism, though the factors considered are same in most of the cases.

(2) Regarding the crack initiation, there is lot of confusion which can be seen in the Introduction. The location and state of soil when the crack is initiated is the cause of discussion and confusion.

Causes:

(3) There is a general agreement over those factors which causes the soil to crack.

(4) Apart from the natural factors like temperature, wind speed, and relative humidity, the characteristics of the soil like the structure, density, clay content, water content, thickness of the desiccating soil and presence of vegetation in relation to the process of desiccation are well studied and a general trend on how these factors affect can be found.

(5) The other main and important properties of soil, Tensile strength and Suction which plays a major role in unearthing the process of cracking are not given due importance and very little information is available on these as concerned to the cracking of soil.

Implications:

(6) Though the advancement in science has given a lot new materials for construction, the use of soil as a construction material has not taken in to the back stage, on the other hand it has found its use in more and more places of vital importance. Thus the cracking in soils is now got implications on settlement of earthen embankment of an high way to the structural integrity of a clay cover of an nuclear repository and from stability of foundations to the water loss in reservoirs and agricultural farm lands.

(7) Environmental risk of cracks in soil is far reaching as the cracks are found to increase the hydraulic conductivity by 2-3 fold in comparison with the intact soil. The increased hydraulic conductivity and preferential flow are found to be the main culprits in transport of contaminants in most of the cases, resulting in contamination of ground as well surface water sources.

Experiments:

(8) Laboratory experiments conducted can be widely grouped as to study the soil mechanics and fracture mechanics properties of soil: in the former the cracking in soils is studied by observation and recording the changes taking place in the drying soil, where as in the later the fracture characteristics of the soil are studied by testing the soil specimens

with established fracture mechanics regulations.

(9) There are not much filed experiments to refer, most of the field experiments are more of post-mortem in nature, that is, study of the cracked soil rather than the cracking soil.

Models:

(10) The models proposed are also of particular application and complex. Here, particular application is meant as, models applied to desiccation of clay liners/compacted soils, models applied to desiccation of mine tailings/soft soils, and etc,. Even though there are some general models the applicability is limited to certain types of soils. The complexity is the use more than one concept to explain the whole mechanism and the inter-relation between the stages, though which are continuous and interconnected.

Chapter 3

Soil Used in the Investigation

3.1 Introduction

Soil used in the present investigation is from the Campus North of the UPC, Barcelona. The soil was collected from the construction site behind the NEXUS-II building at an approximate depth of 4 m from the existing ground surface. The soil was air dried and subsequently sieved with a mechanical sieve.

The Barcelona soil has been studied well for its geological origin and mineralogical composition. The soil has also been studied extensively from the point of view of Thermo-Hydro-Mechanical behaviour. The data and information presented in this chapter is a compilation of these previous studies done at the Soil Mechanics Laboratory of the UPC.

3.2 Origin and Composition

3.2.1 Geological Origin

In descending order of antiquity, the main geological formations that are present in and around Barcelona are Paleozoic, the tertiary and the quaternary. The Paleozoic formation consists mainly of Granite (which can be found at the base of the Collserola mountain range), which generally appear altered due to Mediterranean weather forming white sandy soils. Other types of rocks such as, Slate, Quartzite and Limestone are also commonly found. After a major lapse in the time scale, materials are deposited in the Tertiary

period, which can be subdivided in to Miocene and Pliocene deposits. The Miocene deposit is made up of different levels of sandstone, limestone, marl, usually of colour pink and yellow. The materials that are made up of Pliocene deposit are blue marl fossil interspersed at different levels with sand. The materials that are present in superficial outcrops in the vast plain of Barcelona are from the Quaternary period characterised by a gently sloping surface from the mountains to the sea. In low lying areas/sectors recent deposits of alluvial and deltaic origin are found in the delta region of Besos and Llobregat rivers. Figure 3.1 shows the geological map of Barcelona city, in which the main geological

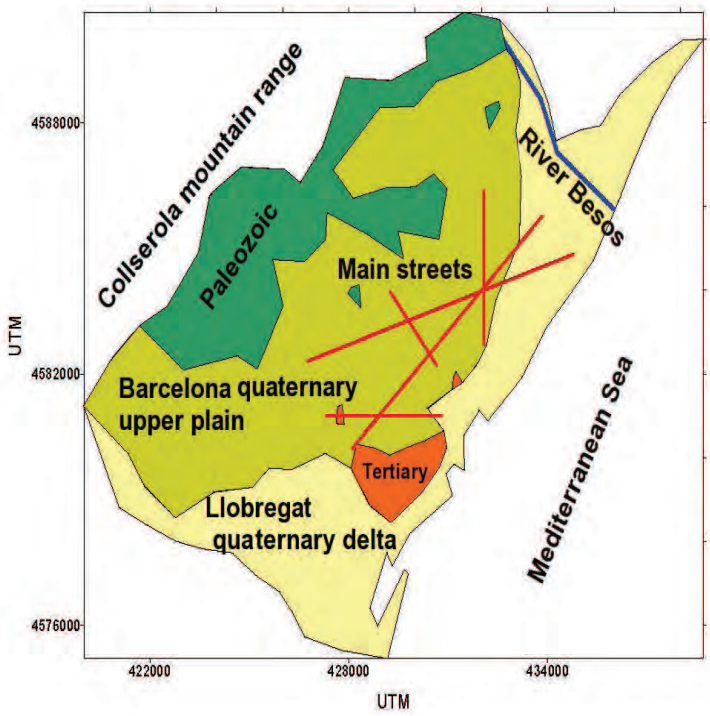

Figure 3.1: Geological map of Barcelona [Vázquez-suñé, 1998]

deposits are shown schematically which is adopted from Vázquez-Suñé, [Vázquez-suñé, 1998].

3.2.2 X-ray diffraction

The fundamental application of the X-ray diffraction technique is for qualitative identification of mineralogical composition of a crystalline sample. Diffraction effects are observed when electro-magnetic radiation impinges on periodic structures with geometrical variations on the length scale of the wavelength of the radiation. The inter-atomic distances in crystals and molecules amount to 0.15-0.4 nm which correspond in the electro-magnetic

spectrum with the wavelength of x-rays having photon energies between 3 and 8 keV. Accordingly, phenomenon like constructive and destructive interference should become observable when crystalline and molecular structures are exposed to x-rays. This is one of the most used methods for the identification of minerals in fine grained soils. Barrera [Barrera, 2002] characterised the mineralogical composition of the Barcelona soil by X-diffraction method. The procedure followed and the results obtained are presented here.

A representative sample of the naturally occurring soil is left to dry in air, this dried soil sample is then sieved with sieve number 200 ($75\mu m$ aperture opening), the material passing through is pulverized for testing.

The equipment used is a Diffractometer commercially called SIEMENS D-500 with a Cu K anode (the wave length of the ray is $\lambda = 1.5406\mathring{A}$), with a step magnitude of 0.05°, a scan speed of $3°/min$ and a starting value of $2\theta = 3.976°$ and up to 69.976°. The pulverized particles were randomly oriented in all directions assuring that at least some will be oriented with respect to the X-ray beams. A characteristic set of continuous reflection was produced at values of θ (angle of the diffracted rays) corresponding to the basal spacing of the prominent planes. Since no minerals have the same spacing of basal planes (d), the angle θ at which the diffraction occurs (which is related to the distance d by Bragg's law: Mitchell [Mitchell, 1993]; Yong and Warkentin [Yong and Warkentin, 1975]) was used for identification. The resulting diffraction pattern is like a "finger print" of the crystalline components. Details of the specimen preparation, mounting and general instructions for the operation of the diffraction unit are described in Willard et al [Willard et al.,].

Figure 3.2 show the results of X-ray diffraction. The mineralogical composition of the fine fraction ($< 2\mu m$) consists predominantly of the following minerals, Quartz, Albite, Calcite, Feldspar and Muscovite. The Muscovite fraction can be matched with that of Illite, but a chemical analysis would be necessary to confirm its presence

3.2.3 Environmental Scanning Electron Microscope (ESEM)

The recent advancements in the field of microscopy has increased the range of magnification immensely. The Environmental Scanning Electron Microscope offers excellent textural characteristics quick and easily. The specimens observed do not need any previous treatment or special preparation. The parameters such as average particle size, their distribution, morphology, textural homogeneity, distribution and approximate quantity

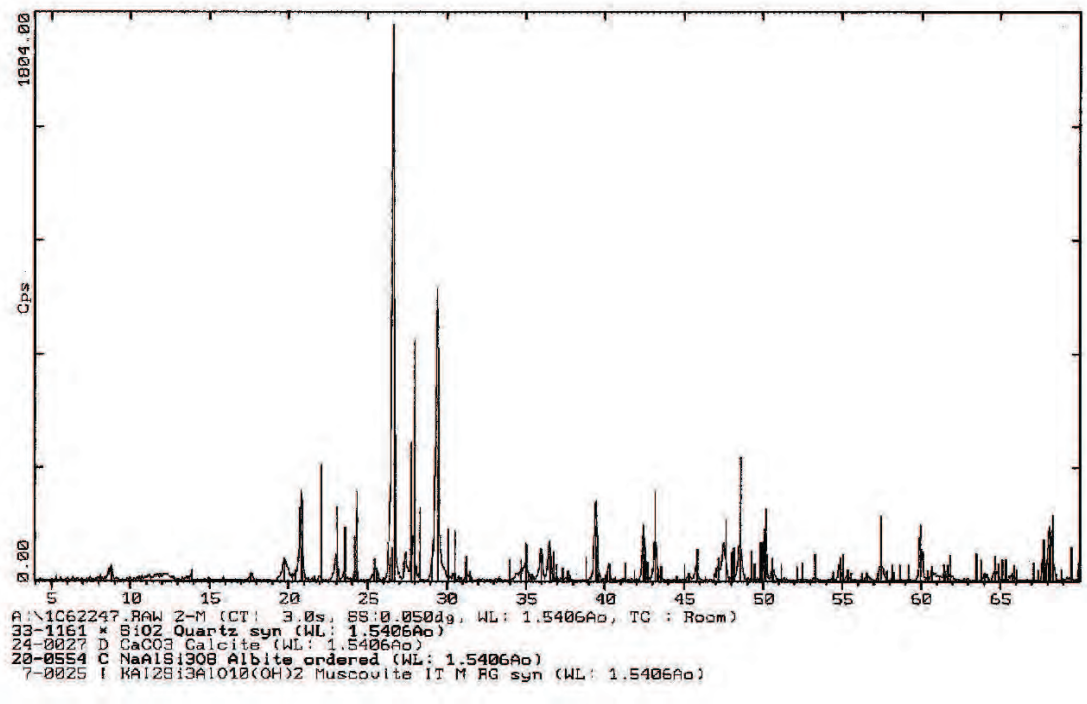

Figure 3.2: X-ray diffraction of Barcelona soil [Barrera, 2002]

of pores can be qualitatively evaluated in very short time.

Figure 3.3 shows the photo of the equipment Electroscan-2020. With this equipment images can be taken with secondary electrons up to a pressure of 50 torr. Specimens were placed in a sample holder with thermoelectric freezing. The testing temperature range is $\pm 20°C$ from the ambient temperature. Additionally samples with moisture can be examined.

Three samples representing three different structures were scanned. The samples were obtained from collapse tests and from isotropic compaction process. Table 3.1 gives the details of the three samples.

Table 3.1: Initial conditions of the specimens observed under ESEM [Barrera, 2002]

Specimen	$\gamma(\frac{g}{cm^3})$	$w(\%)$	$n(\%)$	Stress path
A	1.65	11	38	Isotropic compaction
B	1.53	8	42	Collapse by inundation under constant load
C	1.53	8	42	Collapse by decreasing suction up to saturation

Figure 3.3: Environmental scanning electron microscope(ESEM), ELECTROSCAN-2020

Figures 3.4 and 3.5 show the structure of the specimen A (see table 3.1), this sample was obtained from isotropic static compaction process. Figure 3.6 show the structure of the specimen B obtained from a collapse test due to inundation under a constant load, the sample was taken at the end of the test. Finally, figure 3.7 show the structure of the specimen C, obtained from another collapse test with similar initial conditions as specimen B but with different loading conditions.

The samples B and C show more or less similar structure at the end of the collapse test, though having different hydration. In case of the specimen A, which was isotropically compacted, shows aggregates of clay particles surrounding a silt particle. This was clearly observed in figures 3.4 where the central particle represent an area approximately equal to $37\mu mX80\mu m$, whereas in figure 3.5 the aggregates represent a dimension typically less than $15\mu m$.

3.2.4 Mercury Intrusion Porosimetry (MIP)

The results obtained from the Mercury intrusion porosimetry (MIP) gives the pore sizes and their distribution, which are the essential elements characterising the structure of

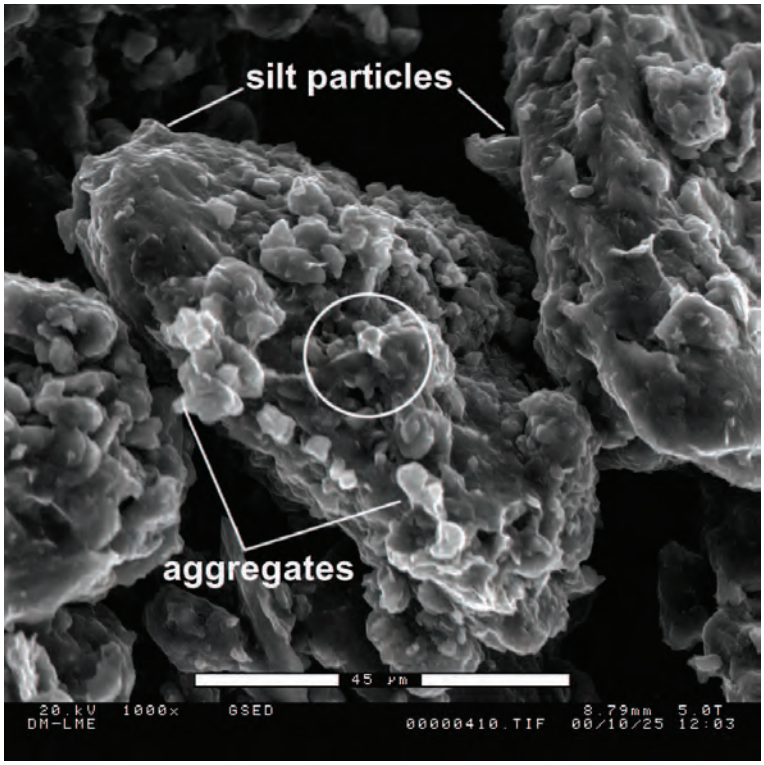

Figure 3.4: Specimen compacted in isotropic conditions (zoom = 1000 times)

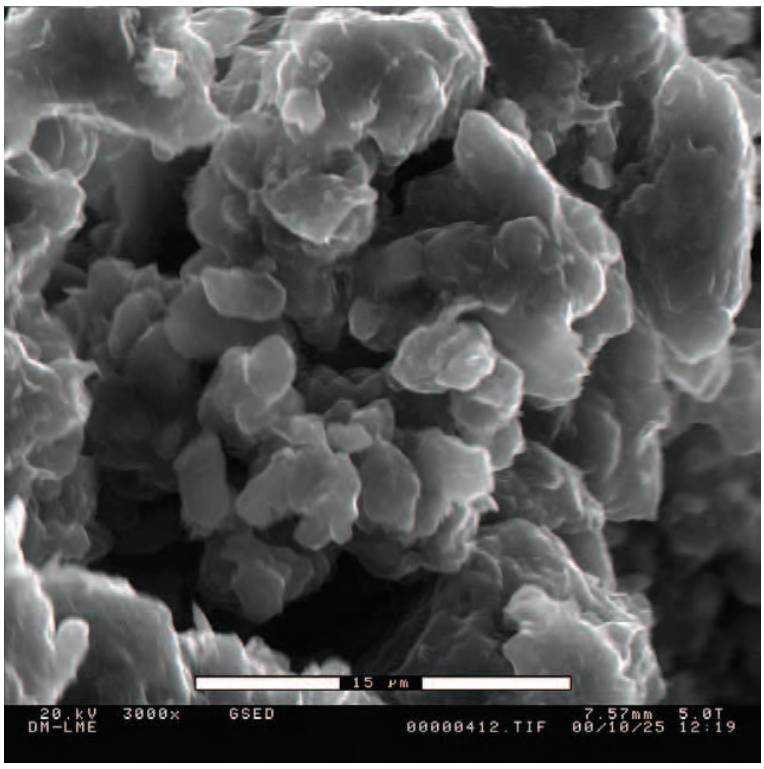

Figure 3.5: 4000 times zoom of the circle in Figure 3.4 showing aggregates [Barrera, 2002]

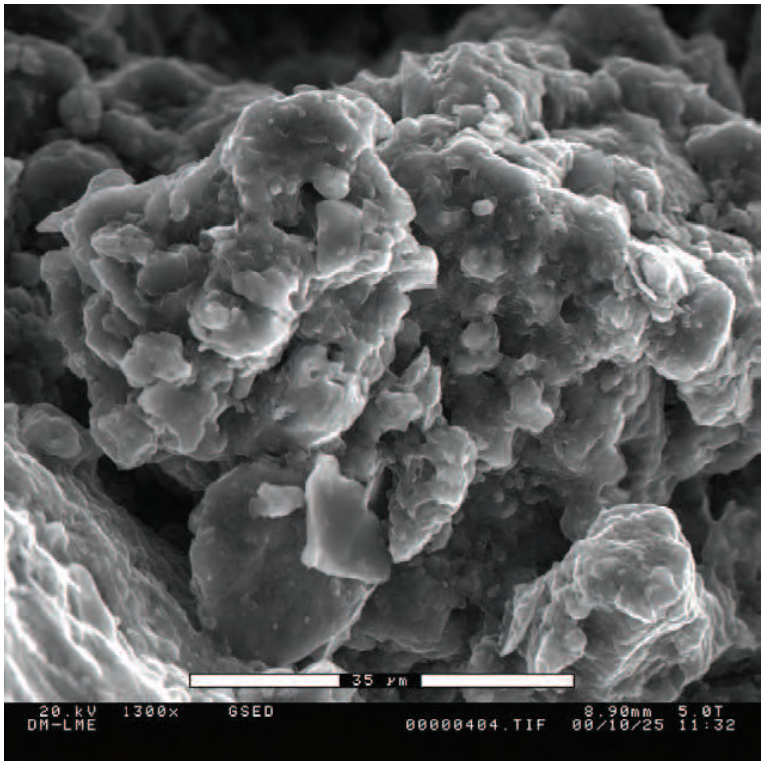

Figure 3.6: Structure of specimen collapsed after inundation [Barrera, 2002]

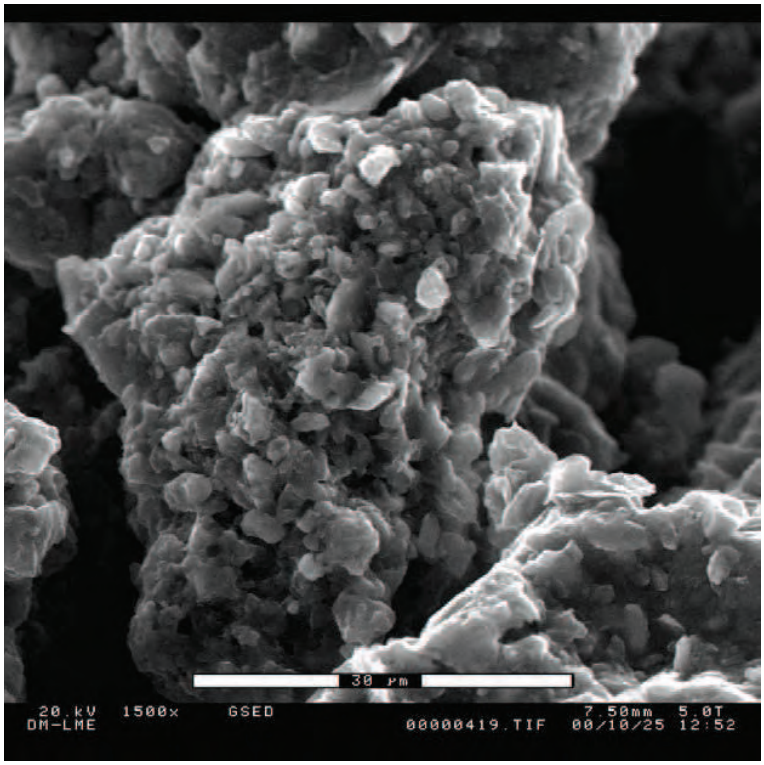

Figure 3.7: Structure of soil collapsed under wetting in stages [Barrera, 2002]

the soil. The pore size distribution is directly related to some the main and important behaviours of the soil, such as hydraulic conductivity, water retention characteristics, and volumetric deformations.

This technique is based on the capillary laws which govern the entrance of a non wetting liquid into the smallest pores. This law, in the case of a liquid like Mercury, is given by the equation of Washburn (Griffiths and Joshi [GRIFFITHS and JOSHI, 1989]):

$$D = -\left(\frac{1}{P}\right) 4\gamma_{mercury} \cos\varphi \tag{3.1}$$

where, D is the diameter of the pore, P is the applied pressure, $\gamma_{mercury}$ is the surface tension of the mercury, φ is the contact angle between the mercury and the sample. The value of surface tension used in this investigation is $\gamma_{mercury} = 0.484 N/m$ at $25°C$. Contact angle value of $\varphi = 140°$ was used (usually a value between 139° and 147° is adopted for clay minerals (Diamond [Diamond, 1970])). Delage and Lefebvre [Delage and Lefebvre, 1984], assumed a value of $\varphi = 141°$ for natural clay, whereas Griffiths and Joshi [GRIFFITHS and JOSHI, 1989] used $\varphi = 147°$ for a Illite and Kaolinite clay. Romero [Romero, 1999] used a value of $\varphi = 140°$ for a Kaolinite-Illite clay.

The volume of mercury V that penetrates in to the pores is directly measured as a function of applied pressure P. This information $(P - V)$, serve as a unique curve characterising the pore structure. The equation by Washburn assumes that all the pores are cylindrical, even though seldom the real soil pores are cylindrical; nevertheless the equation gives a practical solution representing the pore distribution. During the pressure decrease, the extrusion data is also calculated from the equation of Washburn. The extrusion curves of $(P - V)$ are different from that of the intrusion due to the entrapment of the Mercury in the pores with constriction because of the difference in contact angle of mercury for entrance and exit. The two curves of intrusion and extrusion can be used to characterise the pore structure.

The experimental program conducted by Barrera [Barrera, 2002] used a Porosimeter "Micrometrics" (figure 3.8), the important characteristics and specifications of the equipment are given in table 3.2. There is a restriction on the specimen volume used in the MIP equipment, a maximum volume of 5000 mm^3 for the specimen and a maximum pore volume of 292 mm^3 can be tested. The volume restriction for the specimen depends on the volume of the penetrometer.

Three specimens were tested, the first specimen, was obtained by isotropic compaction under a stress of 0.6 MPa, resulting in a dry density of 1.63 g/cm^3 at an initial moisture

Figure 3.8: Mercury intrusion porosimetry equipment (Micrometrics)

Table 3.2: Conditions of the MIP test using "Micrometrics" [Barrera, 2002]

Characteristics	Specifications
Low pressure	
Average	0 to 345 kPa
Sensitivity	69 Pa
Pore diameter	360 to 3.6 μm
High pressure	
Average	up to 228 Mpa atmospheric pressure
Pore diameter	6 to 0.005 μm
transducer precision	$\pm 0.1\%$
Intrusion	
Sensitivity	greater than $0.1 \mu L$
Precision	$\pm 1\%$ of penetrometer volume

content of 11%. The second specimen, the test was done after applying a load of 1.2 MPa resulting in a dry density of 1.8 g/cm^3 with moisture content of 10 %. For the final and third specimen, it was wetted under a constant load of 0.6 MPa resulting in a deformation due to collapse, and the specimen had a dry density of 1.73 g/cm^3 with moisture content of 13.8%. From each of the above mentioned tests, cubical specimens were extracted with extreme care, with an approximate dimension of 10 mm for each side. The specimens were air dried under a relative humidity of 40%. This drying affected the macro pores distributions due to shrinkage.

The corrected cumulative intrusion and extrusion volumes normalised by density of the solid particles (2.71 g/cm^3) plotted against the applied pressure is shown in figure 3.9. It was observed that the volume of pores not penetrated corresponds to a porosity value of 0.22 and 0.16 corresponding to the dry densities 1.63 g/cm^3 and 1.80 g/cm^3 respectively. The un-penetrated volume may correspond to both, the pores in which the pressure did not reach sufficiently high enough so that there can be intrusion and the bigger size pores corresponding to a Mercury pressure much lesser than the lowest applied pressure.

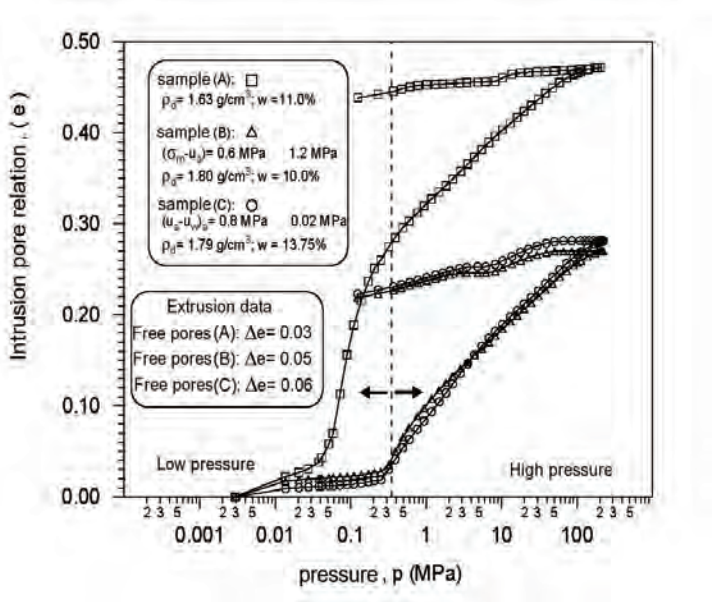

Figure 3.9: Relation between intrusion pressure and voids ratio(Barrera [Barrera, 2002])

Two types of porosity can be determined by two successive intrusions of mercury or alternatively with an intrusion - extrusion cycle. A cycle of intrusion-extrusion was used in the investigation of Barrera [Barrera, 2002]. The intrusion fills all the interconnected and accessible pores, giving a total pore distribution. On the other hand, when the intrusion pressure is relieved this permits the expulsion of only that part of the pore which is free (Delage and Lefebvre [Delage and Lefebvre, 1984]). The difference between the intrusion

and extrusion cycles gives the non-free or trapped porosity. The trapped porosity is attributed to the clay capillary bridges and irregular aggregate or ped formation, which acts as bottle neck for the free movement entrapping the mercury in the inter-aggregate pores (Romero et al [Romero et al., 1999]). Delage and Lefebvre [Delage and Lefebvre, 1984] propose that the free porosity corresponds to the intra-aggregate pores and the entrapped pores correspond to the inter-aggregate pores. The intra-aggregate or free pores can be detected when the pressure is released, in the present tests, it corresponds to 7.4% in the first sample, 18.4 % for the second specimen and 19.5% for the third specimen. These values of percentages correspond to an approximate pore size of 50 nm in the intrusion curve of figure 3.10. This pore size can be accepted to delimit the inter-aggregate and intra-aggregate pore zones (Romero et al [Romero et al., 1999]). Meyer et al [MEYER et al., 1994] present a classification based on the pore diameter, wherein pores with more than 50 nm diameter are classified as macro pores. The dominant pore size in the first specimen is around 15 μm and it is 3 μm for the second and third specimens. Assuming that the volume of pores not filled with mercury correspond to a porosity value

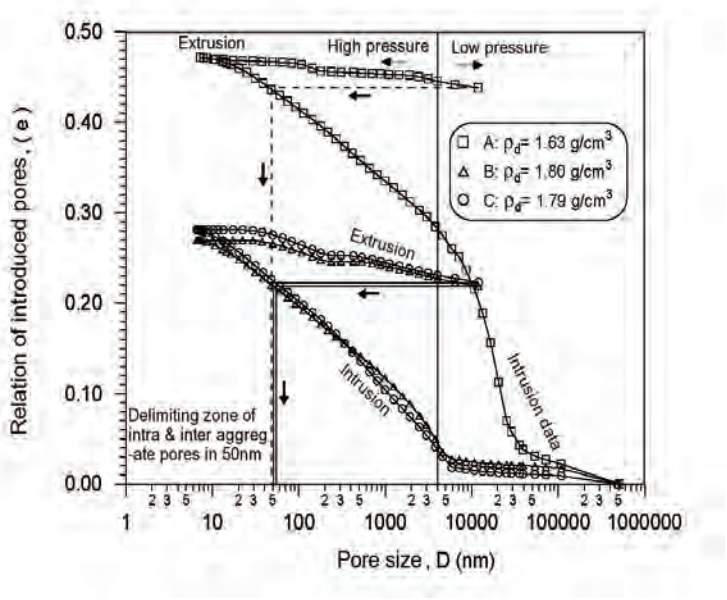

Figure 3.10: Pore diameter under different conditions (Barrera [Barrera, 2002])

of around 0.16, then the intra-aggregate porosity may correspond to a approximately 30% and 50 % of the total pore volume for the two dry densities 1.63 g/cm^3 and 1.8 g/cm^3 respectively.

MIP data can also be used to estimate the specific surface (S_s) of the soil, these values are plotted in figure 3.11 for the soil under study. The specific surface is calculated assuming a cylindrical form of the pores and is calculated using the equation 3.2. This equation for specific surface relates the apparent pore diameter D with the applied pressure P. The

normalised volume increment (dV) in intrusion can be related to the increment of the specific surface by the following expression (Romero [Romero, 1999]):

$$dS_s = \frac{PdV}{\gamma_{mercury} \cos\varphi}; \quad S_s = -\frac{1}{\gamma_{mercury} \cos\varphi} \int_0^{V_{max}} PdV \tag{3.2}$$

where D is the pore diameter, P is the applied pressure, φ is the contact angle between

Table 3.3: Estimation of specific surface from MIP data [Barrera, 2002]

Specimen	$V_{max} of Hg intrusion (\frac{cm^3}{g})$	intrusion voids ratio (e)	$S_s(\frac{m^2}{g})$	$\gamma_d(\frac{g}{cm^3})$
I	0.170	0.47	4.00	1.63
II	0.099	0.27	5.83	1.80
III	0.104	0.29	6.65	1.73

the specimen and the mercury, $\gamma_{mercury}$ is the surface tension of the mercury, and V_{max} is the maximum volume of mercury entered in intrusion.

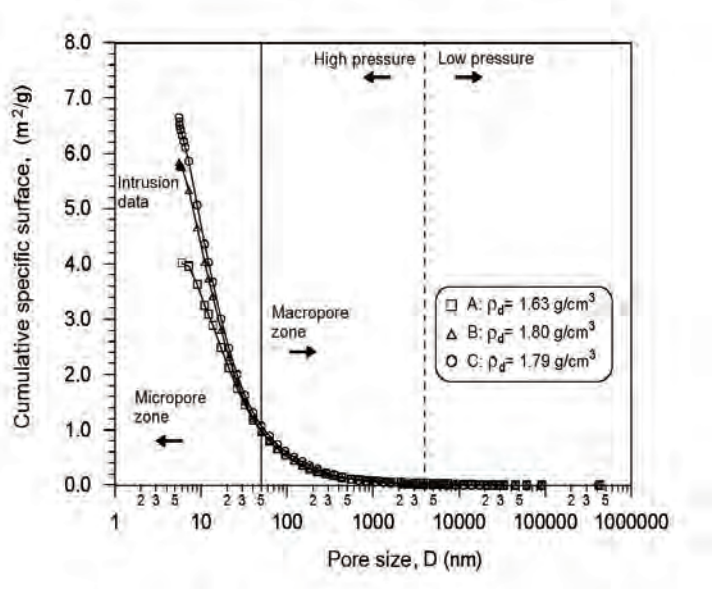

Figure 3.11: Specific surface determined using MIP data under different conditions (Barrera [Barrera, 2002])

3.3 Geotechnical characterisation

3.3.1 Granulometry / Sieve analysis

A large fraction of the Barcelona soil is fine material. In order to determine the gradation curve, two commonly adopted methods were used. Mechanical sieving method was used for the particle size of up to 0.075 mm and for the fraction which is finer than 0.075 mm sedimentation technique was used. By adopting the two methods (see table 3.4)complete granulometirc characterisation of the soil under is study was possible (see figure 3.12). Figure 3.13 shows the results from Gens et al [Gens et al., 1995] and Barrera [Barrera, 2002] for the same soil. Apart from the sieve analysis, some of the other parameters like,

Table 3.4: Results of sieve analysis, sedimentation data from Barrera [Barrera, 2002]

Sieve No.(ASTM)	Opening size (mm)	% passing
4	4.75	100
10	2	97.10
16	1.18	84.56
40	0.425	67.29
100	0.150	58.41
200	0.075	53.19
Sedimentation	0.04	38.77
	0.02	21.27
	0.005	11.44
	0.002	8.65

coefficient of uniformity (C_u) and coefficient of curvature (C_c) were determined. From the combined granulometry curve considering the minimum value of the particle diameter the value obtained for C_u was more than 4 and approximately 1 for C_c., for these values the soil can be considered as well graded one.

The specific weight of the solid particles was determined by the Picnometer procedure as per the ASTM D-854-83 norms and guidelines. The specific weight (ρ_s) of the solid particles determined to be 2.71 $\frac{g}{cm^3}$. Figure 3.13 show the results obtained by Gens et al [Gens et al., 1995], for a soil from the same zone of Barcelona..

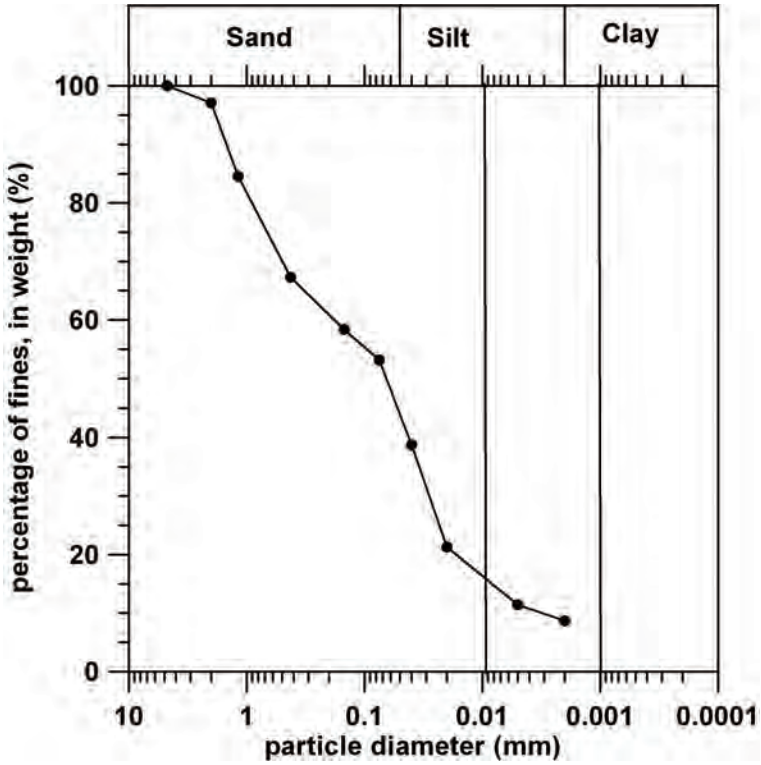

Figure 3.12: Grain size distribution from sieve analysis

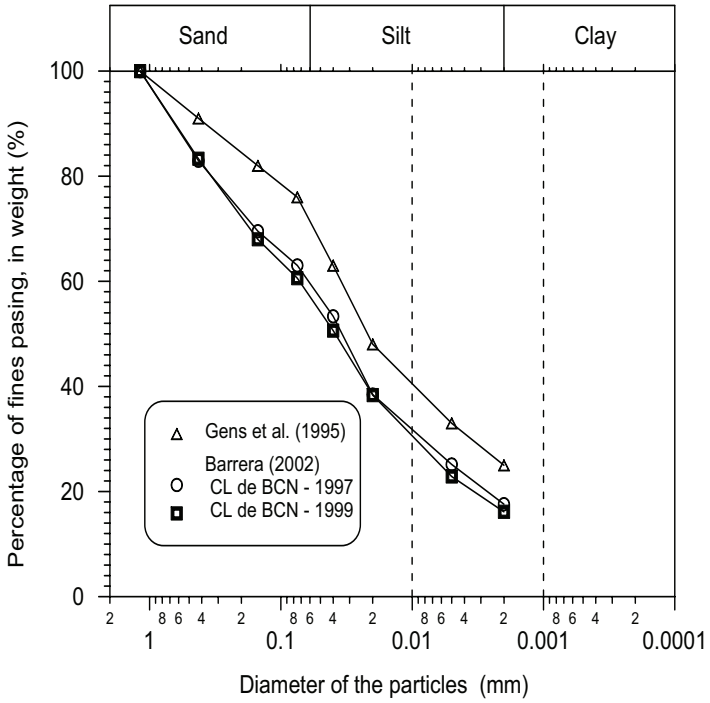

Figure 3.13: Grain size distribution from sieve analysis (data from Gens et al [Gens et al., 1995] and Barrera [Barrera, 2002])

Table 3.5: Grain size characteristics of Barcelona soil

Parameter	Experimental value
Sand	46.8%
Silt	42.7%
Clay	10.5%
C_u and C_c	well graded
ρ_s	2.71 $\frac{g}{cm^3}$

3.3.2 Consistency Limits

Atterrberg's limits also known as consistency limits were determined according to the norm ASTM-D4318. Determination of consistency limits is very important for geotechnical characterisation of a soil, the very basic idea of these simple tests is to determine the relation between the moisture in the soil matrix and its effect on the behaviour of soil. Though they are very empirical in nature, they are the engineer's best tool for a rapid assessment of the soil behaviour.

The values of consistency limits, liquid limit (w_L) and plastic limit (w_P) are given in table 3.6 , where (w_r) is the residual moisture at laboratory conditions and IP is the plasticity index ($w_L - w_P$). The soil at laboratory atmospheric conditions has a residual moisture content between 2% to 2.2%.

Table 3.6: Conditions of the MIP test using "Micrometrics" [Barrera, 2002]

Parameter	Experimental value
w_r	2.2%
w_L	32%
w_P	16%
IP	16%

Figure 3.14 show the plasticity chart including the work of Gens et al [Gens et al., 1995] and Barrera [Barrera, 2002]. Barcelona soil can be classified as low plasticity clay from the plasticity chart in agreement with the Unified system of soil classifications, ASTM-D2487.

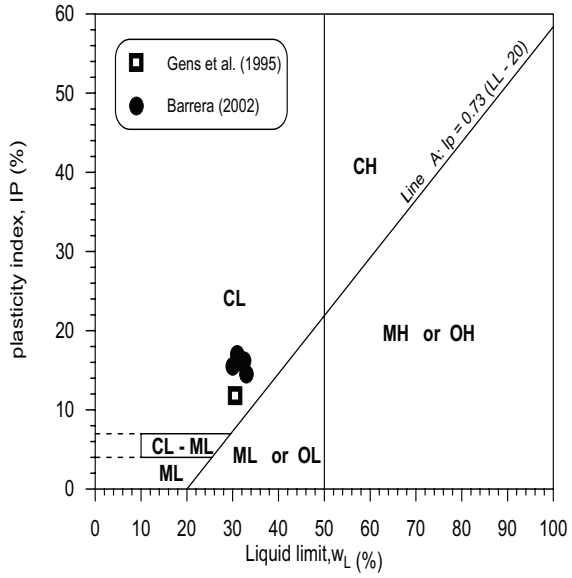

Figure 3.14: Plasticity chart (data from Gens et al [Gens et al., 1995] and Barrera [Barrera, 2002])

3.3.3 Compaction curves

The procedure normally adopted to obtain the compaction curves can be defined as mechanical methods, based on the expulsion of air occupying the soil pores and drastic reduction of voids ratio e at a constant moisture content. The basic idea of soil compaction is to obtain a material with new structure suitable for its intended specific use. The compaction results in permanent changes usually increased mechanical resistance, rigidity and reduction of permeability and thus reducing the propensity to erosion. The compaction tests are summarised in figure 3.15. Table 3.7 gives the summary of the compaction tests done by Barrera [Barrera, 2002] for the Barcelona soil.

Table 3.7: Details of the compaction tests [Barrera, 2002]

Compaction test	$w_{omc}(\%)$	$\gamma_{dmax}(\frac{g}{cm^3})$	$S_r(\%)$	Specification
Normal Proctor	13.0	1.890	81	ASTM D-698
Modified Proctor	9.7	2.040	80	ASTM D-1557
Scaled hammer	16.5	1.750	81	E_e = 600 (kN m/m), N =12, 3 layers
Scaled hammer	10.0	2.020	80	E_e = 6000 (kN m/m), N =27, 3 layers
E_e= Specific energy; N = Number of blows				

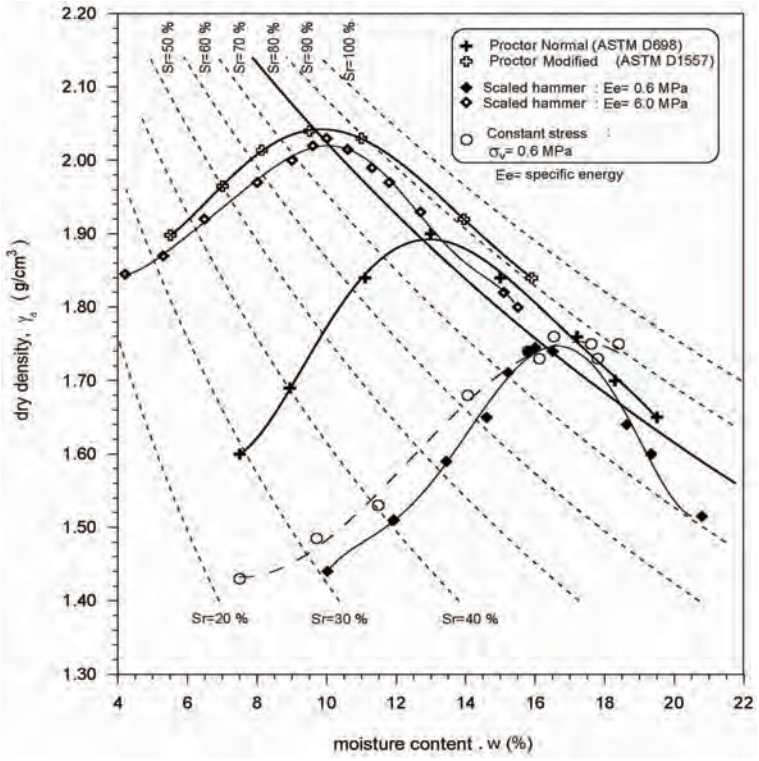

Figure 3.15: Compaction curves (data from Barrera [Barrera, 2002])

3.3.4 Water retention curves

3.3.4.1 Introduction

The relation between the suction and moisture content (or suction with degree of saturation) plays a very important role in the characterisation of partially saturated soils. The graphical representation of this relation is called with different names, like, characteristic curves, water retention curves, suction curves, and soil-water retention characteristic curves, etc. This relation is unique to a soil at a given density. As the name itself suggests "water-retention" these curves are directly related to the grain size distribution, mineralogy and the structure of the soil, these are the factors which influence the distribution of pores and interactions with pore fluid. Geometry of the pores, mineralogy and quantity of fines are decisive factors influencing the shape and slope of the water retention curves. The moisture content of the soil for very low suction values when the pores are saturated depend predominantly on the capillary effect and the distribution of the pores hence will depend on the structure of the soil. On the other hand, at higher values of suction the moisture is partially adsorbed to the particles and the importance of texture and specific surface area is more than that of the structure. This explains the higher values of suction observed in clays when compared to silts and sands.

The water retention curve is not biunivocal (one-to-one) relation. This is due to the hysteresis phenomenon observed between the experimental results of water retention curves obtained from wetting and drying paths. Also, there can be different moisture content values for a determined suction value. This is the reason behind determining the water retention curve in both wetting and drying paths.

van Genuchten [van Genuchten, 1980] proposed an expression to relate the suction and the moisture content, this expression characterise the degree of saturation S_r or normalised moisture content as a function of suction and is given by the following equation:

$$S_r = \frac{w}{w_{sat}} = \left(\frac{1}{1+(\alpha S)^n}\right)^m \tag{3.3}$$

where, the parameters, α: related to the air entry value of the soil, n: is related to the slope of the inflection point, and m: is related to the residual water ratio. The parameter m is related to the porosity n by $m = 1 - (\frac{1}{n})$. In the above expression w is the moisture content and w_{sat} is the saturated moisture content of the soil.

Romero and Vaunat [Romero and Vaunat, 2000] gave a correction factor to the above relation. The correction factor, intends to correlate the relation better taking in to account intra and inter aggregate pores and their interaction and contribution in relation to capillary and specific surface area as a function of moisture. The expression for the correction factor to be multiplied to the right hand side off the equation 3.3 is given by:

$$C(s) = 1 - \frac{\ln\left[1+\frac{S}{a_r}\right]}{\ln\left[1+\frac{a}{a_r}\right]} \quad \text{with} \quad 0.1a < a_r \leq a \tag{3.4}$$

where, S is the suction, a_r is the parameter controlling the shape and slope of the water retention curve at low moisture contents, and a is the intersection parameter. This is similar to the correction factor proposed by Fredlund and Xing [Fredlund and Xing, 1994].

3.3.4.2 Water retention curves for Barcelona soil

The experimental results of the water retention curves (WRC) from the thesis of Barrera are presented. The values of total suction were determined using Pscycrometer technique for isotropically compacted specimens. The data from the experiments are plotted (figures 3.16 and 3.17) as, suction versus compacted moisture content and suction versus degree

of saturation. Figure 3.16 shows that as the compaction moisture content increases the suction decreases, on the other hand figure 3.17 show the same tendency with degree of saturation. High suction values are principally controlled by the intra-aggregate pores. This can be observed with the characteristic curves for different densities, where the effort of compaction affect the macro-pore distribution, which has considerably little effect on high suction values for the soil under study, which was also reiterated in the work of Romero [Romero, 1999]. The moisture in the macro-pores (intra-aggregate pores) can be estimated and was around 6%, which in terms of volume of inter-aggregate pores can be 44%, 35% and 27% of the total volume for the densities $1.77g/cm^3$, $1.65g/cm^3$ and $1.45g/cm^3$ respectively. These values were estimated considering the maximum moisture content obtained in the retention curves.

The experimental retention curve data for the Barcelona soil was fitted with both van Genuchten and Modified van Genuchten equations, by optimising the parameters with a non linear curve-fitting algorithm using the least-square method. A value of 1000 MPa was assumed for a and a_r. The details are given in table 3.8. Figure 3.18 show the experimental values and estimated curves using the relation of van Genuchten [van Genuchten, 1980].

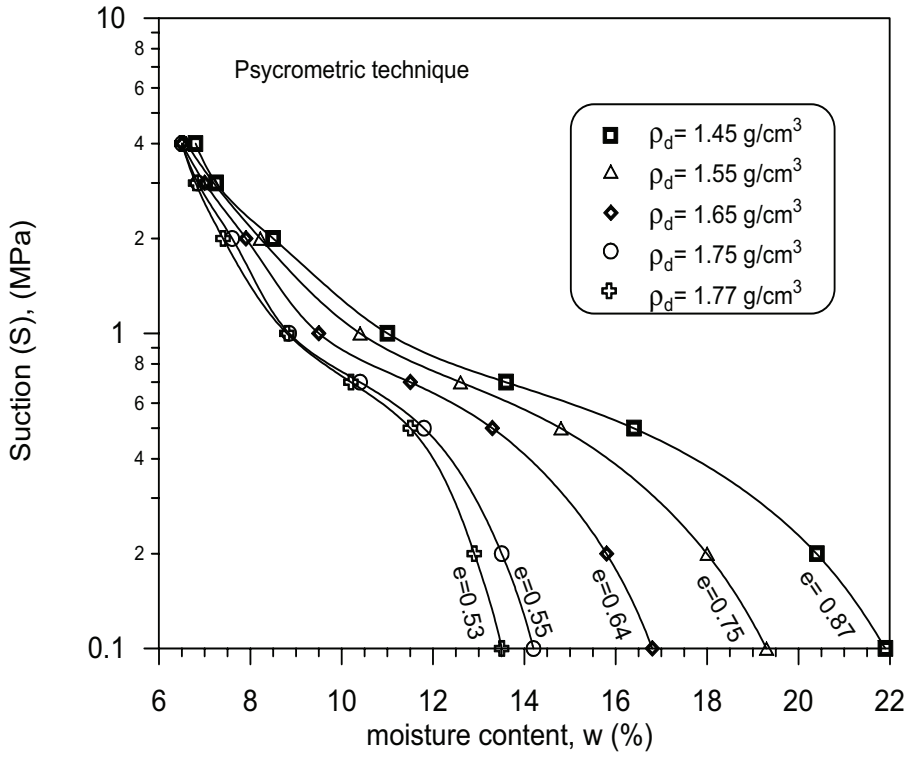

Figure 3.16: Relation between suction and moisture content for different dry densities for a constant porosity (Barrera [Barrera, 2002])

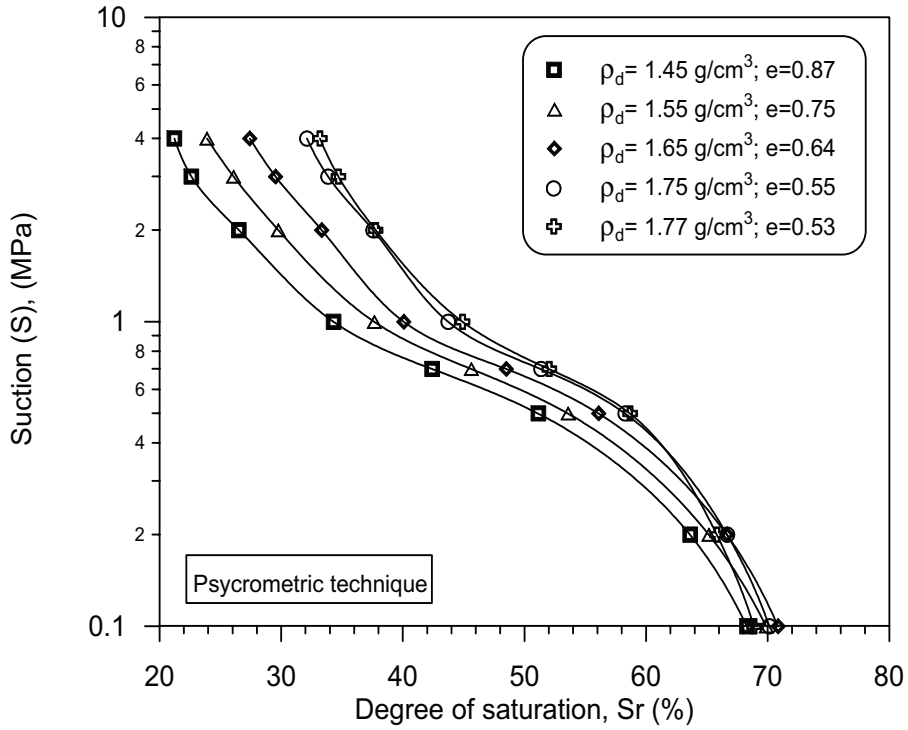

Figure 3.17: Water retention curves for a constant porosity (Barrera [Barrera, 2002])

Table 3.8: Water retention curve parameters from the experimental data of Barrera [Barrera, 2002]

e	$\gamma_d(\frac{g}{cm^3})$	α	m	n
0.87	1.45	0.828	1.524	0.545
0.75	1.55	0.756	1.447	0.527
0.64	1.65	0.485	1.554	0.479
0.55	1.75	0.033	3.052	0.373
0.53	1.77	0.066	2.420	0.380

Parameters determined taking suction values in MPa and using van Genuchten and Modified van Genuchten equations by method of least squares

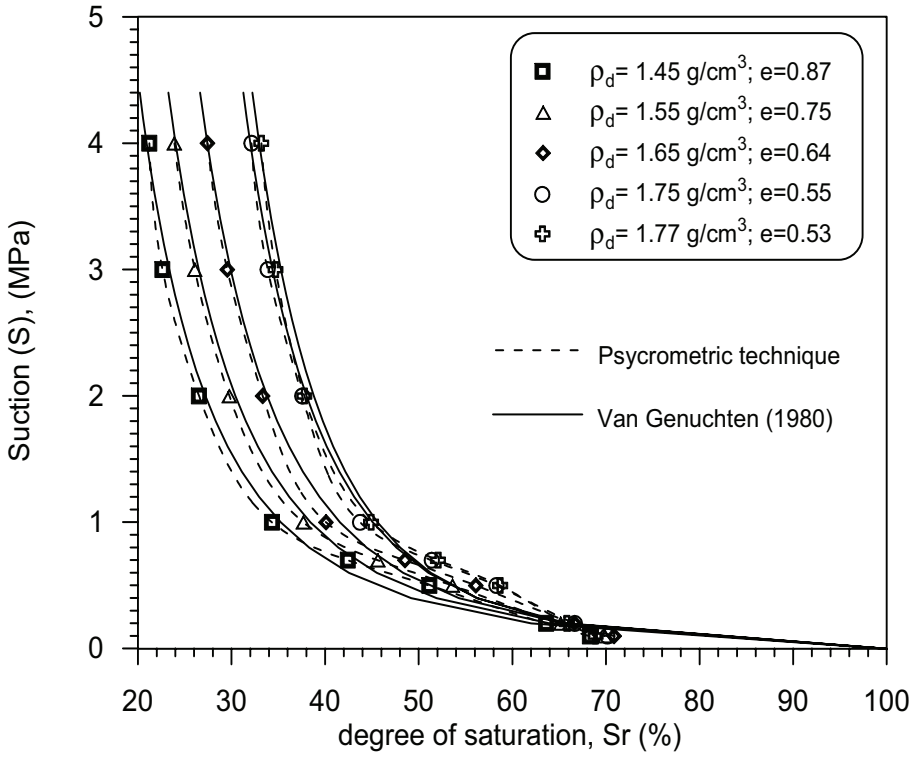

Figure 3.18: Experimental and calculated water retention curves (Barrera [Barrera, 2002])

Chapter 4

Tensile strength and Fracture toughness

4.1 Introduction

In a drying soil crack initiates when the tensile stresses exceed the soil strength. Crack propagation is considered to be governed by the stress state in the crack front and subsequent dissipation of fracture energy, for which fracture mechanics Theory can be used. In this context determination of fracture parameters (tensile strength and fracture toughness) is essential in determining the cracking behaviour. Characterizing the soil for these two parameters require two different testing equipments. The tensile strength was determined using existing equipment (direct method) at the Soil Mechanics Laboratory of UPC whereas new equipment was designed for the fracture toughness determination.

To determine fracture toughness, two sizes (medium and big) of compact tension (CT) tests specimens were used. Originally there was another size (small) of CT test specimen, but due to the problems with sample preparation and handling the tests were not conducted with this size. Apart from the determination of fracture toughness, the effect of moisture content was also studied.

Tensile strength of soils is an important indicator of material strength, as they depend on various other properties of soil. Until recently, determination of the soil's tensile strength had not received the attention it deserved, mainly because of the difficulty in the experimental set-up. It is known that the tensile strength of soils vary with the degree of saturation (moisture content) and as well with the density.

4.2 Tensile strength

4.2.1 Introduction

Tensile strength has not received the due attention it deserves in Geotechnical Engineering practice. Only cohesive materials such as clays, which exhibit both shear and tensile strength, where, following the conventional Mohr-Coulomb failure criterion, the former is captured as a function of normal stress via the friction angle (ϕ) term and the latter is indirectly captured via the cohesion term (C). For design considerations in engineering practice, the worst case scenario is assumed considering the soil to be saturated with null or negligible tensile strength. Nevertheless, there are several phenomenon which can not be resolved by simple assumption as earlier, the problem arises as the soil de-saturates. A classical example is the problem of cracking due to drying or desiccation cracks in soils. Though this is an age old problem but it seems more relevant today than earlier, considering the expected drier climatic conditions due to climate change.

Some published work as early as 1975 have shown that soils exhibit tensile strength which can not be neglected. Several researchers have developed different experimental methods to determine tensile strength directly and indirectly. Also, theoretical models are available to determine tensile strength. Recently, experimental campaign by Avila [Ávila, 2004], determined the tensile strength of Bogota clay at different moisture content with direct suction measurement during the test. Criterion for crack initiation based on the tensile strength was also proposed. Several other researchers ([Morris et al., 1992], [Towner, 1987b],[Konrad and Ayad, 1998],[Rodríguez et al., 2007]) have reported that the crack initiation is governed by the tensile strength, though they don't agree on the prevailing stress expressed in terms of effective or total stresses.

The present section on tensile strength in this chapter deals with direct method of experimental determination. Two experimental campaigns were undertaken, each with two series of tests. The first campaign consists of two series of tests with two different constant natural densities with varying moisture contents. For each natural density and moisture content the tests were repeated with a minimum of two specimens and in some cases three, resulting in 42 tests. The second campaign consists of two series of tests with two different constant dry densities with varying moisture contents. For each dry density and moisture content the tests were repeated with a minimum of two specimens and in some cases three, resulting in 31 tests. As explained earlier, the main objective of these tests is to fallow the drying curve of tensile strength. For suction measurement during the tests considering the moisture range no single sensor or instrument would be able to cover the

full moisture range. Then use of more than one type of sensor will add discrepancy to the experimental data. In the sense, two different sensors will have different cross-sectional area, thus the insertion of two different sensors will have different effect on the specimen. In order to avoid these complications no suction measurement was made during the test.

4.2.2 Unsaturated soils and their behaviour

In the study of soil mechanics since its beginning a greater importance has been devoted to the investigation of saturated soil leaving unsaturated soils to background, even though large extent of land area covers unsaturated soils. Dudley [Dudley, 1970] commented about Terzaghi's concern over the changes in volume of unsaturated soils when subjected to wetting. As of today, there is a broad knowledge and information on the behaviour of saturated soils, both experimental and modelling. On the other hand still there is a scarcity of information on the behaviour of unsaturated soils. One of the reasons attributed to the widespread usage of saturated soil mechanics is the simple concepts used to explain the behaviour. But, still there are many situations where the soil will never reach saturation or if saturated, will not continue to be saturated, especially in arid and semiarid regions of the world. This scenario will be more frequent and prolonged in many parts of the world as an effect of climate change. Unsaturated soils give rise to a variety of problems; they are also called problematic soils, especially when dealing with expansion and collapse, with out forgetting shrinkage and subsequent cracking. Much of these problems are being addressed by the scientific community separately as mentioned by Alonso et al [Alonso et al., 1987], they also suggest to work under a broad umbrella with a single perspective of "suction" as the main parameter controlling the behaviour of partially saturated soils.

The origin of partially saturated soils can be natural or man-made, there are a wide variety of naturally occurring unsaturated soils, for example sedimentary and residual soils. The majority of sedimentary soils are initially deposited in saturated conditions (usually submerged) consequently may dry due to changes in the surrounding environmental and climatic conditions. These types of soils are abundant in arid and semiarid climatic conditions, where the natural seasonal variations are distinct. In the case of residual soils, their formation is associated with agents of weathering and the parent rock which is reflected in the mineralogy of residual soils. On the other hand man made partially saturated soils can be found in each and every construction which uses soil as the base material (normally in compacted conditions).

4.2.2.1 Components of unsaturated soils

Partially saturated soils are a three phase system consisting of; solids, liquids and gases, the relationships between these phases and components of soil according to Yoshimi and Osterberg [Yoshimi and Osterberg, 1963] is presented in figure 4.1. Unsaturated soil structure as proposed by Worth and Houlsby [Wroth and Houlsby, 1984] is shown in figure 4.2. By considering the soil as a three-phase system composed of a solid skeleton, with pores filled with water and air it can be said that, the interactions between these three phase system is the basic point for understanding the behaviour of non-saturated soil. The three phases will be explained briefly considering some basic aspects of each of the constituent phases.

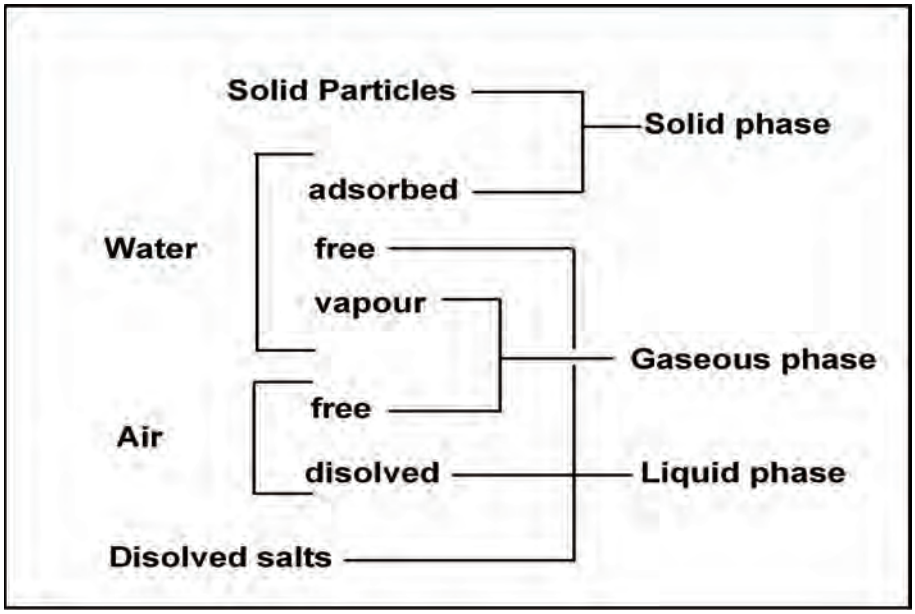

Figure 4.1: Main components of each phase in a partially saturated soil [Yoshimi and Osterberg, 1963]

Solid Phase

The soil particles constituting the solid phase may have highly variable characteristics from one another, such as their size (grain size distribution), shape, texture, mineralogical composition, crystallographic configuration, and so on, which may be critical to their behaviour [Josa, 1988]. The structure of the solid particles is particularly important in the unsaturated state because of the influence they have on the stress state generated in the interfaces between solid particles, water and air controlling the capillary component of suction [Alonso et al., 1987].

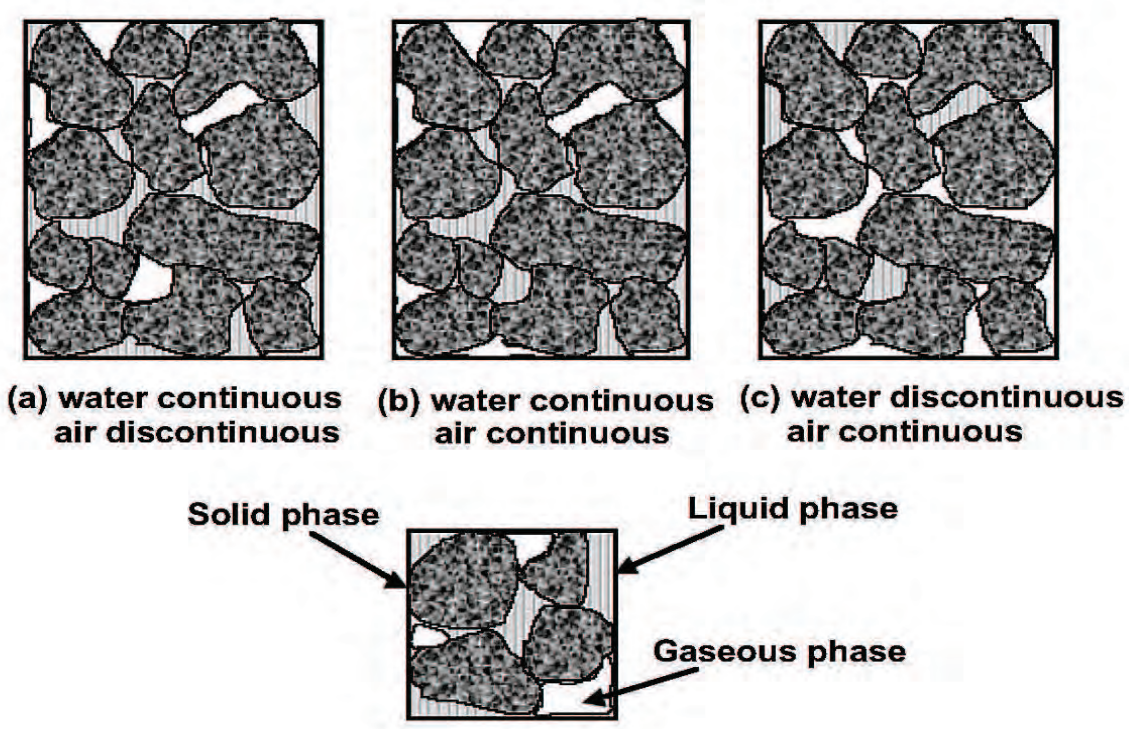

Figure 4.2: Structure of unsaturated soils [Wroth and Houlsby, 1984]

In certain cases the fraction of finer material dictates the overall behaviour, as in the case of clays. In some situations finer clay particles come together to form aggregates, with a different mechanical properties altogether.

In short, the structure of the soil is an important factor determining the response of the soil. As a consequence a sound knowledge of the properties of the individual particles is essential. Though it is quite difficult to model the soil at this micro structural level, researches have elaborated models at an higher macro structural level linking the both.

Liquid Phase

Commonly the liquid phase, which is fluid filling the pores in the soil structure is water. Chemically, this water or pore fluid can be distinguished as: hygroscopic water, capillary water and gravitational water. Hygroscopic water is adsorbed on the surface of the particles or forming a part of the diffused double layer, which can not be separated by hydro-mechanical actions. Capillary water is subjected to the capillary actions of the soil structure. The gravitational water is that part which can move freely as a consequence of gravitational drainage. The last two types of waters can move or flow due to hydro-mechanical actions; which are usually referred to as free water [Lambe, 1958].

The pore fluid normally contain dissolved salts in addition to water, which supply cat-ions. In some cases the presence and the quality of these cat-ions significantly influence the volumetric and strength behaviour of the soil. The presence of salts and changes to their concentration can alter the sensibility of the soil, causing instabilities to the structure; on the other hand in some cases like expansive soils stabilization can be done by adding Sodium silicate up to 1%.

In short, the liquid phase in most of the cases is water and salts dissolved in it.

Gaseous Phase

Basically this phase is composed of air and water vapour, which is how the air is found inside the soil structure. This is related to the moisture content and the degree of saturation. The most important characteristic of this phase with respect to geotechnical point of view is its compressibility in contrast to the incompressible water. The air which dissolves in water according to Henry's law will enter the closed pores with less pressure, and when the system reaches equilibrium; all the air pockets more or less remain at the same pressure. In partially saturated soils, the air can occupy the pore networks, which may be interconnected with one another and as well with external environment. Even though the air is not a perfect gas. For all practical and usual conditions for soils the law of perfect gas can be applied.

4.2.3 Revision of previous studies on tensile strength

4.2.3.1 Introduction

There are three general regimes of saturation in soil with negative pore water pressure or suction (see figure 4.3): the capillary regime, the funicular regime, and the pendular regime. Prior to desaturation, pore water may be under negative pressure within a regime referred to as the capillary regime. When the suction pressure increases, water starts draining from the saturated specimen and air-water interfaces or menisci are produced between and among the soil grains. The suction pressure that first causes air to enter the coarsest pores is known as air-entry pressure. Air-entry pressure depends on the size of the pores, and thus the grain size and grain size distribution of the particle matrix. In general, the finer the grain size, the finer the pore size, and the higher the air entry pressure. During suction increase beyond the air-entry pressure air continues to break into the soil pores but the water still forms a continuous phase.

As indicated in figure 4.3 the pore water resides as menisci or "liquid bridges" between soil particles or groups of soil particles, but may concurrently reside within saturated pores at other locations. This regime is known as the funicular regime. Because the liquid water phase remains continuous, any local change in water pressure is rapidly homogenized throughout the soil. Finally, the pendular regime, which corresponds to relatively high suction pressures describes a regime where water exists primarily as liquid bridges between and among particles and as thin films of water around the particles. The border point between the funicular and the pendular regimes is known generally as residual saturation. After this point, a very large suction change is required to remove additional water from the soil.

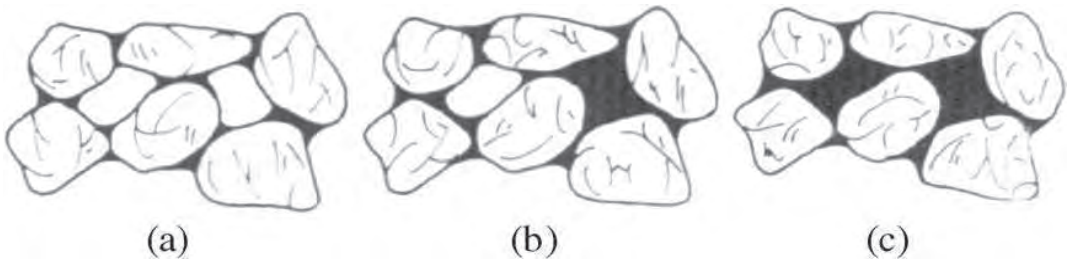

Figure 4.3: States of Saturation in Unsaturated Soils: (a) pendular state, (b)funicular state, and (c) capillary state (after [Kim and Hwang, 2003])

Capillary forces associated with these saturation regimes contribute to tensile strength and shear strength. Capillary forces in the pendular regime result from a surface tension force that acts along the water-solid contact line and the net force due to the pressure deficit in the water bridge with respect to the pore air pressure. In the funicular regime both water bridges and pores filled with water are present. Which means that both capillary forces due to the water bridges, and capillary forces due to regions filled with water, contribute to the total bonding force. Within the capillary regime, negative pore water pressure acts isotropically and contributes directly to total stress. The net tensile force in each of these regimes contributes to macroscopic tensile strength. The net tensile force also contributes to shear strength by increasing the normal forces among the soil particles and thus the frictional resistance of the bulk system.

A first look in to the previous studies on tensile strength of soils will prompt one to divide them in to two broad groups: theoretical models and experimental techniques. The theoretical models are either based on the shear strength of the soil or inter particle contact forces. Models based on the shear strength are quite simple and relatively empirical, whereas the models based on the inter-particle contact forces derive their originality substantiating their claim by comparing with the grain size distribution curves. In the coming

paragraphs the different theoretical models to determine the tensile strength of soils are presented. As far as experimental techniques they are either direct method determining the tensile strength or indirectly from triaxial or shear strength tests.

4.2.3.2 Indirect determination based on shear strength

One of the explanations given for the existence of the tensile strength in soil is due to the cohesion between particles, according to Lambe and Whitman [Lambe and Whitman, 1979] which may be of two kinds: the real cohesion (c'), produced by natural or artificial cementing between particles and apparent cohesion (c_{ap}), produced by the tension of capillary water in pores or suction (S). According to this model, the apparent cohesion is the product of the suction and the tangent of the angle of internal friction (ϕ')

$$c_{ap} = \mathrm{S} \tan \phi' \tag{4.1}$$

And the total cohesion (c) is the sum of real cohesion plus apparent cohesion and is given by:

$$c = c' + \mathrm{S} \tan \phi' \tag{4.2}$$

The apparent cohesion has been called so because its effect is reduced or lost when soil moisture is increased, for that reason to be on the safer side it is not taken in to account as a strength parameter in many geotechnical problems. In the Lambe and Whitman [Lambe and Whitman, 1979] formulation they did not show an explicit link between tensile strength and total cohesion and therefore do not have any expression of tensile strength in terms of suction.

In a Mohr diagram, like the one shown in figure 4.4 the tensile strength (σ_t) can be expressed in terms of real cohesion and the angle of internal friction (ϕ') as:

$$\sigma_t = -c' \cot \phi' \tag{4.3}$$

in this representation the tensile strength is the limit of possible values of normal stress in tension. However, according to Baker [BAKER, 1981] it does not reflect the real behaviour in the negative stress zone which is non linear and thus proposes to limit the magnitude of the tensile strength to a certain limiting value between zero and $-\cot \phi'$.

Fredlund et al [Fredlund et al., 1978] suggest that shear strength in a non-saturated soil can be expressed as:

$$\tau = -c' + (\sigma - u_a) \tan \phi' + (u_a - u_w) \tan \phi^b \tag{4.4}$$

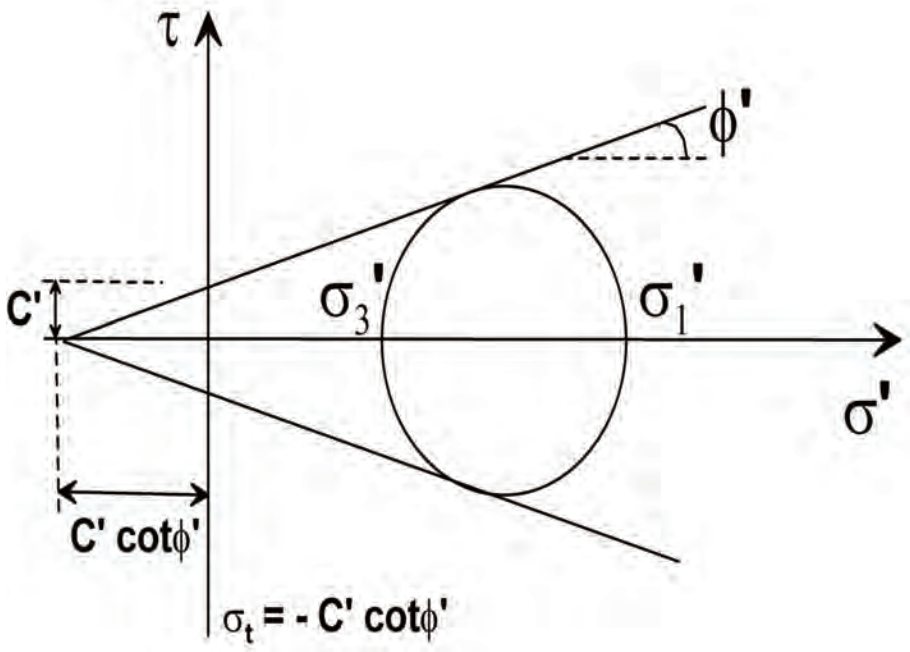

Figure 4.4: Mohr-Coulomb representation of tensile strength as a function of cohesion and angle of internal friction

where σ is the total stress, u_w is the pore water pressure, u_a is the pore air pressure, ϕ' describes the effect of increasing resistance due to the total pressure $(\sigma - u_a)$ and ϕ^b describes the increased resistance to the matrix suction $(u_a - u_w)$. The intercept of total cohesion (C) is defined as the sum of the effective cohesion and the component due to the suction:

$$C = c' + (u_a - u_w) \tan \phi^b \tag{4.5}$$

The term that makes the equations 4.4 and 4.5 different is the value of angle friction, since in the first case ϕ' is used while the second employs friction angle ϕ^b which takes into account that the suction tends to be less important in shear strength than the mechanical compression. Escario Saez [Escario and Sáez, 1986] show, from direct shear tests with suction control,ϕ^b is very close to $\phi'$for states close to saturation and is not constant but decreases with increasing suction, reaching a relatively constant value for very high suctions.

Based on theories by Baker [BAKER, 1981] and Morris et al [Morris et al., 1992] the common failure criteria in compression should be changed when it comes to tensile stresses. Because, the absolute value of the tensile strength σ_t is much smaller than that obtained from equation 4.3 and as shown in figure 4.5. They suggest considering $\sigma_t = -C/2$, where C is total cohesion. Additionally they indicate that to be conservative, in drying soils

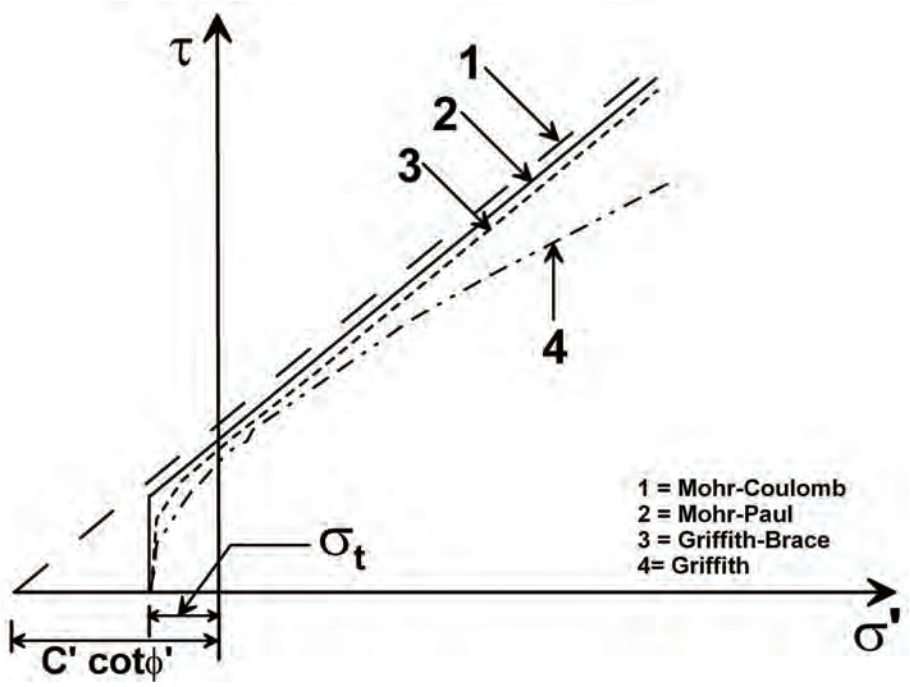

Figure 4.5: Tensile strength from shear strength envelops [Morris et al., 1992]

from very wet conditions, such as sludge/slurry, in the equation 4.5 a value of $c' = 0$ can be assumed, thus:

$$\sigma_t = -0.5(u_a - u_w) \tan \phi^b \tag{4.6}$$

In this case the tensile strength would be obtained from tests such as direct shear with suction control and therefore this is an indirect estimate.

Snyder and Miller [Snyder and Miller, 1985] presented a tensile strength model for unsaturated soils, considering two cases: (a) the soil is uniform without cavities or cracks and (b) the soil has irregularities. In the first case (figure 4.6a), a tensile failure in the soil occurs when tension is zero. To evaluate the tensile strength, equation expressed in effective stress proposed by Bishop [Bishop, 1960a] for unsaturated soils based on the theory of capillary cohesion is used:

$$\sigma' = \sigma - u_a + \chi(u_a - u_w) \tag{4.7}$$

where χ is a dimensionless parameter that depends on the degree of saturation of soil and other variables are the same as defined in equation 4.4. If one considers the air pressure as reference pressure, equal to zero and effective stress equal to zero, the tensile strength obtained in equation 4.7 is in terms of the total stress:

$$\sigma_t = u_w \chi \tag{4.8}$$

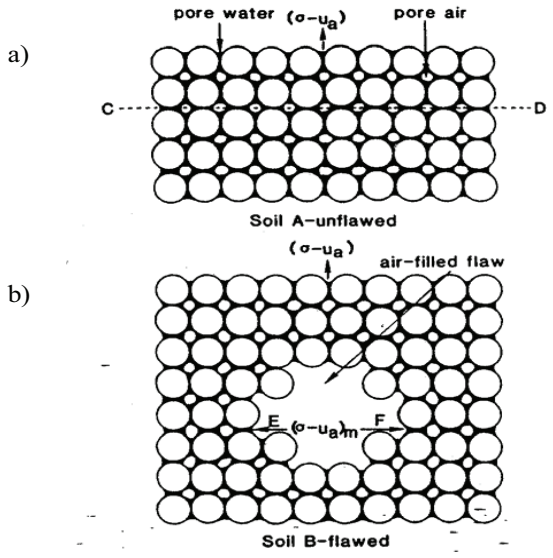

Figure 4.6: Capillary model of soil (a) UN-flawed and (b) flawed [Snyder and Miller, 1985]

In the case of saturated soils $\chi = 1$. Thus, according to this model, the tensile strength is equivalent to the suction. Snyder and Miller [Snyder and Miller, 1985] indicated that "for practical purposes, saturated soil behaves as if it were freely immersed in a water body subjected to tension". However, such an assertion only meets if the suction is zero, since in that case the tensile strength is also zero. But, if the soil is saturated and there is suction acting then in general tensile strength is much less than the suction.

The second case examined by Snyder and Miller [Snyder and Miller, 1985] was the soil with flaws or internal fissures (figure 4.6b), which were attributed to reduce tensile strength with respect to existing suction. This is an analysis that combines earlier formulation of capillary cohesion with fracture mechanics criteria. The main conclusions drawn from the analysis were: the tensile strength was reduced by half to that determined from the theory of capillary cohesion and the experimental results reported for unsaturated soils were well predicted by the model.

Towner [Towner, 1987a] believes that the tensile strength can be understood in the same way as a tensile test in triaxial apparatus, where the effect of confining cell pressure can be similar to the effect of suction. This similarity is valid and compatible with the capillary model and the concepts of apparent cohesion. However, the verifications made to justify the theory were indirect in nature, using the results of drained triaxial compression tests. The Cam Clay model was used with some behavioral assumptions which are difficult to verify.

Abu Hejleh and Znidarčić [Abu-Hejleh and Znidarčić, 1995] in a study of cracking in soils calculated the tensile strength using an exponential equation given for a China clay, based on the un-drained compression strength (s_u) and the voids ratio (e) as:

$$\sigma_t = F10^{1.945-e/0.453} \tag{4.9}$$

where F is a dimensionless factor representing the ratio between the tensile strength and the unconfined compressive strength ($F = \sigma_t/s_u$) and must be obtained independently or adopted from other studies. The value of F adopted in the work of Abu Hejleh and Znidarčić [Abu-Hejleh and Znidarčić, 1995] vary between 0 and 0.5.

The main drawback of the equation 4.9 is without knowing the value of suction it is not possible to determine the overall state of effective stresses. However, in terms of total stresses this kind of relationship between shear strength and tensile strength may be of practical importance because of the ease in conducting a compression test.

Another problem was found in the equation 4.9 which the authors do not specify the units in which it is expressed and assuming that this is kPa (which is a commonly used unit), the values of σ_t obtained are very close to zero.

Ayad et al [Ayad et al., 1997] determined tensile strength parameters of undisturbed clay. A hollow cylindrical sample in triaxial apparatus was used. The sample was initially consolidated isotropically and subsequently subjected to radial deformation by increasing internal pressure and maintaining the vertical and cell pressure constant. The pore pressure was measured in the middle of the sample, which allowed determining the time of failure due to strong pressure drop observed at that instant. Although this is an interesting method because it works in effective stresses. But, the measurements were not direct because the pore pressures was positive and the principal stresses would be the internal pressure on the sample acting parallel to the plane of failure and not perpendicular as in a simple tensile test.

4.2.3.3 Direct methods for determining tensile strength

Farrel et al [Farrell et al., 1967] conducted tensile strength tests on reconstituted soil samples, consisting of clay (12%), silt (17%), fine sand (50%) and gravel (20%). The tests were done with cylindrical samples that were glued (with Araldite) to the loading edges of a compression testing machine. The authors did tests with tensile load and axial compression, both in deformation controlled procedure. Additionally they did bending tests, with prismatic samples to identify tensile strength indirectly. Plot showing stress-strain at different humidity conditions, changes in the tensile strength with moisture (suction

deducted) and the comparison between the tensile strength and unconfined compression strength was determined.

Towner [Towner, 1987b] conducted measurements of tensile strength in samples of reconstituted Kaolin at different humidity. The equipment used for testing was a mold formed two pieces with rounded ends, attached to a dynamo-meter. The tensile load was applied manually until the specimen reached failure (figure 4.7).

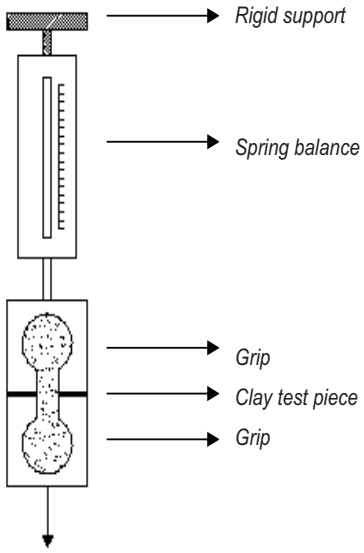

Figure 4.7: experimental setup for direct tensile strength determination [Towner, 1987b]

Tang and Graham [Tang and Graham, 2000] used a tensile strength test device for unsaturated soils as shown in figure 4.8. This device consists of a conventional motor-driven mechanical load frame for applying either compressive or tensile force to specimens at a constant displacement rate. The mold has two separate half-cylindrical forms that are welded to short lengths of channel and connected to the platen and cross-head of the load frame. The results reported correspond to three groups of samples of sand-bentonite, each of them was imposed with a different level of suction (4.0 MPa, 6.5 MPa and 10 MPa) through vapour balance technique. The most important observation was the values of tensile strength were much lower than the overall average suction in the sample, the values of ratio of tensile strength to suction (σ_t/S) varied between 6% (S = 4 MPa) and 3% (S = 10 MPa).

Munkholm et al [Munkholm et al., 2002] used a direct tension test that consists of an automatically operated mechanical press. This device is a two-piece cylinder, where the lower half is fixed in a rigid frame by three screws horizontally driven against the wall of

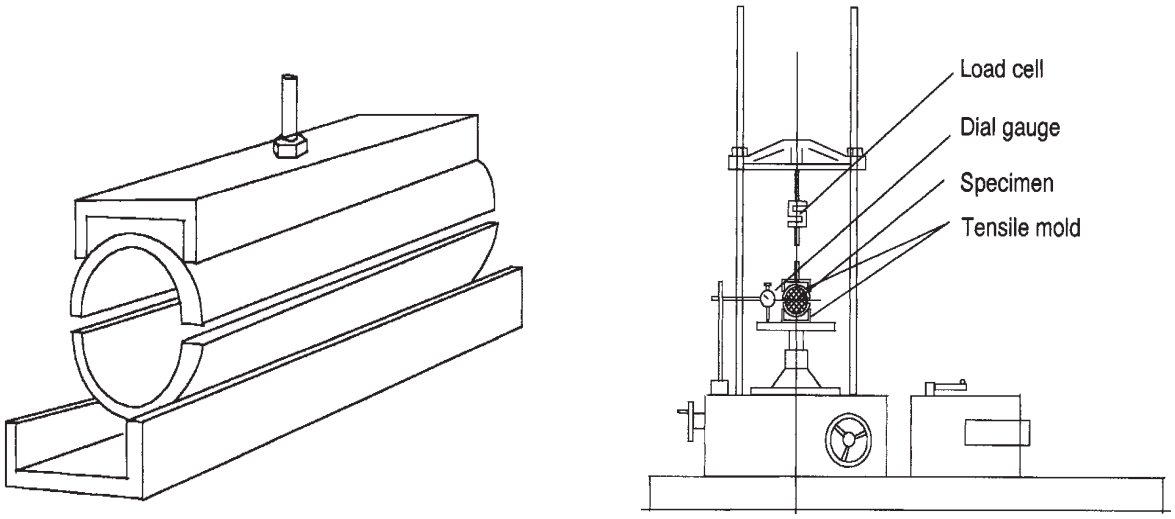

Figure 4.8: Schematics of equipment used by [Tang and Graham, 2000]Left:Mould Right: Loading device

the cylinder. A plastic cap was put in the upper half of the cylinder and is connected to a pressure transducer by an adjustable steel bar.

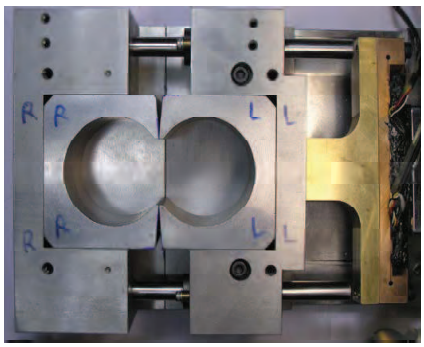

Figure 4.9: experimental setup for direct tensile strength determination [Tamrakar et al., 2005]

Tamrakar et al [Tamrakar et al., 2005] developed an equipment (figure 4.9) that can measure the tensile strength of compacted and saturated soil by a simple and rapid procedure. They conducted experiments with samples of loam, sandy clay, silt, and saturated consolidated clay. The apparatus consists of a horizontal platform with a fixed box and other mobile. Within these boxes, the mold consists of two separate structures in the form of "C"whose internal circular shape, except the portion where they join. Between the mobile box and motor a load cell is placed, which measures the tensile load. The loam samples were tested at dry densities of 0.66, 0.68 and 0.70 g/cm^3, and the maximum tensile strength is obtained for moisture content of between 50 and 60%. Another conclusion from the study was higher the dry density higher is the tensile strength, which was more

pronounced on the drier side than on the wetter side.

Figure 4.10 shows a direct tension device developed by Mikulitsch and Gudehus [Mikulitsch and Gudehus, 1995] that is similar to the one developed by Perkins (1991). The specimen was kept in place by angled walls where one part of the box was fixed and the other part rested on a ball bearing system. The angled internal walls facilitate contact between the specimen and the box to develop tension across the center plane. Tensile forces were imposed by filling a bucket hanging from the movable half of the box with water.

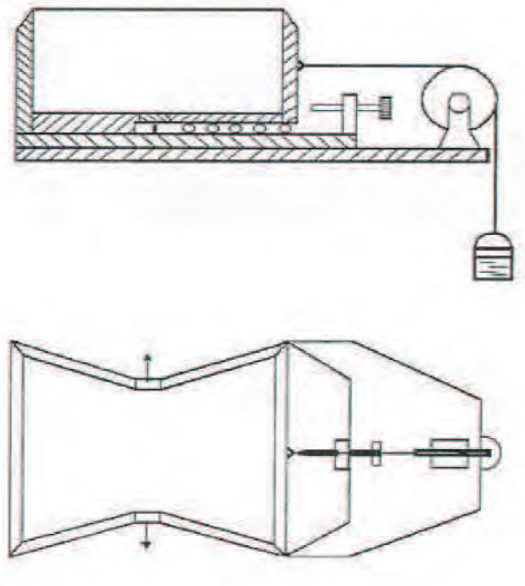

Figure 4.10: Tensile strength determination equipment by Mikulitsch and Gudehus [Mikulitsch and Gudehus, 1995]

Kim and Hwang [Kim and Hwang, 2003] developed the direct tension apparatus shown in figure 4.11. The sample container consists of a 17.8 cm × 17.8 cm × 17.8 cm box split in two equal halves. The movable front half is mounted on two sets of precision roller bearings attached to the bottom of the device. The rear half rests on two aluminium blocks to position it at the same height as the front part. Four wedges are attached inside the box to facilitate contact between the specimen and the box as tensile stresses develop across the plane of separation. The wedges were designed with angles (20°) larger than the dilatancy angle of the material to prevent movement of the soil particles, and to achieve a relatively uniform stress distribution on the failure plane. The device rests on a loading table with two pulleys installed to connect loading wires to the movable half of the box. The rear loading container attached to the movable half is used to initially balance the system against the front loading bucket. Tensile load is applied by introducing water into the front loading container.

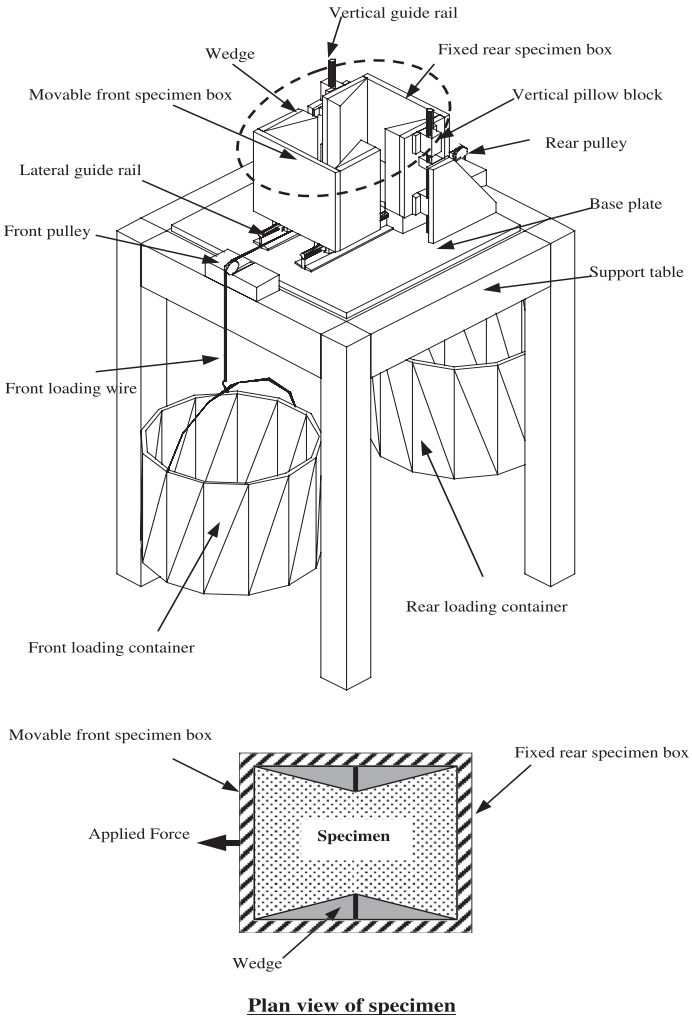

Figure 4.11: Tensile strength determination equipment by Kim and Hwang [Kim and Hwang, 2003]

Lu et.al. [Lu et al., 2007] developed a tensile strength apparatus for cohesion less soils shown in figure 4.12. The apparatus consists of a specimen confining tube (split in the middle), mounting plate, adjustable table for inclining the specimen tube, and a digital probe for measuring inclination angle. The specimen tube has two sections that are clamped together during sample preparation and released prior to testing. One section is fixed on the table, and the other part is free to slide on roller bearings. The table is inclined progressively to increase the gravity force along the longitudinal direction of the sample, thus applying a tensile force. The inclination angle is recorded when the sample fails and used to back-calculate tensile strength from the mass of the movable section.

Heibrock et al [Heibrock et al., 2003] determined tensile strength of medium plastic clay (Kaolin clay with 61% clay and 39% silt. LL = 44.4%, PL = 28.1% and SL = 25%). The set-up used is as shown in the figure 4.13. The tests were conducted for the full

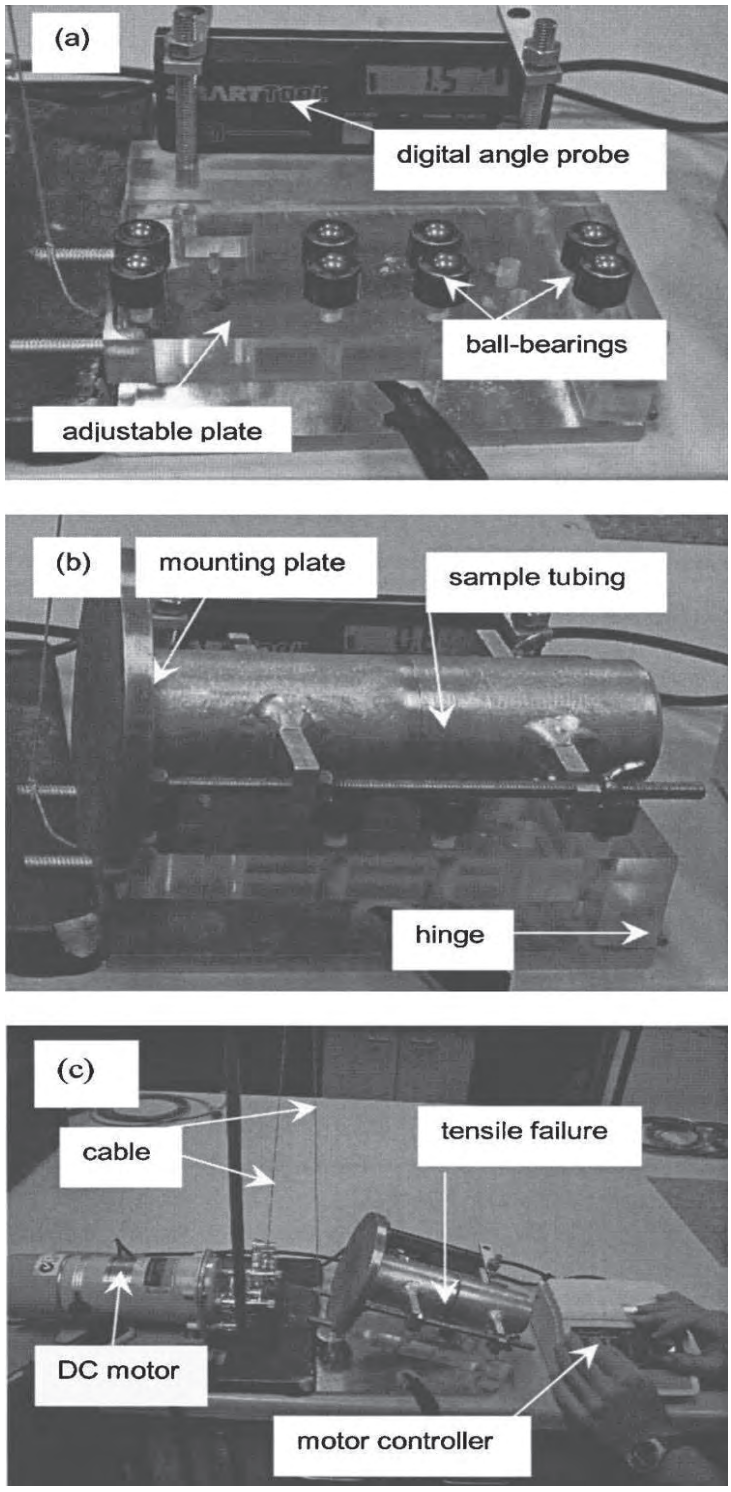

Figure 4.12: Photographic illustration of a simple direct tensile strength apparatus: (a) without sample tubing and mounting plate; (b) with sample tubing and mounting plate; and (c) connected to adjustable rate DC motor for sample tilting [Lu et al., 2007]

range of degree of saturation of the soil. The tensile strength initially increased as the degree of saturation decreased reaching a peak value, further decrease in the degree of saturation of the tested specimens resulted in the decrease of the tensile strength reaching a minimum values comparable with the one on the wet-side. Theoretical explanation was given for this type of behaviour with a single peak by two approaches, one based on the pores size distribution from MIP tests and second by the theory of contact forces between the particles based on the work of: Schubert et al [Schubert et al., 1975], Schubert [Schubert, 1982], and Molenkamp and Nazemi [Molenkamp and Nazemi, 2003]. The model predictions represented well the observed experimental behaviour.

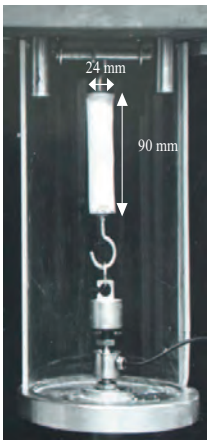

Figure 4.13: Experimental setup for direct tensile strength determination [Heibrock et al., 2003]

Finally, table 4.1 shows the variation of tensile strength depending on the type of test method used. Considering the tensile strength from Ring test to be a unitary reference value and normalizing tensile strength values from rest of the other methods. The direct-pull (dog bone) method seems to give a tensile strength 4.5 times more than the from the Ring test. This table highlights the discrepancy one can expect in the tensile strength data depending on the test method. Also, care should be taken while comparing the data obtained from different experimental techniques.

Table 4.1: Variation of tensile strength with test method [Harison et al., 1994]

Test method	Specimen dimensions (mm)	$V_{95}(mm^3)$	Strength ratio
Ring test	$R_\circ/R_i = 8; R_\circ = 50, and\ t = 25$	8.29	1
Three-point bending	$200 \times 50 \times 25$; $100 \times 50 \times 25$	156; 78.1	1.78; 1.56
Four-point bending	$200 \times 50 \times 25$	2187	3.00
Brazilian test	$R_\circ = 50, and\ t = 25$	10596	4.10
Direct-pull dog bone	$d = 25;\ L = 35$	17181	4.50

4.2.4 Equipment used and its background

Tensile strength was determined using an equipment designed by Rodríguez [Rodríguez, 2002], which is similar to the one explained in [Mikulitsch and Gudehus, 1995]. The equipment is made up of 3 main parts (see figure 4.14). Two pieces of trapezoidal shape, one fixed and another movable freely up on application of external force. The central removable part is removed just before the application of the load, this is the only part of the specimen which will be subjected to tension during the test. Figure 4.15 show the laboratory set-up.

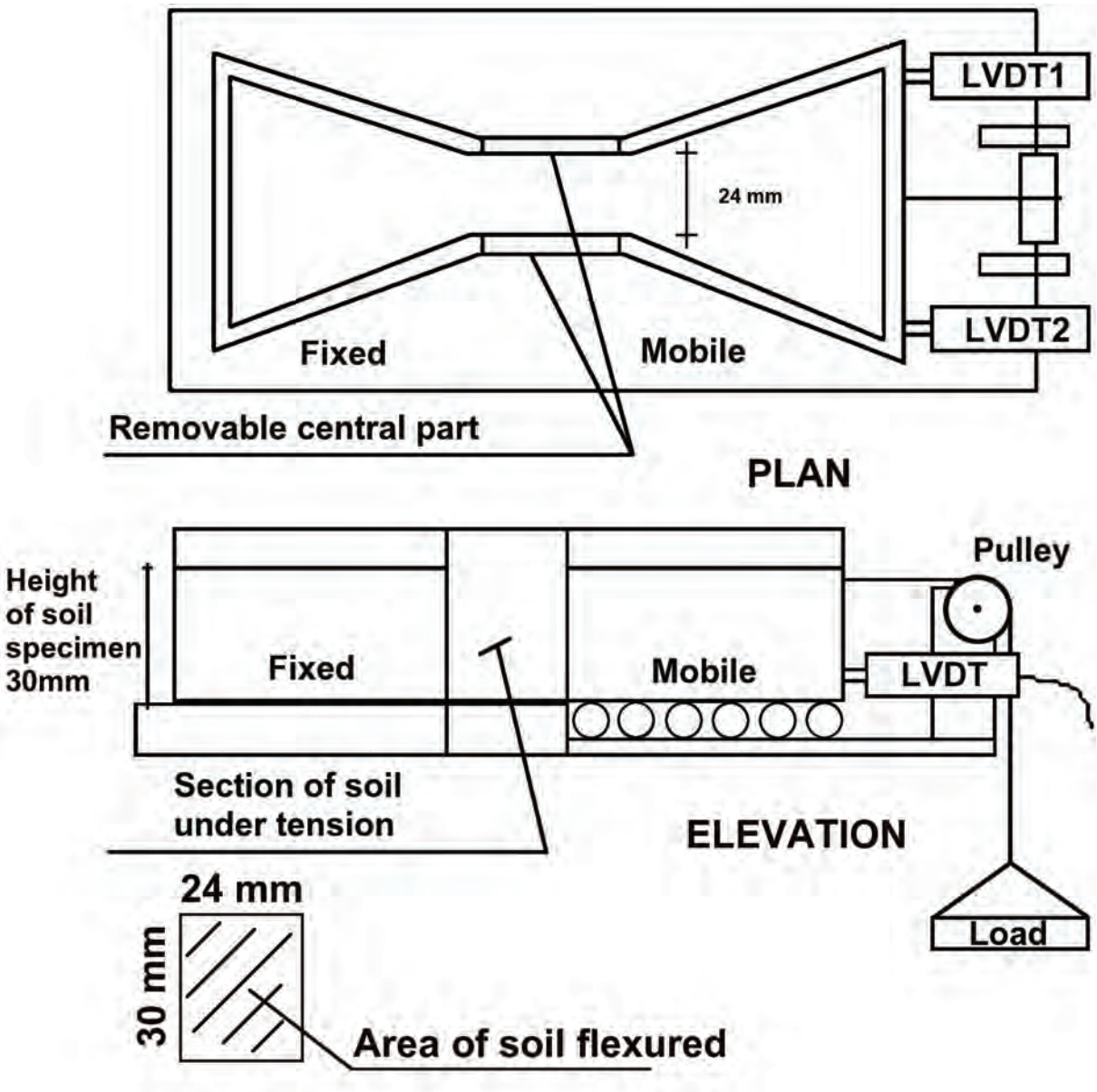

Figure 4.14: Schematic diagram of direct tensile strength equipment

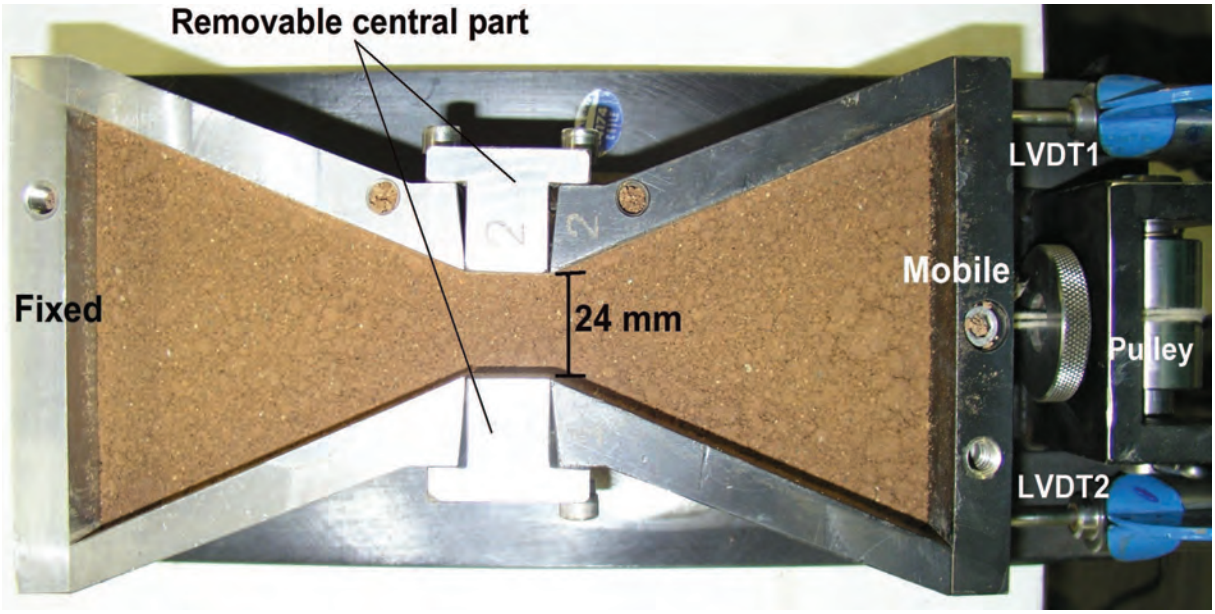

Figure 4.15: Laboratory set-up of direct tensile strength equipment

4.2.5 Experimental program and objectives

As mentioned in the introduction to this section, two campaigns of experiments were carried out. The first campaign consisted in conducting tests with two different constant natural density and varying moisture content, starting with 12% up to 30%, (i.e. 12%, 13.5%, optimum moisture, 16%, 18%, 20%, 22%, 24%, 26%, and 30%). It was decided to start with a moisture content of 12%, below the optimum moisture and gradually increase the moisture up to the liquid limit. For each moisture content and natural density tests were repeated at least twice and in some cases thrice, thus accounting for the repeatability of the tests. Natural densities were 16 kN/m^3 and 19 kN/m^3, chosen from the compaction curves. Table 4.2 gives the summary of the tests conducted for each moisture and natural density of the first campaign.

During the second campaign instead of working with natural density the specimens were prepared with two different dry densities (14 kN/m^3 and 16 kN/m^3) with different moisture contents (11%, 13%, 15%, 17%, 19%, 21%, 23%, 25%, 27%, and 29%). Table 4.3 gives the details of this campaign. Of course it is more realistic to prepare all the samples with the same initial condition and then allowing them to dry and during the process conduct test to find the tensile strength. Due to restrictions with experimental equipments this could not be done and instead the specimens were prepared at different moisture contents.

During drying the soil undergoes very large moisture changes, which induce phase change in the soil structure and change of state from a slurry state with free water to plastic

and finally reaching almost solid state. The objective was to follow how these changes affect the tensile strength of the soil. Another important factor defining the experimental program was to obtain experimental information for a large range of variation of the degree of saturation. The models and theories based on the available experimental data do not account for the full moisture range of the soil. Also, the main focus in most of the studies was crack initiation without dealing with the propagation and formation of secondary and tertiary cracks. It is known that though crack initiation happens when the soil is still saturated or quasi saturated, crack propagation can continue with moistures neas the soil's plastic limit. Most of the tensile strength theories and models fail to address this. Considering all the above factors, the main objective is to give a full picture of the effect of moisture and density.

4.2.6 Sample preparation and experimental procedure

Experiments were conducted in a laboratory with controlled temperature and humidity. The soil was first sieved with sieve number 16 (aperture opening 1.18mm), the sieved soil was left at laboratory conditions for moisture stabilization. The specimens were prepared at the specified moisture content by adding distilled water. The weight of soil and water to be mixed was calculated for each density and predetermined moisture content. Just after the mixing the moisture content was determined and the mixture was left in a humid chamber for 24 hours before testing. At the end of the test the moisture content was determined again.

The specimens were prepared in the equipment by compacting in 3 layers. The area of the mould known, the height of the specimen was fixed at 3 cm, thus fixing the volume of the specimen. To ensure uniform and constant density the mass of soil and water in the mixture was monitored for each trial, moisture content, depending on constant natural or dry densities of the specimens. A leveler was used to check the surface. Thus making sure the correct density was achieved.

As mentioned earlier the specimens were prepared in three layers, for a better distribution and uniformity. Specimens with low water contents were a bit harder to compact to the required densities, where as specimens with high water content it was easier, in the case of very high moisture contents very little compaction was necessary.

Once the specimens were prepared with leveling and density controlled, two electronic strain gauges (LVDT) were installed as shown in the figure 4.14 and 4.15. The load was applied manually. A loading pan was connected to the movable part of the equipment

(figure 4.14 and 4.15). The load application was done with extreem care. Standard weights ranging from 2 grams to 20 grams (specifically, 2g, 4g, 5g, 10g and 20g and several of them) were arranged next to the loading pan sequentially. A dummy test was done for each moisture content and density as a starting point to know approximately the loading sequence. Higher weights were placed during the initial loading following the lower ones towards the failure. Weights were placed into the loading pan with lot of care and with a constant frequency. The procedure was repeated for all the specimens.

Figures 4.16 and 4.17 shows some of the photographs taken during the tests, the captions of the figures explain the details of each one of them.

4.2.7 Results

4.2.7.1 Tests with constant natural density

Two series of tests were done during the first campaign, each with constant natural densities ($\gamma_N = 16KN/m^3$ and $\gamma_N = 19KN/m^3$). The results of the two series are presented in table 4.2. The results presented are average values, as indicated some are average of two trials and others of three. Figure 4.18 and 4.19 shows the load-deformation curves for the two natural densities at different moisture contents. The load-deformation curves corresponds to the moisture contents shown in the table 4.2. Figures 4.18a and 4.19a shows for all the moisture range tested. The figures 4.18b, and 4.19b corresponds to the moisture range 12% to 20% and figures 4.18c and 4.19c to the moisture range 22% to 30%. To reiterate the soil response to the tensile load on wet and dry condtions the load-deformation curves were shown separately for specimens at drier and wetter sides.

The load deformation curves qualitatively show the effect changing soil phase on tensile load. The curves corresponding to 30% moisture content show relatively large deformation since the beginning of the loading and fail at lowest load for the series. The slope of the curves gradually increase with decrease in moisture content, as can be seen for the curves for 26%, 24%, and 22%. On the other hand the curves for moisture contents from 12% to 20% show a rigid failure.

Ávila [Ávila, 2004] conducted tests to determine tensile strength of Bogot clay with saturated samples, with varying suction. Interestingly he observed a similar behaviour. A rigid failure or steep sloped load deformation curves for high suction (180kPa, note that the AEV of Bogat clay is 1000kPa) and flat slope for a specimen with a lower suction value (37 kPa).

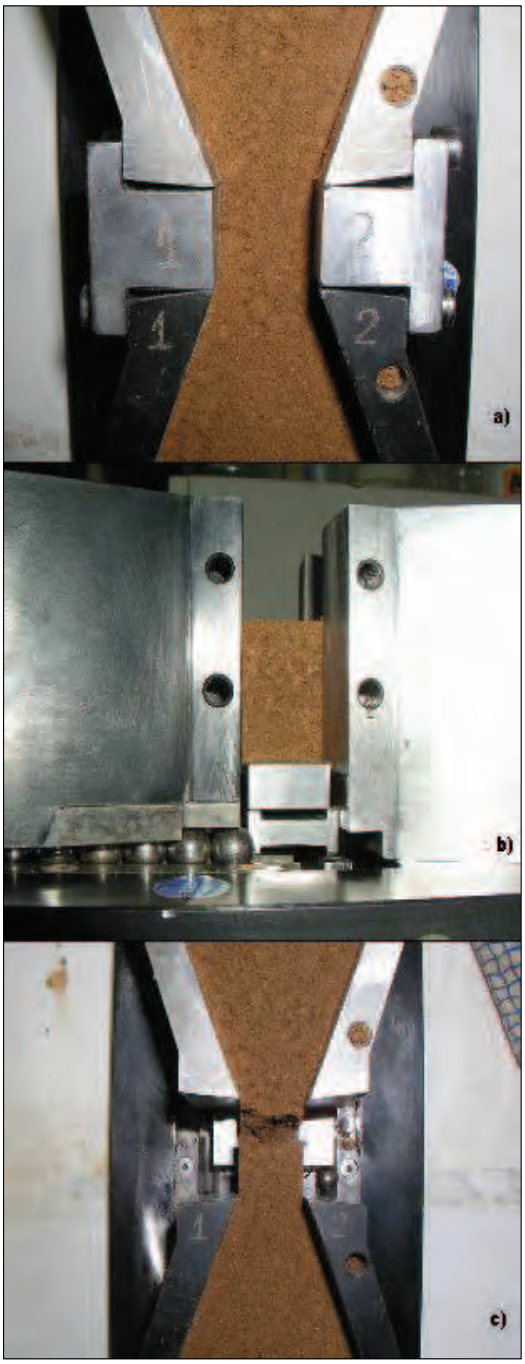

Figure 4.16: Test with constant natural density with moisture content of 12%; (a) plan view of the specimen just before the loading, (b) view from the side, and (c) plan view after failure

Figure 4.17: Test with constant natural density with moisture content of 30%; (a) plan view of the specimen just after the loading, (b) Zoom of the central part, and (c) side view after failure

From different load deformation curves it was observed that at the beginning of each test deformations were very small, hardly significant despite the increment in applied load. This may be because at the beginning of the test on the sample there are two mechanisms acting opposite, on the one hand we have the tensile stresses due to the applied load which tends to extend the sample, and on the other hand suction acting on soil which acts as a contracting force, therefore the material exhibits a rigid behavior trying to keep a balance. This anology can be true for a saturated soil and with varying suction (for example the tests done by Ávila [Ávila, 2004]). In the present investigation, the specimens were tested at various degrees of saturation. The resistance offered by the specimen may be attributed to the capillary forces or capillary bridges for the specimens with degree of saturation 1 or near to 1, whereas for other specimens with degree of saturation less than 1 the resistance is offered by the bonding due to compaction and as well due to some un-broken capillary bridges.

Figure 4.20a,b show the relation between the tensile strength and moisture content for the two natural densities, these graphs were drawn from the average values reported in table 4.2. Figure 4.20c show the variation of tensile strength with moisture content with data from all the trials. Figure 4.20d shows the variation of tensile strength with degree of saturation.

The important observations form these plots can be summarized as: (i) tensile strength reached a peak at a mositure content of 22% (figures 4.20a and b), (ii) tensile strength increased with increasing density (figure 4.20c), but the soil response seems to be similar at wetter side (moisture contents higher than 24%) irrespective of the natural density. The polynomial fit seems to represent well the experimental data (iii) in figure 4.20d, a shift in the tensile strength curve for the higher densitiy, showing the effect of density on degree of saturation, which was masked in figure 4.20c. This behaviour can be compared to a similar trend observed in compaction curves.

Note that the ploynomial fits in figures 4.20 a to d were only to give an idea of the trend of the experimental data, and not to be taken as the final conclusion of the soil's response to moisture change. A detailed analysis is made further in the chapter.

4.2.7.2 Tests with constant dry density

In the second campaign two series of tests were done each with a different dry density. Table 4.3 shows the results of these two series and the values shown are average of two trials and others of three, as indicated. Figures 4.21 and 4.22 shows the load-deformation for the two dry densities at different moisture contents (see table 4.3). Figures 4.21a and

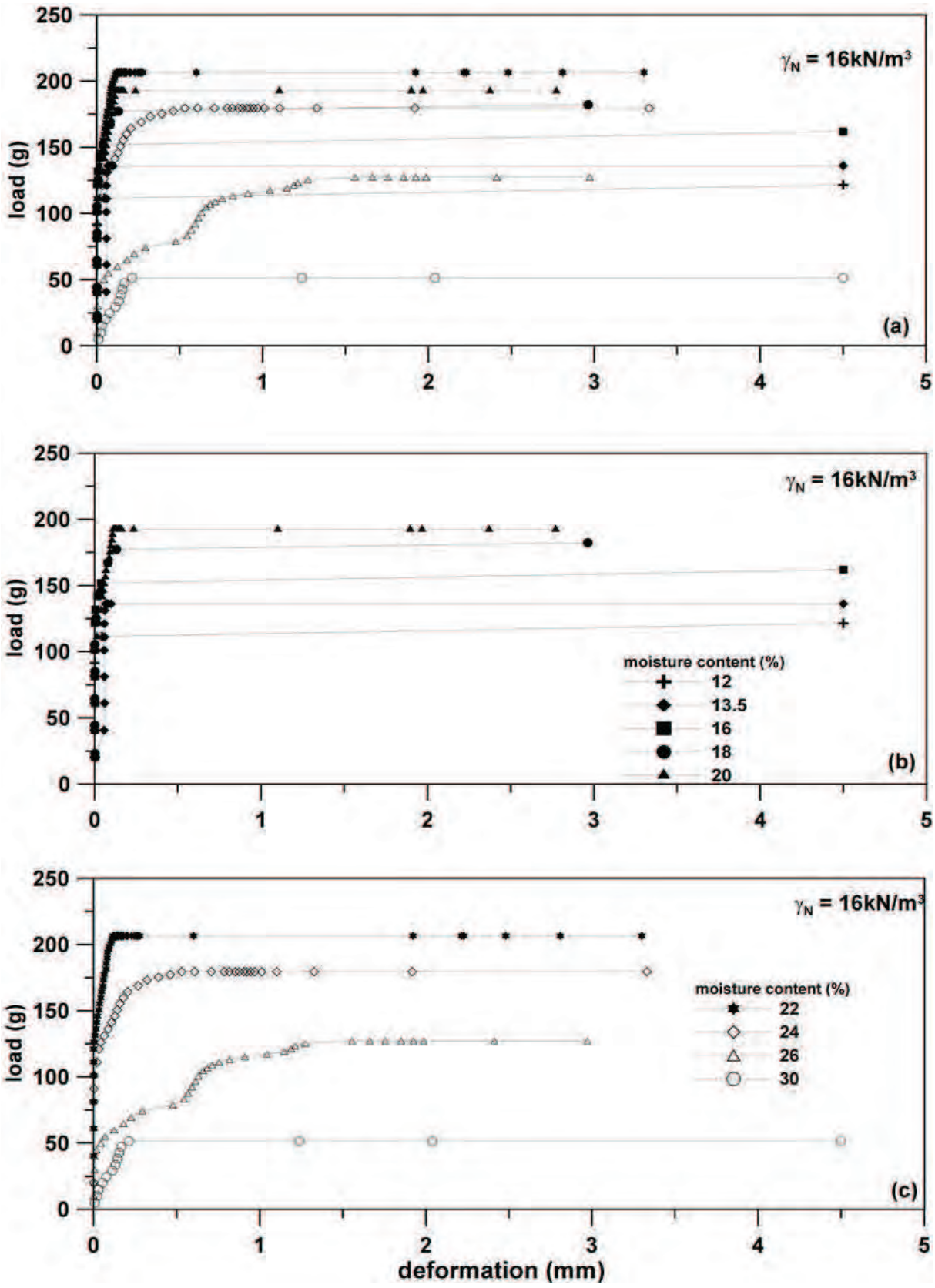

Figure 4.18: Load deformation curves for tests with $\gamma_N = 16kN/m^3$

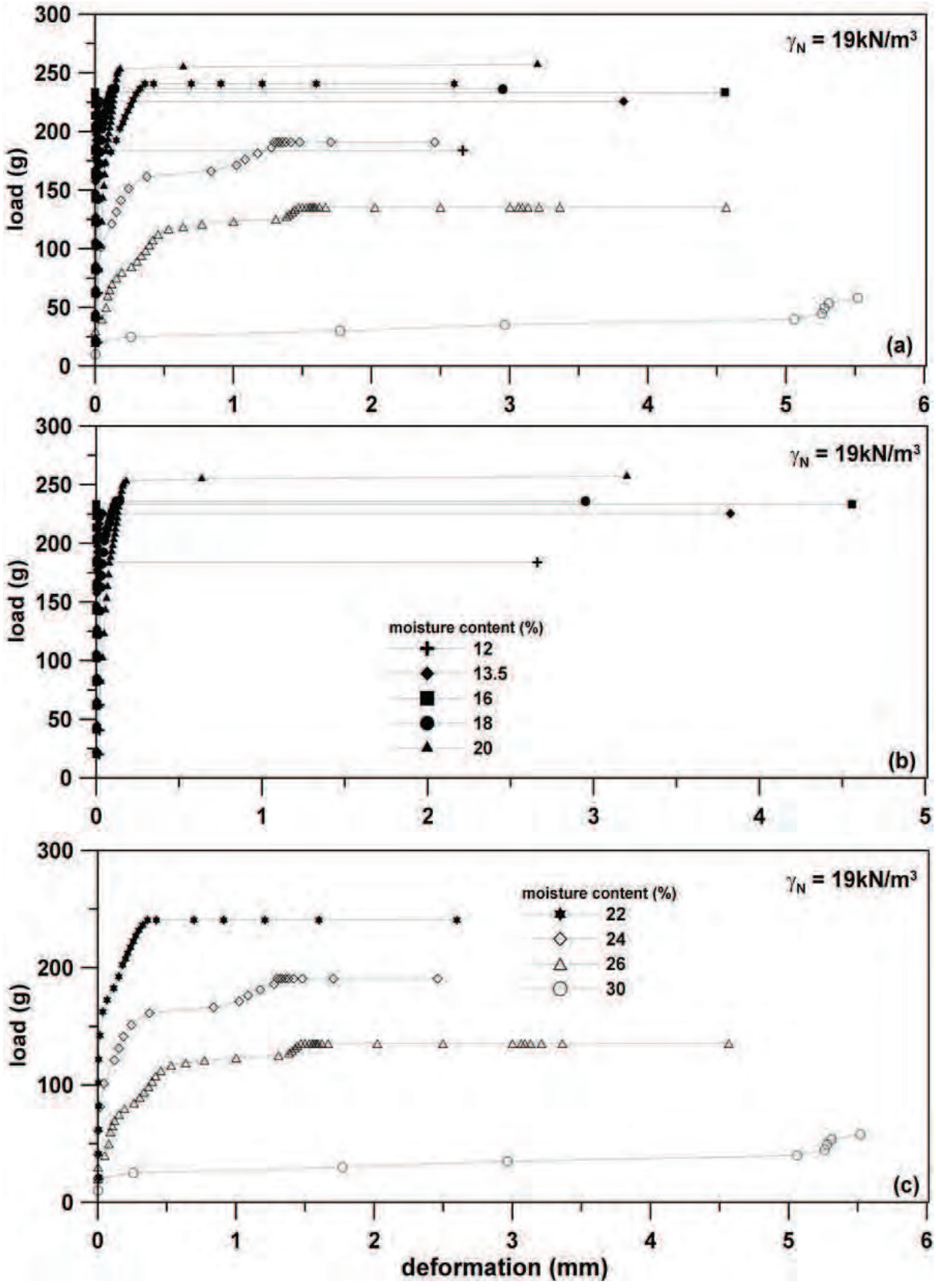

Figure 4.19: Load deformation curves for tests with $\gamma_N = 19kN/m^3$

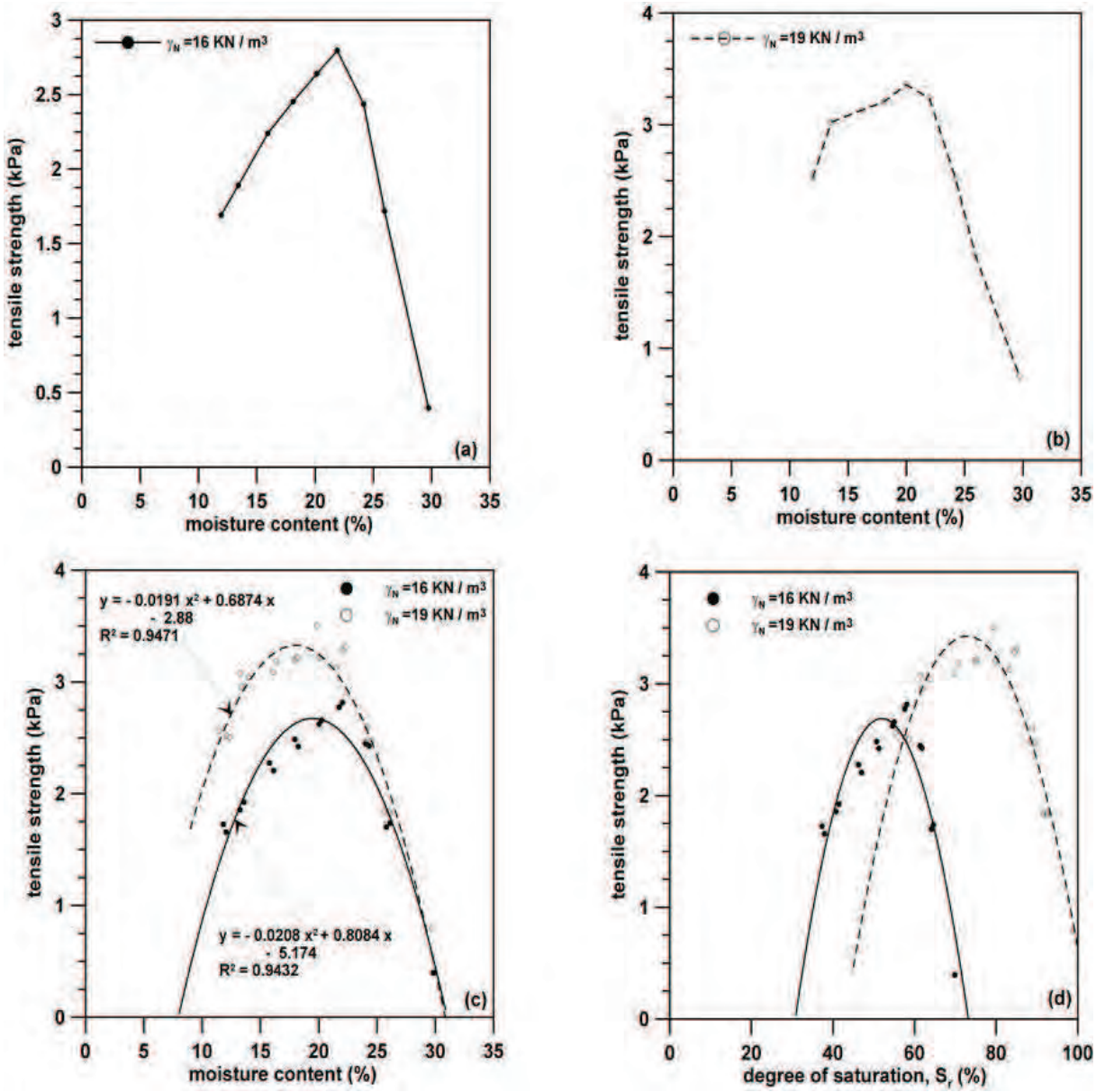

Figure 4.20: Details of tensile strength with constant natural density, (a) and (b) tensile strenth with moisture content (average values) (c) tensile strength with mositure content (all trials included) with ploynomial fit showing the trend (d) tensile strength with degree of saturation (all trails included)

Table 4.2: Details of direct tensile strength tests with constant γ_N

Test#	moisture content before the test $w_i(\%)$	moisture content after the test $w_f(\%)$	average moisture content $w_{ave}(\%)$	maximum load Q_{max} (N)	tensile strength σ_t (kPa)
		$\gamma_N = 16KN/m^3$			
1	12.33	11.56	11.94	1.22	1.69
2	13.64	13.20	13.42	1.36	1.89
3	16.40	15.50	15.95	1.61	2.24
4	18.43	17.79	18.11	1.76	2.45
5	20.48	19.83	20.16	1.90	2.64
6	22.15	21.64	21.90	2.01	2.79
7	24.65	23.69	24.12	1.75	2.43
8	26.30	25.63	25.96	1.24	1.72
9	30.14	29.34	29.74	0.28	0.40
		$\gamma_N = 19KN/m^3$			
10*	12.34	11.60	11.97	1.82	2.53
11*	13.99	13.11	13.55	2.17	3.02
12*	16.47	15.98	16.23	2.26	3.13
13	18.23	17.87	18.07	2.31	3.20
14	20.37	19.58	19.97	2.42	3.36
15*	22.10	21.82	21.96	2.33	3.24
16*	24.50	23.97	24.24	1.80	2.51
17*	26.36	25.46	25.91	1.32	1.83
18*	29.97	29.43	29.70	0.54	0.75

*Average of 3 trials; rest, average of 2 trials

4.22a show the load-deformation curves for all the moisture range tested. The figures 4.21b, and 4.22b for the moisture range 11% to 19% and figures 4.21c and 4.22c for the moisture range 21% to 29%. Once again this distinction is made to show the change in soil response to the tensile load at different moisture contents.

As in the first series of tests with constant natural density, here also the load deformation curves qualitatively show the soil phase change. The curves corresponding to 29% moisture content show relatively large deformation since the beginning of the loading and fail at lowest load for the series. The slope of the curves gradually increase with decrease in moisture content, as can be seen for the curves corresponding to a moisture content of 27%, 25%, 23% and 21%. On the other hand the curves for moisture contents from 11%

Table 4.3: Details of direct tensile strength tests with constant γ_D

Test#	moisture content before the test $w_i(\%)$	moisture content after the test $w_f(\%)$	average moisture content $w_{ave}(\%)$	maximum load Q_{max} (N)	tensile strength σ_t (kPa)
			$\gamma_D = 14KN/m^3$		
1^4	11.50	11.50	11.50	0.61	0.84
2^4	13.30	14.30	13.80	1.85	2.57
3^3	15.60	15.70	15.65	2.90	4.02
4^2	17.50	16.60	17.10	2.94	4.07
5^3	19.20	19.80	19.50	3.11	4.32
6^4	21.30	20.60	21.00	4.63	6.43
7^2	23.40	23.70	23.60	2.44	3.38
8^3	25.70	24.20	25.00	2.67	3.71
9^2	27.50	26.80	27.20	2.64	3.66
10^2	29.60	29.50	29.55	1.94	2.69
			$\gamma_D = 16KN/m^3$		
11^4	11.50	11.70	11.60	2.90	4.07
12^3	13.20	13.50	13.40	4.70	6.50
13^3	15.70	14.60	15.20	4.35	6.05
14^3	17.00	17.30	17.20	5.54	7.70
15^3	19.80	18.60	19.20	3.98	5.53
16^2	21.60	20.50	21.10	2.90	4.03
17^3	23.20	24.00	23.60	2.92	4.06
18^3	25.40	24.70	25.10	2.51	3.49
19^2	27.50	26.70	27.10	2.55	3.54
20^1	28.80	27.80	28.30	1.74	2.41

^{4,3,2} indicate the numebr of trials

to 19% show a rigid failure.

Similar observation can be made from the load deformation curves (figures 4.21 and 4.22) for the tests with constant natural density.

Figure 4.23a and b show the relation between the tensile strength and moisture content for the two dry densities, these graphs were drawn from the average values reported in table 4.3. Figure 4.23c show the variation of tensile strength with moisture content considering data from all the trials. Figure 4.23d shows the variation of tensile strength with degree

of saturation.

Much of the observation made in earlier series with constant natural densities were also observed here, nevertheless, the important observations form these plots can be summarized as: (i) a clear peak in tensile strength was not observed (figures 4.23a and b) as observed in first series of tests with constant natural densities, though the trend is similar (ii) from figure 4.23c shows that the tensile strength increases with increasing dry density. The soil response seems to be similar at higher moisture contents (more than 24%, wetter side) irrespective of the dry density. The polynomial fit seems to represent well the trend (iii) in figure 4.23d, the efffect of density on the tensile strength is shown, the curve for the higher dry density shift to the left showing the effect on degree of saturation as well.

Following the same lines as earlier, the ploynomial fits drawn in Figures 4.23 a to d are only to give an idea of the trend of the experimental data.

4.2.8 Tensile strength as a function of degree of saturation and suction

There is no doubt about the dependence of tensile strength of soils on prevailing suction in the soil matrix. Suction in turn depends on two important parameters: moisture content and the grain size distribution of the soil. Experimental evidences have shown that soil can experience suction when still saturated. This infers the significant role that is played by suction which can be compared to the confining pressure in a triaxial shear test. In agreement to the Mohr-Coulomb theory, the soil offers a greater resistance to shear at greater effective confining stress. Towner [Towner, 1987a] on basis of this theory suggested that a triaxial extension test can be considered as a direct tensile strength determination test, however in saturated conditions. This gives the advantage of applying the existing conventional soil mechanics theory. Several researchers have tried to give equations in terms of total and effective stresses according to their model of tensile strength as a crack initiation criterion.

The state of the art section in this chapter explains some of the theories to calculate tensile strength. However most of them fail to reproduce the observed experimental behaviour reported in this work. As a starting point, figure 4.24 shows a compilation of experimental data from the literature. In all the cases a well defined peak in tensile strength can be observed, especially in figure 4.24e, where the tensile strength and suction in the Y-axis is plotted against moisture content in the X-axis, which clearly shows that although suction keeps increasing with decrease in moisture content, the tensile strength decreases after

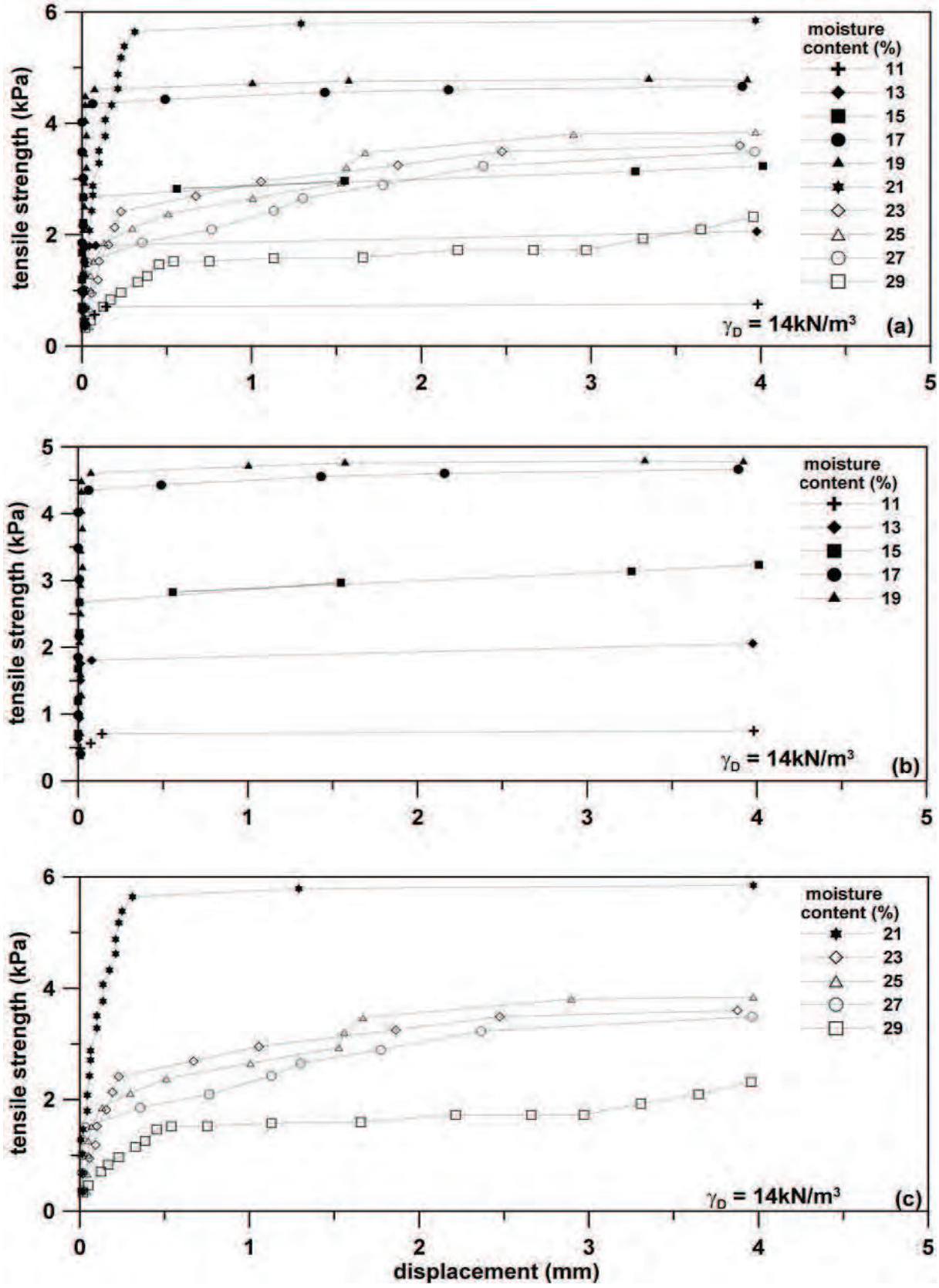

Figure 4.21: Load deformation curves for tests with $\gamma_D = 14kN/m^3$

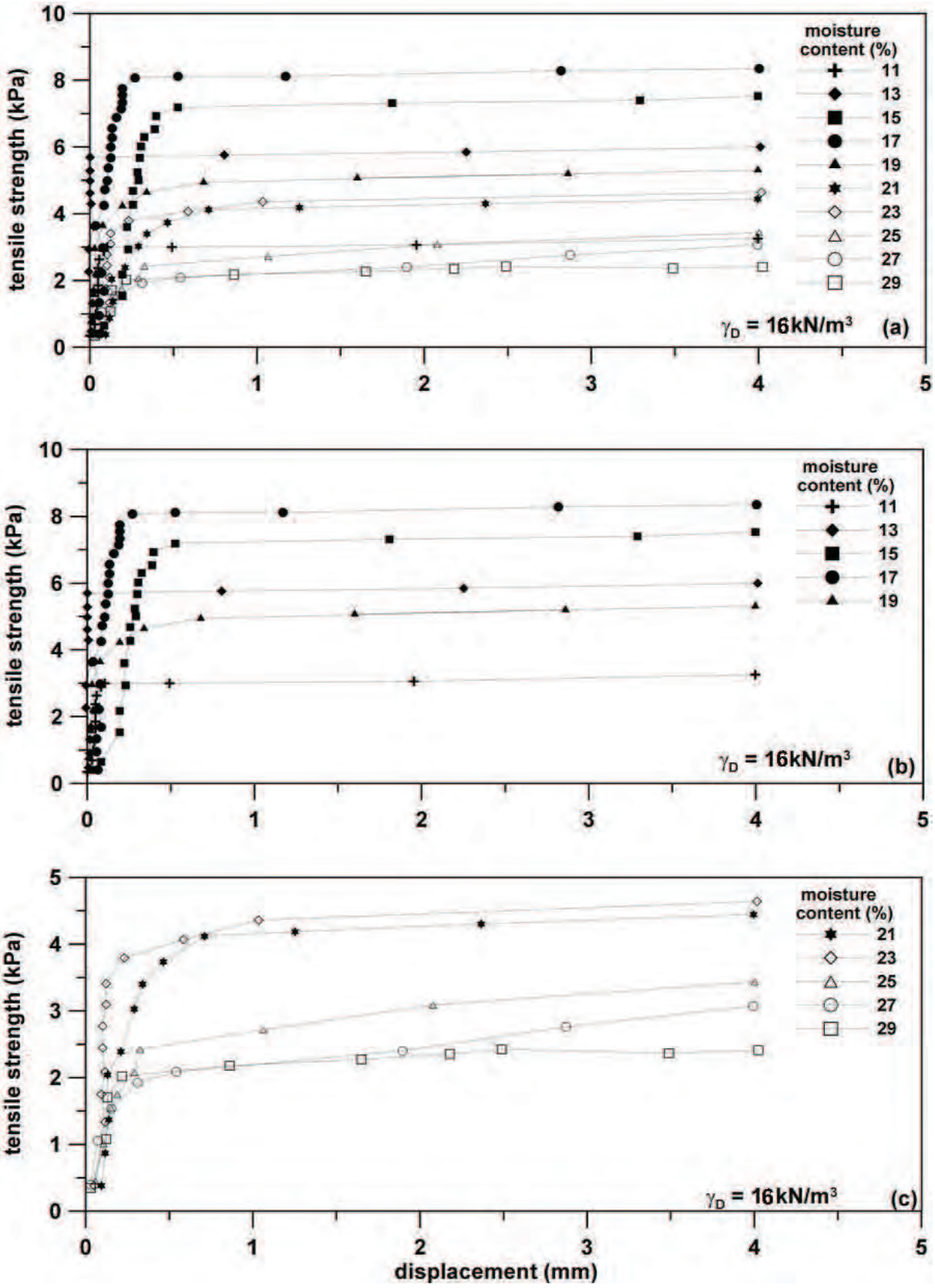

Figure 4.22: Load deformation curves for tests with $\gamma_D = 16kN/m^3$

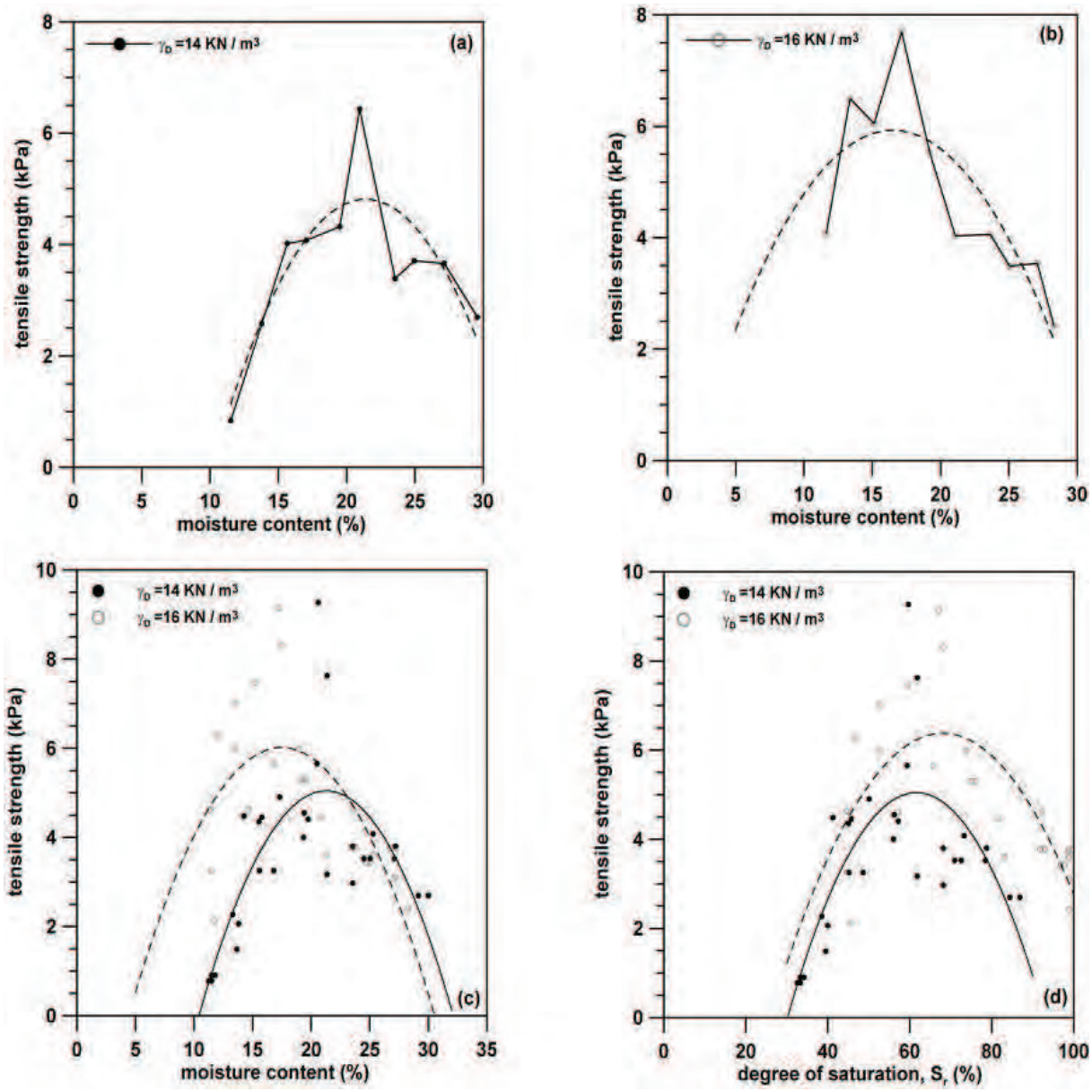

Figure 4.23: Details of tensile strength with constant dry density, (a) and (b) tensile strenth with moisture content (average values) (c) tensile strength with mositure content (all trials included) with ploynomial fit showing the trend (d) tensile strength with degree of saturation (all trails included)

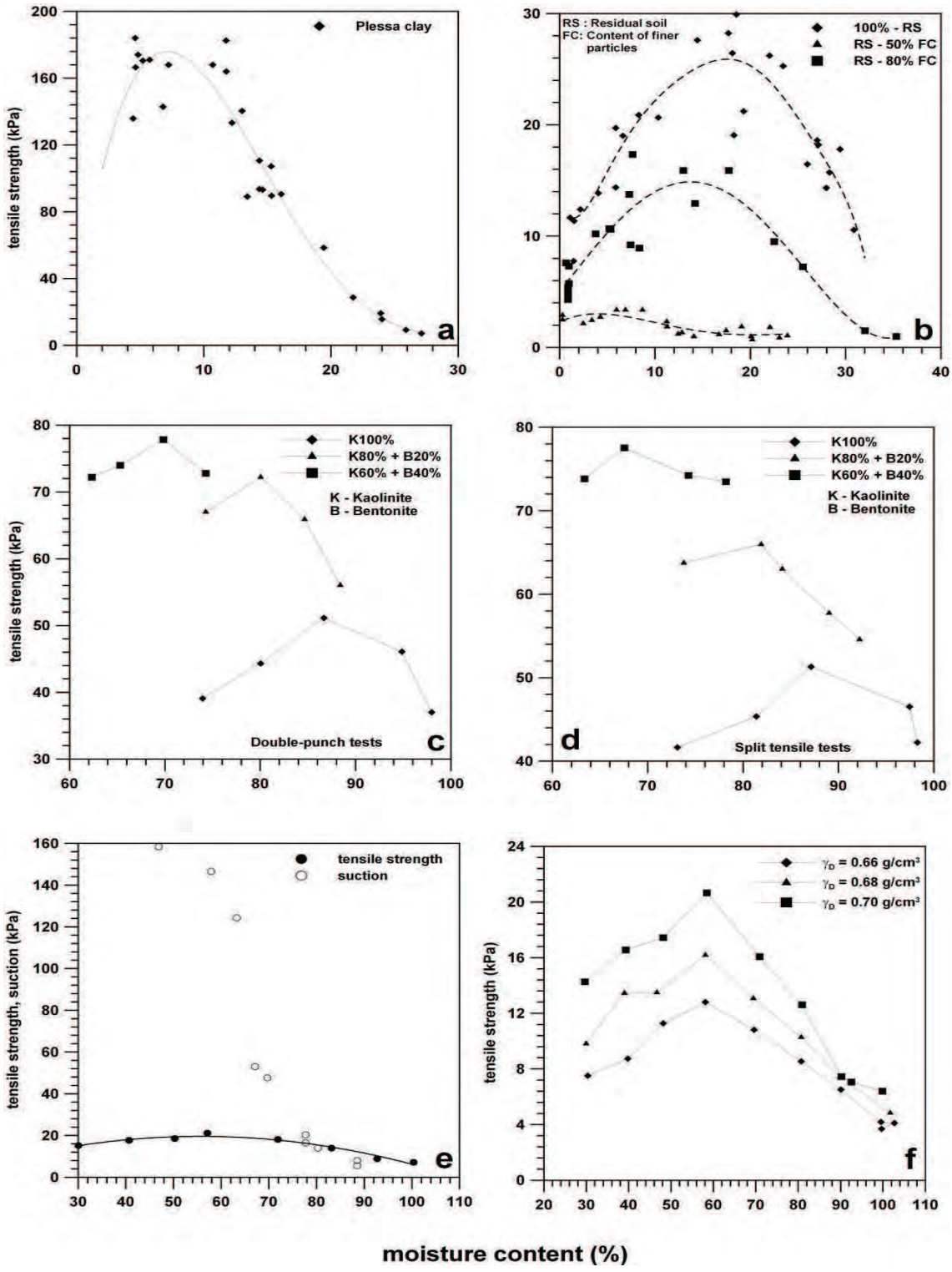

Figure 4.24: Compiled data of tensile strength variation with moisture content from literature, (a) & (b) data from Hagner [Hagner, 2005], (c) & (d) data from Favaretti [Favaretti, 1996] and (e) & (f) data from Tamrakar et al [Tamrakar et al., 2005]

reaching a peak. From the experimental results of the current investigation and the

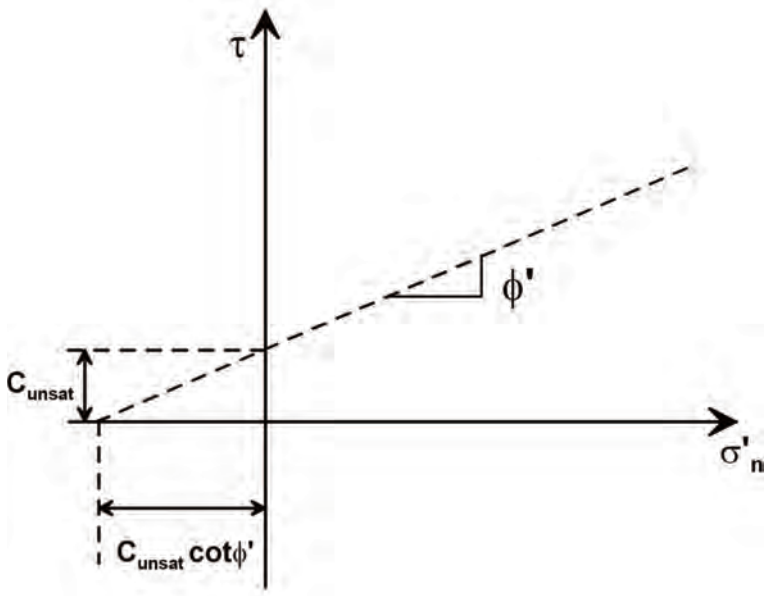

Figure 4.25: Mohr-columb representation of tensile strength as a function of cohesion (C_{unsat}) and effective angle of internal friction (ϕ')

experimental data from the literature it can be concluded that the tensile strength does not increases as the suction increases, instead it decreases after reaching a peak. Thus the tensile strength σ_t for the full range of saturation following the Mohr-Columb theory (figure 4.25)can be defined as:

$$\sigma_t = C_{unsat} \cot \phi' \tag{4.10}$$

Recently Alonso et al [Alonso et al., 2009] have proposed a shear strength equation for unsaturated soils, considering the effect of un-saturation on the soil cohesion as:

$$\tau = C_{unsat} + \sigma_{BBM} \tag{4.11}$$

Where, σ_{BBM} is the normal stress corresponding to the Barcelona Basic Model (BBM) and C_{unsat} is the unsaturated cohesion depending on the degree of saturation and prevailing suction which is given by:

$$C_{unsat} = C_{sat} + \chi(S_r)S \tag{4.12}$$

Where, C_{sat} is the saturated cohesion, S is the suction, which can be obtained from water retention curves (WRC), and $\chi(S_r)$ is a dimensionless parameter depending on the degree of saturation, which can be defined as:

$$\chi(S_r) = S_r^{\alpha} \tag{4.13}$$

where, α is a dimensionless number unique to the soil type. When this value is equal to 1, then the equation 4.11 simply reduces to the Bishop's equation [Bishop, 1960b]. For further detailed information on the theory and its validation against existing experimental data can be obtained from [Alonso et al., 2009].

Experimental WRC data for the Barcelona soil (from chapter 3, section 3.3.4, Figure 3.17) was fitted with van Genuchten [van Genuchten, 1980] and Modified van Genuchten [Romero and Vaunat, 2000] equations. The values of the fitting parameters are shown in table 3.8 of chapter 3. Parameter $\chi(S_r)$ in equation 4.13 was calculated for the data from the fitted curves for different dry densities assuming a value of 7 for α (for silty soils the value can be between 5-7). C_{unsat} was calculated from equation 4.12 by assuming C_{sat}=0. The tensile strength σ_t was calculated from equation 4.10 with $\phi' = 29°$ [Barrera, 2002].

Figure 4.26 shows the experimental data and the calculated tensile strength. The predicted tensile strength seems to follow the trend. Nevertheless the predicted values are higher than the experimental values. A good match between the predicted and the experimental data was obtained for values of S_r less than 0.6. This theory shows an important conceptual change to the previous theories wherein the tensile strength increases with increase in suction. Ávila [Ávila, 2004] observed that an increase of suction results in an increase of tensile strength. However this is only true for saturated or near-saturated conditions. As saturation decreases then tensile strength decreases after reaching a peak, as observed in the experimental work reported in this thesis and the literature. The reduction in tensile strength at lower degree of saturation may be attributed to weak or broken capillary bonds.

ESEM analysis of soils shows two types of voids: namely intra-aggregate voids and inter-aggregate voids. [Alonso et al., 2009] refer to two degrees of saturation, namely macroscopic degree of saturation (referring to the water or pore fluid filling the intra aggregate pores or macro-pores) and microscopic degree of saturation (referring to the inter aggregate pores or micro-pores). They consider that the microscopic degree of saturation is not affected much by the external or internal (suction changes due to desiccation) loads, whereas the macroscopic degree of saturation is greatly affected by desaturation. The intra-aggregate voids depend mainly on the structure of the soil; compaction and moisture content of compaction are two main factors considered in this investigation which affects the voids. This is also true for a desiccating soil, where the volume of the intra-aggregate pores reduce as they desaturate. The moisture in these pores is not affected by the surface forces of the finer particles (clay), rather it is governed by the capillary forces. These capillary forces do not contribute much at saturated conditions; hence a low tensile strength can be expected, as seen in the predicted and experimental results. As the degree of saturation decreases the capillary forces play a important role contributing to the

tensile strength reaching a peak (around $S_r = 0.6$). After, the tensile strength decreases because breaking of capillary bonds. The moisture in the macro-pores reaches a pendular state (see section 4.2). Although the suction keeps increasing, the concept of effective cohesion proposed by Alonso et al [Alonso et al., 2009] captures this phenomenon.

Figure 4.27 shows the calculated tensile strength as compared to the experimental data from Heibrock et al [Heibrock et al., 2003]. Also the WRC is presented in the same graph to highlight the effectiveness of the concept of effective cohesion for unsaturated soils.

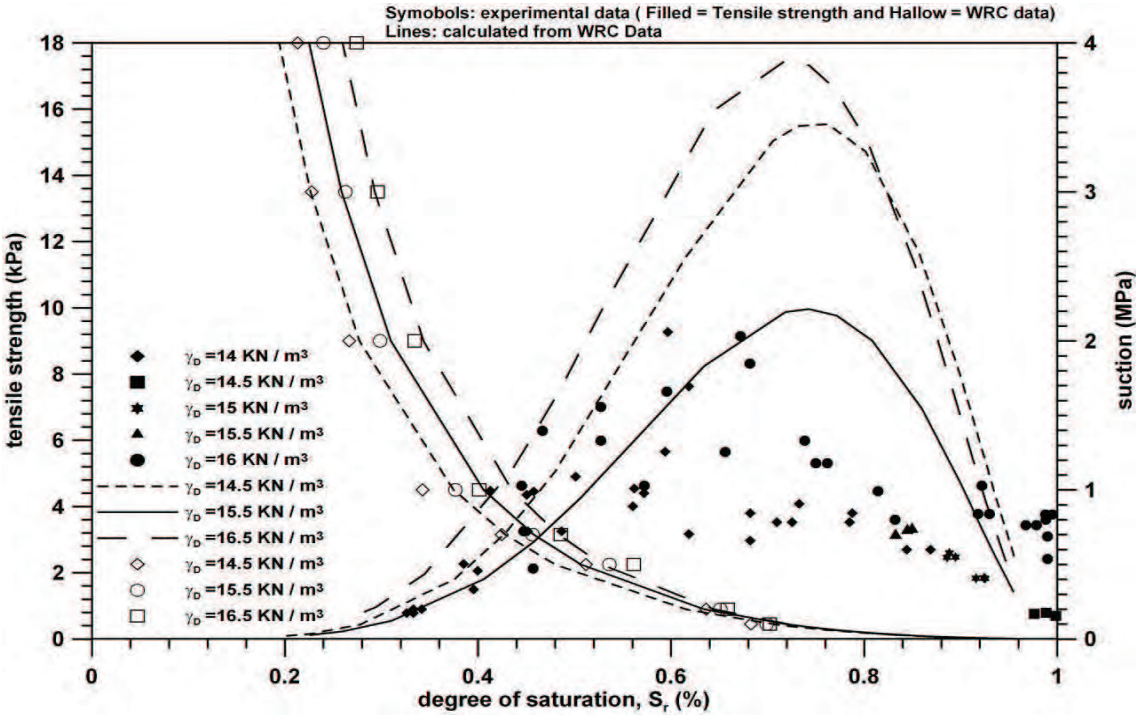

Figure 4.26: Comparison of experimental data with tensile strength calculated from the proposed theory at different degree of saturation for BCN soil and evolution of suction with degree of saturation

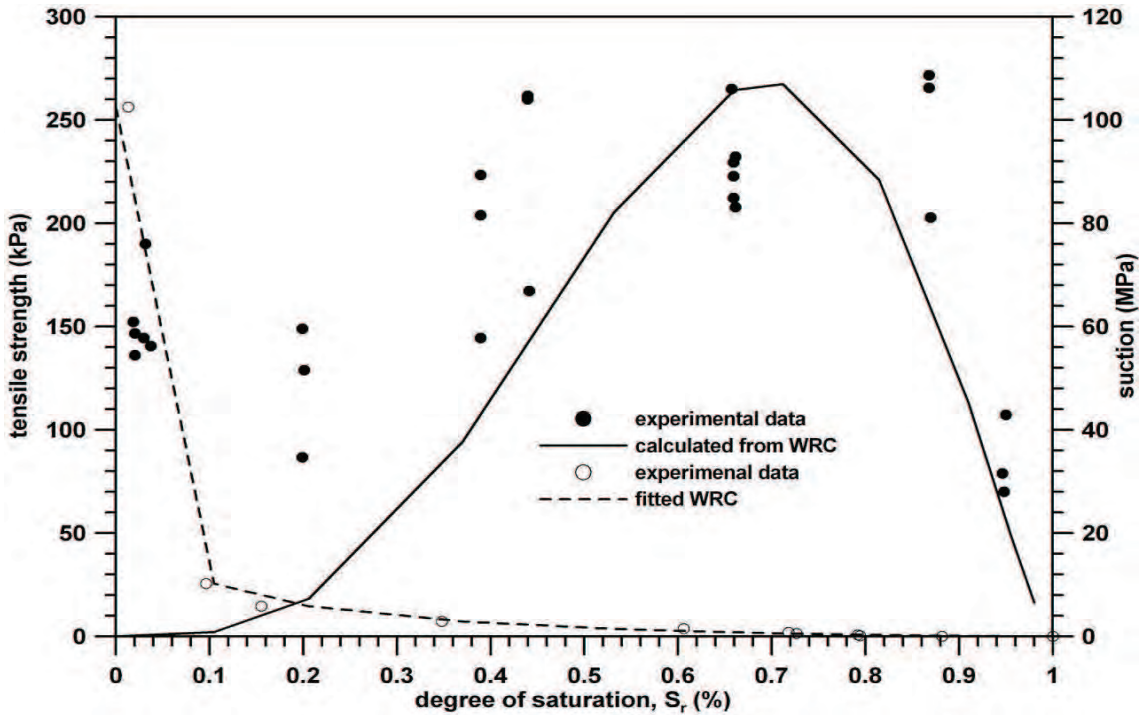

Figure 4.27: Comparison of experimental data from Heibrock et al [Heibrock et al., 2003] with tensile strength calculated from the proposed theory at different degree of saturation and suction evolution with degree of saturation

4.3 Fracture toughness (Compact Tension test)

4.3.1 Introduction

Cracking in drying soils is a complex phenomenon, though the tensile strength determines the crack initiation, crack propagation seems to be a process where concepts of fracture mechanics can be of importance in defining a numerical framework. Application of fracture mechanics concepts is not new to geotechnical engineering but they are scarce. Linear Elastic Fracture Mechanics (LEFM) is the most simple theory to explain a tensile or Mode-I failure (different modes of failure and a simple introduction is given in the next section). Stress intensity factor (K_I) and Energy release rate (G_I) are the basis of this theory. In this chapter fracture toughness (K_{IC}) is determined experimentally for Barcelona soil. There are several methods to determine the fracture toughness; here it is determined by Compact Tension (CT) tests, originally designed for concrete specimens. Though concepts of LEFM have been used for soils but very few experimental data are available, especially with effect of moisture content.

This section concentrates on characterizing the soil for one of the two fracture parameter

hence some basics of LEFM is introduced here, where as Chapter 6 gives a full overview of fracture mechanics as applied/used in Geotechnical engineering.

4.3.2 Basics of Linear Elastic Fracture Mechanics

4.3.2.1 Modes of Fracture

According to Broek [Broek, 1986] a fracture / crack in a solid can be caused by three different modes of fracture and/or by three different stress conditions as shown in figure 4.28.

MODE - I or opening mode: The crack faces separate in a direction normal to the plane of the crack. The displacements are symmetric with respect to the $x-z$ and $x-y$ planes.

MODE - II or (in-plane) shearing/sliding mode: The crack faces are mutually sheared in a direction normal to the crack front. The displacements are symmetric with respect to the $x-y$ plane and anti-symmetric with respect to the $x-z$ plane

MODE - III or (out-of-plane) shearing/tearing mode: The crack faces are sheared parallel to the crack front. The displacements are anti-symmetric with respect to the $x-y$ and $x-z$ planes. The crack faces displacements in modes II and III find an analogy to the motion of edge dislocations and screw dislocations, respectively.

The most complex situation is when more than one of the above said modes is acting in combination, whereas for most of the practical situations, cracking in soils is one among them, the fractures can be classified as predominantly of mode-I type. The subscript used (as I, II, and III) in the nomenclature signifies the mode of fracture opening.

4.3.2.2 Griffith's Fracture Stress

The key aspect of the fracture mechanics is to predict a crack existing in a material will remain stable or whether it will extend under certain stress condition. To be able to predict this behavior, there are two basic approaches, the first in terms of energy balance and the second in terms of stress field.

The energy based criterion for propagation of cracks is the basis of fracture mechanics and was formulated by Griffth [Griffith, 1921] from the solution of the problem of elastic

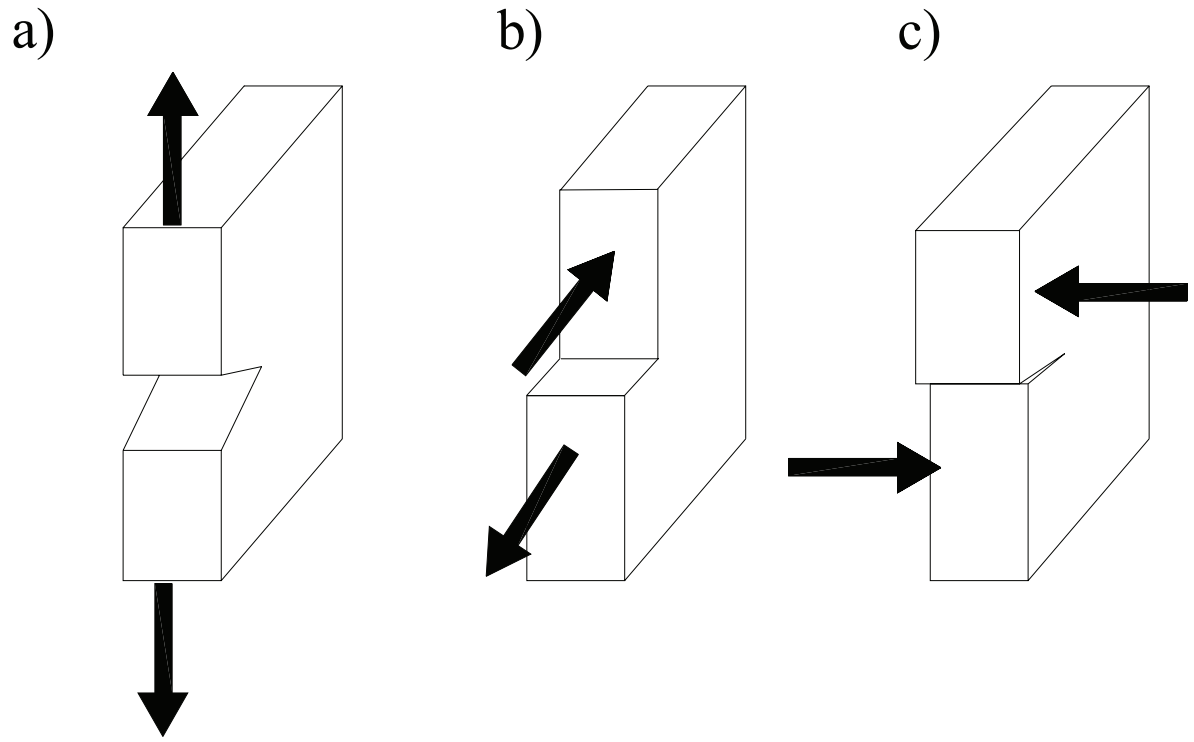

Figure 4.28: Modes of fracture (a) opening mode (b) shearing/sliding mode (in-plane) and (c)shearing/tearing mode (out-of-plane)

stress in the apex of an ellipsoidal cavity in a semi-infinite medium. The elastic analysis indicates that as the vertex of the ellipse become more acute, stresses at this point tend to infinity regardless of the (a very low) value of the applied stress. As this case is similar to a crack in semi-infinite medium, Griffith concluded that because of this singularity, the stress could not be used as a criterion for crack extension instead the problem should be addressed in terms of energy balance.

In order to analyse the Griffith's hypothesis, consider a semi-infinite, homogeneous, isotropic plate with young's modulus E and a central crack of elliptical form with a length $2a$, which is elastically deformed for applied tensile stress σ as shown in the figure 4.29a. In this case, starting from the theory of Inglis [Inglis, 1913], Griffith found that the stored elastic energy (U) in the plate for unit thickness is:

$$U = \frac{\pi^2 \sigma^2 a^2}{E} \tag{4.14}$$

And also defined the surface energy (W) as:

$$W = 4a\gamma_s \tag{4.15}$$

Where, γ_s is the specific surface energy and $4a$ corresponds to the surface area of crack

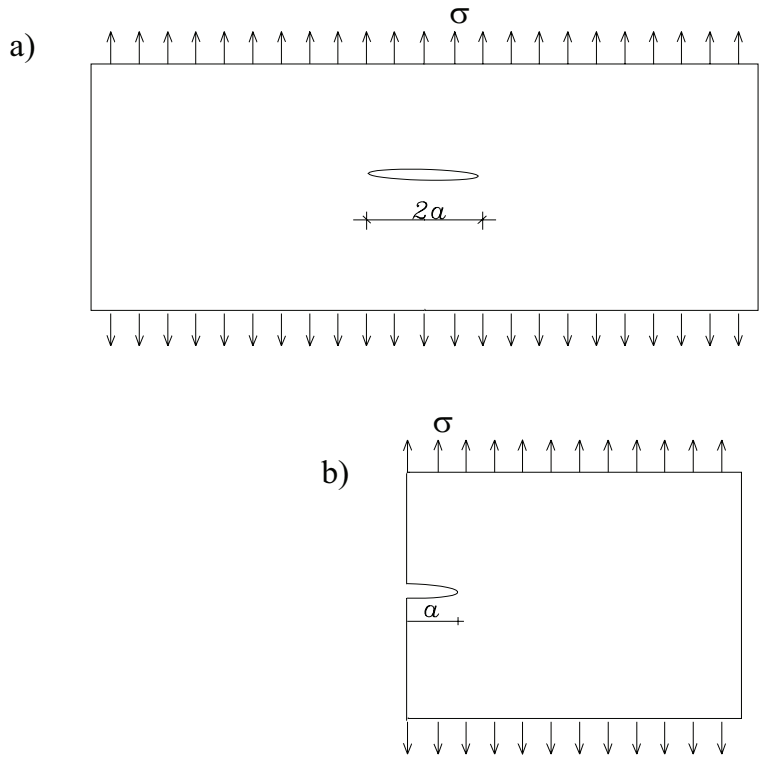

Figure 4.29: (a) Semi-infinite plate with a central crack of length $2a$ (crack with two edges) subjected to a stress σ (b) half plate with a simple crack length a subjected to a stress σ

(in this case, the thickness is considered as unit length and the length of the crack is $2a$ and it is multiplied by 2 as there are two crack surfaces)

When the crack length increases, a state of unstable equilibrium condition is reached under the applied stress and the mechanical system transfers the energy from a non fractured zone to the fractured zone. This occurs through a process of conversion of elastic energy in to surface energy. This energy equivalence can be mathematically expressed as:

$$\frac{dU}{da} = \frac{dw}{da} \tag{4.16}$$

As explained earlier through energy balance, the term dU/da implicitly reflects a reduction in the stored elastic energy of the plate due to the extension of the crack length, and for this reason in the earlier equation negative sign was not included.

Deriving the equations 4.14 and 4.15 with respect the crack length a results in:

$$\frac{dU}{da} = \frac{2\pi\sigma^2 a}{E} \tag{4.17}$$

$$\frac{dW}{da} = 4\sigma_s \tag{4.18}$$

Replacing equations 4.17 and 4.18 in equation 4.16 and rearranging for stress σ, and particularly for a case where the crack starts to grow under this stress is known as Griffith's fracture stress σ_c:

$$\sigma_c = \sqrt{\frac{2\gamma_s E}{\pi a}} \tag{4.19}$$

In general it can be said that according to the Griffith's criterion, for a crack extending a given length da, it is necessary that the elastic energy released by this extension is equal to or greater than the surface energy that is required so that the crack can be extended. If the energy released is less than the energy required for the propagation, then the crack will remain stable.

For the case of point fracture (a condition usually considered), only the half of the plate is sufficient (figure 4.29b), as a consequence equations 4.17 and 4.18 can be respectively rewritten as:

$$\frac{dU}{da} = \frac{\pi\sigma^2 a}{E} \tag{4.20}$$

$$\frac{dW}{da} = 2\sigma_s \tag{4.21}$$

The Griffith's fracture stress equation 4.19 does not seem to be affected, because for a symmetrical plate it is equivalent to analyze either full or half of the plate.

Investigations by Griffith made two fundamental contributions to the fracture mechanics: first a rational approach to crack propagation and show that the fracture is a process of energy conversion which does not depend only on the stress applied, but also on the size of the crack it self. Second, as pointed out by Gonzalez [González, 1998] and in equation 4.19 there is a relation between fracture stress and crack size, which has been repeatedly tested in fragile material.

The main drawback of the Griffith's fracture approach is it only explains fracture mechanisms of very fragile materials such as glass. For other materials in addition to the difficulties in experimental determination of surface energy, the approach generally estimates an energy less than the one required for the real propagation. This rift, because the cracks are not smooth nor straight, but rough and curvilinear and are accompanied by micro-cracks and relative plastic displacements near the crack tip (Broek [Broek, 1986], Bažant and Planas [Bažant and Planas, 1998], Garcia [García, 1997]). Perhaps for this reason LEFM had no great practical application in the beginning and its only major boom began to emerge in the period 1940-1970, when there was a large amount of theoretical, experimental and numerical research, spurred by applications in the shipbuilding industry,

especially during the Second World War (Bažant and Planas [Bažant and Planas, 1998]). The applications were developed with the generalization of the criterion of crack propagation energy and with the addition of stress intensity factor, which will be discussed later.

4.3.2.3 Energy release rate and fracture energy

Griffith's crack extension criterion can be generalized in terms of a balance between the available energy (fundamentally due to the external forces) and the required energy for such an extension to take place.

The available energy for the crack extension usually is denominated as "energy release rate" (G) and as defined by Griffith, is equal to dU/da, thus in the same manner the equation 4.20 can be expressed as:

$$\frac{dU}{da} = \frac{\pi\sigma^2 a}{E} = G \tag{4.22}$$

On the other hand, the required energy (dW/da), also known as fracture energy or critical energy release rate (G_{IC}) is a material property which can be considered as a constant in elastic range. The dimension is force per unit extension of crack, and also for this reason it is denominated as force resisting rupture or crack (R).

The critical condition for G_{IC} is when the stress σ becomes a critical value σ_c satisfying the condition $dU/da = dW/da$, hence from equation 4.22:

$$\frac{dW}{da} = R = G_{IC} = \frac{\pi\sigma_c^2 a}{E} \quad \text{OR} \quad \sigma_c = \sqrt{\frac{G_{IC}E}{\pi a}} \tag{4.23}$$

The above equation is more general form of expressing cracking stress than Griffith's equation (eq. 4.19) and this equation has an advantage as it does not involve the specific surface energy (γ_s).

Thus, the fracture criterion is as follows:

$$\text{If} \quad G < G_{IC} \quad \text{then} \quad da = 0, \quad \text{there is no crack extension (stable)} \tag{4.24}$$

$$\text{If} \quad G = G_{IC} \quad \text{then} \quad da \geq 0, \quad \text{possibly quasi-static crack extension} \tag{4.25}$$

$$\text{If} \quad G > G_{IC} \quad \text{then} \quad da > 0, \quad \text{dynamic crack extension (unstable)} \tag{4.26}$$

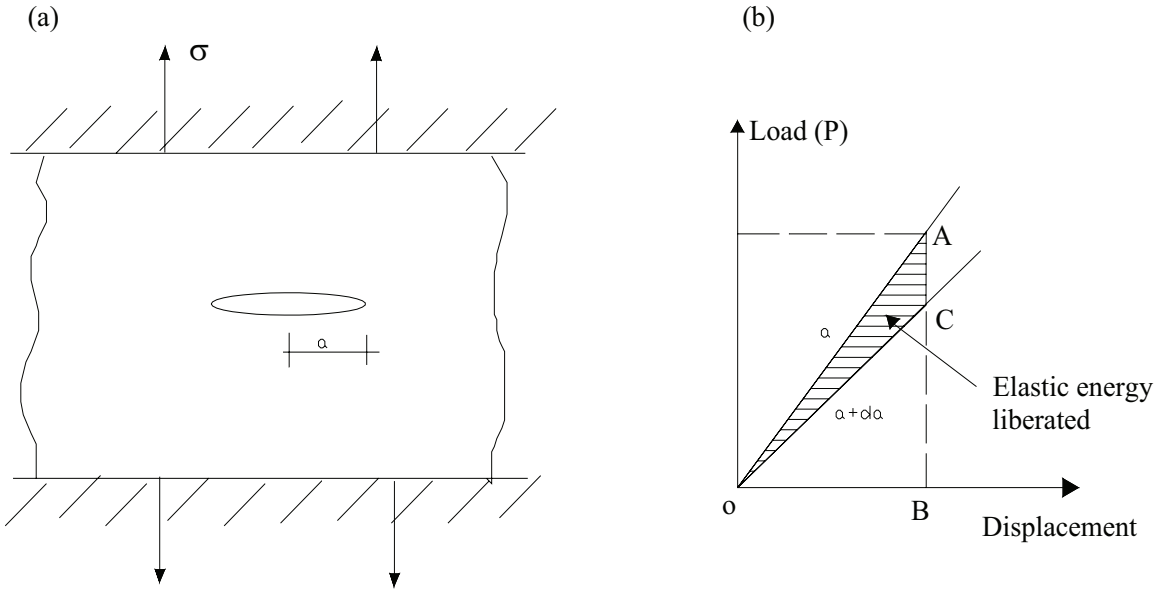

Figure 4.30: (a) Plate with fixed ends and subjected to tension (b) energy reduction due to crack extension

The process of fracture can be graphically represented in the following way, consider a plate like the one in the figure 4.30a, the elastic energy stored due the application of stress σ can be represented by the area under OAB if the figure 4.30b. If the extremes of the plate are fixed (constant deformation) and then the fracture prolong by a length da, then the rigidity reduces, as it originally corresponded to the slope of the line OA and is now to the line OC. This means that part of the load relaxes. The energy that is stored on the plate after the crack spread is now represented by the area OCB, ie, a reduction of elastic energy and the rate of energy release G, is now represented by the area OAC. The crack continues to extend if the energy represented by the area (OAC) is equal to or greater than the one required by the material so that extension can occur.

Note that the plate has been subjected to external stress but is fixed at the ends, thus the external load does not displace, and hence the work done by the external load is zero. In this condition, all the energy required for the crack propagation should be supplied by reducing the elastic energy of the plate as indicated by the equation (4.22) In the case of a plate which is not fixed at the ends and subjected to a constant stress σ or an equivalent constant load P (figures 4.31a and 4.31b), the energy release rate represents the triangle OAEO in the load-deformation curve (figure 4.31c). From figure 4.31c it can be seen that leaving the small infinitesimal area AECA, the energy released under constant deformation or constant load is the same, hence G is independent of the load variation or in general the stress trajectories or paths. (Broek [Broek, 1986]).

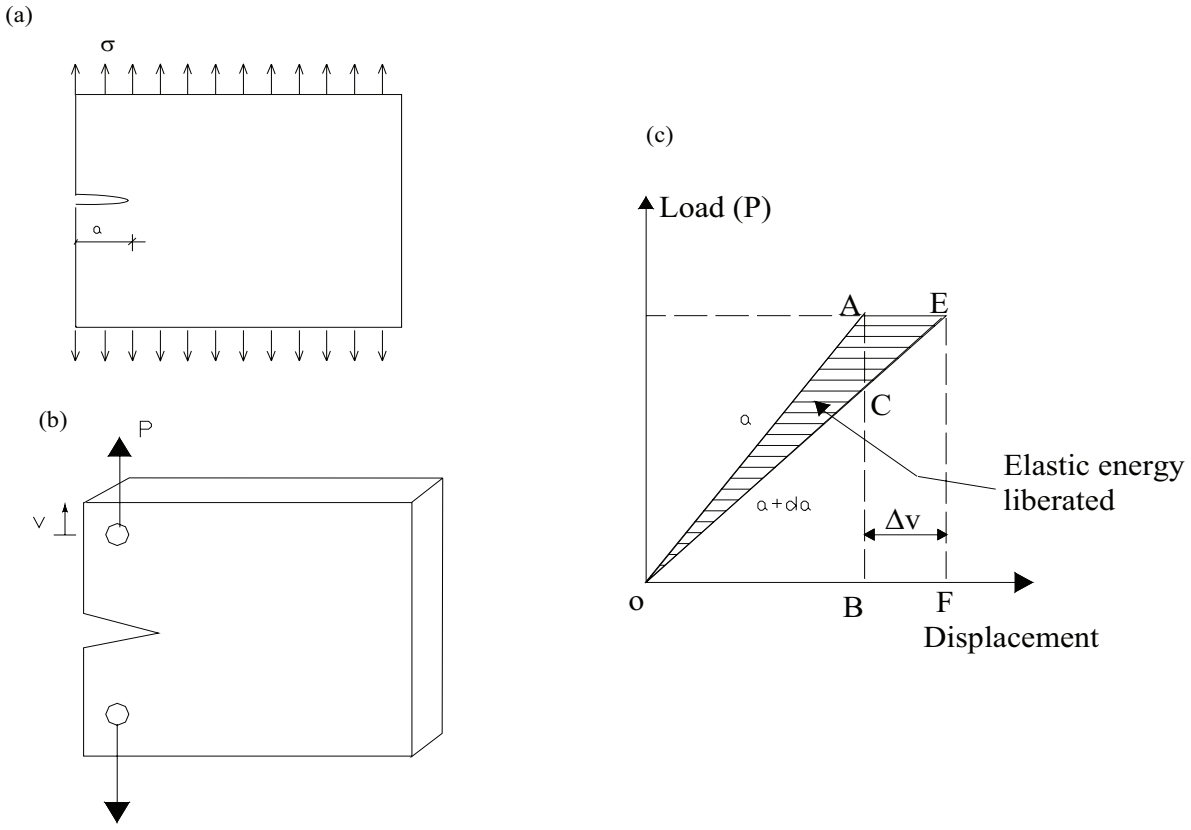

Figure 4.31: (a) Plate with free ends and subjected to uniform stress, (b) plate with free end and subjected to a load P and (c) reduction due to crack extension

In the above case the external loads produced a work, because they contribute to the increment of a crack length of da, in such a way that, with difference to what happens with fixed plate, the stored energy of the plate increases with increased crack extension (this can be seen by comparing the area OCB in fig 4.30b and OEF of the figure 4.31c) and hence the energy balance can be represented as:

$$\frac{d}{da}(U - F + W) = 0 \quad \text{OR} \quad \frac{d}{da}(F - U) = \frac{dW}{da} \tag{4.27}$$

Where, U is the stored energy in the plate, F is the work done by the external loads and W is the energy for the formation of the crack/fracture. Note that in this case the sign of the term dU/da is inverse of what the equation 4.16 has for a fixed plate.

Consider the plate in figure 4.31b, the load P result in a relative displacement ν from the point of load application, hence, when the size of the crack increase with a length da there is an increment $d\nu$ in the displacement y the work done by the load is $F = Pd\nu$, hence G can be expressed as:

$$G = \frac{d}{da}(F - U) = \frac{1}{B}(P\frac{d\nu}{da} - \frac{dU_t}{da}) \tag{4.28}$$

Where, U_t is the total elastic energy in the plate of thickness B (is different from U which is the elastic energy in a plate of unit thickness) and the rest of the terms are the same as defined earlier. If there is no increment in the size of the crack, the displacement ν is proportional to the load P and the proportionality factor is the *compliance* C which is the inverse of the rigidity ($\nu = CP$). Thus the existing elastic energy in a plate with crack like the one in figure 4.31b is:

$$U_t = \frac{1}{2}P\nu = \frac{1}{2}CP^2 \tag{4.29}$$

Replacing equation 4.29 in equation 4.28 and simplifying:

$$G = \frac{P^2}{2B}\frac{\partial C}{\partial a} \tag{4.30}$$

The above equation permit to determine G in terms of variation of compliance, which is described later in the section, this is one of the methods to obtain the LEFM parameters. Additionally, in equation 4.30 the term dP/da does not appear, which indicate that G does not depend on the load variation, hence its value should be equal for the case of the fixed plate and for the one with free ends, like already explained graphically.

4.3.2.4 Stress intensity factor

As mentioned earlier, Griffith formulated the criterion for crack extension based on the energy balance analysis to evade the problem of singularity at the crack tip, where in agreement with the elastic analysis; the stresses tend to infinity up on application of any (quantity) external load.

Irwin [Irwin, 1957] developed one of the most important advances in the LEFM formulation by defining the crack extension in terms of stress state near the crack tip y proved that this approach is in essence same as the energy balance approach and there exists a relation between the two.

Irwin concluded that the fracture could not concentrate on only one point as formulated in the elastic theory, but instead in a small area near the tip, called plastic zone or fracture process zone (FPZ), which, by the effect of deformation, absorbs large amounts of energy and maintains the stresses within a finite value.

In order to determine the distribution of stresses around the crack tip in a plate as in figure 4.29 a, Irwin went to the Airy stress function (ψ), which is special function and

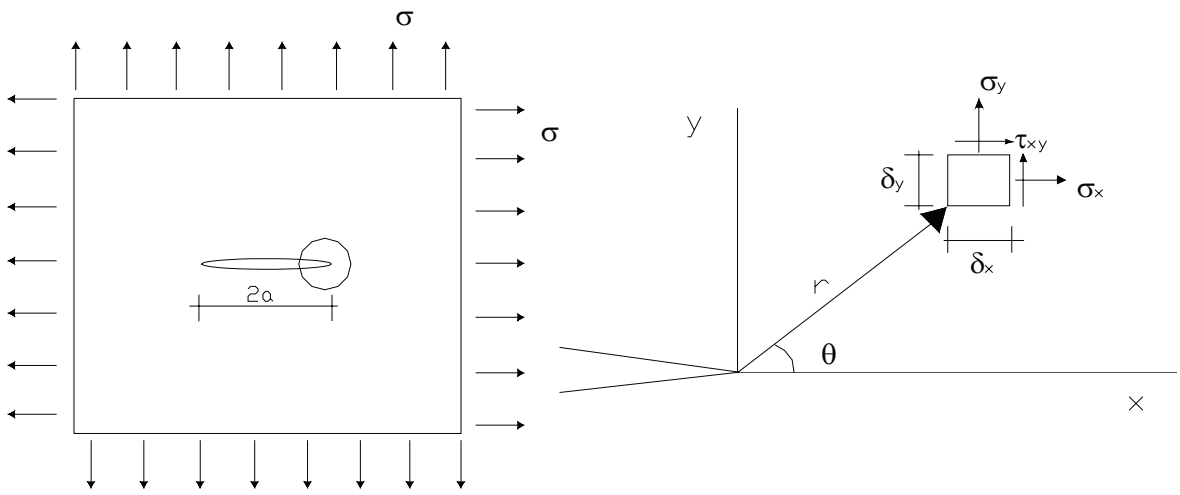

Figure 4.32: Stress field around the crack tip

in this case must simultaneously satisfy the particular stress conditions, deformation and compatibility of stress-deformation (Gonzalez[González, 1998]).

For the solving the Airy's stress function different complex functions can be employed. If the cracking is of Mode-I, then it is convenient to use the solution proposed by Westergaard, in that case the stress field around the crack tip (figure 4.32) is given by:

$$\sigma_x = \sigma\sqrt{\frac{a}{2r}}\cos\frac{\theta}{2}\left[1 - \sin\frac{\theta}{2}\sin\frac{3\theta}{2}\right] \tag{4.31}$$

$$\sigma_y = \sigma\sqrt{\frac{a}{2r}}\cos\frac{\theta}{2}\left[1 + \sin\frac{\theta}{2}\sin\frac{3\theta}{2}\right] \tag{4.32}$$

$$\tau_{xy} = \sigma\sqrt{\frac{a}{2r}}\sin\frac{\theta}{2}\cos\frac{\theta}{2}\cos\frac{3\theta}{2} \tag{4.33}$$

Or in a general form:

$$\sigma_{ij} = \frac{K_I}{\sqrt{2\phi r}} f_{ij}(\theta) \tag{4.34}$$

Where, $f_j(\theta)$ is a known function of θ and K_I is the stress intensity factor (SIF) for the Mode-I crack opening and is expressed as:

$$K_I = \beta\sigma\sqrt{a} \tag{4.35}$$

Where a is the initial crack length and β is a dimensionless factor, which for a infinite

plate corresponds to a $\sqrt{\pi}$ and in such a case,

$$K_I = \sigma\sqrt{\pi a} \tag{4.36}$$

For an element of finite size, β depend on the crack length and the geometry of the body under applied stress/load, and generally expressed in terms of length (L) one of its dimensions. Usually the SIF of these elements is expressed in terms of SIF of an infinite plate, in such a way the factor $\sqrt{\pi}$ derived from β (Broek [Broek, 1986]) and the equation 4.35 can be expressed as:

$$K_I = \beta_{\frac{a}{L}}\sigma\sqrt{\pi a} \tag{4.37}$$

The importance of stress intensity factor lies in after knowing the K_I, one can determine completely the stress field around a crack. Moreover K_I serves as a parameter of similarity to compare the fracture characteristics of a same material but with different geometry and different fracture length. From this principle, which indicates that if two cracks in two different structures have same K_I and submitted to the same mode of crack opening, then one can expect similar behaviour with respect to crack propagation or stability. This is because the stress field in both the cases is same, hence a crack will propagate or advance when the value of stress intensity factor reaches a critical value, known as the "critical stress intensity factor (K_{IC}), also known as the "fracture toughness". The value of K_{IC} can be obtained from the fracture experiments for a condition where the stress is critical ($\sigma = \sigma_c$) and it is considered as a material parameter, mathematically in agreement with equation 4.37 is given by:

$$K_I = \beta_{\frac{a}{L}}\sigma_c\sqrt{\pi a} \tag{4.38}$$

In the a similar way as earlier with the energy release rate, the criterion for the propagation of a crack in terms of stress intensity factor can be explained with the following conditions:

$$\text{If} \quad K_I < K_{IC} \quad \text{then,} \quad \text{there is no crack extension (stable)} \tag{4.39}$$

$$\text{If} \quad K_I = K_{IC} \quad \text{then,} \quad \text{possibly quasi-static crack extension} \tag{4.40}$$

$$\text{If} \quad K_I > K_{IC} \quad \text{then,} \quad \text{dynamic crack extension (unstable)} \tag{4.41}$$

From equations 4.22 and 4.36 the relation between the energy release rate and the stress intensity factor in plane stress conditions can be expressed as:

$$G_{IC} = \frac{K_{IC}^2}{E} \tag{4.42}$$

and for plane strain condition is given by:

$$G_{IC} = (1 - \nu^2)\frac{K_{IC}^2}{E} \tag{4.43}$$

Where, ν is the Poisson's ration. The equations 4.42 and 4.43 are known as the Irwin's equations, which apart from fulfilling for the critical conditions also can be applied for any other conditions less than critical, i.e. they are general relation between G_I and K_I.

An advantage of stress intensity factors is they are additive, i.e. it can be possible to obtain the values of K_I for different parts of a complex geometry and then add the individual values to obtain a global K_I, where as with the energy balance approach this is not possible. Nevertheless as indicated by Bažant and Planas [Bažant and Planas, 1998], the disadvantage is it can only be applied to the linear elastic case only where as the principle of energy release rate does not have this disadvantage.

In most of the materials, like the metals, the properties does not change significantly with normal environmental changes, whereas, in soils the situation is different, as the geo-mechanical properties including the fracture toughness is directly related to the factors like the moisture content and density, the stress history, etc. In such a situation, care should be taken in identifying the critical conditions so that the values reported are representative.

4.3.2.5 Plastic zone or fracture process zone (FPZ)

The stress distribution σ_y near the crack tip, for $\theta = 0$ (figure4.33a) can be obtained from equation 4.34 as:

$$\sigma_y = \frac{K_I}{\sqrt{\pi r}} \tag{4.44}$$

It can be observed from the figure that at the crack tip the stress goes towards infinity and moving farther from this point the stresses reduces gradually. Evidently the stress can not reach infinite value, as the material reaches its yield strength it suffers plastic deformation thus limiting the stress increment. The distance to which the plastic deformations occurs corresponds to a circle with radius r_p^* which is obtained by projecting on the abscissa, the point of intersection between the theoretical stress and the limiting yield strength or the maximum stress value which can be reached under elastic conditions (σ_{ys}) as indicated in the figure 4.33b. This circle is known as the "plastic zone or Fracture Process Zone".

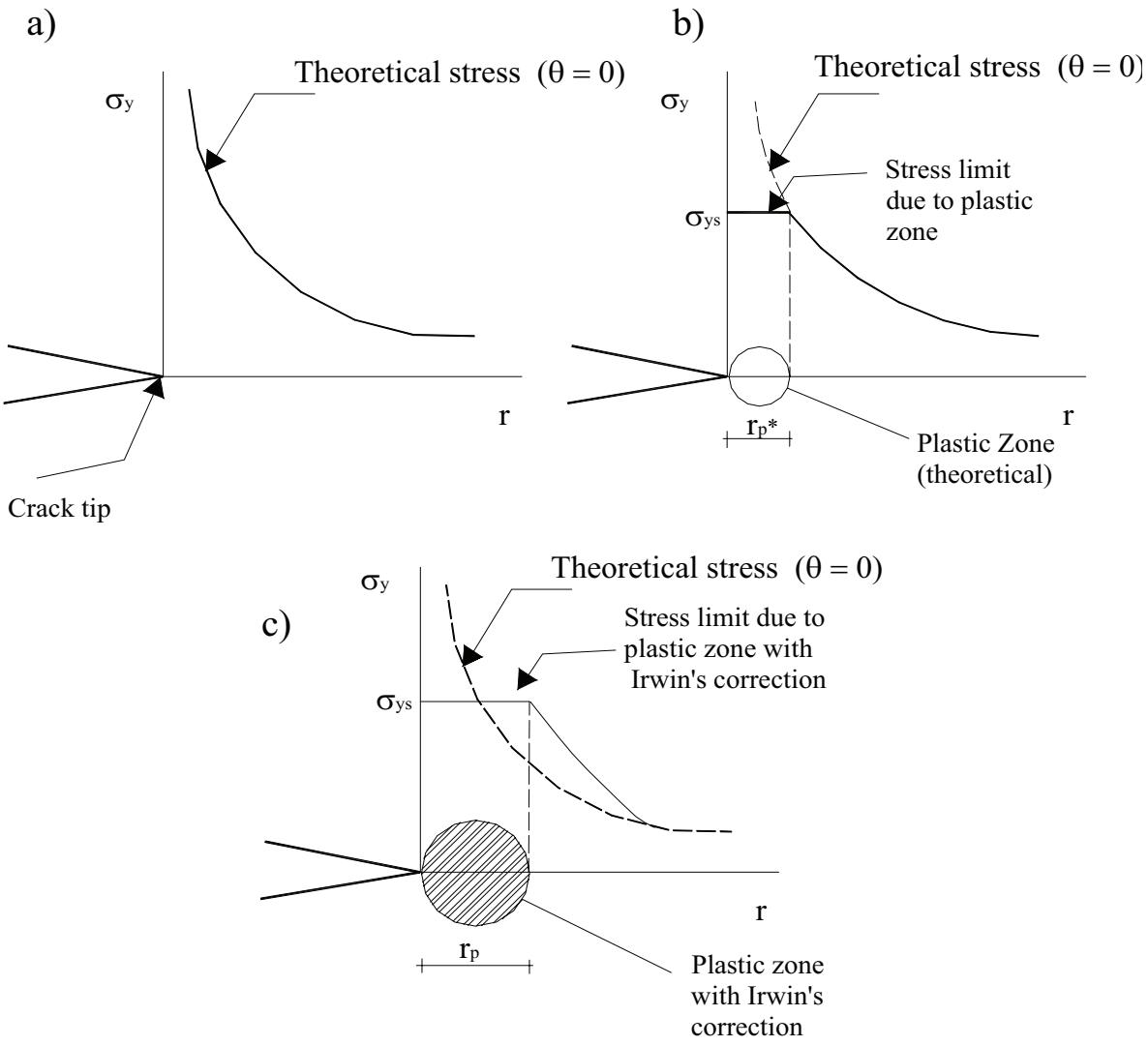

Figure 4.33: Plastic zone in the crack tip (a) theoretical stress in an elastic medium, (b) theoretical plastic zone near the crack tip and (c) plastic zone with Irwin's correction

The value of r_p^* in the stress plane is obtained from the equation 4.44 as:

$$r_p^* = \frac{1}{2\pi}\left(\frac{K_I}{\sigma_{ys}}\right)^2 \tag{4.45}$$

It has been found experimentally that the length of the plastic zone in reality bigger than the r_p^*. Irwin proposed a correction based on assuming that the bigger plastic zone is similar to a bigger/longer crack length, as the rigidity reduces with increment in displacements. From this hypothesis, the corrected value of the radius of plastic zone can be obtained in terms of the crack length as, $a + r_p^*$ and the plastic zone extension is approximately the double with out correction. This modification is called as the Irwin

modification (figure 4.33c) in such a way that:

$$r_p = 2r_p^* = \frac{1}{\pi}\left(\frac{K_I}{\sigma_{ys}}\right)^2 \tag{4.46}$$

The coefficient $\frac{1}{\pi}$ of the above equation was obtained for materials like metals, nevertheless, for quazi-fragile materials like, concrete, with fracture having micro-cracks and non-straight crack extension (curved or curvilinear) and strain softening in such case the value of the coefficient can vary between 2 and 5 (Bažant and Planas [Bažant and Planas, 1998]). In other words, the plastic zone in these materials is much more than in metals. Soils, which have more similarity with concrete than metals, one can expect much bigger plastic zone.

When the fracture process zone is not negligible in comparison with the size of the specimen, then the process is not non-linear. In agreement with Gettu and Shah (after Garcia [García, 1997]), there exists two general models to analyze this type of situations, accordingly the fracture process zone will be modelled implicit or explicit form. The two approaches are, effective models or from effective crack and the cohesive models. The effective models are applicable when the FPZ is not big when compared to the structure or specimen analyzed, in this case the FPZ is simulated in an implicit form up on evaluating the response of the specimen away from the crack tip using a equivalent elastic crack, with its tip some where in side the fracture zone, in what is known as the equivalent field distance (Bažant and Planas [Bažant and Planas, 1998]). The R-curve model, the two parameter fracture model and the size-effect method can be considered in this category.

The cohesive models are applicable when the FPZ is big, compared with the crack length or with the specimen dimensions. In this case the FPZ is modeled in explicit form, for which there are two approximations: the first considering the FPZ is situated in a line and is characterized by a stress-deformation law which exhibits softening and the second, considering the inelastic deformations in the FPZ are distributed in a band with predetermined width, which is imagined to exist in front of the principal crack, which is known as the Crack Band Model (CBM, Bažant and Cedolin [Bažant and Cedolin, 1983]).

4.3.2.6 Experimental determination of LEFM parameters

The two fundamental parameters in LEFM are, the critical stress intensity factor (K_{IC}) and the critical energy release rate (G_{IC}) and these two are mutually related to one another by Irwin's equation. The following paragraphs present the procedure to determine them experimentally.

Determination of Critical stress intensity factor (K_{IC})

In most of the studies in soils with respect to fracture mechanics parameters, specimens with known dimensions have been used. For these known dimensions, the stress intensity factor can be evaluated directly from existing formulas from manuals and codes. Among the most common methods for experimental determination are Compact Tension (CT) tests (figure 4.34a), beam type specimens, Single Edged Notch Bend (SENB) and Three Point Bend (TPB) tests (figure 4.34b), also there are some reported data with non conventional specimens like the one shown in figure 4.34c corresponding to a hollow cylindrical specimen subjected to internal stress.

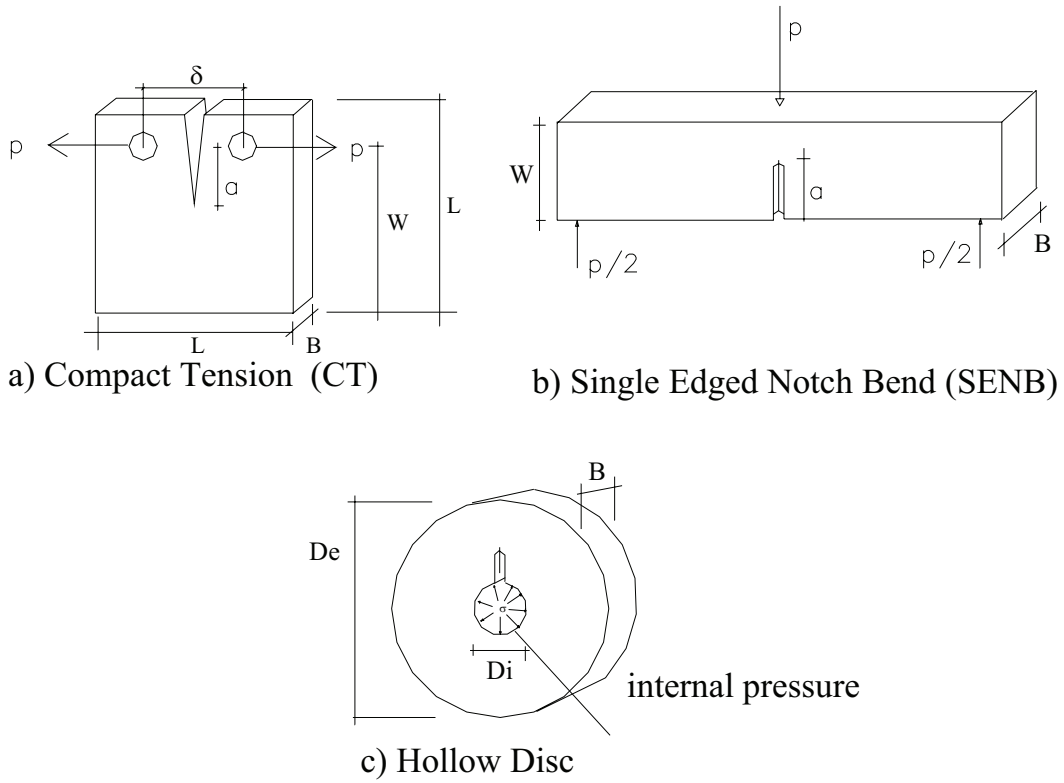

Figure 4.34: Different specimens used for determination of LEFM parameters

A general expression of K_I in terms of stress(σ) and the geometry is given by equation 4.38, nevertheless, most of the manuals which give formulas for stress intensity factor for typical geometries are in terms of load (P) which is usually measured in the experiments. Considering this, in agreement with the nomenclature proposed by Bažant and Planas [Bažant and Planas, 1998]:

$$K_I = \frac{P}{B\sqrt{D}}\hat{k}(\alpha) \tag{4.47}$$

where, D is the characteristic dimension of the specimen or structure, any dimension of the specimen can be considered, for example in a beam, its depth or its span, in a CT

specimen, the initial crack length (a) or the width W, $\alpha = \frac{a}{D}$ and $\hat{k}(\alpha)$ is a function which depend on the geometry.

For a CT specimen in the present case, $W = D$, $\alpha = \frac{a}{W}$ and $\hat{k}(\alpha)$ is calculated both from the equation proposed by Srawley-1976 [Srawley, 1976] and the one recommended by ASTM-E399 [ASTM, 1983]. The equation given by Srawley-1976 [Srawley, 1976] is:

$$\hat{k}(\alpha) = (2+\alpha)\left[\frac{0.886 + 4.64\alpha - 13.32\alpha^2 + 14.72\alpha^3 - 5.6\alpha^4}{(1-\alpha)^{\frac{3}{2}}}\right] \tag{4.48}$$

and the equation given by ASTM-E399 [ASTM, 1983] is:

$$\hat{k}(\alpha) = (30.96\alpha - 195.8\alpha^2 + 730.6\alpha^3 - 1186.3\alpha^4 + 754.6\alpha^5) \tag{4.49}$$

In both the cases the values which are used in the equation 4.52 are: $D = W$ and $\alpha = \frac{a}{W}$.

The expressions for other specimens can be obtained from the manuals and texts on fracture mechanics. If load P corresponds to cracking load P_Q, then from equation 4.52 the critical stress intensity factor (K_{IC}) is obtained directly, for this reason this method can be called as a direct method. This direct method has simple procedure, and it is possible to obtain the fracture energy (G_{IC}) from the Irwin's equations (4.42 or 4.43)

The equation 4.49 has been used by Konrad and Cummings [Konrad and Cummings, 2001] for evaluating the parameters of LEFM with CT specimens of frozen base and sub-base of a pavement. Nicolas and Grismer [Nichols and Grismer, 1997] and Sture et al [Sture et al., 1999a], have used direct methods to determine K_{IC} for soils, with flexion tests.

Determination of critical energy release rate (G_{IC})

Laboratory determination can be done by method of compliance, using the equation 4.30, there are two methods in order to determine the components of this equation. The first method is using a specimen with a initial crack length a subjected to a load P which will be incremented gradually in steps and in each step of the experiment the advance of the crack front is monitored by measuring its length (a), the displacements of the points where the load is applied (δ) and the magnitude of the applied load (P) are also measured, like this it is possible to evaluate the complianza (from the load-displacement curves). The variation of the complianza with respect to the variation of the crack length ($\partial C/\partial a$) can be determined. This method has been used by Lee et al [Lee et al., 1988] with a CT test with a special care taken to measure the crack length advance using a microscope during the test.

The second method is by testing various specimens (minimum three) with different initial crack length for each one with their respective load and displacement curves. In this method it is not required to measure the crack advance as in earlier case, this is an advantage as in many cases it is not clear the so called crack advance even with a microscope one can have some errors, especially when the crack tip advances internally and does not appear on the observing surface. On the other hand the present method minimum of three specimens is required with identical conditions except the initial crack length. Obtaining similar conditions in soils is not always easy; hence extreme care should be taken while preparing the specimens. This method has been used by Ayad et al [Ayad et al., 1997] with CT specimens.

Validity criterion for LEFM experiments

For LEFM experiments to be valid they should satisfy certain requirements with the preparation of the samples, their dimensions and the results obtained. Such requirements are well established for metals, in agreement with ASTM E-399 (1983), nevertheless, for other materials like Polymers, Concrete or Soils, these standards have not yet established, hence it is necessary to adopt the norms available for metals.

The fundamental criterion of validity of the tests established in this norm are based on satisfying the linear elasticity, for which it is necessary to have a very small plastic zone in the crack tip with respect the dimensions of the specimen and the linearity of the load displacement curve should be checked. The conditions that should be satisfied are:

(a) Minimum dimensions for the Specimens: Here the minimum dimension of the specimen (normally it is thickness of the specimen, B) be certain number of times more then the size of the plastic zone. For the case of plain deformations in metals, the norm specifies the following condition:

$$B > 2.5\left(\frac{K_{IC}}{\sigma_{ys}}\right)^2 \tag{4.50}$$

By comparing the equation 4.50 with 4.45 it is clear that the thickness B should be 7.9 times more than the plastic zone ($\frac{B}{r_p} \geq 7.9$) or in other words, the plastic zone can be maximum of 13% of the thickness of the specimen ($\frac{r_p}{B} \leq 0.13$). This is a very rigid restriction and in some cases a very big specimens are required to satisfy this condition. Another inference that can be drawn is, the fulfilment of this condition largely depend on the fracture behavior of the material, hence it is very hard to determine the minimum dimensions of the specimen otherwise a value for K_{IC} can be assumed, and after the experiments are done the dimensions can be checked if they are valid or not. As mentioned earlier for quasi fragile materials or in general materials with micro fissures or having

softening behavior, the minimum thickness indicated by the equation 4.50 are seems to be insufficient because the plastic zone in such materials is much more.

(b) the linearity of the load-deformation curves: During a test to determine the parameter of fracture mechanics, it is necessary to measure the displacements or the crack opening (δ) and the applied load (P). With these data the load-deformation or ($P - \delta$) curves can be drawn, which can have different forms. According to Broek (1986), the ideal case corresponds to a behavior where it is totally linear, with a fragile failure. The load drops drastically once the failure is reached as shown in figure 4.35a. In some cases there can be a small spontaneous extension of the crack with a load little less than the maximum (a phenomenon known as $pop - in$), after which the failure or fracture load is reached which is maximum load resisted P_{max} as shown in figure 4.35b. Finally, there can be elasto-plastic behavior with strain hardening as shown in figure 4.35c. In all these cases for the test done to be valid for LEFM, the plastic deformation should be verified so that it is not more and this is so, when:

$$\frac{P_{max}}{P_Q} < 1.1 \tag{4.51}$$

Where, P_Q is the load determined by the intersection between the stress-deformation and intersecting line drawn from the origin, with 5% reduction in slope from the original initial tangent. In the event this is satisfied, P_Q is termed as the load initiating the crack.

This condition or norm is very demanding, especially with the type of soil studied here. The soil can suffer lot of deformation compared to other materials; moreover the tests were conducted with different moisture contents, the deformation increases with the moisture content, which has been already seen in the tensile strength tests in the first half of this chapter. If this norm is to be followed strictly, then it is obvious that many of the tests or trials can be considered as not valid. However, in the non availability of a norm or standard for soils with large deformations, the results are analyzed with the existing norms.

The values of E (elastic modulus), poisons ratio ν were considered to be 0.3 and 4.2 MPa respectively from the previous study by Barrera [Barrera, 2002].

4.3.3 Previous studies on fracture toughness of soils

Few reported works are available on the fracture properties of soils. Thus, instead of giving a separate account, the available literature is cited where ever it was deemed appropriate.

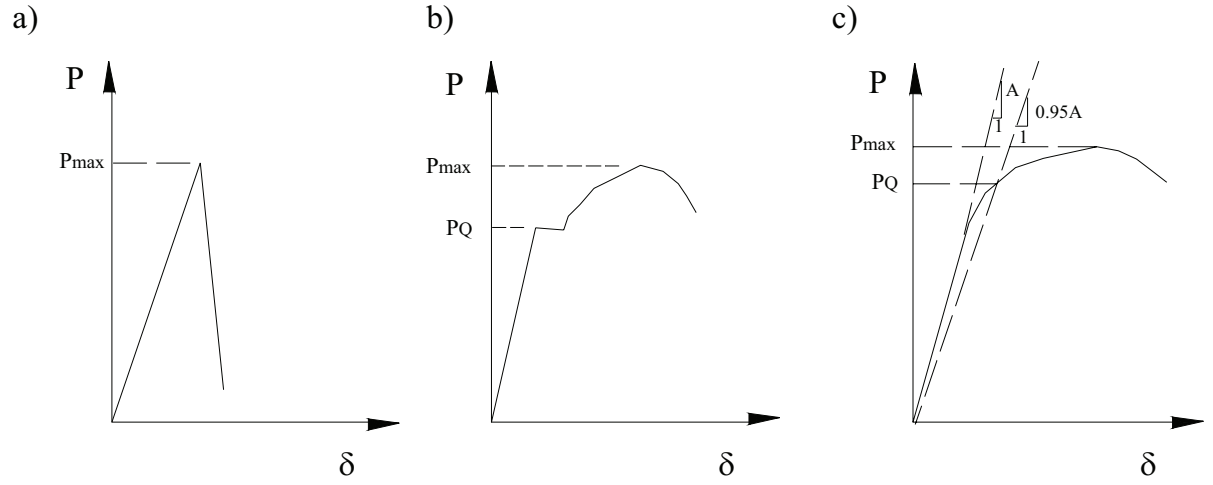

Figure 4.35: Typical load-displacement curves (a)linear behaviour with fragile rupture, (b) pop-in phenomenon and (c) elasto-plastic behaviour and linearity criterion

4.3.4 Equipment used and its background

The equipment for the determination of fracture toughness (K) was developed at soil mechanics laboratory of UPC, following the equipment of Ávila [Ávila, 2004]. Figure 4.37 show the schematic diagram of the equipment.Test specimens of two different sizes were tested (see figure 4.36 and table 4.4) at different moisture contents, with a constant natural density γ =1.95 $\pm 0.05 KN/m^3$. Figure 4.38 show the laboratory set-up with medium size specimen. Figure 4.39 show the three CT moulds. The important parts of the equipment and the functions are explained in the following paragraphs.

Loading pins: The loading pins are shown in figure 4.40, their function is to transmit the applied load to the specimen. They also serve for the application of a uniform load to the desired zone.

Methacrylate plates: Figure 4.41 show the Methacrylate plates used. These plates allow maintaining the form and shape of the specimen during the handling and loading phase. Another important function of using these plates is to assure that the load is applied in the desired zone (near the initial crack) rather than other zones such as near the loading pins. The plates are fixed by the nuts which are placed on the threaded part of the loading pins.

Metal bars: Figure 4.42 show the metal bars. The specimens are placed over the metallic bar to give one single plane of support which allows correct transmission of load just below the initial crack.

Leveling platform: There are two leveling platforms for the medium and small specimens and the big specimen is directly placed.

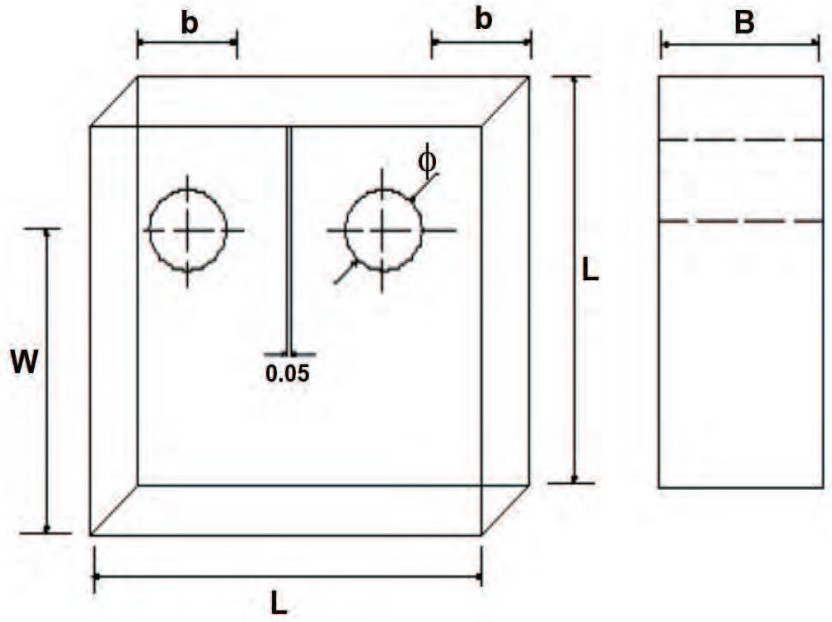

Figure 4.36: Schematic diagram of CT-test specimen

Table 4.4: Details of CT-test specimens

Mould	L (mm)	B (mm)	W (mm)	d (mm)	ϕ (mm)
medium	60	25	45	15	12
big	120	50	90	30	24

$$K_I = \frac{P}{B\sqrt{D}}\hat{k}(\alpha) \tag{4.52}$$

$$G_{IC} = (1-\nu^2)\frac{K_I^2}{E} \tag{4.53}$$

Fracture toughness (K_I) was calculated by equation 4.52, where, D is the characteristic dimension of the specimen (in the present case W = D); P is the fracture load; and B is the breadth of the specimen. $\hat{k}(\alpha)$ is a function depending on the geometry of the specimen ($\alpha = a/W$). $\hat{\text{k}}$ (α) was calculated using two different empirical formulas, given by ASTM-E399 [ASTM, 1983] and Srawley-1976 [Srawley, 1976]. Fracture energy (G) was calculated using the standard relation (equation 4.53) between K, G, and E (elastic modulus), considering $\nu = 0.3$ and E = 4.2 MPa [Barrera, 2002].

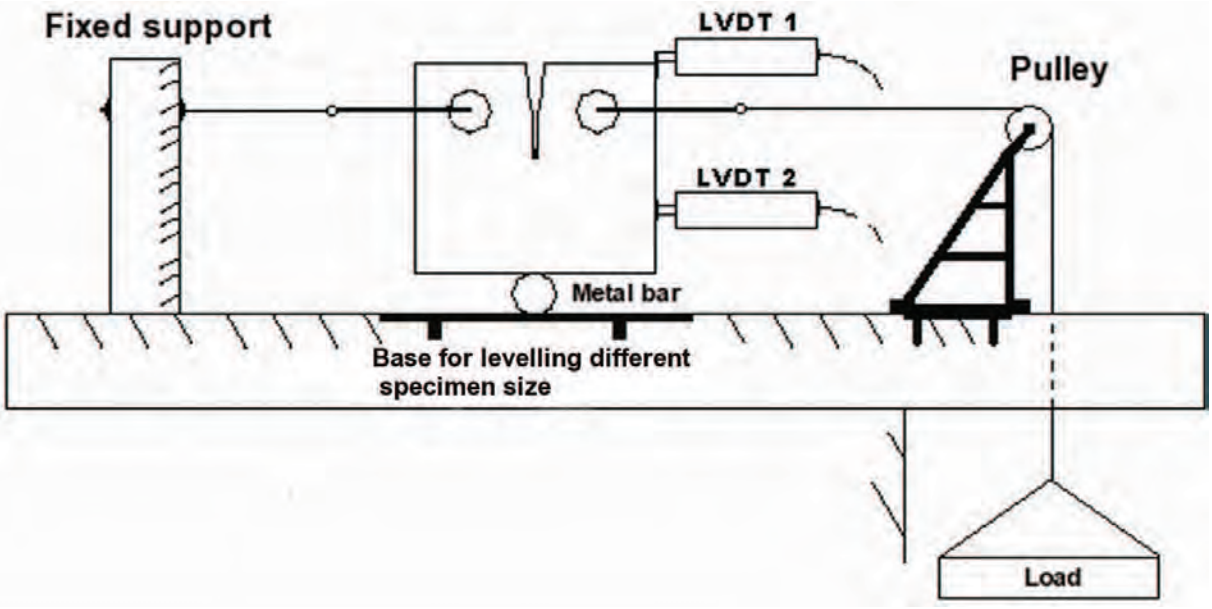

Figure 4.37: Schematic diagram of CT-test equipment

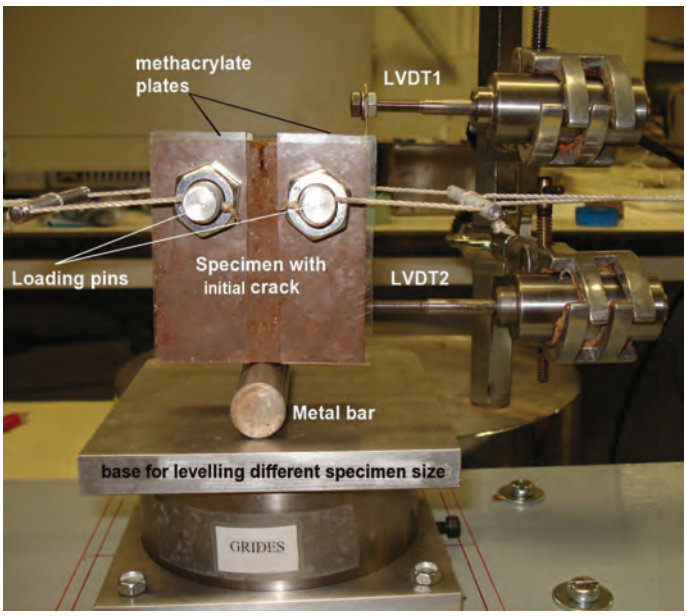

Figure 4.38: Laboratory set-up of CT-test equipment

Figure 4.39: Photograph of CT-Moulds used in the experiments

Figure 4.40: Photograph of loading pins

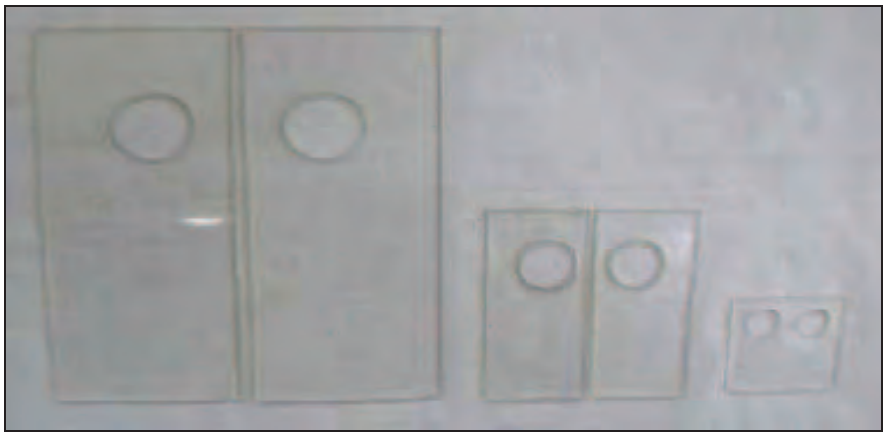

Figure 4.41: Photograph of Methacrylate plates

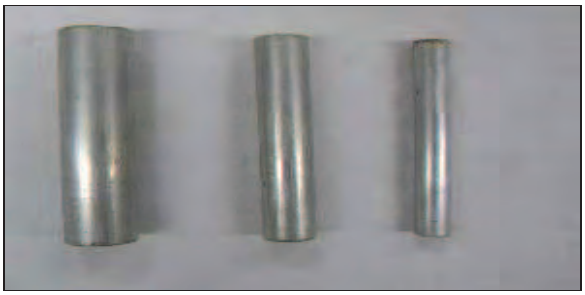

Figure 4.42: Photograph of metal bars

4.3.5 Experimental program and objectives

As mentioned in the introduction to the section 4.3, two campaigns of experiments were carried out. The first campaign consisted in conducting tests with two different specimen sizes (Big and Medium; see table 4.4) and with varying moisture contents (16%, 18%, 19%, and 21%). The length of initial cracks were 10 mm, 15mm and 20mm for the medium sized specimens and 20mm, 30mm, and 40mm for the big size specimen. For each moisture content, specimen size and initial crack length tests were repeated at least twice and in some cases thrice, thus accounting for the repeatability of the tests. All the specimens were prepared at a constant natural density of 19 kN/m^3. Table 4.5 gives the summary of the tests conducted in the first campaign. During the second campaign tests were conducted with only medium size specimens for moisture contents of 15%, 17%, 20%, and 22%. Table 4.6 gives the details of this (second) campaign. It was not possible to test specimens with moisture content less than 15% and more than 22%, because the specimens with low moisture content was very difficult to prepare and for higher moisture content the specimens collapsed just after removing from the mould. Due to these restrictions with

experimental shortcomings experiments were restricted to the moisture contents reported earlier. Initially there were three sizes of specimens; small, medium and big, due to difficulty in handling the small specimens the tests were not conducted with this size.

The motivations for the determination of the fracture toughness are similar to that of tensile strength determination explained (in earlier section 4.2.5). Specimens were tested with different initial crack length which shows how the load required for the propagation of a crack varies with crack length. The objective of this test program was to determine the effect of moisture on the fracture toughness of the Barcelona soil and hence to see the effect on the fracture energy release rate. This would shed more light on the change in the material mechanical behavior during the process of drying. Once again, the test program and its objectives are focused on characterizing the material for the study of mechanism of cracking in drying soils.

4.3.6 Sample preparation and experimental procedure

The details of the specimen preparation is same as explained for specimens of tensile strength. Once the soil-distilled water mixture was taken out from the humid chamber, CT-mould were filled with the prepared material in three layers in order to have a homogeneous density. Initial crack (of a predetermined size) was made depending on the specimen size using a metallic wire 0.5 mm thick. Care should be taken while making the initial crack. The mould has guides to make the initial crack (see, figure 4.43b) and these guides were marked with various lengths of initial crack. With the help of the guide and the reference mark the initial crack was introduced. Figure 4.43 shows the different stages in the preparation of the specimen until extrusion from the mould. Loading pins were inserted to the specimens after removing from the moulds, a methacrylate plate was inserted between the specimen and the nuts of the loading pin in order to ensure the correct load transmission to the right fracture zone just below the initial crack. Figure 4.44 show the different stages after the removal from the mould, like the insertion of loading pins and methacrylate plates.

Once the specimens were ready with loading pins and methacrylate plates in place, the specimen was placed on the base (leveling platform) plate. The loading wires were then attached to the loading pins with extreme care. The loading wires were adjusted depending on the specimen size. LVDT's were then positioned for the measurement of deformation. The next step was to place the metallic bar perpendicular to the face of the specimen at the center. Then load was applied manually with a constant frequency (detailed explanation of the load application can be found in the experimental procedure

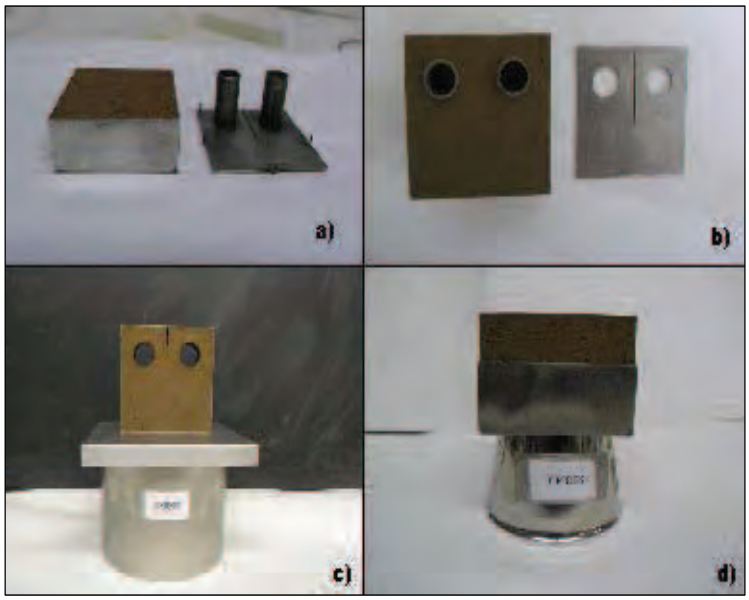

Figure 4.43: Different stages during the preparation of the CT specimen

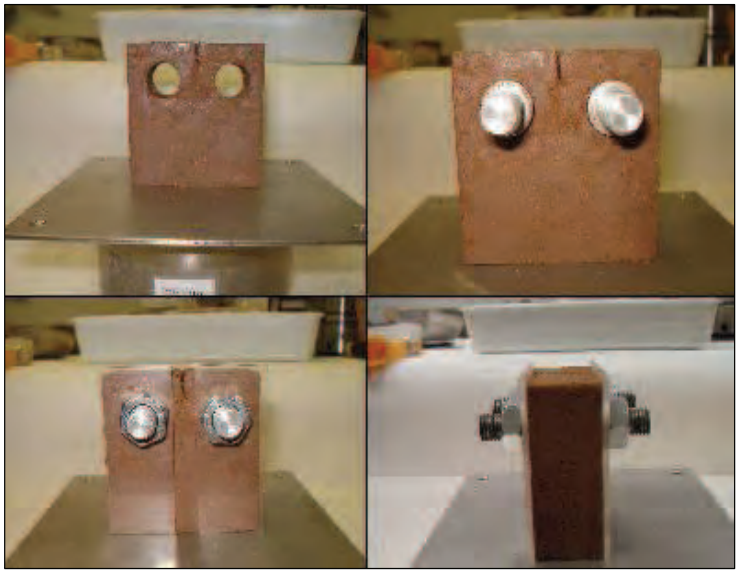

Figure 4.44: Photograph showing the insertion of loading pins and methacrylate plates

explained in section 4.2.6). The specimen was loaded until it tears apart, then fracture load was determined adding all the weights in the loading pan after the specimen was teared apart. The procedure was repeated for rest of the specimens.

4.3.7 Results

The results of the two campaigns are summarised in table 4.5 and 4.6. The values in the tables are average values of three trials or two trials. Figures 4.45, 4.46, and 4.47 show the load-displacement curves for different moisture contents, specimen size and initial crack length.

The load-deformation curves show the effect of moisture and initial crack length. A maximum fracture load at failure was observed for the specimen with least initial crack length, which is consistent with other studies with concrete specimens. The load-deformation curves for moisture contents 16% and 17% with medium size specimen are shown in figure 4.45b and c and for moisture contents 16% and 18% with big size specimen are shown in figure 4.47a and b. It was observed that these curves show a different behaviour when compared to the rest. Interestingly the fracture load increases with decreasing moisture content and reaches a maximum value around a moisture content of 17%, also this is the moisture content near to the plastic limit (PL = 16%) of the tested soil. The specimens were prepared by compacting at a natural density, thus for a specimen at moisture content near the plastic limit the inter granular or inter particle distance is minimum and with least inter capillary bridges. The load resisted by the specimens is mostly by the inter particle friction rather than capillary bonds. The higher deformation of the specimens can be explained as sliding in particle bond due to load increment since the beginning of the loading phase. In case of the specimens with higher moisture contents much of the load is resisted by the capillary and inter particle bonds. During the initial stages the capillary bonds resist with out breaking and thus very less deformation is observed.

The load-deformation curves shown in figures 4.45, 4.46, and 4.47 does not strictly adhere to the criterion of LEFM validity, this is because of the plastic nature of the soil. It is not possible to apply the validity criterion of LEFM which are formulated considering brittle or quazi-brittle materials in view. As explained in the section on basics of linear elastic fracture mechanics, these validity analysis were not done in this study. The fracture load is considered to be as the load at failure.

Table 4.5: Details of CT tests with moisture content 16, 18, 19 & 21 %

average moisture content $w_{ave}(\%)$	specimen size	initial crack length $a(mm)$	maximum fracture load (N)	K_{ASTM} $(KN/m^{1.5})$	$K_{Srawley}$ $(KN/m^{1.5})$	G_{ASTM} (N/m)	$G_{Srawley}$ (N/m)	σ_N (kPa)
16	medium	10*	3.73	1.93	3.21	0.81	2.23	1.84
		15*	2.50	1.93	2.89	0.81	1.81	1.24
		20	1.87	2.12	2.90	0.98	1.82	0.92
	big	20	9.95	1.82	3.02	0.72	1.99	1.23
		30	7.68	2.09	3.13	0.95	2.13	0.95
		40	5.15	2.07	2.82	0.93	1.73	0.64
18	medium	10	2.33	1.21	2.00	0.32	0.87	1.15
		15*	2.15	1.66	2.49	0.60	1.34	1.06
		20	1.38	1.57	2.14	0.54	0.99	0.68
	big	20	8.88	1.62	2.70	0.57	1.58	1.10
		30	7.75	2.11	3.16	0.97	2.17	0.96
		40	3.53	1.42	1.93	0.44	0.81	0.44
19	medium	10	2.12	1.09	1.82	0.26	0.72	1.04
		15	2.06	1.58	2.37	0.54	1.22	1.01
		20*	1.41	1.6	2.18	0.55	1.03	0.69
	big	20	8.45	1.55	2.57	0.53	1.45	1.04
		30	6.96	1.90	2.84	0.78	1.75	0.86
		40	3.85	1.54	2.11	0.52	0.96	0.47
21	medium	10*	1.11	0.57	0.95	0.07	0.21	0.55
		15*	0.89	0.68	1.02	0.10	0.23	0.44
		20*	0.44	0.50	0.69	0.06	0.10	0.22
	big	20	4.71	0.86	1.43	0.16	0.44	0.58
		30	3.68	1.00	1.50	0.22	0.49	0.45
		40	2.30	0.92	1.26	0.19	0.34	0.28

*Average of 3 trials; rest, average of 2 trials

Table 4.6: Details of CT tests with moisture content 15, 17, 20 & 22 %

average moisture content $w_{ave}(\%)$	specimen size	initial crack length $a(mm)$	maximum fracture load (N)	K_{ASTM} $(KN/m^{1.5})$	$K_{Srawley}$ $(KN/m^{1.5})$	G_{ASTM} (N/m)	$G_{Srawley}$ (N/m)	σ_N (kPa)
15	medium	10	2.21	1.14	1.90	0.28	0.78	1.09
		15	1.81	1.39	2.09	0.42	0.94	0.89
		20	1.40	1.59	2.16	0.54	1.01	0.69
17	medium	10*	4.78	2.47	4.11	1.34	3.69	2.36
		15	2.11	1.62	2.44	0.59	1.33	1.04
		20*	1.90	2.16	2.94	1.06	1.98	0.94
20	medium	10*	2.18	1.13	1.87	0.29	0.79	1.08
		15*	1.71	1.31	1.97	0.37	0.84	0.84
		20*	1.40	1.59	2.17	0.55	1.03	0.69
22	medium	10*	1.91	0.99	1.64	0.21	0.59	0.94
		15*	1.84	1.42	2.12	0.44	0.98	0.91
		20	1.53	1.74	2.37	0.65	1.21	0.75

*Average of 3 trials; rest, average of 2 trials

4.3.8 Effect of moisture content

The variation of fracture load for specimens with different initial crack length and specimen size at different moisture contents is shown in figure 4.48. Figure 4.49 show the variation of fracture energy with initial crack length for different moisture contents. A more clear representation of the effect of moisture on fracture energy and fracture toughness is presented in figures 4.50 and 4.51 respectively, where the fracture energy and fracture toughness are plotted against moisture content.

A more known and common behaviour of CT specimens is that the fracture load decreases as the initial crack length increases, this can be observed for medium and big specimens (figure 4.48a and b) irrespective of the moisture content. The objective of the experiments was to see the effect of moisture on the fracture behaviour, which can be seen very clearly in figure 4.48b for big specimens, where a maximum fracture load was observed for a moisture content of 16% and reduces as the moisture content increase. For the medium sized specimen where the experiments were conducted for a more wide range of moisture contents (figure 4.48a); the fracture load increases as the moisture content decreases till a moisture content of 17%, further decrease in moisture content a decrease in the fracture load was observed.

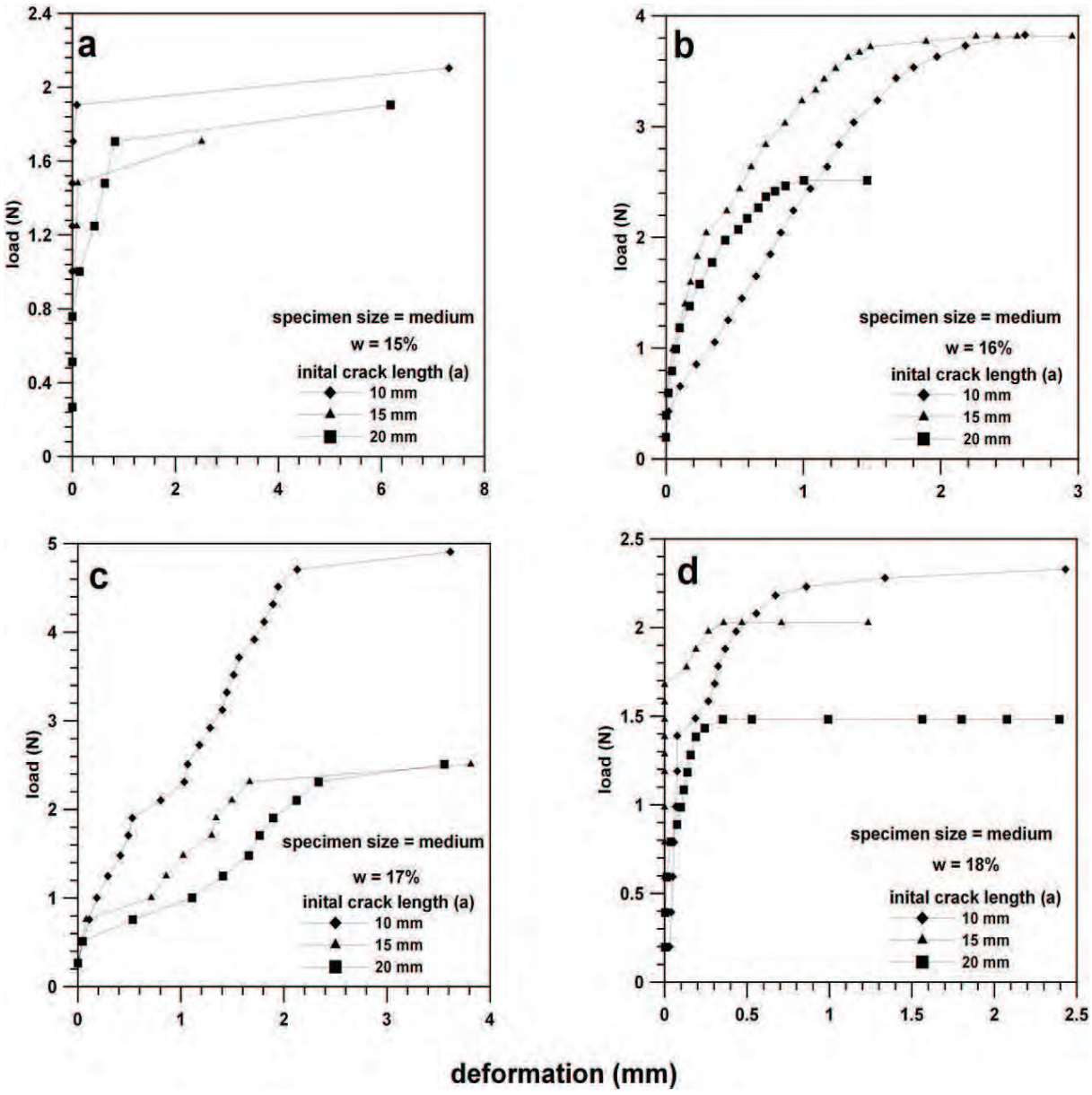

Figure 4.45: Typical load-displacement curves from CT specimen (of medium size) for moisture contents of 15%, 16%, 17%, and 18%

Fracture energy is considered to be a material constant, it is constant for a material. In case of soil, the presence and volumetric content of pore fluid affects greatly the mechanical behaviour. In this context it was assumed that fracture energy varies with moisture content, eventually the results of the test confirmed the hypothesis. Though the fracture energy varies with moisture content, but for a given moisture content it can be considered as a constant which can be seen in figure 4.49. The variation of fracture energy for various moisture content is shown in figure 4.50 and fracture toughness in figure 4.51. In these two figures an exponential curve is fitted for the experimental data and in the next section an attempt is made to give a theoretical explanation for the assumed exponential behaviour

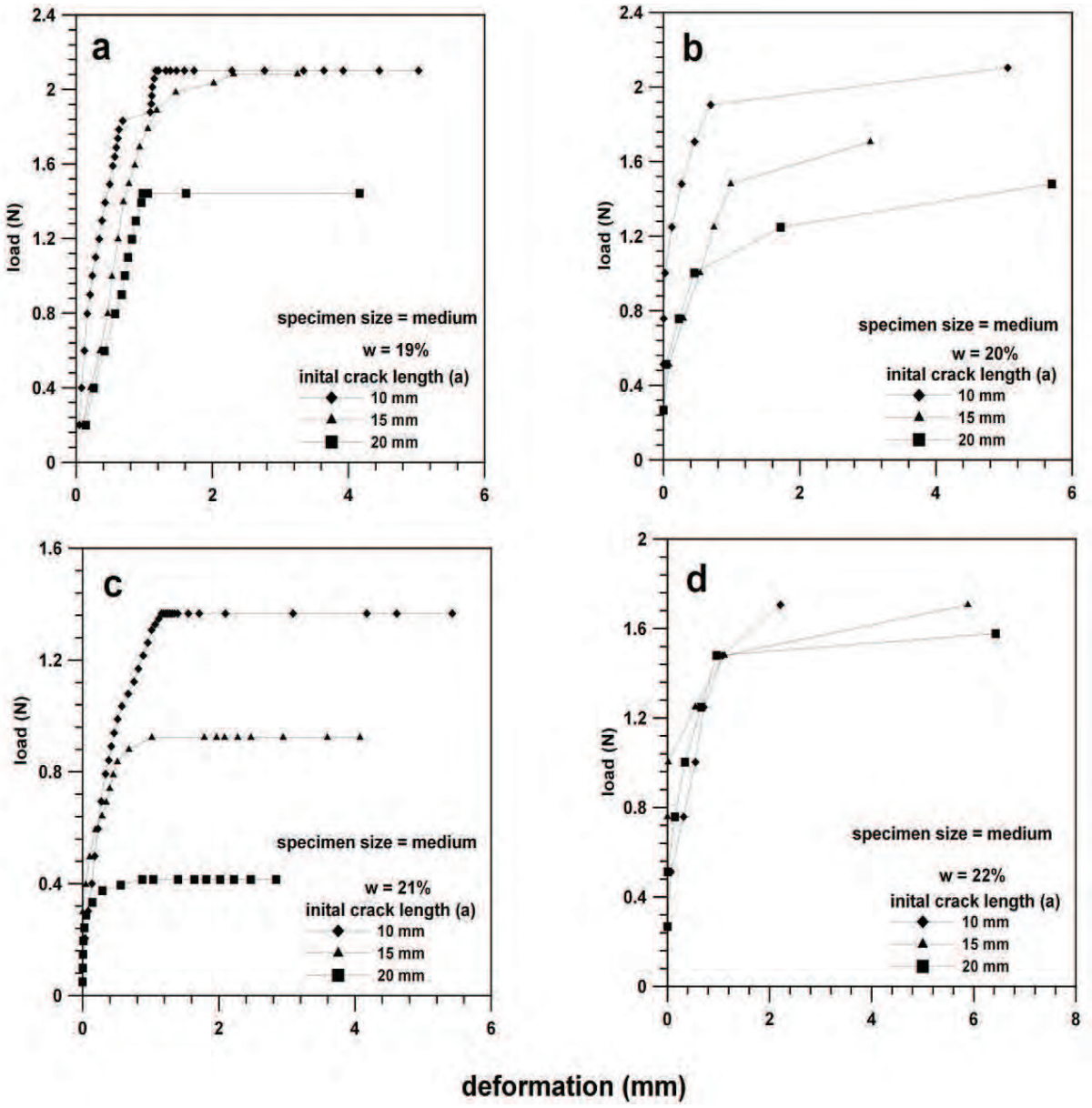

Figure 4.46: Typical load-displacement curves from CT specimen (of medium size) for moisture contents of 19%, 20%, 21%, and 22%

with the concepts of activation energy and rate process theory.

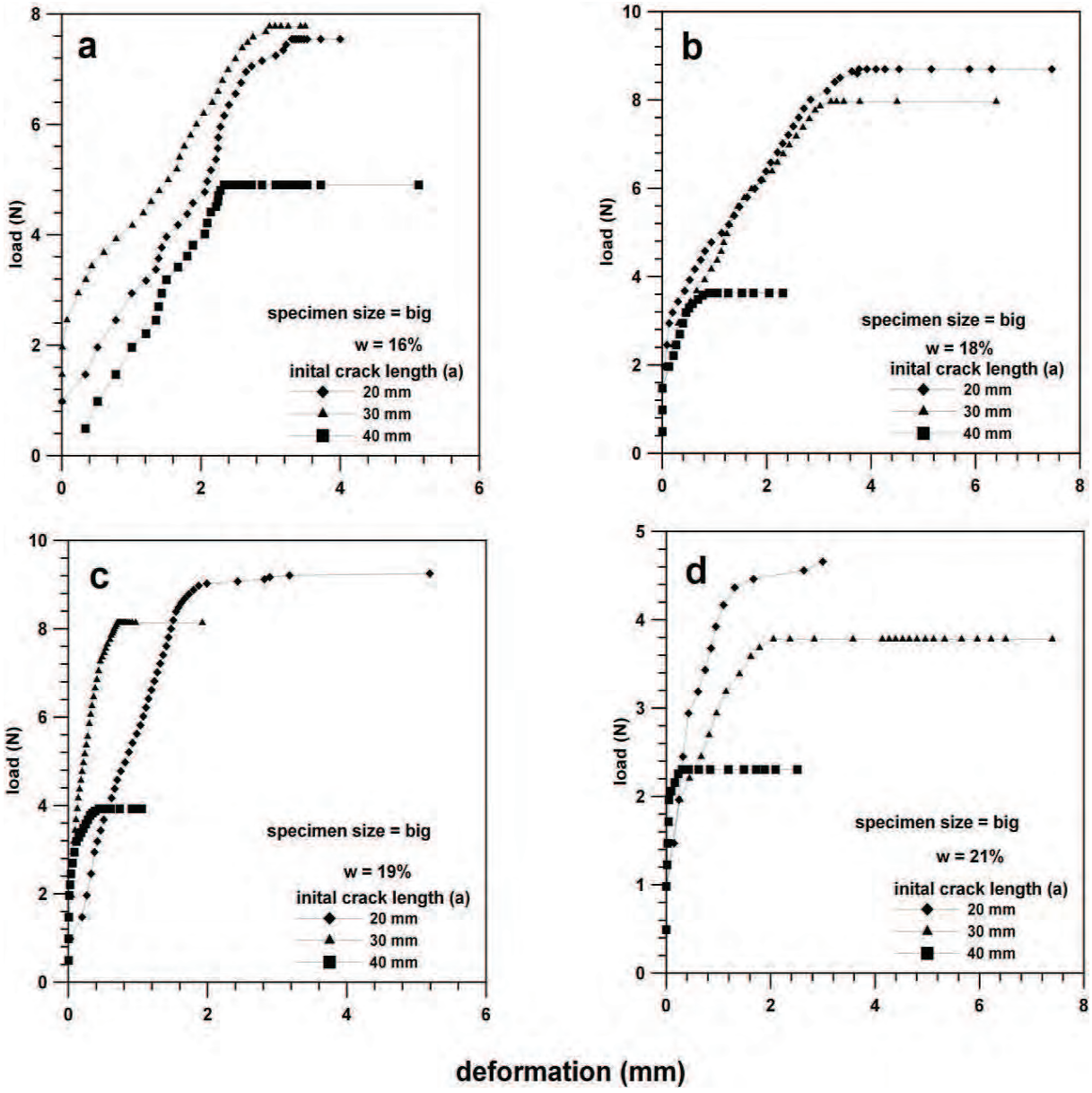

Figure 4.47: Typical load-displacement curves from CT specimen (of big size) for moisture contents of 16%, 18%, 19%, and 21%

4.3.9 Theoretical model

4.3.9.1 Activation energy

It is generally accepted that fracture is a thermally activated rate process. This means that the atomic bond ruptures that constitute the mechanism of fracture are provoked by the energies of thermal vibrations [Cottrel, 1964]. This is valid for many materials: metals, glass, ceramics, rocks, concrete, etc. which can be considered as single phase

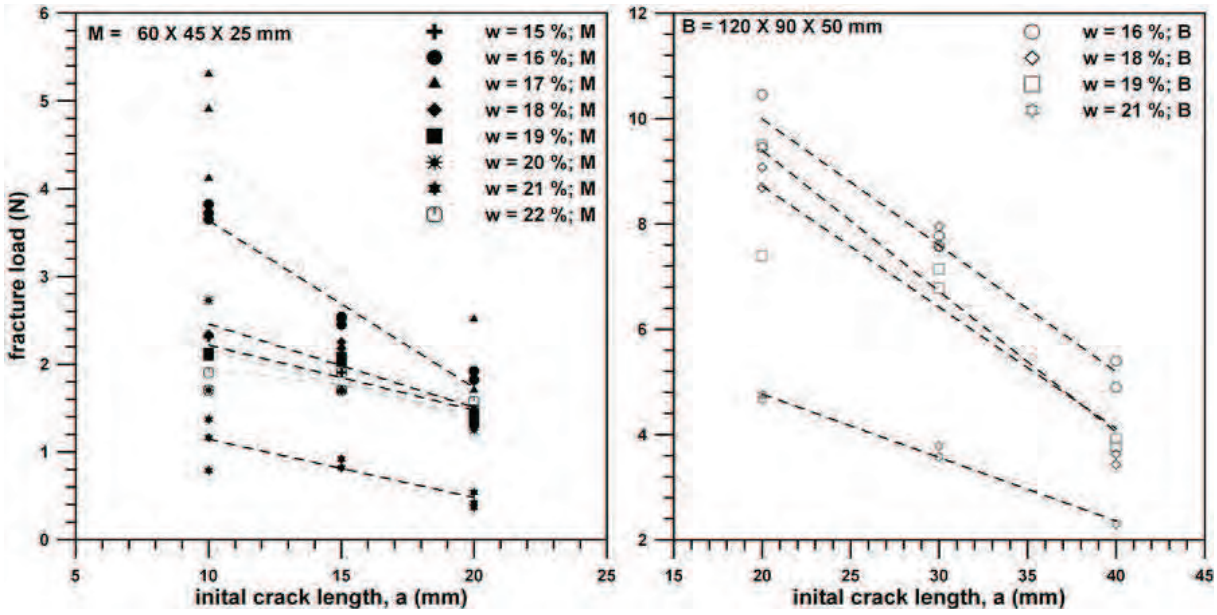

Figure 4.48: Fracture load vs initial crack length for different moisture contents: (a) for medium size specimen and (b) for big size specimen

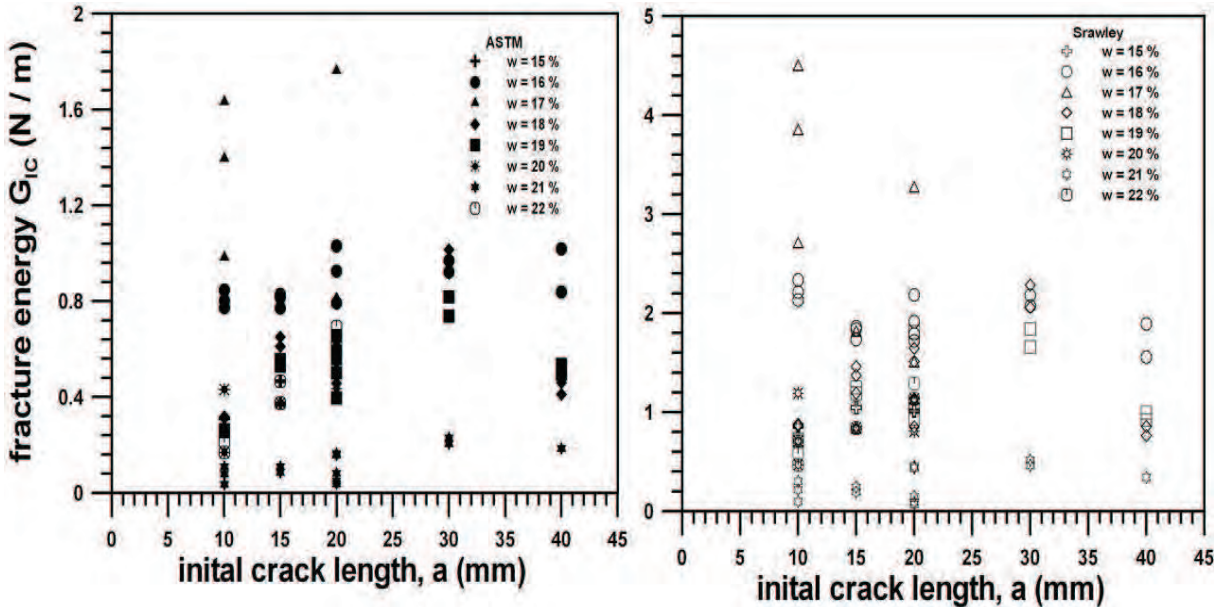

Figure 4.49: Fracture energy vs initial crack length for different moisture contents for medium and big size specimens: (a) calculated from ASTM and (b) form Srawley expressions

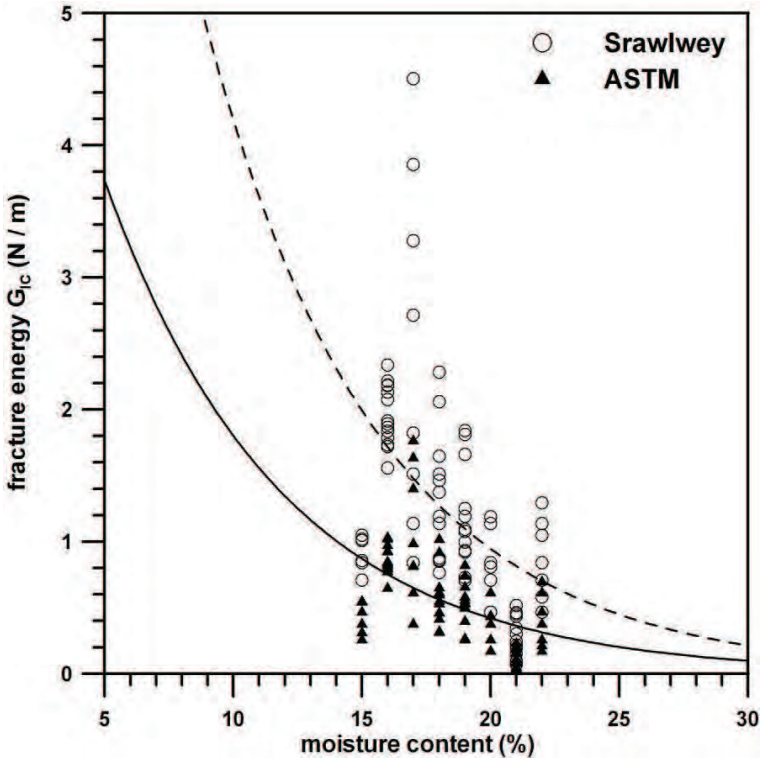

Figure 4.50: Fracture energy variation with moisture content for medium and big size specimens

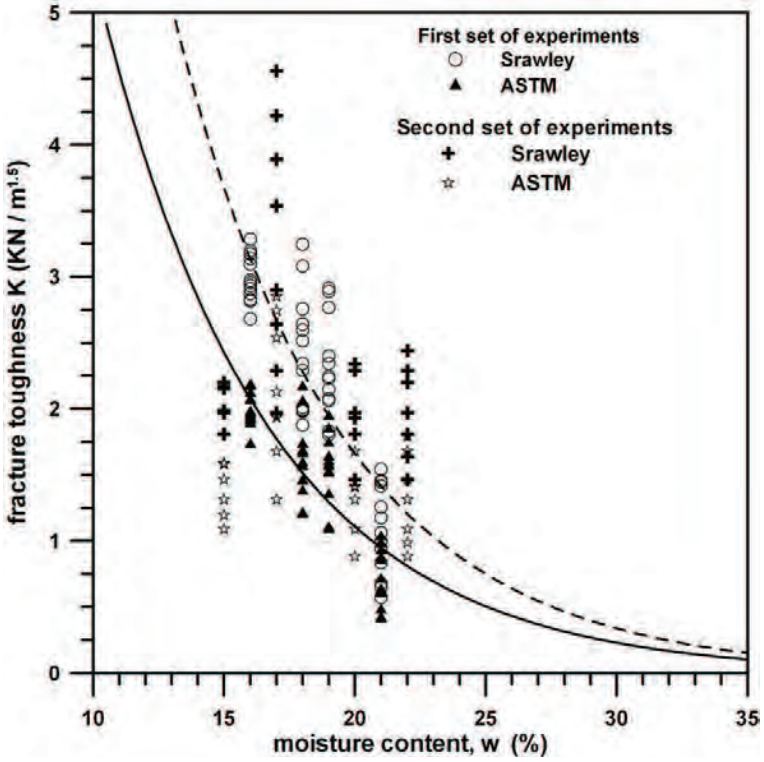

Figure 4.51: Fracture toughness variation with moisture content for medium and big size specimens

and/or continuous medium. Soils are particulate media, and usually two-phase (solid particles and pore fluid when fully saturated) or three-phase systems (solid-pore fluid-air when un-saturated). The most important characteristic of such materials is the effect of degree of saturation on the mechanical properties keeping aside the effect of temperature. Therefore the fracture behaviour of soils depends largely on the variation of degree of saturation (suction and tensile strength) which affects the fracture toughness.

Crack initiation (primary cracks) in desiccating soils occurs when the soil is close to saturation (quasi-saturated) [Lloret et al., 1998]. During the process of drying, the soil matrix absorbs the energy; which is utilized in the evaporation of water from the soil surface. The rate of moisture loss depends on the distribution of pores besides the temperature and relative humidity of the air in contact with the drying surface. Random distribution of pores (depending on grain size distribution and density) results in uneven rate of moisture loss. The differential drying rate with existing boundary conditions results in build up of internal stresses in the soil matrix. When the internal stresses (can be stresses generated due to, internal energy imbalance, differential shrinkage, etc) overcome the soil strength (tensile strength) at the boundary of the air-water-solids, a crack appears. The internal stresses generated in the soil matrix depends on the degree of saturation at that point, in variably the stresses is another form of energy absorbed by the soil matrix. In other words these internal stresses are the energy required to overcome the (soil strength) bond between the air-water-solids in the soil matrix. These energies are statistically distributed, as described by Maxwell distribution, and any variation in saturation should affect the probability (or frequency) that the activation energy (internal stresses developed) would exceed the bonding energy (soil strength). Therefore the activation energy is related to the soil saturation, and in turn the propagation of cracks, which generally follows a formula of the type $\dot{a} = f(K)\exp(-U/RT)$ (Cherepanov, 1979), where U = activation energy of bond rupture; R = universal gas constant; T = absolute temperature; K = stress intensity factor; and $f(K)$ = empirical monotonically increasing function.

Rate process theory has been used in the past by researchers, to explain the variation of strain rate with the deviator stress [Christensen and Wu, 1964];[Mitchell, 1964], to predict the rate of erosion of cohesive soils [Christensen and Das, 1973], to evaluate the effect of temperature and humidity on fracture energy of concrete [Bažant and Prat, 1988], to estimate the temperature effects on water flow in variably saturated soils [Zhang et al., 2003]. Evans and Fu [Evans and Fu,] and Thouless et al [Thouless et al., 1983] have verified for certain ceramics a special form of this formula for rate of growth of fracture ($\dot{a}$):

$$\dot{a} = \nu_c (K/K_c)^n e^{-U/RT} \tag{4.54}$$

in which ν_c and n may be approximately considered as constants characterizing the given material and K_c= critical value of K (fracture toughness). As an approximation, this equation will be used also for soils.

According to [Bažant and Prat, 1988] , this equation is not exact but approximate for two reasons: (1) the proportionality of $\dot{a}$ and K^n is empirical; and (2) more than one mechanism of bond rupture, with different activation energies, might be involved, and the type of this mechanism might change with temperature. Added to this in the case of soil it might change with different saturation. Considering these, equation (4.54) may be re-written as

$$\dot{a} = \nu_w \left(\frac{K}{K_w}\right)^n \exp\left[\frac{-U^*}{RT}\right] \tag{4.55}$$

where U^* is the activation energy depending on the soil moisture or saturation and is expressed as $U^* = (U_0/w)$. U_0 is the reference activation energy independent of moisture change. ν_w and n are new material constant. K_w is the value of K at moisture content w.

Some special considerations should be made before using the equation 4.55. Considering the soil to be in fully dry state (i.e. w=0), at this point there will be no further fracture of the soil media. Another extreme condition is when the soil is at its liquid limit (i.e. w=w_L), at this state soil flows with out resistance or in other words the value of rate of growth of fracture is a very large number.

For $w = 0$; $e^{-\infty}$ $\dot{a} = 0$

For $w = w_L$; $K_w \gg 0$ $\dot{a}$ is a very large number

Note that here the effect of moisture is considered to be the same as temperature, but in the reverse sense, i.e. increase in temperature decreases the activation energy but a decrease in the moisture increases the activation energy for a given temperature. Then equation 4.55 may be written with effect of moisture change for a given temperature.

$$\dot{a} = \nu_w \left(\frac{K}{K_L}\right)^n \exp\left[\frac{-U_0}{RT}\left(\frac{1}{w} - \frac{1}{w_L}\right)\right] \tag{4.56}$$

Where, $w_L$is the reference moisture content equal to the liquid limit of the soil, and w is the any water content between liquid limit and dry state of the soil. K_L is the value of K at moisture content$w_L$and K_w is the value of K at moisture content w. Now considering

the water content w in equation (4.56) to be equivalent to w_L, then the crack growth rate $\dot{a}$ at water content $w = w_L$ is simply expressed as

$$\dot{a} = \nu_w \left(\frac{K}{K_w} \right)^n \tag{4.57}$$

Crack growth rate expressions referred to w or to $w_L$must be equivalent. Equating the expressions in (4.56) and (4.57) , one obtains (equation(4.58) which is similar to Bažant's approximate formula [Bažant, 1987])

$$K_w = K_L \exp\left({}^{\nu}\!/_{w} - {}^{\nu}\!/_{w_{LL}} \right) \tag{4.58}$$

in which

$$\nu = {}^{U_0}\!/_{nRT} \tag{4.59}$$

ν is a constant characterizing the given material (soil in the present case) at temperature T. Equation (4.58) allows a simple determination of material parameters since it may be written in form $Y = \nu X + b$ where $Y = ln(K_w)$; $X = 1/w$; $b = ln(K_w) - \nu/w_L$. So the values of ν and b may be found as the slope and Y-intercept of the regression line in the plot of $ln\ (K_w)$ versus $1/w$.

Experimental determination of the Values of activation energy U for soils is quite difficult. According to equation (4.59), one would also need to determine exponent n. This would require measuring the rate of growth of the crack length at various load values.

The fracture toughness values obtained experimentally at various moisture contents are plotted in figure 4.52a as the data points. The linear regression plot shown in figure 4.52b demonstrates that the present test results indeed fall quite close to a straight line in this plot. This confirms the validity (mathematically) of equation 4.58. Analyzing the physical significance of the linear regression plot with respect to soil has something to do with the behavior of soil. Let us consider the basic and most common parameters used to classify/identify the soil. Atterberg's limits: Liquid limit (w_L), plastic limit (w_P) and Shrinkage limit (w_R). By definition the liquid limit is the water content at which the soil has such small shear strength that it has the consistency of a fluid. The shrinkage limit is the water content below which the soil becomes unsaturated, and further reduction of the water content will not result in volume change. The experiments show that the

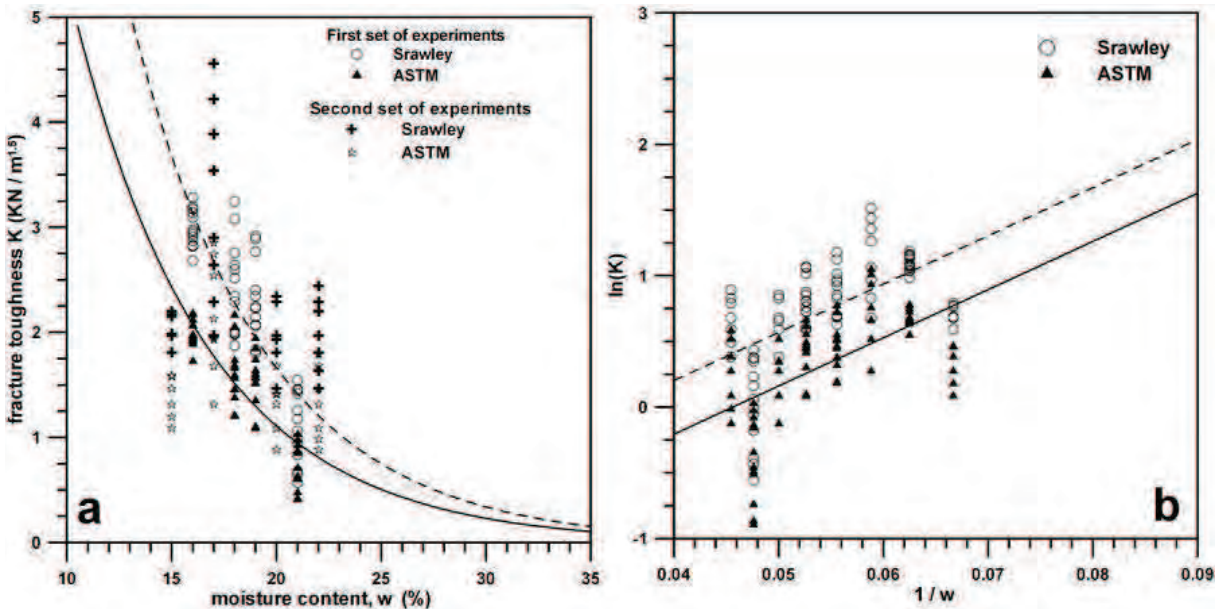

Figure 4.52: Experimental results and theoretical formula for the effect of moisture content on fracture energy: (a) fracture toughness versus moisture content at temperature T (21±0.5°) and (b) linear regression line

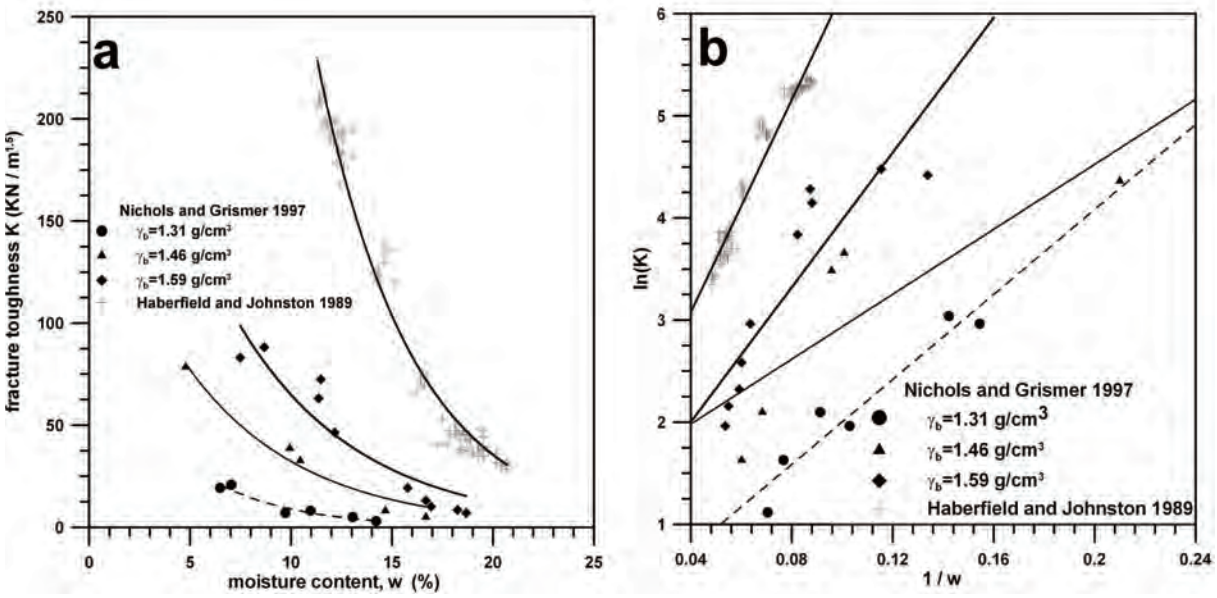

Figure 4.53: Experimental results and theoretical formula for the effect of moisture content on fracture energy for a soil (Nichols and Grismer [Nichols and Grismer, 1997]) and rocks (Haberfield and Johnston [Haberfield and Johnston, 1989]): (a) fracture toughness versus moisture content and (b) linear regression line

majority of cracks appear and develop for moisture contents between these two limits. So, for the physical relevance of the regression line in figure 4.52b for soils has to be limited between the liquid limit and shrinkage limit of the soil. Figure 4.53a and b show the experimental data (for a soil and a rock) and linear regression in support of the present theory to explain the variation of fracture toughness with moisture content. It can be observed that the data points follow a similar tendency.

Initiation and propagation of cracks in soils are complicated mechanisms, involving number of interconnected parameters different from that of other brittle materials. Other unique feature of soils is the change in state from, liquid to plastic, plastic to formation of peds or granular material, involving lot of volume change not observed in other materials. The present study was done keeping in mind the applicability of LEFM (linear elastic fracture mechanics), which is generally applicable to brittle and quasi-brittle materials. The present study also gives an insight in to the other material parameters to be considered when applying the standard theories of LEFM. In the preset case the effect of moisture content was considered, this type of analysis for concretes considering the effect of temperature was done by [Bažant and Prat, 1988].

4.4 Relationship between tensile strength and fracture toughness for (natural) geo-materials

4.4.1 Introduction

Fracture toughness is an important mechanical material parameter in LEFM, which reflects the ability of the material to resist fracture failure under Mode-I load conditions. This material mechanical parameter can be correlated with other material mechanical parameter such as tensile strength. Haberfield and Johnston [Haberfield and Johnston, 1989] determined the fracture toughness and tensile strength of soft rocks and correlated each other. In this section a compilation of data from available literature for soils and rocks and an empirical relation is given to relate fracture toughness and tensile strength.

Although Haberfield and Johnston gave the correlation, they did not propose any empirical relation. Zhang [Zhang, 2002] gave an empirical relation for rocks, proposing a linear relation between the two parameters. In this study power-law relation is proposed instead of a linear one because the relation is linear only over a small range of the moisture contents, whereas it is not linear for a broader ranges of moisture contents. In fracture mechanics the square of the ratio of fracture toughness to tensile strength $(K_{IC}/\sigma_t)^2$ is

used as both an indicator and a basis for estimating a minimum specimen size for the determination of plane strain fracture toughness. In general, the higher the ratio, the higher the ductility and the larger the specimen size required.

4.4.2 Rocks

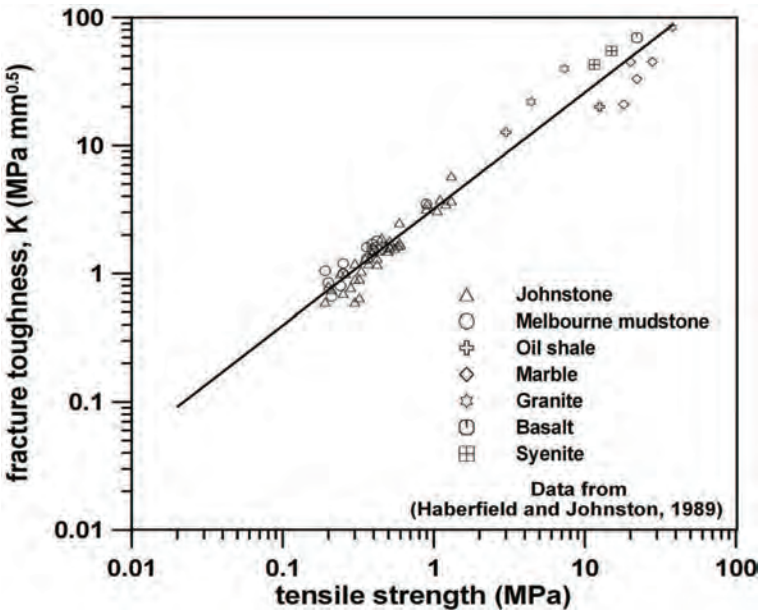

Figure 4.54: Relation between fracture toughness and tensile strength for rocks

The data from Haberfield and Johnston [Haberfield and Johnston, 1989] for a wide range of different types of rocks is plotted in figure 4.54. An empirical relation between K_{IC} and σ_t for rocks (equation 4.60) can be obtained by fitting power law relation to the experimental data.

$$K_{IC} = 3.208\sigma_t^{0.909} \quad \text{and} \quad R^2 = 0.962 \tag{4.60}$$

where, R is the sum of the residual squares. From figure 4.54 the ratio $(K_{IC}/\sigma_t)^2$ is approximately 9 for harder rocks and around 11 for the Johnstone and Melbourne mud stone.

4.4.3 Soils

Figure 4.55 shows the relation between tensile strength and fracture toughness for various soils. The fracture toughness for these soils was determined either by CT specimens or SENB specimens. Equations 4.61 and 4.62 give the empirical relations obtained. The ratio $(K_{IC}/\sigma_t)^2$ ranges from 20 to 500.

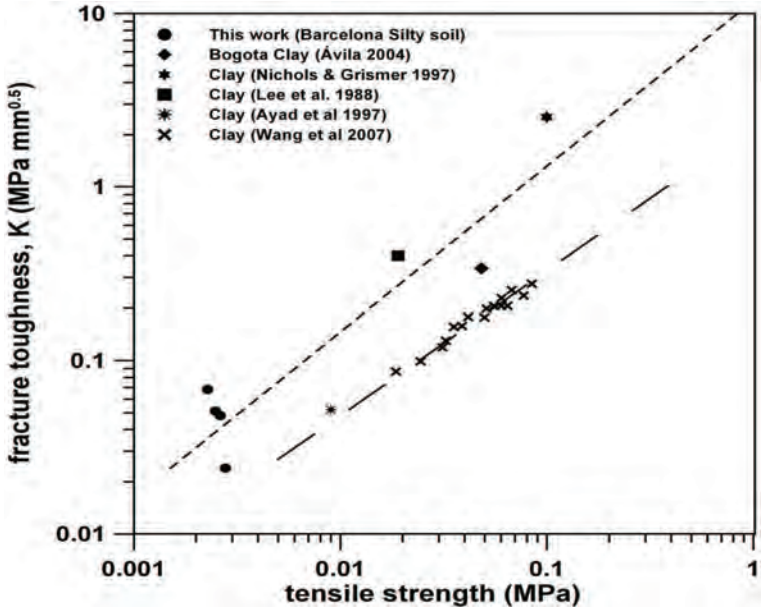

Figure 4.55: Relation between fracture toughness and tensile strength for soils

$$K_{IC} = 11.819\sigma_t^{0.954} \quad \text{and} \quad R^2 = 0.832 \tag{4.61}$$

$$K_{IC} = 2.238\sigma_t^{0.834} \quad \text{and} \quad R^2 = 0.92 \tag{4.62}$$

Figure 4.56 show the relation between tensile strength and fracture toughness for a soil which was determined by a ring test([Harison et al., 1994]) and the other data plotted is for a frozen soil (Li and Zhu, 2002; after [Wang et al., 2007]). Equation 4.63 gives the empirical relations obtained. The ratio $(K_{IC}/\sigma_t)^2$ ranges from 0.5 to 4.5. As these tests were not conducted with usual specimens adhering to LEFM norms, no conclusions are drawn on the ratio $(K_{IC}/\sigma_t)^2$.

Finally, figure 4.57 show a summary of the relation for natural geomaterials, where the difference between rocks, soft-rocks, and soils can be appreciated.

$$K_{IC} = 0.738\sigma_t^{1.202} \quad \text{and} \quad R^2 = 0.906 \tag{4.63}$$

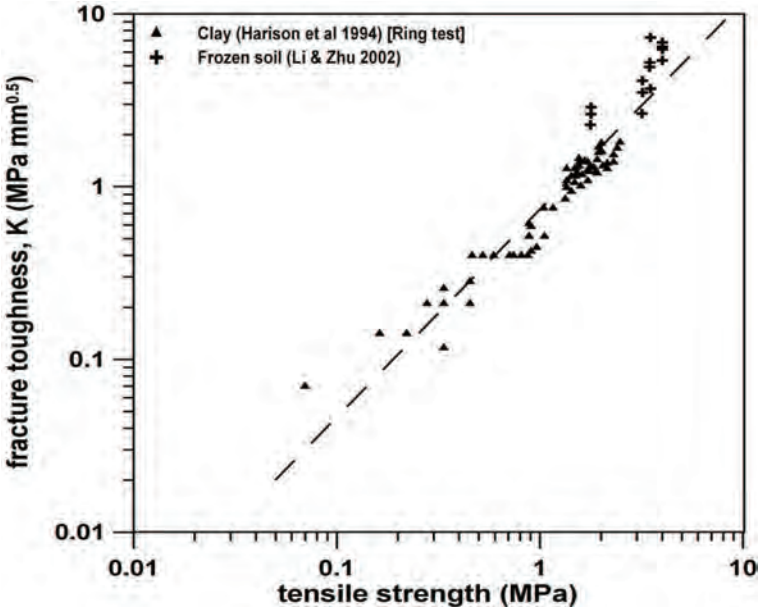

Figure 4.56: Relation between fracture toughness and tensile strength for frozen soil and data from Ring test

4.5 Conclusions

4.5.1 Tensile strength

Tensile strength of soils can be determined either by direct or indirect methods. In this study it was determined by a direct method. Moisture content and density of the soil influences considerably its tensile strength, which increases with increasing density of the soil. The effect of density is more pronounced for specimens with lower moisture contents than those with higher moisture content. Experimental results showed that tensile strength does not increase with increasing suction, but reaches a peak and then reduces with further increase in suction. The load-deformation curves clearly show the transformation of soil stiffness with reduction in moisture content. The theoretical model to estimate the tensile strength from the effective cohesion of an unsaturated soils seems to capture the trend of experimental data very well.

4.5.2 Fracture toughness

Fracture toughness was determined using CT specimens for different moisture contents. Fracture load decreases with increasing initial crack length irrespective of the moisture content, which is in agreement with other studies on concrete and metals. The fracture

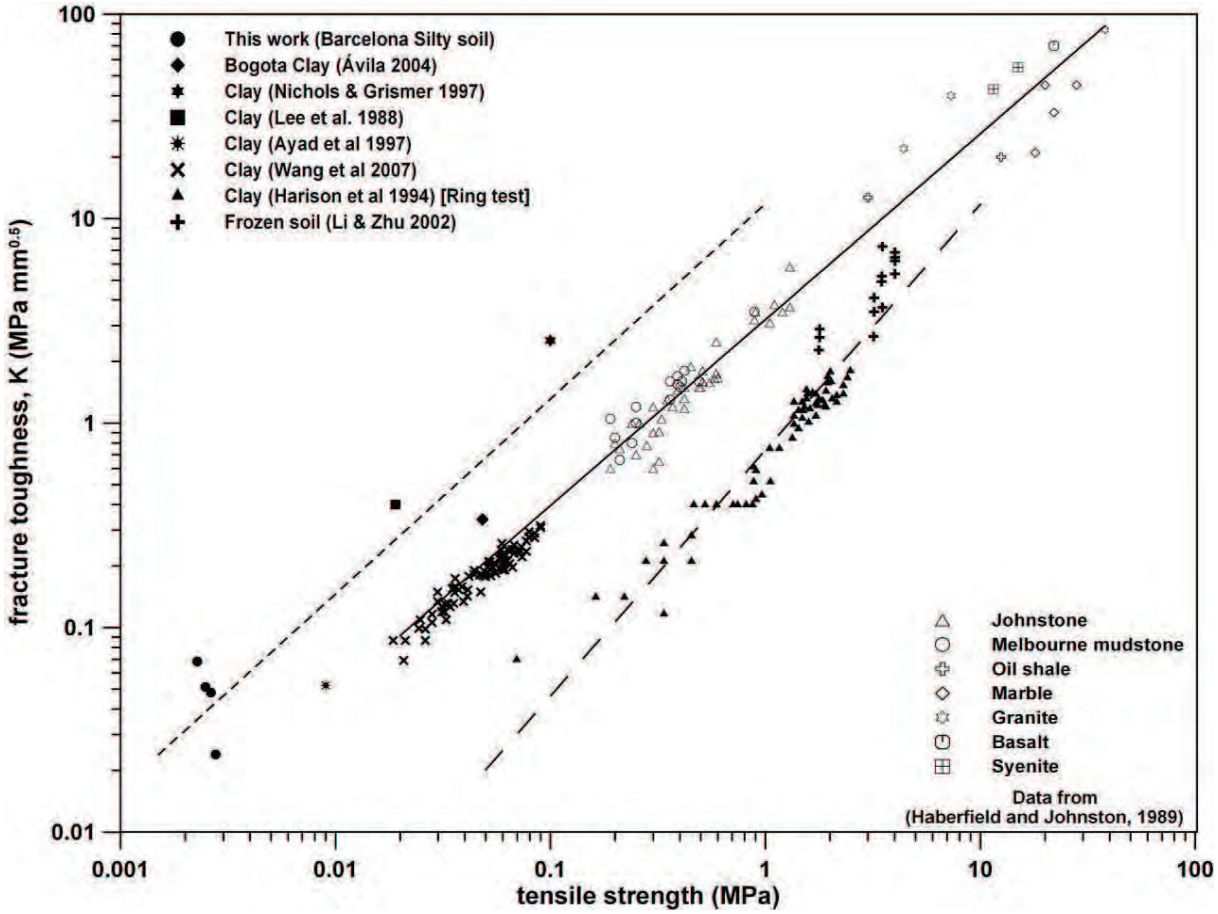

Figure 4.57: Relation between fracture toughness and tensile strength for geo-materials

energy, which is a material constant, can be considered as constant for a given moisture content, though there is a little scatter. Fracture toughness increases with decreasing moisture content until the plastic limit is reached. Further decrease in moisture content results in a decrease of fracture toughness. The theoretical model proposed using the activation energy and rate process theory for soils can be used if a relation between the activation energy and the soil suction is established. In view of very few experimental data available on fracture parameters of soil with effect of moisture content, the present study can be a good reference for the further exploration.

4.5.3 Relation between tensile strength and fracture toughness

There appears to be a strong correlation between fracture toughness and tensile strength. Therefore, a reasonable estimate of the fracture toughness may be obtained if the tensile strength is known. The empirical relations proposed fit reasonably well with the experimental data. This relation seems to be of power-law type, rather than a linear one as

reported in some published literature. In general, the higher the ratio $(K_{IC}/\sigma_t)^2$ higher the ductility, hence larger the specimen size required. The higher values of ratio $(K_{IC}/\sigma_t)^2$ observed for soils indicate that the size of the specimen used may not be sufficiently big.

Chapter 5

Desiccation of thin soil layers

5.1 Introduction

Cracking in soils is a complex phenomena involving physical, chemical, mechanical and hydraulic parameters of soil with respect to its surrounding geo-environment. Cracks develop in soils as they dry to form a complex, random but unique pattern. Apart from the above mentioned parameters the mechanism is also controlled by physical boundary conditions imposed/existing. A single or several cracks can initiate at the same time in the initial stages of drying. As the process continues several new secondary cracks are formed in existence to the earlier primary cracks which are propagating and widening. Desiccation rate and/or desiccation coefficient are two important parameters which indicate the state of desiccation of the drying soil, which in turn depends on the rate of change of moisture content during drying. Moisture content is a direct indication of suction and tensile strength of soil, which are other two key parameters if we want to explain the stress state inside the soil.

Presence of cracks strongly affects the mechanical and hydraulic properties of soil mass. The mechanism of crack formation needs a thorough systematic study taking in to consideration the parameters which govern them. Experimental investigation to study this phenomenon has been an object since early (Corte and Higashi [Corte and Higashi, 1960]) to the present day (Ávila [Ávila, 2004]; Nahlawi and Kodikara [Nahlawi and Kodikara, 2006]; Rodríguez et al. [Rodríguez et al., 2007]). Most of the experiments conducted earlier were for a single geometrical shape of the drying specimen with varying the thicknesses. The effect of different geometrical shapes or boundary conditions have never been the object of study, though they play an important role. The effect of thickness of drying

soil on parameters such as, cracking moisture content, desiccation speed, desiccation coefficient, crack width, and spacing has been widely published. But the final crack pattern has never been dissected to show-up its properties.

In this chapter the results of the laboratory experiments with circular and rectangular specimens are presented. These tests were devised to show the effect of boundary conditions (size, shape and aspect ratio of the trays) on the process of initiation and propagation of cracks and final crack pattern at the end of desiccation.

Circular trays of thicknesses 4, 8 and 16 mm and with three different bottom surface were tested. Two series of tests were carried out with rectangular trays, first with different sizes (11 in totally); aspect ratio and thickness (10 and 15 mm), second with five geometrically similar sizes with two different thicknesses (10 and 20 mm). All the specimens were subjected to drying conditions in a laboratory controlled environment. The results obtained are consistent with the available literature. Desiccation rate and coefficient is known to vary with thickness, but here the effect of surface area of drying and thickness is presented.

5.2 Holding trays

Figure 5.1 shows a schematic diagram to the scale, the shape and size of all the specimens. Three series of tests were performed, C corresponds to the first series of tests, 1 to 7 corresponds to the second series of test and A0 to A4 to third series.

5.2.1 Circular specimens - First series (C)

The first series of tests consisted of circular specimens of 22.5 cm in diameter (C; see figure 5.1 and table 5.1) and three different thicknesses: 4, 8 and 16 mm. Also a set of tests with same thickness (8 mm) were performed with three different roughness of the contact surface between the soil sample and the holding plastic tray; smooth, with circular grooves, and with a square grid pattern. These experimental series were designed to extend the previous research conducted with the same type of circular samples (Lloret et al. [Lloret et al., 1998]; Rodríguez [Rodríguez, 2006]; Rodríguez et al. [Rodríguez et al., 2007]), to include crack pattern analysis.

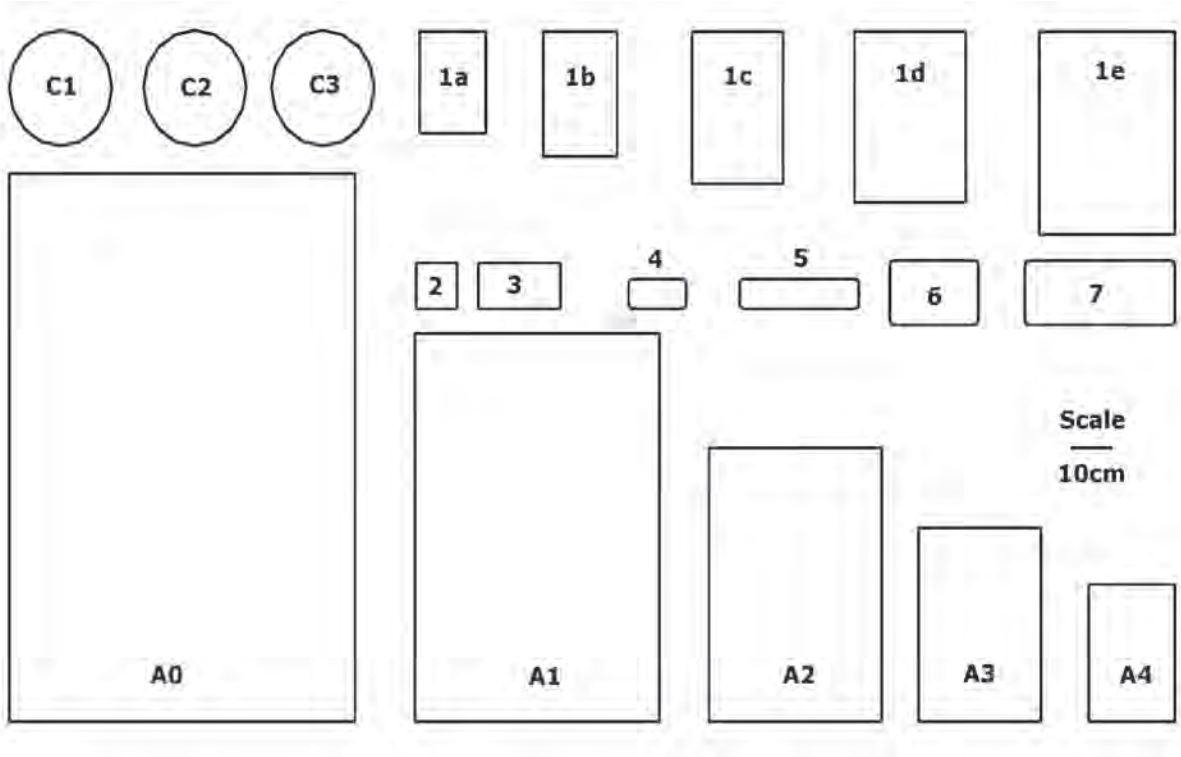

Figure 5.1: Schematics showing the geometry of all the specimens tested

5.2.2 Rectangular specimens of different geometry

The second series of tests was carried out with rectangular samples of different size, aspect ratio and thickness. Test No. 1 is a sequence of five geometrically similar, 10 mm-thick samples with aspect ratio approximately 1.5 and increasing size from 350 cm^2 to 1450 cm^2. Tests No. 2-7 were carried out on three specimens each, with different geometric parameters. Specimens for Tests No. 2 and 3 had a thickness of 10 mm, whereas specimens for Tests No. 4-7 had a thickness of 15 mm. The complete geometric characteristics of the specimens for each test are given in Table 5.2. Because the available laboratory trays were not all equal, the specimens had different cross-sections (trapezoidal, square and rounded bottom edges) as depicted in Figure 5.2. A posteriori this was seen to introduce an extra factor affecting the cracking mechanisms, indicating that laboratory experiments are very much influenced by the boundary conditions and thus leading the way to larger-scale experiments (third series), where the effect of the boundaries will influence less the overall behaviour.

Figure 5.2: Cross section of the holding trays for all tests with rectangular specimens with different geometry

5.2.3 Rectangular specimens of similar geometry

The third series of test specimens consisted of five geometrically similar rectangles of aspect ratio and surface area of 1, 0.5, 0.25, 0.125 and 0.0625 m2 (A0 to A4; see figure 5.1 and table 5.3) in two series of different thickness (10 and 20 mm), subjected to drying conditions in a laboratory controlled environment. The holding trays were made of PVC sheet, and they were glued to wooden base to give the rigidity for handling and placement over the load cell. The wooden base was coated with water-resistant paint.

5.3 Specimen preparation and experimental condition

The soil was allowed to dry in open air and then passed through a mechanical sieve (size 2 mm). The dry material that passed through was then mixed with distilled water until a visibly homogeneous paste was obtained. The prepared soil paste then was poured in the test trays, and small blows were given to the edge of the trays to remove air pockets. The surface of the sample was levelled with a straight edge to get a uniform surface. The soil left on the straight edge was taken to determine the initial moisture content. This procedure was repeated for all the specimens tested. For the first and second series of tests the soil paste was prepared one time and the tests are done simultaneously, where as for the third series the tests were done one specimen after another requiring the soil paste preparation separately for each specimen.

5.3.1 First and Second series

Soon after the placement and leveling of the surface, the samples were weighed to an accuracy of 0.01 g, and placed on a level surface in the environment-controlled room. The weight of the samples was recorded at 30 minutes intervals for the first 24 hours and at

one hour intervals for the remaining period until there was no further change in weight. During the process, the samples were monitored carefully to capture the most relevant features such as the onset of first crack, separation of the soil from the edges of the trays, etc. Photographs were taken at the end of each test, to be used for image analysis. All tests of both series were conducted in a laboratory room with controlled temperature and relative humidity fixed at 21 ± 0.5°C and 52 ± 2% respectively. The initial water content of first and second series were 30 ± 0.5% and 26 ± 0.5% respectively.

5.3.2 Third series

In this series after pouring and levelling of the surface, the samples were placed over three load cells to record the loss of weight at one-minute intervals. A digital camera was positioned directly above the tray to obtain images of the sample at three-minute intervals, to be used for image analysis after the conclusion of the experiments. The experiments were conducted inside an environment-controlled room with temperature and relative humidity fixed at 21± 0.5°C and 52± 2% respectively. The initial water content of the specimens was 24.5± 1%. During the process, the samples were monitored carefully to capture the most relevant features such as the onset of the first crack, separation of the soil from the edges of the trays, and reaching of the fully cracked and fully dry states. This series of tests were conducted to determine the existence of size effect in soil cracking (details in the chapter on size-effect).

5.4 Observations and Morphology of crack pattern

5.4.1 Circular specimens

The first preliminary series of tests with circular samples served to show in a qualitative manner the basic dependencies of the cracking pattern on specimen size and on boundary conditions. Figure 5.3 shows the final crack pattern of samples of varying thickness (4, 8 and 16 mm) with a rough contact surface between the sample and the holding tray. As expected, the spacing and width of the cracks, and the area of cracked cells, increase with the thickness of the sample. Figure 5.4 shows the final crack pattern of 8 mm-thick samples with varying boundary conditions (smooth, rough with circular grooves, rough with square grid). This figure shows that a smooth contact surface results in smaller width and spacing of the cracks (and therefore, a larger number of cracked cells) than the rough contact surfaces. There seems to be no noticeable difference between the cracked

pattern obtained with the two different types of rough contact surface (circular grooves and square grid).

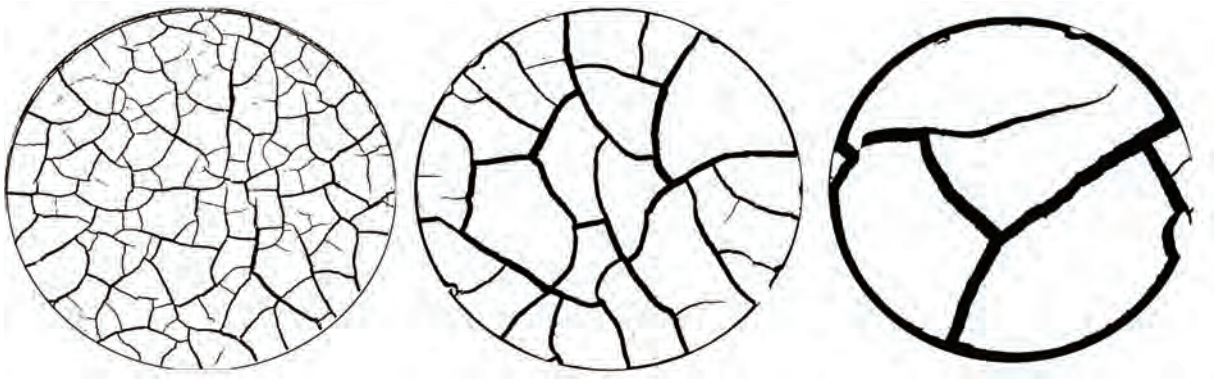

Figure 5.3: Final crack pattern for circular specimens of different thicknesses with circular groove bottom (not to scale)

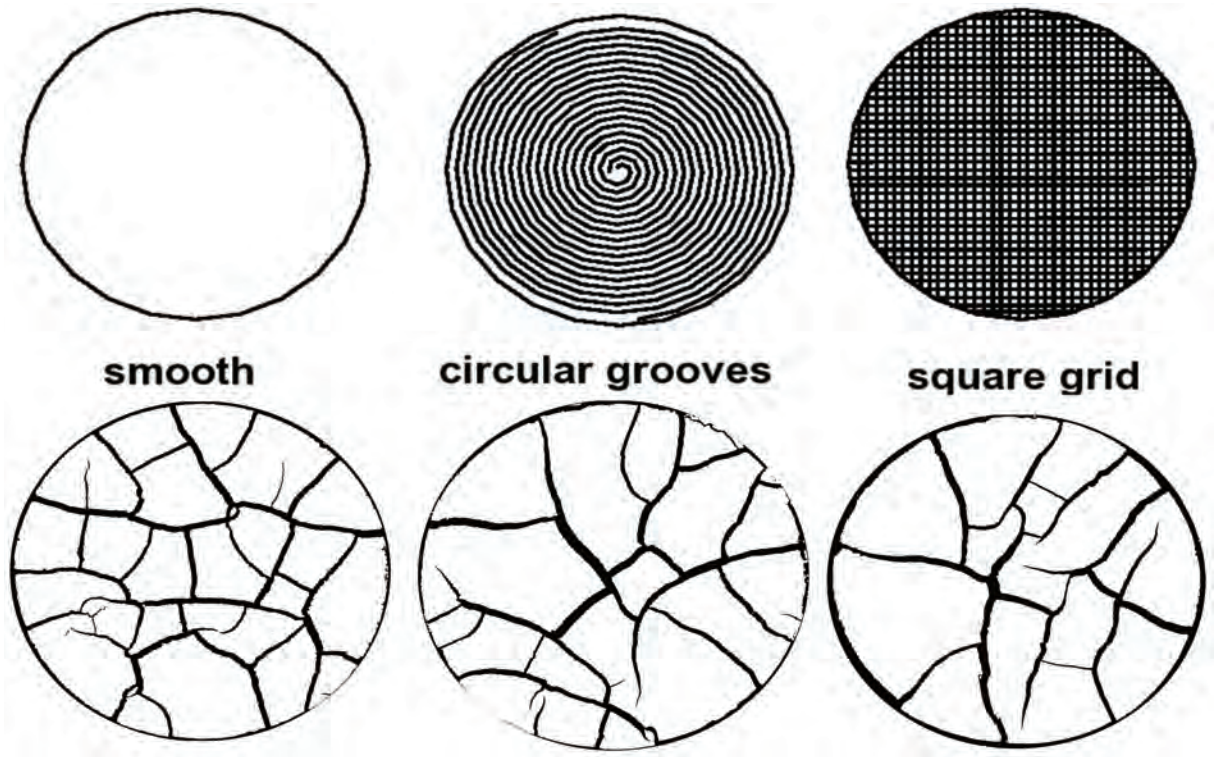

Figure 5.4: Schematic diagram of different contact surfaces and final crack pattern for circular specimen of 8 mm thick (not to scale)

Table 5.1: Specimen geometry and main results form image analysis for circular specimens

Test	nominal area of specimen (cm^2)	thick-ness (mm)	number of cells	average area of cells (cm^2)	average width of cracks (mm)	length of cracks per unit area (cm^{-1})	surface shrinkage (CDF) (%)
$C-4$	398	4	98	3.58	0.112	1.05	11.73
$C-8$	398	8	21	15.31	0.250	0.55	19.16
$C-16$	398	16	6	53.20	0.460	0.32	19.75
$C-Plain$	398	8	25	12.64	0.370	0.56	20.58
$C-Circ$	398	8	19	17.82	0.385	0.52	19.92
$C-Grid$	398	8	12	25.62	0.440	0.46	20.21

5.4.2 Rectangular specimens of different geometry

Figure 5.5 (1a to 1e) shows the crack pattern obtained in the five specimens of Test No. 1 that had approximately the same aspect (length-to-width) ratio. Figure 5.5 (2 - 3) shows the crack pattern obtained in Tests No. 2 and 3, with aspect ratios of 1 and 2 respectively. The above tests had a thickness of 10 mm. Figure 5.5 (4 to 7) shows the crack pattern obtained in Tests No. 4 to 7; all specimens in these tests had a thickness of 15 mm, and varying aspect ratios from 1.5 to 4.5

A first look at Figures 5.5 shows a significant difference between the 10 mm (Tests No. 1-3) and the 15 mm-thick (Tests No. 4-7) specimens: although because space limitations Figure 5.5 (1a to 1e) is presented at a smaller scale than the other two, the evidence shows that the cracked cells are smaller (and therefore the relative number of cells larger) for specimens with a lower thickness.

This was of course expected after the results from the preliminary tests with circular specimens. Closer inspection of these figures show that specimens with trapezoidal (Test No. 1) or rounded (Tests No. 4-7) bottom edges become completely separated from the tray walls during the process of drying, thus increasing the effective area where moisture can be lost. However, specimens with perfectly square (Tests No. 2-3) bottom edges do not separate, and cracking occurs in the bulk of the specimen, without formation of a perimeter crack and therefore preventing moisture loss across the sides of the specimen.

Table 5.2: Specimen geometry and main results form image analysis for rectangular specimens of different geometry

Test	nominal area of specimen (cm^2)	thick-ness (mm)	aspect ratio	number of cells	average area of cells (cm^2)	average width of cracks (mm)	length of cracks per unit area (cm^{-1})	surface shrinkage (CDF) (%)
1a	352	10	1.5	48	6.7	1.06	0.762	8.1
1b	486	10	1.5	43	10.2	1.13	0.832	9.4
1c	726	10	1.5	66	10.1	1.28	0.674	8.6
1d	999	10	1.5	126	7.3	0.95	0.871	8.2
1e	1452	10	1.5	158	8.4	1.08	0.753	8.2
2	100	10	1.0	22	7.1	1.02	0.867	8.9
3	200	10	2.0	30	6.0	1.20	0.753	9.0
4	91	15	2.0	12	6.9	1.94	0.646	12.4
5	188	15	4.5	15	11.9	2.06	0.633	13.0
6	301	15	1.5	10	26.5	4.26	0.352	14.4
7	511	15	2.0	21	20.5	3.43	0.415	14.2

5.4.3 Rectangular specimens of similar geometry

This series of tests were constantly monitored by digital camera since the beginning till the end of the tests. Figure 5.6 shows the final crack pattern for all the specimens, once again the effect of thickness can be clearly distinguished at first look. The specimens got separated from the edge only in tests A4 for both thicknesses. Location of appearance of first crack was random, but never in the middle of the specimen and the drying pattern was from edges towards the centre. Time for the appearance of the first crack varied depending on the size and thickness of the specimen, no clear tendency was observed with respect to the size of the specimen, but it was less for 10 mm than for 20 mm specimen. The cracks were usually vertical in depth, and this may be due to the small thickness of the desiccating specimen. Sequential observation of the digital photos revealed that the three important mechanisms of initiation, propagation, and intersecting of cracks occurred simultaneously. Another mechanism observed was a hierarchy in the crack pattern formation. The primary cracks were the first to form, followed by the secondary and tertiary, some cases quaternary. The primary cracks can be identified in test A0 of 20 mm thick sample, where primary cracks are wider than other cracks. Secondary cracks formed between two primary cracks while the primary crack/s still propagating, similarly in the case of tertiary cracks (especially in the case of tests A0 to A3 of 10 mm thick sam-

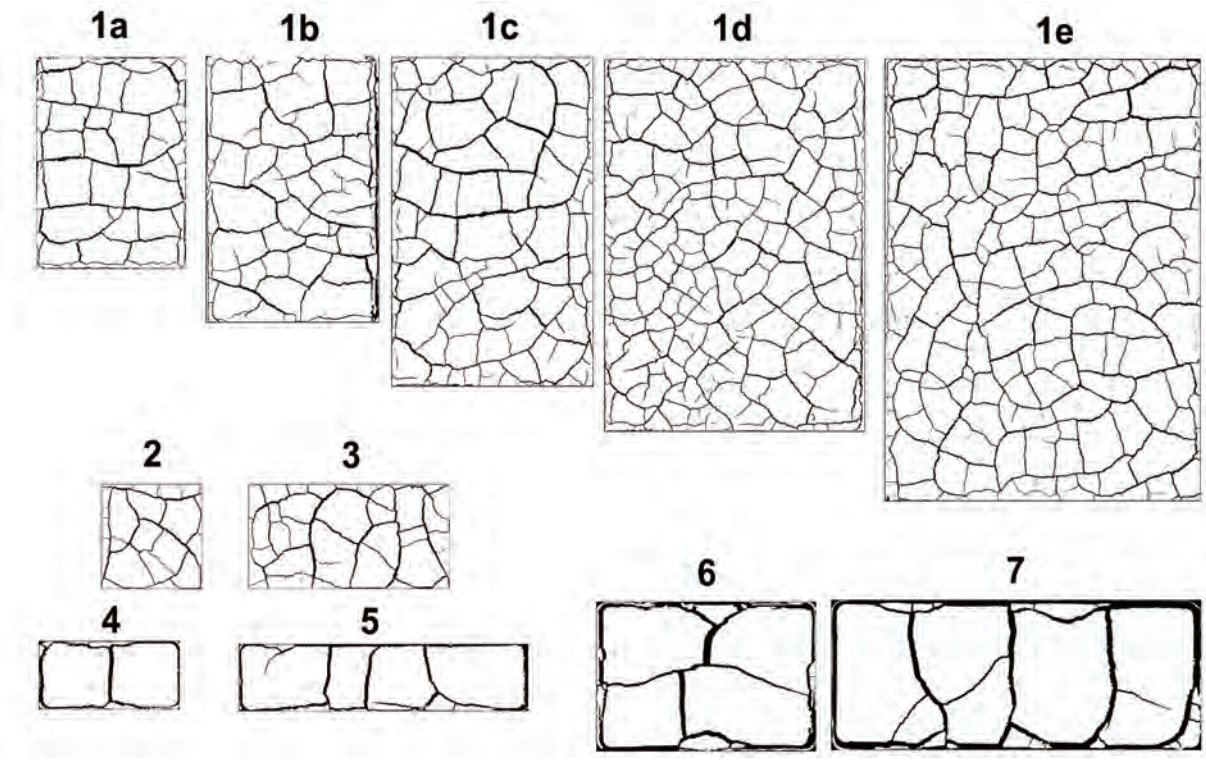

Figure 5.5: Final crack pattern for rectangular specimens of second series (Tests 1 to 7) (not to scale)

ple). Some cracks which initiated lately stopped propagating leaving a dead-end crack with out intersecting. A close observation of the crack pattern (figure 5.6) showed that majority of the cracks are at right angle to the edges. A detailed image analysis of the crack pattern showed that the majority of the cracks intersect at right angle (see section 8.4.3 of Chapter 8). Orthogonal angles (between 80° - 100°) are formed due to tensile failure and non orthogonal angles ($< 80°and > 120°$) due to shear failure (Hartge and Bachmann [HARTGE and BACHMANN, 2000]).

5.5 Moisture loss, Desiccation rate and Coefficient

Another important aspect to consider in the investigation about the mechanics of cracking in soils is the changes in moisture content of the specimen during drying. During the tests, this was monitored by weighing the specimen and recording the weight, from which the loss of moisture can be deduced. For the first and second series of experiments the moisture loss was monitored manually, whereas for the third series, load cells connected to a data acquisition system was used. The desiccation rate and coefficient were calculated using the modified definition from Nahlawi and Kodikara [Nahlawi and Kodikara, 2006]

Table 5.3: Specimen geometry and main results form image analysis

Test	nominal area of specimen (m^2)	thick-ness (mm)	area of un-cracked material (cm^2)	surface shrink-age (CDF) (%)	number of cells	average area of cells (cm^2)	total length of cracks (cm)	average width of cracks (mm)	length of cracks per unit area (cm^{-1})
$A0-10$	1.0000	10	8828.69	11.71	1272	6.94	7280.76	1.61	0.73
$A1-10$	0.5000	10	4460.48	10.79	466	9.57	2746.49	1.95	0.55
$A2-10$	0.2500	10	2208.29	11.67	219	10.08	1460.33	1.96	0.58
$A3-10$	0.1250	10	1135.96	9.12	95	11.96	560.26	1.99	0.45
$A4-10$	0.0625	10	577.22	7.64	34	16.98	232.92	2.00	0.37
$A0-20$	1.0000	20	8850.88	11.49	249	35.55	2793.85	4.11	0.28
$A1-20$	0.5000	20	4333.98	13.32	109	39.76	1545.88	4.28	0.31
$A2-20$	0.2500	20	2176.31	12.95	53	41.06	668.24	4.77	0.27
$A3-20$	0.1250	20	1068.88	14.49	25	42.46	342.08	5.22	0.27
$A4-20$	0.0625	20	545.50	12.72	12	45.46	110.91	7.05	0.18

considering the residual moisture content, over the original definition of Corte and Higashi [Corte and Higashi, 1960].

Figure 5.7a depicts the changes in moisture for the first series (circular specimens). The three specimens have three different thicknesses with same drying surface area. Desiccation rate coefficient increased as the thickness of the specimen decreased, clearly showing the effect of thickness (figure 5.7b), which is extensively reported in the literature (Corte and Higashi [Corte and Higashi, 1960]; Nahlawi and Kodikara [Nahlawi and Kodikara, 2006]). If the thickness increases with the same surface area of drying, it is logical that the rate of moisture loss decreases because moisture has to travel more distance for evaporation (Nahlawi and Kodikara [Nahlawi and Kodikara, 2006]). Another important observation made was that the soil thickness increased with a factor of 2 and the desiccation rate approximately decreased with a factor (1/2). As expected the three specimens reach the same final moisture content, but depending on thickness each specimen reaches this stage at different time, 4mm thick specimen being the first.

Figure 5.8 depicts the changes in moisture for the second series (rectangular specimens of different geometry). For tests No. 2-7 the results are the average of the three specimens used in each test. Figure 5.8 shows two groups of tests having different rate of moisture loss, but having the same final moisture content (residual moisture content of the soil at laboratory conditions). Filled symbols are for specimens of 15 mm thick and the unfilled

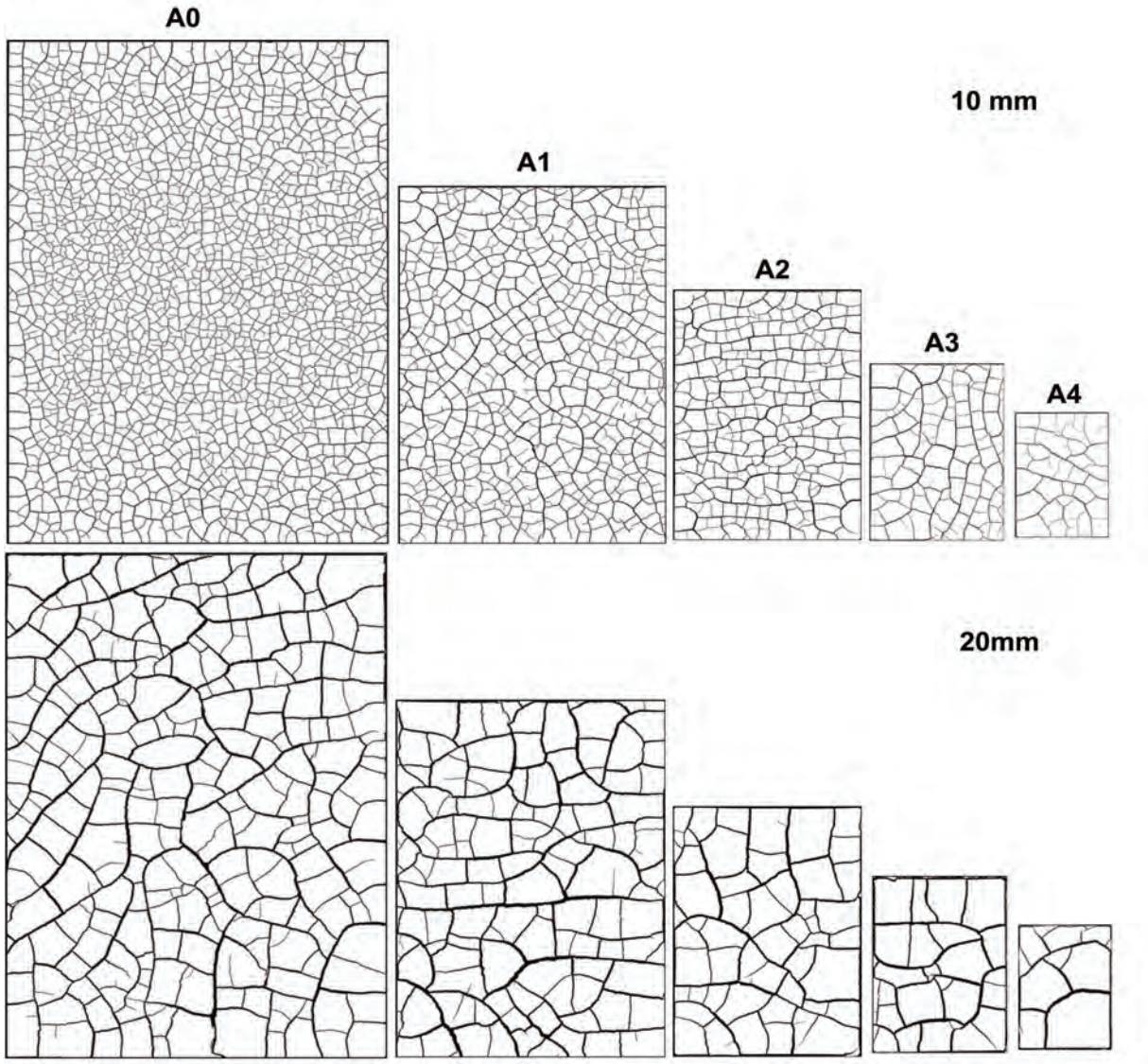

Figure 5.6: Final crack pattern for rectangular specimens of third series (Tests A0-A4) (not to scale)

for 10mm thick. The time taken to reach the final moisture loss ranges from about 75 hours to about 150 hours, depending on the specimen characteristics. The differences in the rate of moisture loss are more difficult to explain. For Tests No. 1a-1d, the rate is 0.29% per hour; for Tests No. 1e and 4, 0.24% per hour; for Tests No. 2, 3 and 5, 0.20% per hour and for Tests No. 6-7, 0.16% per hour. In this case the results suggest that mainly two variables affect the rate of moisture loss, the specimen thickness and its aspect ratio: thicker elements tend to lose water at a slower rate while specimens with larger aspect ratios tend to lose water at a faster rate. Generally, rate of moisture loss also increased with the increase in drying surface.

In the existing literature, desiccation rate coefficient is plotted against the thickness of the

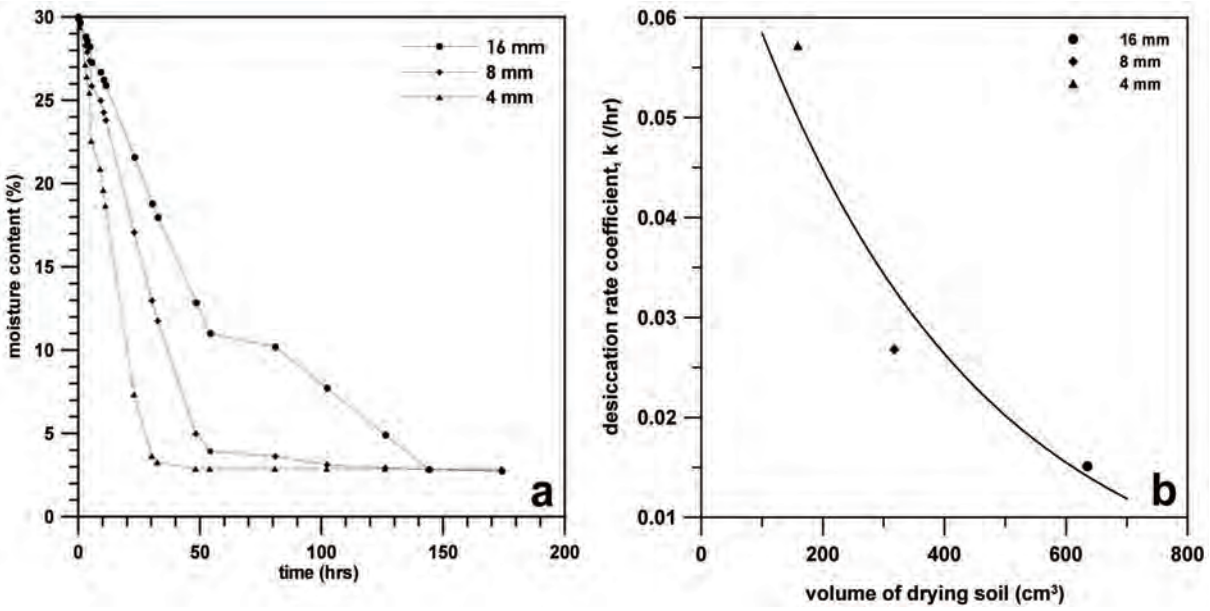

Figure 5.7: (a) Moisture loss with time for circular specimens, 4, 8 and 16 mm thick. (b). Desiccation rate coefficient for circular specimens of same drying surface area with different thicknesses

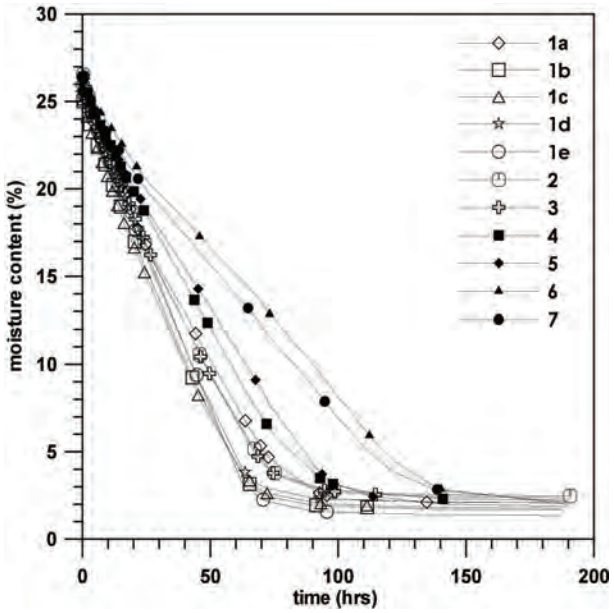

Figure 5.8: Moisture loss with time for rectangular specimens of different geometry, tests 1 to 3 is 10 mm thick and 4-7 is 15mm thick

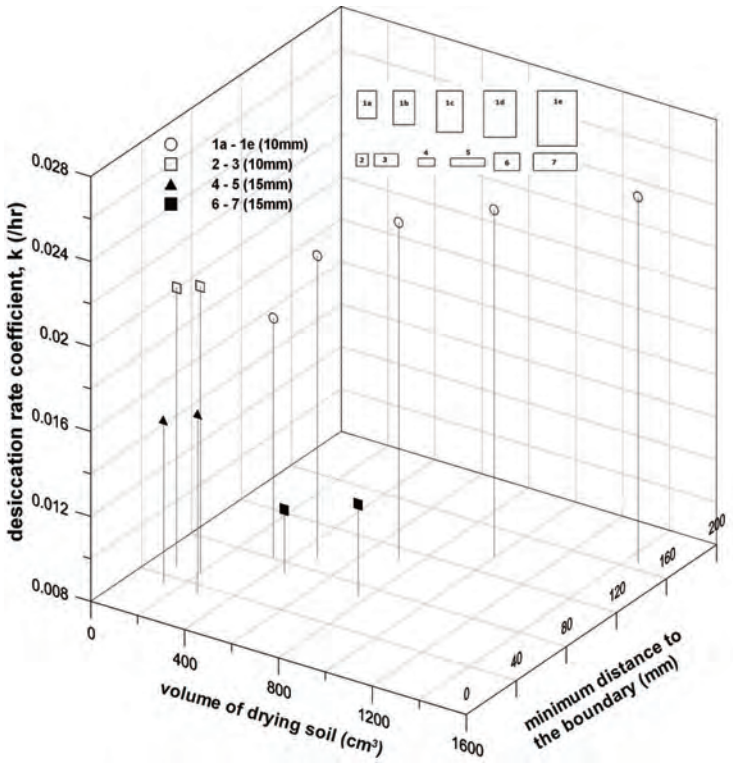

Figure 5.9: Desiccation rate coefficient for rectangular specimens of different geometry

drying soil, as most of the experiments have been performed by varying only thickness. In the present work, when the desiccation rates were calculated, the effect of thickness was evident but the surface area and shape of the specimens seem to affect as well. So, the desiccation rate was plotted considering all these parameters (Figure 5.9).

Second series of experiments, can be grouped based on their geometrical characteristics in to 4 groups, TEST 1, 2 - 3, 4 - 5 and 6 - 7. In Test 1 the area increment is by changing the both dimensions of the rectangle, whereas in rest of the tests is by changing only one dimension while keeping the other equal. For TEST 1, desiccation rate increases with increasing surface area and minimum distance to the boundary (unfilled circular symbols in fig 5.9). In rest of the experiments, while the respective minimum distance to the boundary does not change, the increase in area increases the desiccation rate. In all the tests the classical effect of thickness is clearly marked (filled symbols for 15mm and unfilled symbols for 10mm thick specimens in fig 5.9). Figure 5.10 depicts the changes in moisture for the third series (rectangular specimens of similar geometry). The figure shows two groups of tests having different rate of moisture loss: as expected, the thinner 10 mm-specimens reach equilibrium in about half of the time it takes for the thicker 20 mm specimens. After reaching equilibrium, there remains about 2% of water content that has not been removed by drying. This of course can be expected, since this is water that

could only be removed by forced drying in oven at high temperature.

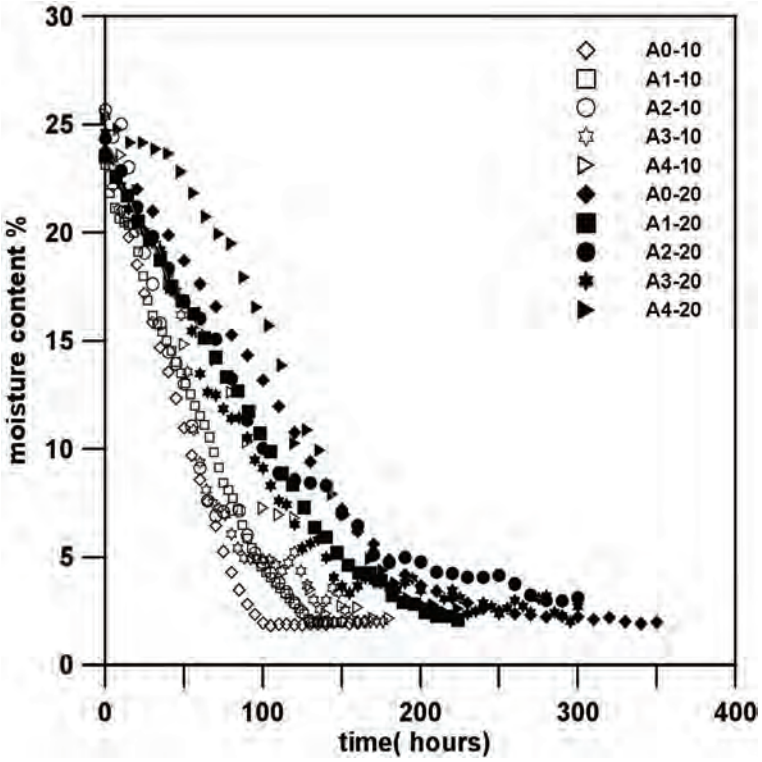

Figure 5.10: Moisture loss with time for rectangular specimens of similar geometry

In agreement with the second series of tests, the third series experiments showed a steady increase in desiccation rate as the area of the holding trays increased, which is more pronounced in 10 mm thick specimens (figure 5.11).

5.5.1 Why desiccation rate changes?

The variation of desiccation rate with the thickness is widely reported. In the present work apart from the thickness effect, the variations due to surface area (volume) of drying soil are also presented. But the basic question, why the desiccation rate changes, has to be answered. The time required to desiccate a soil of same thickness in two different environments is different, and a soil with different thickness in a similar environment is also different. Thus rate of desiccation, depth of drying soil and the environment have interdependence.

Moisture loss from the drying soil surface is by evaporation, which involves a change of state of water from liquid to vapour. For the process of evaporation to take place at a surface, there must be an input of energy to bring about this change of state. Thermal

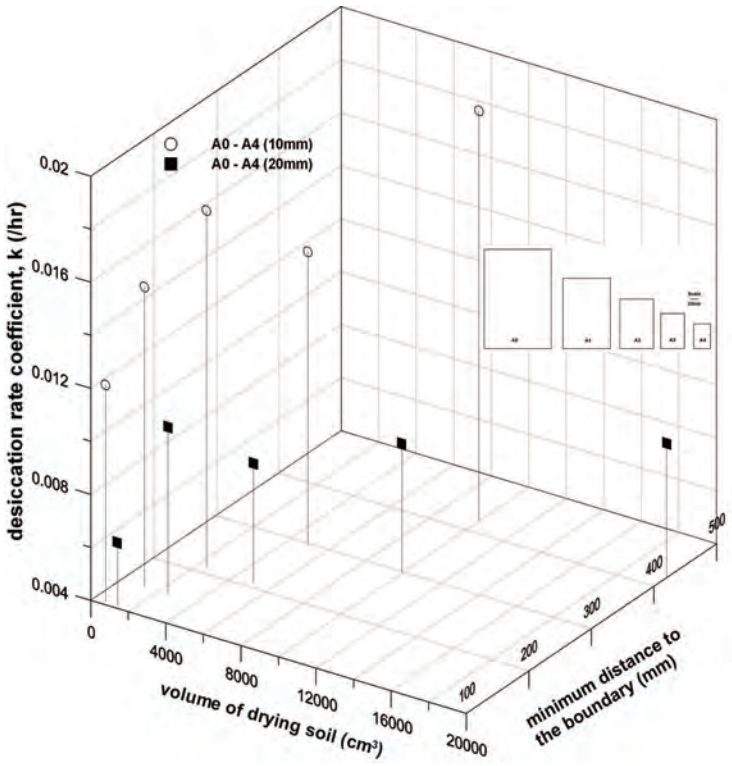

Figure 5.11: Desiccation rate coefficient for rectangular specimens of similar geometry

(heat) energy supplies the energy for the process of state change. Solar radiation is the source of thermal energy in the case of natural phenomenon. Latent heat and Sensible heat are important sources to be considered in the case of evaporation. Both these sources are expressed in terms of energy per unit square meter indicating dependence of surface area. The important bulk of exchange of the energy in case of soil drying takes place by Conduction, the transfer of heat energy by intermolecular contact, once again which depends on the drying surface area in question. With this background, now consider a drying surface (a) with a thickness (d) in an environment with temperature (t) and relative humidity (RH) or suction, which will dry at a desiccation rate coefficient (k). If the thickness is increased (2d), keeping rest of the parameters constant, the decrease in rate coefficient can be explained by the distance travelled by the water to the surface to get evaporated, but the increasing area (2a) keeping rest of the parameters, should increase the desiccation rate (more surface area more air particle to moist soil particle contact). No field data is available considering this effect. So, an attempt is made to explain the obtained laboratory test results. The experiments were conducted in a laboratory room with controlled environment. Considering uniform and constant distribution of temperature and relative humidity inside the room, one can assume that the latent heat and sensible heat available for the evaporation are constant. There was more surface area available for the conduction to take place with the increase in the area of the holding trays,

resulting in faster conduction and high desiccation rate. But, the experimental results (see figure 5.11) obtained were exactly the opposite. The possible explanation may be due to the effect of specimen size. The increase in specimen size has two effects: one, increase of drying surface area increases the desiccation rate; two, increase in specimen size increases the volume of drying soil which decreases the desiccation rate. Thus, if the effect of volume increment is more than the effect of surface area, then the overall desiccation rate decreases for a bigger specimen.

Higher desiccation rates for certain specimens (10 mm thick) of second series with lesser surface area than certain specimens (10 mm thick) of the third series were observed. Except for the initial moisture content (moisture content at the beginning of the test), rest of the test conditions were similar for both series. The initial moisture content of the second series is around 2% more than the third. This means more water was available in a relatively free state for evaporation. Hence water could escape more rapidly with the same available heat energy, so a higher rate of desiccation. The real effect of initial moisture content needs more specific studies. It is explained here as only possible explanation for the difference in desiccation rate observed.

5.6 Cracking moisture content

In the present study, cracking moisture content was determined by indirect method from the moisture loss vs. time curves assuming a uniform moisture loss throughout the drying surface. Cracking water content is considered as the water content at the time of appearance of first crack. It was observed that there was significant change in colour of the moist soil to that of completely dry soil (from the digital photographs, through visual observation, no measurement relating pixel intensity to the moisture content was made). No significant colour change took place at the initial stages of drying and until several primary cracks were developed, even if there was any, it was uniform over the surface. This indicated that the moisture loss was uniform over the surface in the initial stage of drying. Figure 13 shows the relation between the cracking water content and the desiccation rate coefficient for the third series of experiments. Only this test series was observed by digital camera, the other first and second series were not, so the digital photograph indicating the exact time of appearance of first crack was not available hence the cracking water content could not be determined.

Cracking water content is known to increase with the increase in the thickness of the drying soil layer (Corte and Higashi [Corte and Higashi, 1960]; Nahlawi and Kodikara [Nahlawi and Kodikara, 2006]; Rodríguez et al. [Rodríguez et al., 2007]) and also increase

as the desiccation rate coefficient decreases (Corte and Higashi [Corte and Higashi, 1960]; Nahlawi and Kodikara [Nahlawi and Kodikara, 2006]). Both the above two effects were observed in the present tests (figure 5.12). Decrease in the desiccation rate with the decrease in the drying surface (as described in the earlier sub section) is supported by the increase in the cracking moisture content.

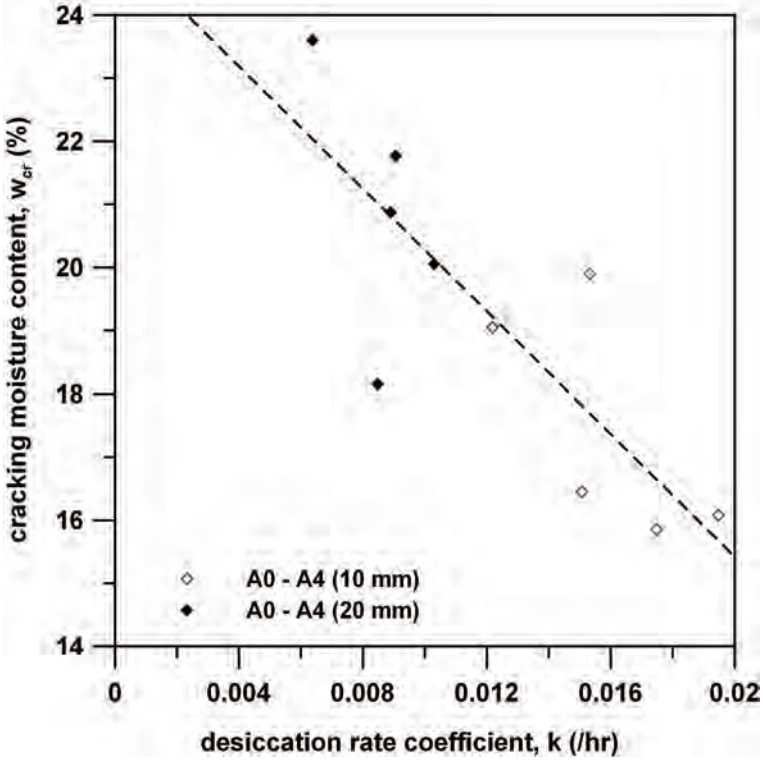

Figure 5.12: Cracking moisture content with desiccation rate coefficient for rectangular specimens of similar geometry

The hypothesis put forward by Nahlawi and Kodikara [Nahlawi and Kodikara, 2006] considering the dependence of cracking water content on the desiccation rate explained by Corte and Higashi [Corte and Higashi, 1960] is summarized here. The crack initiates by coalescence of micro cracks during desiccation. The initiation of a desiccation crack is considered as the probability of coalescence of a micro crack during a small time, which depends on the prevalent stress state at that particular small time. They say that this small time is low for a higher desiccation rate resulting in lower cracking water content. Concluding, higher tensile stresses are needed to initiate cracks when the desiccation rate is higher. In other words the rate of change of stress state is high when the desiccation rate is high.

The results from the chapter on tensile strength and fracture toughness can be used suitably to explain the above hypothesis. In the tensile strength vs. moisture content

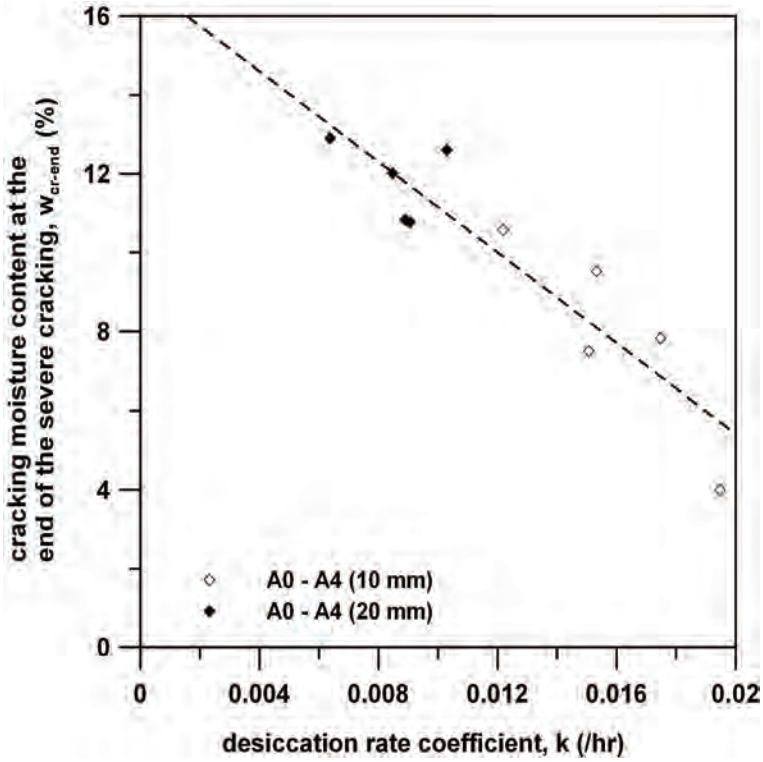

Figure 5.13: Moisture content at the end of severe cracking for rectangular specimens of similar geometry

curve, tensile strength peaked for certain moisture content, a decrease or increase of moisture content was observed with decrease in tensile strength. But the slope of decrease of tensile strength on either side was different; a steeper on the wetter when compared to the drier side, similar observation was made by other researchers (Tamarakar et al. [Tamrakar et al., 2005]; Rodríguez et al. [Rodríguez et al., 2007]; Favaretti [Favaretti, 1996]; Heibrcok et al. [Heibrock et al., 2003]). A steeper slope for tensile strength means faster tensile strength development for a small change in moisture content. Hence, a faster desiccation rate will certainly lower the probability of stress state to prevail over a small time. This indicates that for a soil drying from moisture content higher than the moisture content corresponding to its peak tensile strength, and then a higher desiccation rate will result in lower cracking moisture content. Peak tensile strength was observed around a moisture content of 20-21%, a careful observation of figure 5.12 shows that specimens with 20 mm thickness have cracking moisture content more than 20% and 10 mm thick specimens less than 20%. This gives a hint that the micro crack coalescence might have taken place at the same tensile strength but at different suction or desiccation stress, as suction keeps on increasing with drying process.

From the digital photographs it was observed that at a certain stage during the drying process, no major cracks initiated or propagated resulting in new crack surface. This

point is called end of severe cracking. First crack initiates at moisture content when the tensile stresses prevail sufficient enough time to nucleate a crack. Similar conditions should prevail at different moisture contents (obviously lesser than cracking moisture content) with higher tensile stresses to nucleate more cracks in a drying soil. Finally a point will be reached where further increase in tensile stresses will not nucleate a new crack; this point is the end of severe cracking. The figure 5.13 show the relationship between the desiccation rate coefficients to the moisture content at the end of the severe cracking stage. Results of only third series are plotted, as only this series of tests were observed digitally. In comparison to the cracking moisture content, the moisture content at the end of severe cracking as well decreases with increase in desiccation rate.

5.7 Effect of boundary condition on crack pattern

More detailed information about the mechanics of cracking requires a deeper look into the pattern structure of the crack network as it develops during drying. For that purpose, a public-domain image processing program, ImageJ Rasband [Rasband, 2005], is used. The raw data obtained from pictures taken with a digital camera has been processed with that software, obtaining several parameters that can be used to characterize the crack network: the number of cells into which the specimen is divided, the average area of those cells, their aspect ratio, the average crack width, the crack density factor (CDF) which is the ratio of the surface area of cracks to the total surface area of the soil (Miller et al. [Miller et al., 1998], also see Section 2.5.1.1 of Chapter 2), etc. The summary of the results of the image analysis are given in table 5.1, 5.2, and 5.3 for the 3 series respectively.

5.7.1 Crack density factor

CDF, or crack intensity factor (Miller et al. [Miller et al., 1998]), is used to characterize the extent of surface cracking. This parameter is defined as the ratio of total crack area to the total virgin surface area of the drying specimen. Note that CDF in this context must not be confused with a concept with similar name used in fracture mechanics. The CDF values for the first series of tests will be discussed in the next sub section. The results shown in table 5.2 indicate that, for the second series of tests, the single factor influencing the crack intensity factor is the specimen's thickness: average CDF for 10 mm-thick specimens is $CDF_{10(2)} = 8.63\%$ (s = 0.49), whereas for the 15 mm-thick specimens, $CDF_{15(2)} = 13.50\%$ (s = 0.96). Similar results were obtained for the third series of tests (table 5.3) indicate that the crack density factor depends on specimen's thickness: average

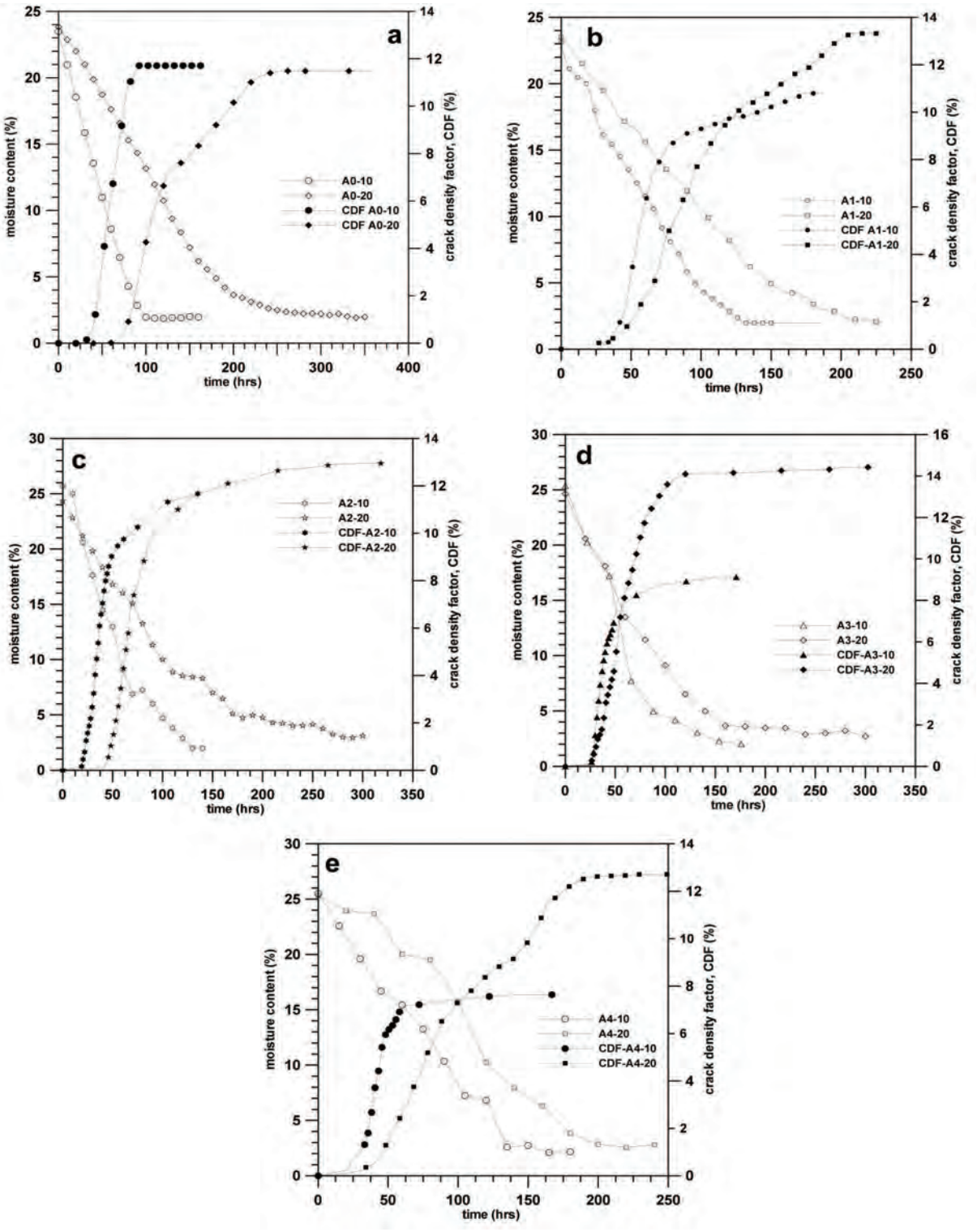

Figure 5.14: Moisture loss and crack density factor with time for rectangular specimens of similar geometry

CDF for 10 mm-thick specimens is $CDF_{10(3)} = 10.19\%$ (s = 1.77), whereas for the 20 mm-thick specimens, $CDF_{20(3)} = 12.99\%$ (s = 1.08), where s is the standard deviation. The difference in the CDF values of 10 mm thick specimens of second and third series of experiments can be attributed to the different initial moisture content and desiccation rate. From the digital photographs taken during the entire duration of the experiment for the third series of tests, some selected photographs were analysed to calculate the extent of crack growth. Figure 5.14 shows the evolution of crack density or area plotted with the evolution of moisture content. The key aspects of these curves is that, they give an overall picture of crack evolution, important stages in the crack pattern formation such as crack initiation, severe cracking period, rate of crack growth and end of cracking. The 20 mm thick samples have a milder slope when compared to the 10 mm thick sample, reflecting the desiccation speed which can be observed in the moisture loss curves as well.

5.7.2 Effect of bottom contact surface

Corte and Higashi [Corte and Higashi, 1960] studied the effect with two different bottom surfaces, wood and glass. The average area of cracked cells were lesser in glass bottom than in one with wood, suggesting, lesser the bottom surface friction smaller the area of cracked cell. Groisman and Kaplan [Groisman and Kaplan, 1994] did some experiments using glass bottom with Coffee-water mixture in order to model mud cracks occurring in nature. Three bottom surfaces were used, uncoated, coated with 2 mm of grease, and with 6 mm of Vaseline. They conclude that lower the bottom friction lower the crack formation. But, severe cracking was observed on uncoated surface when compared to the other two, and the Vaseline coated was more cracked than the grease coated though the bottom friction is less. This indicates that the friction between two soil layers can not be simulated by coatings. In the present work only circular specimens were tested with different bottom contact surfaces. The effect was not seen in CDF (20.58, 19.92, and 20.21 % for plain, circular grooves, and square grid respectively) of the final crack pattern; whereas the number of cracked cell is 25, 19, and 12 respectively and average area of cracked cells are 12.64, 17.82, and 25.62 cm^2 respectively. The smooth surface offered the least friction whereas the square grids the most. The bottom surfaces used in the present method introducing the friction by changing the surface characteristics of the same material seems to be more realistic.

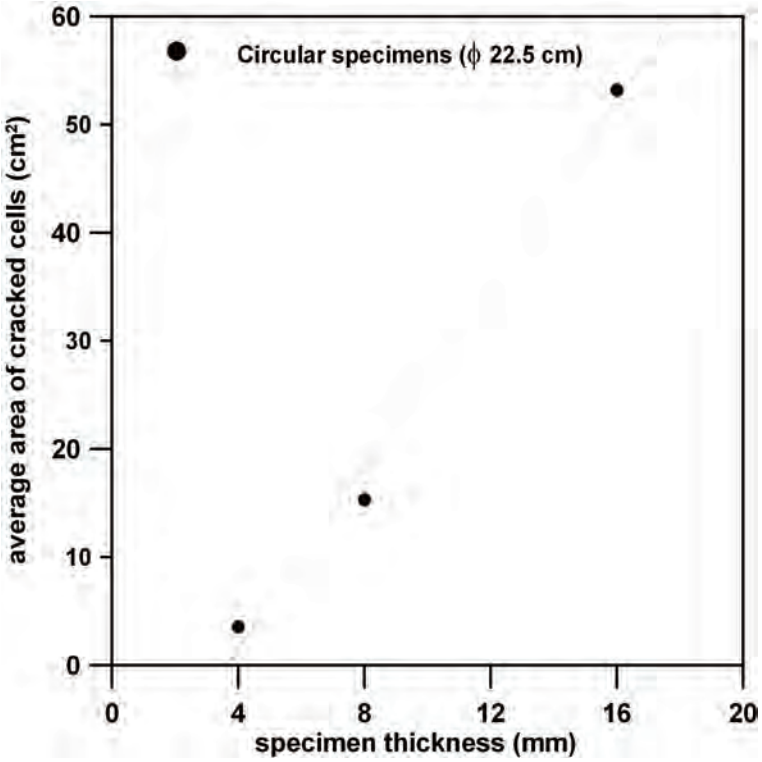

Figure 5.15: Average area of cracked cells for circular specimens

5.7.3 Effect on cracked cells and crack width

Area of cracked cells can be a substitute to the crack spacing measurement. In this paper we have adopted the average area of the cracked cells (AACC) as the standard instead of usually reported crack spacing. It is easier to measure the crack spacing in strip like specimens. Where as, for circular and rectangular specimens as big as 1 m^2 with thousands of cracks, the average area of cracked cells better represented the crack pattern. Another very important factor which influenced this decision was the methods of image analysis. It is easier to determine the area of the cracked cells than the spacing between two cracks. Spacing between two parallel cracks is not difficult to determine, but seldom have we found quite parallel cracks; hence it becomes more complicated to find the distance between the cracks. The methods used to determine the crack spacing in earlier published data, somehow seem too difficult to fit into an automatic method using image analysis. Considering all these factors finally the average area of cracked cells was adopted.

Crack spacing is known to increase with thickness but this increase will decrease the desiccation rate. A similar observation was made with an increase in AACC with thickness (figure 5.15) for the circular specimens. For rectangular specimens the results are plotted

in a similar fashion like the one for desiccation rate earlier. AACC increased with decrease in drying surface (fig 5.16 and 5.17) interestingly the desiccation rate also decreases for the same set of tests (fig 5.9 and 5.11).

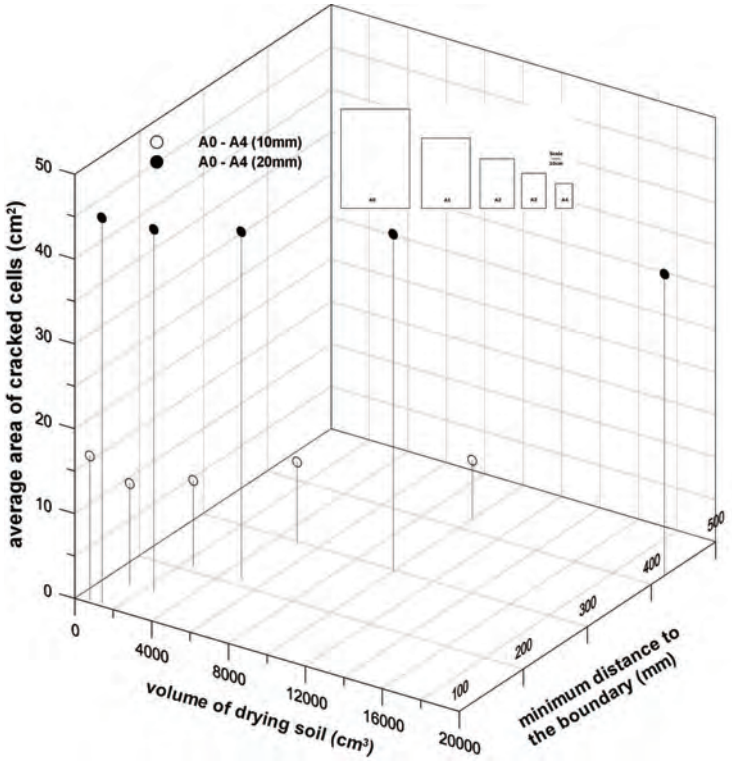

Figure 5.16: Average area of cracked cells for rectangular specimens of similar geometry

It appears that the average crack width (second series, table 5.2) is also basically affected by the specimen's thickness: $w_{10(2)} = 1.10$ mm (s = 0.11) and $w_{15(2)} = 2.92$ (s = 1.12) and similar observation was made for the average crack width of third series (table 5.3): $w_{10(3)} = 1.90$ mm (s = 0.16) and $w_{20(3)} = 5.09$ mm (s = 1.18); w is the average crack width and s the standard deviation. Apart from the thickness effect, for the third series the effect of area was also observed, with average crack width increasing as the area of the specimen decreased.

5.7.4 Unique relation between crack length and area of cracked cell

Finally, it can be shown that only three types of regular polyhedron (triangle, square and hexagon) can produce a uniform tessellation of the plane. For all of them, the relation in the log-log space of figure 5.18 between the area of a cell (A), and the length of crack

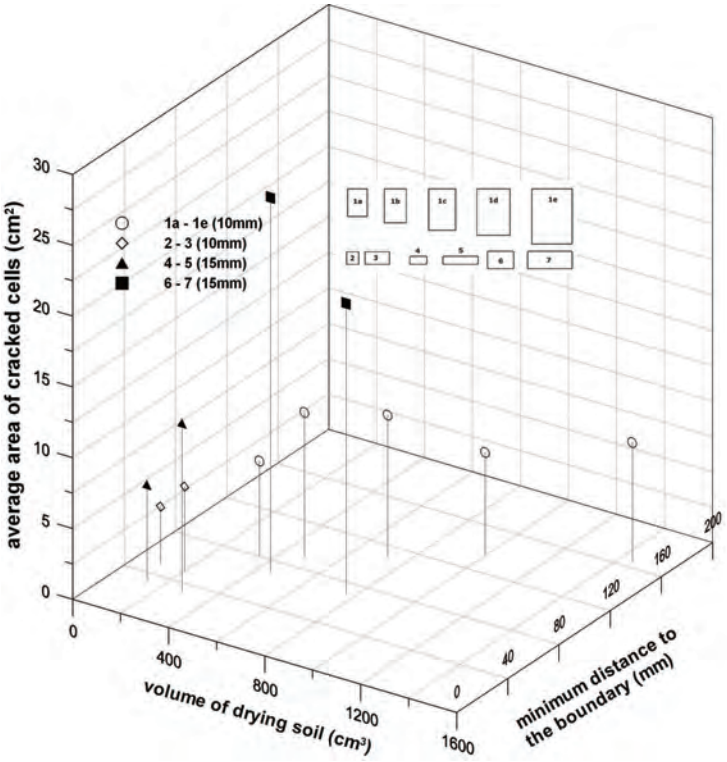

Figure 5.17: Average area of cracked cells for rectangular specimens of different geometry

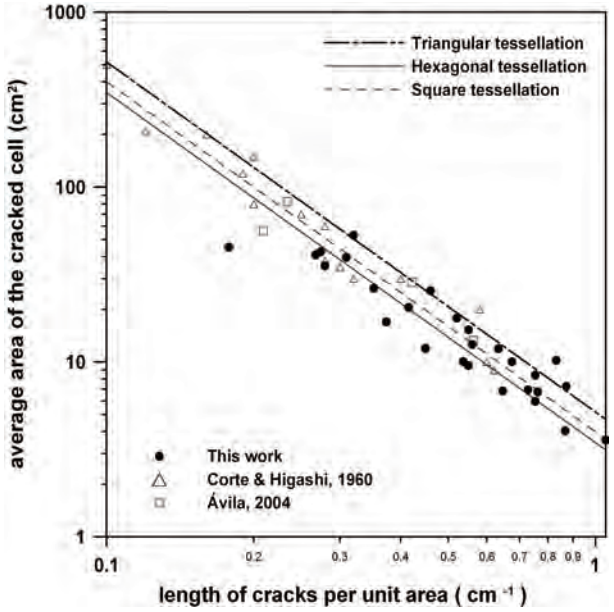

Figure 5.18: Relation between length of cracks and area of cracked cell for all the specimens tested

per unit area (l_c) has a linear form $\log A = B - 2\log l_c$ [Corte and Higashi, 1960] where B is a term that depends on the polyhedron considered. This relation is independent of the size of the cells. Figure 5.18 illustrates that the experiments performed in the present work fall in acceptable accordance with this linear relation for a uniform tessellation, and with other tests found in the literature [Corte and Higashi, 1960];[Ávila, 2004].

5.8 Conclusions

The chapter presents the results of an experimental work devoted to give insight into the mechanics of cracking of thin soil layers under drying conditions. Three series of tests with circular and rectangular specimens of varying geometry have been performed giving qualitative and quantitative information about the main parameters controlling the process of cracking: size, thickness and aspect ratio of the specimen, and boundary conditions (cross-section of the holding tray, and roughness on the contact surface between specimen and tray).

The effect of bottom contact can be studied effectively by different surface roughness rather than different material coatings. The experiments once again reiterate the interwoven effect of thickness, desiccation rate and cracking moisture content on one another.

The effect of geometry of specimen is first time studied in an elaborate manner. Desiccation rate is affected by area of the drying soil. Thickness and area have reverse effect on the desiccation rate, desiccation rate increases with drying area. The observed effect of drying area adds an additional parameter to be analysed while considering the numerical solutions for soils undergoing drying, apart from the thickness of the layer. The increase in desiccation rate with increase in drying area is complimented with crack pattern characteristics. The different geometries had an effect only on the final crack pattern.

Cracking mechanism should be studied in combination with evolving characteristics of crack pattern. Like, in addition to the evolution of CDF, evolution of crack width, individual cracks and their interaction with other cracks leading to the formation of unique crack pattern will broaden the current knowledge. This work is out of scope for the present thesis, but should be considered for future studies. Image analysis is certainly a powerful, efficient and easy tool for this task.

The results are in acceptable agreement with existing literature. The work presented gives the much needed effect of different boundary conditions which are essential towards the development of a model able to predict formation and propagation of cracks in soil under

drying conditions.

Chapter 6

Size-effect in soil cracking

6.1 Introduction

Size-effect is a prominent feature of fracture mechanics. The size-effect in fracture mechanics [Bažant, 1984] takes in to account that in quasi-brittle materials, such as concrete, rocks, some types of ceramics and hard clays, among others, the resistance to fracture depends on the size of the structure or specimen subjected to load. Such behavior is different from the classical theories that predict material resistance to assess the load carrying capacity in terms of strain or deformation criterion. Due to the size-effect, when two geometrically similar structures (of different sizes) are compared, the nominal resistance of the bigger structure is different (usually lower) from that of the small. Size-effect is one of the three main reasons for using fracture mechanics in the analysis of behavior of quasi-fragile materials [García, 1997]. The other two reasons are that fracture mechanics takes a realistic approach towards softening behaviour and also takes into account the energy dissipated in the process of crack formation, in conjunction with stress or deformation, which is closer to reality than the conventional approach based only on the resistance.

Bažant and Planas [Bažant and Planas, 1998] indicate that the size-effect in concrete structures can be due to six different causes such as: the wall effect (dealing with the different sizes of aggregates), diffusion phenomena, heat of hydration, statistical effect, fractal characteristics of the fracture surfaces and the effect of size in fracture mechanics. The latter is by far the most important and is related to release of stored energy in the crack front.

In this chapter evidences of energy-related size-effect on the process of cracking in drying

soil will be presented. An innovative experimental program to study the size-effect was devised and carried out. The most important results of these tests were obtained by Image Analysis (see appendix A). The fracture toughness and fracture energy determined experimentally in the Chapter 4 were used to calculate the cracking stress. The results show that indeed there is a size-effect on the process of cracking in soils.

6.2 Previous studies

Apart from the experiments done by Ávila [Ávila, 2004] on CT specimens of soil, there seems to be no other experimental data available on the size-effect in soils. There are some data related to difference in strength for different sizes of specimens tested but not directly related to fracture mechanics size-effect.

6.3 Size-effect laws

6.3.1 Nominal stress and representation of size-effect

To evaluate the size-effect it is necessary to compare the behaviour of geometrically similar structures of different sizes. For such an analysis it is necessary to define the nominal stress σ_N which will serve as a load parameter and it corresponds to the load divided by the typical transversal section. For bi- and tri-dimensional analysis σ_N can be expressed as:

$$\sigma_N = c_N \frac{P}{bD} \quad \text{(bi-dimensional)} \tag{6.1}$$

$$\sigma_N = c_N \frac{P}{D^2} \quad \text{(tri-dimensional)} \tag{6.2}$$

where P is the failure load, b is the thickness of the structure, and c_N is a coefficient introduced for convenience if needed for some cases of structural analysis, in this study it is taken equal to 1. D is the characteristic dimension of the structure and can be any dimension of the structure. For example, in a beam it can be the thickness or span, in the case of a CT soil specimen it can be the height or thickness, as only the relative values of σ_N is of interest. If the load at crack initiation correspond to a maximum load (P_{max}), also known as the ultimate load (P_u), then the nominal stress is called the nominal ultimate stress σ_{Nu}.

According to the classical failure theories σ_{Nu} is constant for a given geometry, with or without crack, independently of its size. Therefore this relation can be graphically represented, taking logarithm of strength ($\log\sigma_{Nu}$) against the logarithm of size ($\log D$), as a horizontal line (figure 6.1a), which indicates that there is no size-effect

If the analysis is done using LEFM, in contrast to the classical failure theories, a strong size-effect is observed, which is represented in figure 6.1a with the dotted line inclined with a slope of $-1/2$. In case of concrete structures, a curved transition in behaviour from small structures well represented by the strength criterion (nearing asymptotically to a horizontal line) to big structures well represented by LEFM (line with slope of $-1/2$) is needed to represent the size-effect.

Size-effect can also be seen in the ductility of a structure or specimen subjected to loading. In general, small structures fail at a higher relative deflection than bigger structures, as indicated in figure 6.1b [Bažant and Planas, 1998].

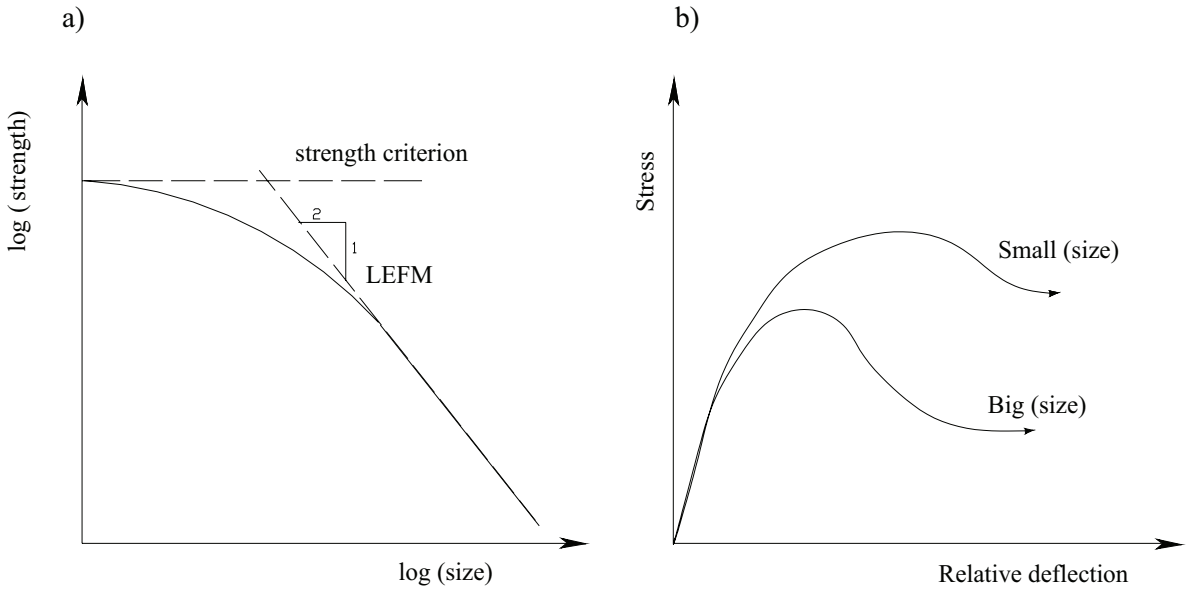

Figure 6.1: (a)Bi-logarithmic relation representing the size-effect of resistance, (b) size-effect in the ductility Bažant and Planas [Bažant and Planas, 1998]

6.3.2 Size-effect in terms of energy balance

In terms of energy size-effect can be explained (in terms of the balance between) energy available and energy required for crack propagation. Now, consider a plate as shown in figure 6.2a, in which the first crack develops within a crack band of width h_f, (area

ABCD). The unit extension of this crack band requires a certain energy per unit thickness, which corresponds to the fracture energy G_{IC}, (which is) a material constant [Bažant and Cedolin, 1983] [Bažant and Planas, 1998].

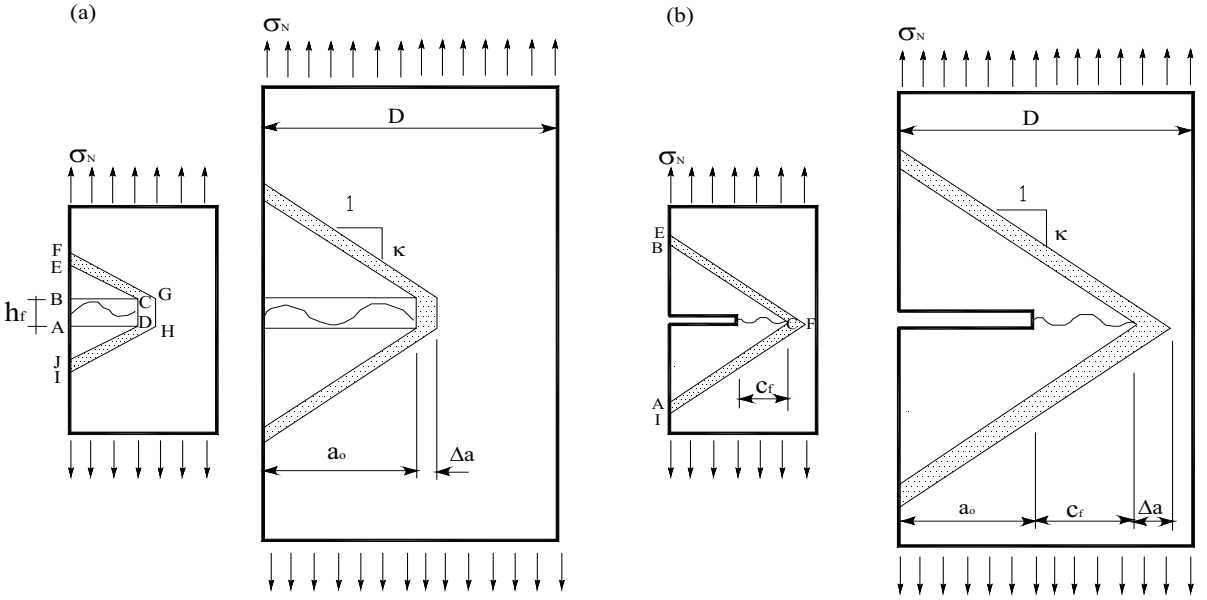

Figure 6.2: Explanation of size-effect (a) crack band, (b)simple longitudinal crack (adopted from Bažant and Planas [Bažant and Planas, 1998])

The energy balance permits to determine the load required for the crack band to propagate: under a constant stress σ_N the stored elastic energy in the plate before cracking is $(\sigma_N^2/2E)$, i.e., the area under the stress-deformation curve. Once the crack band or the first crack has developed, the elastic energy near the crack zone is released, reaching a value equal to zero. According to Bažant and Planas [Bažant and Planas, 1998], the zone in which the energy is released corresponds to the area JECD in the figure 6.2a, which, is limited by two lines with slope k, a value that must be determined empirically.

When the crack band propagates a length Δa, the zone where the elastic energy is released increases to the area IFGH. Now consider another structure geometrically similar, but of larger size, subjected to the same normal stress, as shown in the right-hand side of the figure 6.2a. This structure has a larger initial crack band length, and more energy is released than in the smaller structure.

The shadowed area in figure 6.2a represents the deformation energy liberated due to crack propagation by a length Δa and corresponds to the difference in the outer area (IFGH) and the inner area (JECD). This can be calculated as: $b(h_f \Delta a + 2ka_0\Delta a)(\sigma_N^2/2E)$, where b is the plate thickness and a_0 is the initial length of crack band as shown in figure 6.2a.

This energy should be equal to the energy required to create a fracture, which is: $G_{IC}b\Delta a$. Equating these two expressions the energy balance can be obtained:

$$b(h_f\Delta a + 2ka_0\Delta a)(\frac{\sigma_N^2}{2E}) = G_{IC}b\Delta a \tag{6.3}$$

Solving for the nominal stress for the ultimate condition, Bažant's size-effect law [Bažant, 1984] can be obtained:

$$\sigma_{Nu} = \frac{Bf_t^{'}}{\sqrt{1+\frac{D}{D_0}}} \tag{6.4}$$

where,

$$Bf_t^{'} = \sqrt{\frac{2G_{IC}E}{h_f}} = \quad \text{Constant and} \quad D_0 = \frac{h_f D}{2ka_0} = \quad \text{constant} \tag{6.5}$$

$f_t^{'} = \sigma_{ys}$ is the tensile strength of the material, which is introduced only for the purpose of dimensionality. It should be noted that B is a dimensionless constant and D_0 is a constant with dimensions of length. Both B and D_0 depend on the material fracture properties and the geometry and the shape of the structure, but not on its size.

Equation 6.4 not only satisfies the crack band theory but also the case of a simple longitudinal crack, like the one shown in figure 6.2b. In this case,

$$Bf_t^{'} = \sqrt{\frac{G_{IC}E}{kc_f}} = \quad \text{constant, and} \quad D_0 = c_f\frac{D}{a_0} = \quad \text{constant} \tag{6.6}$$

Where, c_f is the difference between the equivalent crack length and initial crack length (a_0). When c_f tends to zero, the plastic zone becomes very small and hence the behaviour is clearly LEFM.

The size-effect law proposed by Bažant [Bažant, 1984] has been experimentally verified on different quazi-brittle materials using different types of specimens. To obtain the parameters to be used in equation 6.4 a regression analysis has to be carried out on the experimentally measured values of σ_N in the laboratory.

6.4 Other types of size-effect in drying soils

According to Bažant and Planas [Bažant and Planas, 1998] in concrete structures there are five different types of size-effect, besides energy-related size-effect that may influence

the nominal value of strength. These other types of size-effect are equally applicable to the case of soils subjected to drying.

6.4.1 Effect of edge layer or wall effect

This effect can be of three types. The first, which is seen in concrete structures, is attributed to the concentration of relatively finer or smaller sized particle in the walls of the structure where there is also higher cement content and mortar. Therefore, if the structure is small, the layer next to the wall, independently of size of the structure, represents a significant proportion of its cross section, while in big structures such proportion is much less (figure 6.3). However, according to Bažant and Planas [Bažant and Planas, 1998], this size-effect in most cases does not seem to be very significant.

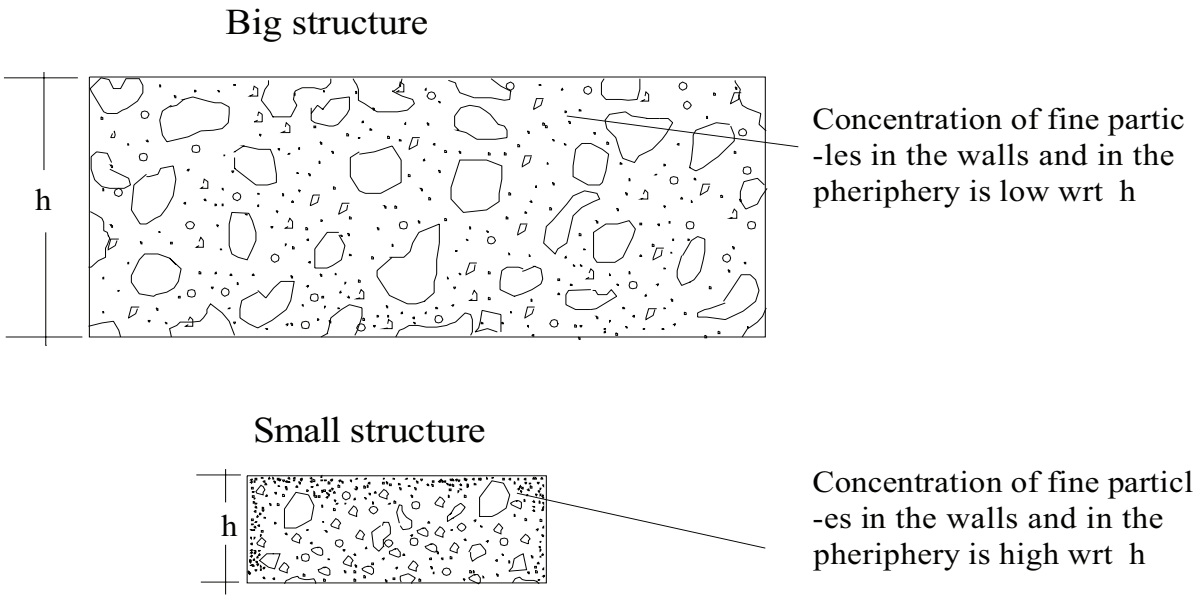

Figure 6.3: Schematic interpretation of the effect of edge layer associated to the concentration of fine particles in the edges of the structure

The second type of edge layer effect appears, because under normal stress parallel to the surface, there is a mismatch between the elastic properties of aggregate and the mortar matrix, thus creating transversal stresses in side the specimen (figure 6.4), while on the surface these stresses are zero. This effect is lower in bigger structures than in smaller structures.

The third type of edge layer effect is attributed to the lateral expansion and is known as Poisson's effect. In which in superficial layer the specimen is close to plane stress

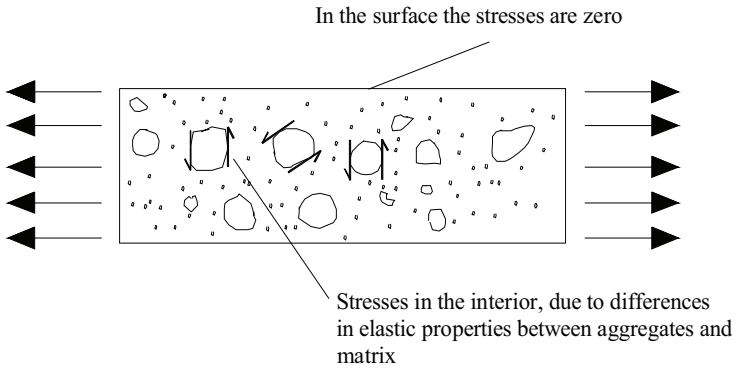

Figure 6.4: Schematic interpretation of the effect of edge layer associated with the transversal stress generation in the interior of a structure

condition, whereas in the inside it is close to plain strain condition. This effect is also more pronounced for smaller specimens or structures.

In soils the size-effect associated to the edge layer can be seen in a soil sample which has higher moisture content like slurries. In such a condition there can be higher concentration of finer particles in edges and superior part of the mould than in the central part. The second effect, related to the mismatch in the elastic properties between the soil matrix and the aggregates can occur in soils which are variably graded, but also in uniformly graded and finely graded materials which usually get cracked due to water loss or desiccation. The capillary phenomenon results in the formation of aggregates or peds and these aggregates act as particles of bigger size interacting with the rest of the soil matrix. The third effect or the Poissons effect can be of great importance in soils, because the process of lateral expansion due to changes in suction causes non-uniform distribution of matrix stresses.

6.4.2 Diffusion phenomenon

This effect is due to the time taken for the process of diffusion. Such as, heat conduction for drying or water transport through the pores. These processes are proportional to the square of the size of the structure. The process of diffusion changes the material properties and generate residual stresses resulting in inelastic deformations and cracking. For this reason, the cracks seen on the surface of the concrete structures due to desiccation can have very different orientation pattern and density, depending on the size of the structure.

A similar behaviour can occur in soils subjected to drying/desiccation. This was observed in the unique random patterns of cracked soils discussed in Chapter 5.

6.4.3 Heat of hydration

The phenomenon is usually seen in concrete structures and is basically associated with the chemical reactions during setting process. This effect is similar to the effect of diffusion, since the average time for dissipation of the heat of hydration in a structure is proportional to the square of its size, hence bigger structures reach higher temperature. This non-uniform increment of temperatures can result in cracks and induce desiccation altering greatly the material properties. Though not to the same extent as in concrete, the heat of hydration in clays trigger various complex chemical reactions (see, Mitchell [Mitchell, 1993]) which probably cause an increment in temperature (as mentioned earlier this is in no way comparable to the increment in concrete). Hence, the heat of hydration in clays can be of very less importance contributing to the size-effect.

6.4.4 Statistical effect

Originally it was thought that this effect was due to the randomness of the strength of a material made up of different constituents. The theory proposed by Weibull (1939) known as the chain model states that the strength of a chain (or of a structure) is governed by the strength of the weakest link, and hence the statistical effect indicate that while longer the chain greater the likelihood of appearance of a weak link and thus lower the value of strength that can be expected.

Traditionally, the statistical effect has been used to explain most of the size-effect in concrete specimens especially in long beams subjected to tension, however it can not be applied for flaws in reinforced concrete structures. As opposed to what happens in metallic structures where the rupture begins in a macro crack (when a micro-fissure becomes macroscopic), in concrete structures the rupture occurs only after a considerable propagation of stable crack causing dissipation and redistribution of stored energy. This process generate strong size-effect which will be much greater than any statistical effect, above this, decisive part of developing cracks concentrate in a very small zone, thus the statistical effect which is related to the size of the whole structure becomes irrelevant.

Certain behaviour observed in soils is quite similar to that seen in concrete. Consider the process of desiccation in soils, the process of desiccation results in micro crack formation, though they are not participate in a decisive way for the cracking in general, and in some cases the micro fissures get closed as the process of drying continues. Only those micro fissures becoming dominant cracks may be because of their location and orientation with respect to the direction of stresses. Hence these micro fissures define the cracking process

in soils. This behaviour is observed in several specimens tested at laboratory, this type of behaviour was observed by Vallejo [Vallejo, 1987] in direct shear tests with hard clays. The direct shear tests were conducted with samples having different orientation of initial cracks. At the end of the test it was observed that the initial cracks had strong effect on the final crack formation. An earlier work by Ávila [Ávila, 2004] on macroscopic and microscopic observation of cracking in soils reported a similar behaviour.

Lo [Lo, 1970] observed that in many specimens tested that the un-drained shear strength of fissured clays was less in smaller specimens when compared to the bigger samples. The observed behaviour was explained as statistical effect, but not over the entire specimen area as in the case of the theory of Weibull instead on a potential area susceptible to rupture. Based on this analysis for clays with fissures an operational strength would be estimated, this value depends on the distribution of fissures and the potential area of rupture. This operational value will fluctuate between the intact strength (equal to or a material with out fissures) and the residual strength. According the explanation given by Bažant [Bažant, 1984] and the process of stable crack growth observed in soils, probably the size-effect of fracture mechanics may be more significant in reducing the strength in big specimens than the statistical effect proposed by Lo [Lo, 1970].

6.4.5 Fractal nature of the crack surfaces

The hypothesis that tries to explain the size-effect from the fractal nature of the crack surfaces was proposed by Carpinteri [Carpinteri et al., 2002]; [Carpinteri, 1994], Carpinteri and Chiaia [Carpinteri and Chiaia, 1995]. However, according to Bažant [Bažant, 1995];[Bažant, 1997] and Bažant and Planas [Bažant and Planas, 1998] the fractal nature or the auto-similitude of the cracking at different scales of observation does not play a significant role in the process and formation of new crack or fracture surface. If they did any influence, it would have modified the size-effect due to fracture mechanics, which incidentally does not reflected in the experimental studies fitting the bilogarithmic curve of figure 6.2a.

In soils, the cracking process or the crack pattern show fractal characteristics of qualitative nature. The cracks preserve their distinctive nature of crack surface at different scales of observation and process in agreement with the auto-similitude of the fractals.

6.5 Size-effect experiments

6.5.1 Specimen geometry

The experiment consist of five geometrically similar rectangles of aspect ratio $\sqrt{2}$ and surface area of 1, 0.5, 0.25, 0.125 and 0.0625 m^2 (see figure 6.5 and table 6.1) in two series of different thickness (10 and 20 mm), subjected to drying conditions in a laboratory controlled environment.

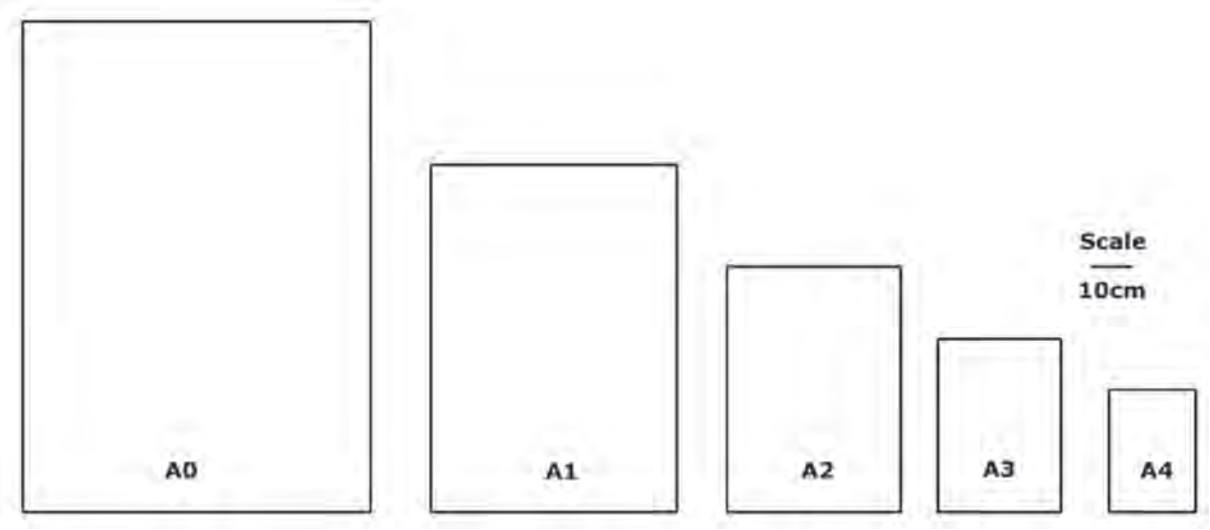

Figure 6.5: Schematic representation of the size-effect specimens

6.5.2 Sample preparation and experimental procedure

The soil was allowed to dry in open air and then passed through a mechanical sieve (size 2 mm). The dry material that passed through was then mixed with distilled water until a visibly homogeneous paste was obtained. The prepared soil paste then was poured in the test trays, and small blows were given to the edge of the trays to remove air pockets. The surface of the sample was levelled with a straight edge to get a uniform surface. The soil left on the straight edge was taken to determine the initial moisture content. This procedure was repeated for all the specimens.

Soon after pouring and levelling of the surface, the samples were weighed to an accuracy of 0.01 g, and placed over three load cells to record the loss of weight at one-minute intervals. A digital camera was positioned directly above the tray to obtain images of the sample at three-minute intervals, to be used for image analysis after the conclusion of

the experiments. The experiments were conducted inside an environment-controlled room with temperature and relative humidity fixed at $21 \pm 0.5°C$ and $52 \pm 2\%$ respectively. The initial water content of the specimens was $24.5 \pm 1\%$. During the process, the samples were monitored carefully to capture the most relevant features such as the onset of first crack, separation of the soil from the edges of the trays, and reaching of the fully cracked and fully dry states. Sequential images of crack development at different stages of drying, from the appearance of the first crack to the final crack pattern, were obtained. Similar images were obtained for the other tests.

6.5.3 Image analysis for quantification of developing crack pattern

Image processing and analysis is not new to geotechnical applications, but technology developments in recent years have made it easier and more efficient. Apart from the characterisation of the crack pattern, crack detection and crack monitoring are the other areas where image analysis techniques are employed.

In this work techniques of image processing and analysis were used to quantify the crack pattern from the size-effect experiments (see table 6.1). The details of steps involved in the image processing and analysis for crack pattern quantification can be found in appendix A on Image analysis.

6.6 Results of size-effect experiments

Figure 6.6 shows the final crack pattern for all tests obtained after fully drying of the specimens. A first look at this figure shows, as expected, a significant difference between the 10 mm and the 20 mm-thick specimens: for a given specimen surface area, the average area of the cracked cells is smaller (and therefore the number of cracked cells larger) for specimens with a lower thickness. More detailed information about the mechanics of cracking requires a deeper look into the pattern structure of the crack network as it develops during drying. For that purpose, a public-domain image processing program, ImageJ [Rasband, 2005], is used. The raw data obtained from pictures taken with a digital camera has been processed with that software, obtaining several parameters that can be used to characterize the crack network: the number of cells into which the specimen is divided, the average area of those cells, their aspect ratio, the average crack width, the crack density factor (or surface shrinkage, see [Miller et al., 1998]), and others. The

summary of the results of the image analysis are given in Table 6.1.

The crack density factor (CDF), or surface shrinkage (see [Miller et al., 1998]), is used to characterize the extent of surface cracking. This parameter is defined as the ratio of total crack area to the total virgin surface area of the drying specimen. The results shown in Table 6.1 indicate that the crack density factor depends on specimen's thickness: average CDF for 10 mm-thick specimens is $CDF_{10} = 10.19\%$ (s = 1.77), whereas for the 20 mm-thick specimens, $CDF_{20} = 12.99\%$ (s = 1.08). Equally, it appears that the average crack width is also basically affected by the specimen's thickness: $w_{10} = 1.90$ mm (s = 0.16) and $w_{20} = 5.09$ mm (s = 1.18); w is the average crack width and s the standard deviation. Figure 6.7 shows the effect of specimen size on several variables measured at the end of the tests. These results have been obtained from image analysis conducted on digital pictures obtained during the experiments.

Table 6.1: Specimen geometry and main results form image analysis

Test	nominal area of specimen (m^2)	length of short side (mm)	aspect ratio	surface shrinkage (CDF) (%)	number of cells	average area of cells (cm^2)	total length of cracks (cm)	average width of cracks (mm)	fractal dimension
$A0-10$	1.0000	841	1.4	11.71	1272	6.94	7280.76	1.61	1.42
$A1-10$	0.5000	594	1.4	10.79	466	9.57	2746.49	1.95	1.44
$A2-10$	0.2500	420	1.4	11.67	219	10.08	1460.33	1.96	1.47
$A3-10$	0.1250	297	1.4	9.12	95	11.96	560.26	1.99	1.48
$A4-10$	0.0625	210	1.4	7.64	34	16.98	232.92	2.00	1.52
$A0-20$	1.0000	841	1.4	11.49	249	35.55	2793.85	4.11	1.47
$A1-20$	0.5000	594	1.4	13.32	109	39.76	1545.88	4.28	1.56
$A2-20$	0.2500	420	1.4	12.95	53	41.06	668.24	4.77	1.63
$A3-20$	0.1250	297	1.4	14.49	25	42.46	342.08	5.22	1.70
$A4-20$	0.0625	210	1.4	12.72	12	45.46	110.91	7.05	1.76

6.7 Evidences of Size-effect

Here Cracking stress were calculated from the generated crack surface and Bažants size-effect law.

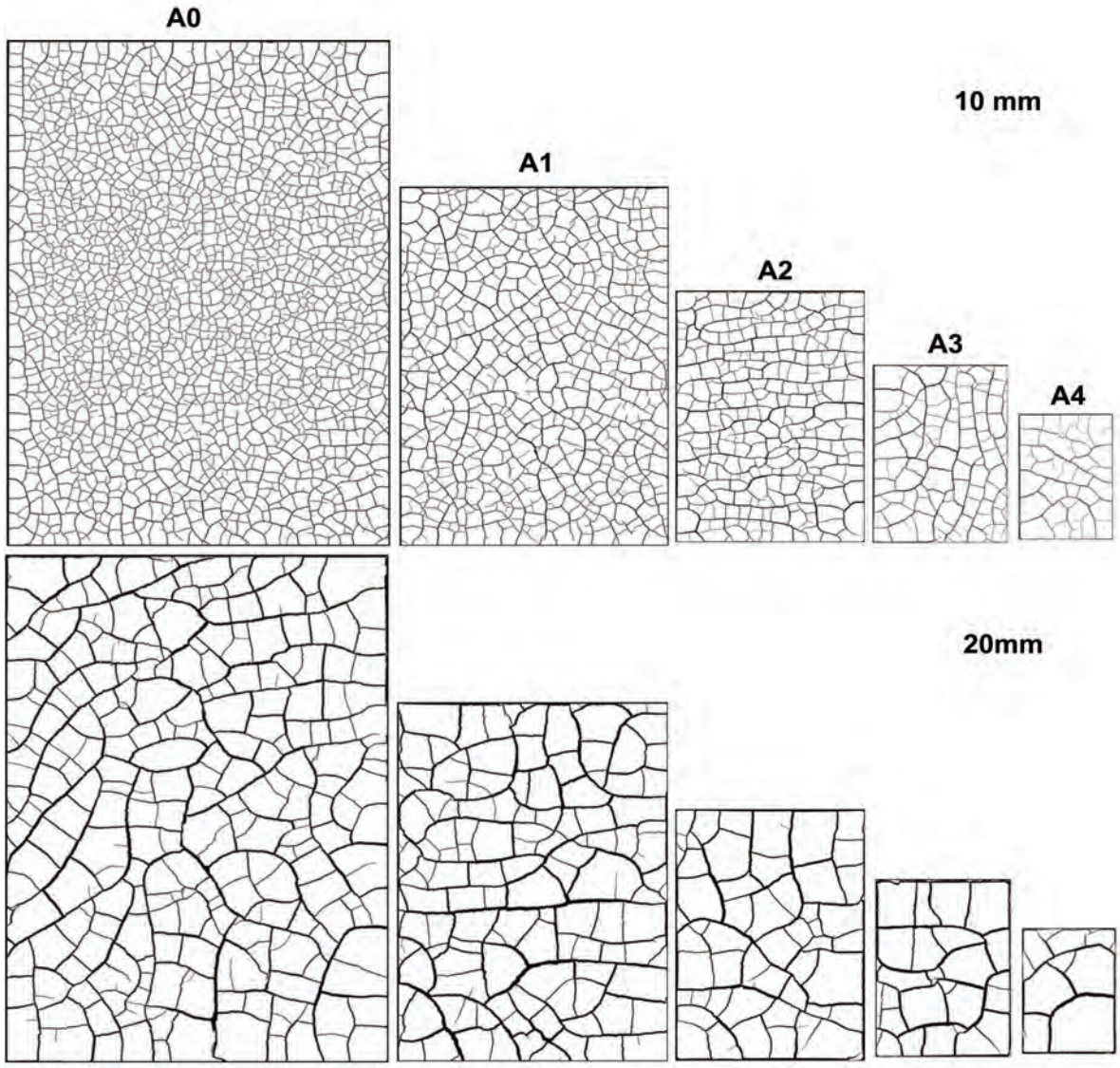

Figure 6.6: Final crack pattern for rectangular specimens of third series (Tests A0-A4)

Although fracture mechanics theory has been developed and applied mostly to brittle or quasi-brittle materials such as concrete, steel, industrial alloys, ceramics, etc. with much larger strength than that of soils, the theoretical and experimental developments in this field may be of application in the analysis of similar behaviour patterns for other materials far less strong and stiff, such as cohesive soils (clay, silt). In fact, there has been recently considerable research using fracture mechanics to study cracking phenomena in clays ([Konrad and Ayad, 1998], [Ávila, 2004], [Prat et al., 2002], [Lee et al., 1988], [Morris et al., 1994]). However, most of the work deals with the application of fracture mechanics methods without justifying that the theory is indeed driving the cracking process. The purpose of this work is to give some insight on the appropriateness of using fracture mechanics for materials such as cohesive soils.

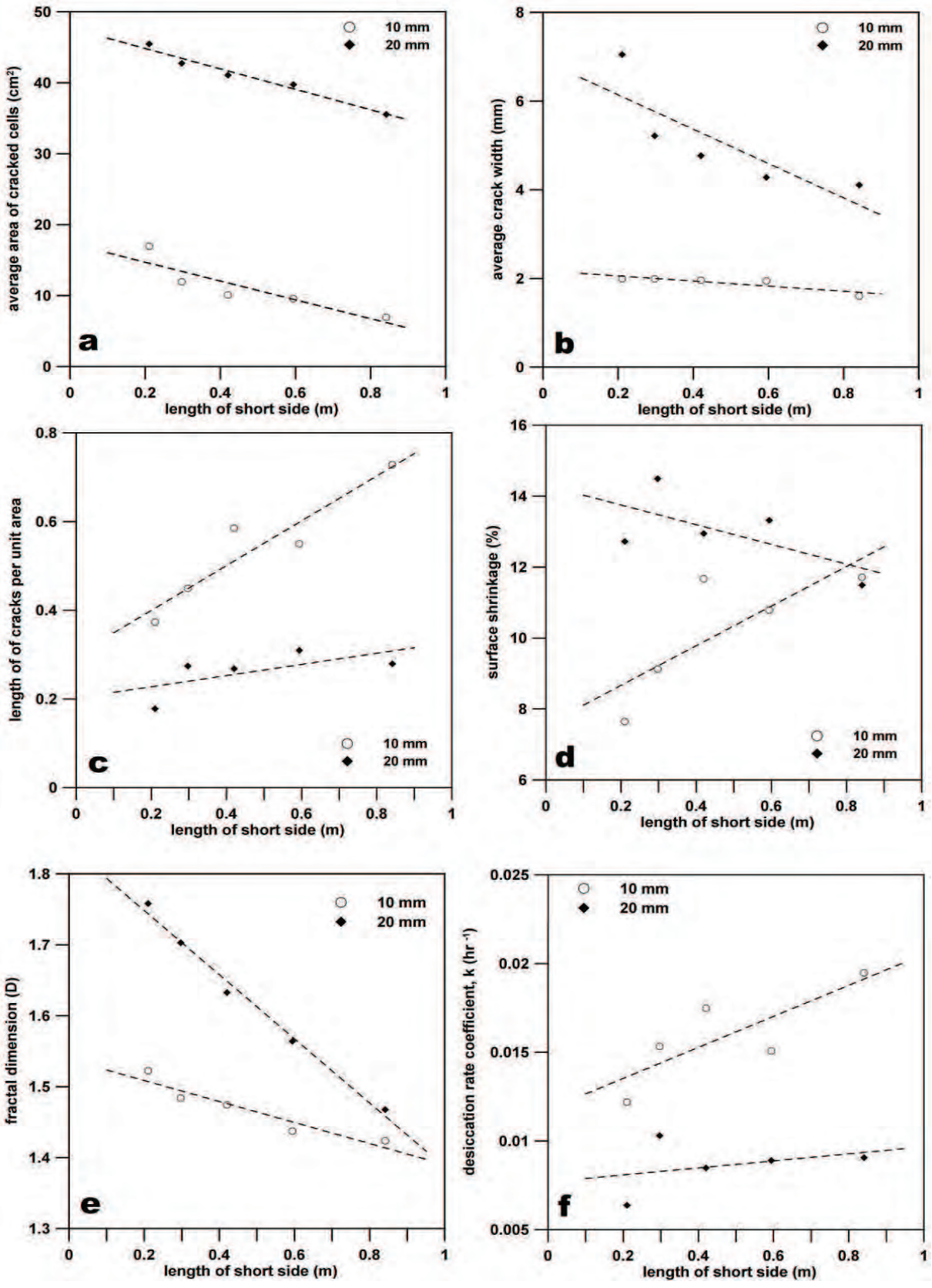

Figure 6.7: Effect of specimen size on several measurements: (a) average area of cells, (b) average crack width, (c) length of cracks per unit area, (d) surface shrinkage, (e) fractal dimension, and (f) desiccation rate coefficient

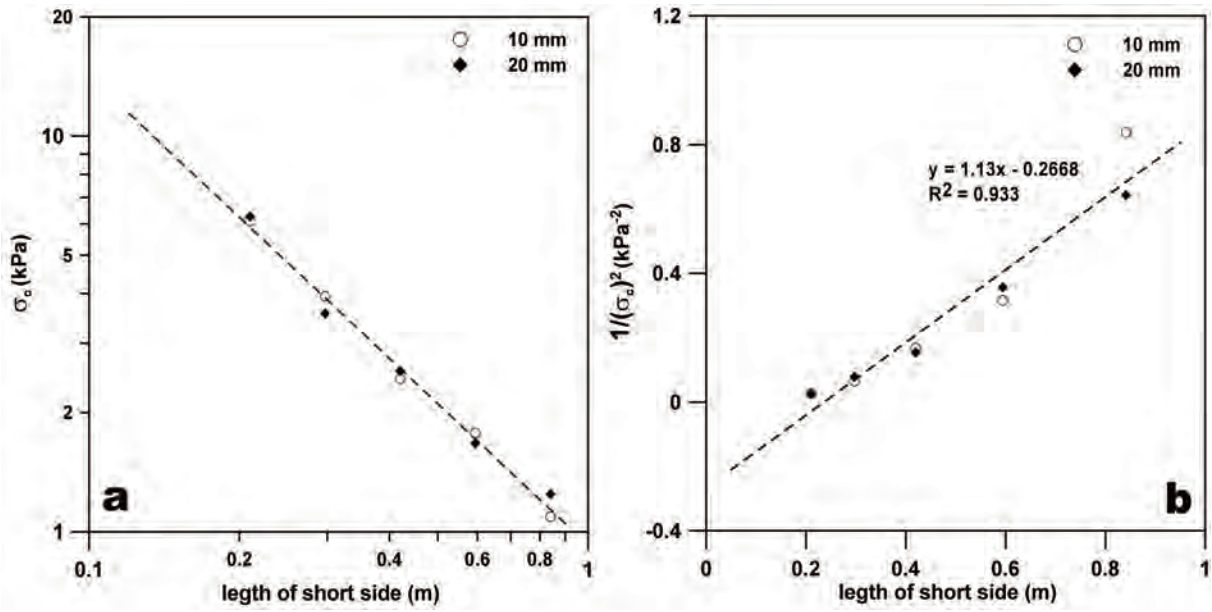

Figure 6.8: Size effect plots: (a)cracking stress decrease with increasing size; (b) linear interpolation to obtain Bažant's size effect law's parameters [Bažant, 1984]

One of the key aspects that differentiates conventional strength of materials from fracture mechanics analysis is size effect: in the latter, strength may change with size of the loaded specimen. There has been, in the recent past, a large amount of published research related to size effect of brittle or quasi-brittle solids [[Bažant and Planas, 1998], [Bažant et al., 1994], [Bažant and Jirásek, 1993], [Mazars et al., 1991], [Bažant and Kazemi, 1990], [Sulem and Vardoulakis, 1989], [Mazars and Bažant, 1989], [Bažant et al., 1988], [Bažant, 1984]]. However, research on this topic related to soils or other geologic media has been scarce [[Ávila, 2004], [Bažant et al., 2003], [Sture et al., 1999b], [Finno, 1989]].

Evidence of size effect in the drying cracking of soils has been shown by Ávila [[Ávila, 2004]], who conducted fracture mechanics tests on geometrically similar samples of Bogotà clay and concluded that there is size-effect, and that the results follow Bažant's size-effect law [Bažant, 1984]. The experimental results described previously in this chapter can be used as well to show that fracture mechanics-related size effect occurs during cracking of clay samples subjected to moisture loss due to drying. This has to be done in a simplified manner, since the tests were simple on purpose and no load-related measurements were made. For soils undergoing desiccation (i.e. water loss due to drying) and becoming partially saturated, suction is the main driving agent causing cracking. Suction is the cause of tensile stresses in the soil matrix that appear when the drying soil mass loses water and experiences considerable shrinkage. An indirect way to estimate the average value of the cracking stress (σ_c) was used. From the image analysis performed on the fully cracked specimens, the total length of cracks can be evaluated for all specimens. Then

the average cracking stress can be estimated using the LEFM relation

$$\sigma_c = \sqrt{\frac{G_{IC}E}{\pi a}} \tag{6.7}$$

where G_{IC} is the fracture energy (assumed a material property), E is the Young's modulus, and a is the total length of cracks. The value of fracture energy $G_{IC} = 0.65$ N/m. Young's modulus has been taken from Barrera [Barrera, 2002] for the clay used: E = 4.5 MPa. With these values, the average cracking stress (σ_c) can be calculated as:

$$\sigma_c = \sqrt{\frac{0.65\frac{N}{m} \cdot 4.5 \times 10^6 \frac{N}{m^2}}{\pi \cdot a}} \simeq \frac{965N \times m^{\frac{-3}{2}}}{\sqrt{a}m^{\frac{1}{2}}} = \frac{0.965}{\sqrt{a}}kPa \tag{6.8}$$

Figure 6.8 shows the results of the analysis with data from the experiments described in previous sections. Figure 6.8a represents the size-effect law, where the cracking stress decreases as the size of the specimen increases. Figure 6.8b is the regression plot used to calibrate Bažant's size-effect law.

6.8 Conclusions

An innovative experimental program to study the fracture mechanics size-effect in soil cracking has been presented. The experimental results show the evidences of size-effect in soil cracking. Soil behavior is neither quasi-brittle nor linear, never the less, LEFM seems to be the most simple fracture mechanics theory for cracking in soils. This is due to ease with which the LEFM parameters can be determined. Experimental evidences of existence of size-effect further strengths the applicability of LEFM. Thus a numerical modeling with these parameters can be implemented with a certain degree of confidence as a first step towards numerical modeling. An experimental determination of non-linear and elasto-plastic fracture parameters for soils is quite difficult and complicated with the existing soil testing equipments.

Chapter 7

Desiccation tests with environmental chamber

7.1 Introduction

Moisture loss in soils under drying conditions commonly causes the soil to shrink and, as a consequence, cracks appear. This has diverse implications on the soil's mechanical and hydraulic properties. These cracks may close during a subsequent wet season, but the soil properties remain at least partially altered. The current global warming scenario suggests that prolonged, severe and frequent dry conditions are expected, increasing the frequency and size of cracks in soils, especially in temperate regions that currently do not reach their full shrinkage potential (Climate Change Impacts Review Group;[CCIRG, 1996]). Shrinking and swelling soils damage building foundations through subsidence, creating problems for householders and insurance companies (Building Research Establishment;[BRE, 1990]). Cracks induced by environmental agents also reduce the bearing capacity of the soil and increase its propensity to erosion. Most of the studies currently available, involving several disciplines, have been performed mostly on already cracked soils instead of focusing on the cracking process. Currently, there is lack of substantial large-scale experimental work in laboratory and variables such as temperature and relative humidity are not systematically controlled; however, these affect the suction and tensile strength of soils which are key factors explaining the cracking process. In this chapter, a new laboratory set-up to investigate the desiccation cracking in soils, designed and constructed at the Soil Mechanics Laboratory of UPC is presented. Soil specimens as big as 800 mm and 200 mm deep, with sensors measuring suction, relative humidity and temperature, can be tested. Load cells record the loss of weight, and a digital camera with

prescribed time frequency records images of the specimen's surface providing a picture of the evolving crack pattern. Air temperature and relative humidity can be controlled or imposed. Computer software controls and logs all the processes and measurements. The experimental program presented in this chapter was devised to develop all the capabilities of the new equipment and to provide new insight to the process of crack formation and propagation in soils. Experiments were carried out to determine the effect of size and bottom surface roughness on the mechanism of crack formation. Starting from the same initial conditions specimens with two different sizes (800 and 400 mm in diameter) and bottom surfaces with plain or circular grooves were tested imposing the same air temperature and relative humidity. One set of experiments was carried out outside the chamber in laboratory conditions similar to the rest of the experimental programs presented in this thesis.

7.2 Environmental chamber and its components

A brief background leading to the visualisation and design of the environmental chamber is given. This section also explains in detail the different components making up the new laboratory set-up specially designed to study the process of desiccation in soils under controlled or imposed environmental conditions. The last section comments on the optional features for improving the testing range of the equipment.

7.2.1 Background

Most of the studies of cracking in soils currently available, involving several disciplines, have been performed on already cracked soils instead of focusing on the cracking process. Currently, there is lack of substantial large-scale experimental work in laboratory and variables such as temperature and relative humidity are not routinely controlled; however, these affect the suction and tensile strength of soils which are key factors explaining the cracking process. The environment chamber described in this section is a key component of long-term research project dedicated to study the mechanisms of cracking in drying soils [Lloret et al., 1998];[Rodríguez, 2002];[Rodríguez, 2006]; [Rodríguez et al., 1999];[Rodríguez et al., 2007];[Ávila, 2004].

Before designing the environmental chamber several tests were carried out with specimens moulded into rectangular, square, and circular holding trays (see Chapter 5). Rectangular specimens of different geometries were tested, with surface areas ranging from 60 cm^2 to

10000 cm^2. The results and experience gained from this work led to the final design of the environmental chamber. The main objective of the environmental chamber is to study the process of desiccation in soils by imposing and controlling environmental conditions and eventually studying the impact of cycle of environmental conditions. The equipment is capable of monitoring the changes with in the soil specimen while the desiccation process is happening as well as taking digital images of the top surface of the specimen.

7.2.2 Holding trays

Trays were specially designed to house the sensors at strategically important locations. Figure 7.1 shows to the scale the schematics of the different types of holding trays to the scale. Figure 7.2 shows a picture of holding trays 80-20, 40-10, and 20-5 (first number is the diameter, the second the depth) with a grooved bottom surface. The holding trays were made of PVC in order to have a minimum temperature effect when placed in the environmental chamber.

7.2.3 Body of the environmental chamber

Figure 7.3 show the schematic diagram of the environmental chamber, with its different parts numbered and explained. Figure 7.4 shows a picture of the chamber in its laboratory position.

The body of the chamber is made up of transparent Methacrylate with dimensions of 1 m $\times$ 1 m $\times$ 1.5 m. This is placed on a much thicker PVC base plate. The exact details of the contact between the base plate and the methacrylate chamber is shown in DETAIL X in figure 7.3. Specially designed rubber tube has been used guarantee air-tightness. The body of the chamber has four circular openings of about 100 mm diameter, two for the entry of dry air from the dehumidifier (marked by number 04 in figures 7.3 and 7.4), and two for the exit of the humid air from the chamber (marked by number 03 in figures 7.3 and 7.4). All the four openings are connected to the dehumidifier in a closed circuit. Apart from these, there are two more air-tight utility openings (see figure 7.4) which are used for minor adjustments during the experiment.

Further equipments required to operate the chamber includes a digital camera to capture the process of formation and propagation of cracks that is fully computer controlled to take pictures automatically at prescribed time frequencies, a sensor to monitor the air inside the chamber for temperature and relative humidity; three load cells supporting the

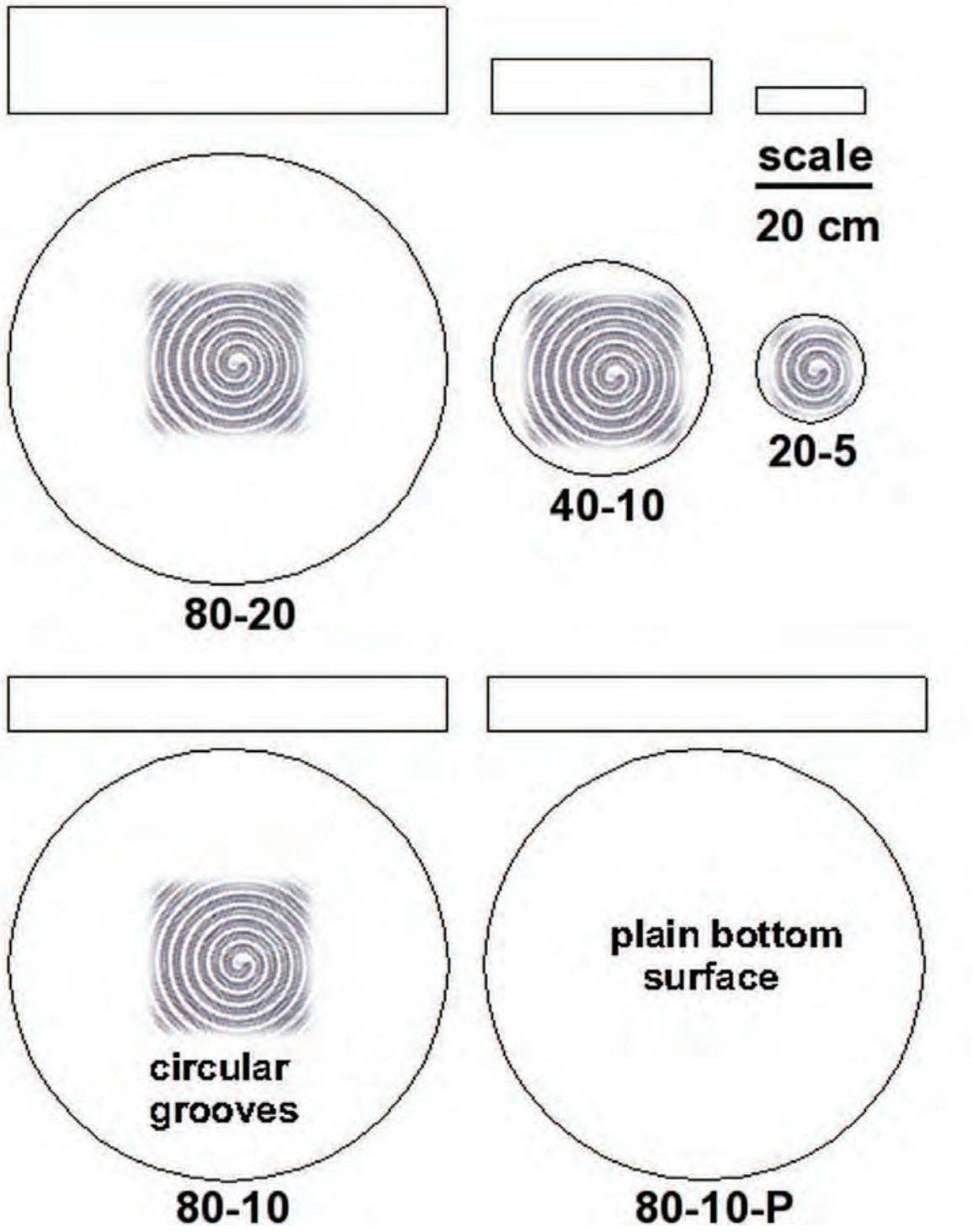

Figure 7.1: Schematics of holding trays for environmental chamber

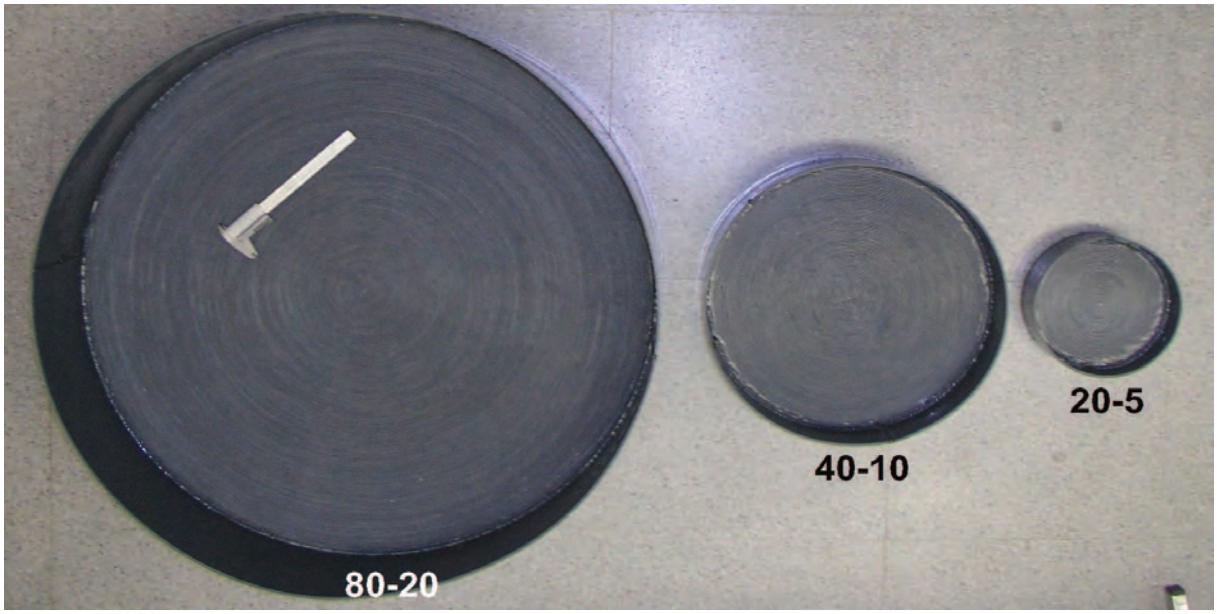

Figure 7.2: Photo of holding trays for environmental chamber

desiccation trays to monitor constantly the loss of weight as the soil sample dries. All the sensors and load cells are connected to the data acquisition system. A computer program in Visual Basic is designed for the purpose.

Experiments with suction and temperature control can be performed by imposing different air temperature and relative humidity inside the chamber. This is a unique feature of this equipment.

7.2.4 Sensors and their placement

Several sensors are used to measure different parameters, as well to impose or control other parameters. This section explains in detail each of those sensors.

7.2.4.1 Tensiometers

Careful recording of suction changes during the process of desiccation is very important because these changes in suction can be closely matched to changes of the degree of saturation. When this data is combined with information about the time when the first crack appears, valuable information about the state of the soil at crack initiation can be obtained.

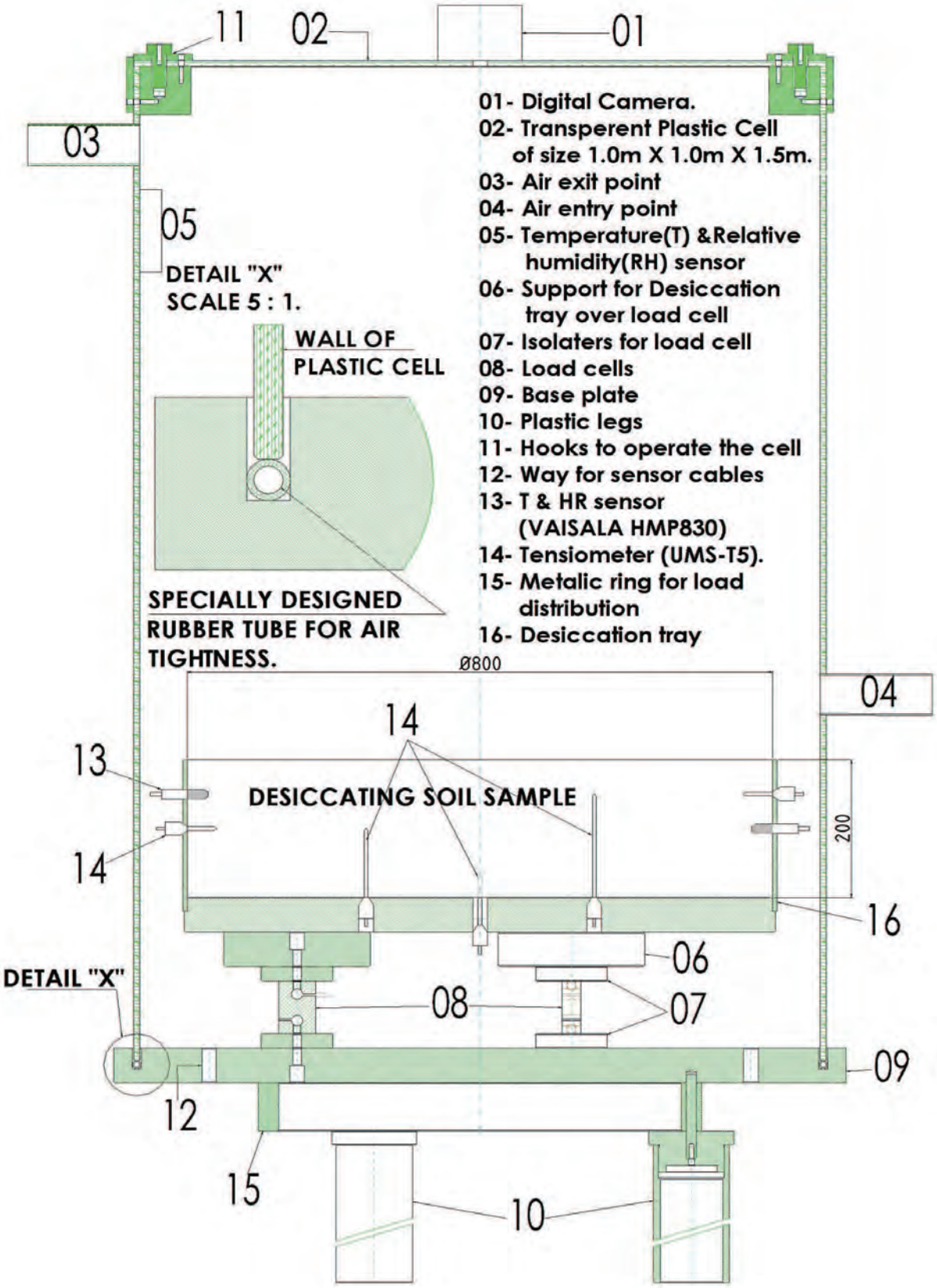

Figure 7.3: Schematics of Environmental Chamber

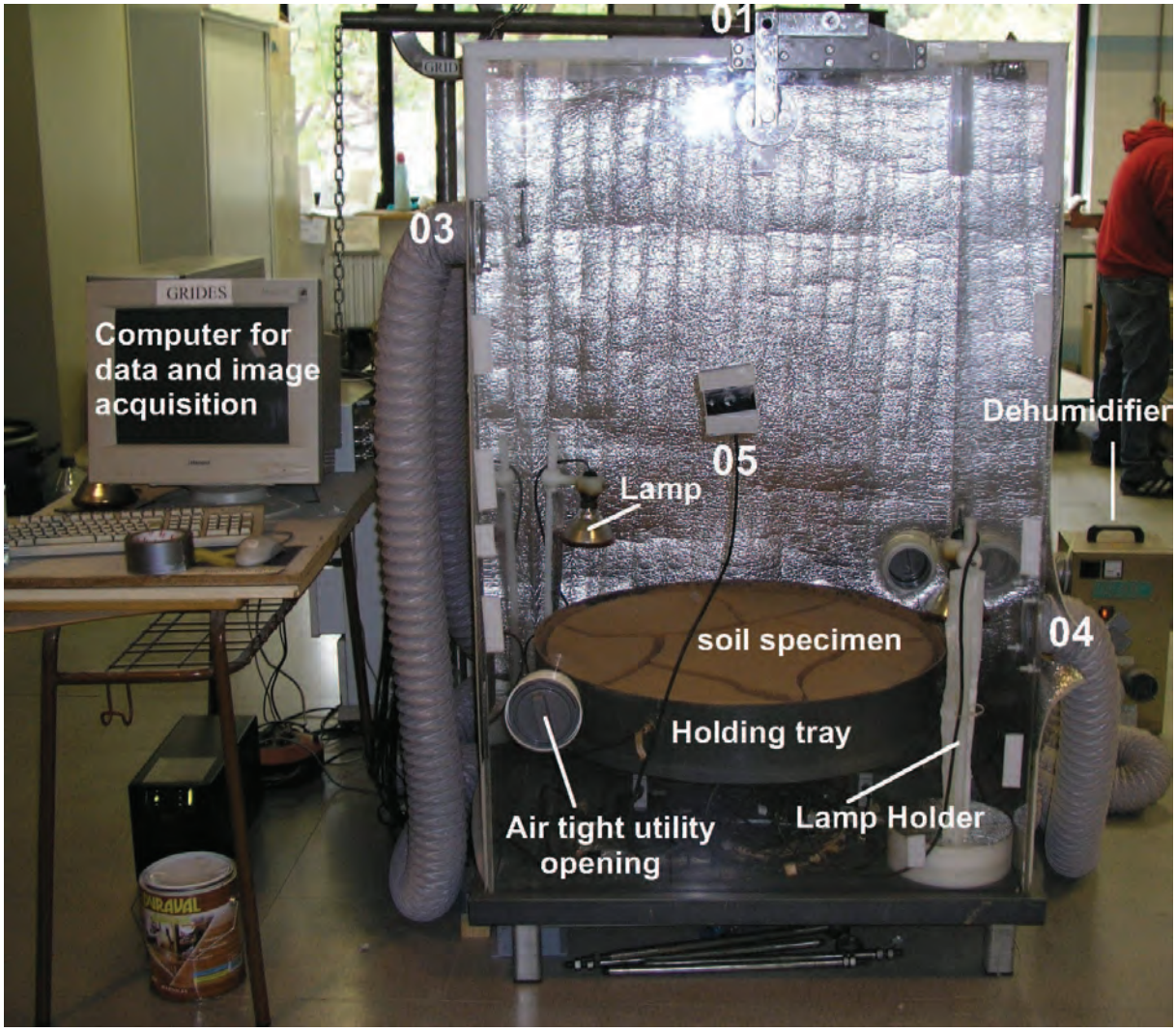

Figure 7.4: Environmental Chamber in the laboratory; the numbers represent the different parts as indicated in figure 7.3

Tensiometers are devices measuring the soil water tension and thus the suction. The tensiometers used are UMS-T5©, with a working range from +100 kPa (water pressure/level) to -85 kPa (suction/soil water tension). A detailed description of their range, electrical, and electronic features can be obtained from the product's data sheet and users manual. The UMS-T5©tensiometer was selected because of its miniature size and accurate measurements at very low suctions. Figures 7.6 and 7.7 show the cross-section and top view respectively of the 80-20 and 80-10-P circular trays with the location of the six tensiometers T1 to T6. On images showing the top surface of specimens, the location of these tensiometers is clearly indicated by their respective label, whereas on the bottom surface, the position of the tensiometers can be identified by the small hole left in the soil where the sensors were located. The position of the tensiometers was planned to facilitates tracking of the evolution of suction in the specimen during the test. Because earlier

Figure 7.5: UMS©-T5 miniature tensiometer

experiments with rectangular and circular trays (Chapter 5) showed that the specimen separates from the edges of the holding trays during the initial stages, two tensiometers (T5 and T6) were place on the wall of the holding tray to record suction during the early stages of desiccation. Four other tensiometers were placed at the bottom surface of the holding tray, among which one tensiometer (T1) at the center and the other (T2-T4) at equal distance from the center tensiometer. The tensiometers are placed at different depths in order to gain detailed information of suction distribution within the specimen. Changes of suction in time recorded by the tensiometers clearly show moisture loss and the location of the drying front.

7.2.4.2 Temperature and relative humidity

Two different types of special sensors measuring temperature and relative humidity were employed. The Vaisala© HMP-230 sensor was used to monitor the changes in soil water pressure and temperature within the soil specimen. Except for the smallest size (20-5), two of these sensors can be fitted to each specimen. The sensors can not be inserted from the beginning of the experiment because of high moisture content in the soil specimen at that time. Therefore a dummy sensor of the same shape and size was placed at the appropriate location (see figure 7.7). Once the tensiometers reached their peak value the dummy sensors were replaced by the real ones. Due to the difficulty in replacement during the experiment it was decided to place the sensors only on the walls of the holding trays. Figures 7.6 and 7.7 show the location of the sensors V1 and V2 for holding trays 80-20 and 80-10-P respectively. The location of this sensors are also clearly labelled in the images showing top and bottom surfaces of the specimen tested.

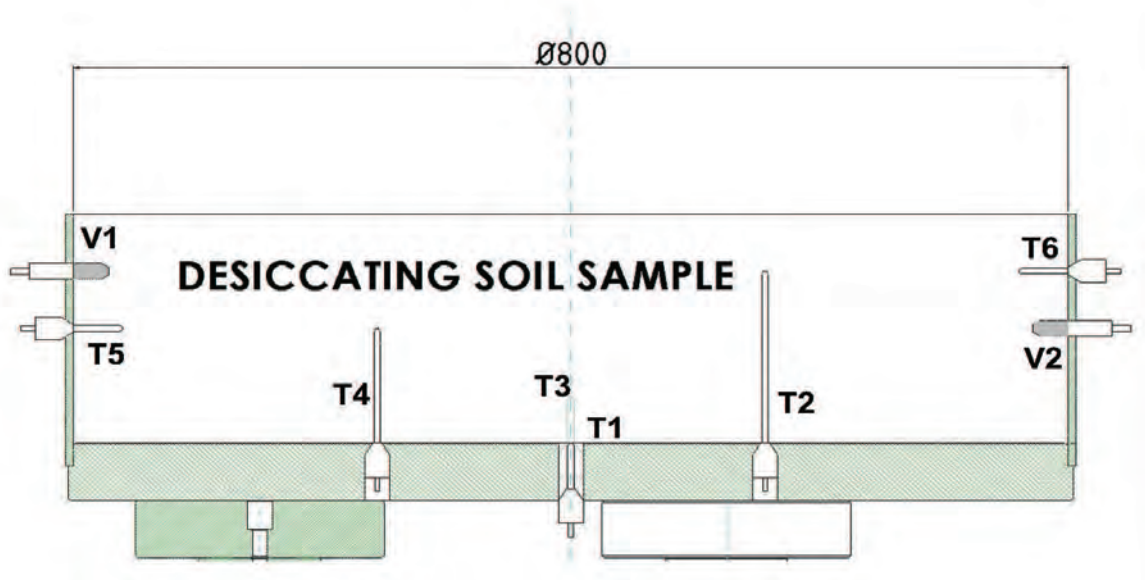

Figure 7.6: Cross-section of the 80-20 circular tray showing the location of tensiometers (T1-T6) and Vaisala humidity sensors (V1-V2)

A second Vaisala© HMD/W70 sensor was used to measure the air temperature and relative air humidity inside the chamber. This sensor is mounted on the interior face of the environmental chamber wall. The location of this sensor is marked as number 05 in figure 7.3.

7.2.4.3 Load cells

Three load cells INTERFACE© SSM series were used to monitor the weight loss due to water evaporation during the tests. The load cells were located on the base plate following an equilateral triangular pattern and sandwiched between the isolators and support plates.

7.2.4.4 Digital camera

An Olympus© C-5050Z was used to record images of the process of formation and propagation of cracks. The camera was fully computer-controlled to take pictures automatically at a prescribed time frequency. To support and position the digital camera, a special purpose mechanical arm was designed and constructed (figure 7.8). This mechanical arm has the shape of an inverted letter "L", consisting of a vertical extensible column supporting a horizontal cantilever arm that can be adjusted to properly position the camera, to get undistorted zenithal images of the specimen during the test.

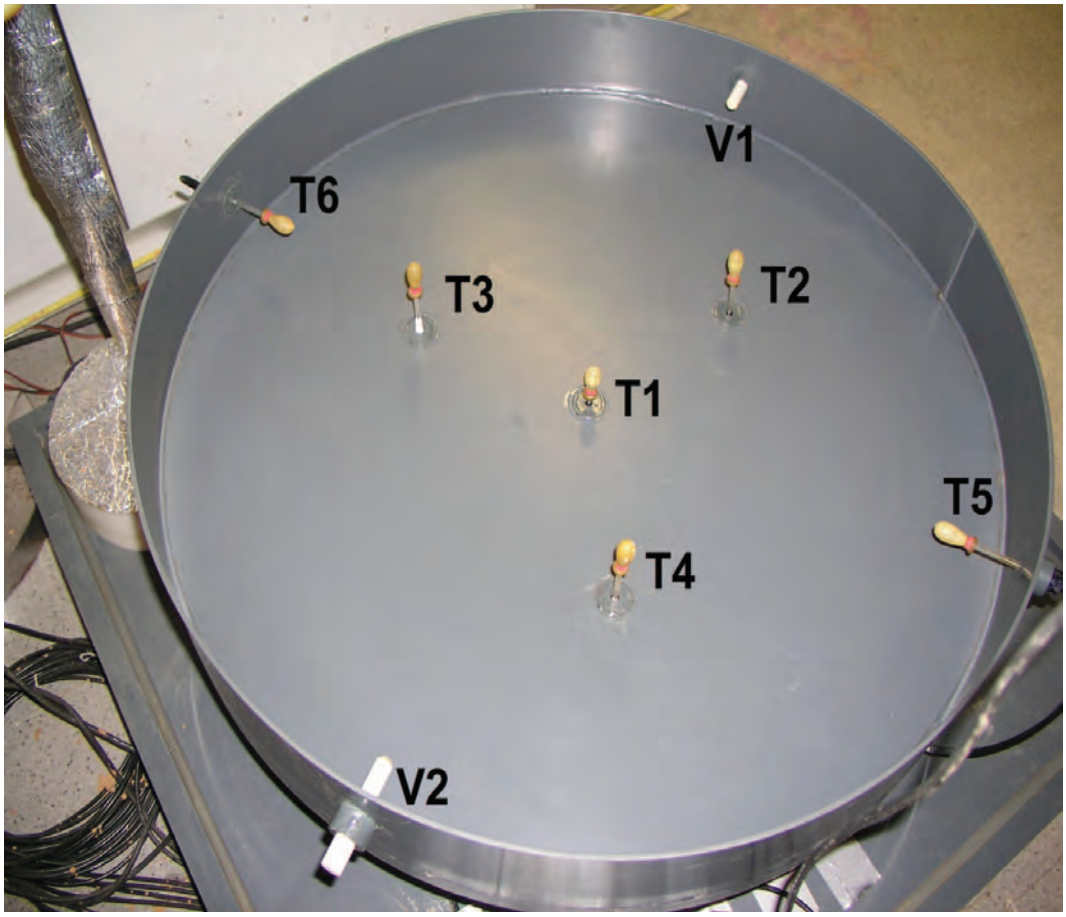

Figure 7.7: Top view of the 80-10-P circular tray showing the location of tensiometers (T1-T6) and Vaisala humidity sensors (V1-V2)

7.2.5 Temperature and relative humidity control equipment

To simulate cracking due to drying in soils high temperature and low humidity conditions are needed. A simple way to impose this conditions is by means of a heating source and a dehumidifier to remove air moisture.

7.2.5.1 Heating source

The chosen heat source are infrared lamps (figure 7.9). The location and placement of the lamps inside the chamber can be seen in figure 7.4. The lamp holders shown in figure 7.4 are made of plastic and are covered with reflecting foil. The lamps are turned on and off according to the prescribed temperature by means of a computer controlled interface. However, in order to maintain the temperature at a prescribed value of around 35°C the lamps have to be switched on most of the time.

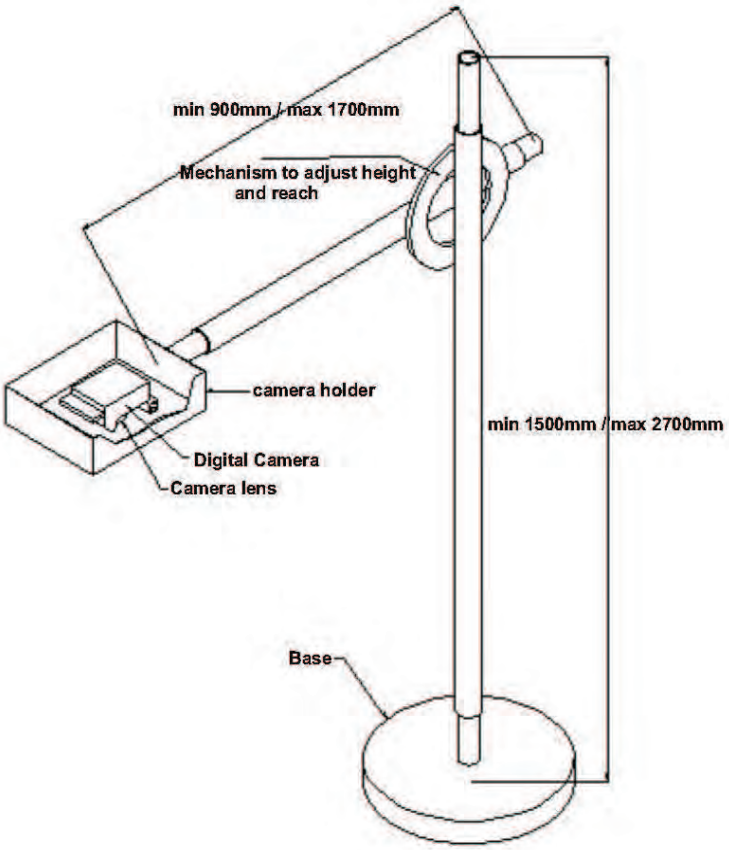

Figure 7.8: Special purpose mechanical arm for positioning the digital camera

Figure 7.9: Infrared lamp used as heating source

7.2.5.2 Dehumidifier

The air moisture in the environmental chamber is removed by means of a commercial dehumidifier DST-Seibu Giken© "RECUSORB DR-010B". This dehumidifier was selected for its power, relative to the largest specimen to be tested (80-20). The dehumidifier was connected in a closed circuit with the environmental chamber, recycling the air from the chamber to economise. The air entering and exiting the dehumidifier has approximately the same temperature so that the heating system in the environmental chamber does not have to work more to compensate the heat loss during the dehumidifying process.

Figure 7.10: Dehumidifier: RECUSORB DR-010B by DST-Seibu Giken©

7.2.6 Software interface

A software interface in Visual Basic© was written especially to control the tests in the environmental chamber. Data acquisition intervals from one second to several days can be set. The software allows incorporation of the calibration curves of the sensors. The data acquired is stored in plain text format and can be imported into spreadsheets for further analysis. The software has also an interface for prescribing the temperature and relative humidity of the environmental chamber.

7.2.6.1 Data acquisition

Two National Instruments© Data Acquisition Cards (PCI Card, NI-PCI:6023) were used for data acquisition. The PCI card was mounted on the CPU of the computer and a separate connection box was constructed to connect all the analog input from the sensors to the different channels of the data acquisition card. The connection box also has digital outputs for controlling the heating and dehumidifier equipment and houses the necessary signal conditioners and electrical installation to power the sensors. The power requirement of the each type of sensors is different and analog output needs amplification and/or conditioning, thus allocation should be made to power all the sensors and conditioning of the analog signal.

7.2.6.2 Control parameters and conditions

The parameters used to control the environmental conditions are the air temperature and the relative air humidity inside the environmental chamber. With just the two devices described above (heating source and dehumidifier) it is only possible to maintain the relative humidity at a prescribed value within a certain tolerance. As soon as the relative air humidity in the chamber is higher than the prescribed value, the dehumidifier is switched on; and when the relative air humidity in the chamber is lower than the prescribed value, the dehumidifier is turned off. A similar procedure is followed by the heating source, following input from the air temperature sensor. The choice of tolerance depends on the accuracy required and the equipment. For example, for temperature control a tolerance of $\pm$ 0.1°C is acceptable while for relative air humidity a tolerance of $\pm$ 0.5% may be needed.

7.2.6.3 Image acquisition

Image acquisition was performed using a software called CAM2COM©. The software detects the camera connected to the computer through a USB port and if the camera has the hardware necessary, the software can be used to control the full camera operation, including prescribed times for taking pictures, setting of frequency-intervals, selecting output devices for storage of images, etc.

7.2.7 Options for additional features

The environmental chamber is fitted with only two devices for air temperature and humidity control: a heating source and a humidifier. However, having full control of this variables and being able to prescribe their cycles to simulate real natural conditions, would require two more devices: a cooling source (such an air conditioner) to lower the temperature, and a humidifier to increase the relative air humidity. The environmental chamber has options for adding these two additional devices for future tests.

7.3 Experimental program and objectives

The main objectives of the experimental program were to test the performance of the environmental chamber and to conduct some preliminary tests on specimens of different sizes under a controlled environment. Three experiments were carried out using the environmental chamber with a temperature of 35°C and a relative humidity of 40%. Some tests were also carried out with the same type of specimens and holding trays while the chamber was being finished.

7.4 Specimen preparation and experimental procedure

The soil was allowed to dry in open air and then passed through a mechanical sieve (size 6 mm). The dry material that passed through was then mixed with distilled water until a visibly homogeneous paste was obtained. The prepared soil paste was then poured in the holding trays, and small blows were given to the edge of the trays to remove air pockets. The surface of the sample was levelled with a straight edge to get a uniform surface. The soil left on the straight edge was taken to determine the initial moisture content. This procedure was repeated for all the specimens tested. For specimens of size 40-10 and 20-5 the soil could be prepared, because of their size, in a single mix. However for specimens 80-10 and 80-10-P the soil-water mixture was prepared in two batches that were later mixed together in a much bigger container, before placing the mix into the testing tray. For the specimen of size 80-20 the soil mix was prepared in a concrete mixing machine, in three batches. Moisture content was monitored for each batch of soil mix and also for the final mix just before pouring it into the testing tray. The initial moisture content for all the specimens tested was around 30% (similar to the specimens tested in Chapter

5). Note that the soil-water mixture prepared (either in a single, double or triple mix) was left for 24 hours before pouring it into the testing tray. Moisture content was again determined at each of these steps.

Before the start of an experiment, the following steps should be taken:

- Tensiometers should be checked to ensure that they are fully saturated and there are no air bubbles inside the tube.
- If a tensiometer is not saturated then care should be taken to saturate it following the instructions given in the device's user manual.
- The temperature and relative humidity sensors (Vaisala) should be checked for its correct functioning.
- Care should be taken that the isolators and the support plates of the load cells are fixed with a correct tightness. A connection that is too tight or too loose may result in damage to the load cell.
- The sensor measuring air temperature and relative air humidity inside the chamber must be checked carefully, because it is the sensor which reading will trigger the heating and dehumidifying devices.
- Checks should be carried out on the software interface, to ensure that change in temperature and relative humidity will trigger the corresponding devices.
- The holding tray should be placed well centered on the three load cells and its weight should be recorded.
- The holding tray has special fittings at the locations where the sensors must be placed. Each fitting is unique to the sensor it houses, and has a rubber washer to ensure airtightness. All the fittings should be checked with care for the presence of the rubber washer and its condition, because a leak in only one sensor might damage the load cells, and the cables of the sensors.
- The tensiometers should be placed in their designated locations. Care should be taken to prevent them from drying till the soil mixture is poured, by placing a rubber cap with distilled water on the ceramic cup at the end of the sensor tube.
- A dummy sensor should be installed in place of Vaisala temperature and relative humidity sensor.
- The weight of the holding tray with the sensors in place should be recorded again.

- Computer controlled data acquisition starts at this point and continues onwards.
- At this point the soil-water mixture, prepared the previous day, is poured into the tray. Care should be taken while pouring the mixture, because the tensiometers are very fragile devices.
- Once the holding tray is full, the top surface is levelled using a straight edge.
- The outer walls of the holding tray and other surfaces outside the tray should be cleaned for any mud spilled over, so that there is no damage to the cables and other sensors.
- During the previous steps the Vaisala temperature and relative humidity sensors should be with its protective cap on.
- Place the lamp holders with the heating lamp in their position, usually at the corner opposite to the utility opening.
- Lower the chamber walls and top very slowly, till it positions itself in the groove with the special rubber sealing tube.
- The air entry and exit points to the chamber must be connected to the dehumidifier in a closed circuit and then make sure that the dehumidifier is in the ON and AUTO mode.
- Set the temperature and relative humidity to their prescribed values, using the software interface.
- The chamber box should be disconnected from the roof pulley and the metallic frame attached to the chamber box should be removed.
- The mechanical arm holding the digital camera should be moved on top of the chamber, positioning it to the center of the top cover. Some test pictures should be taken to check the quality of the images and adjustments should be made for optimal quality. Once set, the camera holder should not be moved for any reason till the end of the test.
- Though the system functions automatically, monitoring of the main functions of the environmental chamber and the software interface is advised during the first few days of the test.
- It is recommended to keep the frequency of image acquisition to a minimum of one image every 30 minutes during the initial period. This frequency may be increased to 3-4 hours after the primary cracking starts developing.

- Some experiments last more than a month. Therefore, the computer auto-update features needs to be disabled and its operating system needs to be manually updated regularly. Attention should be paid in case of spurious reboots of the computer due to power failure or other unforeseen circumstances.
- Regardless of the amount of hard disk space, keeping in the system only the latest and relevant test data would result in better functioning of the system.

7.5 Results of tests in open laboratory conditions

These experiments were carried out while the environmental chamber was being built. Because the holding trays were ready before the environmental chamber was completed, some tests were conducted in an open laboratory atmosphere with controlled air temperature and humidity. Three tests were carried out under such conditions and are described in detail in the following sections.

7.5.1 Specimen size 80-20

This is the largest specimen tested in the present investigation and also the largest the chamber can accommodate. The holding tray for specimen size 80-20 can be seen to the scale in figure 7.2.

The duration of this test was 119 days. The time evolution of the surface crack pattern can be seen in figure 7.11, where 15 selected images of the top surface of the specimen taken during the test are shown. The first image corresponds to the starting of the test. Most cracks were observed during the first 8 days, the first cracks appearing at around $t = 8.24$ days. The images corresponding to $t = 10.05$ days and $t = 12.09$ days show the evolution of these primary cracks. Two new crack appeared at around $t = 14.30$ days, one exactly where sensor V1 (see figure 7.12) was located; the other can be seen at the bottom of the image. These two cracks seemed to propagate simultaneously till $t = 25.31$ days. Further, the crack originating from point V1 seemed to stop while the other crack propagated to reach the crack at the other end. At that point, the crack originating from V1 continued propagating (see image for $t = 39.29$). The rest of the images corresponding to $t = 48.61$ days onward till the end of the test show only minor changes in crack morphology. Figure 7.12 shows the upper surface of the specimen at the end of the test, with the positions of the tensiometers (T1-T6) and the Vaisala temperature and relative humidity sensors (V1-V2) marked. It is interesting to note that the presence of the sensors is not directly causing

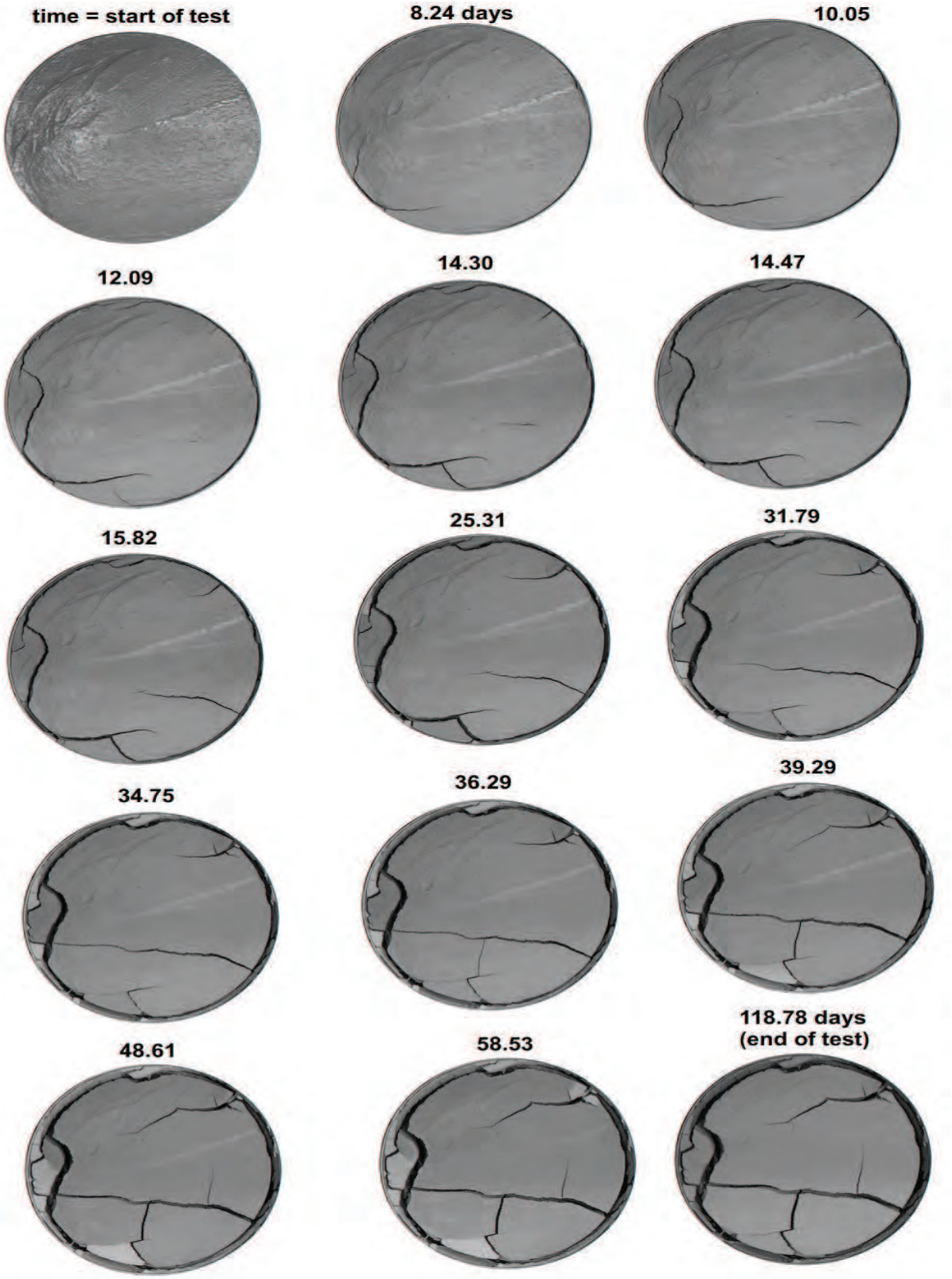

Figure 7.11: Evolution of surface crack pattern of specimen 80-20 under open laboratory conditions

a crack nucleation, the only exception being sensor V1. The crack which appeared last is less wider and the crack which appeared first is the widest. The crack pattern produced in this test is relative simple if compared to more complex patterns, with several levels of crack families, that were seen in the tests reported in Chapter 5. However, a most relevant and unexpected observation was made while dismantling the specimen for recovery of the sensors.

Dismantling of the specimen is a very laborious and time consuming procedure, with much care taken not to damage the sensors which are very fragile. Removing the sensors from the specimen is difficult because during the test it become very hard, and water is injected with a syringe to loosen the areas where the sensors are located. Not much regard was taken about preserving the specimen for further study. However, observation of the bottom surfaces of intact portions of the specimen revealed that a crack pattern had also developed at the bottom surface, even if at the top surface no cracks were visible (see figure 7.13). Because of this observation, care was taken in subsequent tests to preserve the bottom surface so that images could be obtained for further analysis.

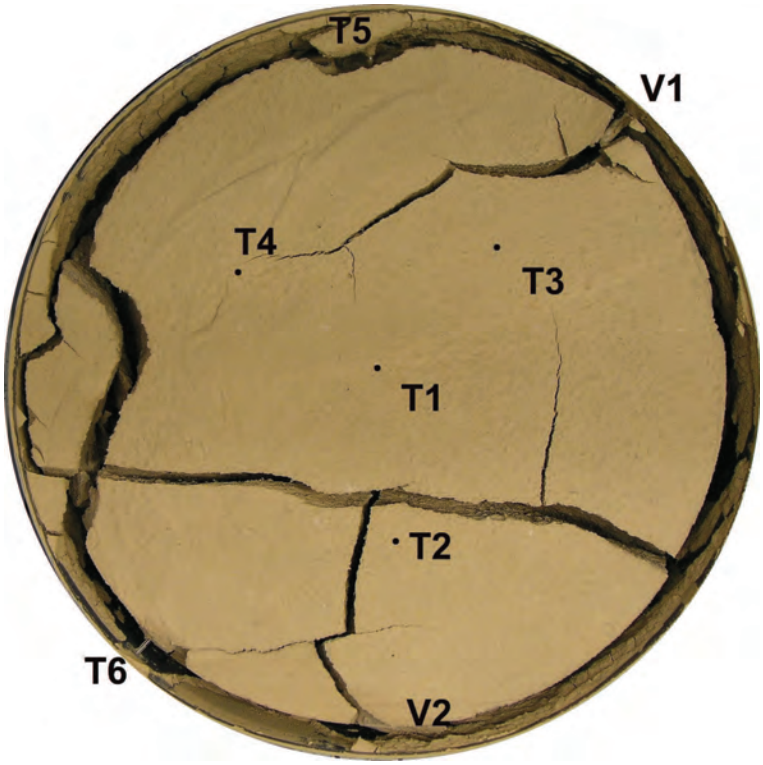

Figure 7.12: Top surface of the specimen 80-20 at the end of the test under open laboratory conditions, with the position of the sensors marked

Time evolution of various parameters are shown in figures 7.14, 7.15, and 7.16. The evolution of both air and soil temperature and relative humidity as well as the moisture

Figure 7.13: Bottom surfaces of intact portions of specimen 80-20 revealing cracks that are not visible on the upper surface

loss or desiccation curve can be seen in figure 7.14. The figures show anomalous readings during the first 50 days of the tests caused by some serious problem with the laboratory air-conditioning equipment. Normally the temperature in the laboratory should be stable at around 21±0.5°C; however, because the air-conditioning failure, the temperature in the laboratory showed much greater oscillations following the environmental cycles. Although after that initial 50-day period the problem was solved and the temperature was stable, most of the cracking had already taken place, making the analysis of the results far more difficult to perform. Nevertheless, regardless of the laboratory air temperature oscillations it appeared that the rate of moisture loss was not much affected. The temperature within the specimen was always less than the air temperature, but the difference decreased from about 4°C at the beginning of the test to about 1°C at the end. The discrepancy in the readings of the Vaisala sensors at $t = 39$ days, when sensor V1 showed a moisture decrease while V2 indicated the soil was continuing to be fully saturated, may be explained by a crack appearing directly above sensor V1.

Figure 7.15 shows the evolution of suction in the specimen measured by the tensiometers T1 to T6, located as indicated in is shown in figure 7.12: T1 is located at the centre of the specimen; T2, T3, and T4 each are located at a distance 18 cm from the centre; T5 and T6 are located at 10 cm and 5cm from the surface respectively as shown in the cross-section view of figure 7.1. A tensiometer measures the water pressure transmitted via a ceramic cup to the deionised water in the tube. If there is loss of contact between the ceramic tip and the water in the soil matrix, then the ceramic tip starts loosing water

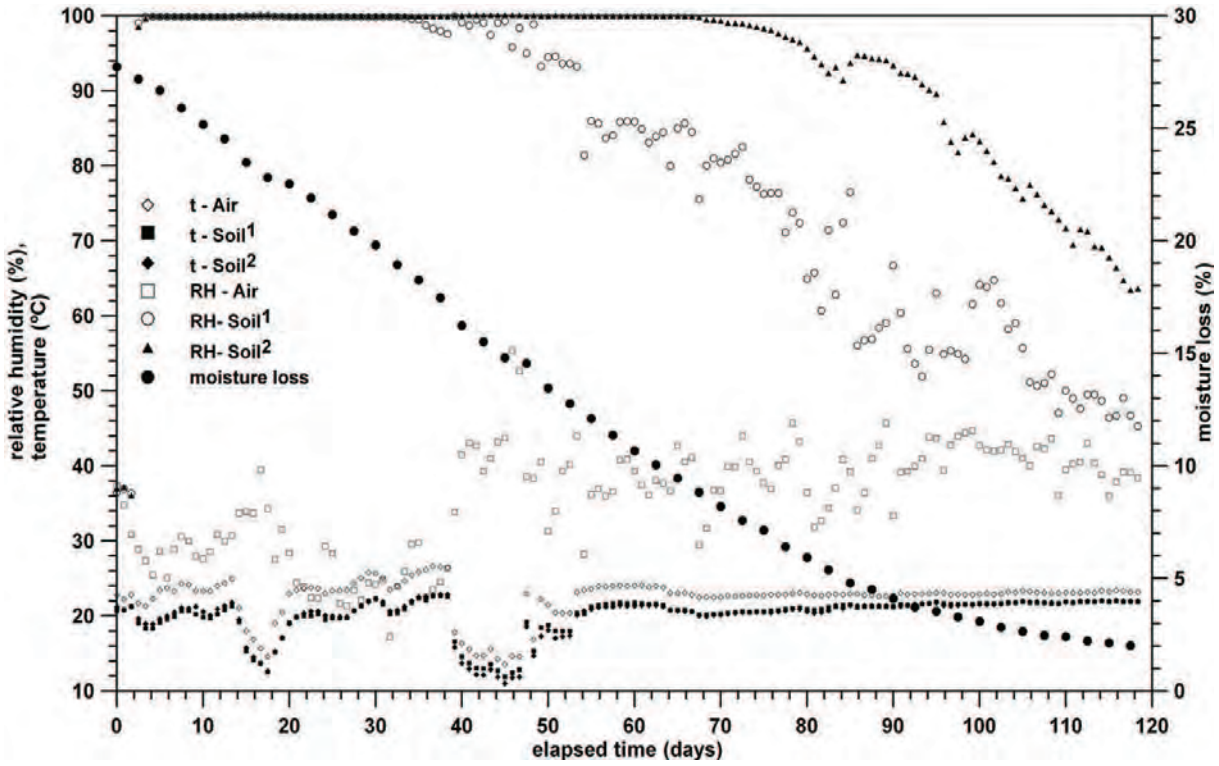

Figure 7.14: Time evolution of various parameters for specimen 80-20 under open laboratory conditions

(cavitation) and the sensor no longer measures the real water pressure. Then the reading from the tensiometer falls to zero. Cavitation occurs some time before the upper limit of the sensor is reached. As explained above, during the first 50 days of the test the laboratory temperature and relative humidity had severe oscillations, which are reflected by the many peaks shown by the measured suction. Because of these quick oscillations in the readings it was difficult to plot all them in one single graph. For clarity each tensiometer reading is plotted as a separate graph. Regardless of the several peaks, only the one before cavitation occurs and the suction falls to zero is considered here. For most of the tensiometers the peak occurred at a suction of about 60-80 kPa, except for tensiometer T6 which reached a suction of 110 kPa before cavitation. An interesting observation is that the time taken to reach the peak increases from the tensiometers on the periphery toward the centre. Tensiometer T6, which is located on the wall and is just 5 cm below the top surface exposed to drying, is the first tensiometer to reach the peak (about 34 days). Tensiometer T1, located at the centre, reaches peak at about 50 days. The rest of the tensiometers, which are in between, reach peak at about 45 to 52 days.

The measured soil relative humidity (shown in figure 7.14) is converted to suction and plotted in figure 7.16. The specimen remains saturated (at least where readings are made by the sensors) till $t = 34$ days. From then onward suction increases are shown by the

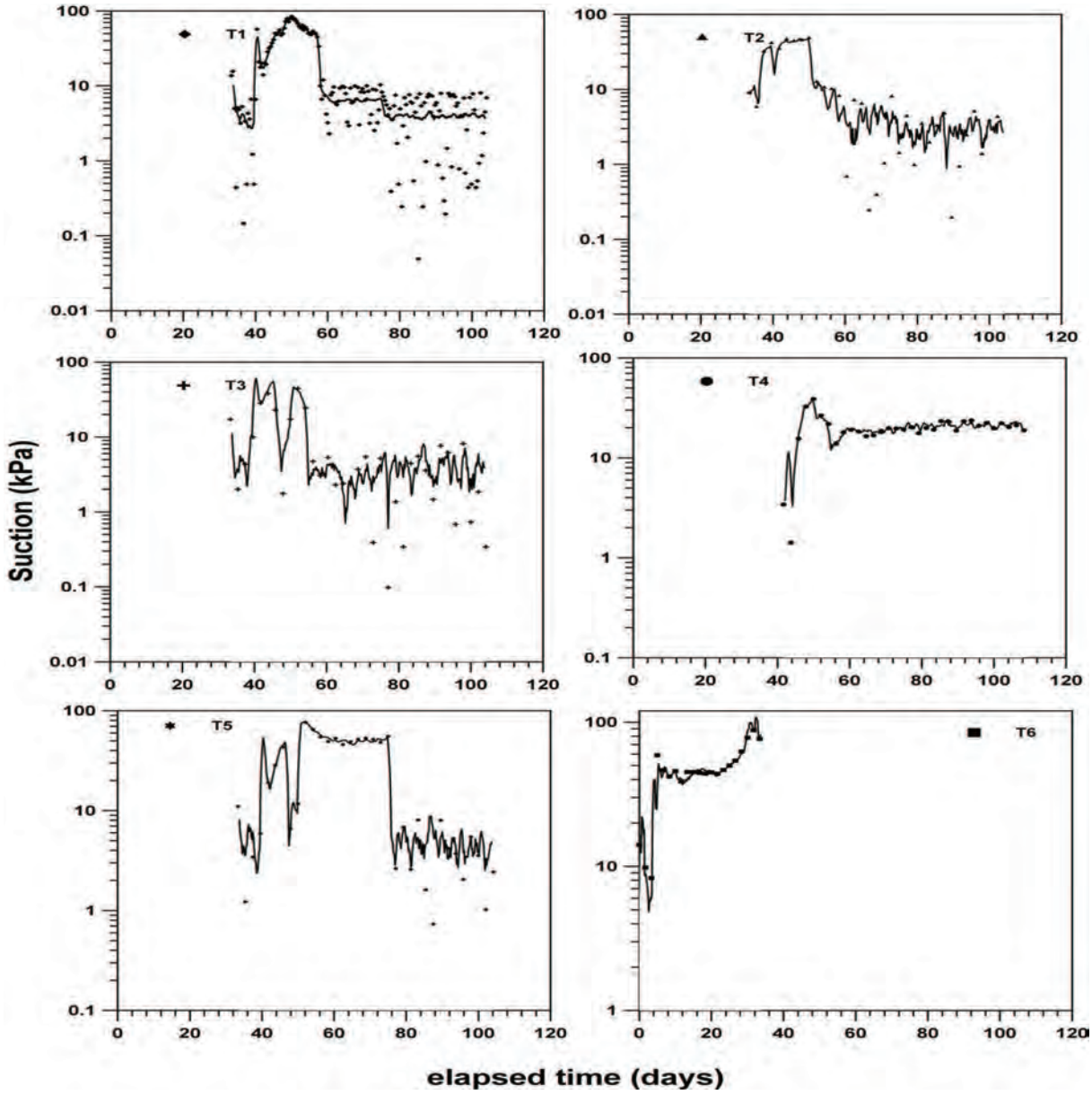

Figure 7.15: Evolution of suction in tensiometers T1 to T6 during the initial stages of the test for specimen 80-20 under open laboratory conditions

readings of sensor V1, while readings from sensor V2 indicated that there the soil remains saturated till $t = 68$ days. This difference in behaviour is due to the a crack starting to develop in the vicinity of sensor V1, thus inducing a faster rate of evaporation and therefore a loss of the saturated state earlier than in the area of sensor V2. Although no quantitative analysis was performed on this observation, this provides evidence of the influence of cracking on the rate of desiccation.

The results of the test were masked by the oscillations of air temperature and relative humidity in the laboratory during the initial and important phases of desiccation. It

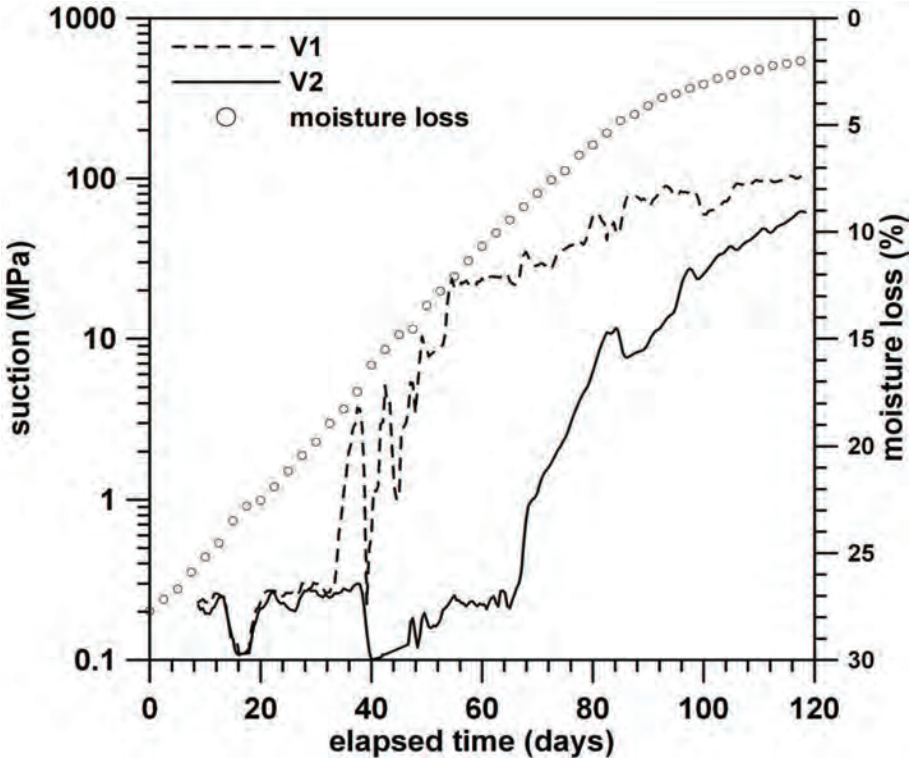

Figure 7.16: Evolution of suction from relative humidity data for specimen 80-20 at laboratory conditions.

seems, however, that the rate of desiccation was not too much affected by these oscillations. A possible reason could be the constant circulation of air provided by the air conditioners even though the temperature was not constant. At the time the first visible crack developed ($t = 8.25$ days) the readings from the tensiometers and the temperature and relative humidity indicated that the soil was still fully saturated. It could be objected that the sensors were at a depth inside the specimen while the crack appeared first on the exposed surface. However, the tensiometers started showing some signs of suction at about $t = 37 - 40$ days, and about the same time several well developed crack could be seen that were not superficial. Thus, first cracking in this test occurred when the soil was still saturated or perhaps quasi-saturated as proposed by Lloret et al [Lloret et al., 1998].

7.5.2 Specimen size 40-10

The holding tray for specimen size 40-10 can be seen to the scale in figure 7.2 Both the diameter and thickness of the specimen are half of the same dimensions in specimen 80-20. The total duration of the test was 110 days, but the moisture content in the soil reached equilibrium after 40 days. The location of the tensiometers and temperature and relative

humidity sensors is marked in figure 7.17. Only the two Vaisala sensors are located at the perimeter of the specimen. No tensiometers are placed at the perimeter for this specimen size. Four tensiometers are placed within the specimen, one at the centre and three at equal distance from the centre as shown in figure 7.17.

The image taken, at the end of the test, of the upper surface that was exposed to drying during the test is shown in figure 7.17. Other than the small perimeter crack, no other surface macro-crack developed during this test. There were very few micro-cracks that cannot be seen at the scale shown in the figure. The perimeter crack propagated from top to bottom making the specimen to fully separate from the tray wall. At the end of the test the sensors were recovered with extreme care not to damage the bottom surface of the specimen, and once the sensors were removed the specimen was turned upside down and photographed (figure 7.18). Contrary to the upper surface, some crack pattern did develop at the bottom one. The main cracks observed here seems to be radial, normal to the perimeter of the specimen. Some non-radial cracks following a circular pattern also developed. In the figure the hole left by the tensiometers can be clearly seen, and no crack seems to be originating from these points indicating that they are not weak points that might have triggered crack initiation. The tray used for this test had circular grooves at the bottom surface. The grooves can be clearly visible in the central part of the image, whereas near the perimeter the marks are less prominent. The reason for that is that as the specimen lost water due to drying, the outer part of the bottom surface of the specimen was slightly lifted due to curling and lost contact with the bottom surface of the tray.

Time evolution of several parameters during the test have been plotted in figure 7.19. Air and soil temperature and relative humidity, together with the desiccation or moisture loss curve are shown in figure 7.19a. The moisture content reaches equilibrium at about $t = 40-42$ days from the start of the test, when the relative humidity inside the specimen at this time is about 60%. The relative humidity sensor shows signs of desaturation beginning at about $t = 20-21$ days, when soil moisture content is about 12%. The relative humidity from day 21 onward decreases constantly till day 61 and thereafter it comes to equilibrium with the air relative humidity that in the laboratory was maintained at around 40% with little variations. The temperature was kept around $21\pm2^{\circ}$. The evolution of suction calculated from relative humidity data is shown in figure 7.19b. Similar to specimen size 80-20, there is a slight difference between the readings of the two sensors due to a crack developing in the vicinity of sensor V1. In this test the difference is much less prominent than in specimen 80-20 because the crack in specimen 40-10 was not exposed to open air. The suctions measured by tensiometers T2, T3, and T5 during the initial stages of the test are plotted together in figure 7.19c. The suction measured by

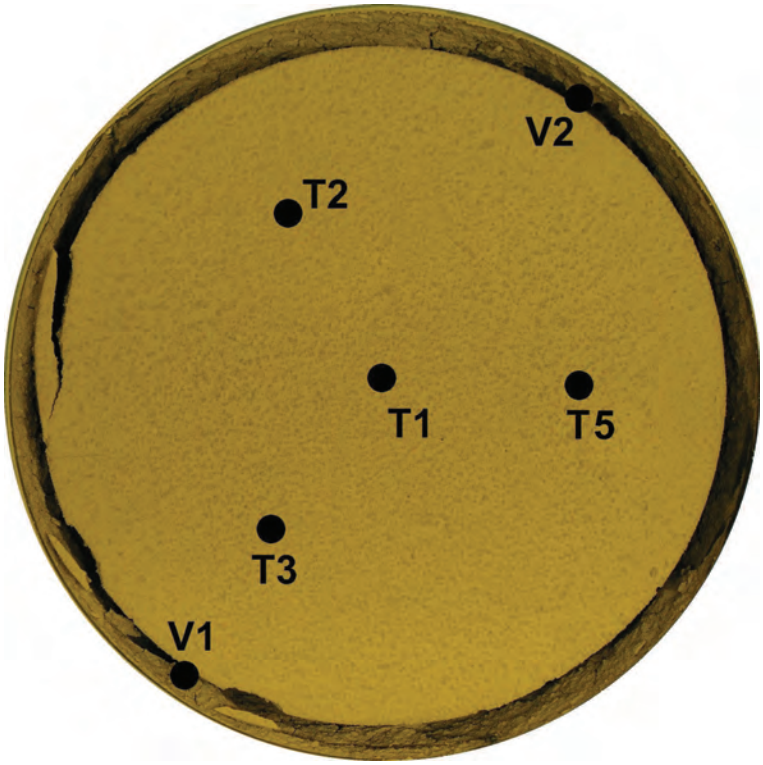

Figure 7.17: Upper surface of the specimen 40-10 at the end of the test under open laboratory conditions

tensiometer T1 is plotted separately in figure 7.19d. The readings from tensiometers reach the peak between 15 and 16 days after the beginning of the test. The suction increases very slowly until $t = 10$ days and from there onward the rate of suction change is quite fast. During the first 10 days the average suction was around 20 kPa, and the peak suction of around 80 kPa was reached at about $t = 15-16$ days. All the four tensiometers reached the peak more or less at the same time may be because the specimen did not crack and the rate of desiccation might have been constant along the upper exposed surface.

7.5.3 Specimen size 20-5

Both the diameter and thickness of the specimen are half of those in specimen 40-10, and one-fourth of those in specimen 80-20. The duration of the test was 28 days, with moisture content reaching equilibrium about 20 days after the beginning of the test. Because of the small size of the specimen, and in order to keep disturbance to a minimum, only three sensors were used in this test. In this case, only tensiometers were used, without the Vaisala sensors because of their big size (these sensors have a diameter of 13.5 mm).

Figure 7.20 shows the upper external surface of the specimen, with the locations of the

Figure 7.18: Bottom surface of the specimen 40-10 at the end of the test under open laboratory conditions

three tensiometers marked. The length of tensiometer T1 is a little under 5 cm, so when it was in place during the test it was barely covered with soil. The tip of this tensiometer was exposed to air during the test due to the vertical shrinkage of the specimen as shown in figure 7.20. Time Evolution of the different parameters during the test is shown in figure 7.21. The laboratory air temperature and relative humidity, as well as the specimen moisture loss during the test is shown in figure 7.21a. Laboratory temperature varied much during the initial 10 days and remained more or less constant at around 19±1°C during the rest of the duration of the test. The relative air humidity remained also constant at around 42±2% throughout the test. The desiccation or moisture loss curve shows the usual behaviour of rapid loss during the initial stages, then gradually decreasing and coming to equilibrium depending on the existing environmental conditions and the residual moisture retaining capacity of the soil (around 2% for the Barcelona soil at laboratory conditions). Figure 7.21b shows the evolution of the readings from the three tensiometers used in the test. Because the tip of tensiometer T1 was exposed to air due to specimen shrinkage, this sensor showed loss of saturation much earlier than for the other two sensor (around six days from the beginning of the test, see figure 7.21b). Tensiometers T3 and T5, which were inside the specimen at a depth 2.5 cm from the upper surface, reached the full range of suction (that the tensiometer can measure before cavitation) around 7 days from the beginning of the test. The evolution of suction during the initial

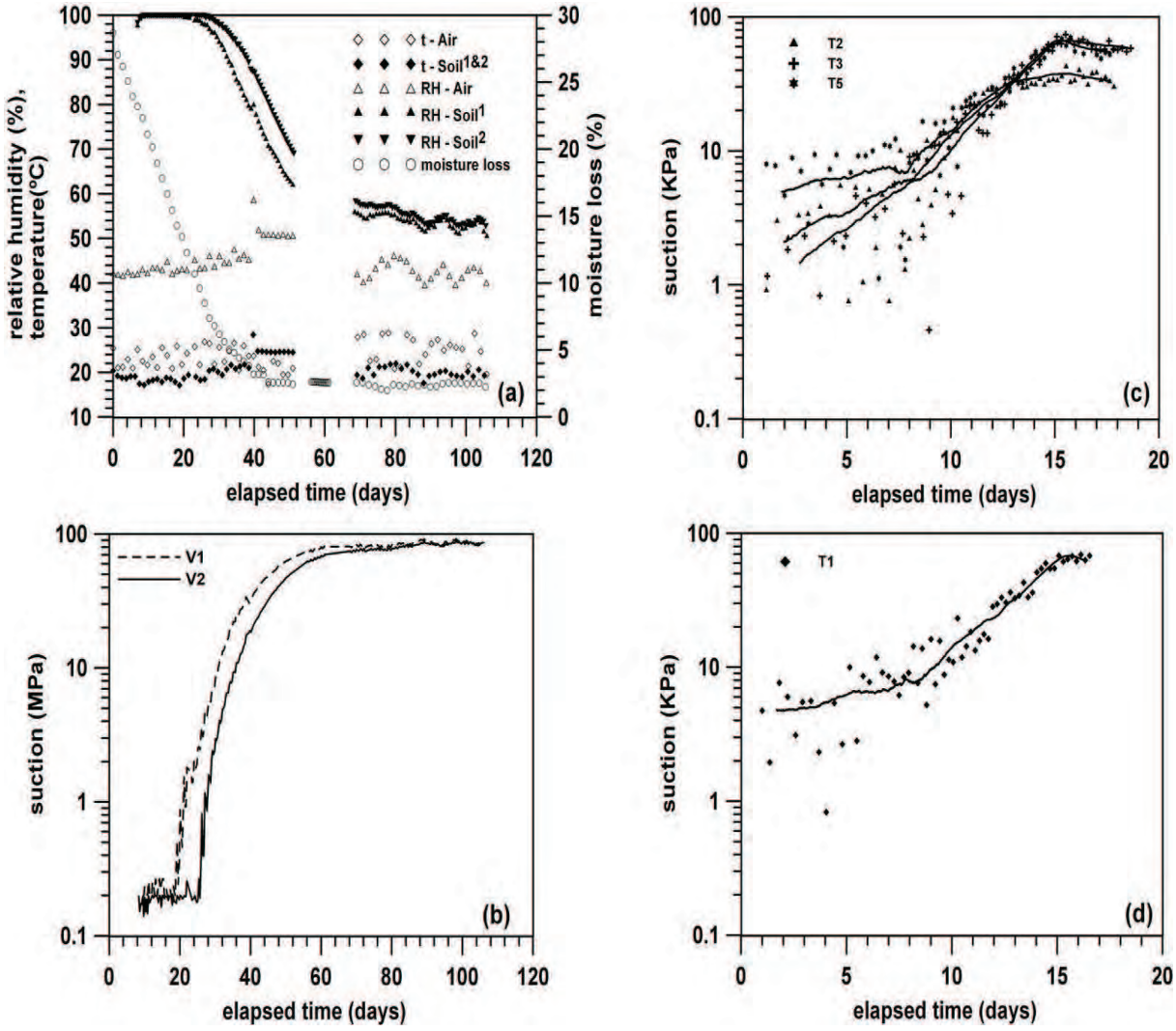

Figure 7.19: Time evolution of different parameters for specimen 40-10 during test under open laboratory conditions: (a) air and soil temperature and relative humidity, and moisture loss; (b) suction changes from relative humidity data; (c) suction at tensiometers T2, T3, and T5; (d) suction at tensiometer T1.

stages of desiccation seems to have been uniform throughout the specimen.

7.6 Suction from relative humidity data

Because of its relatively small range, the measures from the tensiometers could be used to determine suction only during the initial stages of desiccation and crack initiation. To have a complete history of suction throughout the test, suction was calculated from relative humidity measurements, that were carried out continuously during the test, using equation 7.1.

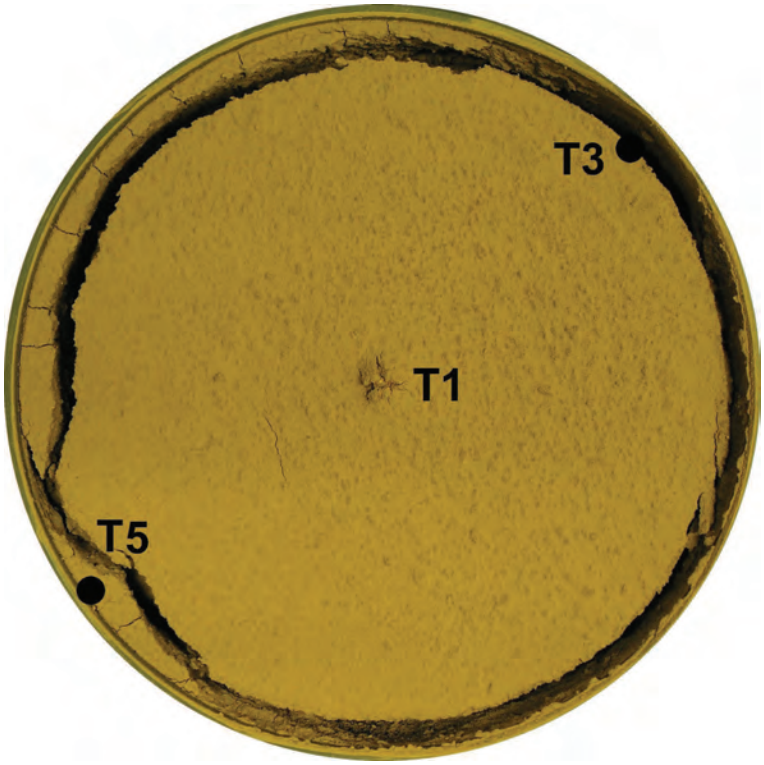

Figure 7.20: Upper surface of the specimen 20-5 at the end of the test under open laboratory conditions

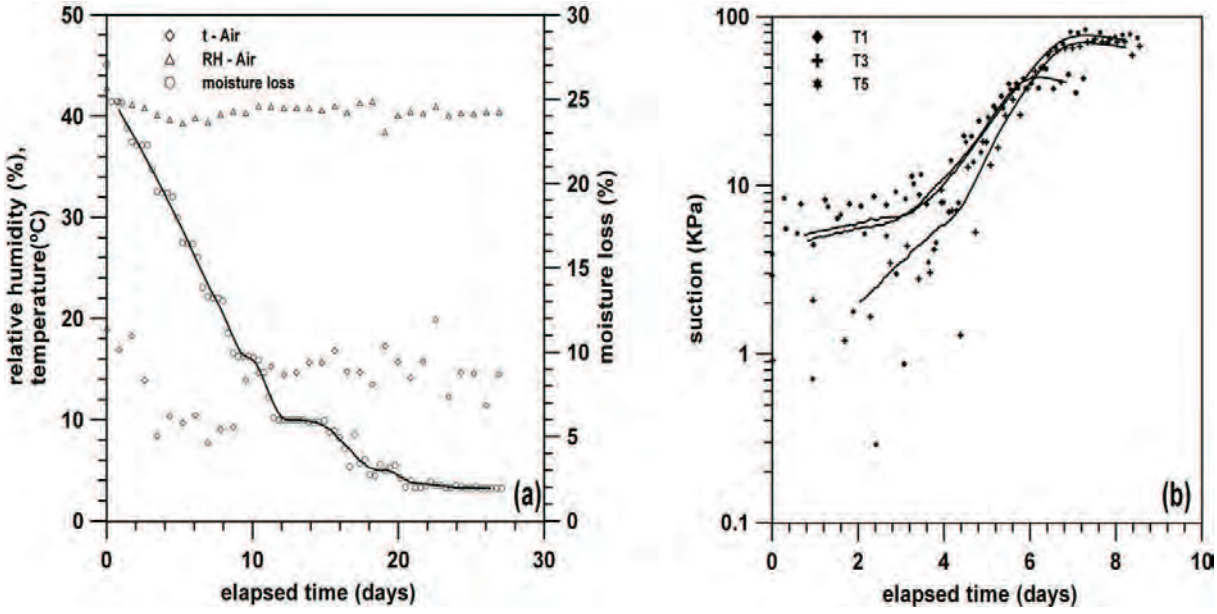

Figure 7.21: Time evolution of different parameters for specimen 20-5 during test under open laboratory conditions: (a) air temperature and relative humidity, and moisture loss; (b) suction at tensiometers T1, T3, and T5.

$$S = -\frac{RT}{V_w} \ln(h_{rh}) \tag{7.1}$$

Where,

S = Suction (Pa)

R = Universal gas constant = 8.314472 m^3 Pa k^{-1} mol^{-1}

T = Absolute air temperature = (t°C + 273.16) °K

V_w = Specific volume of water = 17.9798 $\times$ $10^{-6} m^3$ mol^{-1}at 22°C and 17.9086 $\times$ $10^{-6} m^3$ mol^{-1}at 35°C

h_{rh} = (Relative humidity in %/100)

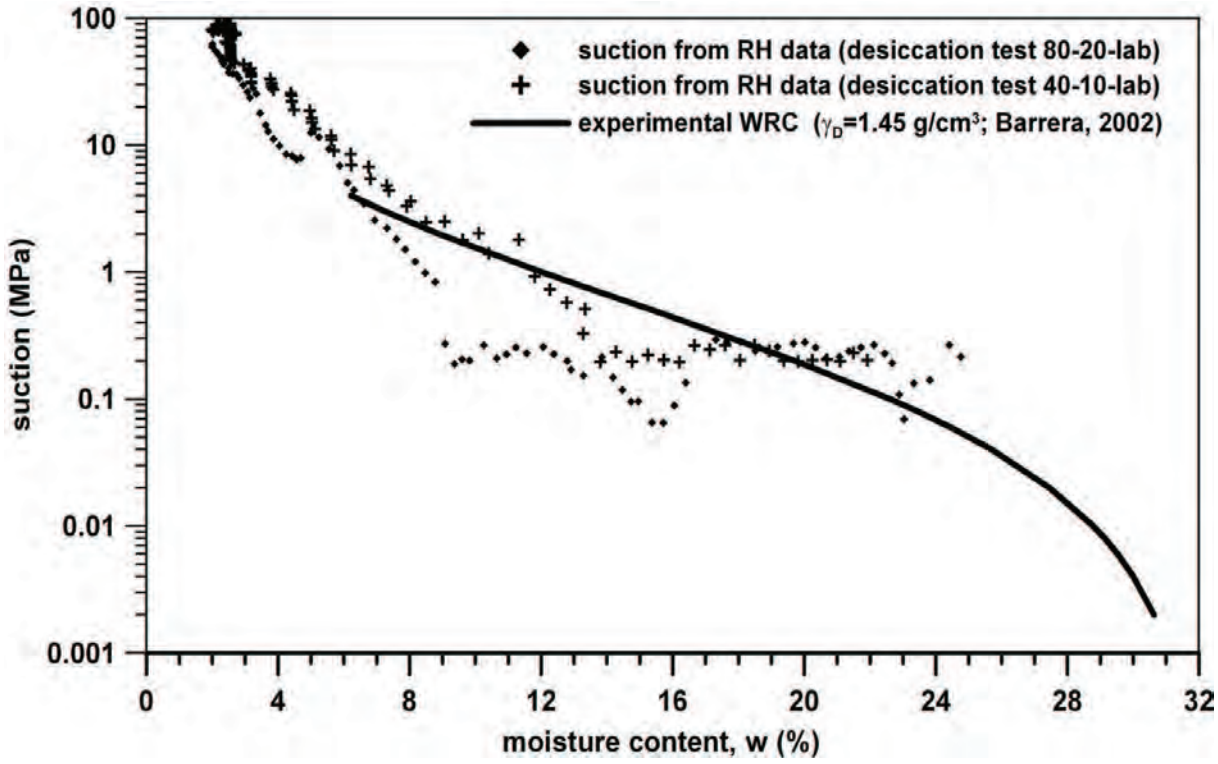

Figure 7.22: Suction calculated from relative humidity and comparison with data from Barrera [Barrera, 2002]

Figure 7.22 shows the suction calculated from relative humidity, compared to the water retention curve for the Barcelona soil determined by Barrera [Barrera, 2002] at a dry density $\gamma_d = 1.45$ g/cm^3 because this dry density is closer to the experimental conditions ($\gamma_d \approx 1.35$ g/cm^3) during the desiccation tests. Suction from test 40-10 (under laboratory

conditions) is in close agreement with the water retention curve. The dispersion observed in the data from test 80-20 may be attributed to the possible anisotropy cause during preparation of this very large specimen (80 cm diameter, 20 cm thickness and a weight of approximately 177 kg) that required mixing soil and water in three batches. Another possible reason to explain the dispersion are the oscillations of air temperature and relative humidity during this test(see figure 7.14). Nevertheless, suction from the measured relative humidity provides a fair estimate of the water retention capacity of the soil.

7.7 Results of tests in the environmental chamber

Three tests were conducted in the environmental chamber. The imposed conditions (temperature of 35°C and relative humidity of 40%) were the same for all the tests. The initial conditions were also the same for all tests (the specimens were prepared at a moisture content near the soil's liquid limit). The first experiment was carried out with a specimen size 40-10 (see figure 7.1). The second and third tests were conducted with a specimen size 80-10 using holding trays 80-10 (with circular grooves at the bottom contact surface) and 80-10-P (smooth bottom contact surface) respectively (see figure 7.1). This section explains in detail the observations during the experiments and the results for the three tests.

7.7.1 Specimen size 40-10

The holding tray 40-10 can be seen to scale in figure 7.2. The total duration of the test was 45 days, but the moisture content in the soil reached equilibrium after 40 days from the beginning of the test. The location of tensiometers and Vaisala temperature and relative humidity sensors is marked in figure 7.23. No tensiometers were located on the perimeter of the specimen, only the temperature and relative humidity sensors. Four tensiometers were placed in the specimen, one at the centre and three at equal distance from the centre as shown in figure 7.23.

Figure 7.23 shows an image of the upper surface of the specimen taken at the end of the test. This surface was exposed to the environmental conditions imposed in the chamber. The picture shows that no cracks developed during the test other than the perimeter crack that started at the upper surface and propagated toward the bottom. In this test the specimen shrank without developing any crack on the surface, similar to the test carried out under open laboratory conditions with the same specimen size (see section

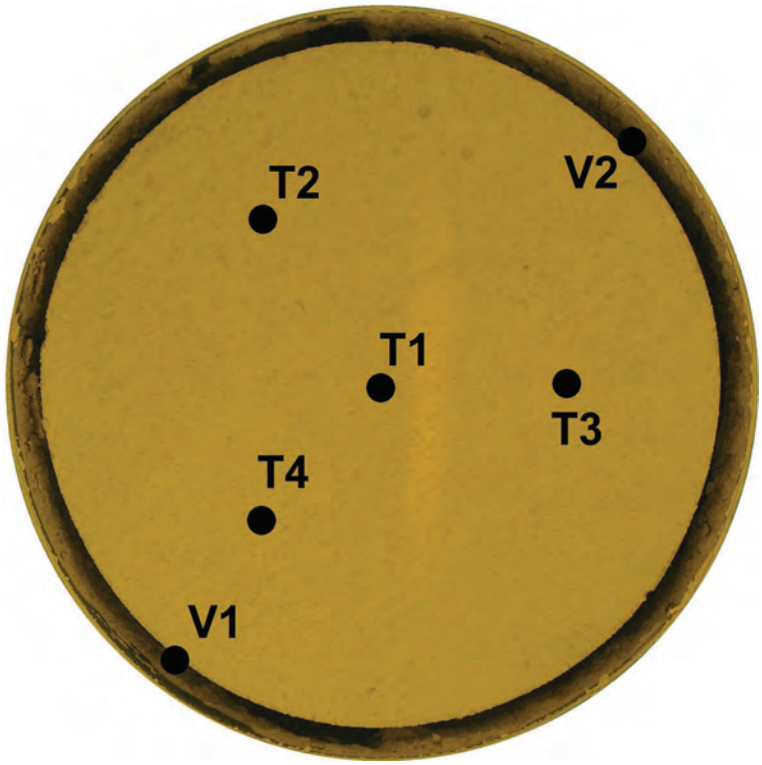

Figure 7.23: Upper surface of specimen 40-10 at the end of the test carried out in the environmental chamber

7.5.2). Very few small micro-cracks were noticed on the surface of the specimen but are not visible at the scale shown in the figure. At the end of the test the sensors were recovered with extreme care not to damage the bottom surface of the specimen. Once the sensors were removed the specimen was turned upside down and photographed (figure 7.24. Contrary to the upper surface, the bottom surface showed numerous cracks, the primary cracks having a radial direction, perpendicular to the outer perimeter. Some secondary cracks were also present, on a circular pattern. These curved cracks concentrate in the central part of the specimen while the radial cracks intersect the curved cracks. The intersections in the crack pattern indicate that the cracks were not formed simultaneously, but successively or hierarchically. Another morphological feature observed was that the curved cracks seems to be seamless, while the radial cracks join the curved cracks at right angles indicating that the radial cracks developed after the curved ones.

The hierarchy in crack formation between curved and radial cracks has wider implications. First, on the conditions for crack initiation and second, on the mechanism of crack initiation. The radial cracks can be assumed to be formed due to the curling phenomenon, but curling usually occurs at a later stage, i.e. during secondary shrinkage. If the curved cracks formed earlier than the radial ones they should have initiated some time during the primary shrinkage. However, during the primary shrinkage the specimen had sufficiently

Figure 7.24: Bottom surface of specimen 40-10 at the end of the test carried out in the environmental chamber

high moisture content to be either saturated or quasi-saturated with very low or negligible suction values. By definition cracks can be called desiccation cracks when they develop on a surface which is exposed to air or sub-aerial. In the present case both radial and curved cracks were on the surface which was in contact with the bottom of the holding tray. However, since the radial cracks were formed due to curling, there were loss of contact between the bottom surface of the specimen and the surface of the holding tray. Therefore, the specimen's bottom surface, in a ring near the outer wall, lifted and became in contact, at lest partially with air. During recovery of the sensors it was observed that the central portion of the specimen never lost contact with the bottom of the holding tray, thus curved cracks were formed without either aerial or sub-aerial exposure, but under sub-surface conditions. The crack formation in sub-surface conditions are attributed to a process called "synaeresis", which will be discussed in detail in section 8.6 of this Thesis.

Figure 7.25 shows the time evolution of several parameters during the test. Figure 7.25a shows the evolution of air and soil temperature and relative humidity as well as the desiccation or moisture loss curve. The moisture content reaches equilibrium at $t = 32-34$ days after the start of the test, but the soil's relative humidity at that time was still around 50%. At $t = 15 - 16$ days after the start of the test the relative humidity starts decreasing, but the change is very slow till $t = 18$ days. The relative humidity from that

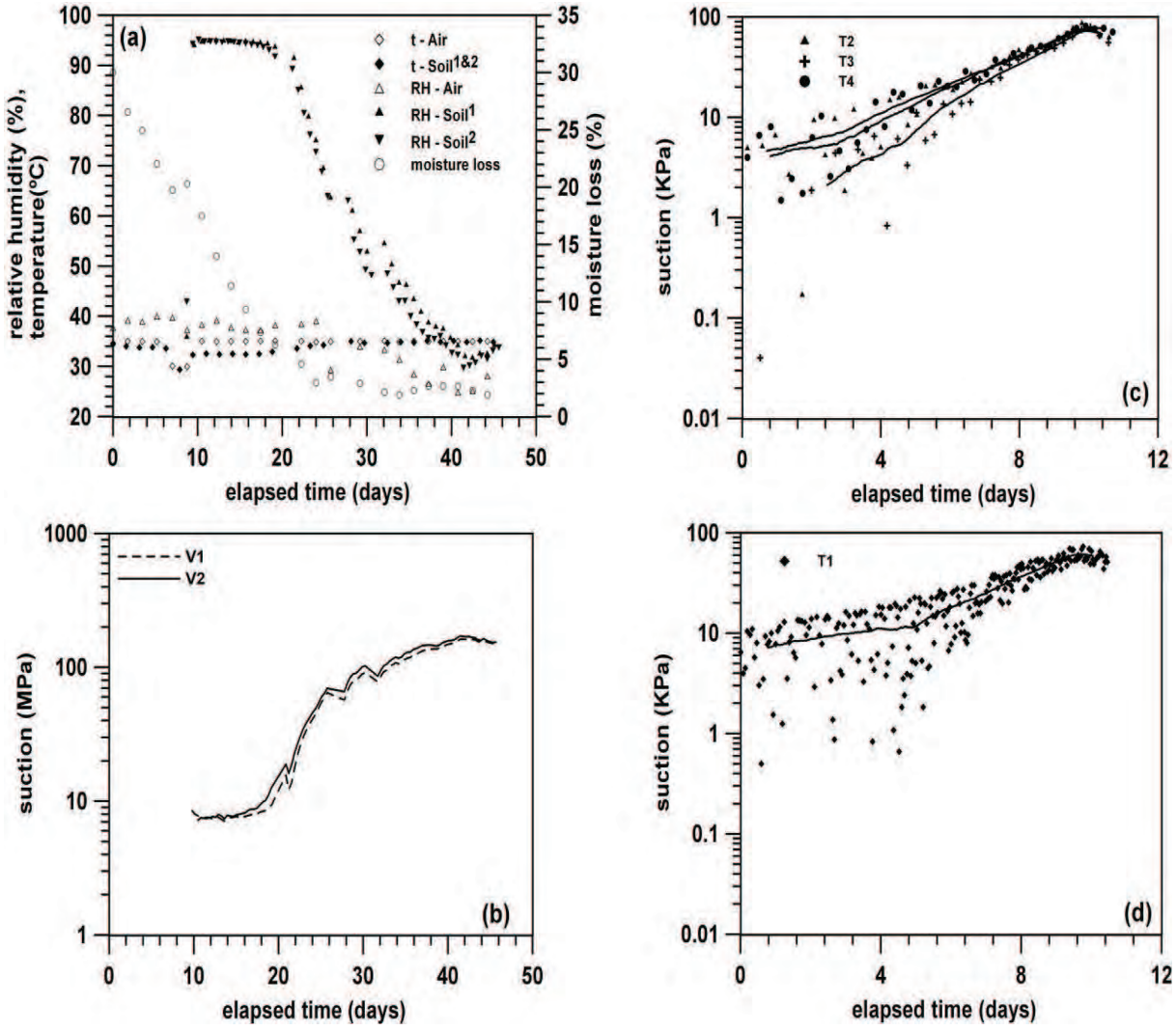

Figure 7.25: Time evolution of different parameters for specimen 40-10 during test in the environmental chamber: (a) air and soil temperature and relative humidity, and moisture loss; (b) suction changes from relative humidity data; (c) suction at tensiometers T2, T3, and T5; (d) suction at tensiometer T1.

time onward decreases constantly till $t = 40$ days and thereafter it comes to equilibrium with the relative air humidity. The relative air humidity in the environmental chamber was maintained at around 40% with little variations, and the temperature was maintained at around 35±0.2°. The evolution of suction calculated from the relative soil humidity data is shown in figure 7.25b, where readings from both the sensors seem to be similar because no crack appeared on the upper surface. This is in contrast to the test carried out under open laboratory conditions with the same holding tray, where a crack at the bottom surface affected the reading of one of the sensors. The suction measured during the initial stages of the test by tensiometers T2, T3, and T5 are plotted in figure 7.25c, while suction measured by the central tensiometer T1 is plotted in figure 7.25d. The

tensiometers reached the peak at $t = 10$ days after the beginning of the test. The suction increase measured by tensiometers T2, T3, and T5 was almost negligible during the first two to three days, but from the fourth day onward suction increased rapidly until reaching the peak. The tensiometer T1, which is located at the centre of the specimen, showed very little increase in the suction up to the 4th day and thereafter it followed the same trend as rest of the tensiometers. The initial slow suction development in tensiometer T1 can be attributed to the fact that the specimen dries from the periphery to the centre.

7.7.2 Specimen size 80-10

The environmental conditions imposed for this test were the same as for the previous test: temperature of 35°C and relative air humidity of 40%. The total duration of the test was 38 days, although moisture content in the soil reached equilibrium after 35 days from the beginning. The location of the tensiometers, temperature and relative humidity sensors is marked in figure 7.26. In this case, four sensors are located on the tray's perimeter wall: two Vaisala temperature and relative humidity sensors and two tensiometers. Four tensiometers were also placed within the specimen, one at the centre and three at equal distance from the center as shown in figure 7.26. The exact details of the location of each sensor in the holding tray is the same as in test 80-10-P, shown in figure 7.7.

Figure 7.26 depicts the image of the upper surface of the specimen at the end of the test. The figure also shows the locations of the sensors used. The presence of the sensors seems not have affected neither crack initiation nor the formation of the final crack pattern. Except for the crack appearing near tensiometer T2, the rest of the cracks intersect the perimeter of the specimen clearly indicating the effect of boundary conditions. The cracked cell at centre (containing tensiometers T1 and T4) is surrounded by relatively smaller cracked cells. The cracks seen at the surface divide the specimen into 7 cells with an average area of 718 cm^2. In the cracked cell with tensiometer T5, two small disconnected cracks developed. Figure 7.27 depicts the bottom surface of the specimen manually re-arranged after removing the sensors. The location where the tensiometers had been can be clearly identified by the hole left after removal of the sensor. On the bottom surface, several smaller cracks were observed apart from the main cracks which run from top to bottom. Observation of these smaller cracks in figure 7.27 is difficult because of the scale at which the image is presented.

The cell marked with a black rectangle in figure 7.27, which had contained the Vaisala sensor V2 (see figure 7.26) is shown in detail in figure 7.28. Groove marks can be seen near the central portion of the sample, but no groove marks appear near the borders.

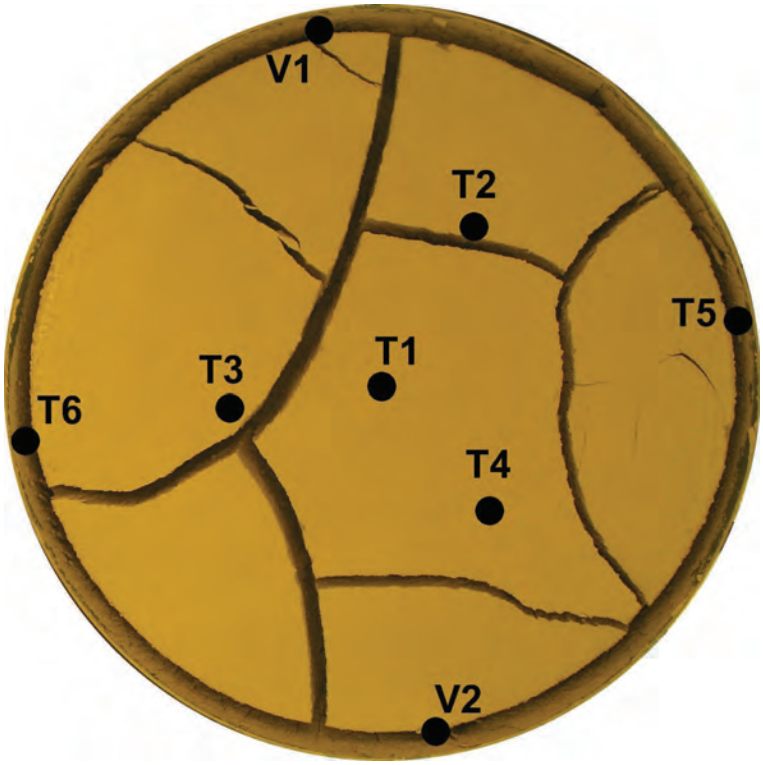

Figure 7.26: Upper surface of the specimen 80-10 at the end of the test carried out in the environmental chamber

The reason, again, is because the edges lifted from the bottom surface due to curling. Along the boundaries of the cell, several cracks originating from the edge toward the centre were observed. Most of the cracks may be also assumed to be due to curling of the sample. Incidentally, these cracks do not fully propagate to the centre of the sample, and seem to be confined to the lifted area where no groove marks are seen. A well developed circular/curved crack can be seen at the centre of the cell. A crack that has developed between opposite edges of the cell is located next to the central circular crack. Closer observation of this crack shows that the its width decreases from the edge corresponding to the perimeter of the original specimen toward the inner newly formed edge. From the morphological point of view, the point where the crack is widest indicates the crack initiation point and the direction along which the crack width decreases indicates the direction of crack growth. Therefore, it would appear that the crack started at the perimeter of the specimen and propagated toward the inner edge of the formed cell. The central circular crack and the edge-to-edge crack are close to each other and for a considerable stretch they are parallel to each other suggesting close interaction between the two cracks during their propagation. Since the edge-to-edge crack is wider, it seems likely that it developed first than the circular crack hence conditioning its development.

Time evolution of several variables recorded during the test are is depicted in figures 7.29,

Figure 7.27: Bottom surface of the specimen 80-10 at the end of the test carried out in the environmental chamber

7.30, and 7.31. Evolution of air and soil temperature and relative humidity as well as the moisture loss or desiccation curve is shown in figure 7.29. The temperature shows slight variations of ±0.2°C from the imposed 35°C. The relative humidity is kept between +0.2% -4% of the imposed 40%. The soil moisture reaches equilibrium after 35 days of drying. The evolution of the various parameters is explained by choosing 6 transition points: (1) the first crack was observed on the 8th day, next to the location of tensiometer T5 (see figure 7.26), but this crack did not develop to be a fully grown crack; (2) a fully developed crack was observed 11.5 days after the beginning of the test, just above sensor V1 (see figure 7.26), which resulted in a much faster rate of relative humidity loss recorded by sensor V1 than sensor V2, indicating the effect of crack formation on the surrounding moisture conditions; (3) on the 20th day more than 80% of moisture loss had taken place and the soil temperature started to increase, the temperature in the soil at this time being about 3°C less than the imposed air temperature, and a change in the slope of the moisture loss curve was observed; (4) the effects of the increment in soil temperature can be seen in the drastic change of the slope of the soil relative humidity curve on day 23, also on the same day another change in the slope of the moisture loss curve was observed; (5) from day 27 onward there was no further increment in soil temperature which remained almost equal to the imposed air temperature, the moisture loss curve was practically flat, the humidity control device was not triggered anymore because the

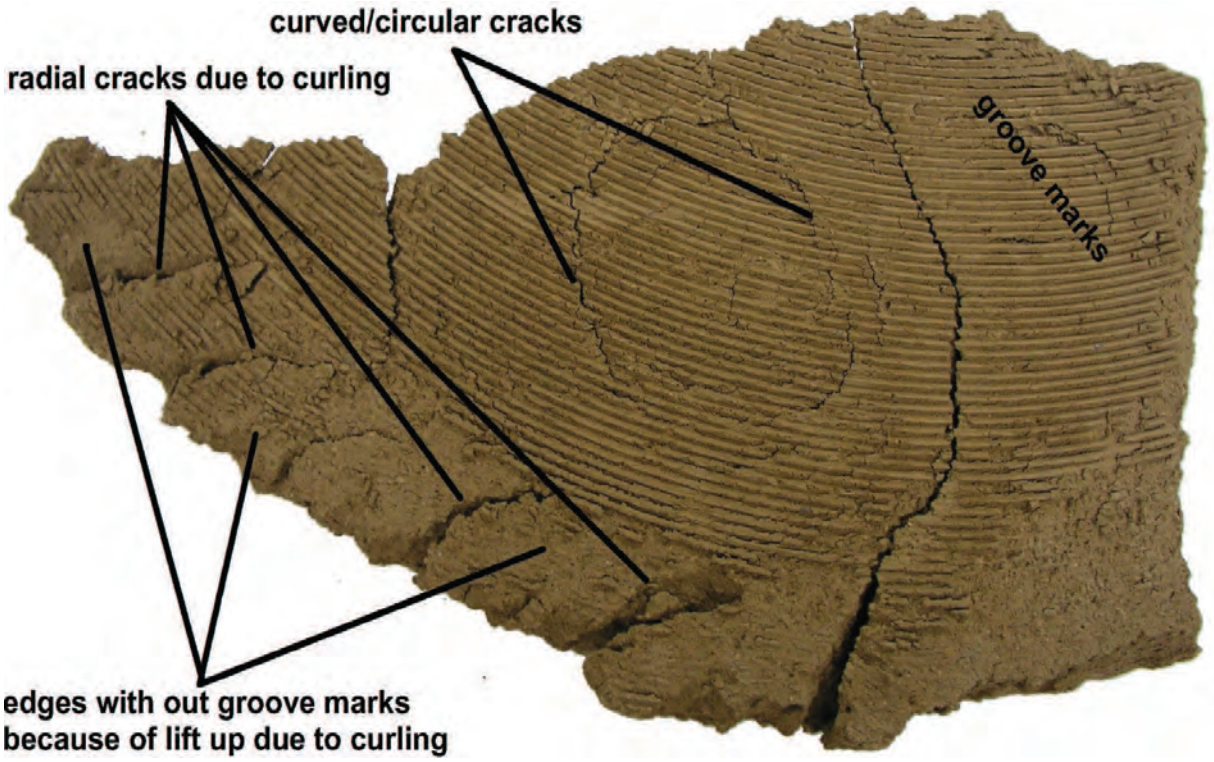

Figure 7.28: Detail of the cell marked with a black rectangle in figure 7.27 containing sensor V2 in figure 7.26

quantity of evaporating water was not enough to increase the humidity of the volume of air inside the environmental chamber; (6) around day 37, equilibrium between the air and soil temperatures and relative humidity was reached and as a result the moisture content of the soil stabilised with no further loss.

Figure 7.30 shows the evolution of suction during the initial stage of the experiment (first 15 days) measured using the tensiometers. The tensiometers can measure suction up to 100 kPa before desaturating, but at certain instances (e.g. loss of contact between the water in the tensiometer ceramic tip and the soil moisture) they may desaturate before reaching 100 kPa. The location of each of the tensiometers is shown in figure 7.26. Tensiometer T1 is located at the centre of the specimen. T2, T3, and T4 each are located at a distance of 18 cm from the centre. T5 and T6 are located at 5 cm from the surface. During the first 4 days the measured suction did not vary much, indicating the soil specimen was fully saturated. At around 5.2 days, the rate of suction variation in tensiometers T5 and T6 was more than for the rest of the tensiometers: suction values until the 8th day were lower than 10±3 kPa in the tensiometers T1 to T4, whereas T5 and T6 showed a suction of around 20 kPa. From the 8th day onward the suction increased very rapidly in tensiometers T4, T5 and T6, while in tensiometers T1, T2 and T3 it evolved at a much lower rate. In most of the tensiometers the peak suction was of 60-80 kPa, except

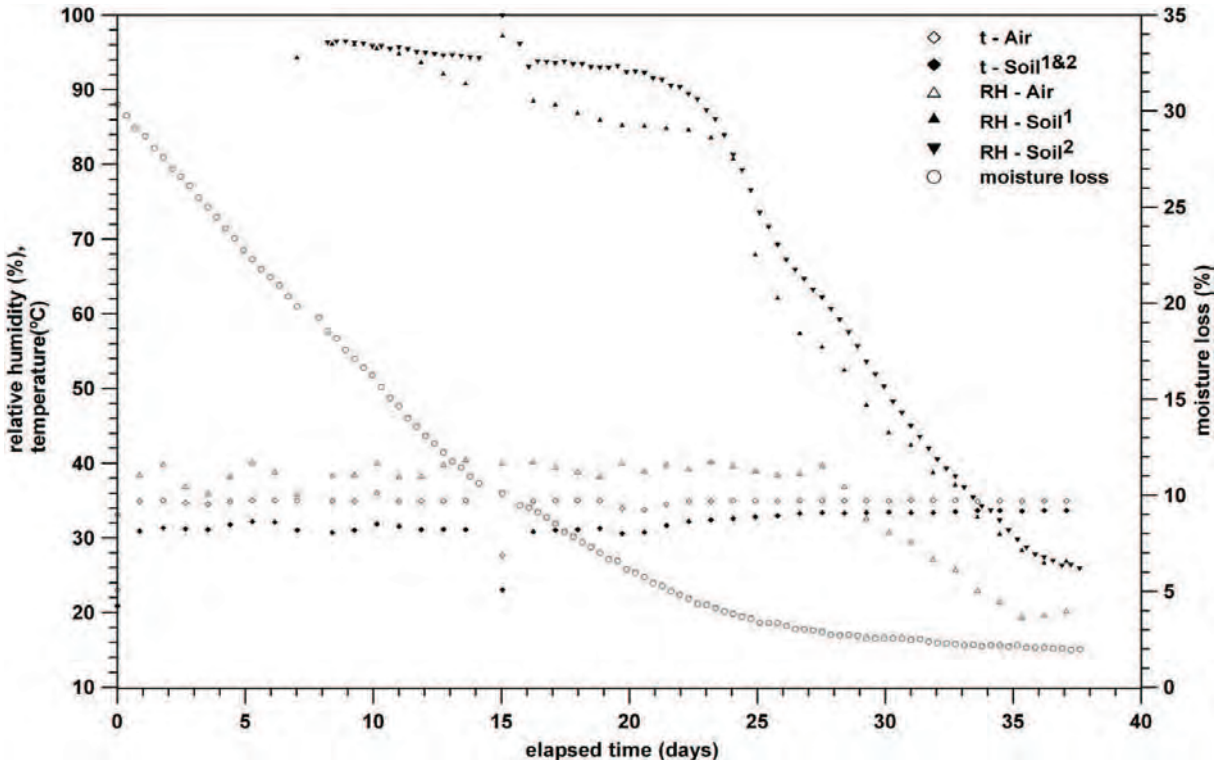

Figure 7.29: Time evolution of air and soil temperature and relative humidity, and of soil moisture loss for specimen 80-10 tested in the environmental chamber

for tensiometer T3 which reached a suction of only 40 kPa before cavitation. Interestingly, the time taken to reach the peak value of suction increases from the tensiometers located on the periphery toward the one at the centre. Tensiometers T5 and T6 were the first to reach the peak at around 9.8 days. Tensiometer T4 reached the peak at 10 days, followed by T3 and T2 at around 12.8 and 13.6 days respectively. Tensiometer T1 was the last to reach the peak at around 14 days. Evolution of suction shows a different behaviour in comparison to the tests with the smaller specimen size 40-10 (both in laboratory and environmental chamber conditions). This behaviour reiterates the visual observation of the drying front progressing from the periphery to the centre.

The relative humidity measured in the soil (see figure 7.29) is converted into suction and plotted in figure 7.31. The specimen remains almost saturated till day 10, at least at the points where the sensors were located. From there onward the suction increases only in the sensor V1, but the sensor V2 desaturates at a little lesser rate. This difference in behaviour is due to the presence of a crack above the sensor V1, showing again the effect of cracking on the rate of desiccation. At around day 25 the rate of suction increase in the two sensors is about same because the crack on the sensor V1 could not develop much further and the soil moisture might be the same throughout the specimen. The evolution of moisture loss is also plotted in the same figure to have a better idea on suction evolution.

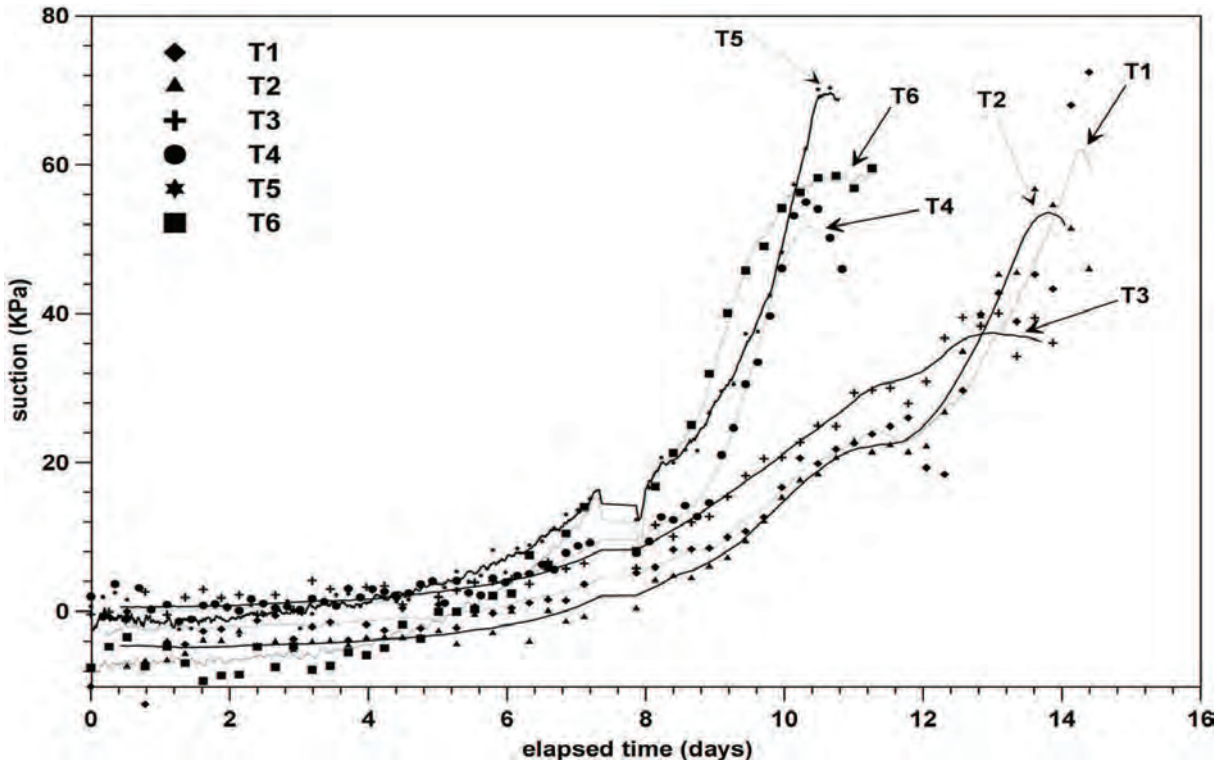

Figure 7.30: Evolution of suction in tensiometers T1 to T6 during the initial stages of the test for specimen 80-10 tested in the environmental chamber

7.7.3 Specimen size 80-10-P

The specimen size is exactly the same as for the previous test, the only difference being the tray used that in this case has a smooth bottom surface instead of a grooved one (see figure 7.1). The conditions during the experiment were also the same, an imposed temperature of 35°C and relative air humidity of 40%. The total duration of the test was 34 days, but the moisture content in the soil reached equilibrium after the 30 days from the beginning. The location of the tensiometers and Vaisala temperature and relative humidity sensors is marked in figure 7.32. In this case, four sensors were located on the tray's perimeter wall: two Vaisala temperature and relative humidity sensors and two tensiometers. Four tensiometers were also placed within the specimen, one at the centre and three at equal distance from the center as shown in figure 7.32. The exact details of location of each sensor in the holding tray 80-10-P is shown in figure 7.7.

The picture of the upper surface of the specimen at the end of the test is shown in figure 7.32. The figure also shows the locations of the different sensors used. The cracks seen at the surface divide the specimen into 10 cells with an average area of 502 cm^2. The cells are indicated with number 1 to 10. The cell at the centre (containing tensiometers T1) is

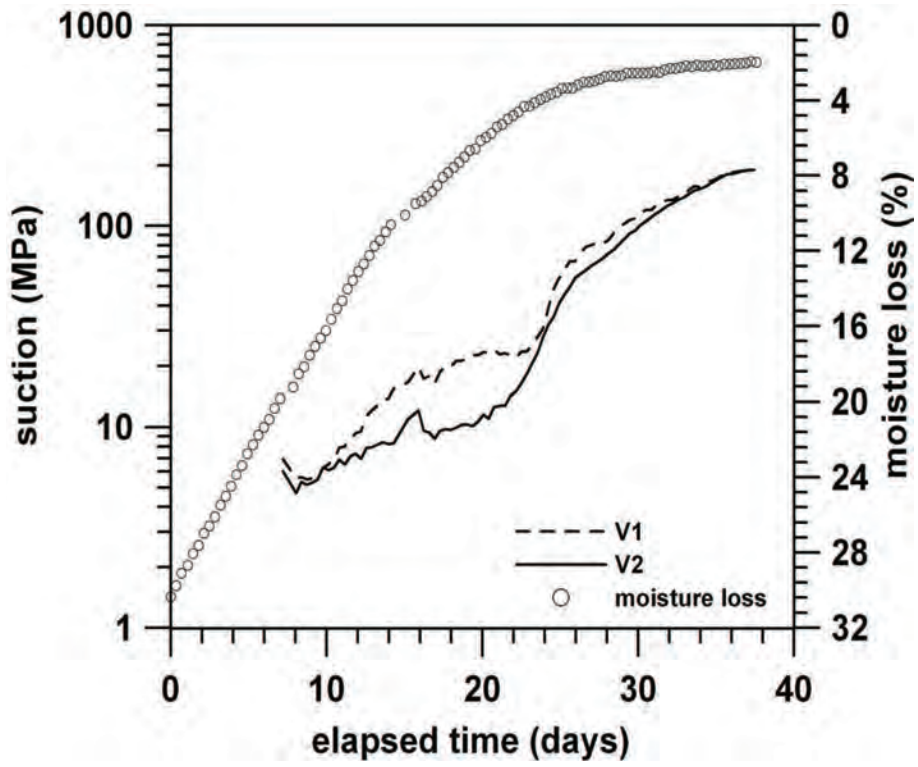

Figure 7.31: Evolution of suction from relative humidity data for specimen 80-10 tested in the environmental chamber

surrounded by cells touching the perimeter of the specimen, except for cell 2. Only two cracks making the edges of cell 1 at the centre do not touch the perimeter indicating the effect of boundary conditions on the crack pattern formation. Several undeveloped cracks can be observed in cells 1, 6, 7 and 9. Some undeveloped cracks in cells 1, 6 and 7 were observed where the sensors had been located. Although figure 7.32 seems to show that the cracks pass through the location of tensiometers T2, T3, and T4, this is only because of the scale at which the image is presented. While recovering the tensiometers at the end of the test, they were found inside the cell and not within the crack. Figure 7.33 shows the bottom surface of the specimen, manually re-arranged after removing the sensors. The marks left by the tensiometers can be identified by the hole left by the devices. On the bottom surface, several cracks can be seen besides the main cracks which run from top to bottom. Smaller cracks in figure 7.33 cannot be seen clearly because of the scale at which the image is presented.

For a better view of the extent of cracking at the bottom surface, the cells marked "cell-1" and "cell-2" in figure 7.33 are shown in detail in figures 7.34 and 7.35 respectively. The morphology of the crack pattern observed in these cells is not easily explained. It would seem that three mechanisms are acting: (1) desiccation from the upper exposed surface; (2) curling (due to differential shrinkage between the top and bottom of the specimen as

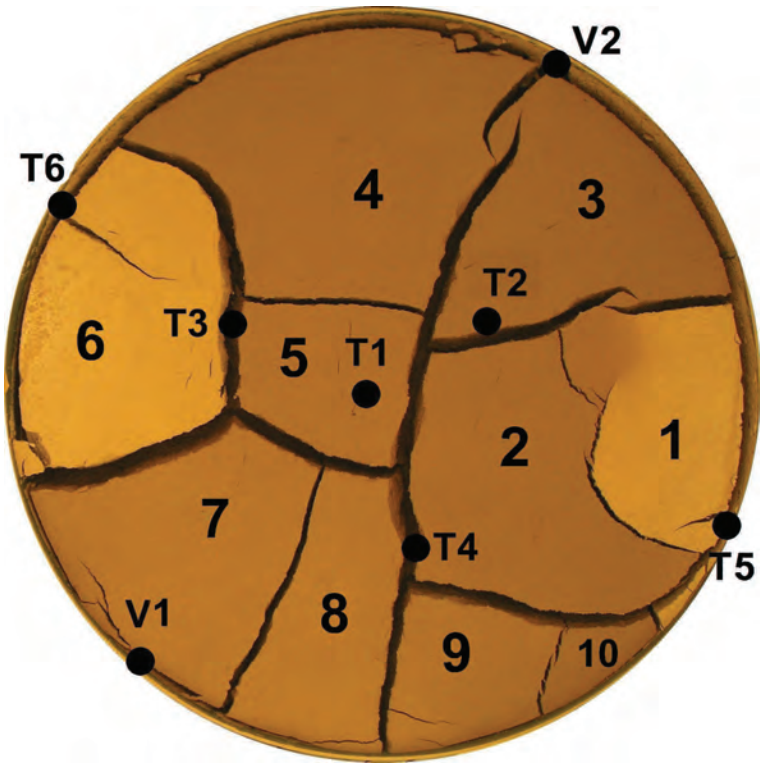

Figure 7.32: Upper surface of specimen 80-10-P at the end of the test carried out in the environmental chamber

a result of desiccation); (3) possibly a synaeresis process. The possibility of a synaeresis process as a mechanism comes from the morphological observations. Sinuous to spindle are associated with ripple marks that are hallmark of synaeresis processes occurring in either submerged or in sub-strata and as a response to volume change due to shrinkage [Plummer and Gostin, 1981]. Morphology of cracks observed in both "cell-1" and "cell-2" (as well as in all the other cells shown in figure 7.33) show spiral cracks and cracks/fissures resembling ripple marks. A detailed analysis of the morphology of the cracks observed on the bottom surface of the cells from different specimens tested in the present work can be found in section 8.6 of Chapter 8.

Time evolution of several variables recorded during the test are shown in figures 7.36, 7.37, and 7.38. Evolution of air and soil temperature and relative humidity as well as the moisture loss or desiccation curve is shown in figure 7.36. The temperature shows slight variations of $\pm 0.2°C$ from the imposed 35°C. The relative humidity is kept between +0.2% -4% of the imposed 40%. The soil moisture reaches equilibrium after 30 days of drying. The evolution of various parameters is explained by choosing 6 transition points: (1) initiation of first crack was observed just after one day from the start originating from the outer perimeter of cell number 6 above tensiometer T1 (figure 7.26); until day 3 no significant development of the crack was observed and not until day 6 a clear developed

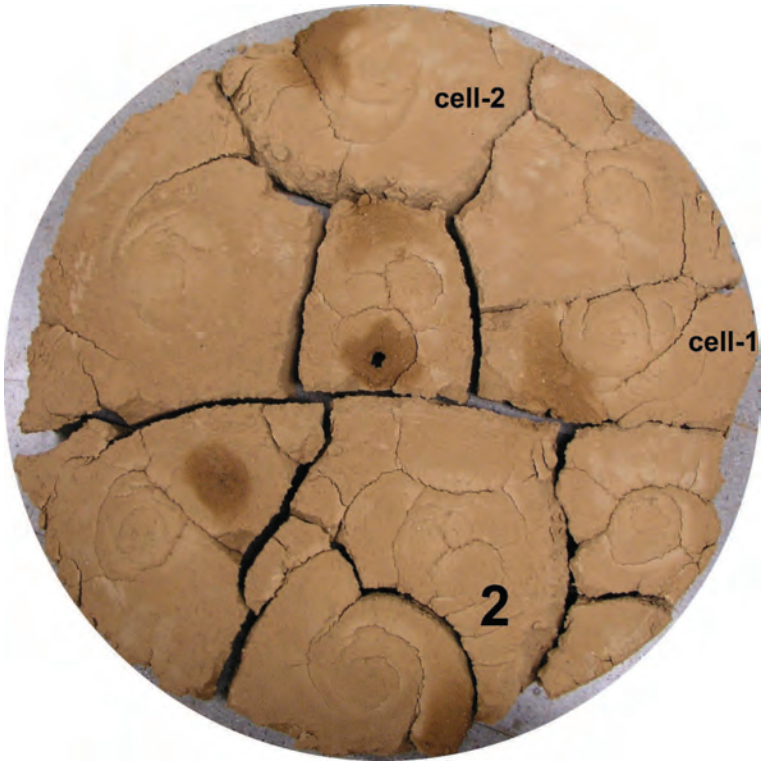

Figure 7.33: Bottom surface of specimen 80-10-P at the end of the test carried out in the environmental chamber

Figure 7.34: Zoom of "cell-1" on figure 7.33 marked as number 8 in figure 7.32

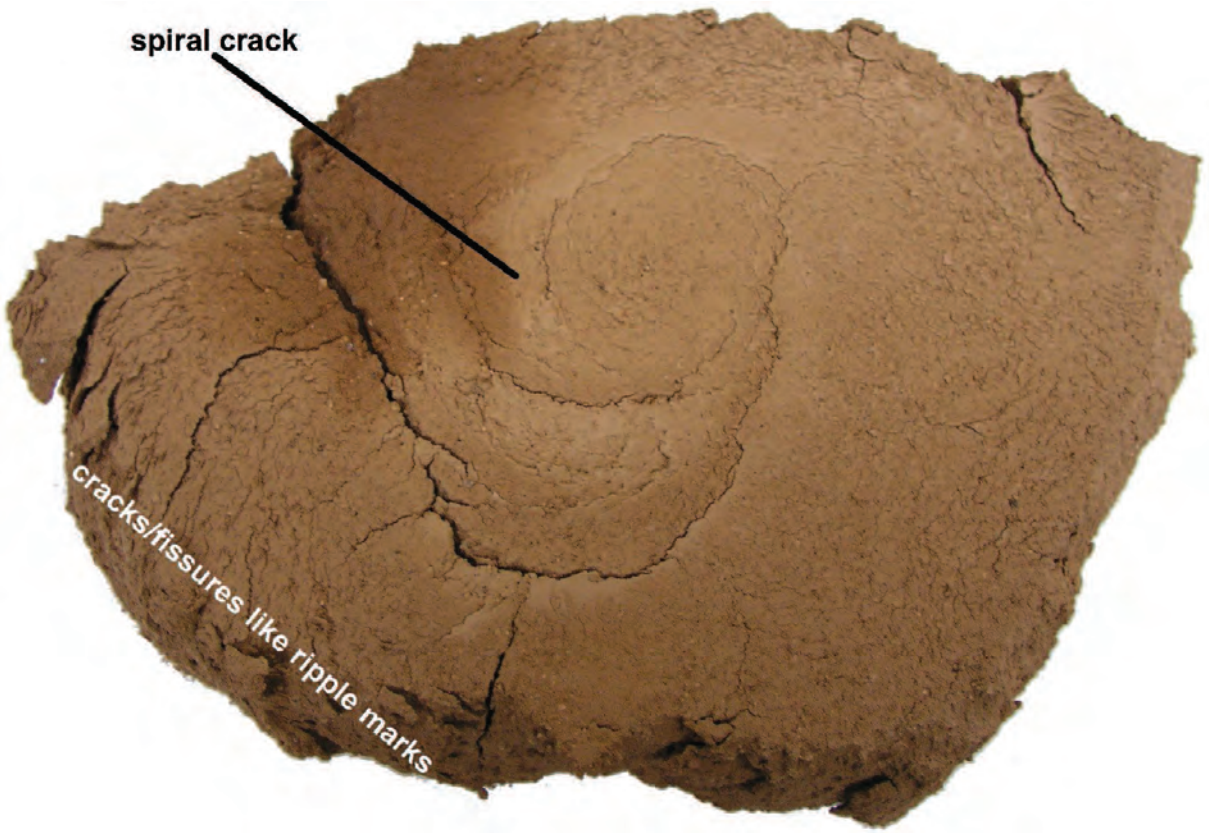

Figure 7.35: Zoom of "cell-2" on figure 7.33 marked as number 6 in figure 7.32.

crack was observed; (2) around day 10 a fully developed crack was observed above sensor V2 (figure 7.32), which resulted in a much faster rate of decrease on the relative humidity compared to sensor V1 indicating the effect of crack formation on moisture conditions; (3) on day 20 around 80% of moisture loss had taken place and the rate of decrease of relative humidity in sensor V2 (measuring around 60%) slowed down; at the same time the relative humidity around sensor V1 was still more than 90%; The soil temperature started to increase, soil temperature at this time being around 3°C less than the imposed air temperature; a change in the slope of the moisture loss curve was observed three days earlier (on day 17); (4) the effect of the increment in soil temperature can be seen in the drastic change of the slope of relative soil humidity on day 22 in sensor V1, whereas the relative humidity around sensor V2 which has a crack above it shows a rate decrease; on the same day another change in the slope of the moisture loss curve was observed; (5) from day 26 onward there was no further increment in soil temperature, remaining almost equal to the imposed air temperature; the moisture loss curve was practically flat and the humidity control device was not triggered anymore because the quantity of evaporating water could not increase the humidity of the volume of air inside the environmental chamber; (6) around day 34 equilibrium between the air and soil temperature and relative humidity was reached and as a result the moisture content of the soil stabilised with no

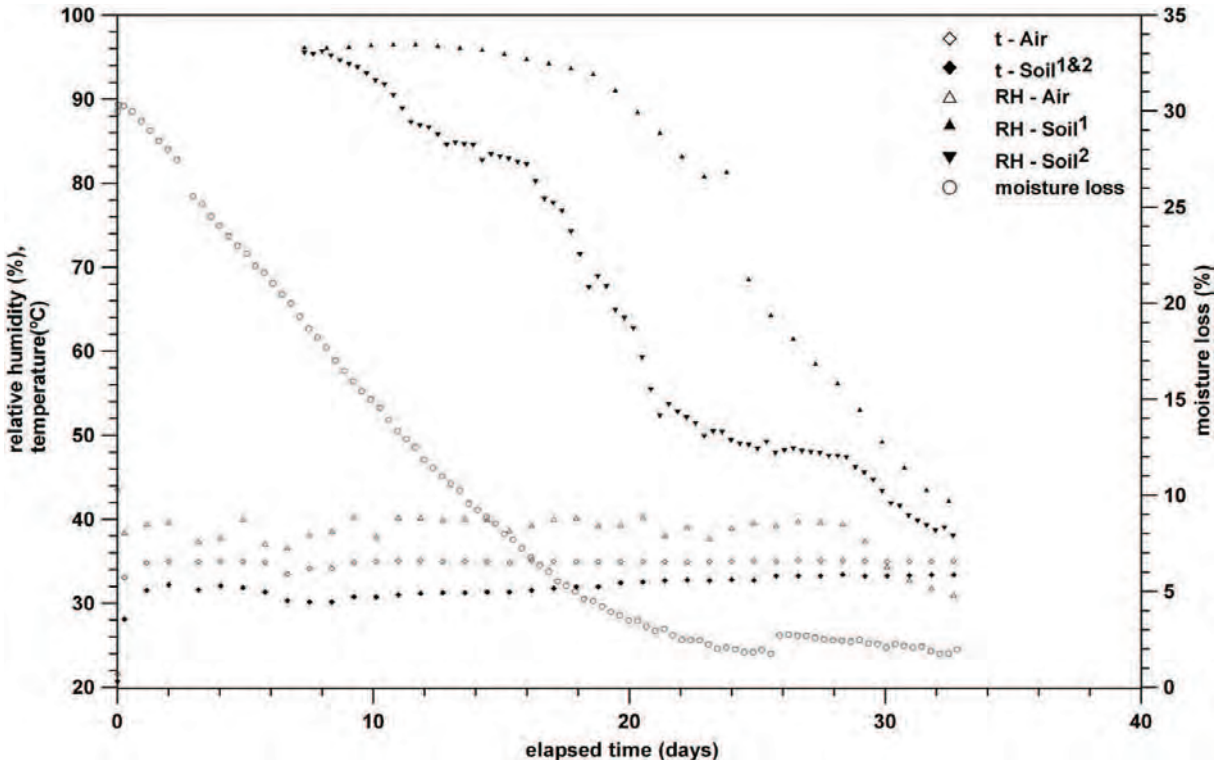

Figure 7.36: Time evolution of air and soil temperature and relative humidity and of moisture loss for test 80-10-P carried out in the environmental chamber

further loss.

Figure 7.37 shows the evolution of suction during the initial stage of the experiment (first 16 days) measured using the tensiometers. The location of each of the tensiometer is shown in figure 7.32. During the first 4 days the measured suction did not vary much, indicating that the soil specimen was fully saturated. After 3.6 days the rate of change in suction in tensiometer T5 was larger than in the rest of the tensiometers. The rate of change in suction in tensiometers T6 and T4 started to increase after 5.6 and 6 days respectively. However, suction values before day 8 were lower than 10±3kPa in the tensiometers T1 to T3 and started to increase thereafter. In most of the tensiometers the peak suction was of 60-100 kPa, except for tensiometer T2 which did not show any change of suction. Time taken to reach the peak increased from the tensiometers on the periphery toward the one in the center. Tensiometer T5 was the first to reach the peak at about 5.6 days, followed by T6 at about 7.2 days, T4 at about 7.6 and T3 at about 10 days. Tensiometer T1 was the last to reach peak at bout 13.6 days. The evolution of suction shows a similar behaviour in comparison to the tests with holding tray 80-10 with grooved bottom surface.

The measured relative soil humidity (figure 7.36) is converted into suction and is plotted in figure 7.38. The specimen remained almost saturated until day 6 at least at the points

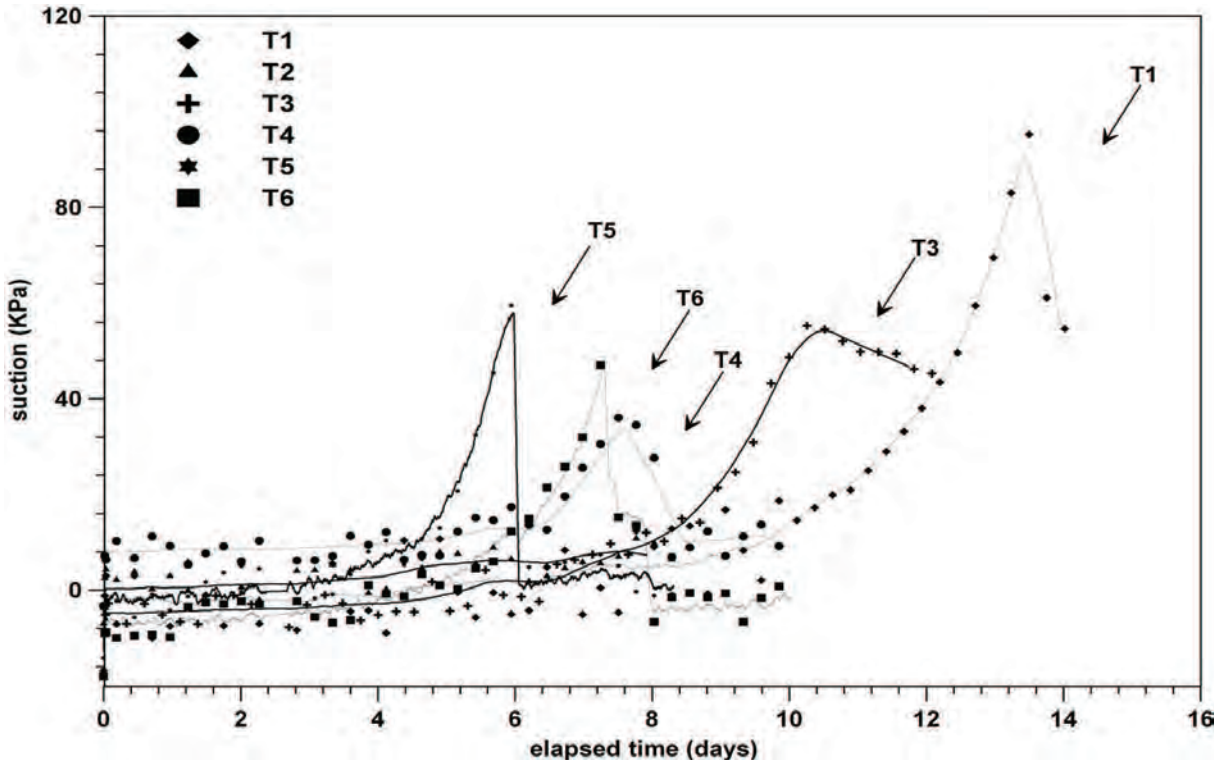

Figure 7.37: Suction evolution in tensiometers T1 to T6 during the initial stages of the test for test 80-10-P carried out in the environmental chamber

where the sensors were located. From there onward the suction increased only in the sensor V2, but the sensor V1 desaturates at a little lower rate. This difference in behaviour is due to the presence of a crack above sensor V2. At around day 24 the rate of suction increase in the two sensors was about the same. The evolution of moisture loss is also plotted in the same figure to have a better idea on suction evolution.

7.8 Location and extent of cracking

7.8.1 Introduction

Many discrepancies exists in the literature regarding the location of crack initiation. Shrinkage cracks may start at the upper or bottom surfaces of the specimen, or at any given point within the specimen thickness. Shrinkage cracks can appear as a result of restraint to volume change due to moisture loss. Desiccation cracks usually appear at the top surface which is exposed to environmental conditions but under certain circumstances they can also initiate inside the specimen. In the experiments of Corte and Higashi [Corte

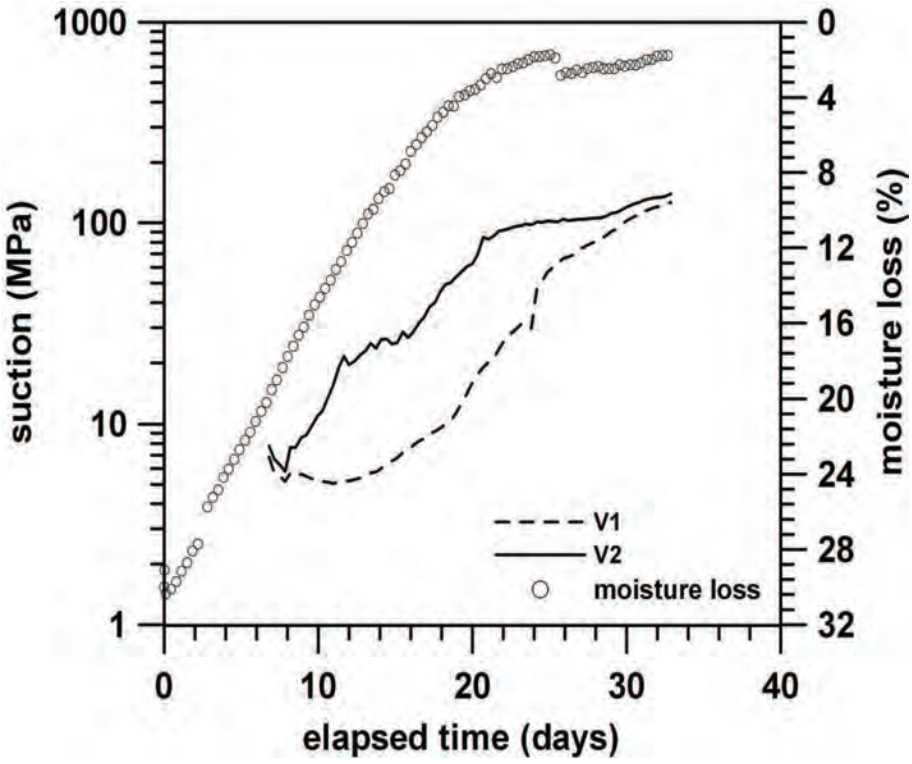

Figure 7.38: Evolution of suction from relative humidity data for specimen 80-10-P tested in the environmental chamber.

and Higashi, 1960] cracking was found to begin from the centre of the soil layer and to propagate to the upper or bottom surface with non-uniform speed. Morris et al [Morris et al., 1992] explain that soils generally dry downward from the surface, where matrix suctions are generally largest and self-weight stresses are zero. The micro-cracking that is present throughout bodies of soil in the form of inter-particle voids is of course also present at the soil surface. Thus, conditions for crack growth are most favourable at the surface of the soil. No doubt the hypothesis of Morris et al is true, but the suction development and presence of micro-cracks cannot satisfactorily explain crack initiation at the bottom surface. Lachenbruch [Lachenbruch, 1961] is of the opinion that crack initiates at a surface of great stress often at or near the ground surface and propagates toward the interior of the medium where tensile stresses decrease and ultimately become compressive. The hypothesis of Lachenbruch of crack initiation at a surface of great stress is true for the cracks generated at the external surface but is not true for the propagation to a compression zone because in the present investigation cracks were observed both at the top (external) and bottom surfaces indicating no prevailing distinguishable compression zone. Most of the recent publications ([Abu-Hejleh and Znidarčić, 1995], [Morris et al., 1992], [Konrad and Ayad, 1998], [Nahlawi and Kodikara, 2006]) assume the hypothesis of Corte and Higashi and Lachenbruch. In contrast to most of the published data, the work of Weinberger [Weinberger, 1999] showed some very interesting morphological fea-

tures observed in desiccation cracking of stratified sediments from the Dead Sea region of Israel. The cracks were nucleated at the bottom and propagated upward (see figures 2.21, 2.22 and 2.23) in the fine sediment layer overlaying a layer of coarser material.

7.8.2 Factors to be considered

Cracking in soils due to desiccation is a complex phenomenon where several coupled processes occur simultaneously. Cracking characteristics depend on the type of soil, the existing boundary conditions, the initial moisture conditions, the thickness of the drying layer and the stress history. Further, mechanisms like curling and synaeresis may play also an important role. Usually there is strong dependence on the physical boundary conditions and existing or imposed environmental conditions.

The four main factors to be considered are: (1) physical boundary conditions; (2) initial moisture conditions and stress history; (3) temperature and relative humidity of the surrounding environment; and (4) thickness of the drying layer. The remaining factors are also important, but are most likely to influence the extent of cracking rather than crack initiation. In the present investigation, the parameters used to assess location and extent of cracking have been the bottom surface roughness, temperature and relative humidity, and thickness.

7.8.3 Initiation and extent of cracking

In naturally drying soils first crack initiation mainly occurs at the exposed outer surface. However, cracks starting at the middle of the drying layer should not be ruled out. If the soil continues drying, further cracks may appear at the layer's bottom interface where contact between curled and not curled layers may exist. In stratified sediments, it is clear from the work of Weinberger [Weinberger, 1999] that cracks nucleate at the bottom of the fine layer of the sediment exposed.

In the present investigation cracks were observed to initiate at both the top (exposed to drying conditions) and bottom (in contact with the holding tray) surfaces of all specimens tested irrespective of thickness, temperature, and bottom surface condition. An extended explanation of the effect of the physical boundary conditions on the extent of cracking on the top surface has been presented in chapter 5. No quantitative analysis was done on the extent of cracking at the bottom surface of the specimens, but a qualitative analysis could be made by crack morphology and is discussed in Chapter 8. A rough tray surface

(with grooves) resulted in less dense cracks at the bottom surface of the specimen in comparison to specimens tested with a smooth tray surface (without grooves) with the same test conditions. An increase in temperature resulted in an increase in the extent of cracking at the bottom surface (see figures 7.18 and 7.24).

7.9 Evolution of suction during desiccation and cracking

7.9.1 Introduction

Suction calculated from the relative humidity data recorded during experiments carried out under laboratory conditions are shown in figure 7.22 where fairly good agreement with the water retention curve determined using psychrometric techniques by Barrera [Barrera, 2002] was observed. Figure 7.39 shows the suction calculated from relative humidity data recorded during experiments carried out in the environmental chamber and under laboratory conditions along with the experimental water retention curve. The initial conditions of all the specimens were the same except for the temperature and relative humidity under which they were subjected to drying.

7.9.2 Temperature and rate of desiccation

Temperature affects the rate of desiccation. An increase in temperature increases the rate of desiccation for a given specimen thickness. Thus, when comparing all tests carried out with 10 cm thick specimens, it can be seen (figure 7.39) that specimens tested in the environmental chamber (40-10, 80-10, 80-10-P) show higher suction profiles than specimen 40-10 tested under laboratory conditions where the temperature was much lower. This observed effect of increase in suction at higher temperature is in contrast with the earlier work of Romero [Romero, 1999].

Temperature is not the only factor affecting the desiccation process. The rate of desiccation (of course influenced by temperature) plays also a role. Figure 7.40 shows the rate of desiccation coefficient for different specimens tested under laboratory conditions and in the environmental chamber. The rate of desiccation coefficient (k) is proportional to the rate of desiccation. The lowest value of k was found for specimen 80-20 under laboratory conditions and the highest value for specimen 20-5. Tests with specimens 40-10 were con-

ducted both under laboratory conditions (at 22°C) and in the environmental chamber (at 35°C). The specimen in the environmental chamber conditions shows a higher value of k in comparison to the specimen tested under laboratory conditions. Looking to the suction evolution seen in figure 7.39, it can be seen that suction is higher for higher values of k. It can be concluded that suction evolution in the desiccating soil is related to the speed of the desiccation process rather than directly to temperature. Of course the influence of cracks already present cannot be ruled out. The water retention curve shown in the figure serves only the purpose of checking the deviation, not to make a match or comparison since the water retention curves are determined with very small specimens (weighing several grams), whereas the suction evolution presented here is determined from specimens weighing several tens of kilogrammes.

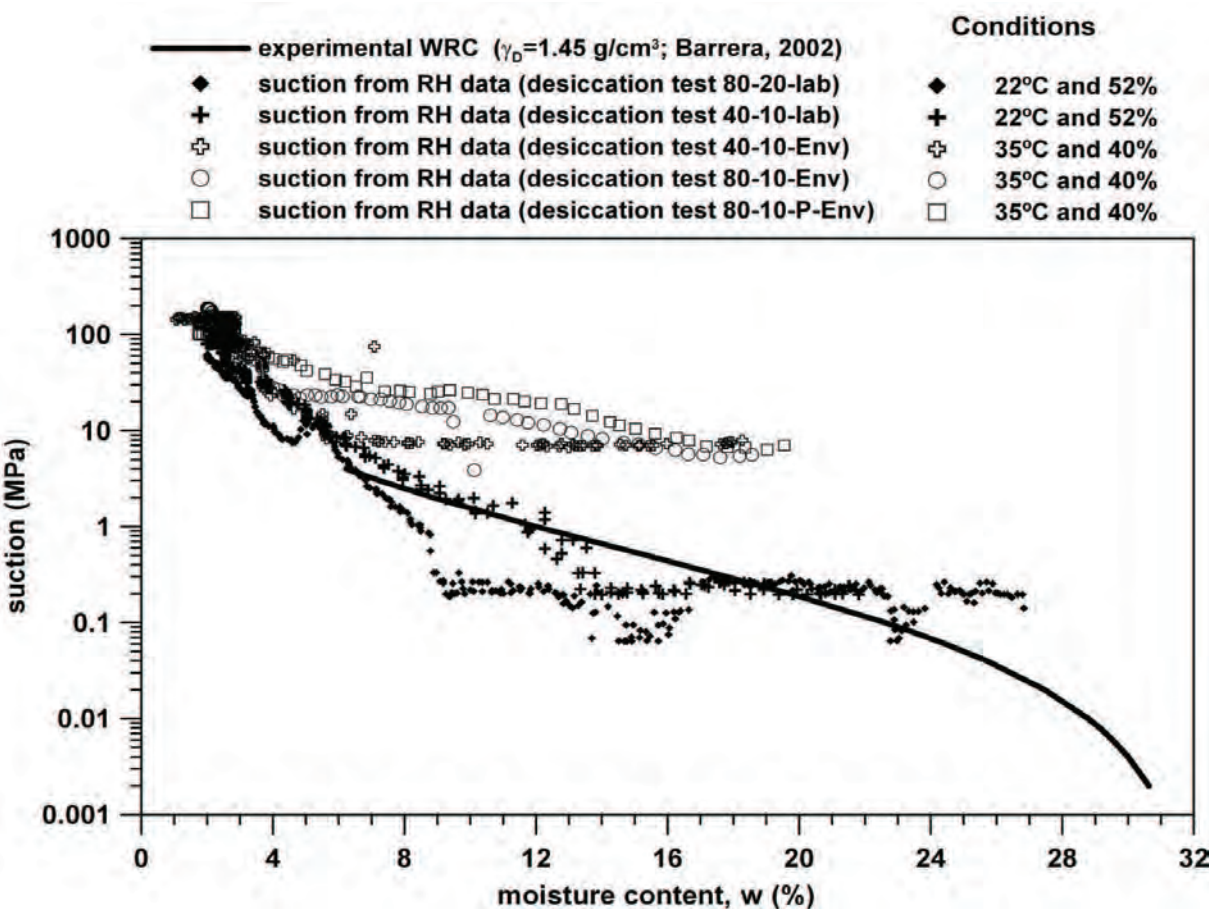

Figure 7.39: Effect of temperature and desiccation rate on suction

7.9.3 Presence of cracks

Presence of cracks has a considerable impact on the relative humidity of the specimens which directly reflects the suction evolution. A summary of the suction evolution observed

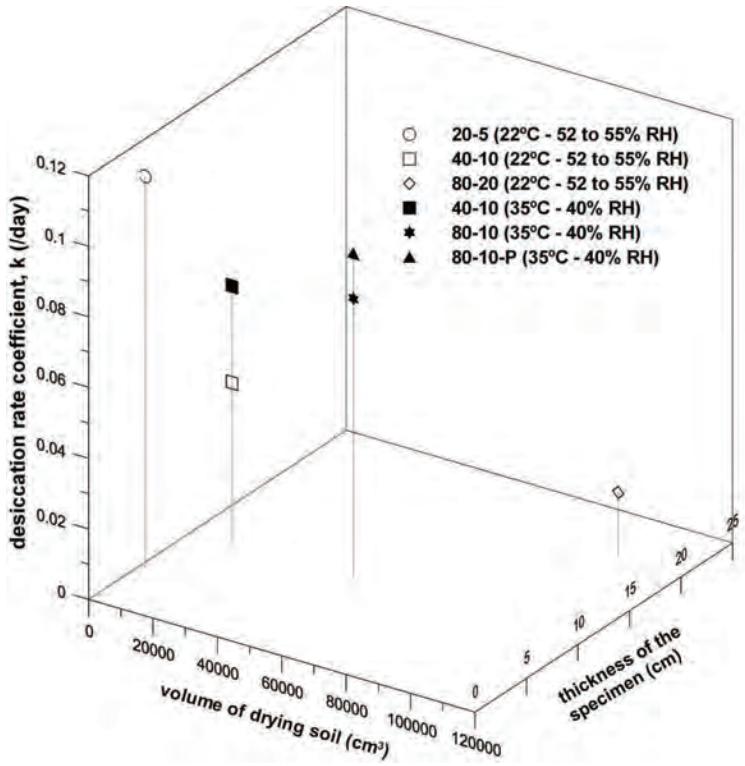

Figure 7.40: Rate of desiccation coefficient k for the specimens tested under laboratory conditions and in the environmental chamber

in the 5 specimens is presented in figure 7.41. No cracks developed on the upper surface of specimens 40-10 under laboratory conditions or in the environmental chamber. The suction evolution is shown in figures 7.41b,c. The presence of cracks increases the surface for evaporation and thus in the vicinity of the cracks a higher rate of evaporation can be expected, resulting in faster drying. This effect can be seen in the higher suction recorded when cracks were present near the sensors.

7.10 Theoretical considerations

After reviewing some of the very widely accepted research papers, disagreement was seen regarding the applicability of classical saturated or unsaturated soil mechanics for the desiccation cracking in soils. In fact, cracks can occur in nature in saturated or unsaturated states, but the disagreement for desiccation cracking is evident in the literature.

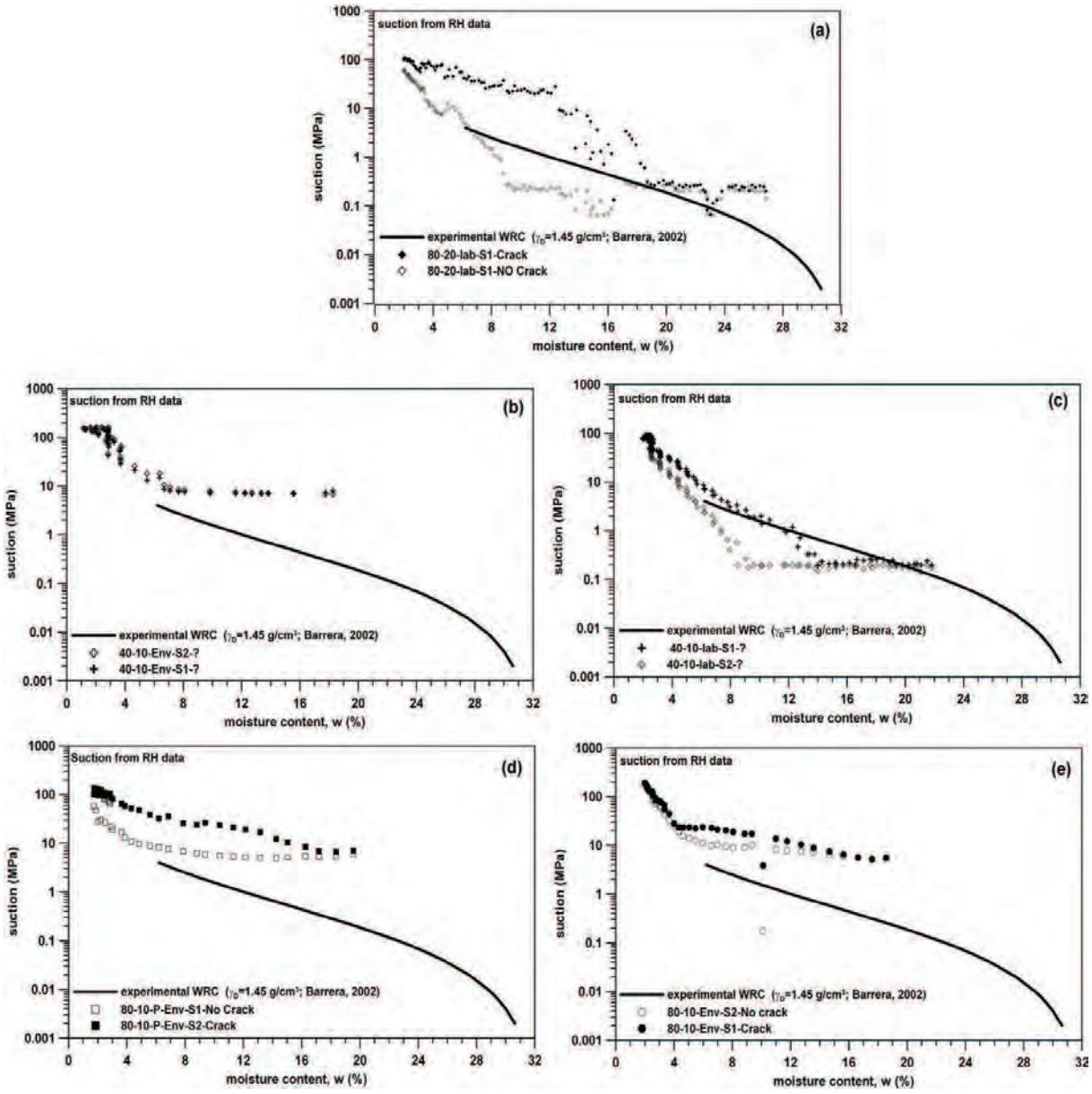

Figure 7.41: Suction evolution at cracks and uncracked portions of the specimens

7.10.1 Unsaturated soil mechanics

Clay soils tend to crack when they dry. In early stages of drying from a horizontal surface, starting with a soft, initially saturated soil, decreases in water content are largely accommodated by reorganisation of the soil particles into successively closer arrangements and reduction of the voids ratio. Experiments have shown that the voids between the particles do not remain indefinitely filled with water, and successively larger proportions of air gradually enter these voids. Surface tension effects at air-water-soil contacts inside the soil generate negative pore water pressures (or matrix suctions) below atmospheric

pressure in the remaining pore water. These matrix suction produce two counteracting effects: at a given point the soil tends to shrink more or less isotropically producing vertical cracks below horizontal drying surfaces; and the soil gains strength and provides increased resistance to crack formation. This mechanism of soil desiccation proposed by Morris et al [Morris et al., 1992] clearly shows that the soil is unsaturated when it cracks. Further, to express the shear strength of an unsaturated soil they utilise the Fredlund's equations [Fredlund, 1979], with some reservations on the validity of the effective stress concept, and Fredlund's state variables to link the pore-air and pore-water pressures in the soil.

7.10.2 Saturated soil mechanics

Saturated clay subjected to evaporation experiences a continuous decrease in water content, while negative pore water pressure or suction develop in the porous network of the soil. If the soil is unrestrained, the suction generates an increase in the effective stresses, which in turn, produces a decrease in the soil volume by consolidation. The relationship between moisture content and voids ratio is often referred to as the shrinkage characteristics of a given soil. Figure 2.25 in Chapter 2 presents a typical shrinkage curve for a soil with a high clay content. During the drying process, several stages can be identified. In the first stage, the reduction of the volume of the soil is equal to the moisture loss and the soil remains saturated over a wide range of water contents. The second stage begins when the capillary tension reaches the bubbling pressure or the air entry pressure of the soil. As the air enters progressively into the soil's pore network, further moisture loss occurs, and the liquid phase becomes more and more discontinuous. At this stage, the moisture loss is greater than the volume decrease, and the shrinkage curve becomes progressively horizontal. In the third, zero shrinkage stage, the soil does not show any further volumetric change. The moisture loss is then equal to the increase in the soil air volume. This mechanism of shrinkage in clays was proposed by Konrad and Ayad [Konrad and Ayad, 1997b] who clearly state that cracking begins when the soil is in the first stage, i.e. still fully saturated, questioning the use of the equations proposed by Morris et al [Morris et al., 1992] on the grounds that they are for unsaturated soils.

7.10.3 Reservations on the applicability of effective theory

Kodikara et al [Kodikara et al., 1998] in their discussion on the framework proposed by Konrad and Ayad [Konrad and Ayad, 1997b] agree that some clays (for example slurried Regina clay) do not desaturate until the soil is subjected to suctions over 1 MPa.

However, referring to Bronswijk [Bronswijk, 1988] they argue that there is evidence that some light clays deviate from this behaviour and primarily show residual shrinkage as the soil desaturates. Further, heavily over-consolidated clays as well as compacted clays predominantly behave in an unsaturated manner during the desiccation. To substantiate this claim they point to the work of Vanapalli et al [Vanapalli et al., 1996a] where soil-water characteristics measured for compacted soil specimens of Indian Head till have shown that the air entry value is less than 100 kPa even for specimens compacted about 6% wet of optimum. Since the tensile strength of these clays is higher than that of unconsolidated clays, suctions exceeding 100 kPa can develop at the point of initial cracking. Under these suctions, these soils are most likely to be unsaturated. Regarding the comment by Konrad and Ayad [Konrad and Ayad, 1997b] on the use of equations for crack initiation and initial depth of propagation given by Morris et al [Morris et al., 1992], Kodikara et al [Kodikara et al., 1998] point that the equation for net horizontal stress used by Morris et al [Morris et al., 1992] can be modified for K_0 loading, and saturated conditions will be the same as the effective stress relation used by Konrad and Ayad [Konrad and Ayad, 1997b]. The only difference is that the coefficient of lateral pressure at rest, K_0, will be given by $\nu/(1-\nu)$ instead of by $(1-\sin\phi)$ as commonly used for normally consolidated soils. This arises from inherent disparity between continuum mechanics elasticity and particulate soil mechanics. On the discussion of Kodikara et al [Kodikara et al., 1998], Konrad and Ayad [Konrad and Ayad, 1998] in their reply totally agree that the model should also consider the unsaturated soil mechanics, but they mention that the model presented holds for soils with a high clay content in which the desiccation cracks appear while the soil is still saturated.

The comments from Kodikara et al [Kodikara et al., 1998] can be substantiated by the experimental work on crack initiation in drying soils by Lloret et al [Lloret et al., 1998]. According to them cracking occurs in quasi-saturated conditions. They carried out experiments with different initial water contents and different imposed suctions and concluded that in soils with high initial water content crack initiation occurs with degrees of saturation close to 1, and for soils with lower initial water content with degrees of saturation close to 0.8; in both cases crack initiation happens under quasi-saturated or saturated conditions. Their conclusion is fully corroborated by the evidence gained from the present research.

7.10.4 Saturated soils with suction

Bronswijk and Evers [Bronswijk and Eversvermeer, 1990] conducted shrinkage experiments on Dutch clay soil aggregates and noted that some clay soils show normal shrinkage

from saturation until suctions much lower than 1.57 MPa. An extreme example of this is the Bruchem C11g horizon, one of the clay soil they tested, which aggregates, under Dutch climatic conditions always remain fully saturated. Air is only present at inter-aggregate pores like shrinkage cracks.

Another example of saturated soils with suction can be seen in the work of Fleureau et al [Fleureau et al., 1993]. They conducted experiments on 11 different types of soils, from natural loams to pure kaolinite and montmorillonite. In their experiments they observed that when the water content is reduced below the air entry point, the degree of saturation decreases very sharply, almost linearly with water content as long as the void ratio remains approximately constant. The point of saturation at which the curve begins to deviate from the straight line corresponds to the shrinkage negative pressure as seen in figure 2.26B in Chapter 2. Figure 2.26D shows the variation of the degree of saturation with suction (expressed in terms of the logarithm of the negative pore water pressure given in cm of water): the soil remains quasi-saturated up to a suction of 1MPa, then the degree of saturation decreases rapidly to reach approximately 0.1 for negative pore water pressures of 10 MPa.

7.11 Conclusions

Experimental studies on cracking soil are very scarce and practically there are no published data relative to evolution of parameters such as moisture content and suction. In the present work an environmental chamber was designed and constructed to study the desiccation process and cracking of drying soils. A particular combination of temperature and relative humidity can be imposed to the desiccating specimen by controlling the air temperature and relative humidity inside the chamber.

7.11.1 The environmental chamber

Four devices (for heating, cooling, humidifying and dehumidifying) are required to impose and control different temperature and relative humidity combinations and cycles. If cycles of drying and wetting need to be imposed to simulate seasonal climatic variations, then an extra device to wet the specimen would be necessary. This additional device could be a sprinkler with discharge and velocity control. Currently there are only two of these devices (for heating and dehumidifying) built into the chamber.

The experimental program and the results presented in this chapter were focused on demonstrating the capabilities of the environmental chamber. However, very interesting results were obtained from the tests performed. A set of three experiments were carried out under laboratory conditions (21 ± 0.5°C and 52 ± 2%) while the environmental chamber was being built. Another three experiments were carried out in the environmental chamber with temperature around 35 ± 0.1°C and relative humidity of 40 + 0.2 & - 4%.

This equipment is extremely well suited to study the mechanisms of cracking in soils due to drying. Air temperature and relative humidity can be controlled with minimal variations from the imposed values. Digital images taken by a camera during the tests provides very valuable data for the later analysis. Tailor-made holding trays with its sensors are excellent for continuous monitoring. Provision to add cooling and humidifying sources makes it more versatile for future research as cycles of wetting-drying can be imposed coupled with warm-cool cycles.

7.11.2 Desiccation of thick layers

The tests have provided some new insights into the mechanics of the process of formation of cracks in a drying soil. Cracks can be seen starting either at the top, bottom or at both surfaces of the drying specimen. The mechanism responsible for the initiation at the top surface is usually desiccation, while the cracks starting at the bottom surface may be a product of curling and/or synaeresis processes. An increase in temperature increases the extent of cracking at both top and bottom of the specimen. Though a direct link between the temperature and suction evolution was not found, an interesting relation between the desiccation rate and suction evolution was seen. The presence of crack affect the suction evolution with increased desiccation speed. The suction profiles during the initial stages of the desiccation showed that the drying front moves from the periphery toward the centre and from top to bottom. Extent of cracking was larger with a smooth bottom surface than with a rough one, both at the top and bottom surfaces but more noticeable at the bottom surface of the specimen. Cracking initiated near saturation or at quasi-saturated conditions. From a theoretical perspective, modelling should consider the effect of suction. It can be argued that although crack initiation may occur near saturation, no doubt crack propagation takes place in unsaturated conditions for drier and warmer conditions. At the same time exceptions should be allowed for extreme cases like highly plastic clay and for dry-cold environments.

Chapter 8

Macro-morphology of 2D crack networks

8.1 Introduction

Drying soils often crack as a result of water loss, mostly due to evaporation. Examples can be found in irrigated land, tailing ponds for mining waste, landfill liners, earth embankment, reclaimed land, reservoir beds, etc. Although cracking in desiccating soils is a common phenomenon, the causes and mechanisms involved are very complex with several interacting factors playing a coupled role. An important aspect of the study of cracking soils is quantifying the characteristics of the crack network or finding the similarities among these apparently random but unique patterns.

Characterisation of crack patterns is useful in different fields of science and engineering. In Soil Mechanics structural cracks are of much interest: their shape, size, and ruggedness carry with them clues to past stresses and strains imposed to the soil, with implications into their future stability and functionality [Preston et al., 1997]. In agriculture, study of crack patterns can help determine whether different soil management treatments are having an effect on soil structure. Crack patterns act as an indicator of state of soil structure. If crack patterns are different between soil treatments, other structural properties of soil are also likely to be different, but not vice-versa. Crack pattern measurements together with bulk density can be used to calculate the volume changes during drying and this can increase the accuracy of water balance calculations for soils that shrink as they dry [Voase and Sanidad, 1996]. In Concrete technology it is crucial to understand the pattern formation of surface cracks in structures, in particular for their aging properties.

Surface cracks are easy paths for chemical species which may react with the material or reinforcement [Colina and Roux, 2000]. There is also a need to monitor the cracks in cases such as highway engineering where pavement cracking is an important issue.

Observation of crack patterns on different materials immediately points to clear geometrical similarities between the patterns over a wide range of scale, from microns to kilometres. This suggests the existence of some universal mechanism and therefore that microscopic details may be not so important. Therefore, similar to phase transition, a mesoscopic coarse-grained description may be sufficient and more useful than a microscopic one provided essential features are captured.

There is an established relation between the macroscopic parameters of a typical crack pattern such as crack width, polygon size or cracked cell size and the depth or thickness of drying soil. Crack width and polygon size seems to increase with thickness of the drying soil [Corte and Higashi, 1960]. Interestingly, a similar phenomenon was noticed on a much larger scale by Vogt [Vogt, 1974] who showed that the distances between fractures in the Earth's Lithosphere, which originate volcanoes, are essentially equal to the thickness of the Lithosphere plate.

In this chapter macroscopic characteristics of the observed crack patterns in different desiccation tests are analysed. Existing theories for the study of similarities of two-dimensional crack patterns are applied to explain the results. Other macroscopic features such as crack intersection angle and time evolution of the crack pattern are explained. An attempt is made to explain formation at the bottom unexposed surface of the specimens, a unexpected morphological feature.

8.2 Mechanism of successive domain division or hierarchical crack pattern development

8.2.1 Introduction

A large variety of morphologies of crack patterns can be found in nature. In many cases the cracks or joints form a closed network and thus divide a two dimensional surface in to distinct domains. Very different mathematical, physical, biological or social processes give rise to two-dimensional space dividing patterns. Examples include the Voronoi tessellation of randomly distributed points, the two-dimensional soap froth confined between glass plates, the reticulum formed by cracks in thin layers, the cellular structure of two-

dimensional living tissue, the leaf ventilation, or the division of large geographical areas by roads, streets, or political borders. These networks have a well known common property expressed by Euler's theorem which states that in the plane each domain has, on average, six neighbours. For many cellular networks, it follows that the average number of sides per cell is also six ([Bohn, 2004],[Bohn et al., 2005a]).

There exists a subset of the above explained two-dimensional space dividing networks, where geometry imposes that the domains are, on average, four sided. While compatible with Euler's theorem, the average of four sides is the signature of hierarchy. It is the consequence of a formation process that can be described as the successive division of domains and the absence of any further reorganisation ([Bohn et al., 2005b], [Bohn et al., 2005c]).

Two-dimensional space dividing patterns do not always result in hierarchical patterns, a classical example being the pattern formed by soap bubbles. Whereas the process of successive division of two-dimensional domains results in hierarchical patterns in some cases, the patterns formed by soap bubbles are relatively instantaneous and dynamic. Some morphologies/patterns show an astonishing similarity to two-dimensional soap foams which have often been considered to be the model system for space dividing patterns. The geometric structure of soap foams is given by reorganisation phenomena. Being mobile, the soap films adapt the shape that minimises the surface. In two-dimensional foams, the lines corresponding to the films are arcs of circles and the angles at the intersections are adjusted to 120° (laws of Plateau). These angles are the signature of quasi-instantaneous force equilibrium at the edge contacts [Bohn, 2004].

Figure 8.1 summarises the most salient feature of a hierarchical crack pattern compared to a soap foam pattern. The histogram in the figure shows clearly that the majority of the cracked cells have four sides but the majority of these four-sided polygons have six neighbours which is a typical feature of the hierarchical patterns. A pictorial comparison between the hexagonal foam cells with six neighbour and a typical hierarchical crack pattern is made in figures 8.1b,c.

8.2.2 Hierarchical patterns in soil cracks

Hierarchical patterns are natural phenomenon in drying soils where they form and evolve driven by changes in material strength due to natural inhomogeneities, or due to cycles of stress increase and decrease following seasonal environmental changes.

Usually hierarchical patterns are semi-dynamic or quasi-static when considered in a rel-

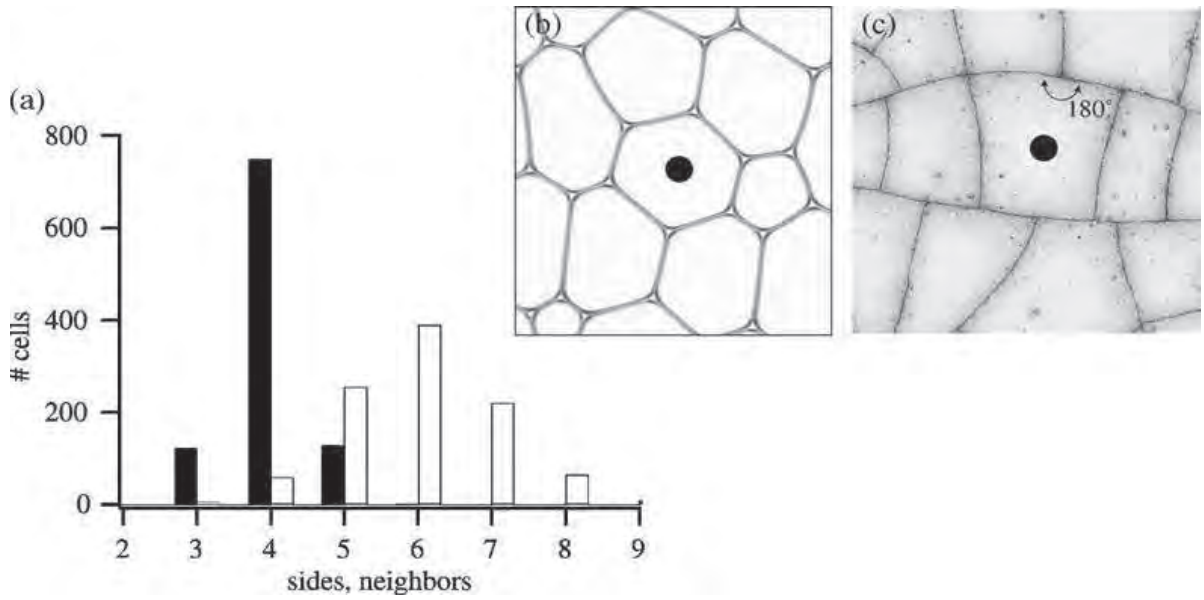

Figure 8.1: (a) Histogram of the number of sides (black) and the number of neighbors (white) of 1000 domains in a ceramic crack pattern. (b) A six sided cell in foam. (c) A four sided cell in a crack pattern (after [Bohn, 2004]).

ative frame of elapsed time from their formation. The domains formed by soap bubbles usually attain equilibrium in a very short time and are dynamic, constantly redistributing or repositioning themselves to maintain the equilibrium. In contrast, crack patterns formed in drying soils attain equilibrium relatively slowly depending on the rate of desiccation. This pattern formation is not dynamic, because there is no rearrangement of domain shape and normally the size of the domains remain fixed in time.

The process of division of domains usually follows a pattern that suggest the existence of some hierarchy. The hierarchical nature can be explained by three important processes: (1) stress generation beyond the material strength; (2) direction of stress generation; and (3) stress re-distribution in the vicinity or inside the newly formed domain. Following there is a discussion on the physics involved in these processes. Note that if the drying soil mass is sufficiently large (relative to surface area, aspect ratio and thickness), then all the three processes can occur simultaneously in different subdivided domains. This should not be confused with the first crack generation, because all the divided domains are part of a single hierarchical structure.

Stress generation in a drying soil and crack nucleation: Several factors can be listed as responsible for stress generation in a drying soil. Soils are neither continuous, homogeneous or isotropic materials. The very granular or particulate nature of the soils is the main cause for stress generation. Soils are usually two- or three-phase systems with

pore fluid and pore gas being main constituents of the complex pore system in the soil matrix. Due to these factors, weak points or points of possible crack nucleation exists in the soil structure. These points are randomly distributed throughout the soil matrix and the strength at these points vary depending on the time evolution of cracking. The crack nucleation process itself has also a random component. In drying soils the stress generation is primarily caused by desiccation and the resistance to free shrinkage. Usually the shrinkage is not uniform over the drying surface. The differential shrinkage results in differential stress generation at different points. The stress at certain points may reach the soil strength earlier than at others resulting in nucleation at those points where the strength has been reached.

Direction of stress generation: The direction of stress generation governs the direction of crack growth. Note that it takes some time to crack nucleation as the stress at nucleation point should exceed the material strength.

8.2.3 Experimental evidences of hierarchy in soil cracks

The existence of a hierarchy in crack formation was reported from experimental studies in desiccating latex gel [Bohn, 2004] and starch-water mixtures [Bohn et al., 2005b],[Bohn et al., 2005c]. However, no attempt has been made previous to the present work to study experimentally the existence of hierarchy in soil crack pattern formation. For this purpose, the laboratory equipment and experimental techniques developed to study size-effect (Chapter 5) have been used. Identification of hierarchical crack pattern formation requires continuous time-images of the evolving crack pattern as the soil dries, as was routinely carried out in those experiments.

For simplicity and clarity, only images corresponding to one specimen are presented. However, the process described was observed in all the specimens tested. The final crack pattern on specimen A0-20 is shown in figure 8.2. The numbers marked inside some cracked polygons indicate the cells selected for in-depth morphological analysis. Some of these numbered cells will be discussed later in this chapter. The time evolution of the cracked polygons within the white boundary in figure 8.2 is shown in figure 8.3. The nine images of this figure show the process of successive crack formation that divides the surface into cells. The first image (taken 99 hours after test initiation) shows a crack initiating nearly at the centre of the cracked polygon. In the second image (taken at 103 hours) the crack in the earlier image has fully grown and is already meeting the cell's boundary cracks. It is interesting to notice that the crack divides the cracked cell in half and that there is no crack formation anywhere else inside the cell. This newly formed

Figure 8.2: Final crack pattern on specimen A0-20. The numbers indicate the cracked polygons selected for further detailed analysis and the white border marks the area selected for monitoring of its time evolution.

crack meets the cell's boundary cracks at right angles and is more or less perpendicular to the longest boundary cracks. From this point, crack formation within the two newly formed cells will proceed separately without influencing each other.

Let us look now into the bottom half cell where two cracks can be seen in the third image (taken at 107 hours). These two cracks divide the bottom half cell into three more sub-cracked domains, which can be seen fully formed in the fourth image (taken at 111 hours) named respectively as 1, 2, and 3. Further a new crack formation is seen at 115 hours on the right side of cell number2, resulting in another cell sub-division as indicated (2-1 and 2-2) in the image corresponding to 115 hours. Finally the last division in the bottom polygon takes place in the cell numbered 3, the resulting sub-division formed (3-1 and 3-2) is marked in the image corresponding to 119 hour. A final division was observed in the cracked cell 2-1 in the image corresponding to 131 hours: the cell divided further into three new cells 2-1-1, 2-1-2 and 2-1-3.

Now, consider the top cracked cell in the image corresponding to 103 hour. A new crack

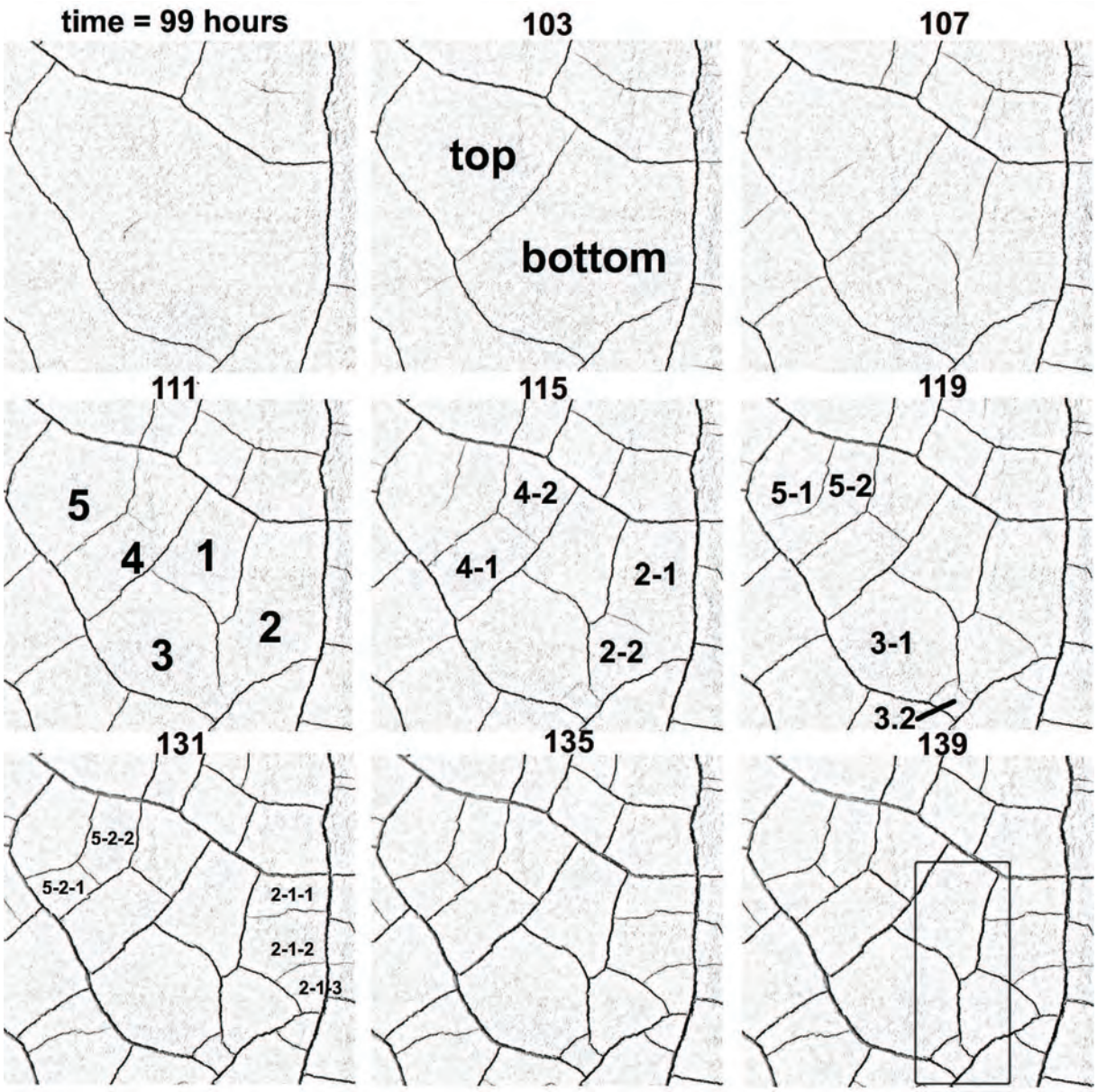

Figure 8.3: Temporal evolution of the white border in figure 8.2 indicating the successive hierarchical nature of crack formation.

originating as observed in image corresponding to 107 hour divides the cracked cell in to two, the newly formed cracked cells are marked as 4 and 5 in image of 111 hour. As soon as the crack resulting the cracked polygons 4 and 5 reaches the boundary cracks of the cell a new crack is seen nucleating in the cracked cell numbered 4. The image of 115 hour show another crack developing in the cracked cell numbered 5, and also the two newly formed cracked cells 4-1 and 4-2 is also seen. In the image corresponding to 119 hour the crack in the cracked cell 5 divides it in to 5-1 and 5-2, in the subsequent image a further sub-division of the cracked cell 5-2 in to 5-2-1 and 5-2-2 is observed.

From these experimental observations it is very clear that there exists a marked hierarchy during crack pattern formation in drying soils. This hierarchical order provides much information that helps explaining the way in which crack patterns are formed. Stepping back from the final crack pattern, knowledge of the hierarchical order makes possible to trace the changing stress states during the process of cracking.

An important characteristic feature of the crack pattern is the angle at which cracks intersect. The area within the black rectangular border marked in the last image of the figure 8.3 will be used for the purpose of studying this process.

8.3 Time evolution of crack pattern

8.3.1 Introduction

This section gives an insight into the evolution of two-dimensional cracks resulting in the formation of a crack network. Data to study the evolution in time of the developing crack networks presented in this section are taken from the size-effect tests presented in Chapter 6. A detailed description of the experimental procedure, test conditions and specimen types is given in Chapter 5 (Sections 5.2.3 & 5.3.2) where an exhaustive image analysis of the final crack pattern by is performed.

The specimens were monitored for the duration of the tests by taking digital photographs at regular intervals. These images were further treated to enhance the regions of interest (in this case the cracks). Time evolution of 10 specimens of 5 different surface areas (each with two different thickness) are presented here. Each figure contains 15 images taken at different stages of crack evolution. The first image always corresponds to a time when a crack becomes clearly visible. The last image shows the final crack pattern for the test, when there is no further moisture loss and the crack network no longer changes.

8.3.2 Time evolution of crack patterns on 20 mm thick specimens

Figures 8.4 to 8.8 show the evolution of the crack patterns developing on the surface of the five 20 mm thick specimens, ranging from size A0 to A4.

Figure 8.4 shows the evolution of the crack pattern on specimen A0-20 (area = 1 m^2). A

clearly visible crack was visible 59 hours after the starting of the test. After 119 hours the crack pattern was completely formed except for some tertiary or dead-end cracks. The cracking initiated from the edges and progressed toward the centre, this being visible in the second row of images from 87 to 95 hours. The majority of the cracks formed at this stage can be considered to be primary cracks, as they are the longest and widest cracks in the network. A careful observation shows that the majority of these cracks are approximately perpendicular to the longest side of the specimen. Subsequent images from 99 to 119 hours show the formation of secondary and some tertiary cracks that are usually formed between two primary cracks. In the last row of images from 132 hours to the end of the test very few new cracks are formed, whereas a widening of the existing cracks was observed. Although the size of the images is small in this figure, a distinction of primary and secondary cracks can be made according to their thickness.

Figure 8.5 shows the evolution of the crack pattern on specimen A1-20 (area = 0.5 m^2). The first image of the figure was taken 25.2 hours from the start of the test. The next two images in the same row show a crack forming from the right side of the specimen. The image taken at 43.2 hours shows a crack perpendicular to the longer side approximately dividing the specimen in half. In the last image of the second row, taken at 53.2 hours, cracks forming on the left side of the specimen can be seen. The three images of the third row show the gradual crack formation all over the specimen. The majority of the cracks were completely formed at around 100 hours after test initiation. The images from 70 to 100 hours show the formation of secondary cracks further dividing the space between the primary cracks.

Figure 8.6 shows the evolution of the crack pattern on specimen A2-20 (area = 0.25 m^2). The crack formation seems to be influenced by the boundary conditions. The images taken from 45 to 60 hours show the formation of primary cracks. The images in the third and fourth row show the formation of the rest of the primary cracks and the secondary cracks. It is interesting to note that there are very few tertiary cracks. The majority of the crack formation had been completed after about 85 hours. After that time, only widening of the existing cracks was observed.

Figure 8.7 shows the evolution of the crack pattern on specimen A3-20 (area = 0.125 m^2). A clear influence of the boundary conditions on the crack formation and the final pattern can be seen throughout the sequential images. The majority of the cracks meet the boundary of the specimen. The number of boundary cells (i.e. with at least one edge being at the boundary) is larger than the number of inner cells. Therefore the shape of the polygons limiting the cells is heavily influenced by the boundary conditions. The final crack pattern was formed at about 74 hours. After that time, further drying only results in widening of the existing cracks.

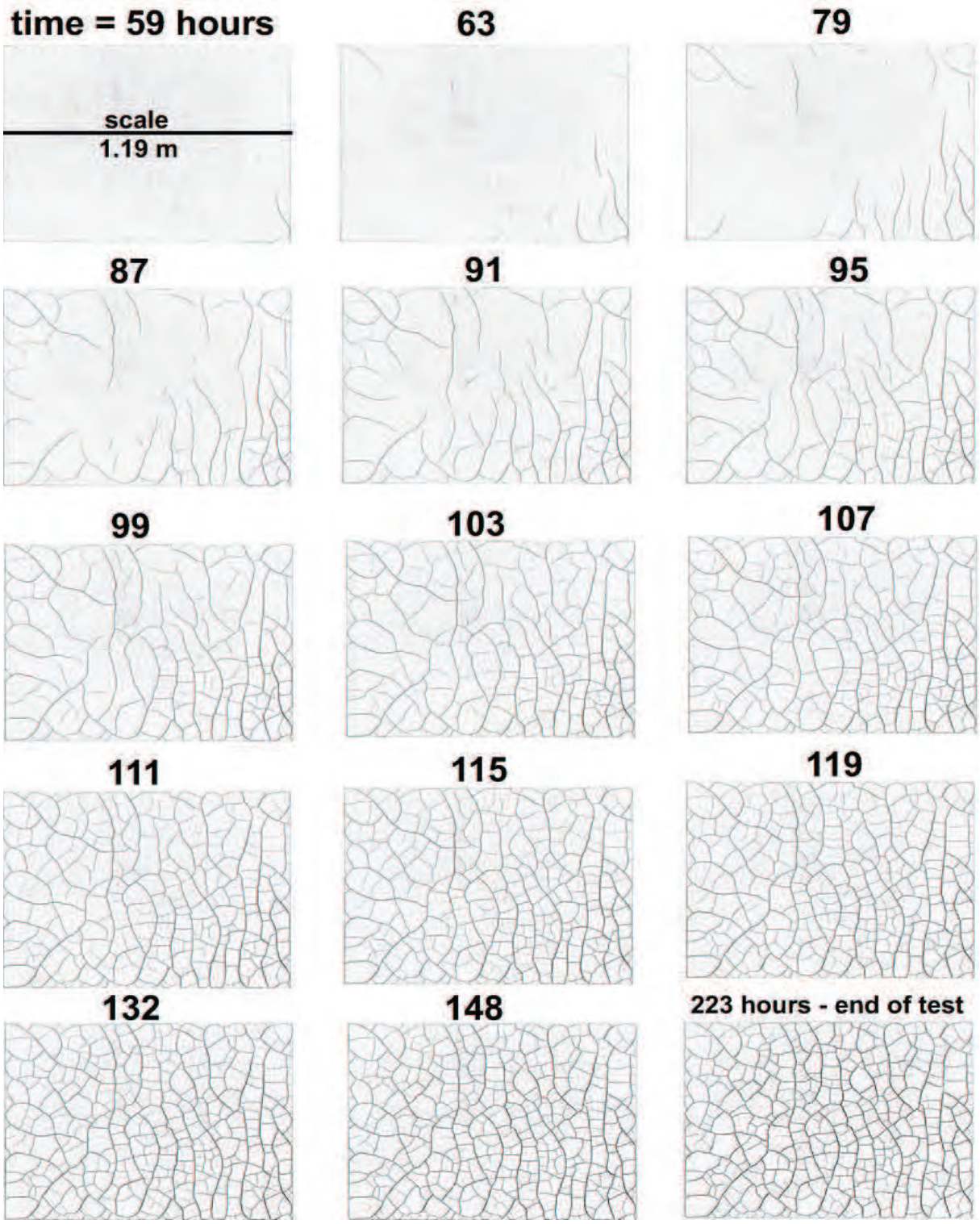

Figure 8.4: Evolution of crack pattern for specimen A0-20

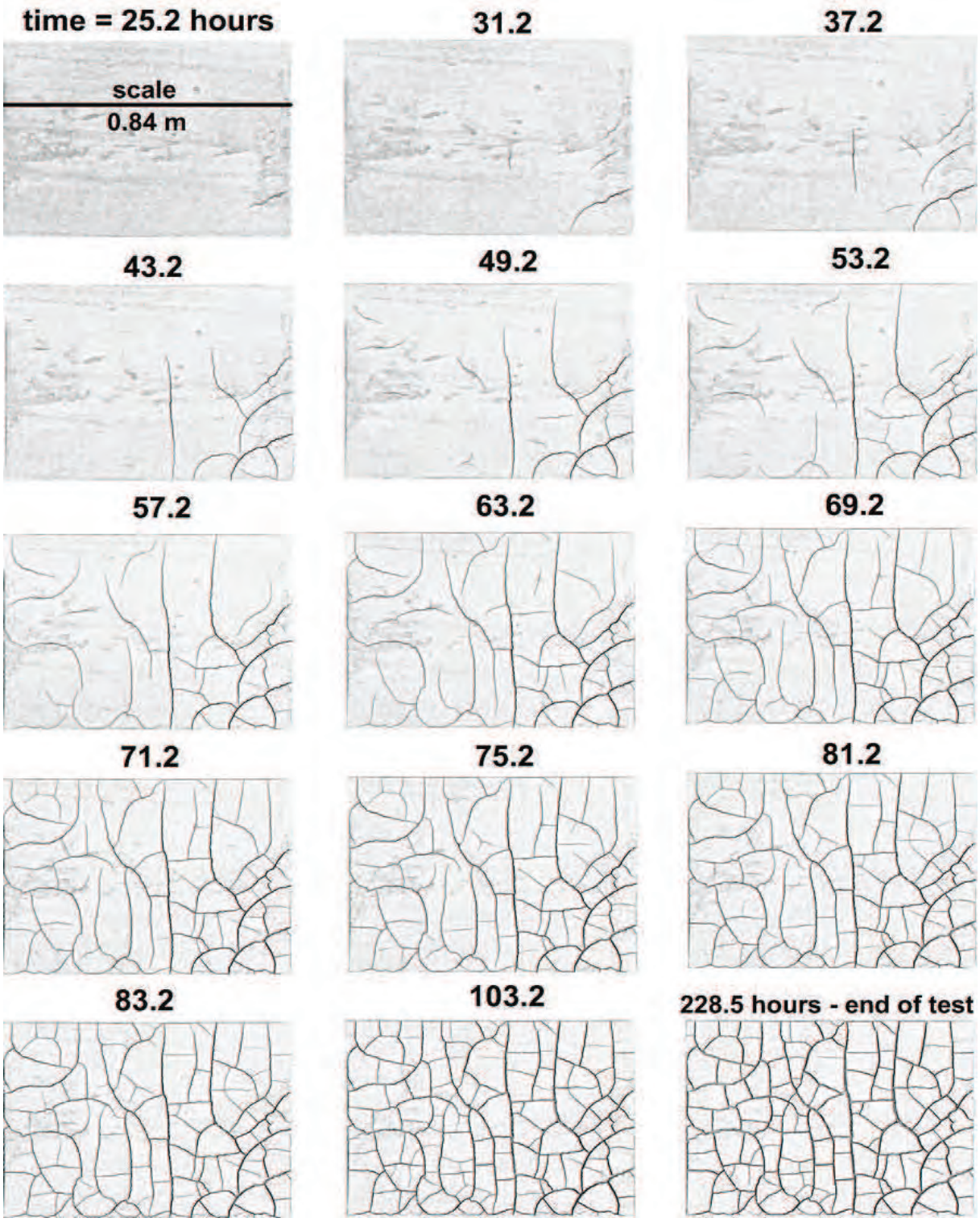

Figure 8.5: Evolution of crack pattern for specimen A1-20

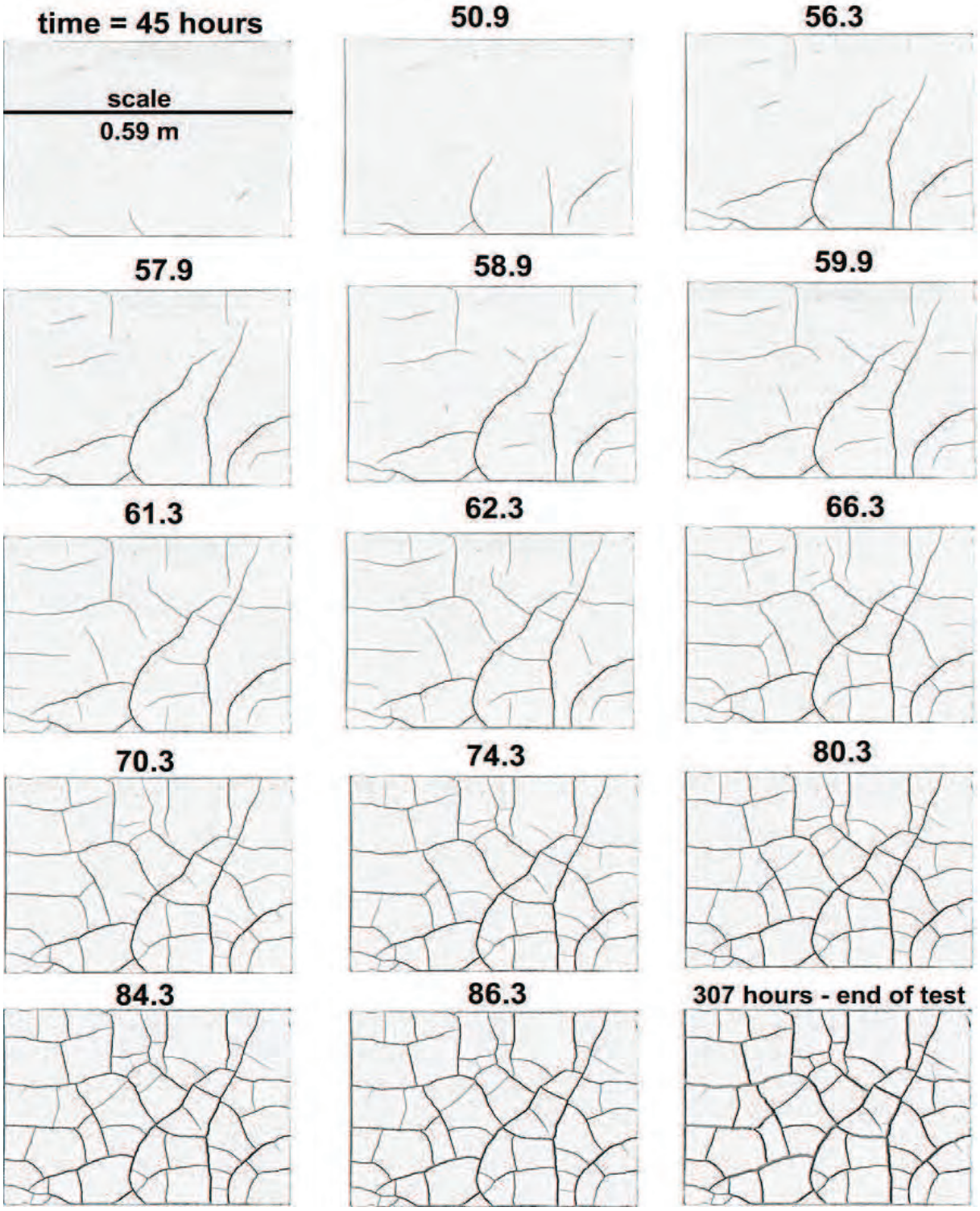

Figure 8.6: Evolution of crack pattern for specimen A2-20

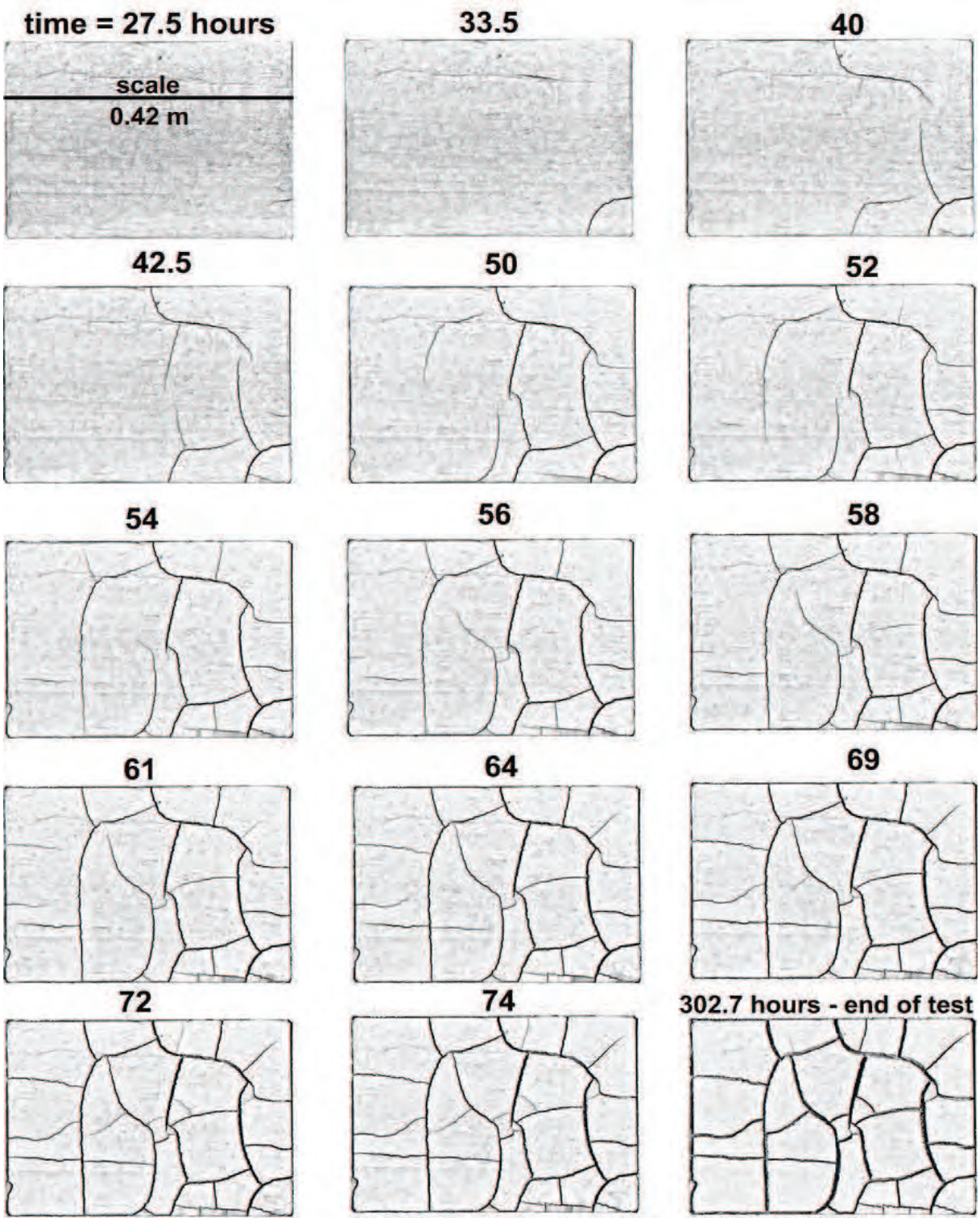

Figure 8.7: Evolution of crack pattern for specimen A3-20

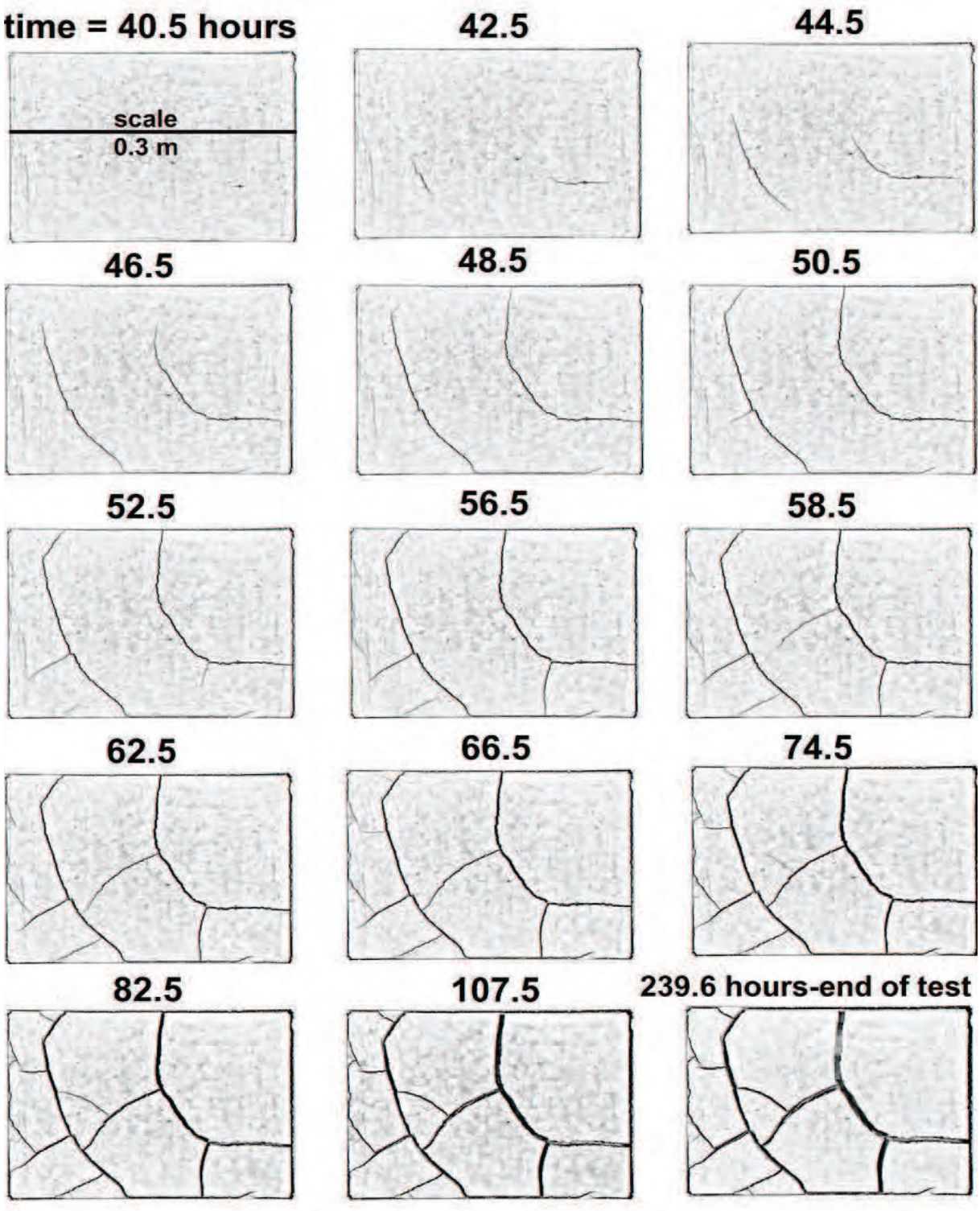

Figure 8.8: Evolution of crack pattern for specimen A4-20

Finally, figure 8.8 shows the evolution of the crack pattern on specimen A4-20 (area = 0.0625 m^2). The first image shows a crack starting as a dot on the bottom-right corner of the specimen. The second image shows another crack developing on the left side. The third image, taken at 44.5 hours, show two developing cracks. The crack on the left-hand-side seems to start parallel to the longer side of the specimen but changes direction more or less 90°. This change in the direction is due to the presence of another crack on the left side. The influence of an existing crack on a developing crack depends on the characteristic distance (crack spacing) that separates them. The influence of the crack on the left side on the developing crack on the right side can be seen from the sequence of images taken at 42.5, 44.5 and 46.5 hours. The last image on the second row taken at 50.5 hours shows two fully formed cracks, one on the left side that is approximately perpendicular to the longer side and another L-shaped crack on the right side. A simple observation of this crack allows identification of three segments: the first one is parallel to the longer side while the third one is perpendicular, with a curved segment joining the first and third segments.

Prediction of a crack path is extremely difficult because of the interaction between the developing and existing cracks. The direction of crack propagation depends on the stress state: cracks propagate in the direction perpendicular to the maximum tensile stress. However, existing or developing cracks in the vicinity of another newly forming crack change the stress state in unpredictable, seemingly random manners, thus forcing the new crack to change direction according to the rotating principal stresses. On the other hand, crack bridging between two existing cracks can be more deterministic. Consider the last image of the second row, taken at 50.5 hours. Two primary cracks have been formed and both touch the boundary of the specimen. From the morphological analysis of the final crack pattern it is very much clear that the secondary crack originating from a primary crack intersects the existing crack at a right angle. Also other secondary or tertiary crack meet the existing crack at right angles. The first image of the third row taken at 52.5 hours shows nucleation of a secondary crack to the crack on the right-hand side exactly at the point where the crack changed its direction. Though this crack nucleates to the crack on the right-hand side its propagation is influenced by the left-hand side crack and by the specimen's boundary. This can be seen in the image taken at 58.5 hours where the crack meets the longer side of the specimen's boundary at a right angle. A similar explanation can be made for another crack seen between the two primary cracks in the image taken at 58.5 hours, which finally meets other cracks at the image taken at 66.5 hours.

The mechanism of successive divisions of domains and the hierarchical nature of the crack pattern formation in drying soils can also be explained using analysis of these time-

evolution images.

8.3.3 Time evolution of crack patterns on 10 mm thick specimens

Figures 8.9 to 8.13 show the evolution of the crack patterns developing on the surface of the five 10 mm thick specimens, ranging from size A0 to A4.

Figure 8.9 shows the evolution of the crack pattern on specimen A0-10 (area = 1 m^2). Although the scale at which the images are printed is rather small, the sequence of the images provides an overall idea on how the crack pattern evolved. An interesting observation is that the larger-sized cells between polygonal cracks concentrate mostly on the edges of the specimen, while smaller-sized cells are found near the centre. This phenomenon may be attributed to boundary effects extending to a certain distance from the edges and therefore having no influence on the inner region of the specimen. Comparison to specimen A0-20, the test duration with A0-10 was considerable less. Also, comparison between figures 8.9 and 8.4 shows that the size of the cells between cracks is much larger in the 20 mm thick specimen, thus making more difficult to establish a visual distinction of primary and secondary cracks in the 10 mm thick specimen. In this case. many dead-end cracks were observed after the formation of the tertiary cracks. Very little or no widening of the primary and secondary cracks was observed.

Figure 8.10 shows the evolution of the crack pattern on specimen A1-10 (area = 0.5 m^2). Because of the scale, the images taken during this test and shown in the figure allow for a better visual analysis. The first image of the first row shows that the crack pattern starts at the bottom right-hand side. The subsequent images taken at 38.2 and 47.17 hours show cracks propagating from all four edges of the specimen toward the centre. Images in the second row taken at 50 to 55 hours show that although cracking propagates toward the centre, fully formed crack polygons can be seen in all four corners especially in the image taken at 55.17 hours. Though this type of crack propagation was also observed in specimens of 20 mm, there only primary cracks were propagating and no fully formed polygons were seen. In 10 mm thick samples crack density is higher, resulting in smaller cells and more cracks. It is appropriate to mention here that the rate of desiccation is almost double in 10 mm thick specimens than in 20 mm thick ones. However, the cracking front does not propagate twice as fast. It would seem that because of the increased desiccation rate the stresses develop faster, resulting in rapid formation of secondary cracks.

Another important morphological characteristic of test A1-10 is the absence of long primary cracks, some stretching from one end to another of the specimen boundary, that were seen in test A1-20. The absence of long primary cracks may be explained by the well known fact that crack spacing decreases as the thickness decreases. This indicates that stress concentration necessary for crack nucleation is more closely spaced in 10 mm specimens resulting in more number of cracks closely spaced. The area of the drying surface being the same for both 10 mm and 20 mm thick specimens, more cracks per unit area are observed in 10 mm thick samples, thus resulting in shorter primary cracks.

Figure 8.11 shows the evolution of the crack pattern on specimen A2-10 (area = 0.25 m^2). Like in most of the other tests, the crack initiates from the right-hand side bottom of the specimen, which can be seen in the first image taken at 21.1 hours. Following images of the first and second row show the temporal evolution until 32.1 hours. The final crack pattern was already visible at about 36.1 hours. In this test the crack pattern propagates from right to left. It is interesting to note that the primary crack formation is perpendicular to the longer side, clearly seen in the last image of the third row taken at 36.1 hours. The right half of the specimen shows crack polygons and the left half shows cracks parallel to the short side and no polygon formation yet. The final crack pattern is shown in the last image taken at 138 hours. It is very clear from these images that the primary crack formation is perpendicular to the longer side and that secondary cracks were formed between two primary cracks parallel to the longer side. As a result of this type of crack formation the majority of the cracked cells have four sides. This type of crack formation is very particular and it was not observed at such scale spanning all the specimen. In some way this type of pattern formation seems to be deterministic.

The cracking pattern in soils seems to be affected by external loads or perturbations if applied just before the drying process. Figures 8.14, 8.15 and 8.16 show the effect of external loading or perturbation. The soil sample, in its plastic state before the start of drying, "remembers" the load or perturbation. This memory is reflected during the formation of the crack pattern as it dries. In the present investigation crack patterns which seem not to be random, but have some definite order, were observed only in specimens A2-10 and A3-10. It is interesting to mention here that during the preparation of the specimens some blows were given to the sides of the holding trays to facilitate the spreading of the soil and to remove entrapped air. Also, at the end a smooth surface was obtained by passing a straight edge over the holding trays, and several passes were needed before getting a smooth surface. It might be argued that this had some effect on the crack pattern formation, although the procedure was the same for all the specimens.

Figure 8.12 shows the evolution of the crack pattern on specimen A3-10 (area = 0.125 m^2). Though some cracks already appeared at 26 hours, they can be better viewed in

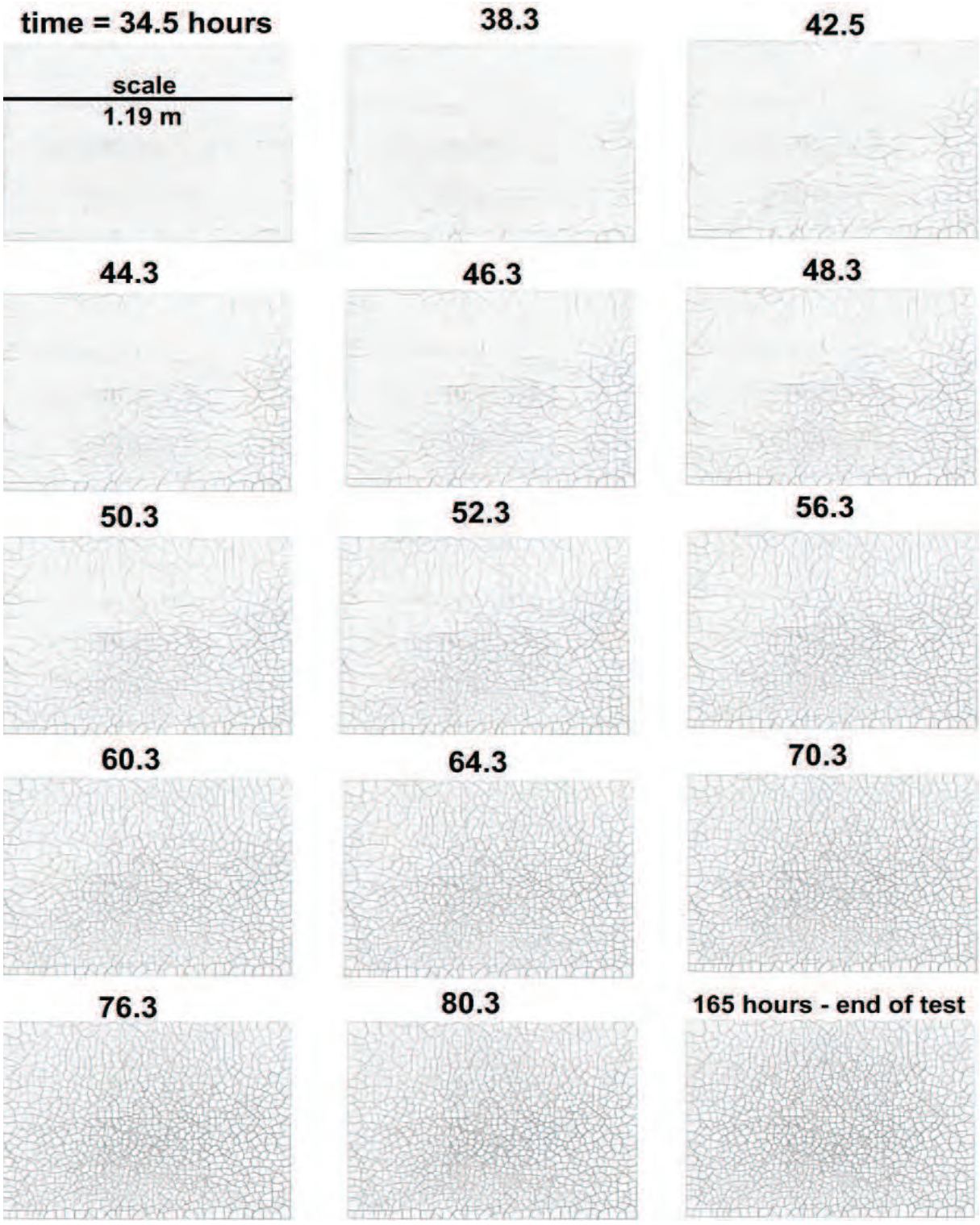

Figure 8.9: Temporal evolution of crack pattern for specimen A0-10

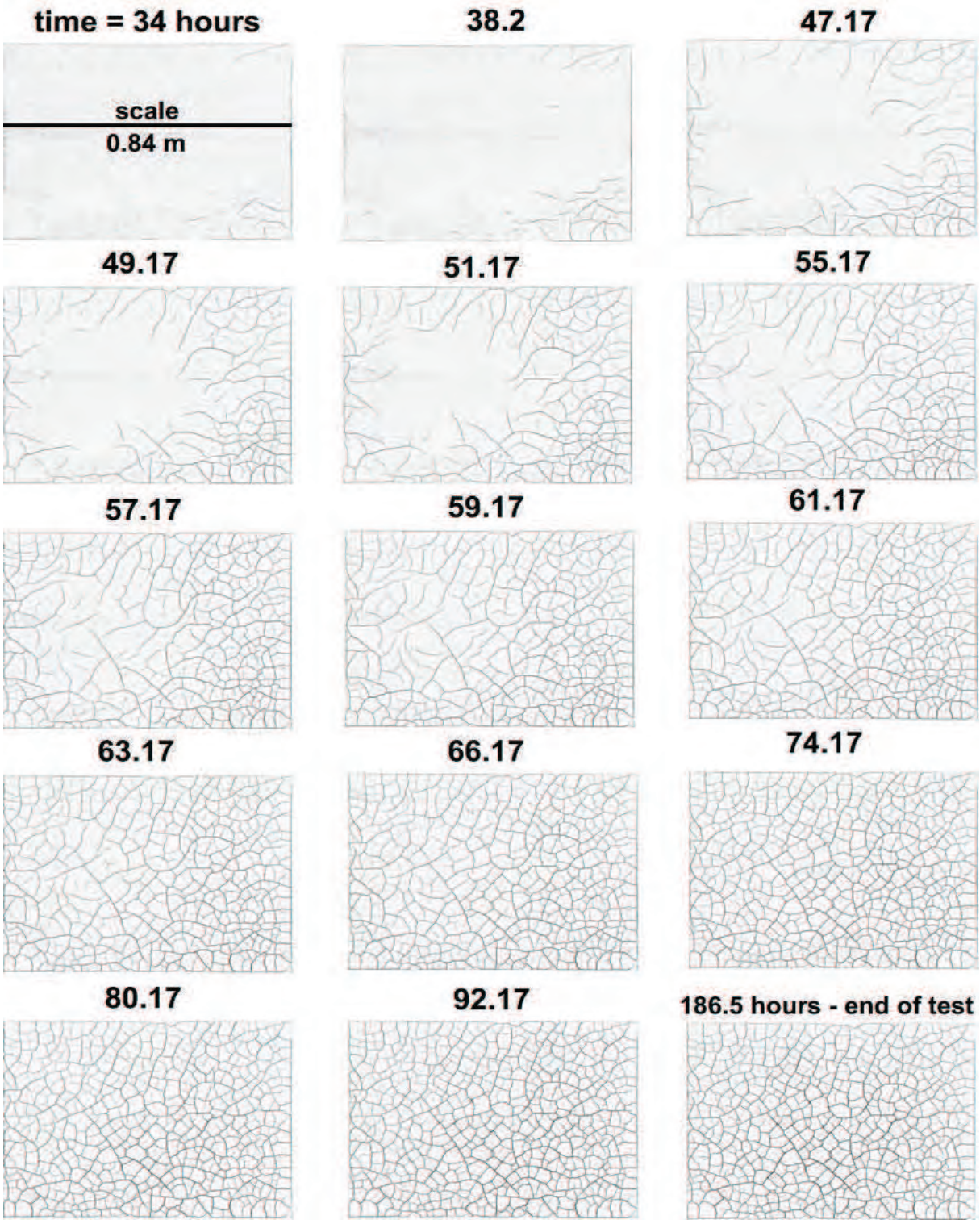

Figure 8.10: Temporal evolution of crack pattern for specimen A1-10

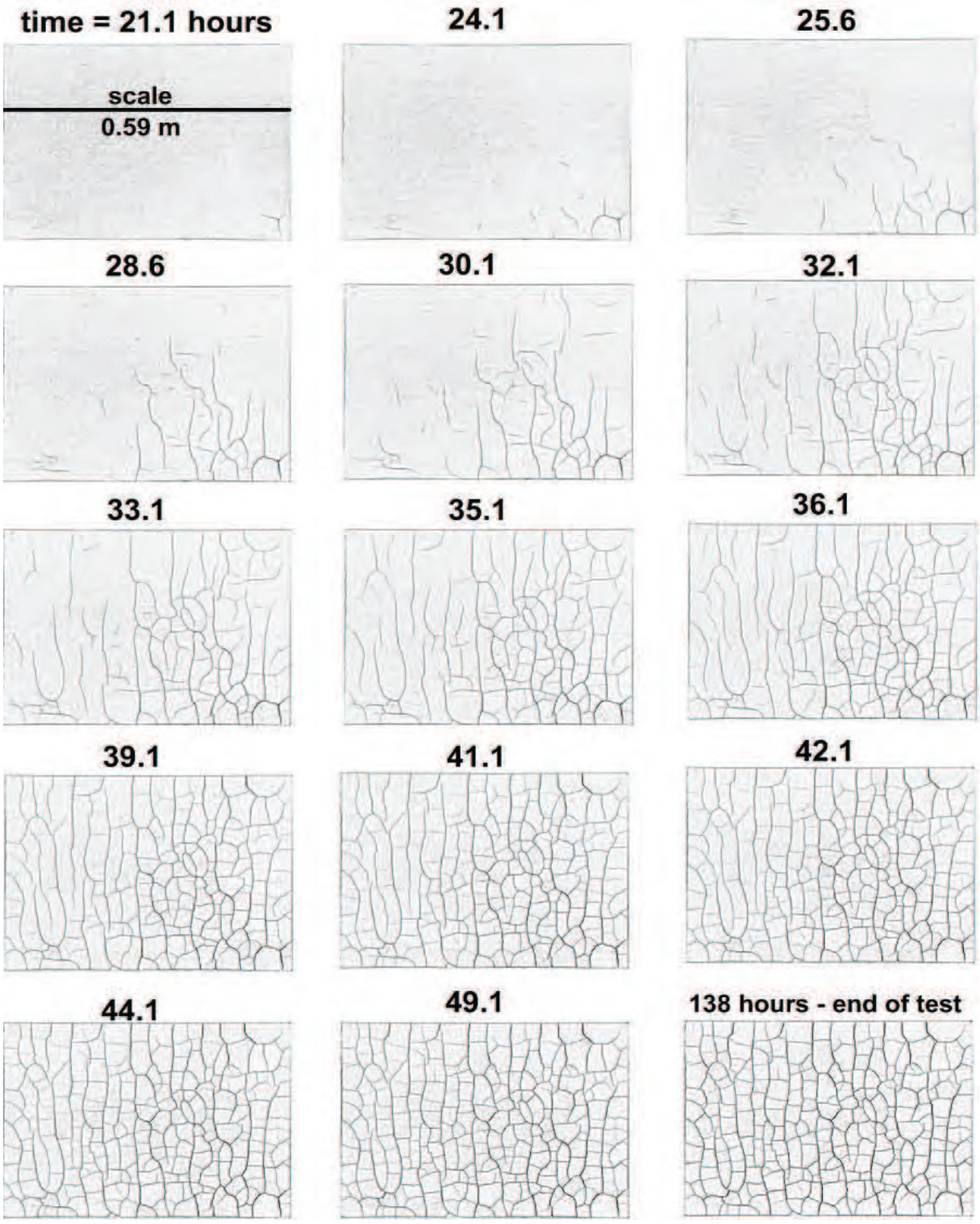

Figure 8.11: Temporal evolution of crack pattern for specimen A2-10

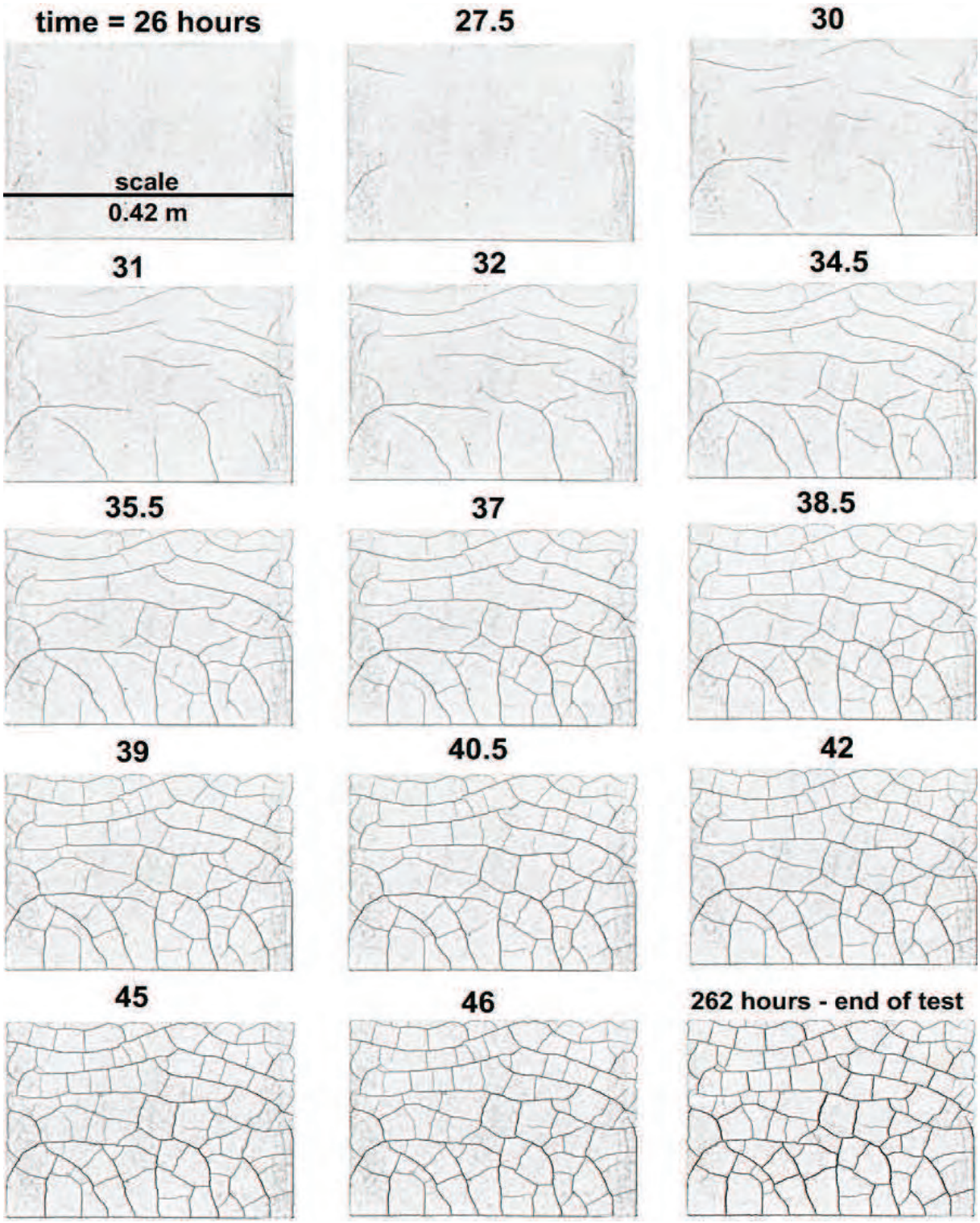

Figure 8.12: Temporal evolution of crack pattern for specimen A3-10

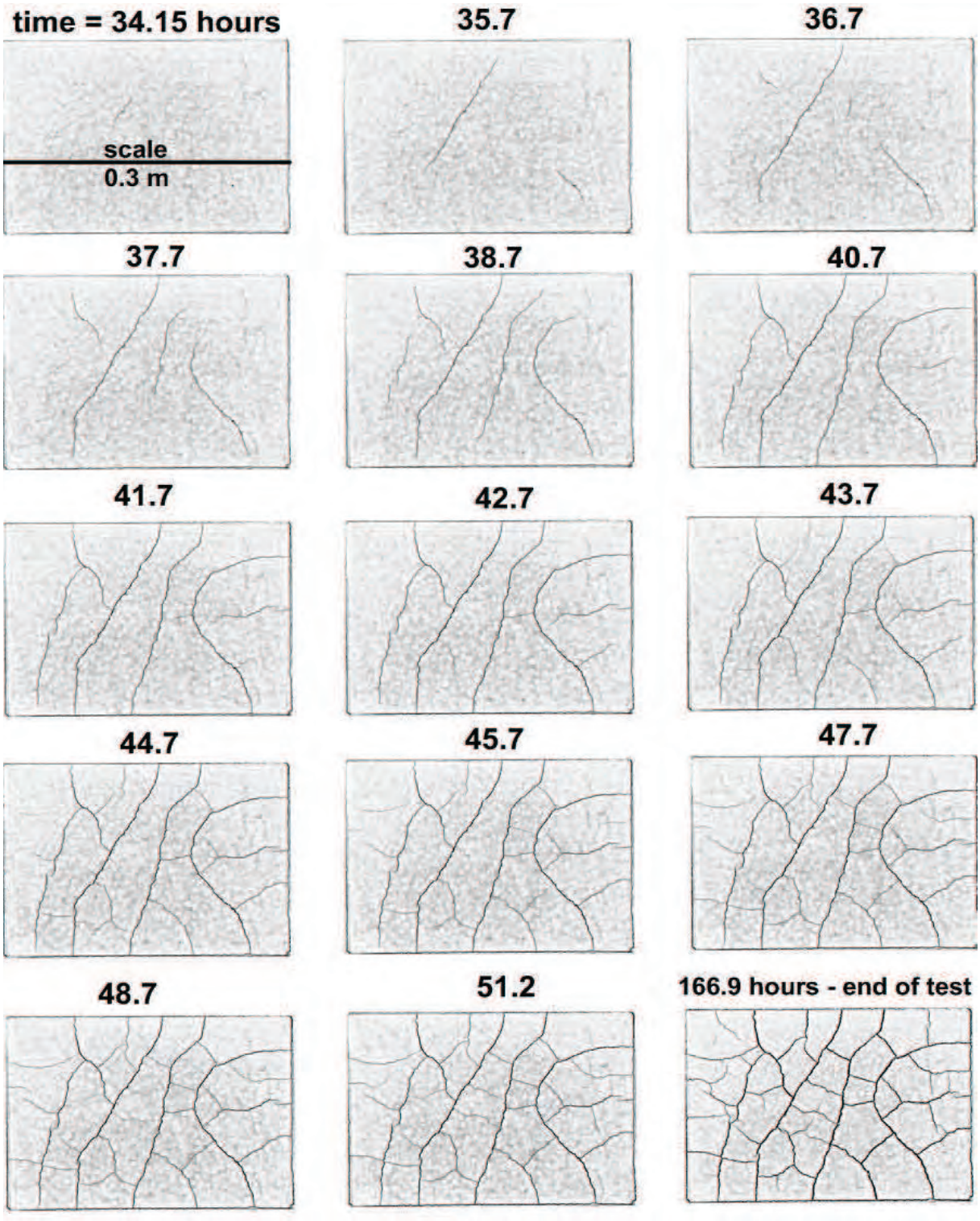

Figure 8.13: Temporal evolution of crack pattern for specimen A4-10

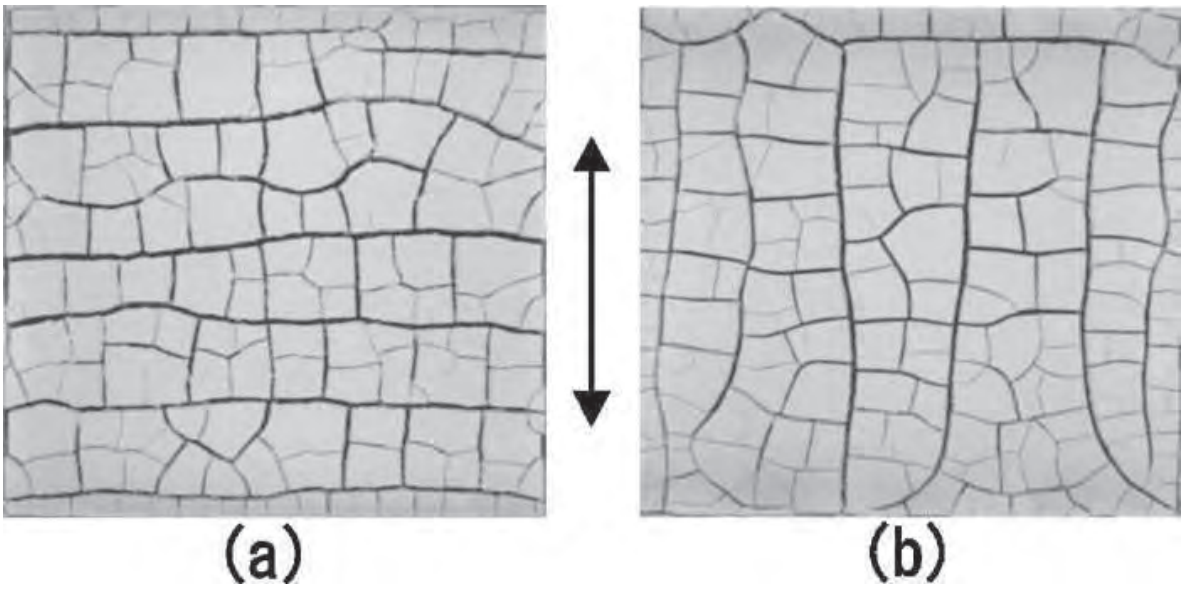

Figure 8.14: Transition in the direction of lamellar crack patterns. The arrow between (a) and (b) indicates the direction of the initial vibration, where the amplitude r and the frequency f of the vibration are 15 mm and 2 Hz, respectively, i.e., the strength $4\pi^2 r f^2$ is 2.4 m/s^2. The lengths of the sides of both square containers are 200 mm. (a) The solid volume fraction is 12.5%. The direction of the lamellar cracks is perpendicular to the direction of the initial vibration. (b) The solid volume fraction is 6.7%. The direction of the lamellar cracks is parallel to the direction of the initial vibration (after [Nakahara and Matsuo, 2006]).

the image taken at 27.5 hours. The three images of the second row taken from 31 to 34.5 hours, show the formation of primary cracks. In these images the specimen can be divided into two distinct zones: the top portion where cracks are seen parallel to the longer edge and the bottom portion where the cracks are approximately perpendicular to the longer edge. The subsequent images of the third row taken from 35.5 to 42 hours show the formation of cracks between the primary cracks resulting in four-sided polygonal cracked cells. The image taken at 46 hours shows a fully formed crack network. After this time no more cracks appear and existing ones increase their width.

Finally, figure 8.13 shows the evolution of the crack pattern on specimen A4-10 (area = 0.0625 m^2). The mechanics of crack formation in this test is similar to the mechanics explained for the earlier specimen of same size but double thickness. The effect of the boundary drives the process of crack formation. Formation of the primary cracks can be seen in the images taken from 35.7 to 43.7 hours. Further, the secondary cracks formation can be seen in the subsequent images up to 51.2 hours. No more crack formation was observed after that time, only widening of the existing cracks.

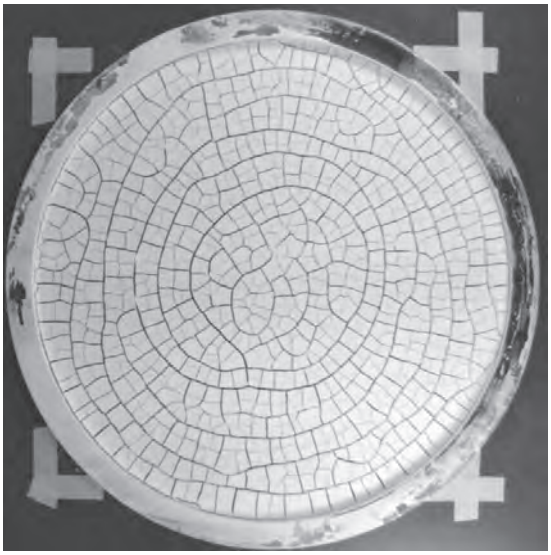

Figure 8.15: A ring pattern. Here, the solid volume fraction is 7.7%. The diameter of the circular container is 500 mm. Before drying, a cover on the paste was placed and rotated counterclockwise at a period of 1 s for 10 s, and then removed for drying. It can be seen that no surface wave or vibration is necessary for the formation of a flow pattern (after [Nakahara and Matsuo, 2006]).

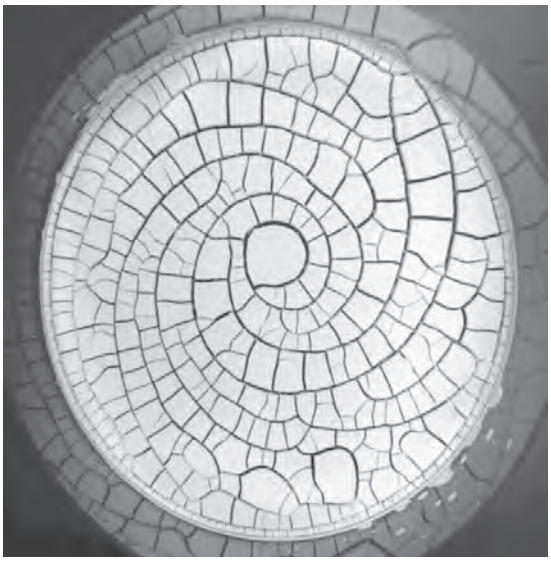

Figure 8.16: A spiral crack pattern. Here, the solid volume fraction is 7.7%. The diameter of the circular container is 500 mm. Before drying, the container was translated along a circuit with a radius of 15 mm clockwise at a period of 1 s for 60 s, so that the container pushes the paste inward and clockwise simultaneously to produce a spiral flow. Note that the container was not rotated around its center (after [Nakahara and Matsuo, 2006]).

8.4 Crack intersection angle

Crack intersection angle is one of the most significant parameters that characterise a crack network. This values provides information about the direction of the principal stresses during the formation and propagation of individual cracks and also help in explaining the pattern as a whole.

8.4.1 Junction formation during desiccation cracking

There are three types of junctions that can be formed during desiccation cracking. The first type of junction is formed when a developing crack meets an existing crack. The second type of junction is formed when a crack nucleate or bifurcates from an existing crack. In both of the above types of junctions the angle of intersection is more likely to be around 90°, this is because the stress relaxation occurs only in the direction perpendicular

to the direction of cracking and the stress parallel to the direction of cracking can only contribute in nucleation of a crack in a direction perpendicular to the existing crack. The third type of junction is formed when a crack nucleates and there is more than one crack developing as shown in figure 8.17. The intersection angle in this last type of junction is not 90° as in the earlier two cases.

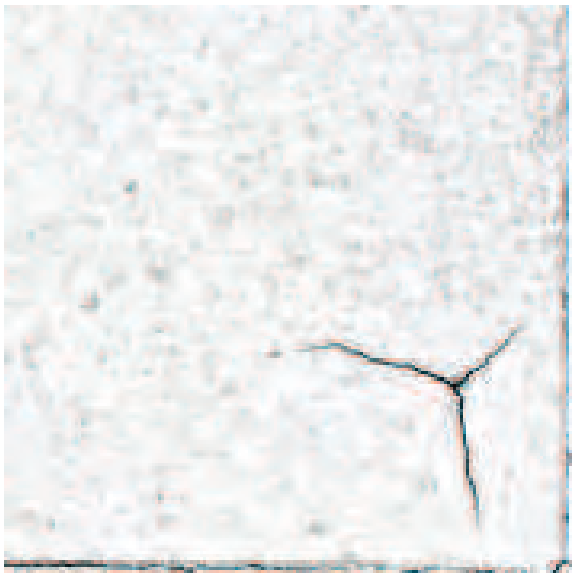

Figure 8.17: Junction formation during the crack nucleation in specimen A2-10

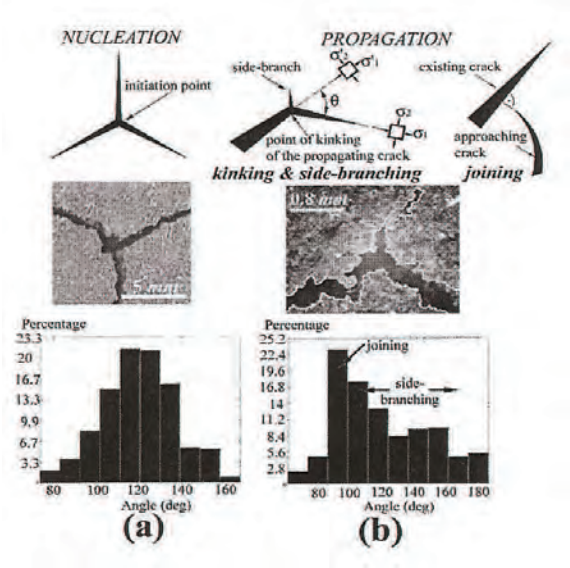

Figure 8.18: (a) Nucleation dominated cracking; (b) Propagation dominated cracking (after [Toga and Alaca, 2006])

Toga et al [Toga and Alaca, 2006] studied the formation of junctions during desiccation cracking. The desiccation experiments were carried out with coffee:water suspensions (1:2 by mass) on a Poly-Methyl-Methacrylate (PMMA) substrate. In the experiment depicted in figure 8.18a, a network of needles was used to pattern the surface of the PMMA substrate prior to casting the suspension. Distance between the needles is kept small enough to suppress crack propagation. Once cracks initiate at one particular point, stresses around its immediate vicinity are relieved, and hence, neighbouring cracks cannot propagate into the relaxed region. During drying, each needle serves as such a nucleation point, and this is reflected by the dominance of 120° in the histogram of junction angles.

On the other hand, if the surface was not patterned with needles and the crack network was left to evolve under ambient conditions, kinking and side branching and joining at 90° were observed as in figure 8.18b. The peak angle was observed to be 90°, indicating the dominance of joining cracks in forming triple junctions. Other angles are due to kinking and side branching and, to a certain extent, due to nucleation. The rather broad distribution indicates the inhomogeneity in the system, in particular the stress state, with kink angles or intersection angles taking a variety of values. In contrast to this, systems

of reduced inhomogeneity, usually soil coatings such as glazed surfaces on ceramics, do not exhibit sharp kinks, and almost all junction angles are observed to be 90°, while only a minority of 120° triplets exist ([Bohn et al., 2005b], [Bohn et al., 2005c]).

Considering the above explanation on the formation of junctions and the angle of intersection, it can be asserted that crack nucleation occurs at an angle 120° and side-branching and joining occurs with an intersection angle of 90°. Hartge and Bachmann [HARTGE and BACHMANN, 2000] also studied the angle between cracks developed during primary shrinkage of fine-grained soil materials, and according to them the intersection angle can be of two types: orthogonal angles (OA) and non-orthogonal angles (NOA). According to them OA were caused by tensile failure and NOA by shear failure. Recalling now the histograms in figure 8.18a,b it can be concluded that crack nucleation is predominantly driven by shear failure and that side-branching and joining is predominantly driven by tensile failure. This provides a different view from the widely accepted theory for crack nucleation occurring when the tensile stresses are larger than the tensile strength of the material at a given point.

Figure 8.19 shows the evolution of cracking in the area within the rectangle marked in the last image of the figure 8.3. These images show the formation of triple junctions when a developing crack meets an existing crack (images taken from 107 to 108 hours and from 111 to 113 hours). In both cases the developing crack changes direction quite abruptly to meet the existing crack at 90°. In the final image taken at 114 hours, a side branching crack can be observed which is just nucleating with an intersection angle of 90°. The abrupt change in direction of the developing cracks suggest the influence of higher order cracks and also of the stress perturbation.

8.4.2 Determination of the intersection angle

The intersection angle was determined by analysing the digital images taken during the experiments. The details on how the images were obtained are given in Appendix A. The experimental techniques are described in Chapter 5. The image processing and analysis used in determining the angle of intersection throughout the crack pattern is also described in Appendix A.

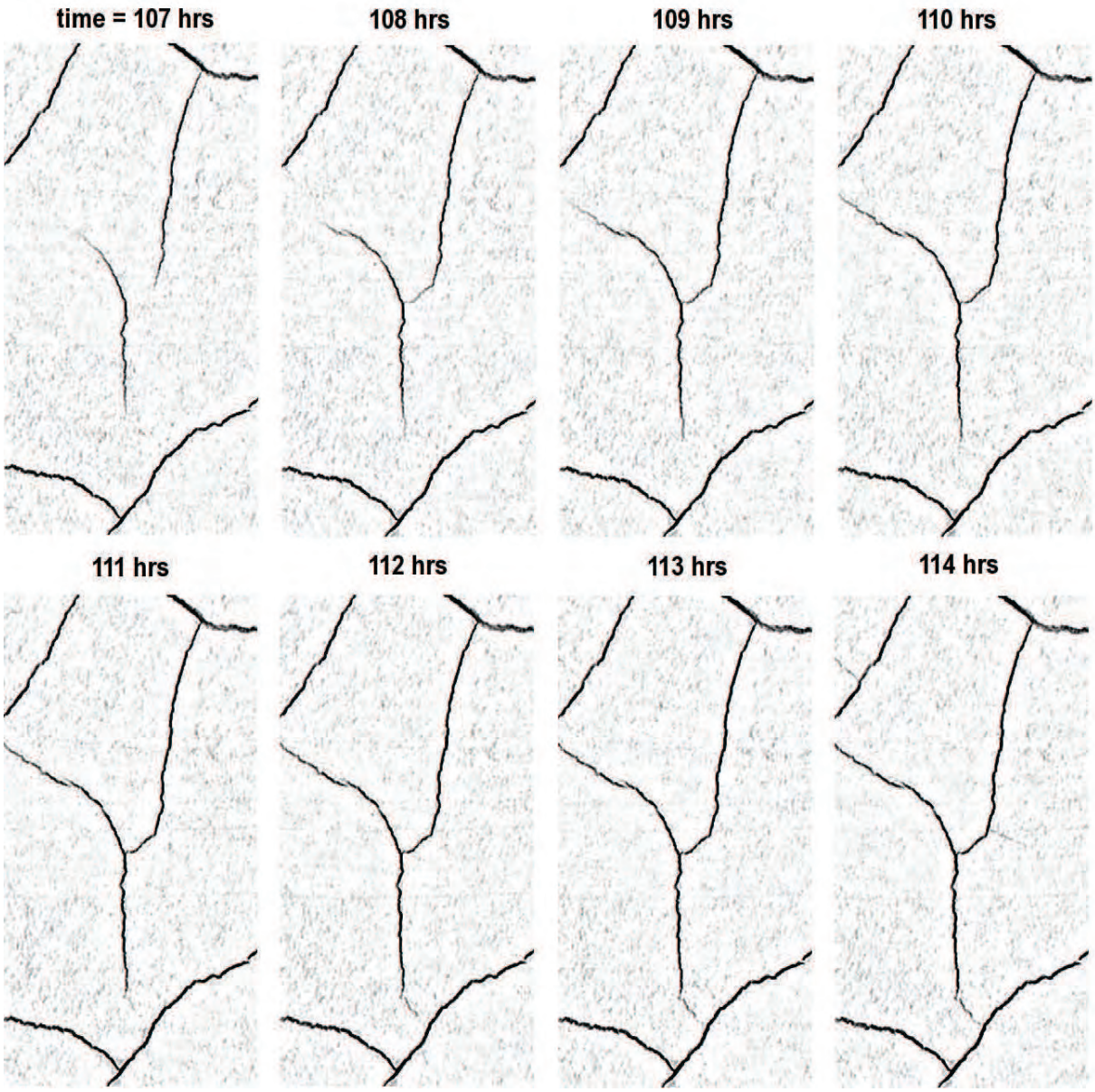

Figure 8.19: Evolution of cracking in the area within the rectangle marked in figure 8.3 showing formation of junctions (joining and side-branching) during desiccation cracking

8.4.3 Frequency distribution of crack intersection angles

Figure 8.20 shows the frequency distribution of the angles between intersecting cracks. The peaks of the distribution are found at 90° and 120°, indicating that these were the most frequent angles. Formation of a crack pattern involves crack initiation, crack propagation and crack bridging and joining. These three processes may happen simultaneously after cracking begins. Depending on the existing stress conditions cracks are likely to meet forming a Y or T joint, resulting in an intersection angle that varies between 90°

and 120° (Vogel et al.[Vogel et al., 2005]). The intersection angle (orthogonal or non orthogonal) indirectly indicates at which stage of desiccation the crack has formed as well as the local stress state (drying conditions). Orthogonal angles ($80° - 100°$) are formed due to tensile failure and non-orthogonal angles ($< 80°$ or $> 120°$) due to shear failure (Hartge and Bachmann [HARTGE and BACHMANN, 2000]). Though non-orthogonal angles are formed during desiccation of soils, their frequency is much less and from this one can conclude that tensile failure is responsible for the majority of cracks. However, evidence from experimental observation indicates that there are always some non-orthogonal angles and Y joints, indicating that there is always some cracking triggered by shear stress.

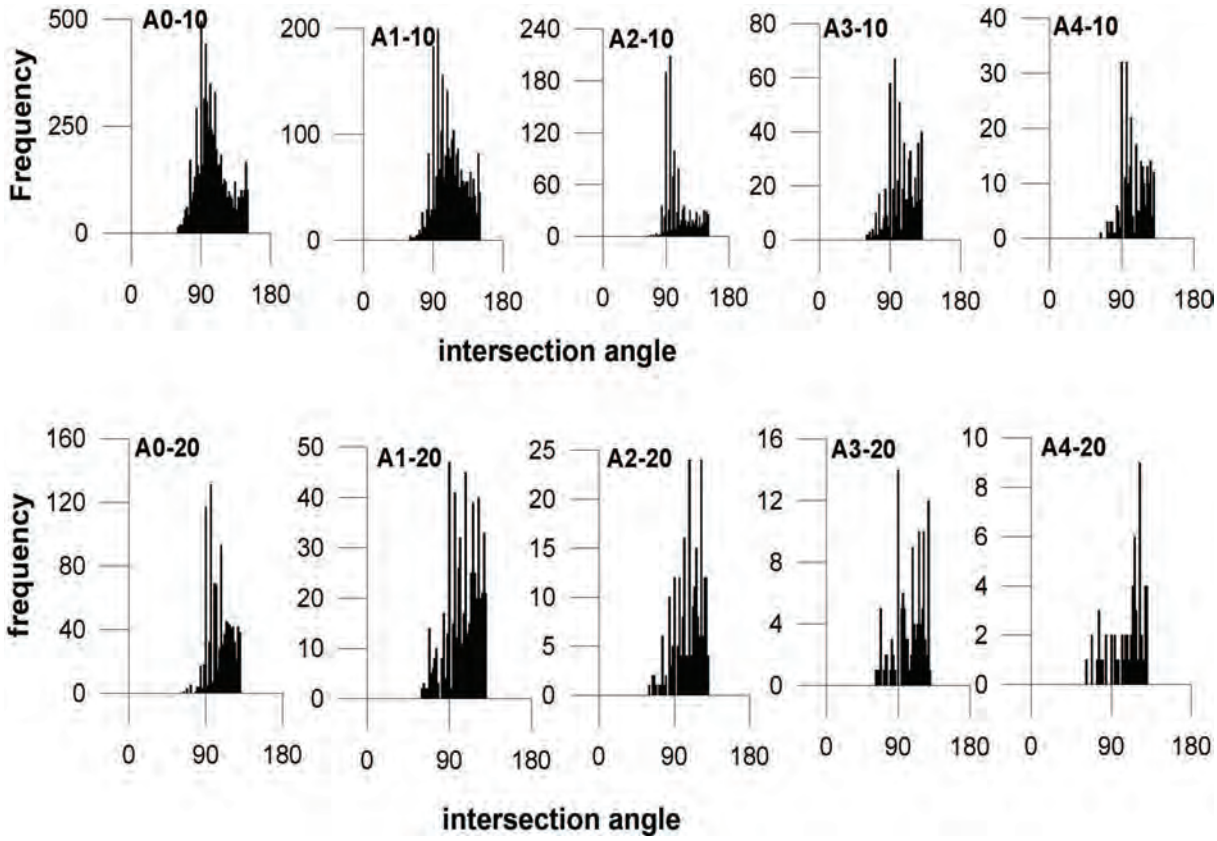

Figure 8.20: Frequency of crack intersection angles

8.5 Soil cracking: from disorder to determinism?

8.5.1 Introduction

Unless a physical phenomenon may be explained in a strict deterministic manner no theories can be formulated. When the parameters governing a certain phenomenon can

be described in a systematic way which is independent from time and spatial position, then the phenomenon is likely to be deterministic. In some cases the parameters may change in time but remain independent of spatial position. Then the phenomenon still may be deterministic. Another important characteristic of deterministic phenomenons is the repeatability.

Cracking is difficult to classify: on one side, it is almost impossible to obtain the same crack pattern even for two identical desiccation tests carried out at the same time next to the other, making the final crack pattern a disordered phenomenon. However, there are certain aspects of the cracking process which can be deterministic, such as the crack initiation mechanism which can be predicted with great accuracy, although it seems almost impossible to predict the exact location of crack initiation: Cracks initiate on the drying surface in a very disordered manner. It is well known that crack initiation occurs when the tensile stresses are greater than the tensile strength, however, if these points where the crack initiates are weak points they are indeed distributed in a very disordered way.

8.5.2 Disorder and deterministic parameters

Table 8.1 lists the deterministic and disordered parameters that have a role during the process of drying/desiccation of a soil resulting in the formation of a crack pattern.

Table 8.1: Parameters that can be deterministic and disorder

Deterministic	Disordered
Mechanics or conditions of crack initiation	The location of crack initiation
Crack propagation	Direction of crack propagation of primary cracks
Termination or end of cracking process	Final crack pattern network
Geometric or morphologic characteristics of the final crack pattern	Geometry or morphology of individual cracks
Moisture content and its evolution for the system	Distribution of moisture content over the system
Overall volumetric shrinkage	Localised differential shrinkage
Soil moisture evaporation	Mechanisms for soil moisture transportation and its path/s
Stress concentration	Fabric / structure of soil and its contribution
Macroscopic morphological insight	Microscopic reorganisation or changes

Although the agents governing crack initiation and the conditions for crack propagation and nucleation are well known, it is still highly difficult to predict the location where a crack will start in a drying soil mass. Crack propagation is deterministic: cracks *will* grow as a consequence of differential shrinkage and desiccation. On the other hand the direction of crack growth at least in the case of primary cracks is difficult to determine. Although some crude estimate, depending on the boundary effect, can be made it is still not accurate. However, the direction of most of the secondary cracks (between two primary cracks as well as subsequent cracking) can be more precisely determined.

The end of the cracking process can be determined based on knowledge of the soil type, its thickness and the imposed or existing environmental and boundary conditions during desiccation. Although looking at the final crack pattern of two identical specimens tested simultaneously under the same conditions it may seem that the patters are different (and therefore random), a detailed analysis proves that there is actually a great deal of similarity between the desiccation crack patterns and much of the morphological features can be predicted with certain accuracy. In the same line of investigation, it is interesting to note that the morphology of individual cracks is far from deterministic.

It is very easy to follow the evolution of moisture loss of the specimen during the process of drying, but it is virtually impossible to accurately measure the distribution of moisture over the drying surface. However, this would be valuable information because the differences in moisture distribution due to differential drying, resulting in differential shrinkage, leads to the stress concentration for crack nucleation. Similarly, the overall volumetric shrinkage can be determined, but not the localised differential shrinkage. Known theories can determine with accuracy the quantity of soil moisture evaporation, but it would be only a crude guess the prediction on how the soil moisture is transported in the developing crack network and inside the developing cracked cells. Finally it is possible (and has been adopted in this work) to observe the macroscopic response but it seems far more difficult to observe the microscopic reorganisation that takes place.

8.5.3 The transition

Several of the agents discussed in the previous paragraphs will remain disordered till the end of the cracking process. Nevertheless certain parameters, especially the macroscopic morphology of crack pattern formation, seem to make a transition from a disorder to a deterministic state. The degree of determinism seems to grow from the beginning of the desiccation process. This transition takes place as more and more cracks nucleate and grow and, in the process, the drying soil domain divides into many smaller domains.

During this process, the newly formed cracks act as new boundaries which in turn affect the formation and propagation of new cracks within the new cells. IT would therefore appear that the process of successive domain division explained in previous sections of this chapter is the key to make the system deterministic.

8.6 Shrinkage cracks: Desiccation or Synaeresis?

8.6.1 Introduction

Plummer and Gostin [Plummer and Gostin, 1981] explained that shrinkage cracks form within the soils or sediments (weather exposed or buried) in response to tension(s) produced within the soil by volumetric decrease induced by water loss. The water loss can be due to variations in the salinity of the depositing media, sediment compaction and temperature. According to Lachenbruch [Lachenbruch, 1962] two systems of cracks can be formed in such a system: (a) in a non-homogeneous, plastic medium an orthogonal system of cracks is formed; in this orthogonal pattern cracks are formed at the loci of low strength or high stress concentration and they do not form or propagate simultaneously; (b) in a homogeneous, non-plastic or relatively less plastic medium, a non-orthogonal system of cracks is formed; in this non-orthogonal pattern cracks propagate simultaneously and bifurcation occurs at obtuse angles.

Sinuous to spindle structures are associated with ripple marks whose width is proportional to their spacing. These types of structures are very common in sediments deposited in fully submerged conditions, indicating that a synaeresis process must be responsible, whereas desiccation cracks are formed under sub-aerial exposure. Table 8.2 gives a detailed description of the origin and characteristics of shrinkage cracks, which is directly taken from the work of Plummer and Gostin [Plummer and Gostin, 1981]. As the table is self explanatory no further discussion is elaborated here.

Although all the specimens tested in this work were sub-aerial exposed (and not submerged), some questions may be raised after observing the crack cells on the bottom specimen surfaces, where some ripple marks were seen. Hence an attempt is made here to explain their possible cause. Curling is also an important phenomenon observed in drying soils, and a possible link between curling and some cracks observed on the bottom surface of the specimens is also explored.

Table 8.2: Summary of shrinkage crack origins and characteristics (after Plummer and Gostin [Plummer and Gostin, 1981])

Type of shrinking crack and plan shape			Cross-sectional shape	Derivation of infill	Number of generations of cracks	Preferred orientation	Associated features (diagnostic)	Frequency encountered in geologic record	Origin and depositional environment
DESICCATION	Polygon	rectangular	V or U shaped	from above	can be multiple	?	rain drop imprints hailstone imprints bubble tracks foam impressions gypsum and/or salt casts flat-topped ripples vertebrate tracks etc.	uncommon	Algal or mud shrinkage by atmospheric drying Exposed
		hexagonal				none		rare	
		irregular						common	
	Non-polygonal	incomplete						uncommon	
		radial				?		rare	
		ribbon				parallel to water retreat			
SYNAERESIS		Polygon		from above or below	generally one	none	none	rare	Surface or Sub-stratal dewatering of submerged muds Submerged
		spindle				can be aligned	often with load phenomena	common	
		sinuous				along ripple troughs	ripple marks		

8.6.2 Definitions

Shrinkage cracks that form when muds loss water can appear in at least three kinds of settings:

1. Mud cracks that form under the open atmosphere (sub-aerial). These are the common cracks of dried mud puddles: they are called "desiccation cracks." Shrinkage takes place when water evaporates into the atmosphere. The resulting cracks often form a polygonal pattern (individual polygons may reach up to 300 meters across) and present typically a V-shaped cross-section of up to 15 meters deep. In some cases, but certainly not in all cases, mud curls (either upward or downward) can form between the cracks; these can be picked up and redeposited if the surface is flooded.

2. Mud cracks that form underwater (sub-aqueous). Synaeresis is a term used by chemists to describe the separation of liquid from a gel (as in cheese making). Its importance as a process for de-watering muds has been known by geologists for many years. "Synaeresis cracks" are known to form in the muddy bottoms of some lakes, settling

ponds, and even in lime muds beneath shallow marine waters in the Bahamas. Water loss is driven by osmosis, and so it is especially known to occur in saline lakes (immerse your hands long enough in a salty brine and you will get cracks of the same kind). Unless mud curls are present, these are extremely difficult to distinguish from desiccation cracks. Figure 8.21 shows different crack morphology formed due to synaeresis, the caption gives a detailed explanation for each morphology observed.

3. Mud cracks that form while buried (sub-stratal). This kind of cracks are generated when a mud loses its water while in a buried state. Water can be pressed from the mud layer gradually by compaction from above, or released suddenly by earthquake shock. The resulting cracks tend to form a polygonal pattern (when exposed from above), with either a lens-shaped or straight-sided cross-section. They may penetrate upward, downward or both. Synaeresis can also play an important role in some sub-stratal cracks when one layer differs from another in the salinity of its inter-particulate water. Sub-stratal cracks have been positively identified in multiple levels in the Hermit and Hakatai Shale groups of the Grand Canyon.

Mud cracks can certainly form in a variety of environments and distinguishing them in the field is not easy. It is a gross error to assume by default that mud-cracks in ancient strata formed by desiccation when it is known that they can form both sub-stratally and sub-aqueously. Mud cracks provide no evidence of "drought" during the Flood. The above definitions are after William [William, 2006].

8.6.3 Morphology of cracked polygons

In this section, a detailed analysis is presented of the cracked polygons formed during test A0-20 (figure 8.2) and from specimen 80-10-P tested in the environmental chamber. The cracked polygons are photographed separately with details from top, bottom and sides. Figures 8.22 to 8.30 show some of the selected cells.

Figure 8.22 shows the details of the cracked polygon No. 20 of the specimen A0-20 shown in figure 8.2. Figure 8.22 shows (a) the top, (b) the bottom and (c) & (d) the sides where the crack is present. These images were taken from a digital camera fixed at a constant distance and the cracked polygons were placed on a surface lit from below. Figure 8.22a: shows the top surface that was exposed to the air during the desiccation test. The edges of this polygon are defined by either primary of secondary cracks. No visible cracks or fissures can be seen on this surface. While this polygon was picked from the specimen, it was felt that the polygon was still adhering to the holding tray. Just after it was separated

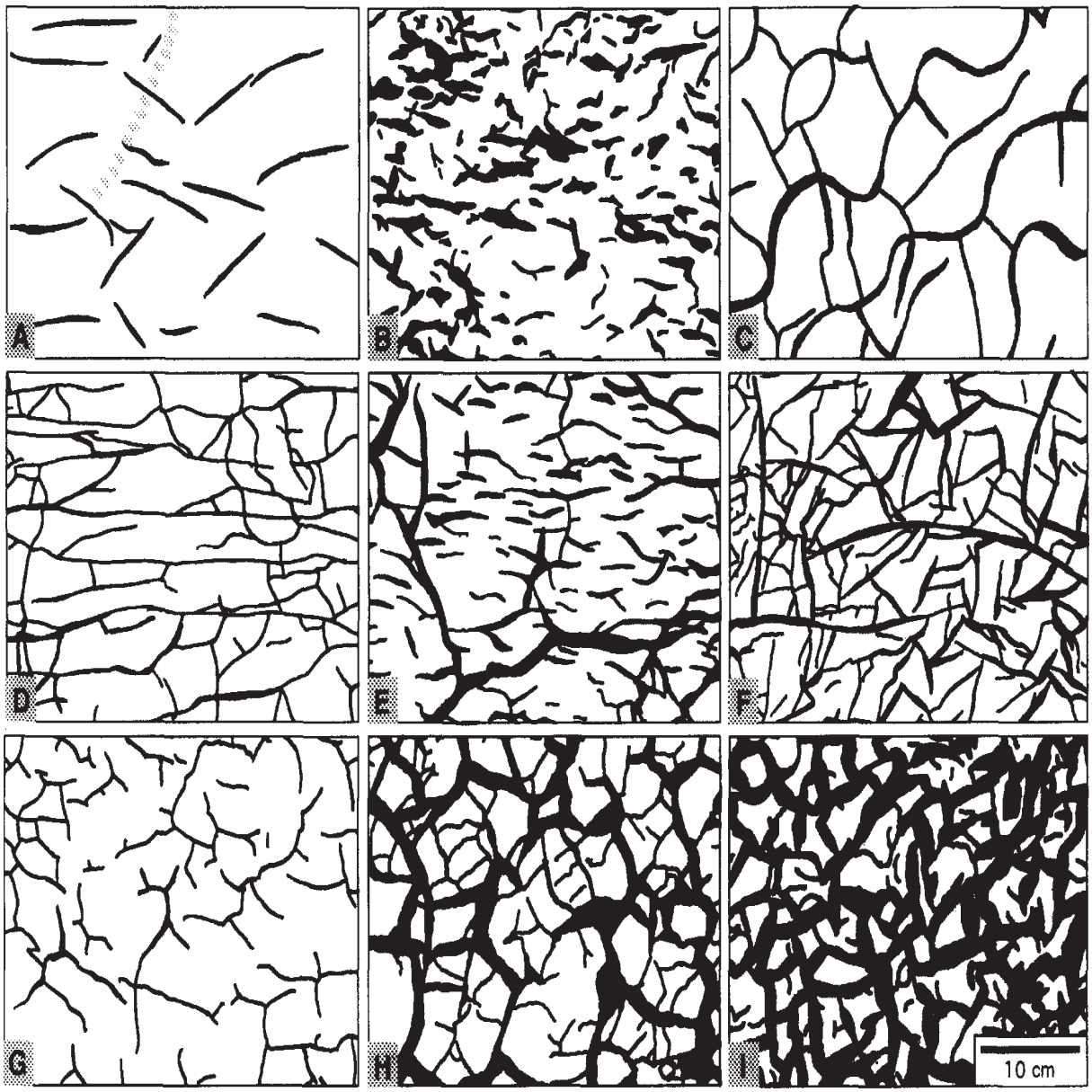

Figure 8.21: Shapes of synaeresis cracks on bedding planes traced from photographs. All are developed in terrigenous facies, except for (B) which is in calcareous siltstone, and (F) which is in argillaceous lime mudstone. (A) Sub-parallel lenticular, cross-cutting Cruziana arthropod trace (upper centre); Mahto Formation, Gog Group (Lower Cambrian), Moraine Lake, Banff National Park, Alberta. (B) Sub-parallel, irregularly lenticular; Cass Fjord Formation (Upper Cambrian), Ellesmere Island, Northwest Territories. (C) Sinusoidal in ripple troughs (conforming to Manchuriophycus pseudofossil); Grinnell Formation, Purcell (=Belt) Supergroup (Mesoproterozoic), Waterton Lakes National Park, Alberta. (D) Orthogonal reticulate, Appekunny Formation (Belt Supergroup), Glacier National Park, Montana. (E) Polygonal with parallel lenticular, Appekunny Formation, Glacier National Park. (F) Irregular reticulate and lenticular, Boat Harbour Formation, St. George Group (Lower Ordovician), Western Newfoundland. (G) Incomplete polygonal, Appekunny Formation, Glacier National Park. (H) Polygonal, Appekunny Formation, Glacier National Park. (I) Polygonal, Grinnell Formation, Glacier National Park (after Pratt [Pratt, 1998]).

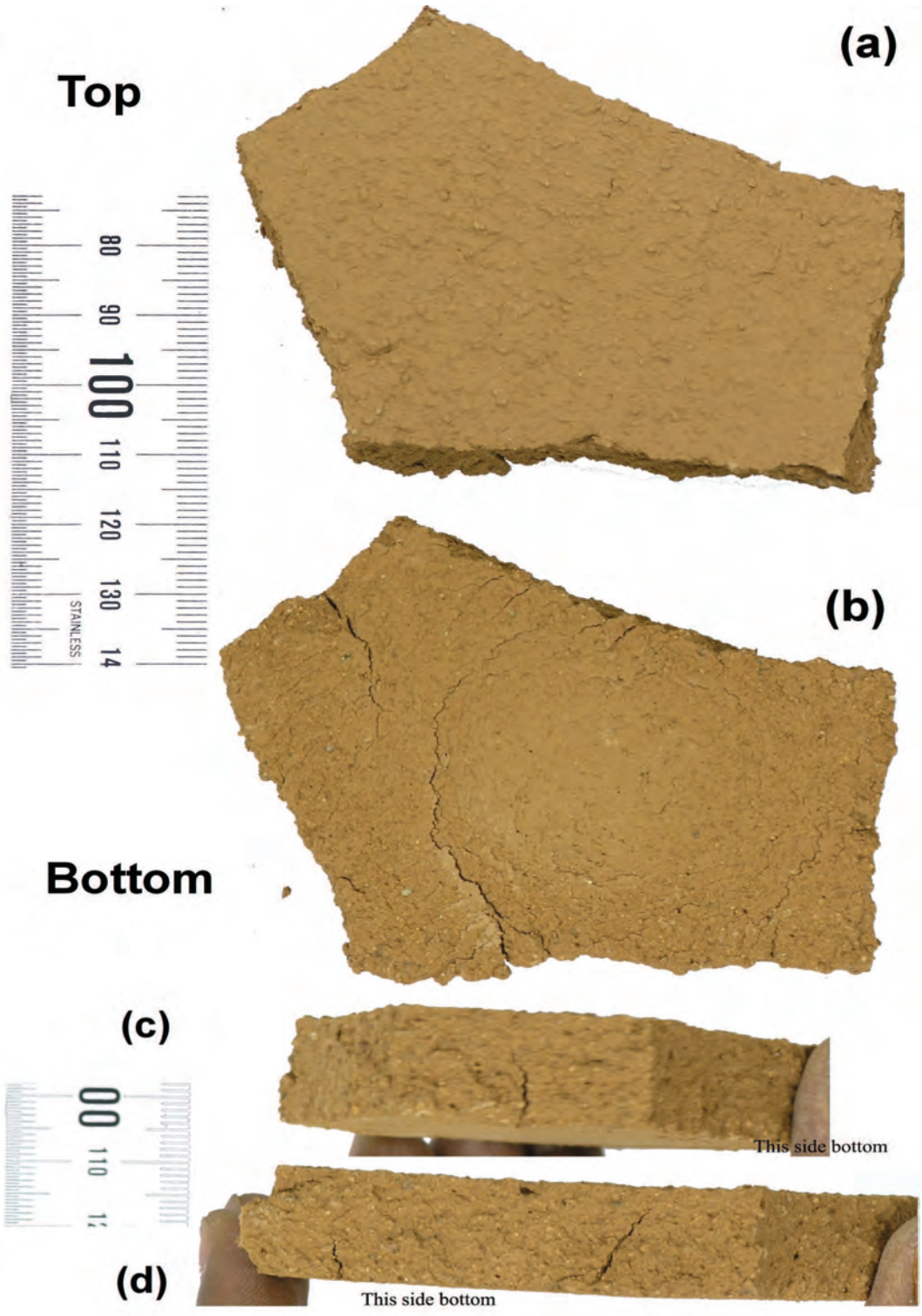

Figure 8.22: Details of cracked polygon No.20 of figure 8.2: (a) top surface without cracks; (b) bottom surface with curving cracks; (c) and (d) side view, with straight and oblique cracks originating from the bottom without reaching the top surface.

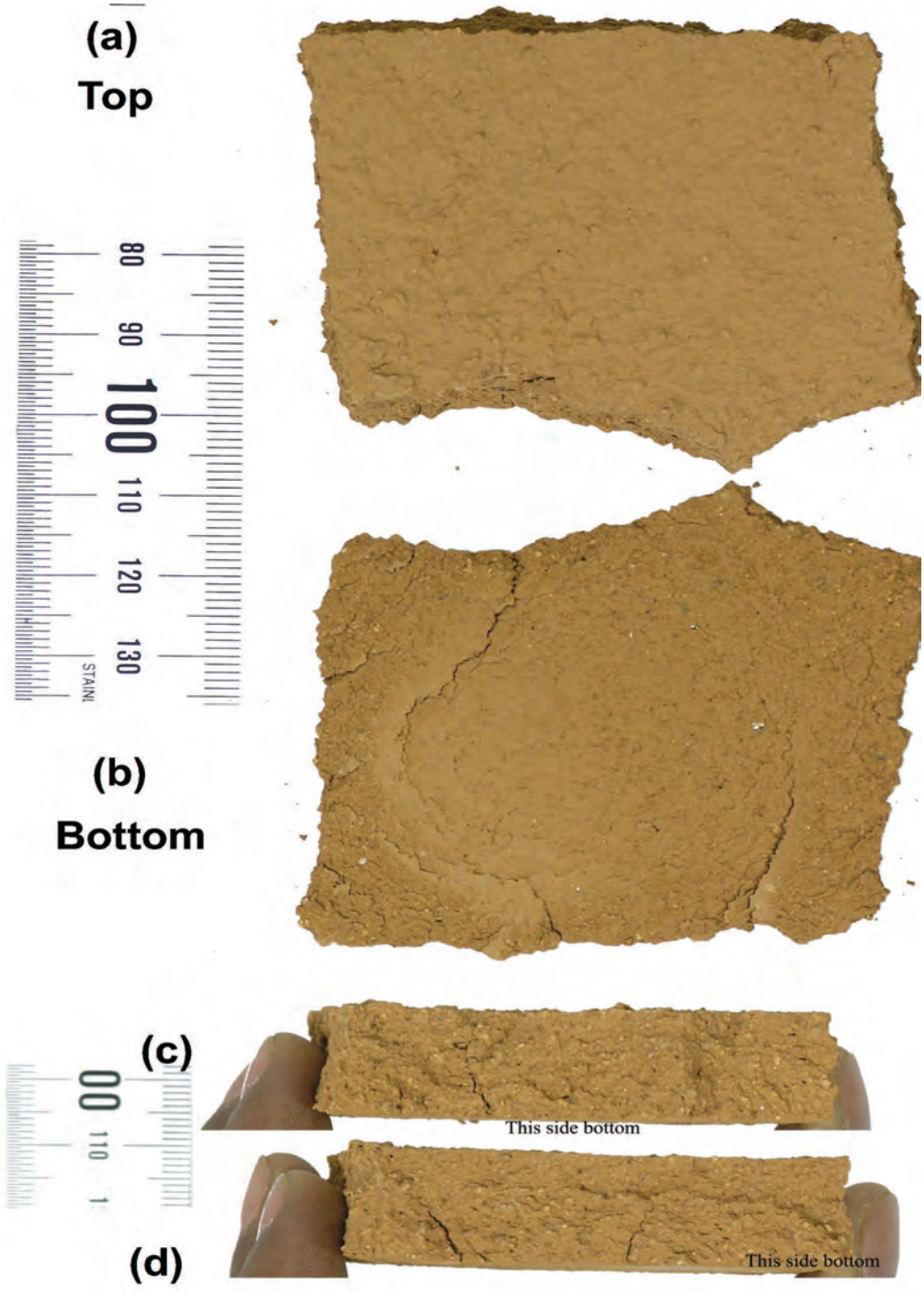

Figure 8.23: Details of cracked polygon No.5 of figure 8.2: (a) top surface without cracks; (b) bottom surface with curving cracks; (c) and (d) side view, with straight and oblique cracks originating from the bottom without reaching the top surface.

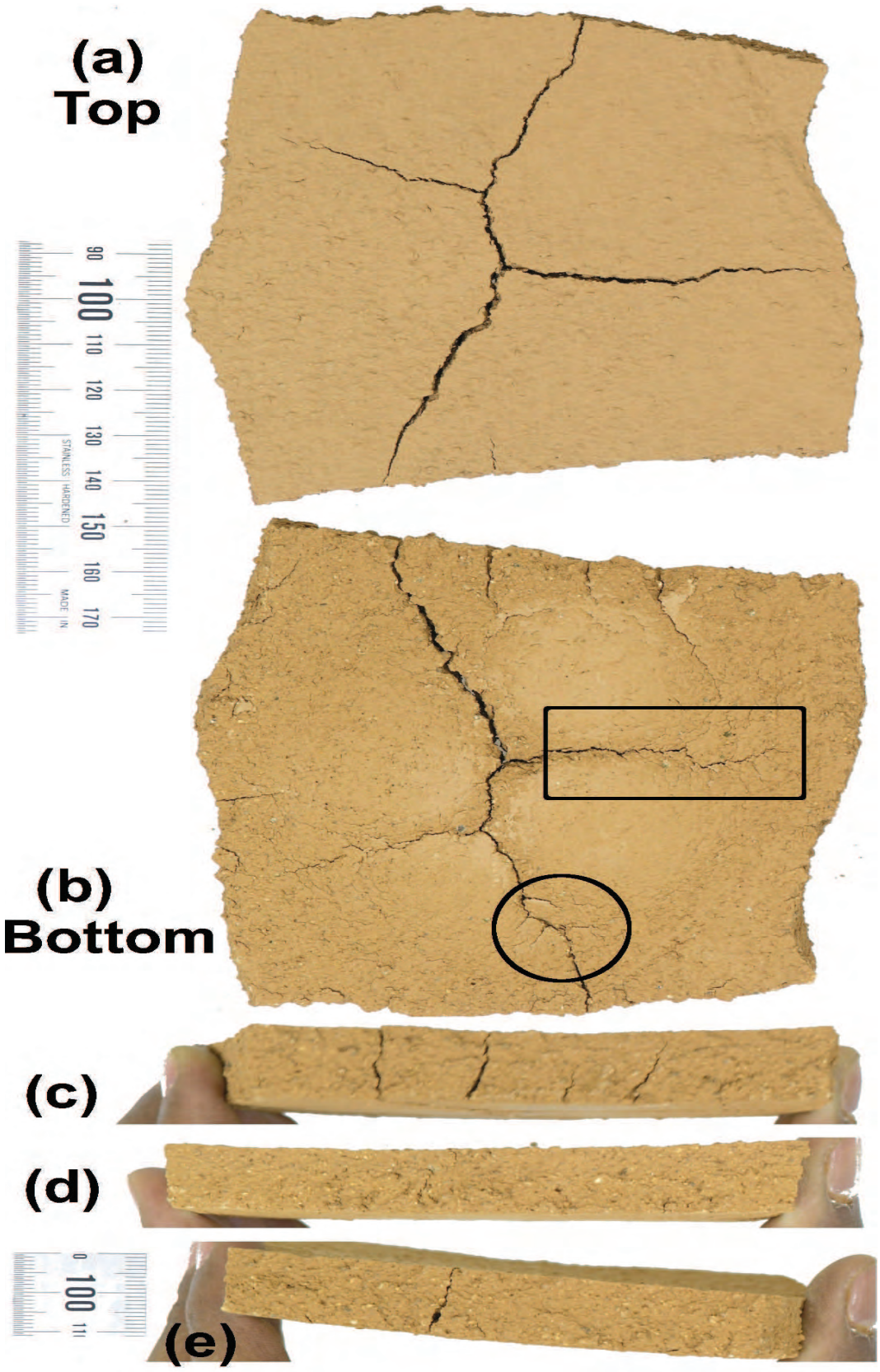

Figure 8.24: Top, bottom and side view of cracked polygon 7 from figure 8.2

Figure 8.25: Zoom of the region marked by the rectangle in figure 8.24b

Figure 8.26: Zoom of the region marked by the circle in figure 8.24b

from the holding tray, a more or less circular impression was observed on the holding tray indicating the surface which was still in contact. Figure 8.22b: shows the bottom surface where two important cracks can be observed. These cracks do not seem to be developing continuously, rather they seem to be developing in steps, preceding one another. All along the edges of the cell small fissures can be observed, some are marked on the upper part. Here also the surface which was in contact with the holding tray till to the end of the test can be seen in the centre, where the cracks and fissures seems to follow a circular pattern. A very slight difference in colour can also be observed. Figures 8.22c,d: show the sides of the cell where cracks were found. These two images show that the cracks can originate either from the top or bottom of the drying specimen. Notice that the cracks do not reach

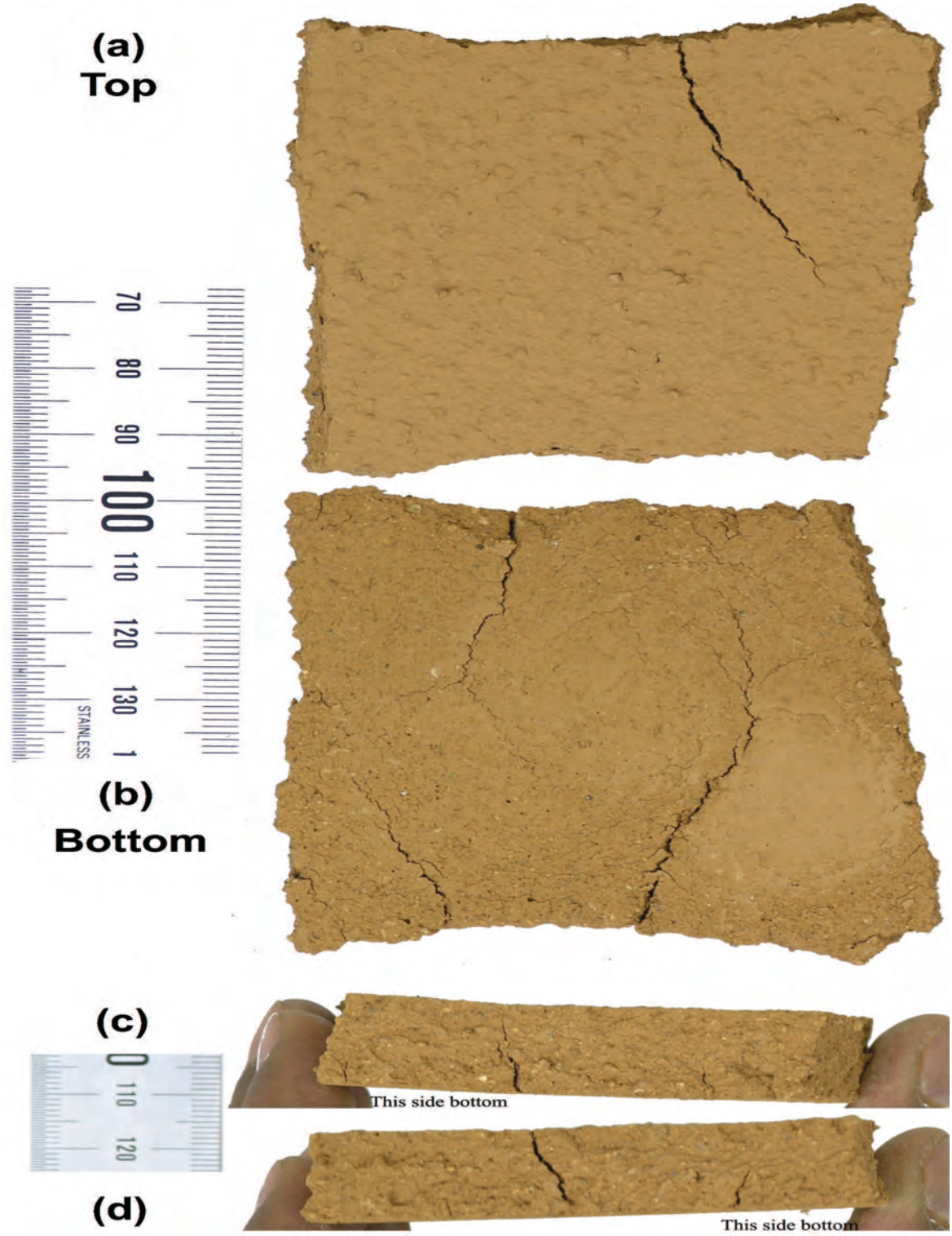

Figure 8.27: Top, bottom and side view of cracked polygon 8 from figure 8.2

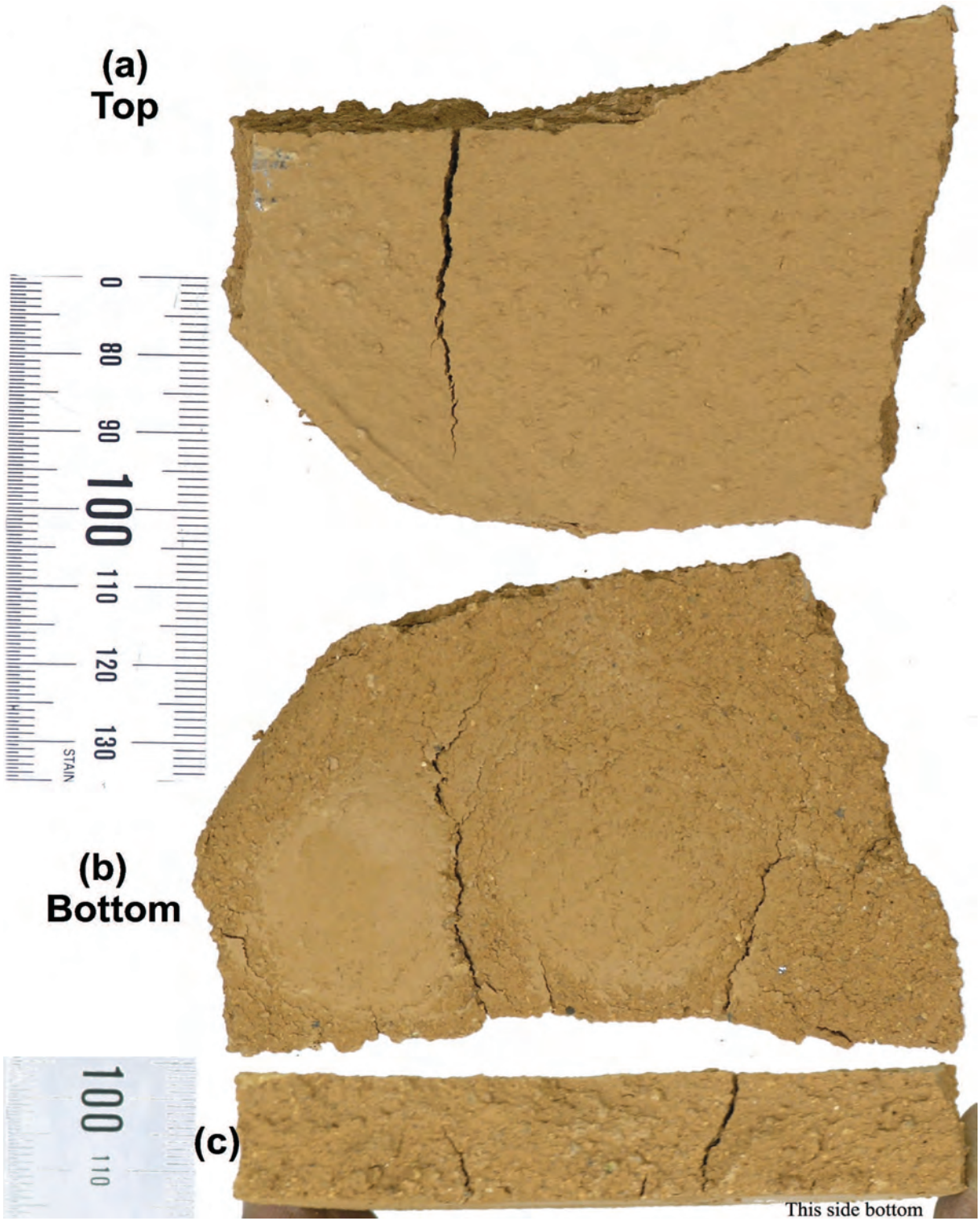

Figure 8.28: Top, bottom and side view of cracked polygon 22 from figure 8.2

Figure 8.29: Bottom view of cracked polygon 1 from specimen 80-10-P (figure 7.32)

the top surface and some cracks are not perpendicular to the thickness. The specimen is 20 mm thick at the beginning of the test and oblique cracks are observed even with this small thickness. This implies that vertical propagation of cracks is not always straight.

The cracked polygon numbered 5 in the figure 8.2 is shown with details in figure 8.23. The top and bottom of the cracked cell is shown in figures 8.23a,b while the sides where cracks were present are shown in figures 8.23c,d. Figure 8.23a: shows the top surface of the cracked cell with no visible cracks or fissures. Figure 8.23b: shows the bottom surface where the crack on the left-hand side seems to avoid something in the centre and takes a deviation to the left and another deviation toward right to meet the crack from the other side. The other crack on the right-hand side also follows a curved path, though it does not propagate fully to meet the other side. Small fissures along the edges can be observed as in the earlier cracked cell No. 20 (figure 8.22). Figures 8.23c,d: the three cracks observed in earlier image are oblique in the vertical plane. They does not reach the top surface.

Figure 8.24 shows the top, bottom and sides of the cracked polygon numbered 7 in figure

Figure 8.30: Bottom view of cracked polygon 2 from specimen 80-10-P (figure 7.33)

8.2. Figure 8.24a shows the top surface of the cell with one crack extending from one edge to the other and two more side-branching cracks, which do not reach the edge of the cell. The crack extending from edge to edge on the surface show several kinks. Figure 8.24b shows the bottom surface which was in contact with the holding tray. Several cracks can be observed near the edges. Several side-branching cracks can be observed on the cracks. Two regions marked by a black rectangle and a circle on this figure are selected for further observation: Figure 8.25 shows the zoom of the region marked by the rectangle and figure 8.26 shows the zoom of the region marked by the circle. The cracks originating from the crack in the zoomed images do not seem to make an intersection angle of 90°. Morphologically, these images seem like a river with its tributaries sketched as a line diagram. Figures 8.24c,d,e: show the sides of the cracked cell. Some cracks propagate the full depth of the soil specimen, while some cracks arrest at an inner point.

Figure 8.27 shows the details of the cracked cell numbered 8 in figure 8.2. Figure 8.27a: shows the top surface of the cracked cell, apart from a single crack no other important feature can be seen. Figure 8.27b: shows the bottom surface of the cracked cell, where

Figure 8.31: Surface of the holding tray with smooth bottom showing the paths left by the cracks and fissures, the image was taken at the end of test 80-10-P after careful removal of the cracked cells. The black lines correspond to the cracks which were seen in the top and bottom and the white line correspond to the spiral cracks observed only at the bottom.

two more cracks other than the one observed on the top surface can be seen. Once again the small fissures along the main crack resemble the crack morphology observed in figures 8.25 and 8.26. Figures 8.27c,d: show the sides of the cracked cell 8. As explained earlier only one crack can be seen on the top while three cracks can be seen in the bottom, this being also visible in the images showing the sides of the cracked cell. In figure 8.27c a crack can be seen which does not reach the top surface and in figure 8.27d two cracks can be seen, only one reaching the top.

The cracked cell numbered 22 in figure 8.2 is shown with details in figures 8.28a (top), 8.28b (bottom), and 8.28c (side). In figure 8.28a a single crack is the only important morphological feature on this surface. Figure 8.28b shows two cracks of important size and some minor fissures on the edges. On the left side of the image a more or less round area with a different shade can be observed: this was the area that was attached to the tray till the end of the desiccation process. Figure 8.28c shows two cracks, one is the

crack that reaches the top surface, while the can be seen only on the bottom surface.

Two images from the desiccation tests carried out in the environmental chamber are presented. Both images correspond to test 80-10-P. The images show some very interesting morphological features: figure 8.29 shows the bottom surface of the region marked with number 1 in figure 7.32 and figure 8.30 shows the region marked with number 2 in figure 7.33. Both these images show spiral crack formations at the bottom surface, the spiral being more prominent in figure 8.29. Similar morphological features were observed in most of the cracked polygons from the specimens tested in the environmental chamber.

Figure 8.31 shows the trail left by the moisture movement at the bottom of the specimen 80-10-P. The black lines are drawn on the crack paths seen both on the top and bottom surfaces while the white lines are shown only on one of the spiral marks left by the cracks seen only on the bottom surface. In most of the cracked polygons spiral marks can be seen at the centre. The sub-aerial or desiccation cracks form polygonal patterns and the crack intersection angle is more or less at right angles and figure 8.21 shows the different crack patterns caused by synaeresis processes or sub-aqueous cracks. The cracks (in figures 8.25, 8.26, 8.29, and 8.29) do not resemble any of the crack morphologies observed so far. It would be difficult to pinpoint the exact cause for these types of crack formations, but a qualitative analysis could be done to find the possible mechanisms. The cracks were formed on the bottom surface which was in contact with the holding tray and obviously this surface was not exposed to desiccation. Therefore it can be suspected that the cracks may be formed due to synaeresis. Another cause for these cracks may be due to a curling phenomenon, which will be explained in the next section in detail. It is more likely that a combination of curling and synaeresis would better explain the morphology observed.

8.6.4 Curling during drying

According to Kodikara et al. [Kodikara et al., 2004] curling is due to differential shrinkage between the top and bottom layers caused by differential drying of the soil layer. During the initial stages of drying curling of crack edges results in a concave surface due to top surface shrinking more than the bottom one. At a later stage of the drying process, lifting up of the central part results in a convex surface due to the bottom surface shrinking more than the top one. Curling in soils or sediments can vary with the salinity: upward curling was observed in sediments deposited with low-salinity where the edges are curled upward. Downward curling was observed in sediments deposited in water with high-salinity where the edges are curled downwards. Figure 8.32 shows the curling of soft Werribee clay at the end of a test [Kodikara et al., 2004] and the mechanism responsible is explained pictorially

in figures 8.33a,b.

Figure 8.32: Curling of soft Werribee clay at the end of test 3 (after Kodikara et al. [Kodikara et al., 2004]).

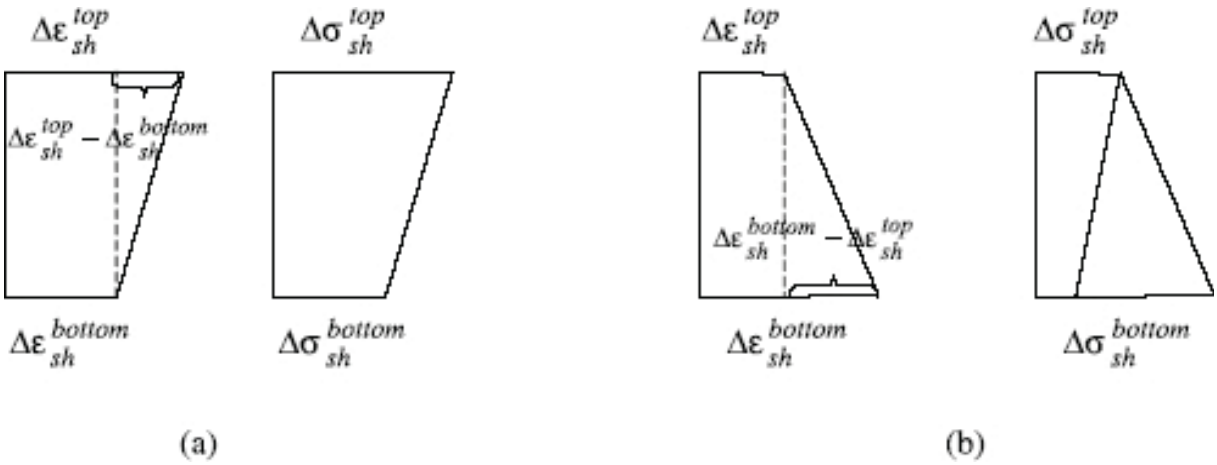

Figure 8.33: Idealized profiles of shrinkage strain and shrinkage stress for (a) upward edge curling, and (b) upward curling at the middle (after Kodikara et al. [Kodikara et al., 2004]).

Figures 8.34a,b,c show the curling of Barcelona silty soil for specimen thicknesses of 10 mm, 20 mm, and 100 mm respectively. These images were taken at the end of the test. Unlike the curling of the soft Werribee clay (figure 8.32) where curling resulted in a convex surface, the curling of the Barcelona silty soil used in the experiments resulted in a concave surface that was similar in all the specimens tested with variety of different surface area and thickness. This means that the mechanism given by Kodikara et al. [Kodikara et al., 2004] could be applied in part, only considering the first part where the curling caused by the lifting of the edges results in concave surfaces.

Kodikara et al. [Kodikara et al., 2004] did some desiccation experiments in Perspex moulds of rectangular cross section measuring 250 mm long, 25 mm wide, and 12.5 mm deep to study the curling of soils, similar to the procedure proposed by Standards Australia

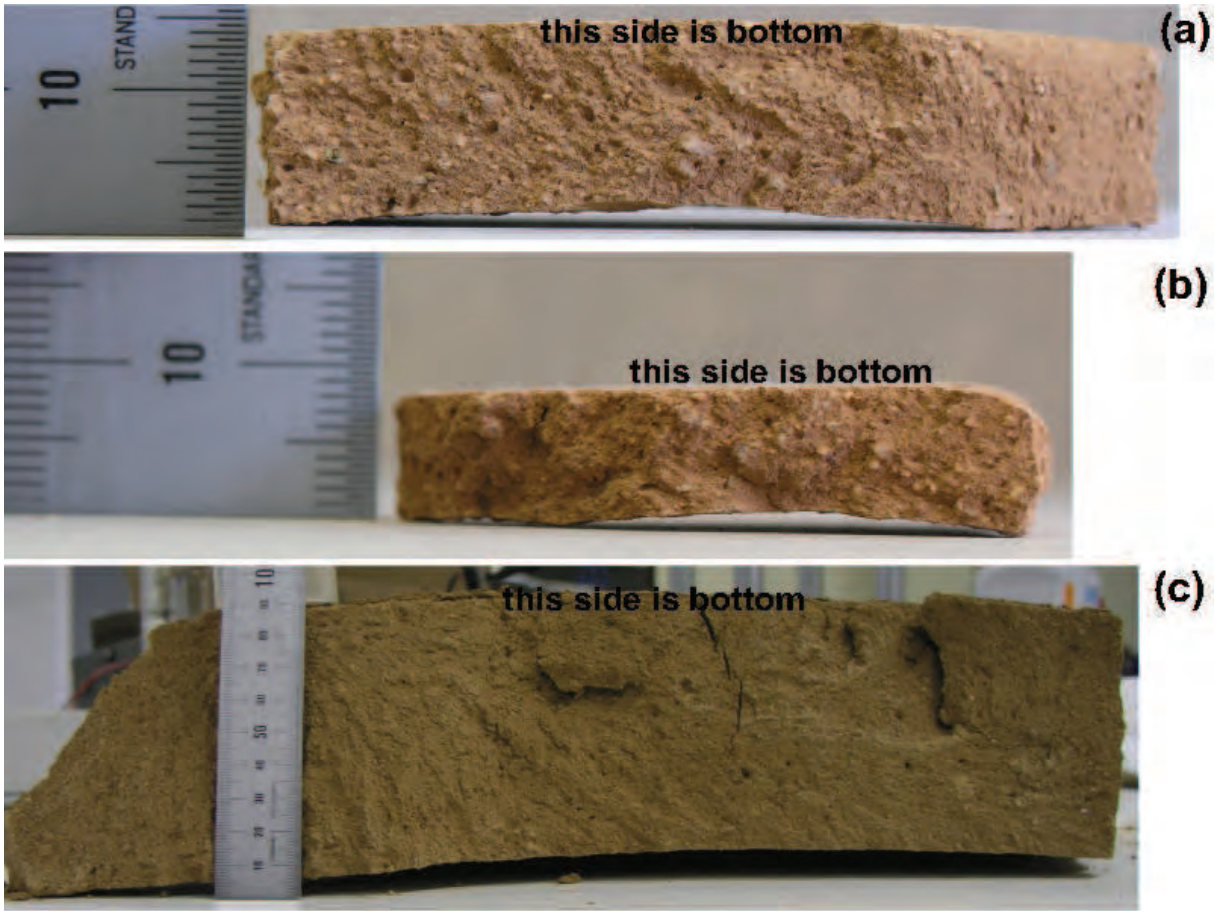

Figure 8.34: Curling of Barcelona silty soil during the desiccation tests with different thicknesses.

(1995) for linear shrinkage measurement. The main characteristics of the soil used are: specific gravity = 2.66; clay content = 62%; liquid limit = 127%; plastic limit = 26%; and plasticity index = 101%. Figure 8.35 shows the moisture loss with time for two tests. In both tests they observed the onset of significant curling with a moisture content near the plastic suggesting that curling starts when the desiccating soil reaches its plastic limit. This helps explaining the cracks at the bottom of the specimens. Lifting of the edges during desiccation due to differential shrinkage between top and bottom surfaces will result in a concave surface with tensile stresses at the bottom layer and compressive stresses at the top layer. Because drying starts at the top layer, there is a moisture gradient across the thickness of the specimen, dryer at the top and wetter at the bottom, with implications on the soil's strength. A drier soil has more strength than a moist one, thus it makes sense that the cracks which originate at the bottom surface may not reach the top one.

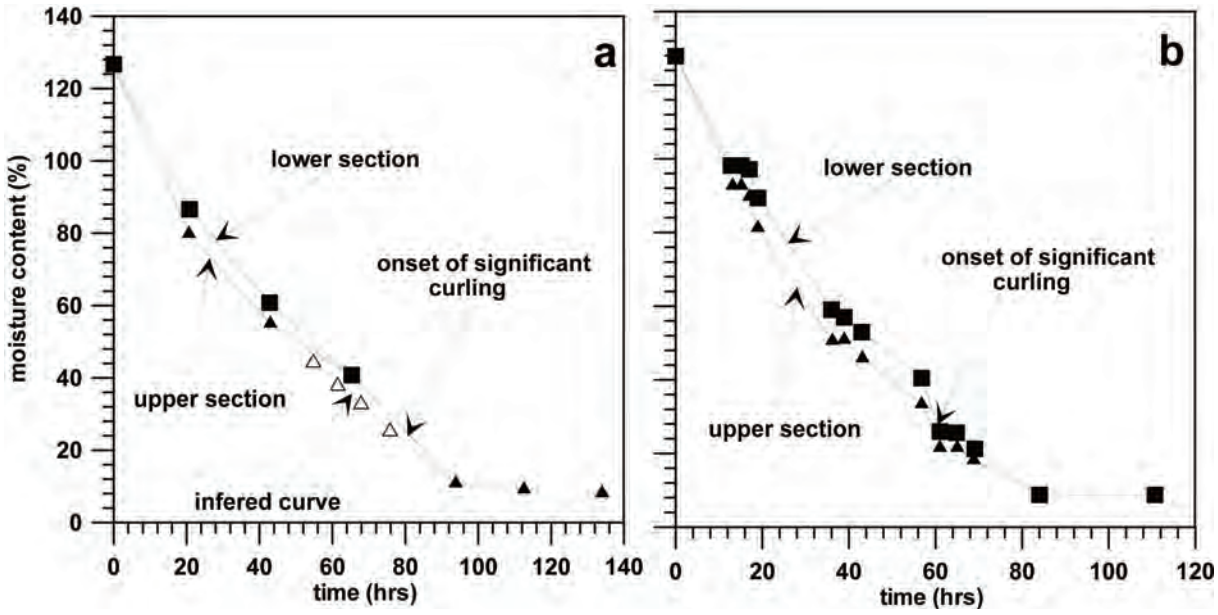

Figure 8.35: Moisture content versus drying time for (a) curling test 1, and (b) curling test 3 (after Kodikara et al. [Kodikara et al., 2004]).

8.7 Conclusions

This chapter gives an overview of the macro-morphology of the cracks and crack pattern. Some of the most important morphological features are explained in a detailed way, that may lead to further exploration. Morphology can help determining the origin of the cracks in geological time and also clarify the mechanisms involved in the formation of such crack patterns. It can also determine the stress state that might have been responsible for such pattern formation, and help explaining crack growth and direction of propagation.

Many researchers who are attempting to model this complex mechanism of cracking in drying soils formulate equally complex mathematical laws, but ignore or oversee the basic physical phenomenon behind the process. The theory of successive domain division or the hierarchical nature of crack pattern formation gives essential parameters for a stress relaxation criterion in modelling; as a consequence, to a large extent the spacing of the cracks is also established. Intersection angle determines, or indirectly indicates, which failure mechanism governed the formation of such a crack or crack pattern. The effect of the presence of other cracks on the direction of crack growth and stress state is an important parameter to be considered while modelling.

Chapter 9

Conclusions

9.1 Introduction

The chapter presents the conclusions drawn from the present investigation. The following section gives a brief summary of the contributions of the present investigation to the advancement in understanding desiccation and cracking behaviour of soils. The summaries of conclusions on specific topics investigated are presented in the subsequent section. Some recommendations for the continuation of the investigation and to improve the capabilities of the new equipment constructed are presented as future lines of investigation. Finally, some comments leading to the probable development of a theoretical framework and its possible implementation are discussed.

9.2 General remarks

The present research is a clear example of how the combination of different disciplines and experimental techniques help to a better understanding of this complex problem. In this research unsaturated soil mechanics principles, fracture mechanics and a number of advanced experimental techniques have been used to advance the current understanding on the subject [Lakshmikantha et al., 2006];. Experiments with a new equipment (environmental chamber with large scale experiments; [Lakshmikantha et al., 2008b]), simulating the in situ conditions with real time monitoring by sensors and observation by digital camera have been carried out. To obtain fracture mechanics parameters, new equipment was constructed for the compact tension test which was originally developed for concrete

specimens. A fully computer controlled image acquisition system was designed and image processing and analysis techniques were developed [Lakshmikantha et al., 2009b] for real time observation of soil specimens and to study the crack and crack pattern formation during the drying process. Tensile strength was experimentally determined [Lakshmikantha et al., 2008d] and evidence of size-effect was established [Prat et al., 2006]. The experimental results helped to increase knowledge on the physics involved in the phenomenon of desiccation cracks and also to advance the state-of-the-art in experimental studies. Furthermore, this experimental investigation is very valuable for the development and validation of advanced numerical models.

9.3 Specific remarks

9.3.1 State-of-the-art

The following are the conclusions after the extensive literature survey.

Definition and mechanism:

(1) The definition on how the mechanism of cracking occurs, each researcher has his own definition of mechanism, though the factors considered are same in most of the cases.

(2) Regarding the crack initiation, there is lot of confusion. The location and state of soil when the crack is initiated is the cause of discussion and confusion.

Causes:

(3) There is a general agreement over those factors which causes the soil to crack.

(4) Apart from the factors like temperature, wind speed, and relative humidity, the characteristics of the soil like the structure, density, clay content, water content, thickness of the desiccating soil and presence of vegetation in relation to the process of desiccation are well studied and a general trend on how these factors affect can be found.

(5) The other main and important properties of soil, Tensile strength and Suction which plays a major role in unearthing the process of cracking are not given due importance and very little information is available on these as concerned to the cracking of soil.

Implications:

(6) Though the advancement in science has given a lot new materials for construction, the use of soil as a construction material has not taken in to the back stage, on the other hand it has found its use in more and more places of vital importance. Thus the cracking in soils is now got implications on settlement of earthen embankment of an high-way to the structural integrity of a clay cover of a nuclear waste repository, and from stability of foundations to the water loss in reservoirs and agricultural lands.

(7) Environmental risk of cracks in soil is far reaching as the cracks are found to increase the hydraulic conductivity by two to three fold in comparison with the intact soil. The increased hydraulic conductivity and preferential flow are found to be the main culprits in transport of contaminants in most of the cases, resulting in contamination of ground as well surface water sources.

Experiments:

(8) Laboratory experiments reported can be widely grouped to study the soil mechanics and fracture mechanics properties of soil: in the former the cracking in soils is studied by observation and recording the changes taking place in the drying soil, where as in the later the fracture characteristics of the soil are studied by testing the soil specimens with established fracture mechanics specifications.

(9) There are not much filed experiments to refer, most of the field experiments are more of post-mortem in nature, that is, study of the cracked soil rather than the cracking soil.

Models:

(10) The models proposed are also of particular application and complex. Particular application models are: applied to desiccation of clay liners/compacted soils, applied to desiccation of mine tailings/soft soils, and etc,. Even though there are some general models but the applicability is limited to certain types of soils.

9.3.2 Fracture parameters

9.3.2.1 Tensile strength

Tensile strength of soils can be determined either by direct or indirect methods. In this study it was determined by a direct method. Moisture content and density of the soil influences considerably its tensile strength, which increases with increasing density of the soil. The effect of density is more pronounced for specimens with lower moisture

contents than those with higher moisture content. Experimental results showed that tensile strength does not increase with increasing suction, but reaches a peak and then reduces with further increase in suction. The load-deformation curves clearly show the transformation of soil stiffness with reduction in moisture content. The theoretical model to estimate the tensile strength from the effective cohesion of an unsaturated soils seems to capture the trend of experimental data very well.

9.3.2.2 Fracture toughness

Fracture toughness was determined using CT specimens for different moisture contents. Fracture load decreases with increasing initial crack length irrespective of the moisture content, which is in agreement with other studies on concrete and metals. The fracture energy, which is a material constant, can be considered as constant for a given moisture content, though there is a little scatter. Fracture toughness increases with decreasing moisture content until the plastic limit is reached. Further decrease in moisture content results in a decrease of fracture toughness. The theoretical model proposed using the activation energy and rate process theory for soils can be used if a relation between the activation energy and the soil suction is established. In view of very few experimental data available on fracture parameters of soil with effect of moisture content, the present study can be a good reference for the further exploration.

9.3.2.3 Relation between tensile strength and fracture toughness

There appears to be a strong correlation between fracture toughness and tensile strength. Therefore, a reasonable estimate of the fracture toughness may be obtained if the tensile strength is known. The empirical relations proposed fit reasonably well with the experimental data. This relation seems to be of power-law type, rather than a linear one as reported in some published literature. In general, the higher the ratio $(K_{IC}/\sigma_t)^2$ higher the ductility, hence larger the specimen size required. The higher values of ratio $(K_{IC}/\sigma_t)^2$ observed for soils indicate that the size of the specimen used may not be sufficiently big.

9.3.3 Desiccation of thin soil layers

The results of an experimental work devoted to give insight into the mechanics of cracking of thin soil layers under drying conditions is presented. Three series of tests with circular and rectangular specimens of varying geometry have been performed giving qual-

itative and quantitative information about the main parameters controlling the process of cracking: size, thickness and aspect ratio of the specimen, and boundary conditions (cross-section of the holding tray, and roughness on the contact surface between specimen and tray).

The effect of bottom contact can be studied effectively by different surface roughness rather than different material coatings. The experiments once again reiterate the interwoven effect of thickness, desiccation rate and cracking moisture content on one another.

The effect of geometry of specimen is first time studied in an elaborate manner. Desiccation rate is affected by area of the drying soil. Thickness and area have reverse effect on the desiccation rate, desiccation rate increases with drying area. The observed effect of drying area adds an additional parameter to be analysed while considering the numerical solutions for soils undergoing drying, apart from the thickness of the layer. The increase in desiccation rate with increase in drying area is complimented with crack pattern characteristics. The different geometries had an effect only on the final crack pattern.

Cracking mechanism should be studied in combination with evolving characteristics of crack pattern. Like, in addition to the evolution of CDF, evolution of crack width, individual cracks and their interaction with other cracks leading to the formation of unique crack pattern will broaden the current knowledge. This work is out of scope for the present thesis, but should be considered for future studies. Image analysis is certainly a powerful, efficient and easy tool for this task.

The results are in acceptable agreement with existing literature. The work presented gives the much needed effect of different boundary conditions which are essential towards the development of a model able to predict formation and propagation of cracks in soil under drying conditions.

9.3.4 Image analysis

Image analysis is a powerful tool for the qualitative and quantitative description of 2D patterns. Manual methods of quantifying the crack pattern are time consuming, expensive, and boring affair. Real-time observation was done using a simple laboratory set-up. The method proposed, using image analysis techniques, gives the main parameters needed to describe qualitatively and quantitatively the crack pattern. A complete description of the crack pattern can be obtained. Results obtained are direct measure of the state of the soil, for example the area of cracks represents the increased porosity of the soil surface due to presence of cracks. The intersection angles give an insight to the possible mechanisms

of crack formation. CDF curves of different soil types in combination with the moisture evolution during drying can be very useful in water management scheme in irrigation. CDF is also a measure of the topology of the evolving crack pattern. As well the results can be used to calibrate the existing numerical models with respect to formation and propagation of crack patterns.

The method is simple, cost-effective and gives reliable results. It is simple because, the method uses well established algorithms in the field of image processing and analysis. It is cost effective because the software used is freely available and it is written in Java being platform independent.

9.3.5 Size-effect

An innovative experimental program to study the size-effect in soil cracking has been presented. The experimental results show the evidences of size-effect in soil cracking. Soil behavior is not quasi-brittle and linear, never the less, LEFM seems to be the most simple fracture mechanics theory for cracking in soils. This is due to ease with which the LEFM parameters determination. Experimental evidences of existence of Size-effect further strengths the applicability of LEFM. Thus a numerical modeling with these parameters can be implemented with a certain degree of confidence and a first step towards numerical modeling. An experimental determination of Non-linear and Elasto-plastic fracture parameters for soils is quite difficult and complicated with the existing soil testing equipments.

9.3.6 Environmental Chamber

Experimental studies on cracking soil are very scarce and practically there are no published data relative to evolution of parameters such as moisture content and suction. In the present work an environmental chamber was designed and constructed to study the desiccation process and cracking of drying soils. A particular combination of temperature and relative humidity can be imposed to the desiccating specimen by controlling the air temperature and relative humidity inside the chamber.

Four devices (for heating, cooling, humidifying and dehumidifying) are required to impose and control different temperature and relative humidity combinations and cycles. If cycles of drying and wetting need to be imposed to simulate seasonal climatic variations, then an extra device to wet the specimen would be necessary. This additional device could

be a sprinkler with discharge and velocity control. Currently there are only two of these devices (for heating and dehumidifying) built into the chamber.

The experimental program and the results presented were focused on demonstrating the capabilities of the environmental chamber. However, very interesting results were obtained from the tests performed. A set of three experiments were carried out under laboratory conditions (21 ± 0.5°C and 52 ± 2%) while the environmental chamber was being built. Another three experiments were carried out in the environmental chamber with temperature around 35 ± 0.1°C and relative humidity of 40 + 0.2 & - 4%.

This equipment is extremely well suited to study the mechanisms of cracking in soils due to drying. Air temperature and relative humidity can be controlled with minimal variations from the imposed values. Digital images taken by a camera during the tests provides very valuable data for the later analysis. Tailor made holding trays with its sensors are excellent for continuous monitoring. Provision to add cooling and humidifying sources makes it more versatile for future research as cycles of wetting-drying can be imposed coupled with warm-cool cycles.

9.3.7 Desiccation of thick layers

The tests have provided some new insights into the mechanics of the process of formation of cracks in a drying soil. Cracks can be seen starting either at the top, bottom or at both surfaces of the drying specimen. The mechanism responsible for the initiation at the top surface is usually desiccation, while the cracks starting at the bottom surface may be a product of curling and/or synaeresis processes. An increase in temperature increases the extent of cracking at both top and bottom of the specimen. Though a direct link between the temperature and suction evolution was not found, an interesting relation between the desiccation rate and suction evolution was seen. The presence of crack affect the suction evolution with increased desiccation speed. The suction profiles during the initial stages of the desiccation showed that the drying front moves from the periphery toward the centre and from top to bottom. Extent of cracking was larger with a smooth bottom surface than with a rough one, both at the top and bottom surfaces but more noticeable at the bottom surface of the specimen. Cracking initiated near saturation or at quasi-saturated conditions. From a theoretical perspective, modelling should consider the effect of suction. It can be argued that although crack initiation may occur near saturation, no doubt crack propagation takes place in unsaturated conditions for drier and warmer conditions. At the same time exceptions should be allowed for extreme cases like highly plastic clay and for dry-cold environments.

9.3.8 Morphology of crack and crack network

An overview of the macro-morphology of the cracks and crack pattern is presented in this thesis. Some of the most important morphological features are explained in a detailed way, that may lead to further exploration. Morphology can help determining the origin of the cracks in geological time and also clarify the mechanisms involved in the formation of such crack patterns. It can also determine the stress state that might have been responsible for such pattern formation, and help explaining crack growth and direction of propagation.

Many researchers who are attempting to model this complex mechanism of cracking in drying soils formulate equally complex mathematical laws, but ignore or oversee the basic physical phenomenon behind the process. The theory of successive domain division or the hierarchical nature of crack pattern formation gives essential parameters for a stress relaxation criterion in modelling; as a consequence, to a large extent the spacing of the cracks is also established. Intersection angle determines, or indirectly indicates, which failure mechanism governed the formation of such a crack or crack pattern. The effect of the presence of other cracks on the direction of crack growth and stress state is an important parameter to be considered while modelling.

9.4 Future lines of investigation

9.4.1 Experimental investigation

Tensile strength:

Barcelona soil has been characterised for tensile strength, but it would be interesting to know the behaviour of different types of soils. The existing equipment could be modified to carry out the tests with deformation control, since the present tests were done with load control. Triaxial extension tests could be carried out for the Barcelona soil to compare the results with the direct method results from the present work. Also, determining the tensile strength of soil-cement mix would be very valuable as soil-cement mix is used routinely in a variety of construction projects.

Fracture toughness:

Determination of fracture toughness at constant dry density varying moisture content would be a good addition to the present data. In the present work the tests were con-

ducted with load control, it would be very interesting to know the behaviour under strain controlled testing. Determination of fracture toughness by SNEB specimens for Barcelona soil could be very helpful in combination with the present data. The relation between fracture toughness to moisture content fits fairly well with the proposed exponential relation. In this regard it would be interesting to conduct experiments (similar to those done in the present work) with different types of soils to check and/or validate the proposed theory.

Desiccation experiments:

Preliminary tests with circular and rectangular specimens are very simple at the same time gave a good understanding of the cracking behaviour of soils. To see the effect of seasonal variations tests could be carried out at different combination of temperature and relative humidity. The same tests with circular and rectangular specimens could be conducted for: soil-cement mix and other soils.

Image analysis:

Image analysis techniques adopted in the present work are simple and quick. The next step would be correlating the images taken at time t with time t +1, t+2, etc to have a more accurate quantification by automating the procedure.

Environmental Chamber:

The most important future work to enhance the capability of the equipment would be incorporating a cooling source and a humidifying source. This will make the equipment more versatile since any desired climatic condition could be imposed. Further, a system to wet the specimen to simulate raining would allow imposing drying-wetting cycles. The lamps used as heating sources should be replaced by a different heating source such as hot air. The use of hot air would allow more uniform distribution of temperature eliminating any localised effect of temperature by a light source.

Incorporating a strain gauge to the equipment would give additional data on one-dimensional vertical shrinkage. The data from the strain gauge could be combined with the two-dimensional shrinkage data (including the cracks) from the image analysis, thus a better quantification of volumetric shrinkage during the desiccation could be obtained.

To explore the mechanism of cracks observed at the bottom of the specimen, experiments could be conducted with the same specimen size but terminating the test at different stages of drying and observing for the presence of cracks at the bottom. The data of different sensors at different locations in the specimen for a number of tests at different drying

stage along with the observation from the images would lead to identify the mechanism of crack initiation at the bottom.

The effect of initial moisture conditions of soil and climatic conditions could be determined by preparing specimens at different initial conditions and imposing different air temperature and relative humidity.

Crack Morphology:

Morphology of cracks and crack pattern presented in this work is based on the final crack pattern at the end of the desiccation process. The work can be extended to account for the dynamic nature of crack pattern formation. This can be done by considering the crack patterns at different stages of cracking and identifying the stress states and prediction of appearance of new cracks and propagation of existing cracks based on the proposed theory of successive domain divisions and the hierarchical nature of crack pattern formation.

9.4.2 Modelling desiccation cracks

As far as modelling is concerned, a review of the literature shows that several researchers tend to use models based on the theory of continuum media [Coussy et al., 1998], whereas other authors adopt the theory of LEFM [Harison et al., 1994];[Vallejo, 1994];[Hallet and Newson, 2001]. Studies from the point of view of soil mechanics are few [Morris et al., 1992];[Abu-Hejleh and Znidarčić, 1995];[Konrad and Ayad, 1997b] while application of unsaturated soil mechanics principles is still minimal [Lloret et al., 1998];[Rodríguez et al., 2007]. However, in the latter works it has been shown that to include the effect of suction and the dependence of soils properties on the degree of saturation is crucial to describe correctly the desiccation process and the time of crack initiation. Therefore, it can be concluded that several well established lines of investigation such as classical soil mechanics, unsaturated soil mechanics, fracture mechanics and stochastic models that have been traditionally employed separately should be integrated into an interdisciplinary study. As mentioned, in today's literature there is no reference framework that allows a comprehensive analysis of the kind of laboratory tests performed in this work, let alone real-life field problems. Existing models are often tailored to particular applications and the most general models are themselves restricted to certain types of soil and usually not suitable for their implementation in numerical codes. In addition they are not able to deal with the generation and propagation of cracks in soils. It is evident that a multidisciplinary approach is much needed.

There are two important issues to be addressed, one is the development of a reference

mathematical framework able to include the main physical phenomena that control the behaviour of soils submitted to drying and second, its implementation in a numerical tool to solve practical problems. Perhaps the difficulties to model correctly this problem comes from the complexity of the phenomenon under study, as several and simultaneous coupled physical phenomenon take place during crack formation. For example, during the drying process the pores do not remain saturated, but are progressively filled with air, which induces a negative pore water pressure due to surface tension effects. The desiccation process, mainly governed by the hydraulic properties, has an influence on the mechanical behaviour because the material tends to contract. Restriction to free shrinkage of the surface layer of soil during desiccation (imposed by the subsoil) induces an increment of horizontal tensile stress, which is followed by the generation of vertical cracks when a critical tensile strength is reached. In addition to that, this critical tensile strength depends on the degree of saturation of the material, confirming the strong coupling that exists between the soil water flow and the resulting stress field. When the desiccation process takes place under non-isothermal conditions (as in the field) several Thermo-Hydro-Mechanical (THM) interactions become evident and they could significantly influence the water transfer process.

For the first issue, the approach proposed by Rodríguez et al [Rodríguez et al., 2007] is an excellent starting point. In that work a fully coupled HM framework is proposed to solve the problem of desiccation cracks in soils. A non-linear elastic law is used to describe the mechanical behaviour and a number of hydraulic models are proposed to solve the non-saturated flow during water evaporation. For the validation of the approach the transient behaviour observed during desiccation tests in soil specimens has been modelled. A very good agreement between the results from their numerical approach and experimental data suggests that the main physical phenomena that control the behaviour of soil during desiccation crack have been well contemplated. The assumption of the soil as a continuous medium is a clear limitation of the framework proposed by Rodríguez et al [Rodríguez et al., 2007]; implying that the behaviour during water loss in soils can be only modelled until the onset of crack generation (i.e. when discontinuities appears).

The second issue will be the implementation in a numerical code. Modelling the onset and development of multiple cracks is still a formidable challenge for numerical analysis, and standard methods such as the FEM are ill-suited to these problems because all discontinuities (cracks) must be meshed as they appear, and re-meshed as they evolve. Some recent numerical techniques, such as eXtended Finite Element (XFEM) [Bordas et al., 2007] and mesh-free methods [Rabczuk et al., 2007] are very promising to tackle this kind of problems. The XFEM was invented to alleviate the shortcomings of the FEM when dealing with evolving discontinuities. XFEM has two advantages: (1) discontinuities do

not need to be meshed; and (2) in the presence of singularities special functions may be added to increase the convergence rate for coarse meshes. These two advantages are of paramount importance for the problem at hand in which many cracks (possibly hundreds or more) are likely to nucleate, grow, and coalesce.

Appendix A

Image Analysis Techniques

A.1 Introduction

Drying soils often crack as a result of water loss, mostly due to evaporation. Examples can be found in irrigated land, tailing ponds for mining waste, landfill liners, earth embankment, reclaimed land, reservoir beds, etc. Although cracking in desiccating soils is a common phenomenon, the causes and mechanisms involved are very complex with several interacting factors playing a coupled role. An important aspect of the study of cracking soils is quantifying the characteristics of the crack network or finding the similarities among these apparently random but unique patterns.

Characterization of crack patterns is useful in different fields of science and engineering. In soil mechanics, structural cracks are of much interest: their shape, size, and ruggedness carry with them clues to past stresses and strains imposed to the soil, with implications into their future stability and functionality [Preston et al., 1997]. In agriculture study of crack patterns can help determine whether different soil management treatments are having an effect on soil structure. Crack patterns acts as an indicator of the state of soil structure. If the crack patterns are different between the soil treatments, other structural properties of the soil are also likely to be different, but not vice versa. Crack pattern measurements together with bulk density can be used to calculate the volume changes during drying and this can increase the accuracy of water balance calculations for soils which shrink as they dry [Voase and Sanidad, 1996]. In concrete technology it is crucial to understand the pattern formation of surface cracks in structures, in particular for their aging properties. Surface cracks are easy paths for chemical species which may react with the material or reinforcement [Colina and Roux, 2000]. There is also a need to monitor the

cracks in cases such as in highway engineering where pavement cracking is an important issue.

Techniques for quantification of developing crack networks have evolved in recent years from direct field measurement to more sophisticated techniques such as the image analysis which will be presented in this paper.

Empirical formulas relating crack development to soil properties which can be determined from conventional soil survey reports were developed after studying crack formation in irrigated soils of alluvial plains (Yassoglou et al. 1994). A method for direct measurement of surface cracks development in soils has been proposed [Voase and Sanidad, 1996] as an improvement over earlier methods [Dasog and Shashidhara, 1993];[Zein-El-Abedine and Robinson, 1971]. With all these methods measurements are made manually over the crack pattern in the field.

Another form of characterising the morphology of two- and three-dimensional patterns is in terms of geometrical and topological descriptors based on concepts of integral geometry. According to integral geometry, there are three additive image functionals, called Minkowski functionals [Minkowski, 1991], that describe the morphological content of the 2D pattern, namely the area A, the perimeter U, and the Euler characteristic , the latter describing the topological connectivity of the pattern. Minkowski densities are calculated from the frequencies of different Minkowski numbers over the entire image or pattern. The detailed theory and simple examples to calculate these functionals step by step can be found in the literature [Michielsen and De Raedt, 2001]. The result of this approach is an objective numerical characterization of a given pattern. A new approach to recalculate the Minkowski densities for a series of morphological erosion [Serra, 1988] using circular structuring elements of increasing size [Mecke, 2000] has been used recently to characterise the crack pattern of soil [Vogel et al., 2005].

Image analysis is not new to geotechnical engineering; however, the advancement in the computer hardware and software capabilities has made it a new and efficient tool that can be automated and applied to series of images. In recent years many researchers have used image analysis in various applications for direct and indirect estimation of soil properties, including characterisation of crack patterns, crack detection and crack monitoring ([Horgan, 1998];[Preston et al., 1997]; [Puppala et al., 2004];[Sarmah et al., 1996];[Velde, 1999];[Velde, 2001];[Vogel et al., 2005]). The technique of distance map/distance transform data has been used to describe the soil structure [Holden, 2001] while image analysis of X-ray microtomograms has been used to study the behaviour of soft materials during 2-D [Léonard et al., 2002] and 3-D [Léonard et al., 2005] convective drying measurements. A CCD camera was used to study the cracking and dynamics of crack opening

in one-dimension desiccation experiments ([Lecocq and Vandewalle, 2002];[Lecocq and Vandewalle, 2003]).

In this appendix a technique to characterize the 2D crack network developing on the surface of a desiccating soil sample tested in the laboratory has been presented. A fully automatic, computer controlled, image acquisition system has been developed in order to monitor the crack pattern in real time with continuous monitoring during the experiment, using a high resolution digital camera placed straight above the sample, mounted on a specially designed mechanical arm. The camera was computer controlled and it was programmed to acquire and store images at a predetermined time frequency.

The image analysis technique is made in two basic steps. The first involves the preparation of the image for quantification, in which the digital image taken is processed in various stages, including conversion of the original RGB colour image to gray-scale image and then to a binary (black-and-white) image obtained by thresholding the gray-scale image. The second step consists of the analysis of the processed image to quantify the many parameters that characterize the crack pattern such as average crack width, total crack length, total area of cracks, total number of un-cracked cells, aspect ratio and area of the un-cracked cells, total number of crack segments and crack intersection angle. Crack initiation and time evolution of the cracking pattern (surface shrinkage with time) can also be determined. For the image analysis a public domain Java image processing program, ImageJ [Rasband, 2005], was used.

A.2 Image analysis

The image analysis technique is made in two basic steps. The first involves the preparation of the image, in which the original colour digital image is processed in various stages, including conversion of the colour image to gray-scale image, and then to a binary (black-and-white) image obtained by thresholding the gray-scale image. The second step consists of the analysis of the processed image to obtain the parameters that characterize the crack pattern. This is done by performing several types of binary operations depending on the desired magnitude. The public domain program ImageJ [Rasband, 2005], with plug-ins and additions has been used to carry out these operations.

The two main objectives of the image analysis were: a) the study of the evolution of the crack density factor or surface shrinkage [Miller et al., 1998] with time, for which sequences of images representing the initiation, formation, and evolution of cracks during the experiment were used; and b) the determination of the parameters characterizing the

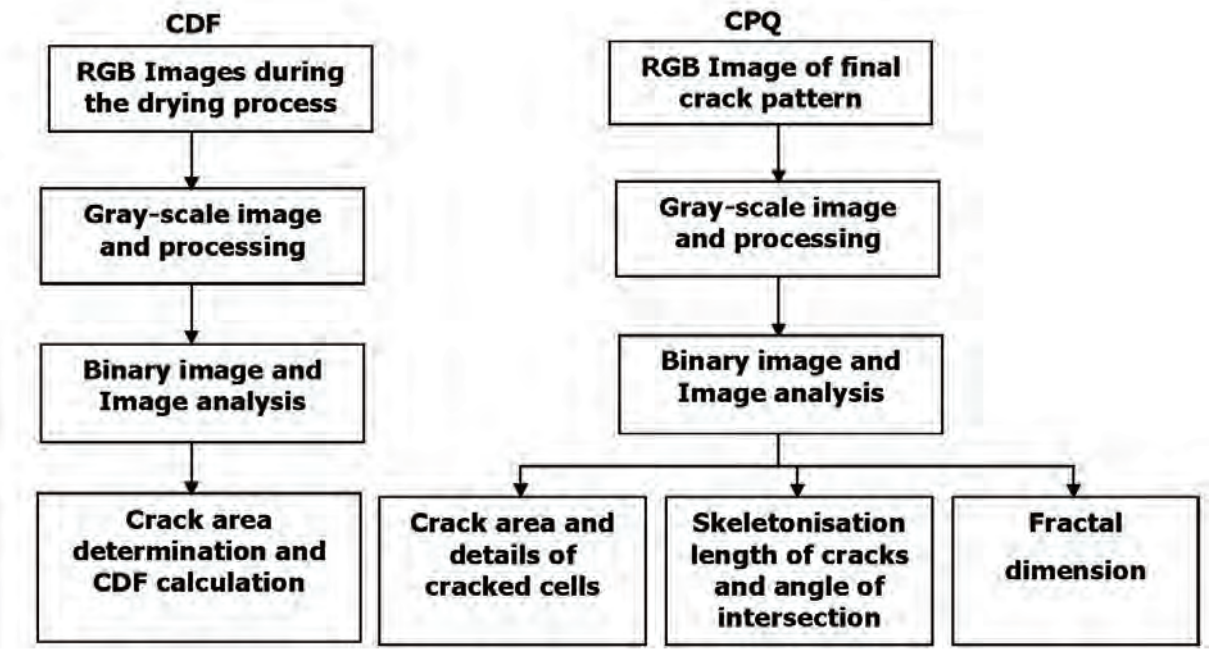

Figure A.1: Flow chart showing the image processing and analysis. Flow chart in the left shows the steps to quantify Crack Density Factor (CDF) and in the right shows steps for Crack Pattern Quantification (CPQ)

final crack pattern for which only the final image at the end of the experiment was used. Figure A.1 shows the flowcharts for these two procedures. The basic binary operations carried out on the images are summarized here.

A.2.1 Conversion RGB to gray-scale

A 2D continuous image is divided into an array of N rows by M columns. The intersection of a row and a column is termed a pixel. The value assigned to the integer coordinates [m, n] with m [0, M-1] and n [0, N-1] is A[m, n]. An RGB image of size mn pixels is stored as an mn3 data array that defines the red, green and blue colour components of each individual pixel. The colour of each pixel is determined by the combination of the red, green and blue intensities stored in each colour plane at the pixel's location. A gray-scale image is simply one in which the only colours are shades of gray. A gray colour is one in which the red, green and blue components all have equal intensity in the RGB space and so it is only necessary to specify a single intensity value for each pixel, as opposed to the three intensities needed to specify each pixel in a full colour image. In the present method the RGB images were converted to gray-scale by using the formula:

$$gray = 0.299 \times red + 0.587 \times green + 0.114 \times blue. \tag{A.1}$$

A.2.2 Gray-scale processing

The experiments had to be carried out in the laboratory with controlled environmental conditions. Therefore, no extra illumination on the surface of the drying soil could be used because it would have affected the test conditions. This resulted in images with uneven illumination. To correct this and to enhance the details of interest (to distinguish the cracks and the un-cracked areas) gray-scale processing was performed. This operation includes two single operations: a) subtract background that removes smooth continuous backgrounds using a rolling ball algorithm; the rolling ball radius should be at least as large as the radius of the largest object in the image that is not part of the background [Sternberg, 1983]; and b) un-sharpen mask that sharpens and enhances edges by subtracting a blurred version of the image (the un-sharp mask) from the original.

The un-sharp mask is created by Gaussian blurring the original image and then multiplying by a mask weight parameter. The Gaussian blur radius can be increased to increase contrast. An increase of the mask weight will result in additional edge enhancement. The process is described with the following equations:

$$U(m,n) = O(m,n) - \lambda(m,n) \tag{A.2}$$

where U(m,n) and O(m,n) are the modified and original images respectively, is the mask weight parameter ($\lambda > 0$) and G(m,n) is the Gaussian blur of the original image:

$$G(m,n) = g_{bk}(u,v) \cdot G(m,n) \tag{A.3}$$

where g_{bk} is the blur kernel function:

$$g_{bk}(u,v) = \left(\frac{1}{2\pi\sigma^2}\right) \exp\left(-\frac{r^2}{2\sigma^2}\right) \tag{A.4}$$

and,

$$r = (u^2 + v^2)^{1/2} \tag{A.5}$$

σ is the standard deviation of the Gaussian distribution, and r is the blur radius. Thus the Gaussian blur image G(m,n) is obtained by convolution of the Gaussian function in equation A.3 and the original image O(m,n).

A.2.3 Segmentation

Segmentation is the partitioning of a digital image into multiple regions or sets of pixels, according to a given criterion. The goal of segmentation is typically to locate objects of interest such as, in the case of the present work, separating the cracks and the un-cracked cells. There are different methods of image segmentation, the simplest one being the thresholding of a gray-scale image with a fixed threshold. Individual pixels in a gray-scale image U(m,n) are marked as 'object' pixels if their value is within the threshold range (assuming an object to be brighter than the background) and as 'background' pixels otherwise. Typically, an object pixel is given a value of '1' while a background pixel is given a value of '0'.

A.2.4 Binary processing

In order to be familiar with the binary operations, a brief description of each operation is given here: ERODE replaces each pixel with the minimum (lightest) value in a 33 neighbourhood, effectively removing pixels from the edges of black objects. DILATE replaces each pixel with the maximum (darkest) value in a 33 neighbourhood, effectively adding pixels to the edges of black objects. OPEN performs an ERODE operation followed by a DILATE operation, smoothing objects and removing isolated pixels. CLOSE performs a DILATE operation followed by an ERODE operation, smoothing objects and filling in small holes. More detailed information on these operations can be found in the literature [Serra, 1988]. The sequence of these operations is shown in figure A.2 , starting with a colour RGB image (figure A.2a) which is first converted to a gray-scale image (figure A.2b). Figure A.2c is the thresholded black-and-white image prior to any binary operations. It can be seen that this image has much unwanted data or noise. To eliminate this noise the binary operations described above are carried out. Figure 4d shows the result of an OPEN operation performed on the previous image (figure A.2c). Since it still shows some noise, a CLOSE operation is then carried out (figure A.2e), but this operation removes some valuable data.

To avoid the loss of valuable data, the CLOSE operation may be replaced with a DESPECKLE median filter. This filter replaces each pixel with the median value in its 33 neighbourhood. This is a time consuming operation because for each pixel in the selection, the nine pixels in its 33 neighbourhood must be sorted and the centre pixel replaced with the median value (the fifth). Median filters are good at removing "salt and pepper" noise. The binary image after this operation has conserved all the relevant information, while the unwanted data has been deleted (figure A.2f).

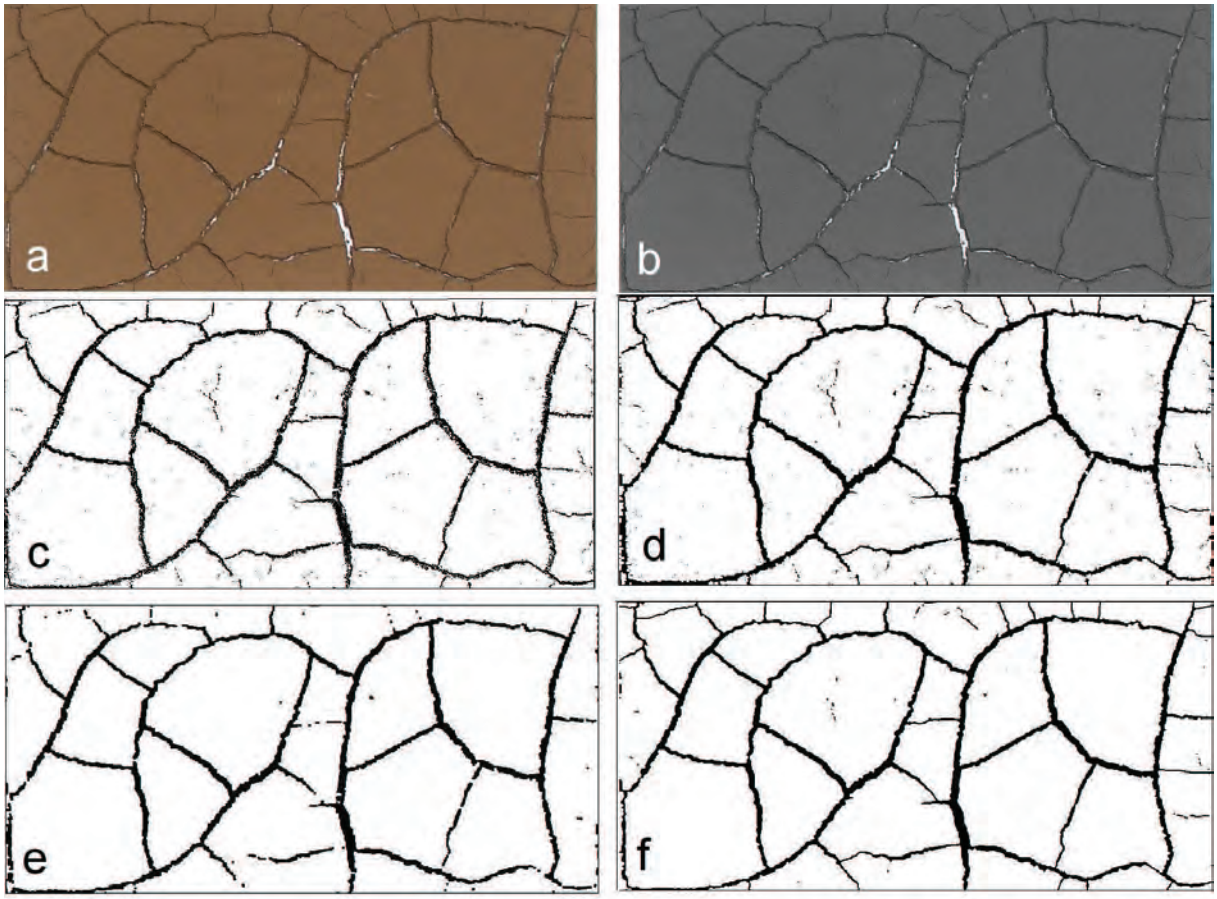

Figure A.2: Different stages of image processing (a) RGB colour image (b) gray scale image (c) Thresholded (binary) image (d) after opening (e) after Opening-closing (f) after opening-despackle.

A.2.5 Further specific processing

A.2.5.1 Characterization of the crack pattern

The crack pattern characterization is performed only on the final stage image, after the pattern has reached its final shape. Therefore, the image analysis has to be performed only on one single image, but the information that needs to be extracted is more elaborate, and further binary operations have to be carried out for specific measurements, with specific plug-ins to the basic ImageJ code.

ANALYZE: This plug-in counts and measures objects in binary images and is used to count the number of intact cells and their area. It works by scanning the image or selection until it finds the edge of an object. It then outlines the object, measures it using the measure command and resumes scanning until it reaches the end of the image or selection. Figure A.3 shows the intact cells numbered, while their area is produced as

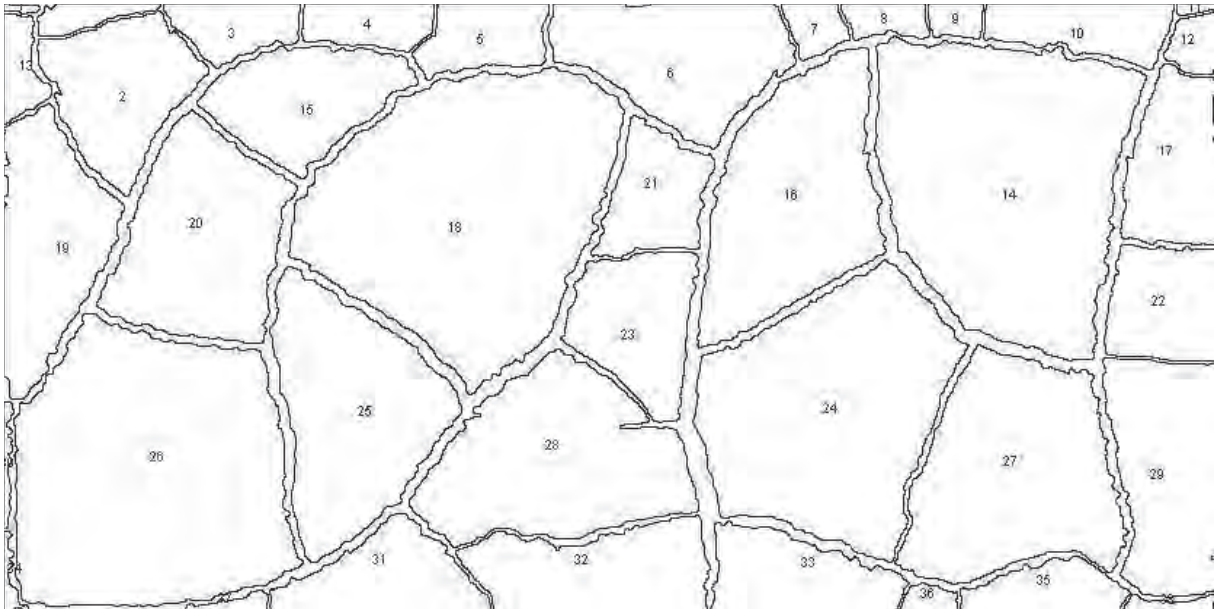

Figure A.3: Binary image of the Trial-image showing the boundaries of the cells

a separate file. Subtracting the total area of intact cells from the total initial area of the sample will give the area of cracks. Alternatively by counting the black and the white pixels the total area of cracks and the total area of intact cells can also be determined as a cross check. Additionally, the aspect ratio and the size distribution of the intact cells are also obtained.

SKELETONISE: It works by repeatedly removing pixels from the edges of objects in a binary image until they are reduced to single-pixel-wide skeletons. Figure A.4a shows the result of applying this plug-in on the image shown in Figure A.2f. Isolated single pixels that do not contribute to the total length of cracks have to be manually removed (figure A.4b).

SKELETAL DISSECTION: This plug-in [Joss, 2001] is used to measure the number of intersections, segments, and the total length of cracks. It dissects binary skeleton images, detecting the nodes where cracks intersect (figure A.4c). The result is given in a separate file that contains a row for each segment with the coordinates of both ends, number of pixels, length of the segment, and inter-nodal distance in pixel units. The sum of lengths of all segments will give the total length of cracks. The average width of cracks is obtained dividing the total area of cracks by the total length.

ANGLE CALCULATOR: In order to determine intersection angles a macro code [Joss, 2006] was used. This macro locates and isolates the intersection nodes and then calculates the angles between the intersecting lines. The macro calls the skeletal dissection

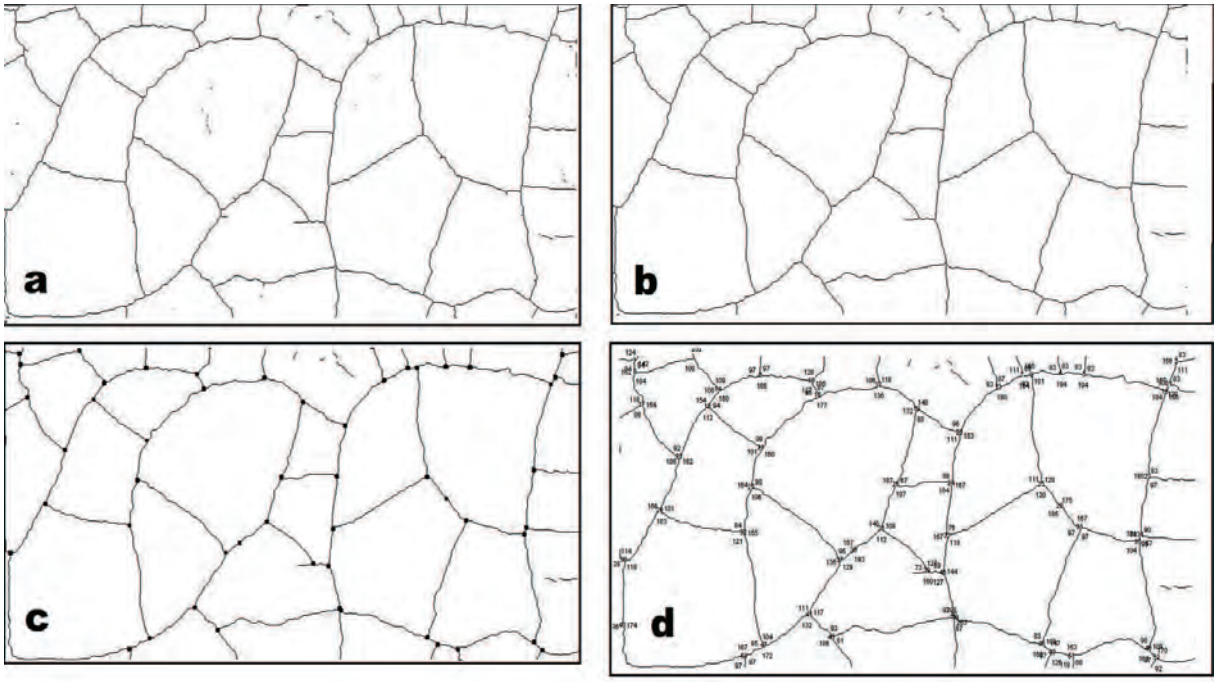

Figure A.4: Trial-image showing the Skeletal-crack-network (a)Before processing (b) after processing (c)after dissection (d)with intersection angles

plug-in to mark the intersection nodes on the skeletonised image (figure A.4b), and then a rolling ball kernel runs through the image isolating the already marked nodes and vertices (figure A.4c). Finally angles between successive segments around the node are determined in anticlockwise direction. The results are given in visual format with each intersection details (figure A.4d). Care should be taken while assigning the radius of the rolling ball kernel; a radius too small (e.g. less than 10 pixels) gives meaningless results due to pixilation and a radius too big while scanning the curved segments will distort the measured intersection angle.

A.2.5.2 Surface shrinkage or Crack Density Factor (CDF)

Figure A.5 shows sequential images of crack development at different stages of drying, from the appearance of the first crack to the final crack pattern, corresponding to test A0-20. Similar images were obtained for the other tests. Images captured at various stages of drying were used to calculate the crack density factor (CDF). The process involved a batch processing macro, which can sequentially execute a set of predetermined image conversion, processing and analysis operations on several images taking one at a time.

The processed images were stored in a new file while keeping the original image intact. A text file was created with results for each image. No image correlation technique was used in this work. Of course, relating an image at time t with the same image at time t-1 would result in better estimates of the surface shrinkage evolution. However, this would involve much computational time and development of a new algorithm for batch processing of the image correlation, which is beyond the scope of the current work.

Figure A.5: Sequence showing crack development from appearance of the first crack to the completion of drying and crack pattern formation corresponding to test A0-20

Appendix B

Publications

Journals

1. [Lakshmikantha et al., 2008d], Lakshmikantha, M. R., Prat, P. C., and Ledesma, A. (2008). Discussion on experimental study on fracture toughness and tensile strength of a clay. Engineering Geology, 101:295-296. doi:10.1016/j.enggeo.2008.07.001.

   Abstract

   The paper [Wang, J.-J., Zhu, J.-G., Chiu, C.F., Zhang, H., 2007. Experimental study on fracture toughness and tensile strength of a clay. Engineering Geology 94, 64-75.] focuses on two important fracture parameters of soils: tensile strength and fracture toughness. These parameters control the behaviour of soils in a wide range of situations, from the design of a simple footing to much complicated fracture behaviour of clay liners or covers. The authors have done extensive laboratory work to determine these two parameters and their laborious and complicated experimental program needs praise. However, some of the points raised in their conclusions, based on the analysis and comparison with the data from the literature, need to be discussed.

2. [Lakshmikantha et al., 2009a], Lakshmikantha, M. R., Prat, P. C., and Ledesma, A. (2009). Experimental evidences of size-effect in soil cracking. Canadian Geotechnical Journal, Under Review.

   Abstract

   Results of an experimental study on the formation of crack patterns during drying of a soil paste are presented. The test's aim is to ascertain whether Fracture Mechanics plays a significant role in the process of formation and/or propagation

of cracks during drying of soils due to changes in environmental conditions such as temperature and/or humidity. The experiments consist of five geometrically similar specimens in two series of different thickness, subjected to drying conditions in a laboratory controlled environment. Cracking initiates shortly before the soil reaches a near-solid quasi-brittle state of consistency/firmness. Although crack initiation can be explained by classical Soil Mechanics effective stress theory, crack development and propagation appears to be energy-driven. The results prove, in a qualitative and quantitative manner, that cracking stress (stress generating crack/s) depends on the size of the specimen. Fracture toughness values were determined for the same soil by compact tension tests at different moisture contents. Tensile strength was also determined by a direct method for two specific weights at different moisture contents.

3. [Lakshmikantha et al., 2009b], Lakshmikantha, M. R., Prat, P. C., and Ledesma, A. (2009). Image analysis for the quantification of a developing crack network on a drying soil. Geotechnical Testing Journal, Under Review.

Abstract

Image analysis techniques can be applied to study the crack patterns that appear in cohesive soils under drying conditions due to changes in the environmental conditions. Qualitative and quantitative characterization of these crack networks is needed to study the mechanical behaviour of a cracking soil, how cracks generate and propagate. For this purpose a simple laboratory set-up has been developed for real-time monitoring of the process of cracking due to desiccation of a cohesive soil, and to study the final crack pattern. The paper describes a simple technique to process sequences of images obtained during the laboratory tests, and how information can be gathered by means of image analysis, providing values for such parameters as average crack width, total crack length, total area of cracks, number, area and aspect ratio of un-cracked cells, or evolution of surface shrinkage with time

Proceedings of International conferences

1. [Lakshmikantha et al., 2006], Lakshmikantha, M. R., Prat, P. C., and Ledesma, A. (2006). An experimental study of cracking mechanisms in drying soils. In Thomas, H. R., editor, Environmental Geotechnics V., pages 533-540, London, UK. Thomas telford.

Abstract

Results of laboratory tests of cracking of a clayey soil due to desiccation are presented. Circular and rectangular soil samples of different sizes and boundary conditions were used in the tests. The samples were monitored while desiccating in laboratory-controlled conditions, taking pictures at regular intervals for image analysis. The analysis reveals that specimen size, thickness and aspect ratio have a strong influence on the crack pattern, total moisture loss and rate of moisture loss. Boundary conditions have also a considerable impact in the mechanism of drying. The results of the presented work provide the foundation for large-scale, fully monitored tests needed to develop predictive models for cracking of soils under drying conditions.

2. [Prat et al., 2006], Prat, P. C., Ledesma, A., and Lakshmikantha, M. R. (2006). Size effect in the cracking of drying soil. In Gdoutos, E. E., editor, Failure Analysis of Nano and Engineering Materials and Structures., pages 1373-1374, (abstract); full paper in accompanying CD-ROM, Alexandroupolis. Springer.

   Abstract

   The paper presents the results of an experimental study on the formation of crack patterns during drying of a clay paste. The tests aim is to ascertain whether Fracture Mechanics plays a significant role in the process of formation and/or propagation of cracks during drying of soils due to changes in environmental conditions such as temperature or humidity. The experiments consists of five geometrically similar specimens in two series of different thickness, subjected to drying conditions in a laboratory controlled environment. Cracking initiates shortly before the soil reaches a near-solid quasi-brittle consistency. Although crack initiation can be explained by classical Soil Mechanics effective stress theory, crack development and propagation appears to be energy-driven. The results prove, in a qualitative manner, that cracking stress depends on the size of the specimen.

3. [Lakshmikantha et al., 2007], Lakshmikantha, M. R., Prat, P. C., and Ledesma, A. (2007). Characterization of crack networks in desiccating soils using image analysis techniques. In Pande, G. N. and Pietruszczak, S., editors, Proceedings of the 10th International Symposium on Numerical Models in Geomechanics (NUMOG X)., pages 167-176, Rhodes, Greece. Balkema.

   Abstract

   Image analysis techniques can be applied to study the crack patterns that appear in cohesive soils under drying conditions due to changes in the environmental conditions. Qualitative and quantitative characterization of these crack networks is needed to study the mechanical behavior of a cracking soil, how cracks generate and propagate. The paper describes a simple technique to process sequences of images

ob-tained during laboratory tests, and how information can be gathered by means of image analysis, including average crack width, total crack length, total area of cracks, number, area and aspect ratio of un-cracked cells, surface shrinkage, etc. Crack initiation and time evolution of the crack pattern can also be determined. An example of application that shows size-effect in the drying of soils is presented.

4. [Lakshmikantha et al., 2008a], Lakshmikantha, M. R., Prat, P. C., Tapia, J., and Ledesma, A. (2008d). Effect of moisture content on tensile strength and fracture toughness of a silty soil. In D.G. Toll, and etal., editors, Unsaturated Soils - Advances in Geo-Engineering, pages 405-409, Durham, UK. Taylor and Francis.

   Abstract

   Determination of fracture parameters (tensile strength, fracture toughness) is essential in determining the cracking behaviour of soils. In drying soils, a crack initiates when the tensile stresses exceed the soil strength. Crack propagation is considered to be governed by the stress state in the crack front and subsequent dissipation of fracture energy, for which Fracture Mechanics Theory can be used. In this context characterizing the soil for these two parameters require two different testing equipments. The tensile strength was determined using existing equipment (direct method) at the Soil Mechanics Laboratory of UPC whereas new equipment was designed for the fracture toughness determination. The results of tensile strength tests are consistent with published literature. Fracture toughness decreases as the moisture content increases; an attempt is made to explain this using the concept of Rate Process Theory and Activation Energy of soils.

5. [Prat et al., 2008],Prat, P. C., Ledesma, A., Lakshmikantha, M. R., Levatti, H., and Tapia, J. (2008). Fracture mechanics for crack propagation in drying soils. In Singh, D. N., editor, GEOMECHANICS IN THE EMERGING SOCIAL TECHNOLOGICAL AGE, pages 1060-1067; in accompanying CD-ROM, Goa, India.

   Abstract

   Fracture parameters (Fracture toughness and Tensile strength) are determined experimentally at different moisture contents. The tensile strength was determined using existing equipment (direct method) at the Soil Mechanics Laboratory of UPC whereas new equipment was designed for the fracture toughness determination. The results of tensile strength tests are consistent with published literature. Fracture toughness decreases as the moisture content increases. A numerical model is presented for crack initiation and propagation in drying soils. The model combines the concepts of soil mechanics and fracture mechanics. Crack initiation and propagation criterions are based on fracture parameters. Experimental values of fracture parameters are used to trigger the crack initiation and propagation.

6. [Lakshmikantha et al., 2008b], Lakshmikantha, M. R., Prat, P. C., and Ledesma, A. (2008b). A new laboratory set-up to investigate desiccation cracking in soils. In Magnan, J.-P., and etal. editors, SEC 2008 (Scheresse et constructions/Drought and constructions), pages 163-168, Paris, France. LCPC.

Abstract

A laboratory set-up to study the mechanisms of cracking in drying soils is presented. The new equipment is capable of, imposing a prescribed environment, testing unusual big soil samples, monitoring the drying surface using a digital camera, recording the suction changes and the evolution of moisture loss. The set-up involves in fact an environmental chamber where a particular history of temperature and relative humidity can be imposed, and the evolution of the soil sample as well as its interactions with the chamber atmosphere can be monitored. The set-up was designed and constructed at the Soil Mechanics Laboratory of Tech. University of Catalonia (UPC) and the results of some preliminary drying tests are presented as well.

7. [Lakshmikantha et al., 2008c], Lakshmikantha, M. R., Prat, P. C., and Ledesma, A. (2008). Relation between tensile strength and fracture toughness for soils and rocks. In Pereira, J. M., and etal., editors, W(H)YDOC08 (3rd International Workshop of Young Doctors in Geomechanics), pages 75-78, Paris, France. Ecole des Ponts ParisTech.

Abstract

Tensile strength and Fracture toughness are two important material parameters characterising the fracture behaviour. Failure mechanism during experimental determination of both these parameters is by tensile failure. Tensile strength is a failure parameter of classical mechanics principles, where as fracture toughness is failure parameter of fracture mechanics laws. An empirical relation is proposed relating these two fracture parameters after a careful interpretation of experimental data from authors previous work and available data in literature.

Bibliography:

NOTE: The numbers at the end of each reference indicate the sections where they are cited in the text.

[Abu-Hejleh and Znidarčić, 1995] Abu-Hejleh, A. N. and Znidarčić, D. (1995). Desiccation theory for soft cohesive soils. *ASCE J.Geotech.Engrg.*, 121 6:493–502. 2.3.5, 2.6.1, 4.2.3.2, 4.2.3.2, 7.8.1, 9.4.2

[Albrecht and Benson, 2001] Albrecht, B. A. and Benson, C. H. (2001). Effect of desiccation on compacted natural clays. *ASCE,J. of Geotech. And Geoenvir. Engrg.*, 127 1:67–75. (document), 2.3.1.1, 2.3.1.2, 2.6, 2.2, 2.3.1.4, 2.5, 2.3.2, 2.3.2.1, 2.7, 2.3.3.2, 2.9, 2.5.1.1

[Alonso et al., 1987] Alonso, E. E., Gens, A., and High, D. W. (1987). Special problem soils: General report. i ecsmfe. In *Ground water effects in Geotechnical engineering, E. T. Hanrahan, T. L. L. Orr, and T. F. Widdis, eds*, pages 1087–114, Dublin. 4.2.2, 4.2.2.1

[Alonso and Lloret, 1995] Alonso, E. E. and Lloret, A. (1995). Settlement of a 12 storey building due to desiccation induced by trees. a case study. In *1st Intl.Conf. on Unsaturated Soils*, Paris,France. 2.3.6

[Alonso et al., 2009] Alonso, E. E., Pereira, J. M., Vaunat, J., and Olivella, S. (2009). A microstructurally-based effective stress for unsaturated soils. (submitted). *Géotechnique*. 4.2.8, 4.2.8

[Armstrong et al., 1994] Armstrong, A., Matthews, A., Portwood, A., Addiscott, T., and Leeds-Harrison, P. (1994). Modelling the effects of climate change on the hydrology and water quality of structured soils. *Soil Responses to Climate Change. NATO ASI Series 23*, pages 113–136. 1.1

[ASTM, 1983] ASTM (1983). Stanard test method for plane-strain fracture toughness of metallic materials. (e399-83). *American Society for Testing and Materials*. 4.3.2.6, 4.3.2.6, 4.3.4

[Ávila, 2004] Ávila, G. (2004). *Estudio de la retracción y el agrietamiento de arcillas. Applicación a la arcilla de Bogotá(In Spanish)*. PhD thesis, Technical University of

Catalonia, Barcelona, Catalonia(Spain). 4.2.1, 4.2.7.1, 4.2.8, 4.3.4, 5.1, 5.7.4, 6.2, 6.4.4, 6.7, 7.2.1

[Ávila et al., 2002] Ávila, G., Ledesma, A., and Lloret, A. (2002). Measurement of fracture mechanics parameters for the analysis of cracking in clayey soils. In *Third International Conference on Unsaturated Soils*, pages 547–552, Recife,Brasil. 2.5.1.1

[Ayad et al., 1997] Ayad, R., Konrad, J. M., and Souliè, M. (1997). Desiccation of a sensitive clay: application of the model CRACK. *Canadian Geotechnical Journal*, 34:943–951. 4.2.3.2, 4.3.2.6

[Babu and Gartung, 2001] Babu, G. L. S. and Gartung, E. (2001). Methodology for prediction of desiccation of clay liners. In *Clay science for Engineering, Adachi and Fukue eds.*, pages 187–190, Rotterdam. Balkema. 2.3.2, 2.3.2.1

[BAKER, 1981] BAKER, R. (1981). TENSILE STRENGTH, TENSION CRACKS, AND STABILITY OF SLOPES. *Soils and Foundations*, 21(2):1–17. 4.2.3.2, 4.2.3.2

[Barrera, 2002] Barrera, M. (2002). *Estudio experimental del comportamiento hidromecánico de suelos colapsables(In Spanish)*. PhD thesis, Technical University of Catalonia, Barcelona, Catalonia(Spain). (document), 3.2.2, 3.2, 3.1, 3.5, 3.6, 3.7, 3.2.4, 3.2, 3.9, 3.2.4, 3.10, 3.3, 3.11, 3.3.1, 3.4, 3.13, 3.6, 3.3.2, 3.14, 3.3.3, 3.7, 3.15, 3.16, 3.17, 3.8, 3.18, 4.2.8, 4.3.2.6, 4.3.4, 6.7, 7.22, 7.6, 7.9.1

[Bažant and Cedolin, 1983] Bažant, Z. and Cedolin, L. (1983). Finite Element Modeling of Crack Band Propagation. *Journal of Structural Engineering*, 109(1):69–92. 4.3.2.5, 6.3.2

[Bažant, 1984] Bažant, Z. P. (1984). Size effect in blunt fracture: Concrete, rock, metal. *ASCE J. Engrg. Mech.*, 110:518–535. (document), 6.1, 6.3.2, 6.3.2, 6.4.4, 6.8, 6.7

[Bažant, 1987] Bažant, Z. P. (1987). Fracture energy of heterogeneous materials and simillitude. In *International Conference on Fracture of Concrete and Rock, Houston, USA*, pages 390–402, Bethel. Society for Experimental Mechancis. 4.3.9.1

[Bažant and Jirásek, 1993] Bažant, Z. P. and Jirásek, M. (1993). R-curve modeling of rate and size effects in quasibrittle fracture. *Int. J. Fracture.*, 62:355–373. 6.7

[Bažant and Kazemi, 1990] Bažant, Z. P. and Kazemi, M. T. (1990). Size effect in fracture of ceramics and its use to determine fracture energy and effective process zone length. *J. Am. Ceramics Soc.*, 73(7):1841–1853. 6.7

[Bažant et al., 1994] Bažant, Z. P., Ozbolt, J., and Eligehausen, R. (1994). Fracture size effect: review of evidence for concrete structures. *ASCE J. Struct. Engrg.*, 120(8):2377–2398. 6.7

[Bažant and Planas, 1998] Bažant, Z. P. and Planas, J. (1998). Fracture and size effect in concrete and other quasibrittle materials. In *New Directions in Civil Engineering. W.F. Chen. Boca Ratn Eds.*, pages 29–37, Evanston IL. Northwestern University. (document), 4.3.2.2, 4.3.2.4, 4.3.2.5, 4.3.2.6, 6.1, 6.3.1, 6.1, 6.3.2, 6.2, 6.3.2, 6.4, 6.4.1, 6.4.5, 6.7

[Bažant and Prat, 1988] Bažant, Z. P. and Prat, P. C. (1988). Effect of temperature and humidity on fracture energy of concrete. *ACI Materials Journal*, July-August:262–271. 4.3.9.1, 4.3.9.1, 4.3.9.1

[Bažant et al., 1988] Bažant, Z. P., Sener, S., and Prat, P. C. (1988). Size effect tests of torsional failure of plain and reinforced concrete beams. *Materials Structures RILEM*, 21:425–430. 6.7

[Bažant et al., 2003] Bažant, Z. P., Zi, G., and McClung, D. (2003). Size effect law and fracture mechanics of the triggering of dry snow slab avalanches. *J. Geophys. Res*, 108(B2):2199. 6.7

[Bažant, 1995] Bažant, Z. (1995). Scaling of quasi-brittle fracture and the fractal question. *TRANSACTIONS-AMERICAN SOCIETY OF MECHANICAL ENGINEERS JOURNAL OF ENGINEERING MATERIALS AND TECHNOLOGY*, 117:361–361. 6.4.5

[Bažant, 1997] Bažant, Z. (1997). Scaling of quasibrittle fracture: hypotheses of invasive and lacunar fractality, their critique and Weibull connection. *International Journal of Fracture*, 83(1):41–65. 6.4.5

[Biddle, 1983] Biddle, P. G. (1983). Patterns of soil drying and moisture deficit in the vicinity of trees on clay soils. *Geotechnique*, 33-2:107–126. 2.3.6

[Bishop, 1960a] Bishop, A. (1960a). The measurement of pore pressure in the triaxial test. *Pore pressure and suction in soils*, pages 38–46. 4.2.3.2

[Bishop, 1960b] Bishop, A. (1960b). *The Principles of Effective Stress.* Norges Geotekniske Institutt. 4.2.8

[Blight, 1997] Blight, G. E. (1997). Interactions between the atmosphere and the earth. *Gotechnique*, 47 4:715–767. (document), 2.1, 2.3.3.3, 2.12

[Bohn, 2004] Bohn, S. (2004). Hierarchical crack patterns: a comparison with two-dimensional soap foams. *Colloids and surfaces A*, 263:46–51. (document), 8.2.1, 8.1, 8.2.3

[Bohn et al., 2005a] Bohn, S., Douady, S., and Couder, Y. (2005a). Four sided domains in hierarchical space dividing patterns. *Physical Review Letters*, 94:054503:1–4. 8.2.1

[Bohn et al., 2005b] Bohn, S., Pauchard, L., and Couder, Y. (2005b). Hierarchical crack pattern as formed by successive domian divisions. i. temporal and geometrical hierarchy. *Physical Review E*, 71:046214:1–7. 8.2.1, 8.2.3, 8.4.1

[Bohn et al., 2005c] Bohn, S., Platkiewicz, J., Andreotti, B., Adda-Bedia, M., and Couder, Y. (2005c). Hierarchical crack pattern as formed by successive domian divisions. ii. form disordered to deterministic beavior. *Physical Review E*, 71:046215:1–7. 8.2.1, 8.2.3, 8.4.1

[Bordas et al., 2007] Bordas, S., Rabczuk, T., and Zi, G. (2007). Three-dimensional crack initiation, propagation, branching and junction in non-linear materials by an extended meshfree method without asymptotic enrichment. *Engineering Fracture Mechanics*. doi:10.1016/j.engfracmech.2007.05.010. 9.4.2

[BRE, 1990] BRE (1990). *Assessment of damage in low rise buildings*, volume BRE Digest 251. Building Research Establishment, London. 1.1, 7.1

[Broek, 1986] Broek, D. (1986). *Elementary Engineering Fracture Mechanics*. Kluwer Academic Pub. 4.3.2.1, 4.3.2.2, 4.3.2.3, 4.3.2.4

[Bronswijk, 1988] Bronswijk, J. J. B. (1988). Modeling of water balance, cracking and subsidence in clay soils. *J. Hydrology*, 97 3 4:199–212. 2.6.2, 7.10.3

[Bronswijk, 1990] Bronswijk, J. J. B. (1990). Shrinkage geometry of a heavy clay soil at various stresses. *Soil Sci. Soc. Am. J*, 545:1500–1502. 2.5.3

[Bronswijk, 1991a] Bronswijk, J. J. B. (1991a). Drying,cracking and subsidence of a clay soil in a lysimeter. *Soil Science*, 1522:92–99. 2.5.3

[Bronswijk, 1991b] Bronswijk, J. J. B. (1991b). Relation between vertical soil movements and water-content changes in cracking clays. *Soil Sci. Soc. Am. J*, 555:1220–1226. 2.4.3, 2.5.3

[Bronswijk and Eversvermeer, 1990] Bronswijk, J. J. B. and Eversvermeer, J. J. (1990). Shrinkage of dutch clay soil aggregates. *Netherlands Journal of Agricultural Science*, 382:175–194. 2.5.3, 2.6.2, 7.10.4

[Carpinteri, 1994] Carpinteri, A. (1994). Scaling laws and renormalization groups for strength and toughness of disordered materials. *International journal of solids and structures*, 31(3):291–302. 6.4.5

[Carpinteri and Chiaia, 1995] Carpinteri, A. and Chiaia, B. (1995). Multifractal nature of concrete fracture surfaces and size effects on nominal fracture energy. *Materials and Structures*, 28(8):435–443. 6.4.5

[Carpinteri et al., 2002] Carpinteri, A., Spagnoli, A., and Vantadori, S. (2002). An approach to size effect in fatigue of metals using fractal theories. *Fatigue Fract Engng Mater Struct*, 25:619–627. 6.4.5

[CCIRG, 1991] CCIRG (1991). *The Potential Effects of Climate Change in the UK: Climate Change Impacts Review Group*. Department of the Environment, Her Majesty's Stationary Office, London. 1.1

[CCIRG, 1996] CCIRG (1996). *The Potential Effects of Climate Change in the UK: Climate Change Impacts Review Group*. Department of the Environment, Her Majesty's Stationary Office, London. 1.1, 7.1

[Christensen and Das, 1973] Christensen, R. W. and Das, B. M. (1973). Hydraulic erosion of remoulded choesive soils. *Highway Research Board*, Special Report 135:9–19. 4.3.9.1

[Christensen and Wu, 1964] Christensen, R. W. and Wu, T. H. (1964). Analysis of clay deformation as a rate process. *J. of soil Mech. Found. Eng. Div., ASCE*, 90SM(6):125–157. 4.3.9.1

[Chudnovsky et al., 1988] Chudnovsky, A., Saada, A., and Lesser, J. A. (1988). Micromechanics of deformation in fracture of overconsolidated clays. *Canadian Geotechnical Journal*, 25:213–221. (document), 2.5.1.1, 2.19, 2.6.1

[Colina and Roux, 2000] Colina, H. and Roux, S. (2000). Experimental model of cracking induced by drying shrinkage. *The European physical journal E EDP Sciences Springer-Verlag Societ Italiana di Fisica*, 1 2/3:189–194. 8.1, A.1

[Corte and Higashi, 1960] Corte, A. and Higashi, A. (1960). Experimental research on desiccation cracks in soil. *U. S. Army Snow Ice and Premafrost Research Establishment*, Report No. 66:Corps of Engineers Wilmette Illinois U. S. A. (document), 1.1, 2.1, 2.2.1, 2.3.1.3, 2.3, 2.3.1.4, 2.6, 2.3.3.2, 2.3.3.2, 2.10, 2.3.3.3, 2.11, 2.5, 2.5.1.1, 2.5.2, 5.1, 5.5, 5.6, 5.7.2, 5.7.4, 7.8.1, 8.1

[Cottrel, 1964] Cottrel, A. H. (1964). *The Mechanical Properties of Matter*. John Wiley Sons, New York. 4.3.9.1

[Coussy et al., 1998] Coussy, O., Eymard, R., and Lassabatère, T. (1998). Constitutive modeling of unsaturated drying deformable materials. *Journal of Engineering Mechanics*, 124(6):658–667. 9.4.2

[Dasog and Shashidhara, 1993] Dasog, G. S. and Shashidhara, G. B. (1993). Dimension and volume of cracks in a Vertisol under different crop covers. *Soil science*, 156:424–428. A.1

[Delage and Lefebvre, 1984] Delage, P. and Lefebvre, G. (1984). Study of the structure of a sensitive Champlain clay and of its evolution during consolidation. *Canadian Geotechnical Journal*, 21(1):21–35. 3.2.4, 3.2.4

[Diamond, 1970] Diamond, S. (1970). Pore size distributions in clays. *Clays and Clay Minerals*, 18(1):7–23. 3.2.4

[Driscoll, 1983] Driscoll, R. (1983). The influence of vegetation on the swelling and shrinkage of clays soils in Britain. *Geotechnique*, 33-2:93–105. 2.3.6

[Drumm et al., 1997] Drumm, E. C., Boles, D. R., and Wilson, G. V. (1997). Desiccation cracks result in preferential flow. *Geotechnical news*, June:22–25. (document), 1.1, 2.4.1.3, 2.16, 2.4.2, 2.17

[Dudley, 1970] Dudley, J. (1970). Review of Collapsing Soils. *Journal of the Soil Mechanics and Foundations Division*, 96(3):925–947. 4.2.2

[Escario and Sáez, 1986] Escario, V. and Sáez, J. (1986). The shear strength of partly saturated soils. *Canadian Geotechnical Journal*, 36(13):453–456. 4.2.3.2

[Evans and Fu,] Evans, A. G. and Fu, Y. *The Mechanical Behavior of Alumina*. Noyes Publications, Park Ridge. 4.3.9.1

[Fang, 1994] Fang, H. Y. (1994). Cracking and fracture behavior of soil. *Fracture Mechanics Applied to Geotechnical Engineering. ASCE, Geotechnical Special publication*, 43:102–117. (document), 2.4, 2.5.1.1

[Fang, 1997] Fang, H. Y. (1997). *Introduction to Environmental Geotechnology*, volume 14 of *New Directions in Civil Engineering*. CRC Press. (document), 2.1, 2.2.3, 2.1, 2.3.1.3, 2.3.3.1, 2.8

[Farrell et al., 1967] Farrell, D., Greacen, E., and Larson, W. (1967). The Effect of Water Content on Axial Strain in a Loam Soil under Tension and Compression. *Soil Science Society of America Journal*, 31(4):445. 4.2.3.3

[Favaretti, 1996] Favaretti, M. (1996). Tensile strength of compacted clays. In *State of the art in Unsaturated Soils, E. E. Alonso and P. Delage, eds*, pages 51–56, Rotterdam. Balkema. (document), 4.24, 5.6

[Finno, 1989] Finno, R. J. (1989). Field measurements of strain localization in soft clay. In *Cracking and damage: localization and size effect*, pages 42–54, Cachan France. J. Mazars and Z. P. Bažant, eds. 6.7

[Fleureau et al., 1993] Fleureau, J. M., Kheirbeksaoud, S., Soemitro, R., and Taibi, S. (1993). Behavior of clayey soils on drying wetting paths. *Canadian Geotechnical Journal*, 302:287–296. (document), 2.3.5, 2.6.2, 2.26, 7.10.4

[Flury et al., 1994] Flury, M., Leuenberger, J., Studer, B., Fluhler, H., Jury, W., and Roth, K. (1994). *Pesticide Transport Through Unsaturated Field Soils: Preferential Flow*. Swiss Federal Institute of Technology. 1.1

[Fredlund, 1979] Fredlund, D. (1979). Second Canadian Geotechnical Colloquium: Appropriate concepts and technology for unsaturated soils. *Canadian Geotechnical Journal*, 16(1):121–139. 7.10.1

[Fredlund et al., 1978] Fredlund, D., Morgenstern, N., and Widger, R. (1978). The shear strength of unsaturated soils. *Canadian Geotechnical Journal*, 15(3):313–321. 4.2.3.2

[Fredlund and Xing, 1994] Fredlund, D. and Xing, A. (1994). Equations for the soil-water characteristic curve. *Canadian Geotechnical Journal*, 31(4):521–532. 3.3.4.1

[Frookes and Denness, 1969] Frookes, P. G. and Denness, B. (1969). Observational studies of fissure patterens in cretaceous sediments of south-east England. *Geotechnique*, 19:453–477. (document), 2.2.2, 2.1, 2.2, 2.3, 2.4, 2.5

[Fujiyasu et al., 2000] Fujiyasu, Y., Fahey, M., and Newson, T. (2000). Field investigation of evaporation from freshwater tailings. *ASCE J. Geotech. and Geoenvironmental Engrg.*, 1266:556–567. 2.5.1.2

[García, 1997] García, V. (1997). *Estudio de la fractura en modo mixto de los materiales cuasifrágiles: aplicación al hormigón convencional y al hormigón de alta resistencia*. PhD thesis, Ph. D. Thesis, Technical University of Catalunya (UPC), Spain. 4.3.2.2, 4.3.2.5, 6.1

[Gens et al., 1995] Gens, A., Alonso, E., Suriol, J., and Lloret, A. (1995). Effect of structure on the volumetric behaviour of a compacted soil. *Proc. 1 stInt. Conf. On Unsaturated Soils, Paris. EE Alonso and P. Delage (eds.), Balkema/Presses des Ponts et Chaussées*, 1:83–88. (document), 3.3.1, 3.3.1, 3.13, 3.3.2, 3.14

[González, 1998] González, J. (1998). *Mecánica de Fractura, bases y aplicaciones*. Editorial Limusa-Noriega, México. 4.3.2.2, 4.3.2.4

[Griffith, 1921] Griffith, A. (1921). The phenomena of rupture and flow in solids. *Philosophical Transactions of the Royal Society of London. Series A, Containing Papers of a Math. or Phys. Character (1896-1934)*, 221(-1):163–198. 4.3.2.2

[GRIFFITHS and JOSHI, 1989] GRIFFITHS, F. and JOSHI, R. (1989). Change in pore size distribution due to consolidation of clays. *Geotechnique*, 39(1):159–167. 3.2.4, 3.2.4

[Groisman and Kaplan, 1994] Groisman, A. and Kaplan, E. (1994). An experimental study of cracking induced by desiccation. *EUROPHYSICS LETTERS*, 25(6):415–420. 5.7.2

[Haberfield and Johnston, 1989] Haberfield, C. and Johnston, I. (1989). Relationship between fracture toughness and tensile strength for geomaterials. *Proceedings of the 12th International Conference on Soil Mechanics and Foundation Engineering, Rio de Janeiro, Brazil*, 1:47–52. (document), 4.53, 4.4.1, 4.4.2

[Hagner, 2005] Hagner, T. (2005). Shrinkage characteristics and tensiel strength of choesive soils. Master's thesis, Bauhaus University, Weimar, Germany and Nanyang Technological University, Singapore. (document), 4.24

[Haines, 1923] Haines, W. (1923). The volume-changes associated with variations of water content in soil. *J. of Agricultural science*, 13:296–310. 2.3.3.2

[Hallet and Newson, 2001] Hallet, P. D. and Newson, T. A. (2001). A simple fracture mehcanics approach for assessing ductile crack growth in soil. *Soil Sci. Soc. Am. J.*, 65:1083–1088. 9.4.2

[Harison and Hardin, 1994] Harison, J. A. and Hardin, B. O. (1994). Cracking in clays - solutions to problems in earth structures. *Int. J. Num. Anal. Methods in Geomechanics*, 187:467–484. 2.1

[Harison et al., 1994] Harison, J. A., Hardin, B. O., and Mahboub, K. (1994). Fracture toughness of compacted cohesive soils using ring test. *Journal of Geotechnical Engineering*, 120 5:872–891. (document), 2.3.4, 2.8, 2.5.1.1, 4.1, 4.4.3, 9.4.2

[HARTGE and BACHMANN, 2000] HARTGE, K. and BACHMANN, J. (2000). Angles between cracks developed at primary shrinkage of finegrained soil material. *International agrophysics*, 14(1):43–51. 5.4.3, 8.4.1, 8.4.3

[Heibrock et al., 2003] Heibrock, G., Zeh, R. M., and Witt, K. J. (2003). Tensile strength of compacted clays. In *From experimental evidence towards numerical modeling of unsaturated soils. Schanz (ed.). ICSMGE Int. Conf. 18-19 September-2003.*, Weimar, Germany. Springer Verlag. (document), 4.2.3.3, 4.13, 4.2.8, 4.27, 5.6

[Hendriks et al., 1999] Hendriks, R. F. A., Oostindie, K., and Hamminga, P. (1999). Simulations of bromide tracer and nitrogen tgransport in a cracked caly soil with the FLOCR/ANIMO model combination. *Jouranl of Hydrology*, 215:94–115. 2.4.2

[Holden, 2001] Holden, N. M. (2001). Description and classification of soil structure using distance transform data. *European Journal of Soil Science*, 52:529–545. A.1

[Holtz, 1983] Holtz, W. G. (1983). The influence of vegetation on the swelling and shrinkage of clays in the United States of America. *Geotechnique*, 33-2:159–163. 2.3.6

[Horgan, 1998] Horgan, G. W. (1998). Mathematical morphology for analysing soil structure from images. *European Journal of Soil Science*, 49:161–173. A.1

[Horgan and Young, 2000] Horgan, G. W. and Young, L. M. (2000). An empirical stochastic model for the geometry of two-dimensional crack growth in soil with discussion. *Geoderma*, 96:263–268. (document), 2.6.3, 2.27

[Inglis, 1913] Inglis, C. (1913). Stresses in a plate due to the presence of cracks and sharp corners: Transactions of the Institution of Naval Architects, v. 55. 4.3.2.2

[Irwin, 1957] Irwin, G. (1957). Analysis of stresses and strains near the end of a crack traversing a plate. *J. of Applied Mech, T of ASME*, 24:361–364. 4.3.2.4

[Josa, 1988] Josa, A. (1988). *Un modelo elasto plástico para suelos no saturados*. PhD thesis. 4.2.2.1

[Joss, 2001] Joss, G. (2001). Skeletal Dissection Macro. A.2.5.1

[Joss, 2006] Joss, G. (2006). Personal communication. A.2.5.1

[Kim and Hwang, 2003] Kim, T.-H. and Hwang, C. (2003). Modeling of tensile strength on moist granular earth material at low water content. *Engineering geology*, 69:233–244. (document), 4.3, 4.2.3.3, 4.11

[Kodikara et al., 1998] Kodikara, J., Barbour, S. L., and Fredlund, D. G. (1998). An idealized framework for the analysis of cohesive soils undergoing desiccation: Discussion. *Canadian Geotechnical Journal*, 356:1112–1114. 2.6.2, 7.10.3

[Kodikara et al., 1999] Kodikara, J., Barbour, S. L., and Fredlund, D. G. (1999). Changes in clay structure and behaviour due to wetting and drying. In *Proc. of the 8th Australian-New Zealand conf. on Geomechanics*, pages 179–186. 2.1

[Kodikara et al., 2004] Kodikara, J., Nahlawi, H., and Bouazza, A. (2004). Modelling of curling in desiccating clay. *Canadian Geotechnical Journal*, 41(3):560–566. (document), 8.6.4, 8.32, 8.33, 8.6.4, 8.6.4, 8.35

[Konrad and Cummings, 2001] Konrad, J. and Cummings, J. (2001). Fracture toughness of frozen base and subbase soils in pavement. *Canadian Geotechnical Journal*, 38(5):967–981. 4.3.2.6

[Konrad and Ayad, 1997a] Konrad, J. M. and Ayad, R. (1997a). Desiccation of a sensitive clay: Field experimental observations. *Canadian Geotechnical Journal*, 34:929–942. (document), 2.5.1.1, 2.5.2, 2.20

[Konrad and Ayad, 1997b] Konrad, J. M. and Ayad, R. (1997b). An idealized framework for the analysis of cohesive soils undergoing desiccation. *Canadian Geotechnical Journal*, 34:477–488. (document), 2.3.5, 2.5.1.1, 2.6.1, 2.24, 2.6.2, 2.25, 2.6.2, 7.10.2, 7.10.3, 9.4.2

[Konrad and Ayad, 1998] Konrad, J. M. and Ayad, R. (1998). An idealized framework for the analysis of cohesive soils undergoing desiccation: Reply. *Canadian Geotechnical Journal*, 35:1115–1115. 2.6.2, 4.2.1, 6.7, 7.8.1, 7.10.3

[Lachenbruch, 1962] Lachenbruch, A. (1962). *Mechanics of Thermal Contraction Cracks and Ice-wedge Polygons in Permafrost*, volume 70. [Geological Society of America]. 8.6.1

[Lachenbruch, 1961] Lachenbruch, A. H. (1961). Depth and spacing of tension cracks. *Journal of Geophysical Research*, 66 12:4273–4292. 2.1, 2.5.2, 2.6.1, 7.8.1

[Lakshmikantha et al., 2006] Lakshmikantha, M. R., Prat, P. C., and Ledesma, A. (2006). An experimental study of cracking mechanisms in drying soils. In Thomas, H. R., editor, *Environmental Geotechnics V.*, pages 533–540, London, UK. Thomas telford. 9.2, 1

[Lakshmikantha et al., 2007] Lakshmikantha, M. R., Prat, P. C., and Ledesma, A. (2007). Characterization of crack networks in desiccating soils using image analysis techniques. In Pande, G. N. and Pietruszczak, S., editors, *Proceedings of the 10th International Symposium on Numerical Models in Geomechanics (NUMOG X).*, pages 167–176, Rhodes, Greece. Balkema. 3

[Lakshmikantha et al., 2008a] Lakshmikantha, M. R., Prat, P. C., and Ledesma, A. (2008a). Discussion on experimental study on fracture toughness and tensile strength of a clay. *Engineering Geology*, 101:295–296. 4

[Lakshmikantha et al., 2008b] Lakshmikantha, M. R., Prat, P. C., and Ledesma, A. (2008b). A new laboratory set-up to investigate desiccation cracking in soils. In Magnan, J.-P. and etal., editors, *SEC 2008 (Scheresse et constructions/Drought and constructions)*, pages 163–168, Paris, France. LCPC. 9.2, 6

[Lakshmikantha et al., 2008c] Lakshmikantha, M. R., Prat, P. C., and Ledesma, A. (2008c). Relation between tensile strength and fracture toughness for soils and rocks. In Pereira, J. M. and etal., editors, *W(H)YDOC'08 (3rd International Workshop of Young Doctors in Geomechanics)*, pages 75–78, Paris, France. Ecole des Ponts ParisTech. 7

[Lakshmikantha et al., 2009a] Lakshmikantha, M. R., Prat, P. C., and Ledesma, A. (2009a). Experimental evidences of size-effect in soil cracking. *Canadian Geotechnical Journal*, Under Riview. 2

[Lakshmikantha et al., 2009b] Lakshmikantha, M. R., Prat, P. C., and Ledesma, A. (2009b). Image analysis for the quantification of a developing crack network on a drying soil. *Geotechnical Testing Journal*, Under Review. 9.2, 3

[Lakshmikantha et al., 2008d] Lakshmikantha, M. R., Prat, P. C., Tapia, J., and Ledesma, A. (2008d). Effect of moisture content on tensile strength and fracture toughness of a silty soil. In Toll, D. G. and etal., editors, *Unsaturated Soils - Advances in Geo-Engineering*, pages 405–409, Durham, UK. Taylor and Francis. 9.2, 1

[Lambe, 1958] Lambe, T. (1958). The structure of compacted clay. *Journal of the Soil Mechanics and Foundations Division, ASCE*, 84:1–34. 4.2.2.1

[Lambe and Whitman, 1979] Lambe, T. and Whitman, R. (1979). *Soil Mechanics, SI Version*. Wiley. 4.2.3.2, 4.2.3.2

[Lecocq and Vandewalle, 2002] Lecocq, N. and Vandewalle, N. (2002). Experimental study of cracking induced by desiccation in one-dimensional systems. *The European physical journal-E EDP Sciences, Springer-Verlag, Societ Italiana di Fisica*, 8 4:445–452. 2.6.3, A.1

[Lecocq and Vandewalle, 2003] Lecocq, N. and Vandewalle, N. (2003). Dynamics of crack opening in a one-dimensional desiccation experiment. *Physica A: Statistical Mechanics and its Applications*, 321:431–441. A.1

[Lee et al., 1988] Lee, F. H., Lo, K. W., and Lee, S. L. (1988). Tension crack development in soils. *ASCE J. Geotech. Engrg.*, 114 8:915–929. (document), 2.1, 2.5.1.1, 2.18, 2.5.1.1, 4.3.2.6, 6.7

[Léonard et al., 2002] Léonard, A., Blacher, S., Marchot, P., Pirard, J. P., and Crine, M. (2002). Image analysis of X-ray microtomograms of soft materials during convective drying. *Journal of Microscopy*, 212:197–204. A.1

[Léonard et al., 2005] Léonard, A., Blacher, S., Marchot, P., Pirard, J. P., and Crine, M. (2005). Image analysis of X-ray microtomograms of soft materials during convective drying: 3D measurements. *Journal of Microscopy*, 218:247–252. A.1

[Li et al., 2000] Li, H., Yang, H., and Liu, Z. (2000). Experimental investigation of fracture toughness K_{IIC} of frozen soil. *Canadian Geotechnical Journal*, 37:253–258. 2.5.1.1

[Lloret et al., 1998] Lloret, A., Ledesma, A., Rodríguez, R. L., Sánchez, M. J., Olivella, S., and Suriol, J. (1998). Crack initiation in drying soils. In *2nd Int. Conference on Unsaturated Soils*, pages 497–502, Beijing China. 2.5.1.1, 2.6.2, 4.3.9.1, 5.2.1, 7.2.1, 7.5.1, 7.10.3, 9.4.2

[Lo, 1970] Lo, K. (1970). The operational strength of fissured clays. *Geotechnique*, 20(1):57–74. 6.4.4

[Lu et al., 2007] Lu, N., ASCE, M., Wu, B., and Tan, C. (2007). Tensile Strength Characteristics of Unsaturated Sands. *Journal of Geotechnical and Geoenvironmental Engineering*, 133:144. (document), 4.2.3.3, 4.12

[Mazars and Bažant, 1989] Mazars, J. and Bažant, Z. P. (1989). *Cracking and damage: localization and size effect*. Elsevier. 6.7

[Mazars et al., 1991] Mazars, J., Pijaudier-Cabot, G., and Saouridis, C. (1991). Size effect and continuous damage in cementitious materials. *Int. J. Fracture*, 51:159–173. 6.7

[McKay et al., 1993a] McKay, L. D., Cherry, J. A., and Gillham, R. W. (1993a). Field experiments in a fractured clay till-1. hydraulic conductivity and fracture aperture. *Water Resources Research*, 29-4:1149–1162. 2.4.1.3

[McKay et al., 1993b] McKay, L. D., Gillham, R. W., and Cherry, J. A. (1993b). Field experiments in a fractured clay till-1. solute and colloid transport. *Water Resources Research*, 29-12:3879–3890. 2.4.2

[Mecke, 2000] Mecke, K. (2000). Additivity, Convexity, and Beyond: Applications ofMinkowski Functionals in Statistical Physics. *Statistical Physics and Spatial Statistics*, pages 12–1. A.1

[Mesri and Ali, 1999] Mesri, G. and Ali, S. (1999). Undrained shear strength of a glacial clay overconsolidated by desiccation. *Gotechnique*, 49 2:181–198. 2.4.1.2

[MEYER et al., 1994] MEYER, K., LORENZ, P., BOHL-KUHN, B., and KLOBES, P. (1994). POROUS SOLIDS AND THEIR CHARACTERIZATION: METHODS OF INVESTIGATION AND APPLICATION. *Crystal research and technology(1979)*, 29(7):903–930. 3.2.4

[Michielsen and De Raedt, 2001] Michielsen, K. and De Raedt, H. (2001). Integral-geometry morphological image analysis. *Physics Reports*, 347(6):461–538. A.1

[Mikulitsch and Gudehus, 1995] Mikulitsch, W. A. and Gudehus, G. (1995). Uniaxial tension, biaxial loading and wetting tests on loses. In *First International Conference on Unsaturated Soils, Paris*, pages 145–150. Balkema / Presses des Ponts et Chaussées. (document), 4.2.3.3, 4.10, 4.2.4

[Miller et al., 1998] Miller, C. J., Mi, H., and Yesiller, N. (1998). Experimental analysis of desiccation crack propagation in clay liners. *J. Am. Water Resources Assoc*, 34 3:677–686. 5.7, 5.7.1, 6.6, A.2

[Minkowski, 1991] Minkowski, H. (1991). Verhandlungen des III internationalen mathematiker-kongresses in Heidelberg, 1904. *Also in Gesammelte Abhandlungen*, 2:50–51. A.1

[Mitchell, 1993] Mitchell, J. (1993). *Fundamentals of Soil Behaviour*. Wiley & Sons, London. 3.2.2, 6.4.3

[Mitchell, 1964] Mitchell, J. K. (1964). Shearing resistance of soils as a rate process. *J. Soil Mech. Found. Eng. Div., ASCE*, 90(SM1):29–61. 4.3.9.1

[Molenkamp and Nazemi, 2003] Molenkamp, F. and Nazemi, A. (2003). Interactions between two rough spheres, water bridge and water vapour. *Géotechnique*, 53(2):255–264. 4.2.3.3

[Morris et al., 1992] Morris, P. H., Graham, J., and Williams, D. J. (1992). Cracking in drying soils. *Canadian Geotechnical Journal*, 29:263–277. (document), 2.1, 2.5.2, 2.6.2, 2.6.2, 4.2.1, 4.2.3.2, 4.5, 7.8.1, 7.10.1, 7.10.2, 7.10.3, 9.4.2

[Morris et al., 1994] Morris, P. H., Graham, J., and Williams, D. J. (1994). Crack depths in drying clays using fracture mechanics. *Fracture Mechanics Applied to Geotechnical Engineering ASCE Geotechnical Special Publication*, pages 40–53. 2.1, 2.5.2, 6.7

[Munkholm et al., 2002] Munkholm, L. J., Schjnning, P., and Kay, B. D. (2002). Tensile strength of soil cores in relation to aggregate strength, soil fragmentation and pore characteristics. *Soil and tillage research*, 64:125–135. 4.2.3.3

[Murdoch, 1993] Murdoch, L. C. (1993). Hydraulic fracturing of soil during laboratory experiments. 1: Methods and observations. 2: Propagation. 3: Theoretical analysis. *Gotechnique*, 43 2:255–287. 2.5.1.2

[Nahlawi and Kodikara, 2002] Nahlawi, H. and Kodikara, J. (2002). Experimental observations on curling of desiccating clay. In *Third International Conference on Unsaturated Soils*, pages 5553–5556, Brasil. Recife. 2.1

[Nahlawi and Kodikara, 2006] Nahlawi, H. and Kodikara, J. (2006). Laboratory experiments on desiccation cracking of thin soil layers. *Geotechnical and Geological Engineering*, 24(6):1641–1664. 2.3.3.2, 5.1, 5.5, 5.6, 5.6, 7.8.1

[Nakahara and Matsuo, 2006] Nakahara, A. and Matsuo, Y. (2006). Transition in the pattern of cracks resulting from memory effects in paste. *Physical Review E*, 74(4):45102. (document), 8.14, 8.15, 8.16

[Nearing et al., 1991] Nearing, M. A., Parker, S. C., Bradford, J. M., and Elliot, W. J. (1991). Tensile strength of thirty-three saturated repacked soils. *Soil Sci. Soc. Am. J.*, 55:1546–1551. 2.3.4

[Nichols and Grismer, 1997] Nichols, J. R. and Grismer, M. E. (1997). Measurement of fracture mechanics parameters in silty-clay soils. *Soil Science*, 162 5:309–322. (document), 2.1, 2.4.3, 4.3.2.6, 4.53

[Omidi et al., 1996] Omidi, G. H., Thomas, J. C., and Brown, K. W. (1996). Effect of desiccation cracking on the hydraulic conductivity of a compacted clay liner. *Water, Air and Soil Pollution*, 89:91–103. (document), 2.3.1.2, 2.3.2, 2.4.1.3, 2.9

[Plummer and Gostin, 1981] Plummer, P. and Gostin, V. (1981). Shrinkage cracks; desiccation or synaeresis? *Journal of Sedimentary Research*, 51(4):1147–1156. (document), 7.7.3, 8.6.1, 8.2

[Prat et al., 2002] Prat, P. C., Ledesma, A., and Cabeza, L. (2002). Drying and cracking of soils: numerical modeling. In *8th Int. Conference on Numerical Models in Geomechanics NUMOG VIII*, pages 705–711, Rome, ltaly. 2.1, 2.5.2, 2.6.1, 6.7

[Prat et al., 2006] Prat, P. C., Ledesma, A., and Lakshmikantha, M. R. (2006). Size effect in the cracking of drying soil. In Gdoutos, E. E., editor, *Failure Analysis of Nano and Engineering Materials and Structures.*, pages 1373–1374, (abstract); full papaer in accompanying CD–ROM, Alexandroupolis. Springer. 9.2, 2

[Prat et al., 2008] Prat, P. C., Ledesma, A., Lakshmikantha, M. R., Levatti, H., and Tapia, J. (2008). Fracture mechanics for crack propagation in drying soils. In Singh, D. N., editor, *GEOMECHANICS IN THE EMERGING SOCIAL TECHNOLOGICAL AGE*, pages 1060–1067; in accompanying CD–ROM, Goa, India. 5

[Pratt, 1998] Pratt, B. (1998). Syneresis cracks: subaqueous shrinkage in argillaceous sediments caused by earthquake-induced dewatering. *Sedimentary Geology*, 117(1-2):1–10. (document), 8.21

[Preston et al., 1997] Preston, S., Griffiths, B. S., and Young, I. M. (1997). An investigation into sources of soil crack heterogeneity using fractal geometry. *European Journal of Soil Science*, 48 1:31–37. 1.1, 8.1, A.1

[Puppala et al., 2004] Puppala, A. J., Katha, B., and Hoyos, L. R. (2004). Volumetric shrinkage strain measurement in expansive soils using digital imaging technology. *Geotechnical testing journal*, 27 6. A.1

[Rabczuk et al., 2007] Rabczuk, T., Bordas, S., and Zi, G. (2007). A three-dimensional meshfree method for continuous crack initiation, nucleation and propagation in statics and dynamics. *Computational Mechanics*, 40(3):473–495. doi:10.1007/s00466-006-0122-1. 9.4.2

[Rasband, 2005] Rasband, W. S. (1995-2005). ImageJ. *National Institute of Health, Bethesda, Maryland, USA*, http://rsb.info.nih.gov/ij/. 5.7, 6.6, A.1, A.2

[Ravina, 1983] Ravina, I. (1983). The influence of vegetation on moisture and volume changes. *Geotechnique*, 33-2:151–157. 2.3.6

[Richards et al., 1983] Richards, B. G., Peter, P., and Emerson, W. W. (1983). The effects of vegetation on the swelling and shrinkage soils in Australia. *Geotechnique*, 33-2:159–163. 2.3.6

[Rodríguez, 2002] Rodríguez, R. (2002). *Estudio experimental de flujo y transporte de cromo, níquel y manganeso en residuos de la zona minera de Moa (Cuba): Influencia del comportamiento hidromecánico(In Spanish).* PhD thesis, Technical University of Catalonia, Barcelona,Catalonia(Spain). (document), 1.1, 2.3.4, 2.14, 2.3.5, 2.15, 2.4.2, 4.2.4, 7.2.1

[Rodríguez, 2006] Rodríguez, R. (2006). Hydrogeotechnical characterization of a metallurgical waste. *Can. Geotech. J.*, 43:1042–1060. 5.2.1, 7.2.1

[Rodríguez et al., 1999] Rodríguez, R., Candela, L., Lloret, A., and Ledesma, A. (1999). Preliminary study of crack formation in a mining tailing dam to evaluate transport of contaminants. *Geophysical Research Abstracts*, 12. 7.2.1

[Rodríguez et al., 2007] Rodríguez, R., Sánchez, M., Ledesma, A., and Lloret, A. (2007). Experimental and numerical analysis of desiccation of a mining waste. *Canadian Geotechnical Journal*, 44(6):644–658. 4.2.1, 5.1, 5.2.1, 5.6, 5.6, 7.2.1, 9.4.2

[Romero, 1999] Romero, E. (1999). Characterisation and thermo-hydro-mechanical behaviour of unsaturated Boom clay: an experimental study. *PhD Thesis, Polytechnical University of Catalunya, Barcelona, Spain.* 3.2.4, 3.2.4, 3.3.4.2, 7.9.2

[Romero et al., 1999] Romero, E., Gens, A., and Lloret, A. (1999). Water permeability, water retention and microstructure of unsaturated compacted Boom clay. *Engineering Geology*, 54(1-2):117–127. 3.2.4

[Romero and Vaunat, 2000] Romero, E. and Vaunat, J. (2000). Retention curves of deformable clays. *Experimental evidence and theoretical approaches in unsaturated soils (eds A. Tarantino and C. Mancuso)*, pages 91–106. 3.3.4.1, 4.2.8

[Rounsevell et al., 1999] Rounsevell, M., Evans, S., and Bullock, P. (1999). Climate Change and Agricultural Soils: Impacts and Adaptation. *Climatic Change*, 43(4):683–709. 1.1

[Saada et al., 1994a] Saada, A. S., Bianchini, G. F., and Liang, L. (1994a). Cracks, bifurcation and shear bands propagations in saturated clays. *Gotechnique*, 44 1:35–64. 2.1, 2.5.1.1

[Saada et al., 1994b] Saada, A. S., Liang, L., and Bianchini, G. F. (1994b). Fracture mechanics and plasticity in saturated clay. *Fracture Mechanics Applied to Geotechnical Engineering ASCEGeotechnical Special Publication*, 43:21–39. 2.5.1.1

[Sarmah et al., 1996] Sarmah, A. K., Pillai-McGarry, U., and McGarry, D. (1996). Repair of the structure of a compacted vertisol via wet/dry cycles. *Soil & Tillage Research*, 38:17–33. A.1

[Schubert, 1982] Schubert, H. (1982). *Kapillarität in porösen Feststoffsystemen*. Springer. 4.2.3.3

[Schubert et al., 1975] Schubert, H., Herrmann, W., and Rumpf, H. (1975). Deformation Behaviour of Agglomerates under Tensile Stress. *Powder Technol*, 11(2):133–146. 4.2.3.3

[Serra, 1988] Serra, J. (1988). Image Analysis and Mathematical Morphology, volume 2. A.1, A.2.4

[Snyder and Miller, 1985] Snyder, V. A. and Miller, R. D. (1985). Tensile Strength of Unsaturated Soils. *Soil Sci Soc Am J*, 49(1):58–65. (document), 4.2.3.2, 4.6, 4.2.3.2

[Srawley, 1976] Srawley, J. E. (1976). Wide range stress intensity factor expressions for astm e-399 standard fracture toughness specimens. *Int. J. Fracture*, 95:475–476. 4.3.2.6, 4.3.4

[Sridharan and Prakash, 2000] Sridharan, A. and Prakash, K. (2000). Shrinkage limit of soil mixtures. *Geotechnical Testing Journal*, 23 1:3–8. 2.5.3

[Sternberg, 1983] Sternberg, S. (1983). Biomedical image processing. *IEEE Computer*, January:22–34. A.2.2

[Sture et al., 1999a] Sture, S., Alqasabi, A., and Ayari, M. (1999a). Fracture and size effect characters of cemented sand. *International Journal of Fracture*, 95(1):405–433. 4.3.2.6

[Sture et al., 1999b] Sture, S., Alqasabi, A., and Ayari, M. (1999b). Fracture and size effects characters of cemented sand. *Int. J. of Fracture*, 95:405–433. 6.7

[Sulem and Vardoulakis, 1989] Sulem, J. and Vardoulakis, I. (1989). Bifurcation analysis of the triaxial test on rock specimens, in cracking and damage: localization and size

effect. In *J. Mazars and Z.P. Bazant Eds.*, pages 308–322. Elsevier Applied Science. 6.7

[Swarbrick, 1994] Swarbrick, G. E. (1994). The use of small scale experiments to predict desiccation of tailings. In *First International Congress on Environmental Geomechanics*, pages 563–568, Edmonton Alberta Canada. BiTech. 2.5.1.2

[Swarbrick and Fell, 1992] Swarbrick, G. E. and Fell, R. (1992). Modeling desiccating behavior of mine tailings. *ASCE J. of Geotech. Engrg.*, 118 4:540–557. 2.5.1.2

[Tamrakar et al., 2005] Tamrakar, S. B., Toyosawa, Y., Mitachi, T., and Itoh, K. (2005). Tensile strength of compacted and saturated soils using newly developed thesnile strength measuring apparatus. *Soils and Foundations*, 45-6:103–110. (document), 4.9, 4.2.3.3, 4.24, 5.6

[Tang and Graham, 2000] Tang, G. X. and Graham, J. (2000). Soil volumetric shrinkage measurements - a simple method. *Geotechnical testing journal*, 23-3:377–382. (document), 4.2.3.3, 4.8

[Thorne, 1984] Thorne, C. P. (1984). Strength assessment and stability analyses for fissured clays. *Gotechnique*, 34-3:305– 322. 2.4.1.2

[Thouless et al., 1983] Thouless, M. D., Hsueh, C. H., and Evans, A. G. (1983). A damage model of creep crack growth in polycrstals. *Acta Metallurgica*, 31(10):1675–1687. 4.3.9.1

[Toga and Alaca, 2006] Toga, K. B. and Alaca, B. E. (2006). Junction formation during desiccation cracking. *Physical Review E (Statistical, Nonlinear, and Soft Matter Physics)*, 74(2):021405. (document), 8.18, 8.4.1

[Towner, 1987a] Towner, G. (1987a). The tensile stress generated in clay through drying. *Journal Agricultural Engineering Research, New York*, 37(4):279–289. 4.2.3.2, 4.2.8

[Towner, 1987b] Towner, G. D. (1987b). The mechanics of cracking of drying clay. *J. agric. Engrg. Res*, 36:115–124. (document), 2.1, 2.3.3.2, 2.7, 2.3.4, 2.13, 2.5.1.1, 2.6.1, 4.2.1, 4.2.3.3, 4.7

[Vallejo, 1987] Vallejo, J. (1987). Influence of fissures in a stiff clay subjected to direct shear. *Geotechnique*, 37(1):69–82. 6.4.4

[Vallejo, 1994] Vallejo, L. E. (1994). Application of fracture mechanics to soils: An overview. *Fracture Mechanics Applied to Geotechnical Engineering ASCE Geotechnical Special Publication*, 43:1–20. 2.1, 2.3, 2.5.1.1, 9.4.2

[van Genuchten, 1980] van Genuchten, M. (1980). A closed-form equation for predicting the hydraulic conductivity of unsaturated soils. *Soil Sci. Soc. Am. J*, 44(5):892–898. 3.3.4.1, 3.3.4.2, 4.2.8

[Vanapalli et al., 1996a] Vanapalli, S. K., Fredlund, D. G., and Pufual, D. E. (1996a). The relationship between the soil water charactersitc curve and the unsaturated shear strength of a compacted glacial till. *Geotechnical Testing Journal,GTJODJ*, 19 3:259–268. 2.6.2, 7.10.3

[Vanapalli et al., 1996b] Vanapalli, S. K., Fredlund, D. G., Pufual, D. E., and Clifton, A. W. (1996b). Model for the prediction of shear strength with respect to soil suction. *Canadian Geotechnical Journal*, 33 3:379–392. 2.3.5

[Vázquez-suñé, 1998] Vázquez-suñé, E. (1998). Les aigües subterrànies del plà de barcelona. Master's thesis, ETSECCPB-UPC. School of Civil Engineering - Barcelona. (document), 3.1, 3.2.1

[Velde, 1999] Velde, B. (1999). Structure of surface cracks in soil and muds. *Geoderma*, 93:101–124. A.1

[Velde, 2001] Velde, B. (2001). Surface cracking and aggregate formation observed in a Rendzina soil, La touche(vienne) France. *Geoderma*, 99:261–276. A.1

[Voase and Sanidad, 1996] Voase, A. J. R. and Sanidad, W. B. (1996). A method for measuring the development of surface cracks in soils: Application to crack development after lowland rice. *Geoderma*, 71 3 4:245–261. 8.1, A.1

[Vogel et al., 2005] Vogel, H. J., Hoffmann, H., and Roth, K. (2005). Studies of crack dynamics in clay soil i. experimental methods, results, and morphological quantification. *Geoderma*, 125:3-4:203–211. 8.4.3, A.1

[Vogt, 1974] Vogt, P. (1974). Volcano spacing, fractures, and thickness of the lithosphere. *Earth Planet. Sci. Lett*, 21:235–252. 8.1

[Wang et al., 2007] Wang, J., Zhu, J., Chiu, C., and Zhang, H. (2007). Experimental Study on Fracture Toughness and Tensile strength of a Clay. *Engineering Geology*, 94:65–75. 4.4.3

[Weinberger, 1999] Weinberger, R. (1999). Initiation and growth of cracks during desiccation of stratified muddy sediments. *Journal of Structural Geology*, 21:379–386. (document), 2.1, 2.5.2, 2.21, 2.22, 2.23, 7.8.1, 7.8.3

[Wells et al., 2001] Wells, R. R., Prasad, S. N., and Romkens, M. J. M. (2001). Cracking modes of an expansive Mississippi delta soil. Technical report, TEKTRAN,USA, The Agricultural research service of the U. S. Department of Agriculture. 2.5.2

[Wendling and Meibner, 2001] Wendling, S. and Meibner, H. (2001). Soil water suction and compaction influence on desiccation cracks of mineral liners. In *Clay science for Engineering, Adachi and Fukue eds.*, pages 191–198, Rotterdam. Balkema. 2.5.1.2

[Willard et al.,] Willard, H., Merritt, L., and Dean, J. Instrumental methods of analysis. *New York*. 3.2.2

[William, 2006] William, A. (2006). Mudcracks and the flood. *Institute for creation research*, http://www.icr.org/article/3111/. 8.6.2

[Wroth and Houlsby, 1984] Wroth, C. and Houlsby, G. (1984). *Soil Mechanics: Property Characterization and Analysis Procedures.* University of Oxford Department of Engineering Science. (document), 4.2.2.1, 4.2

[Yesiller et al., 2000] Yesiller, N., Miller, C. J., Inci, G., and Yaldo, K. (2000). Desiccation and cracking behavior of three compacted landfill liner soils. *Engineering Geology*, 57:105–121. 1.1, 2.5.1.2

[Yong and Warkentin, 1975] Yong, R. and Warkentin, B. (1975). *Soil properties and behaviour*. Elsevier. 3.2.2

[Yoshida and Adachi, 2001] Yoshida, S. and Adachi, K. (2001). Influence of the distribution of soil suction on crack patterns in farmlands. In *Clay science for Engineering, Adachi and Fukue eds.*, pages 191–198, Rotterdam. Balkema. 2.4.3

[Yoshimi and Osterberg, 1963] Yoshimi, V. and Osterberg, J. (1963). Compression of partially saturated cohesive soils. *J. of Soil Mech. And Found. Div. ASCE*, 89:1–24. (document), 4.2.2.1, 4.1

[Zein-El-Abedine and Robinson, 1971] Zein-El-Abedine, A. and Robinson, G. H. (1971). A study on cracking in some vertisols of the sudan. *Geoderma*, 5:229–241. A.1

[Zhang et al., 2003] Zhang, F., Zhang, R., and Kang, S. (2003). Estimating temperature effects on water flow in variably saturated soils using activation energy. *Soil Sci. Soc. Am. J*, 67:1327–1333. 4.3.9.1

[Zhang, 2002] Zhang, Z. (2002). An empirical relation between mode I fracture toughness and the tensile strength of rock. *International Journal of Rock Mechanics and Mining Sciences*, 39(3):401–406. 4.4.1

Back cover:
Final crack pattern
(desiccation test A0-20)